The background image shows an aerial perspective of a wide river system. The river flows from the top right towards the bottom left, creating several large, sweeping curves. The banks of the river are densely covered with green trees and vegetation. The water is a deep blue-grey color. In the top left corner, there is a solid yellow square.

World Water Resources

Guillermo Q. Tabios III

---

# Water Resources Systems of the Philippines: Modeling Studies

 Springer

# **World Water Resources**

**Volume 4**

## **Series Editor**

V. P. Singh, Department of Biological and Agricultural Engineering & Zachry  
Department of Civil Engineering, Texas A&M University, College Station, TX, USA

This series aims to publish books, monographs and contributed volumes on water resources in the world, with particular focus per volume on water resources of a particular country or region. With the freshwater supplies becoming an increasingly important and scarce commodity, it is important to have under one cover up to date literature published on water resources and their management, e.g. lessons learnt or details from one river basin may be quite useful for other basins. Also, it is important that national and international river basins are managed, keeping each country's interest and environment in mind. The need for dialog is being heightened by climate change and global warming. It is hoped that the Series will make a contribution to this dialog. The volumes in the series ideally would follow a "Three Part" approach as outlined below: In the chapters in the first Part *Sources of Freshwater* would be covered, like water resources of river basins; water resources of lake basins, including surface water and under river flow; groundwater; desalination; and snow cover/ice caps. In the second Part the chapters would include topics like: *Water Use and Consumption*, e.g. irrigation, industrial, domestic, recreational etc. In the third Part in different chapters more miscellaneous items can be covered like impacts of anthropogenic effects on water resources; impact of global warning and climate change on water resources; river basin management; river compacts and treaties; lake basin management; national development and water resources management; peace and water resources; economics of water resources development; water resources and civilization; politics and water resources; water-energy-food nexus; water security and sustainability; large water resources projects; ancient water works; and challenges for the future. Authored and edited volumes are welcomed to the series. Editor or co-editors would solicit colleagues to write chapters that make up the edited book. For an edited book, it is anticipated that there would be about 12–15 chapters in a book of about 300 pages. Books in the Series could also be authored by one person or several co-authors without inviting others to prepare separate chapters. The volumes in the Series would tend to follow the "Three Part" approach as outlined above. Topics that are of current interest can be added as well.

### **Readership**

Readers would be university researchers, governmental agencies, NGOs, research institutes, and industry. It is also envisaged that conservation groups and those interested in water resources management would find some of the books of great interest. Comments or suggestions for future volumes are welcomed.

### **Series Editor:**

V. P. Singh, Department of Biological and Agricultural Engineering & Zachry Department of Civil Engineering, Texas A&M University, College Station, TX, USA.  
vsingh@tamu.edu

More information about this series at <http://www.springer.com/series/15410>

Guillermo Q. Tabios III

# Water Resources Systems of the Philippines: Modeling Studies

Guillermo Q. Tabios III

Institute of Civil Engineering and National Hydraulic Research Center  
University of the Philippines, Diliman  
Quezon City, Philippines

National Academy of Science and Technology  
Taguig City, Philippines

ISSN 2509-7385

World Water Resources

ISBN 978-3-030-25400-1

<https://doi.org/10.1007/978-3-030-25401-8>

ISSN 2509-7393 (electronic)

ISBN 978-3-030-25401-8 (eBook)

© Springer Nature Switzerland AG 2020

This work is subject to copyright. All rights are reserved by the Publisher, whether the whole or part of the material is concerned, specifically the rights of translation, reprinting, reuse of illustrations, recitation, broadcasting, reproduction on microfilms or in any other physical way, and transmission or information storage and retrieval, electronic adaptation, computer software, or by similar or dissimilar methodology now known or hereafter developed.

The use of general descriptive names, registered names, trademarks, service marks, etc. in this publication does not imply, even in the absence of a specific statement, that such names are exempt from the relevant protective laws and regulations and therefore free for general use.

The publisher, the authors, and the editors are safe to assume that the advice and information in this book are believed to be true and accurate at the date of publication. Neither the publisher nor the authors or the editors give a warranty, expressed or implied, with respect to the material contained herein or for any errors or omissions that may have been made. The publisher remains neutral with regard to jurisdictional claims in published maps and institutional affiliations.

This Springer imprint is published by the registered company Springer Nature Switzerland AG.  
The registered company address is: Gewerbestrasse 11, 6330 Cham, Switzerland

*To my papa, Nono, and mama, Nida, who  
kindly nurtured me  
and  
to my wife, Aida, and daughter, Gillian, who  
endearingly bring out the best in me*

# Preface

Modeling of water resources systems is essential to develop science-based information, policies, and management actions for effective water resources planning design and operations. Models have been utilized for descriptive and prescriptive purposes such as understanding the behavior of the water resources system; evaluation of strategies to restore, enhance, maintain, or control the integrity of the water resource; detection and surveillance for water resources regulation; as well as forecasting for real-time operations or prediction for possible future behavior of the water resources systems. These days, water resources models and modeling tools have become more sophisticated since one must not only consider the physical and ecological component of the water resources system but also its interaction with the socioeconomic and human systems. In linking science and public policy toward an effective integrated water resources management (IWRM), the decision support system (DSS) which essentially evolves around models and modeling tools is an integral part of IWRM process as a platform or vehicle to link science and technology advances to public policy and management decisions. Water resources planners, managers, and other specialists who are responsible for the development and operation of water resources systems as well as stakeholders can use the DSS in understanding, articulating, and building *a shared vision* of how the water resources system functions; how to evaluate feasible, alternative management options including their impacts or consequences; and finally how to develop consensus for its sustainable development and utilization.

In the Philippines, modeling of water resources systems for planning, design, and management is not quite a common practice especially in government agencies involved in managing the country's water resources. One of the reasons is that the Philippines still lacks investments in science-based management and decision tools. Most water-related agencies in the Philippines do not have a dedicated scientific division in their offices to employ science-based analysis or modeling tools although some agencies employ consultants to conduct water resources modeling but on project basis. Having a permanent modeling group will ensure continuous updating and adaptive master planning and operational studies of water resources system

because watersheds or natural resources systems in general are evolutionary in nature due to land use change, anthropogenic activities, economic change, and climate change. Another challenge is that the country lacks investments in sustained and regular monitoring of water-related data. Thus, model development can be hardly calibrated against the observed data so that the art of modeling plays a significant role to judiciously use experience, knowledge, and insights into the physics of the process and, to some extent, imagination to validate and qualify the results of the modeling studies.

This book presents several modeling experiences and studies of water resources systems of the Philippines and advocates the use of modeling tools to ensure science-based, policy formulations and management decisions in water resources planning and management. The suite of water resources modeling studies includes surface and groundwater modeling for water utilization, reservoir planning and operations studies with optimization-simulation models, reservoir sedimentation studies, hydrodynamic and water quality modeling of bays and lakes, flood and dambreak modeling studies, pipe network distribution modeling with optimization, climate change studies for reliability of reservoir operations, and modeling for environmental assessment studies. The storylines of the motivation and/or purpose of the various modeling studies conducted are also presented for certain water resources systems studied.

Several models used here are available as public domain models and were designed with various optional methods that can be used for hydrologic, hydraulic, and water quality analysis. These public domain models require familiarity and hands-on experience; thus, using these models is more of an art rather than purely the science of modeling. Some models used here were also developed by the author himself and, in certain cases, with collaborators. For these latter models, the author is not only proficient in using them but also very much familiar with the theoretical basis, structure, and algorithms of these models.

The book is intended for professionals, practitioners, as well as undergraduate and graduate students to learn the art and science of modeling water resources systems, in general, and water resources systems of the Philippines, in particular. As the book contains details of model structures and solution algorithms, the various models can likewise be utilized to other water resources systems one wishes to study. With the unique settings and conditions of the Philippines with humid, maritime, tropical climatology and hydrology, as well as with its archipelagic or islandic watersheds typified by short, steep mountain-to-coast river systems, this book offers different perspectives and experiences in modeling these types of water resources systems.

Quezon City, Philippines

Guillermo Q. Tabios III

# Acknowledgments

The author was a graduate student at Colorado State University (CSU) in Fort Collins at the onset of 1980, and the development of water resources models highly proliferated because personal computers (especially the iconic IBM-PC) became available right at graduate student room's desktop. Thus, doing computer work became quicker from developing, testing, and debugging computer programs, instead of the routine of going to the computer center, with decks of cards, and the turnaround time of computer jobs is several hours or a day later. The author was fortunate to be in that era, and in fact, there was a saying then that "anyone who knows how to write Fortran programs those days can finish a PhD in no time." Evidently so, many hydrologic and hydraulic computer programs were developed during that period, and until now, they still remain as the heart of major water resources computer software, significantly enhanced only with nice graphical user interfaces.

Being a PhD graduate student then at CSU, the author was exposed to several schools of thought with regard to his modeling know-how and experiences. In particular, his major influences came from his PhD adviser, Prof. Jose D. Salas, on stochastic analysis and modeling of hydrologic processes; Prof. Warren A. Hall, his initial PhD adviser on optimization and simulation models of water resources systems; and some members of his PhD guidance committee, specifically Prof. Hubert J. Morel-Seytoux on deterministic hydrology and Prof. Vujica Yevjevich on stochastic hydrology. After graduate school, he worked with Prof. Hsieh Wen Shen as postdoctoral fellow at CSU and later as research faculty at the University of California, Berkeley, on river and reservoir sediment transport processes as well as ecology-based river engineering by physical and mathematical modeling.

For the many projects and modeling works conducted at the National Hydraulic Research Center (NHRC) of the University of the Philippines at Diliman (UPD), especially those presented in this book, the author gratefully acknowledges several people that include David S. Rojas, Jr., Odyssey C. Herrera, Edmundo P. Vargas, Eugene C. Herrera, Abner M. Adraneda, Arlene B. Inocencio, Proserfina A. Mariano, Cornelio Q. Dizon, Peter Paul M. Castro, and Genandrialine L. Peralta.

Furthermore, the author is sincerely grateful to the following people:

To Springer International Publisher, Ms. Petra van Steenbergen, executive editor of Earth Sciences, Geography, and Environment, for bringing this book in form and in shape; Ms. Margaret Deignan, senior editor of Global Environmental Change, Climatic Change, Polar Science, and International Journal of Biometeorology for finally putting this book in print; and Prof. Vijay P. Singh, series editor in chief of Springer World Water Resources series.

To Luz R. Ang for carefully editing the chapters of the first draft and subsequent drafts of this book, to Odyssey C. Herrera for his valuable assistance to enhance the quality of figures in this book, and to Dr. Augustus Resurreccion and Dr. Eugene C. Herrera, both from the Institute of Civil Engineering (ICE) of UPD, for the critical reading and suggestions to improve this book.

Finally, to the late Prof. Leonardo Q. Liongson, cousin, mentor, and colleague at ICE and NHRC, who had been the greatest influence to the academic work and professional being of the author. The author certainly missed those endless talks and discourses with him.

# Contents

<b>1</b>	<b>Introduction . . . . .</b>	<b>1</b>
1.1	Purpose, Science, and Art of Water Resources Modeling . . . . .	1
1.2	Status of Modeling Water Resources Systems of the Philippines . . . . .	6
1.3	Organization of this Book . . . . .	7
	References . . . . .	8
<b>2</b>	<b>Physical Features and State of Water Resources and Status of Water Governance in the Philippines . . . . .</b>	<b>9</b>
2.1	Physical Features and State of Water Resources in the Philippines . . . . .	9
2.1.1	General Physiography, Climate, and Weather in the Philippines . . . . .	9
2.1.2	Water Resources Regions and Major River Basins in the Philippines . . . . .	12
2.1.3	Quantity and Quality of Surface and Groundwater Resources . . . . .	14
2.1.4	Water Use Demands and Water Permits . . . . .	15
2.1.5	Irrigation Services . . . . .	17
2.1.6	Flooding Issues and Concerns . . . . .	18
2.1.7	Design Level of Protection for Major Flood Control Projects . . . . .	19
2.1.8	Environmental Problems and Conditions . . . . .	21
2.2	Water Governance in the Philippines . . . . .	22
2.2.1	Current Water Governance and Institutional Arrangement	22
2.2.2	National Water Policy . . . . .	25
2.2.3	Other Issues and Concerns on Water Governance in the Philippines . . . . .	27
	References . . . . .	28

<b>3 Science and Art of Water Resources Modeling in the Philippines . . . . .</b>	<b>29</b>
3.1 Linking Science, Policy, and Management Decisions with Decision Support System . . . . .	29
3.2 Models and Modeling Tools in Decision Support System . . . . .	31
3.3 Simulation and Optimization Models . . . . .	33
3.4 Sample Water Resources Optimization-Simulation Modeling Problems . . . . .	34
3.4.1 Determination of Water Supply Firm Yield . . . . .	36
3.4.2 Allowable Groundwater Withdrawal Rate . . . . .	37
3.4.3 Optimal Cropping Patterns for Effective Water Use . . . . .	37
3.5 Overview of Modeling Studies and Experiences . . . . .	38
References . . . . .	40
<b>4 Surface and Groundwater Modeling for Water Utilization . . . . .</b>	<b>41</b>
4.1 Introduction . . . . .	41
4.1.1 Watershed Model . . . . .	42
4.1.2 Groundwater Model . . . . .	44
4.2 Pampanga River Basin . . . . .	45
4.2.1 Watershed Delineation and Surface Water Modeling . . . . .	47
4.2.2 Groundwater Aquifer Characteristics and Groundwater Modeling . . . . .	49
4.2.3 Estimation of Surface Water and Groundwater Demands . . . . .	55
4.2.4 Surface Water and Groundwater Model Simulation Studies . . . . .	57
4.3 Agno River Basin and Vicinity . . . . .	63
4.3.1 Surface Water Modeling of Agno River Basin . . . . .	67
4.3.2 Groundwater Modeling of Agno River Basin . . . . .	70
4.3.3 Surface Water and Groundwater Demands . . . . .	73
4.3.4 Surface Water and Groundwater Model Simulation Studies . . . . .	74
References . . . . .	93
<b>5 Reservoir Planning and Operations Studies with Optimization-Simulation Models . . . . .</b>	<b>95</b>
5.1 Angat Reservoir System . . . . .	95
5.1.1 Angat Reservoir Optimization-Simulation Model . . . . .	98
5.1.2 Optimization-Simulation Scenarios . . . . .	101
5.1.3 Results of Optimization-Simulation Studies . . . . .	101

<b>5.2</b>	<b>Angat Reservoir Monthly Allocation with Optimization-Simulation Model and Autoregressive Model to Forecast Inflows . . . . .</b>	<b>105</b>
5.2.1	Existing Release Policy Using Storage Rule Curve . . . . .	106
5.2.2	Reservoir Optimization-Simulation Model . . . . .	107
5.2.3	Optimization-Simulation Runs with Historical Inflows . . . . .	107
5.2.4	Optimization-Simulation Runs with Forecasted Inflows . . . . .	109
<b>5.3</b>	<b>Upper Agno River Basin Reservoir Operations Studies . . . . .</b>	<b>114</b>
5.3.1	Ambuklao, Binga, and San Roque Reservoirs of the Upper Agno River Basin . . . . .	116
5.3.2	Assessment of Adequacy of Rainfall Sampling Network . . . . .	118
5.3.3	Upper Agno River Watershed Model . . . . .	122
5.3.4	Upper Agno Reservoir Optimization-Simulation Studies . . . . .	125
5.3.5	Reservoir Storage-Elevation Curve over the Years . . . . .	127
5.3.6	Results of Upper Agno Reservoir Optimization-Simulation Studies . . . . .	127
5.3.7	Optimization-Simulation of San Roque Dam Flood Operations During Typhoon Parma . . . . .	139
5.3.8	Some Discussions on Upper Agno Reservoir Operations . . . . .	147
<b>5.4</b>	<b>Proposed Agos Reservoir System Optimization-Simulation Studies for Reliability Analysis and Project Sequencing and Staging . . . . .</b>	<b>149</b>
5.4.1	Agos River Basin Watershed and River Network . . . . .	150
5.4.2	Alternative Water Resources System Configurations . . . . .	151
5.4.3	Agos River Basin Watershed Model . . . . .	153
5.4.4	Results of Optimization-Simulation Studies of Proposed Agos River Reservoir System . . . . .	158
5.4.5	Recommended Project Sequencing and Staging of the Agos River Reservoir System . . . . .	160
	References . . . . .	163
<b>6</b>	<b>Reservoir Sedimentation Studies . . . . .</b>	<b>165</b>
6.1	Balog-Balog Reservoir Reliability and Cost-Benefit Analysis of a Single, High Dam Versus a Multiple Dam System . . . . .	165
6.1.1	Balog-Balog Multipurpose Project with Single, High Dam . . . . .	167
6.1.2	Balog-Balog Multiple Dam System . . . . .	167

6.1.3	Reservoir Optimization-Simulation Model and Watershed Modeling . . . . .	169
6.1.4	Comparison of Balog-Balog Multipurpose Project (BBMP) with Single, High Dam, Versus Balog-Balog Multiple Dam System (BBMDS) . . . . .	170
6.2	San Roque Reservoir Sedimentation and Operations Study Using a Two-Dimensional Hydraulic Model . . . . .	178
6.2.1	Two-Dimensional Flow and Sediment Hydraulic Model . . . . .	181
6.2.2	Watershed Flow and Sediment Yield Modeling . . . . .	183
6.2.3	Stochastic Rainfall Modeling . . . . .	185
6.2.4	Reservoir Simulation Scenarios . . . . .	187
6.2.5	Results of Reservoir Flow-Sediment Simulations . . . . .	188
6.2.6	Some Highlights of San Roque Flow-Sediment Modeling and Simulation Studies . . . . .	190
6.3	Pulangi Reservoir Sediment Flushing Studies with Two-Dimensional Hydraulic Model . . . . .	192
6.3.1	Reservoir Sedimentation and Sediment Flushing Operations . . . . .	195
6.3.2	Pulangi Reservoir Modeling for Sediment Flushing Operations . . . . .	197
6.3.3	Reservoir Inflow and Sediment Discharge Rating Curve . . . . .	199
6.3.4	Simulation Scenarios and Results of Sediment Flushing Studies . . . . .	200
	References . . . . .	207
<b>7</b>	<b>Hydrodynamic and Water Quality Modeling for Bays and Lakes . . . . .</b>	<b>211</b>
7.1	Introduction . . . . .	211
7.2	Manila Bay-Laguna Lake and Watershed System . . . . .	212
7.3	Brief Observation on Manila Bay-Laguna Lake Hydrodynamics . . . . .	214
7.4	Manila Bay-Laguna Lake Modeling . . . . .	218
7.4.1	Watershed Model of Manila Bay-Laguna Lake System . . . . .	219
7.4.2	Hydrodynamic Model of Manila Bay . . . . .	220
7.4.3	Hydraulic Model of Laguna Lake and Bataan-Pampanga-Bulacan Coastal Areas . . . . .	223
7.4.4	Advection-Dispersion Water Quality Model of Manila Bay and Laguna Lake . . . . .	224
7.5	Watershed Modeling and Streamflow Simulation . . . . .	228
7.6	Manila Bay Hydrodynamic and Water Quality Modeling and Simulations . . . . .	229
7.7	Laguna Lake 2-d Coupled Lake Flow-Salinity Modeling . . . . .	240

7.8	Other Water Quality Issues on Laguna Lake . . . . .	248
7.8.1	Lake Pollution Control and Effects on Fisheries . . . . .	249
7.8.2	Optimal Lake Use Zoning . . . . .	251
	References . . . . .	251
<b>8</b>	<b>Flood and Dam-Break Modeling Studies . . . . .</b>	<b>253</b>
8.1	Influence of Storm Rainfall Movement in Pasac Delta Flooding . . . . .	253
8.1.1	One-Dimensional, Unsteady Flow, Network Modeling of Pasac Delta . . . . .	254
8.1.2	Stochastic, Space-Time Rainfall Modeling of Moving Storm . . . . .	257
8.1.3	Results of Pasac Delta Flooding with Moving Storm . . . . .	259
8.1.4	Brief Remarks on Pasac Delta Flooding with Moving Storm . . . . .	259
8.2	Flood Modeling of Marikina River Basin During Typhoon Ketsana in September 2009 . . . . .	264
8.2.1	Pasig-Marikina River Basin Flood Calculations . . . . .	267
8.2.2	Suggestions for Holistic Flood Management in Pasig-Marikina River System . . . . .	271
8.3	Assessment of Alternative Flood Control Plans for Cagayan de Oro River . . . . .	275
8.3.1	Watershed and Flood Inundation Modeling of the Cagayan de Oro River Basin . . . . .	276
8.3.2	Storm Rainfall and Computed Inflow Flood Hydrograph . . . . .	276
8.3.3	Alternative Flood Mitigation Plans for the Cagayan de Oro River . . . . .	283
8.3.4	Results of Flood Simulations of the Alternative Flood Mitigation Plans . . . . .	285
8.3.5	Remarks on Cagayan de Oro River Flood Mitigation Simulations . . . . .	287
8.4	Dam-Break Model Studies of a Dam Removal Problem and Butas Dam of Cavite Province with Flow and Sediment Movement . . . . .	288
8.4.1	Dam Removal Problem in a Rectangular Reservoir . . . . .	289
8.4.2	Dam-Break Simulation of Butas Dam of Cavite in September 2006 . . . . .	291
	References . . . . .	295
<b>9</b>	<b>Pipe Network Distribution Modeling with Optimization . . . . .</b>	<b>299</b>
9.1	Introduction . . . . .	299
9.2	Description of EPANET Model . . . . .	300
9.3	Enhancement of EPANET with COMPLEX Optimization . . . . .	302

9.4	Enhanced Model Capabilities . . . . .	304
9.5	Application of EPANET-Optimization Model for Model Calibration . . . . .	306
9.6	Brief Final Remarks . . . . .	307
	References . . . . .	310
<b>10</b>	<b>Reliability Studies of Reservoirs Under Climate Change . . . . .</b>	<b>311</b>
10.1	Upper Agno Reservoir Operations with Climate Change . . . . .	311
10.1.1	2050 Climate Change Scenario . . . . .	313
10.1.2	Reliability Analysis of Upper Agno Reservoirs Under Climate Change . . . . .	314
10.1.3	Comparison of Hydropower Generation Between Existing and 2050 Climate Change Scenarios . . . . .	324
10.1.4	Other Issues and Challenges of the Upper Agno Reservoir Operations . . . . .	326
10.2	Angat Reservoir Reliability Analysis with Climate Change and Future Reservoir Sedimentation . . . . .	332
10.2.1	Angat River Basin 2050 Climate Change Parameters . . . . .	332
10.2.2	Angat Reservoir Sedimentation in 2050 . . . . .	333
10.2.3	Results of Angat Reservoir Operations Under 2050 Climate Change and Future Sedimentation . . . . .	334
	References . . . . .	337
<b>11</b>	<b>Modeling for Environmental Assessment Studies . . . . .</b>	<b>339</b>
11.1	Subic Bay Hydrodynamic-Water Quality Modeling as a Tool for Developing Integrated Coastal Management Plan (ICMP) . . . . .	339
11.1.1	Subic Bay Hydrodynamic-Water Quality Model . . . . .	340
11.1.2	Major Components of the Subic Bay Hydrodynamic-Water Quality Model . . . . .	342
11.1.3	Subic Bay Hydrodynamic-Water Quality Simulations . . . . .	346
11.2	Risk of Polluting Novaliches Reservoir from Payatas Dumpsite Through Groundwater Contaminant Transport . . . . .	351
11.2.1	Groundwater Flow and Contaminant Transport Model with FEMWATER . . . . .	352
11.2.2	Groundwater Modeling of Novaliches Reservoir-Payatas Dumpsite . . . . .	353
11.2.3	Stochastic Modeling of Reservoir Levels and Rainfall Sequence . . . . .	355
11.2.4	Results of Groundwater Contaminant Transport Simulations . . . . .	357

11.2.5 Atmospheric Pollution Posing a Bigger Concern than Groundwater Contamination in Novaliches Reservoir . . . . .	360
References . . . . .	361
<b>12 Imperatives of Water Resources Modeling and Applications in the Philippines . . . . .</b>	<b>363</b>
12.1 Key Considerations in Modeling Water Resources Systems . . . . .	363
12.1.1 Modeling Approach: Scientific Versus Data Analytic Method . . . . .	363
12.1.2 Incorporating the Hydrologic, Geomorphologic, and Ecologic Interactions . . . . .	365
12.2 Monitoring and Data Needs for Future Modeling Efforts . . . . .	366
12.3 Science-Based Management and Decision Tools and Capacity Building . . . . .	367
12.4 Need for Sustainability Science and Transdisciplinary Approach for Sustainable Water Resources Development . . . . .	368
12.4.1 Holistic Water Resources Management . . . . .	369
12.4.2 Role of Sustainability Science . . . . .	369
12.4.3 Transdisciplinary Approach to Holistic Flood Risk Management . . . . .	372
12.4.4 Planning Horizon for Sustainable Development of Water Resources Systems: Case of Reservoir and Dam Projects . . . . .	374
12.5 On Building Urban Resilience to Water-Related Disasters . . . . .	375
12.5.1 Engineering Resilience . . . . .	375
12.5.2 Ecological Resilience . . . . .	375
12.5.3 Evolutionary Resilience . . . . .	375
References . . . . .	377
<b>Appendices . . . . .</b>	<b>379</b>

## List of Boxes

Box 3.1	Combined Optimization-Simulation Model with Simulation Model Embedded in the Optimization Model .....	35
Box 9.1	Objective Functions and Decision Variables of the EPANET-Optimization Model .....	304
Box 12.1	Elements of Physical, Social, and Human Systems Inherent in a Complex, Dynamic, and Uncertain Flood Problem .....	373
Box 12.2	Differences of Monodisciplinary, Multidisciplinary, Interdisciplinary, and Transdisciplinary Approaches .....	373
Box 12.3	Platform of Transdisciplinary Approach .....	373

# List of Figures

Fig. 1.1	Hierarchy of the various media and constituents of the soil, water, and air environments and interactions with flora, fauna, and human settlements including the built environment. (Adapted from Nadaoka and Tabios 2009) .....	3
Fig. 1.2	Water resource management and related scientific and engineering disciplines. (From Mays 2001) .....	4
Fig. 2.1	Map of the Philippines showing political regions and provinces. (Taken from <a href="http://www.map-of-the-world.net">www.map-of-the-world.net</a> ) .....	10
Fig. 2.2	Twelve (12) water resources regions (WRR) of the Philippines designated by the National Water Resources Council in 1978 for purposes of planning, development, and water regulation. (From NWRB website: <a href="http://www.nwrb.gov.ph">www.nwrb.gov.ph</a> ) .....	12
Fig. 2.3	Major river basins (RB) in the Philippines. (From NWRB website: <a href="http://www.nwrb.gov.ph">www.nwrb.gov.ph</a> ) .....	13
Fig. 2.4	Surface water and groundwater resources of the Philippines. (Background picture taken from <a href="http://www.prairievers.org">www.prairievers.org</a> ) .....	14
Fig. 2.5	Water use for various purposes based on water permit granted by the National Water Resources Board (NWRB) as of December 2010. Values shown are average annual flows (in m <sup>3</sup> /s), and values in parenthesis are for the total water permit granted of 2727.40 m <sup>3</sup> /s .....	16
Fig. 2.6	Projected regional supply and demand situation in 1000 m <sup>3</sup> for 2005 and 2025 according to WRR in Fig. 2.2. (Source: JICA 1998 Master Plan Study on Water Resources Management in the Philippines submitted to NWRB) .....	16
Fig. 2.7	Water-related agencies in the Philippines and their functions ...	23
Fig. 3.1	Linking science and public policy for effective integrated water resources management. (Adapted from Georgakakos 2004) .....	30

Fig. 3.2	Components of an IWRM decision support system (DSS). (Taken from Loucks and van Beek 2017) .....	32
Fig. 4.1	Schematic diagram of surface water and groundwater model used in this study .....	42
Fig. 4.2	Watershed delineation into overland flow planes and river network. For each overland flow plane (rectangular area), the Sacramento soil-moisture accounting model which is schematically shown in Fig. 4.3 below is used .....	43
Fig. 4.3	Schematic of the Sacramento soil-moisture accounting model and the model components representing different hydrologic processes .....	44
Fig. 4.4	Spatial discretization of the groundwater aquifer in the 3-d, saturated groundwater flow, MODFLOW finite difference model. (From McDonald and Harbaugh 1984) .....	45
Fig. 4.5	Assembly of 1:50,000 Scale NAMRIA topographic maps covering the entire Pampanga River Basin .....	46
Fig. 4.6	Major sub-basin delineations and river network of the Pampanga River Basin .....	48
Fig. 4.7	Sub-basin delineations of Pantabangan River Basin .....	50
Fig. 4.8	Sub-basin delineations of Lower Pampanga River Basin .....	51
Fig. 4.9	Land cover map of Pampanga River which is used to derive certain model parameters in the watershed model .....	52
Fig. 4.10	Digital elevation map of Pampanga River Basin .....	53
Fig. 4.11	Finite-difference grid system of groundwater model of the Pampanga River Basin .....	54
Fig. 4.12	Sample three-dimensional rendering of the geologic structure of the groundwater system to create the geometry of the groundwater model .....	54
Fig. 4.13	Map of groundwater material codes for layers –100 to –80 m, –20 to 0 m, 0 to +20, and + 80 to +100 m for the Pampanga River basin .....	55
Fig. 4.14	Locations in the Pampanga River Basin with existing surface water and groundwater permits issued by the National Water Resources Board (NWRB) of the Philippines .....	58
Fig. 4.15	Amounts granted (in MLD) for surface water permits issued by NWRB in the Pampanga River Basin .....	59
Fig. 4.16	Amounts granted (in MLD) for groundwater permits issued by NWRB in the Pampanga River Basin .....	60
Fig. 4.17	Spatially interpolated rainfall over the Pampanga River Basin for a particular 24-hour rainfall (in mm) .....	62
Fig. 4.18	Long-term average daily flows (m <sup>3</sup> /s) of Talavera River Sub-basin .....	63
Fig. 4.19	Long-term 80% dependable daily flows (m <sup>3</sup> /s) of Coronel River Sub-basin .....	64

Fig. 4.20	Schematic representation of water deficit events and surplus events below or above the demand levels, respectively .....	64
Fig. 4.21	Average flow deficit ( $m^3/s$ ) for Talavera River Sub-basin by runs analysis at a demand level equal to mean daily flows ( $m^3/s$ ) .....	65
Fig. 4.22	Average number of days in deficit for Talavera River Sub-basin by runs analysis at a demand level equal to mean daily flows ( $m^3/s$ ) .....	66
Fig. 4.23	Simulated groundwater heads (in meters at mean sea level) of Pampanga River Basin at the end of year 2025 and 2050 starting in 2010 at extraction rates according to NWRB existing water permits and increased every 5 years based on population projection .....	67
Fig. 4.24	Location of demand points (cities/municipalities as indicated by round dots) and possible abstraction points of major potential rivers (as indicated by square dots) within Pampanga River Basin .....	68
Fig. 4.25	Potential hydropower sites and estimated capacity in megawatts (MW) within Pampanga River Basin .....	69
Fig. 4.26	Map of Agno River Basin covering the entire Pangasinan Province and portions of Benguet, Tarlac, Pampanga, and Zambales. The watershed delineations into sub-basins are also indicated in the figure .....	71
Fig. 4.27	Major rivers and river network of Agno River Basin .....	72
Fig. 4.28	Digital elevation map of Agno River Basin .....	74
Fig. 4.29	Land cover map of Agno River basin which is used to derive the model parameters in the watershed model .....	75
Fig. 4.30	Location of rainfall stations (with round dots) within and around the Agno River Basin .....	77
Fig. 4.31	Finite difference grid system of Agno River Basin groundwater model .....	78
Fig. 4.32	Maps of material codes for layers 0 to +20, +60 to +80, +120 to +140, and + 160 to +180 .....	79
Fig. 4.33	Maps of material codes for layers -40 to -20, -120 to -100, -240 to -220, and - 320 to -300 .....	80
Fig. 4.34	Locations of municipalities/cities (indicated by round dots) with surface water and groundwater demands in the Agno River Basin .....	81
Fig. 4.35	Amounts granted (in MLD) in the existing surface water permits issued by NWRB .....	82
Fig. 4.36	Amounts granted (in MLD) in the existing groundwater permits issued by NWRB. (Data updated to 2010) .....	83
Fig. 4.37	Projected groundwater demand (in MLD) for 2050 based on existing groundwater permits in 2010 and population projection .....	84

Fig. 4.38	Long-term average daily river flows ( $\text{m}^3/\text{s}$ ) over the Lower Agno River Sub-basin .....	85
Fig. 4.39	Long-term 80% dependable daily river flows ( $\text{m}^3/\text{s}$ ) over the Central Agno River Sub-basin .....	86
Fig. 4.40	Average flow deficit ( $\text{m}^3/\text{s}$ ) of rivers in Lower Agno River Sub-basin by runs analysis at a demand level equal to the long-term daily mean .....	87
Fig. 4.41	Average number of days in deficit for rivers in the Lower Agno River Sub-basin by runs analysis at a demand level equal to the long-term daily mean .....	88
Fig. 4.42	Average flow deficit ( $\text{m}^3/\text{s}$ ) for rivers in the Central Agno River Sub-basin by runs analysis at a demand level equal to the 80% dependable daily flow .....	89
Fig. 4.43	Average number of days in deficit for rivers in the Central Agno River Sub-basin by runs analysis at a demand level equal to the 80% dependable daily flow .....	90
Fig. 4.44	Groundwater heads in 2025 computed from the groundwater model with imposed base demands and the demands, 25% and 50% more than the base demand .....	91
Fig. 4.45	Groundwater heads in 2050 computed from the groundwater model with imposed base demands and the demands, 25% and 50% more than the base demand .....	91
Fig. 5.1	Watershed delineation and river network of the Angat-Ipo-Bustos-Umiray water resources system. (From Tabios and David 2014; Tabios 2018) .....	96
Fig. 5.2	Physical components and water demand of the multipurpose Angat Multipurpose Reservoir System for domestic water supply, irrigation water supply, hydropower generation, and flood control. (From Tabios 2016, 2018) .....	97
Fig. 5.3	Watershed delineation and river network of the Angat-Ipo-Bustos-Umiray water resources system. The sub-basin numbers indicated in the figure are used in watershed modeling. (From Tabios 2016) .....	98
Fig. 5.4	Schematic of Angat-Ipo-Bustos Reservoir system indicating the nodes and links. (From Tabios 2008) .....	100
Fig. 5.5	6-month ahead forecasts using seasonal AR(1) and seasonal AR(2) models including observed data for year 1997 .....	112
Fig. 5.6	Monthly reservoir storages of cases: optimization-simulation cases OS1 and OS3, existing rule curve ERC1 case, and proposed rule curve PRC1 case in 2008 with forecasted Angat River inflows from May (month 4) to October. Envelope curves are upper and lower target storage elevations of existing and proposed rule curve operating procedures .....	115

Fig. 5.7	Assembly of 1:50,000 scale NAMRIA topographic maps covering the Upper Agno River Basin. Also shown is the watershed delineation into sub-basins and the three (3) major reservoirs Ambuklao, Binga, and San Roque (in the order from north or upstream to south or downstream) and ARIIP Dam .....	117
Fig. 5.8	Location of rainfall gaging stations in the Upper Agno River Basin and vicinity .....	119
Fig. 5.9	Observed and fitted power model of the spatial correlation function of the daily rainfall in the Upper Agno River Basin . . . . .	120
Fig. 5.10	Contour map of root mean square errors of spatial interpolation of daily rainfall (in mm) in the Upper Agno River Basin and vicinity .....	121
Fig. 5.11	Digital elevation map of Upper Agno River Basin using SRTM data .....	123
Fig. 5.12	Slope map of Upper Agno River Basin derived from the digital elevation map .....	124
Fig. 5.13	Landcover map of Upper Agno River Basin .....	125
Fig. 5.14	Ambuklao Reservoir elevation-storage curve .....	127
Fig. 5.15	Binga Reservoir elevation-storage curve .....	128
Fig. 5.16	San Roque Reservoir elevation-storage curve .....	128
Fig. 5.17	Tract of Typhoon Parma, locally called Pepeng during the period October 1–10, 2018 from PAGASA .....	140
Fig. 5.18	Time series plots of observed rainfall, reservoir levels, inflows, and spills of San Roque Dam during Typhoon Parma provided by NAPOCOR .....	142
Fig. 5.19	Time series plots of rainfall, inflows, power releases, spillway releases, power plus spillway releases, and reservoir elevations of San Roque Dam during Typhoon Parma computed from the optimization-simulation model .....	143
Fig. 5.20	Time series plots of rainfall, inflows, power releases, spillway releases, power plus spillway releases, and reservoir elevations of San Roque Dam using the optimization-simulation model. The top (Case 1) and bottom (Case 2) figures are plots when spillway releases are made after 8AM on October 5, 2009 when the reservoir elevations are above 280 m and 282 m, respectively .....	145
Fig. 5.21	Time series plots of rainfall, inflows, power releases, spillway releases, power plus spillway releases, and reservoir elevations of San Roque Dam using the optimization-simulation model. The top (Case 3) and bottom (Case 4) figures are plots when spillway releases are made after 8AM on October 6, 2009 when the reservoir elevations are above 280 m and 282 m, respectively .....	146

Fig. 5.22	Kaliwa-Kanan-Agos River System watershed boundary and river network .....	150
Fig. 5.23	Nine (9) alternative water resources configurations or schemes denoted by WRC1 through WRC9 of the Agos River Basin composed of combinations of reservoirs and/or water conveyance systems .....	152
Fig. 5.24	Elevation-area-storage data for the proposed Kaliwa Low Reservoir .....	153
Fig. 5.25	Elevation-area-storage data for the proposed Laiban Reservoir .....	154
Fig. 5.26	Watershed delineation of Agos River Basin resulting in 182 sub-basins for watershed modeling. The sub-basin numbers indicated are for purposes of watershed modeling .....	155
Fig. 5.27	Land cover map of Agos River Basin .....	156
Fig. 5.28	Location of rainfall gaging stations in the Agos River Basin and vicinity .....	157
Fig. 5.29	Time series plots of simulated daily flows from 1961 to 2011 at proposed Laiban Dam and Kaliwa Low Dam sites .....	158
Fig. 5.30	Recommended project sequencing and staging at 85% reliability of the projected Metro Manila water demand for years 2012–2060 .....	162
Fig. 6.1	Map of Balog-Balog irrigation system service area .....	166
Fig. 6.2	Location of Balog-Balog multipurpose project (BBMP) with single, high dam, and its reservoir elevation-storage curve .....	168
Fig. 6.3	Location of the nine Balog-Balog multiple dam systems (BBMDS) denoted by S1 through S9 and their corresponding reservoir elevation-storage curves .....	169
Fig. 6.4	Map of the study area showing the watershed delineation and the locations of the proposed reservoirs .....	171
Fig. 6.5	Digital elevation map of the study area .....	172
Fig. 6.6	Land cover map of the study area .....	173
Fig. 6.7	Flood frequency curves of uncontrolled flows (in $m^3/s$ or CMS) at S9 location for both Balog-Balog single, high dam, multipurpose project (BBMP) and multi-dam (BBMDS) including natural flow (without dam project) .....	178
Fig. 6.8	Map showing the Balog-Balog Irrigation System service area traversing three major watersheds, namely, O'Donnell, Rio Chico, and Talavera river basins .....	179

Fig. 6.9	San Roque Reservoir and watersheds. Also indicated is the Ambalanga watershed .....	180
Fig. 6.10	Time series plots of simulation of rainfall input, watershed flows, and sediment yield for Ambalanga sub-basin on 29th year of simulation .....	185
Fig. 6.11	Time series plots of stochastically generated rainfall aggregated on a daily basis using the Poisson rectangular pulse model for 70 years (first three plots) and the historical daily rainfall data at Binga Dam (bottom plot) .....	186
Fig. 6.12	Time series plots of annual sediment inflow to San Roque Reservoir .....	187
Fig. 6.13	Change in bed elevations for Case 3 from year 0 to end of years 25 (left) and 70 (right). Positive values indicate sediment deposition .....	189
Fig. 6.14	Time series plots of reservoir inflows, levels and spills for Case 1 .....	190
Fig. 6.15	Time series plots of reservoir inflows, levels, and spills for Case 2 .....	191
Fig. 6.16	Time series plots of reservoir releases, energy generation, and power release sediment load for Case 1 .....	192
Fig. 6.17	Time series plots of reservoir releases, energy generation and power release sediment load for Case 3 .....	193
Fig. 6.18	Pulangi River Basin and location of Pulangi Reservoir in Maramag, Bukidnon, at the southern part in the map created from a collage of 16, 1:50,000 scale NAMRIA maps .....	194
Fig. 6.19	Schematic sketch of depositional patterns in the longitudinal direction. (From Fan and Morris 1992) .....	196
Fig. 6.20	Schematic diagram of flushing processes with deltaic deposition during drawdown flushing. (From Fan and Morris 1992) .....	197
Fig. 6.21	Schematic diagram of flushing processes with wedge-shaped deposition during drawdown flushing. (From Fan and Morris 1992) .....	197
Fig. 6.22	Pulangi Reservoir 2-d model geometry and associated hydraulic structures and hydropower components .....	198
Fig. 6.23	Pulangi Reservoir finite volume grid system superposed on the bathymetry data provided by NAPOCOR, Pulangi Office, last November 2010 .....	199
Fig. 6.24	Time series of plots of flows ( $\text{m}^3/\text{s}$ ), water elevations (m), sediment flushed ( $\text{m}^3$ ), sediment concentrations (%), and hydropower (MW) generated at pertinent locations in the Pulangi Reservoir system at inflow of $150 \text{ m}^3/\text{s}$ and gate opening of (a) 0.5 m and (b) 2.0 m .....	204

Fig. 6.25	Time series plots of sediments flushed (in cubic meters) and reservoir capacity (in million cubic meters) for 360-day simulation run with fifty-seven (57) 12-h flushing operations . . . . .	205
Fig. 6.26	Areas in the reservoir with net bed deposition (in m) from (a) days 30 to 90, (b) days 30 to 180, (c) days 30 to 240, and (d) days 30 to 360 . . . . .	206
Fig. 6.27	Areas in the reservoir with net bed erosion (in m) from (a) days 30 to 90, (b) days 30 to 180, (c) days 30 to 240, and (d) days 30 to 360 . . . . .	207
Fig. 7.1	Manila Bay-Laguna Lake system and surrounding watersheds . . . . .	213
Fig. 7.2	Elevation map of Manila Bay-Laguna Lake Basins generated from NASA-STRM digital elevation data . . . . .	215
Fig. 7.3	Land use/cover map of Manila Bay-Laguna Lake watershed system . . . . .	216
Fig. 7.4	Temporal distribution of hydrodynamic condition: (a) water elevation; (b) near surface velocity at South Channel (U northing and V easting components); (c) near bottom velocity at South Channel; (d) near surface velocity at North Channel; and (e) near bottom velocity at North Channel. (Data from IMSWES, October 11–12, 2001) . . . . .	217
Fig. 7.5	Program flowchart of Manila Bay-Laguna Lake hydrodynamic and water quality model . . . . .	219
Fig. 7.6	Schematic of dissolved oxygen model and its interactions with other chemicals and other sink/source terms or processes. (Taken from HEC-RAS User's Manual, USACE 2008) . . . . .	225
Fig. 7.7	Major sub-basin delineations of the Bataan, Pampanga (including Guagua), Bulacan, Manila-Cavite, and Laguna River Basins. Also indicated are areas handled by 2-d hydraulic model and 3-d Princeton Ocean Model . . . . .	229
Fig. 7.8	Location of rainfall gaging stations within and around Manila Bay-Laguna Lake watersheds . . . . .	233
Fig. 7.9	Sample time series plots of daily flows calculated from the watershed modeling of two sub-basins in the Pampanga River Basin . . . . .	234
Fig. 7.10	Average daily flows ( $m^3/s$ ) in the Pampanga River Basin calculated from the watershed model simulation using rainfall data from 1972 to 2012 . . . . .	235
Fig. 7.11	Average daily flows ( $m^3/s$ ) in the Bataan sub-basins calculated from the watershed model simulation using rainfall data from 1972 to 2012 . . . . .	236
Fig. 7.12	Average daily flows ( $m^3/s$ ) in the Laguna River Basin calculated from the watershed model simulation using rainfall data from 1972 to 2012 . . . . .	237

Fig. 7.13	Average daily flows ( $\text{m}^3/\text{s}$ ) in the Manila-Cavite sub-basins calculated from the watershed model simulation using rainfall data from 1972 to 2012 .....	238
Fig. 7.14	Finite difference grid of Manila Bay consisting of 16 (sigma-delta) layers of 11,967 square grids of size 400 m x 400 m each together with bathymetric map .....	239
Fig. 7.15	Detailed 2-d model geometry and elevation map of Bataan-Pampanga-Bulacan Delta consisting of 4927 finite elements .....	240
Fig. 7.16	Detailed 2-d model geometry and bathymetric map of Laguna Lake-Pasig River composed of 3572 finite elements .....	241
Fig. 7.17	Plot of BOD and DO loadings versus discharge of Imus River .....	242
Fig. 7.18	Plot of BOD and DO loadings versus discharge of Orion River .....	243
Fig. 7.19	Locations of rivers with outflows to Manila Bay .....	244
Fig. 7.20	Population density map of the study area .....	245
Fig. 7.21	Time series plots of derived BOD and phosphate loadings of Pampanga River .....	248
Fig. 7.22	Time series plots of derived BOD and phosphate loadings of Limay River .....	248
Fig. 7.23	Simulated dissolved oxygen concentrations around Manila Bay using the derived BOD and phosphate loadings using the water quality model with components DO, BOD, and phosphate .....	249
Fig. 7.24	Typical vector plot of lake velocities (a) with spatially varying wind field and (b) with uniform wind field (taken from Tabios et al. 2000b) .....	249
Fig. 7.25	Salinity concentration around Laguna Lake 10, 30, 57, and 96 hours from start of simulation which is typical during the dry month of April when the freshwater inflows are low and the lake can have significant saline intrusion from Manila Bay .....	250
Fig. 8.1	Pasac Delta network located northwest of Manila. [The river reaches are denoted by the letter R (e.g., R38 is reach 38).] .....	255
Fig. 8.2	Maximum water stages (m) resulting from storms coming from (1) northeast, (2) east, (3) southeast, and (4) south directions (all storms at speed of 20 kph) .....	260
Fig. 8.3	Maximum flow velocities (m/s) resulting from storms coming from (1) northeast, (2) east, (3) southeast, and (4) south directions (all storms at speed of 20 kph) .....	261
Fig. 8.4	Maximum discharges ( $\text{m}^3/\text{s}$ ) resulting from storms coming from (1) northeast, (2) east, (3) southeast, and (4) south directions (storms at speed of 20 kph) .....	262

Fig. 8.5	Maximum water surface elevations (m) resulting from storms coming from the south direction at speeds of (1) 10 kph, (2) 20 kph, (3) 30 kph, and (4) 40 kph .....	263
Fig. 8.6	Time series plots of water stages (m), velocities (m/s), and discharges ( $m^3/s$ ) at Guagua River (Reach 8, Sect 3 km) and Pasac River (Reach 22, Sect 3.4 km) for storms coming from northeast, east, and south directions (all moving at 20 kph) .....	264
Fig. 8.7	Empirical cumulative distribution functions (CDF) of water stages (m), velocities (m/s), and discharges ( $m^3/s$ ) at Guagua River (Reach 8, Sect 3 km) and Pasac River (Reach 22, Sect 3.4 km) based on 50 traces of stochastic generated storms coming from northeast, east, and south directions (all moving at 20 kph) .....	265
Fig. 8.8	Map of Metro Manila showing Pasig-Marikina River system with Manggahan Floodway, Laguna de Bay (Laguna Lake), and Napindan River .....	266
Fig. 8.9	Major flood-prone areas in Metro Manila (JICA Report) .....	267
Fig. 8.10	Path of Tropical Storm (TS) Ketsana (international name) locally called in the Philippines as Typhoon Ondoy passing through Metro Manila on September 26, 2009 .....	268
Fig. 8.11	Hourly rainfall (mm/h) during TS Ketsana at five gaging stations around Marikina River Basin .....	269
Fig. 8.12	TS Ketsana's hourly rainfall fields (in mm) by multiquadric spatial interpolation from 8 AM to 2 PM on September 26, 2009 .....	269
Fig. 8.13	Laguna Lake levels at Angono station during TS Ketsana .....	270
Fig. 8.14	Pasig-Marikina River Basin with the unsteady flow, network model geometry (mesh area) .....	270
Fig. 8.15	Marikina River Basin hourly flood hydrograph as upstream inflow ( $m^3/s$ ) of the Pasig-Marikina River flood model and associated average (composite) basin rainfall (mm/h) during TS Ketsana .....	272
Fig. 8.16	Maximum river stages (m) along the alignment Pasig-Marikina River from Sto. Niño Bridge (km 34) to Manila Bay (km 0) superposed on (a) left and (b) right river overbank ground elevations .....	273
Fig. 8.17	Pictures taken a day after the TS Ketsana at Marcos Highway Bridge near SM Mall (km 31 in Fig. 8.16) where flood heights above the overbank ground elevation reached as high as 8 m .....	273
Fig. 8.18	Flood inundation map along Marikina River between Marikina City and Pasig City near Rosario Weir (km 34 to km 27 in Fig. 8.16) .....	274
Fig. 8.19	Watershed boundary and river network of the Cagayan de Oro River Basin .....	277

Fig. 8.20	Cagayan de Oro River Basin delineation for a total of 68 sub-basins .....	278
Fig. 8.21	Cagayan de Oro River Basin topographic map .....	279
Fig. 8.22	Land use/cover map of Cagayan de Oro River Basin .....	280
Fig. 8.23	Finite element grid representation composed of 6092 elements and 6158 nodes of the 2-d flood inundation model covering the lower portion of Cagayan de Oro River Basin. Shown in the inset is the location of the 2-d model geometry relative to the river basin .....	281
Fig. 8.24	Eight flood mitigations plans or scenarios for Cagayan de Oro River Basin .....	284
Fig. 8.25	Class posting of maximum water depths (m) for the eight flood simulation scenarios. Note that only depths of greater than 0.5 m are posted .....	286
Fig. 8.26	Profiles of maximum river stage water surface elevations along the center line of the Cagayan de Oro River for the eight flood simulation scenarios .....	287
Fig. 8.27	Sediment-filled reservoir before and after removal of dam by design or accident. (Taken from Cui et al. 2006b) .....	290
Fig. 8.28	Dam removal problem in a rectangular reservoir in plan view (right figure) and perspective partially showing the reservoir (left figure). The finite volume mesh is 450 m by 60 m composed of 3000 elements, and the 13-m-high dam is located at vertical ordinate 150 m in the figure. The color/grayscale scale is bed elevation in meters .....	290
Fig. 8.29	Bed elevations (m) at time steps (a) -10, (b) 10, (c) 30, and (d) 60 min from time of dam-break of the rectangular reservoir. The color scale is for bed elevations .....	291
Fig. 8.30	Difference between bed elevations (m) and original bed elevations at time steps (a) 10, (b) 30, (c) 60, and (d) 120 min from time of dam-break of the rectangular reservoir. The color scale is for differences in bed elevations, and a negative value indicates scour .....	292
Fig. 8.31	Pictures taken at Butas Dam on October 9, 2006, about 2 weeks after the dam-break in which (a) looking downstream into the dam that broke and (b) looking upstream from the damsite .....	293
Fig. 8.32	Plan view of dam configuration and the finite volume grid representation composed of 1140 irregular grids .....	293
Fig. 8.33	Velocity vectors 10 min after dam-break plotted over the image of river channel and bank geometry. Note that dam is approximately located at ordinates $x = 1250$ m (long side) and $y = 1780$ m (short side) .....	294

Fig. 8.34	Bed elevations (m) at time steps (a) 0, (b) 10, (c) 20, (d) 40, (e) 60, and (f) 120 min from time of dam-break of Butas Dam. The color scale is for bed elevations .....	294
Fig. 8.35	Differences between bed elevations (m) and original bed elevations at time steps (a) 10, (b) 30, (c) 60, and (d) 90 min from time of dam-break of Butas Dam. The color scale is for differences in bed elevations, and a negative value indicates scour .....	295
Fig. 9.1	Typical water distribution pipe network .....	300
Fig. 9.2	Typical time series plot of hourly main water use and non-revenue water (NRW) pilferage and leakage water (in million liters per day, mld) as well as hourly pressure head (in m) at a node .....	301
Fig. 9.3	Flowchart of EPANET-Optimization model .....	302
Fig. 9.4	Water distribution concession area of Maynilad Water Service Incorporated (MWSI) which is on the west zone of Metro Manila .....	307
Fig. 9.5	Time series plots of observed flows and computed flows with optimization including pure simulation for gaging station 22SMA-L008 .....	308
Fig. 9.6	Time series plots of observed flows and computed flows with optimization including pure simulation for gaging station 22SMA-L007 .....	308
Fig. 9.7	Time series plots of observed pressures and computed pressures with optimization including pure simulation for gaging station 22SMA-4P-4Q .....	309
Fig. 9.8	Time series plots of observed pressures and computed pressures with optimization including pure simulation for gaging station 22SMA-1G .....	309
Fig. 10.1	Assembly of 1:50,000 scale NAMRIA topographic maps covering the Upper Agno River Basin. Also shown is the watershed delineation into sub-basins and the three (3) major reservoirs Ambuklao, Binga, and San Roque (in the order from north or upstream to south or downstream) and the AIIP Dam .....	312
Fig. 10.2	Ratios of 2050 future climate daily rainfall and historical daily rainfall on monthly basis based on global climate change model, FGOALS .....	314
Fig. 10.3	Monthly average discharges to Angat Reservoir for past (Q-past) and future (Q-future) climate change scenarios from GFDL_0 GCM including the monthly ratios (Q-future/Q-past) of monthly past and future climate inflows .....	333

Fig. 10.4	Angat Reservoir elevation-volume curves for existing case (circa 2013) and with 2050 future reservoir sedimentation .....	334
Fig. 11.1	Major factors affecting Subic Bay hydrodynamics and water quality process .....	340
Fig. 11.2	Program flowchart of Subic Bay hydrodynamic and water quality model .....	342
Fig. 11.3	Subic Bay land use map with superimposed river network and watershed sub-basin delineation .....	343
Fig. 11.4	Subic Bay hydrodynamic-water quality model finite-difference grids composed of 4133 active horizontal grids and 15 vertical layers .....	345
Fig. 11.5	Subic Bay bathymetry in downward depths (m) from mean low-low water (MLLW) .....	345
Fig. 11.6	China Sea tidal forcing southwest of Subic Bay .....	347
Fig. 11.7	Typical velocity vector of Subic Bay .....	347
Fig. 11.8	Spatial distribution of BOD concentrations after 20, 90, and 150 days for a specific waste discharge scenario around Subic Bay with significant concentration from Olongapo City and Hanjin Shipyard .....	349
Fig. 11.9	Spatial distribution of BOD concentrations after 90 days for three (3) BOD waste discharge scenarios around Subic Bay depending on sewerage and septage reduction schemes specially in the identified hot spot areas .....	350
Fig. 11.10	Oil spill simulation with almost, purely advective (no advection) transport assuming that oil is a conservative tracer. This simulation was motivated by an actual ship oil spill incident indicated in the lower, left-hand portion of the figure and actual sighting of oil had been observed 5 days after the incident the White Rock Resort indicated in the upper, right-hand side of the figure .....	351
Fig. 11.11	Aerial photo of Novaliches Reservoir and the location of the Payatas open dumpsite and a closeup view of the dumpsite looking northeast .....	351
Fig. 11.12	Topographic perspective of Novaliches Reservoir-Payatas dumpsite .....	353
Fig. 11.13	Finite element discretization of the Novaliches Reservoir-Payatas dumpsite .....	354
Fig. 11.14	Observed (a) daily rainfall and (b) water level at Novaliches Reservoir .....	355
Fig. 11.15	Stochastically generated daily water levels for 30 years at Novaliches Reservoir .....	357
Fig. 11.16	Stochastically generated daily rainfall for 30 years in the vicinity Novaliches Reservoir-Payatas dumpsite .....	358
Fig. 11.17	Contaminant concentration after 24-hour simulation .....	359

Fig. 11.18	Contaminant concentration after 2-year simulation .....	359
Fig. 11.19	Contaminant concentration after <b>(a)</b> 24 h, <b>(b)</b> 3 years, <b>(c)</b> 8 years, and <b>(d)</b> 25 years from start of simulation .....	360
Fig. 12.1	Illustrative definition of modeling approaches by <b>(a)</b> scientific method and <b>(b)</b> data analytic method .....	364
Fig. 12.2	Panarchy model of adaptive change to illustrate evolutionary resilience. [Taken from Davoudi (2012); Davoudi et al. (2013)] .....	376
Fig. A.1	Model structure of Sacramento soil-moisture accounting model. Also indicated are key model parameters described in the main text (from Burnash et al. 1973) .....	380
Fig. D.1	Schematic diagram of the SWATCII model structure and components .....	397

# List of Tables

Table 2.1	Flood control design level of protection in terms of return period and other pertinent information of major DPWH flood control projects .....	20
Table 2.2	Current roles and responsibilities of water-related agencies in the Philippines .....	24
Table 3.1	Distinction between simulation model and optimization model . . . . .	33
Table 4.1	Summary of drainage areas and number of sub-basin units for the major sub-basins of the Pampanga River system .....	49
Table 4.2	Groundwater properties of associated material codes. (From Boulding and Ginn 2004) .....	56
Table 4.3	Available rainfall data for Pampanga River Basin .....	61
Table 4.4	Summary of prospective service areas located within the sub-basins having water deficit which have to be supplied from the surplus of major potential rivers .....	67
Table 4.5	Potential hydropower sites and pertinent information with capacities of less than 5 MW based on mean river flows .....	70
Table 4.6	Summary of drainage areas and number of sub-basin units for the major sub-basins of the Agno River Basin .....	73
Table 4.7	List of rainfall stations in Agno River Basin and vicinity .....	76
Table 4.8	Groundwater properties for each material code used in the groundwater model .....	79
Table 4.9	Summary of assessment of surface water availability and projected surplus of major potential river sources within the potential sub-basins of Agno River Basin .....	92
Table 4.10	Potential hydropower sites and pertinent information with capacities between 5 to 7 MW based on average daily flow (Q Average) and 80% (Q 80%) dependable daily flow .....	92
Table 4.11	Potential hydropower sites and pertinent information with capacities between 10 and 15 MW based on average daily flow (Q Average) and 80% (Q 80%) dependable daily flow ....	93

Table 5.1	Angat Reservoir daily flow releases to Ipo Dam for MWSS domestic water supply and to Bustos Dam for NIA-AMRIS irrigation water for the two optimization-simulation model scenarios: (1) with MWSS demand of 46 CMS and (2) with MWSS demand of 50 CMS .....	103
Table 5.2	Auxiliary and main hydropower plant generation from Angat Reservoir daily flow releases for the two optimization-simulation model scenarios: (1) with MWSS demand of 46 CMS and (2) with MWSS demand of 50 CMS .....	104
Table 5.3	Penalty coefficients for MWSS demand violations, NIA demand violations, reservoir spills, as well as hydropower generator benefit coefficient applied in the objective function for four optimization-simulation (OS) cases .....	107
Table 5.4	Results of optimization-simulation runs (OS cases) for 58 years (1946–1963, 1968–2007) of historical data in terms of MWSS demand violations, NIA demand violations, and hydropower generation for various runs (cases). Also given are results for the pure simulation with existing rule curve-based (ERC case) and proposed rule curve-based (PRC case) operating procedures .....	108
Table 5.5	Hydropower generation and demand violations (or surplus if positive values) for year 2008 for cases (i) OS1, (ii) OS3, (iii) existing rule curve ERC1, and (iv) proposed rule curve PRC1. Note that Angat River flows from January to April are observed data and those from May to October are forecasted inflows .....	113
Table 5.6	Summary of drainage areas and number of sub-basin units for the major sub-basins of the Upper Agno River System .....	122
Table 5.7	Three (3) sets of target releases ( $m^3/s$ ) for Ambuklao, Binga, and San Roque reservoirs used in the optimization-simulation studies .....	129
Table 5.8	Reservoir end-of-month elevations (m); inflows, releases, and spills ( $m^3/s$ ); and hydropower generation (MW) for Ambuklao, Binga, and San Roque and outflow to ARIIP Reservoir at 90, 80, 50, 20, and 10 percent-of-time on monthly basis for target release policy Set 1 .....	130
Table 5.9	Reservoir end-of-month elevations (m); inflows, releases, and spills ( $m^3/s$ ); and power generation (MW) for Ambuklao, Binga, and San Roque and outflow to ARIIP Reservoir at 90, 80, 50, 20, and 10 percent-of-time on monthly basis for target release policy Set 2 .....	133

Table 5.10	Reservoir end-of-month elevations (m); inflows, releases, and spills ( $m^3/s$ ); and power generation (MW) for Ambuklao, Binga, and San Roque and outflow to ARIIP Reservoir at 90, 80, 50, 20, and 10 percent-of-time on monthly basis for target release policy Set 3 .....	136
Table 5.11	Time and reservoir inflows, spills, outflows, and reservoir elevations at the occurrence of maximum outflows (spills plus power releases) for the actual case, Case 1, Case 2, Case 3, and Case 4 .....	147
Table 5.12	Time and reservoir inflows, spills, outflows, and reservoir elevations at the occurrence of maximum reservoir elevations for the actual case, Case 1, Case 2, Case 3, and Case 4 .....	147
Table 5.13	List of hydrometric stations within and near the Agos River Basin where hydrologic data have been gathered .....	157
Table 5.14	Kaliwa Low Dam reliability analysis of <b>a</b> water supply deliveries and <b>b</b> hydropower generation for the WRC1 configuration (case with Kaliwa Low Dam only) .....	159
Table 5.15	Reliability analysis of <b>a</b> water supply deliveries at Kaliwa Low Dam, <b>b</b> hydropower generation at Kaliwa Low Dam, and <b>c</b> hydropower generation at Laiban Dam for WRC2 configuration (case with Laiban Dam and Kaliwa Low Dam in tandem) .....	161
Table 6.1	Specifications of the nine reservoirs of Balog-Balog multiple dam system (BBMDS) .....	169
Table 6.2	Comparison of irrigation water deliveries ( $m^3/s$ ) of BBMP and BBMDS (six reservoirs) including lower Bulsa River natural flows for the case with no sedimentation at S1 location .....	174
Table 6.3	Comparison of flow duration curves of daily irrigation water deliveries ( $m^3/s$ ) of BBMP system and BBMDS (nine reservoirs) for the case with no reservoir sedimentation at S9 location .....	175
Table 6.4	Reservoir life computations due to sedimentation with a sediment inflow of $3500 \text{ m}^3/\text{year}/\text{km}^2$ for BBMP and BBMDS reservoirs .....	175
Table 6.5	Comparison of flow duration curves of daily irrigation water deliveries ( $m^3/s$ ) of BBMP system and BBMDS (six reservoirs) for the case with 50 years reservoir sedimentation at S1 location .....	176
Table 6.6	Hydropower generation (in MW) at BBMP (one hydropower plant) versus BBMDS project (five hydropower plants located at S1, S2, S3, S4, and S5) .....	176

Table 6.7	Estimates of benefit/cost (B/C) ratio, net present value (NPV), and economic internal rate of return (EIRR) for BBMP and BBMDS for base case and after 25 years and after 50 years with sedimentation. [Irrigation benefits for rice, sugarcane, corn, potato, eggplant, tomato, string beans, and ampalaya (bitter gourd) but excludes hydropower] .....	177
Table 6.8	San Roque Reservoir capacities and sediment deposited (in MCM) for Cases 1, 2, and 3 .....	188
Table 6.9	Total water yield (in MCM), total energy generation (in GWH), and sediment load of power releases (in MCM) in 70 years for Cases 1, 2, and 3 .....	188
Table 6.10	Historical average daily inflows and number of day under spilling conditions of Pulangi Reservoir HP IV based on 1995–2003 data .....	201
Table 6.11	Estimates (including high and low) of sediments flushed for 12-h flushing operations at various sustained reservoir inflows and sluice gate openings .....	202
Table 7.1	Summary of drainage areas and number of sub-basin units of the modeled area .....	230
Table 7.2	List of rainfall gaging stations within and around the Manila Bay-Laguna Lake River Basins and pertinent information of these stations .....	231
Table 7.3	List of rivers around Manila Bay with derived BOD and phosphate loadings .....	246
Table 8.1	Space-time rainfall model parameters for the Pasac Delta network .....	258
Table 8.2	Rainfall-duration-frequency Curve Lumbia Airport based on 26 years of data from PAGASA. Note: rainfall total (mm), duration (mins or h), and frequency or return period T (years) .....	282
Table 8.3	Rainfall hyetographs (mm) corresponding inflow flood hydrographs ( $m^3/s$ ). The peak rainfall and peak runoff are highlighted below, and the time 1 corresponds to 8 AM–9 AM, December 16, 2011 .....	282
Table 9.1	Capabilities of enhanced EPANET with optimization model .....	305
Table 10.1	Reservoir end-of-month elevations (m); inflows, releases, and spills ( $m^3/s$ ); and power generation (MW) for Ambuklao, Binga, and San Roque and outflow to ARIIP Reservoir for target release policy Set 1 with climate change scenario .....	315

Table 10.2	Reservoir end-of-month elevations (m); inflows, releases, and spills ( $m^3/s$ ); and power generation (MW) for Ambuklao, Binga, and San Roque and outflow to ARIIP Reservoir for target release policy Set 2 with climate change scenario .....	318
Table 10.3	Reservoir end-of-month elevations (m); inflows, releases, and spills ( $m^3/s$ ); and power generation (MW) for Ambuklao, Binga, and San Roque and outflow to ARIIP Reservoir for target release policy Set 3 with climate change scenario .....	321
Table 10.4	Comparison of Ambuklao Reservoir generated hydropower (MW) for the existing reservoir and 2050 climate change scenarios for the three sets of target release policies (RP).....	325
Table 10.5	Comparison of Binga Reservoir generated hydropower (MW) for the existing reservoir and 2050 climate change scenarios for the three sets of target release policies (RP).....	327
Table 10.6	Comparison of San Roque Reservoir generated hydropower (MW) for the existing reservoir and 2050 climate change scenarios for the three sets of target release policies (RP).....	329
Table 10.7	Annual average discharge to Angat Reservoir for past and future climate scenarios from six global climate models (GCMs) .....	332
Table 10.8	Angat Reservoir daily releases to Ipo Dam for MWSS domestic water supply for the three optimization-simulation scenarios: (a) with 46 CMS MWSS demand; (b) with reservoir sedimentation and 46 CMS demand; and (c) with climate change and 46 CMS demand .....	335
Table 10.9	Angat Reservoir daily flow releases to Bustos Dam for NIA-AMRIS irrigation water supply for the three optimization-simulation model scenarios .....	336
Table 11.1	Physical variables and model parameterization of Subic Bay hydrodynamic and water quality model including the watershed model .....	341
Table 11.2	Number of sub-sub-basins and drainage areas of Subic Bay River sub-basin delineation .....	344
Table 11.3	BOD loadings in mg/l at various locations in the Subic Bay as indicated in Fig. 11.2 .....	348
Table 11.4	Groundwater flow and contaminant transport model parameters of Novaliches Reservoir-Payatas dumpsite .....	354
Table 12.1	Flood risk management in the context of sustainability science (SS) versus traditional science (TS) .....	370
Table 12.2	Building urban resilience in the context of sustainability science .....	377

# Chapter 1

## Introduction



**Abstract** This chapter presents an overview of the purpose, science, and art of water resources modeling in general and discussion on elements of water resources systems that encompass soil, water, and air and the target constituents that include flora, fauna, and human settlements. Some historical perspectives on the science versus the art of water resources modeling are also discussed in this first section. An overview of the status of modeling of water resources systems of the Philippines and the perceived lack of modeling including data collection efforts and investments in the country are discussed in the second section. The organization of this book especially the list of the various modeling studies presented ends this chapter.

### 1.1 Purpose, Science, and Art of Water Resources Modeling

Nowadays, modeling has become mainstream as an appropriate tool to deal with large-scale and complex dynamics and uncertainty of water resources systems. Modeling is an essential tool to generate science-based information that is useful to develop policies and management actions and subsequently implementing strategies and operational rules for effective water resources planning, design, and management. Specifically, modeling has been utilized for various purposes such as (1) understanding the behavior as well as general assessment of status and performance of water resources systems; (2) evaluation of alternative strategies to restore, enhance, maintain, and/or control the quantity and quality of the water resources system; (3) development of operational policies to sustain adequate water quantity with desirable water quality; (4) monitoring, detection, and surveillance for water resources regulation; (5) forecasting of water quantity and quality for real-time operations of water resources systems; and (6) prediction of possible behavior and performance of water resources systems to future conditions.

Models and modeling studies of water resources systems have become sophisticated in the past few years since one must not only consider the physical and ecological component of the water resources system but also its interaction with the socio-economic and human systems. For instance, in modeling studies for flood mitigation plans in urban areas like Metro Manila in the Philippines (Tabios 2010),

the factors to be considered in the flood modeling studies are the *meteorological factors* such as extreme rainfalls due to typhoons and monsoons; the *hydrological factors* which include river modification (i.e., straightening, confinement, widening), river sedimentation, and inadequately designed infrastructures; and the *human factors* such as indiscriminate disposal of solid wastes into the waterways, river and floodplain encroachment due to illegal settlement or poor flood zoning, and even obliteration of natural waterways due to urban developments. Another example is water quality modeling of Laguna Lake, located south of Metro Manila, Philippines, which has competing water uses for fish production, domestic water supply, irrigation, and flood control function including hydropower generation with pumped-storage system (Tabios and David 2004). Fisheries is a big industry in Laguna Lake, and saltwater intrusion from Manila Bay is desirable to the fishing industry. On the other hand, lake withdrawal for domestic water supply requires minimum salinity. With the need to extract more domestic water supply from the lake, the question of how much more can be sustainably extracted from the lake should consider not only the hydrology and hydraulics of the lake but other aspects such as ecological considerations (lake flora and fauna) as well as socio-economic considerations (livelihoods, fish farming practices). With regard to the flood control function of the lake, the Marikina River Basin is the biggest contributing watershed to the lake during the flood season when the floodwaters in the Marikina River are diverted to be temporarily stored in the lake through the Manggahan Floodway (a man-made canal built in 1982). While this flood control scheme protects the city of Manila from being flooded, it creates flooding problems in low-lying towns around Laguna Lake as well as it brings pollutants from the urban cities in the Marikina River Basin.

In the two examples above, a major component in the modeling study is the development and application of analytical and/or numerical models to describe, simulate, and predict the watershed hydrology and urban local (inland) and river flood hydraulics to provide the scientific basis for developing policies and management decisions for these water resources systems. Of course, nowadays, the importance of stakeholders cannot be overemphasized for the results of the modeling studies to be effectively utilized and fully appreciated. Also, the active engagement and participation of stakeholders (i.e., government, community, academe, professionals, civil society) in the entire course of the modeling study are necessary to provide not only the technical, ecological, and economic inputs but especially the social, political, and cultural components of the study. On this subject of stakeholder involvement, the transdisciplinary approach in holistic water resources planning, design, and management is advocated, and its framework is discussed in the last chapter of this book.

In modeling water resources systems, it is worthwhile to examine and appreciate the various media and constituents of the natural environment (soil, water, and air), built environment, flora, and fauna as well as human settlement. Figure 1.1 provides a graphic illustration of how the soil, water, and air environments mutually interact and support the terrestrial and aquatic flora and fauna as well as the human settlements.

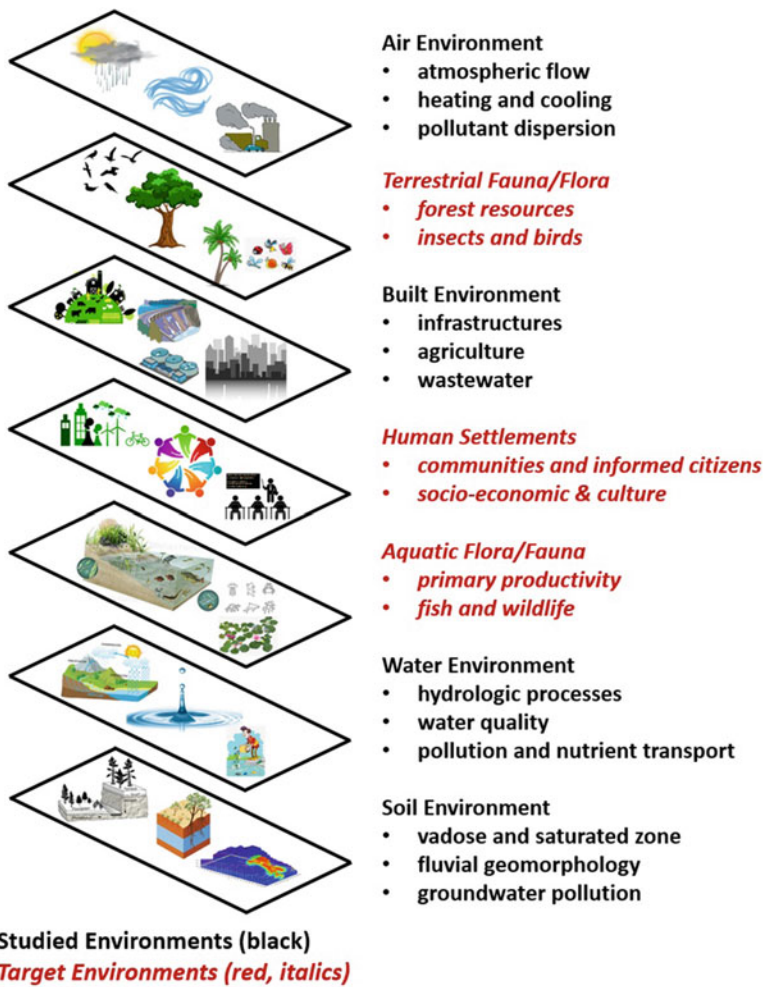


**Fig. 1.1** Hierarchy of the various media and constituents of the soil, water, and air environments and interactions with flora, fauna, and human settlements including the built environment. (Adapted from Nadaoka and Tabios 2009)

In particular, Fig. 1.1 demonstrates how the chain of various media and elements such as soil, water, and air environments interact with the flora, fauna, and human settlements. Each element is linked to one another, forming a web of intertwined dependencies. For instance, the soil environment (including the subsurface or lithosphere) is the medium of the water environment. In a like manner that both soil and water environments are mediums of air environment, which in turn derives elements or constituents like moisture, aerosols, and minerals from both soil and water. Plants, animals, and humans are important constituents of the soil, water, and air environments; they also contribute to the built environment. The soil, water, and

air environments are usually the studied environments (modeled entities), while the flora, fauna, and human settlement are the target environments (model clients or beneficiaries).

The illustration depicted in Fig. 1.1 emphasizes the importance of science/art/practice of modeling water resources to recognize the soil-water-air system as one contiguous system with components (the three different environments) interacting with each other to support humans as well as flora and fauna. For instance, when modeling river flood hydraulics, one should consider that the soil is the medium of water (*thus, the streamflow talks to the streambed*) rather than ignore river sediment transport processes by assuming pure water flow, fixed streambed model formulation. Likewise, in the case of lake water quality modeling, while the objective may be to ensure that dissolved oxygen (DO) is sufficient for fish production, a simple model of DO and biochemical oxygen demand (BOD) interaction may not be adequate if other constituents like nitrogen, phosphorus, sediment, and algae which are significant variables that could affect the DO evolution are not considered in the model. In Chap. 12, more discussion is given about the importance of recognizing the interactions of hydrology, geomorphology, and ecology in modeling of water resources systems.

As an aside but related to the above discussion, it has long been recognized that water resources management and engineering studies encompass various scientific and engineering disciplines. In the context of water resources management, Fig. 1.2 shows the three areas of concern, namely, water supply management, water excess management, and environmental restoration. This latter concern emphasizes the need for environmental-based planning, design, and operation of water resources

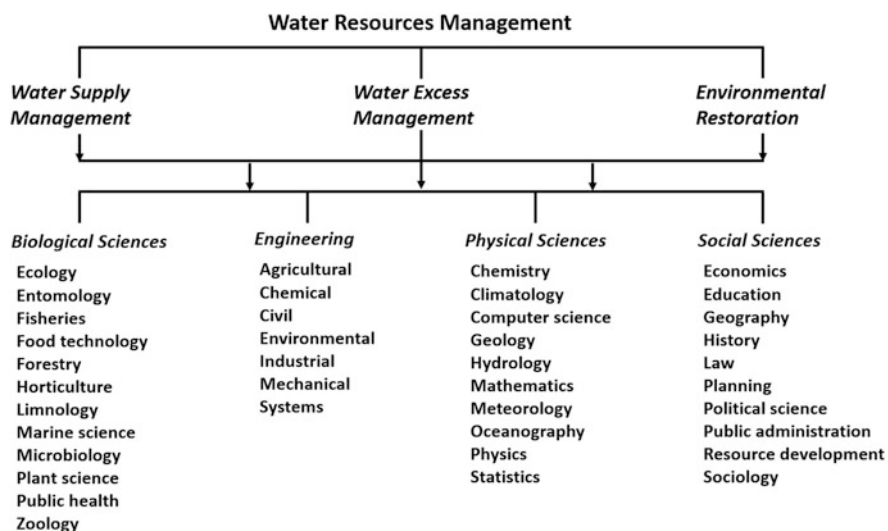


**Fig. 1.2** Water resource management and related scientific and engineering disciplines. (From Mays 2001)

systems to ensure that these water resources systems are not only technically sound but are environmentally friendly.

In view of both Figs. 1.1 and 1.2, the science, art, and practice of modeling water resources systems nowadays demand some level of sophistication with easily accessible data (through the internet), advances in research with efficiently organized knowledge, and especially computing power (speed and storage), compared to a few decades ago. In those days, there is an adage that models are designed for a given purpose, so that even a simple model, as long as it satisfies that purpose, is equally as good as a sophisticated one. Perhaps that can be a convenient excuse during that time, but it is no longer valid these days since there are already available water resources models (public domain or commercial), designed and operational with various optional methods that can be used for hydrologic, hydraulic, and water quality analysis and simulation studies. Utilizing readily available models of varying levels of sophistication and complexity has become more of an art and practice rather than purely science. Thus, it is important that the model user or analyst must somehow examine also the engine or heart of the model rather than merely become proficient at the input and output components of the model.

In the past, the art or ingenuity in utilizing models was necessary because some models were formulated without a particular feature or option to handle such physical process or the computer platform to run these models had limited storage and restrictively low processing speeds. For instance, there were hydraulic models in the past that compute the water surface profile of a river without the capability of handling bridge structures. So the art or ingenuity then was to assign an artificially high roughness coefficient in this bridge section to somehow capture the effect of the bridge crossing in the river flow dynamics. These days however, there are already models that explicitly handle bridge structures with so-called bridge routines. Another example is the art of optimization modeling especially with the use of linear programming (with linear objective function and constraints). With only linear programming computer software available then, a nonlinear optimization problem was linearized mathematically to fit the canonical form of linear programming. Again, these days, there are already a lot of optimization techniques (in readily available computer softwares) with nonlinear formulations.

Despite the advances in the model formulations and computing facilities, there are still modeling studies that require some art rather than pure science. For instance, flood inundation studies, with the availability of LIDAR-acquired elevation data at 1 by 1 m grids that allow for high-resolution spatial model discretization to capture no-flow areas such as presence of building structure, but because of the tremendous computing power needed to do this, the model discretization is reduced to say 20 by 20 m grids. In this case, a grid with a building structure with a footprint of 8 by 10 m is treated either with an artificially high roughness coefficient or with an artificial porosity parameter to account for this no-flow interior boundary and especially to ensure mass conservation in that grid cell.

Another example is a modeling study to assess if the ecological integrity of a river that has been bypassed due to flow diversion, say for hydropower generation, is maintained. But instead of conducting a high-level ecological modeling to evaluate

directly impacts of river flow diversion on flora/fauna population and in particular the survival of specific fish variety in the bypassed river, the modeling is conducted to assess the effects and changes of water temperature, dissolved oxygen (DO), and sediment concentration in the bypassed river. In this case, the art lies in how to translate the results of this temperature-DO-sediment water quality model into some metric or index as surrogate measure of the ecological integrity of the bypassed river.

## 1.2 Status of Modeling Water Resources Systems of the Philippines

In the Philippines, modeling of water resources systems for planning, design, and management is not quite common especially in government agencies involved in managing the country's water resources. One of the reasons is that the Philippines still lacks investments in science-based management and decision tools. Most water-related agencies in the Philippines do not have a dedicated scientific division in their offices to employ science-based analysis or modeling tools. A permanent or regular modeling group can develop, maintain, and update models as an everyday routine to aid in water resources planning and management decisions of the water resources agency. Some related discussions on this and issues relating to water governance in the Philippines where there is practically only one government agency that conducts modeling studies are given in Sect. 2.2.1, Chap. 2. In most cases, modeling studies are done by consulting firms as part of big-ticket water resources projects with associated foreign loans so that the budget allocation for the modeling tasks is either only provided in the required feasibility studies or, in some cases, only in the required master planning studies. Having a permanent modeling group will ensure continuous updating and adaptive master planning and operational studies of water resources system since plans cannot remain static because watersheds or natural resources systems in general are evolutionary in nature due to land use/cover change, anthropogenic activities, economic change, and climate change. Adaptive planning or master planning is best employed under the framework of sustainability science and transdisciplinary approach which is discussed in Chap. 12.

One final challenge of water resources modeling in the Philippines is lack of observed data especially streamflow, groundwater levels, river stages, and water quality data. Thus, model development can hardly be calibrated against the observed data so that the art here is to judiciously use experience, knowledge, and insights into the physics of the process and, to some extent, imagination to validate the results of the modeling studies. Again, the country lacks investments in sustained and regular monitoring of water-related data, more so at adequate and appropriate sampling frequencies in time and space. With this constraint, to conduct reliability analysis of rivers for water supply, the required long sequences of streamflow are generated through rainfall-runoff watershed model since rainfall is more available than streamflow, but the watershed model may not be properly calibrated since no

streamflow data is available. Ideally, models and data can complement each other so that models can fill in data gaps since there are always resource and budget constraints, while any available data can be used to calibrate the model or to fill in gaps not captured in modeling. However, in the Philippines, this is not always the situation because both data collection and modeling efforts may be lacking and, in certain cases, completely missing. Thus, this book advocates the use of modeling tools to ensure science-based policy formulations and management decisions in water resources planning and management in the country by presenting several modeling studies of water resources systems of the Philippines.

### 1.3 Organization of this Book

Chapter 2 presents a background of the state of water resources followed by the status of water governance in the Philippines, and Chap. 3 expounds on the science and art of water resources modeling in general and in the Philippines in particular. Chapters 4 through 11 present the various modeling studies as follows:

- (i) Surface and groundwater modeling for water utilization of the Pampanga River Basin as well as for Agno River Basin in Chap. 4.
- (ii) Reservoir planning and operations studies with optimization-simulation models on Angat Reservoir, Upper Agno Reservoirs, and the Agos Reservoir system in Chap. 5.
- (iii) Reservoir sedimentation studies in Chap. 6 of San Roque Reservoir for long-term sedimentation management, Pulangi Reservoir for sediment flushing operations studies, and comparison of Balog-Balog Reservoir system with single, high dam versus multiple dam system for irrigation and hydropower generation with reservoir sedimentation.
- (iv) Hydrodynamic and water quality modeling of Manila Bay with dissolved oxygen and Laguna Lake salinity intrusion modeling in Chap. 7.
- (v) Flood and dam break modeling studies on effect of moving storm in Pasac Delta flooding with space-time stochastic rainfall, on Marikina River Basin flooding during Typhoon Ketsana, assessment of alternative flood control mitigation plans for Cagayan de Oro River modeling, and dam break studies of a dam removal problem and Butas Dam of Cavite Province in Chap. 8.
- (vi) Pipe network distribution modeling with optimization of the southwest portion of Manila in Chap. 9.
- (vii) Climate change studies for reliability of Upper Agno Reservoir system and Angat Reservoir in Chap. 10.
- (viii) Modeling for environmental assessment studies of Subic Bay for developing an integrated coastal management plan and risk assessment of possible pollution of Novaliches Water Supply Reservoir from leachate of Payatas dumpsite.

Finally, Chap. 12 discusses imperatives of water resources modeling and applications in the Philippines that include monitoring and data need, research and capacity building, the role of sustainability science and transdisciplinary approach for sustainable water resources development, and building urban resilience to water-related disasters.

## References

- Mays LW (2001) Water resources engineering. Wiley, New York
- Nadaoka K, Tabios GQ III (2009) In: Kusakabe O, Aramraks T, Sigua RG, Takemura J, Diola NB, Yodsudjai W (eds) Air, water, groundwater and soil environments, section 2.2 of characterizing the environment: monitoring, analysis and assessment, sustainable civil engineering. University of the Philippines Press, Quezon City
- Tabios GQIII (2010, December) Urban dimensions of flood management: case of Pasig-Marikina River Basin of Metro Manila, Philippines. *J Hydrol Environ, IHES* 6(1):1–9
- Tabios GQIII, David CC (2004) Chapter 5 in winning the water war. In: Rola AC, Francisco HA, Liguton JPT (eds) Competing uses of water: cases of Angat reservoir, Laguna Lake and groundwater systems of Batangas City and Cebu City. Philippine Institute for Development Studies, Makati, pp 105–131

## Chapter 2

# Physical Features and State of Water Resources and Status of Water Governance in the Philippines



**Abstract** This chapter presents an overview of water resources in the Philippines. In particular, the physiographic, climate, and weather features including the water resources regions and river basins of the Philippines. Then, the state of water resources in the Philippines in terms of water quantity and quality of surface and groundwater resources, water use demands, irrigation services, flooding issues and concerns, and environmental problems and conditions are discussed. The status of water governance in terms of policies, processes, and institutional arrangement is discussed followed by a brief summary of the recently revisited national water policy of the Philippines and, finally, other issues and concerns of water governance in the Philippines.

## 2.1 Physical Features and State of Water Resources in the Philippines

### 2.1.1 General Physiography, Climate, and Weather in the Philippines

The Philippine archipelago lies in the Southeast Asia with a total land area of 343,448 km<sup>2</sup> and stretches about 1850 km from south at 5°N to north at 20°N latitudes and traversing about 925 km from west at 116°E to east at 124.5°E longitudes, as shown in Fig. 2.1. The Philippines is divided into three principal regions Luzon, Visayas, and Mindanao where the two biggest islands are Luzon and Mindanao with areas of 105,000 and 95,000 km<sup>2</sup>, respectively, while Visayas is composed of a cluster of islands located between these two big islands. The entire archipelago is composed of over 7600 islands and claims an exclusive economic zone of 370 km from its shores. The country is known to have one of the longest coastlines in the world.

The Philippines is in the Pacific Ring of Fire, and the western rim is characterized by active volcanoes. Among the most notable, active volcanoes are Mount Mayon and Taal Volcano. Mayon with its almost a perfect cone is near Legazpi City, while Taal Volcano, located southwest of Metro Manila, is inside Taal Lake with its crater



**Fig. 2.1** Map of the Philippines showing political regions and provinces. (Taken from [www.map-of-the-world.net](http://www.map-of-the-world.net))

walls enclosing a smaller lake. Both volcanoes erupt almost on decadal basis. Another notable volcano is Mt. Pinatubo just north of Manila which violently erupted in 1991 after about 500 years in hiatus. The country's highest peaks are Mt. Apo that rises 2954 m followed by Mt. Dulang-Dulang of the Kitanglad Mountain Range which rises 2938 m; both are located in Mindanao. There are

prominent mountain ranges such as the Sierra Madre (along the eastern seaboard of Luzon), the longest in the Philippines as well as the Cordillera Central (north western seaboard), and both of them are connected by Caraballo Mountains around 16°N latitude, traversing from east to west. The steepest slope between land and sea is the Philippine Trench, which descends to a depth of 10,430 meters. It is located off the coast of eastern Mindanao.

Among the notable rivers of the country are Cagayan River in Northern Luzon; Pampanga River in Central Luzon which flows from north to south into Manila Bay; Pulangi River in Central Mindanao that becomes Mindanao River (Rio Grande de Mindanao) which flows from north to southwest into Celebes Sea; and Agusan River in mid-eastern Mindanao which flows north into Mindanao Sea. The largest fresh-water lake in the Philippines is Laguna de Bay which is located south of Metro Manila and east of Manila Bay.

The climate in the Philippines is described according to five climate types, namely, tropical rainforest, tropical savanna, tropical monsoon, humid subtropical, and maritime or oceanic. With this, the climate in the country is generally characterized by relatively high temperature, oppressive humidity, and plenty of rainfall. In terms of climate seasons, the Philippines is classified into four types, based on Coronas classification, depending on the location in the country, namely, Type I climate with pronounced dry season from November to April and wet from May to October which is mostly in the China Sea side or western part of the country; Type II with no dry season and very pronounced rainy period from December to February in the Pacific side or eastern part of the country; Type III climate with relatively dry season from November to April and wet during the rest of the year occurs in the inner part of the country from Luzon to Mindanao; and Type IV with rainfall evenly distributed throughout the year occurs in the west inland part of Visayas and mostly in the southern part of Mindanao.

The Philippines receives an average annual rainfall of 2400 mm, and it spatially varies so that 30 and 10% of the country, mostly in northern and southern Philippines, respectively, receive this annual rainfall amount. The remaining 60% of the country receives as much as 5000 mm annually in the mountain regions, while 1000 mm are received in shielded plains and valleys. The Philippines sits across the typhoon belt, and around 28 storms and/or typhoons visit the country per year, but, on the average, only 19 typhoons make landfall. Monsoon also brings several days of heavy rains to most of the archipelago during the months of May to October.

Based on all available weather stations in the Philippines, the average annual temperature for the entire country is 26.6 °C. The coolest month falls in January with a mean temperature of 25.5 °C, while the warmest month occurs in May with a mean temperature as high as 32.0 °C. Temperatures are lower at locations with high elevations like Baguio City, at 1500 m above sea level. It enjoys a mean temperature of 18.3 °C. Essentially, near the sea level, there is no difference in the mean annual temperature in Luzon, Visayas, or Mindanao. With the high temperature and the country virtually surrounded by water bodies, the Philippines has a high relative humidity which averages monthly between 71% in March and 95% in September. Over most parts of the country, it is generally uncomfortable

during the dry months of March to May, especially when temperature and associated humidity attain their maximum levels.

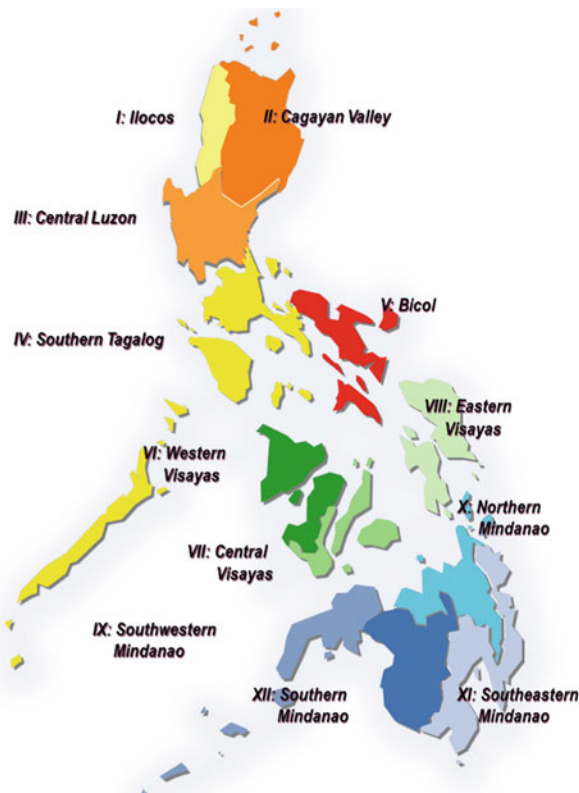
With the above climate and physiography, the Philippines has unique settings and conditions typical of humid, maritime, tropical climatology, and hydrology as well as with its archipelagic or islandic watersheds typified by short, steep mountain-to-coast river systems.

### **2.1.2 Water Resources Regions and Major River Basins in the Philippines**

For purposes of water resources planning, development, and water regulation, the country is divided into 12 water resources regions (WRR) as shown in Fig. 2.2. From the 2008 survey, there are a total of 623 water bodies consisting of 283 principal rivers, and the remaining 340 are classified as lakes, bays, and small rivers.

Figure 2.3 shows the major river basins in the Philippines. Four of the largest river basins in the order of their drainage areas are (1) Cagayan River Basin (RB) in

**Fig. 2.2** Twelve (12) water resources regions (WRR) of the Philippines designated by the National Water Resources Council in 1978 for purposes of planning, development, and water regulation. (From NWRB website: [www.nwrb.gov.ph](http://www.nwrb.gov.ph))



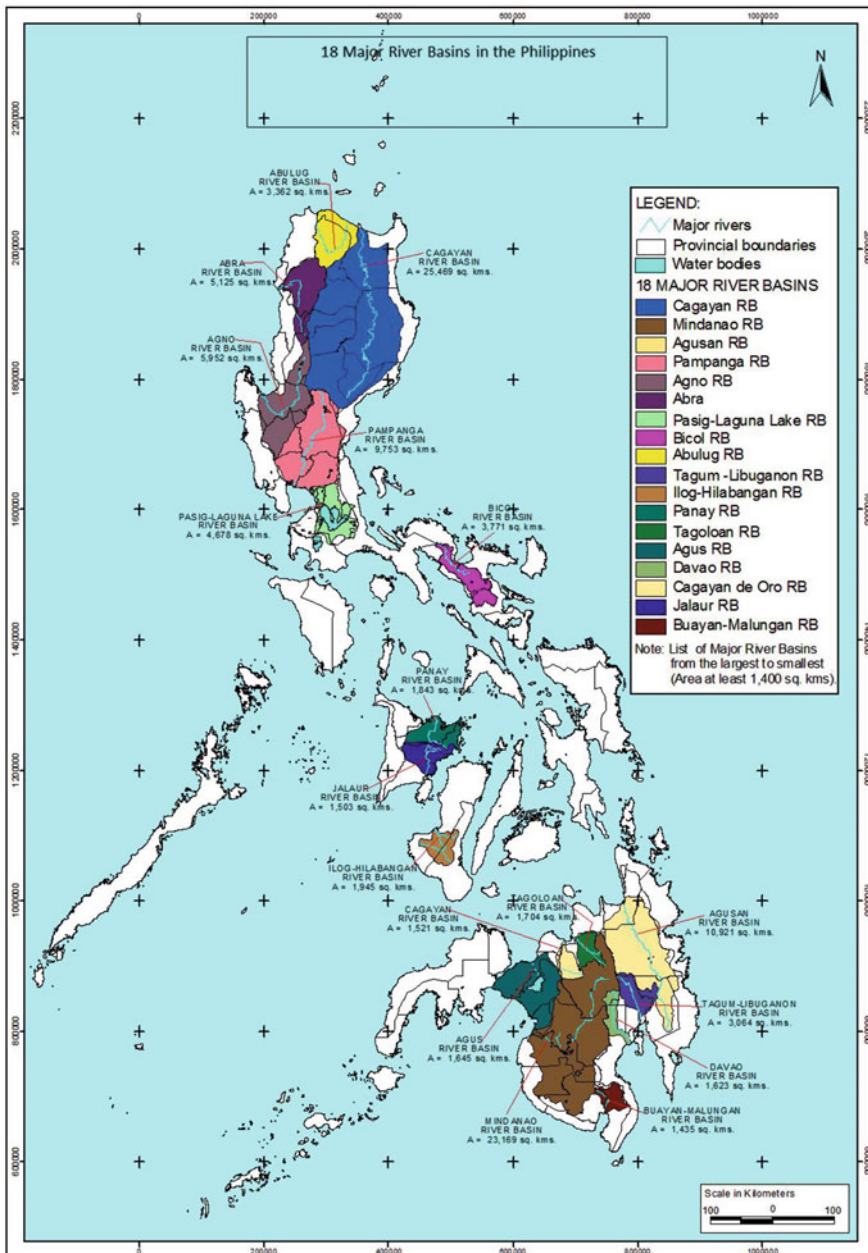
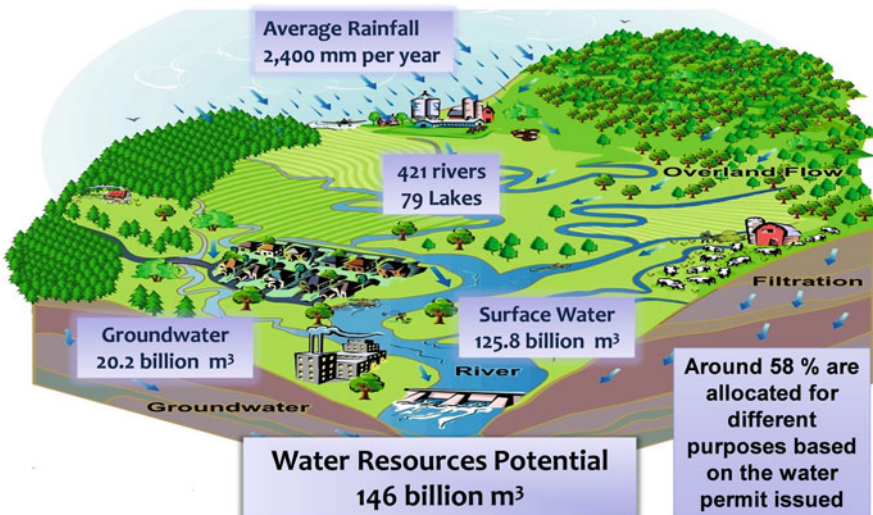


Fig. 2.3 Major river basins (RB) in the Philippines. (From NWRB website: [www.nwrb.gov.ph](http://www.nwrb.gov.ph))



**Fig. 2.4** Surface water and groundwater resources of the Philippines. (Background picture taken from [www.prairievers.org](http://www.prairievers.org))

water resources region 2 (WRR 2) with drainage area, DA = 25,649 km<sup>2</sup>; (2) Mindanao River Basin (WRR 12) with DA = 23,169 km<sup>2</sup>; (3) Agusan River (WRR 10) with DA = 10,921 km<sup>2</sup>; and (4) Pampanga River Basin (WRR 3) with DA = 9245 km<sup>2</sup>. The smallest among these major river basins shown in Fig. 2.3 is Buayan-Malungon River Basin (RB) with a drainage area of 1434 km<sup>2</sup>. The major lakes include Laguna de Bay and Taal Lake in Southern Luzon, Naujan Lake in Mindoro, and Lake Mainit and Lanao Lake in Mindanao.

### 2.1.3 *Quantity and Quality of Surface and Groundwater Resources*

As shown in Fig. 2.4, the Philippines has a total freshwater resource of about 146 billion m<sup>3</sup> in which 86% is from surface water and the remaining 14% is from groundwater. From 2000 data, the Philippines has 1907 m<sup>3</sup> per capita water availability per year with a population of 77 million people, ranking second to lowest in Asia and almost half of the Southeast Asian per capita of 3668 m<sup>3</sup> or about a third of the global average of 7045 m<sup>3</sup>. In 2016, the per capita water availability per year is reduced to about 1400 m<sup>3</sup> with the population of 103 million (Rongavilla 2017).

With regard to quality of water, only a very small percentage of the six water resources regions (WRR) have Class AA most potable, 36% of 623 are classified as Class C suitable for fisheries, and 33% are classified as Class D, that is, needing

complete water treatment to be potable. Fifty years ago, most river waters were potable and fishes in these rivers abound.

According to the Environmental Management Bureau of the Department of Environment and Natural Resources (EMB-DENR), out of the 688 classified water bodies in the country, only about 27% have potable water. Many of the major rivers and lakes are heavily polluted. Of the 40 water bodies monitored as sources of drinking water supply, only 28% conform to the criterion for total suspended solids, signifying the effects of sand and gravel quarrying activities and runoff sediments from denuded forest and agricultural lands.

Domestic sewage has contributed about 52% of the pollution load, while industries account for the remaining 48%, according to available data. On the other hand, pollution of groundwater occurs when contaminants coming from domestic wastewater, agricultural runoffs, and industrial effluents reach the aquifer or water table in the form of leachate. Of these, domestic wastewater is the main contributor of bacterial contamination to the groundwater supplies. Waterborne diseases such as diarrhea, cholera, dysentery, hepatitis A, and others can be caused by the presence of coliform bacteria in drinking water supplies.

Increasing urbanization, industrialization and inadequate sewerage and sanitation facilities are causing massive pollution to the country's water bodies. This effluent is in the form of raw sewage, detergents, fertilizer, heavy metals, chemical products, oils, and even solid waste.

Saline water intrusion has likewise emerged as a problem in some areas that reduces the availability of groundwater supply. This is caused by overexploitation or excessive withdrawal of groundwater. As salt water enters into the water table, water availability for domestic use, including drinking and agricultural usage, is reduced. This poor water quality plus the dwindling water supply due to environmental degradation and climate change can result in the looming water scarcity in the country.

#### **2.1.4 Water Use Demands and Water Permits**

From the National Water Resources Board (NWRB) data of December 2010, there were 21,812 water permit grantees accounting for a total of 2727.40 m<sup>3</sup>/s or about 86.0 billion m<sup>3</sup> annually (i.e., 59% of the total water available of 146 billion m<sup>3</sup> as indicated in Fig. 2.4). As shown in the pie chart in Fig. 2.5, the biggest water consumer is the irrigation sub-sector, accounting for 78% of total water use, followed by industrial water users at 12%, and then 8% domestic water use. Currently, the total area with irrigation facilities is only about 48.47% of the country's potential irrigable land estimated at 2.9 million ha. Considering that over the next 25 years, food will be required for another 25 million more Filipinos (from 103 million), this is a cause for concern. Hydropower accounts for 57.34% of the water permits granted, however, as hydropower is non-consumptive, most of the hydropower water grants are also part of the irrigation water grants.

**Fig. 2.5** Water use for various purposes based on water permit granted by the National Water Resources Board (NWRB) as of December 2010. Values shown are average annual flows (in  $\text{m}^3/\text{s}$ ), and values in parenthesis are for the total water permit granted of  $2727.40 \text{ m}^3/\text{s}$

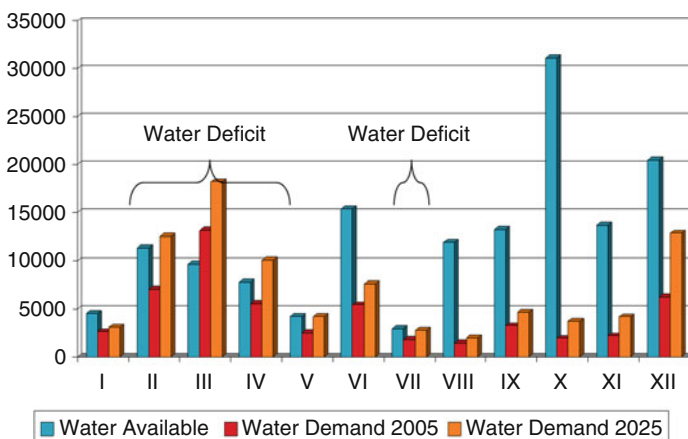
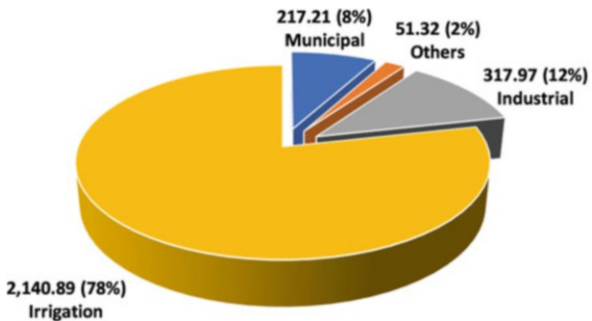


**Fig. 2.6** Projected regional supply and demand situation in  $1000 \text{ m}^3$  for 2005 and 2025 according to WRR in Fig. 2.2. (Source: JICA 1998 Master Plan Study on Water Resources Management in the Philippines submitted to NWRB)

NWRB estimates that over 90% of the domestic water supply is drawn from groundwater, while almost all irrigation water supply is from surface waters. NWRB further reports that not all water extractions have water permits so the rest are unaccounted for by numerous users. This implies that the actual water consumption could even be more than the amounts given above. Furthermore, NWRB with its meager budget and no regional offices, it is unable to properly monitor and subsequently penalize violations due to over-extraction.

Figure 2.6 shows the water available plotted along with the water demands for years 2005 and 2025 from JICA (1998) derived using a high economic growth scenario. As seen here, the estimated water availability is unequally distributed among the different water resources regions of the Philippines (see Fig. 2.2) due to spatial variability and differences in local climate, physiographic, and geographic features. Based on these data, water deficit is expected to happen in the Cagayan Valley (II), Central Luzon (III), Southern Tagalog (IV) and Central Visayas (VII) water resources regions. Water-stressed cities include Baguio, Angeles, Metro

Manila, Iloilo, Bacolod, Metro Cebu, Davao, Cagayan de Oro, and Zamboanga. With extreme climate such as those relating to El Niño, La Niña, and, to some extent, climate change, the country experienced effects on the availability of water supply, raising public alarm on the possibility of water shortages in some areas and extreme flooding in others.

### ***2.1.5 Irrigation Services***

The Philippines has invested heavily in irrigation systems for rice production during the mid-1960s to late 1980s. After this, there was no longer a significant expansion in irrigated agriculture. Post-evaluation studies of these irrigation systems by World Bank in 1992 and well documented by Delos Reyes (2017) showed a host of problems and issues concerning these irrigation systems, such that (1) the actual irrigated areas were only 56% of the design service areas in contrast to 94% areas served before 1965; (2) the economic rates of return were much lower than those estimated in the project planning stage; (3) the rapid deterioration of the irrigation facilities due to inadequate maintenance and unrealistic design assumptions; and (4) the operation of most irrigation canals significantly failed to distribute water efficiently and equitably despite employing the participatory irrigation management; thus nearly half of the farmers refused to pay their assessed irrigation fees.

In response to these irrigation delivery problems, certain farmers resorted to illegal tampering of water control structure to manipulate the distribution of irrigation water, unauthorized pumping from waterways and irrigation canals, and the proliferation of swallow tubewell irrigation water extraction. The rampant use of swallow tubewell in particular has led to overexploitation of groundwater resource resulting in significant decline in groundwater table, thus rendering other swallow tubewells inoperable as well as depriving mangroves and other coastal ecosystems from groundwater flow and inducing saltwater intrusion into groundwater aquifer near coastal areas.

In 1997, the Agriculture and Fisheries Modernization Act (AFMA) was passed to rationalize irrigation development in the country and called for the development of additional irrigation service areas, rehabilitation and maintenance of existing irrigation canals, efficient operation of irrigation canals, institutional capacity and strengthening to improve overall irrigation water delivery, devolution of activities, and service to local government units and private sector to increase productivity of irrigation water. However, AFMA was rather not satisfactory since from years 1998 to 2004; the total irrigation service area increased only by 62,000 ha (from 1.165 to 1.227 million ha) despite a total of 132,000 ha of service area was created and almost one million ha were rehabilitated. The major reason is that only 40–50% of these newly generated irrigation service areas including areas associated to the rehabilitated irrigation system had available water supply from the source.

In the recent past, the public questioned investments in the development and rehabilitation of irrigation system due to the disappointing performance of such irrigation systems, the subsequent foreign debt burden since farmers could not pay

the irrigation fees, and the negative impact of the uncontrolled proliferation of swallow tubewell irrigation water source. Despite these pitfalls, the construction of new irrigation system and rehabilitation or modernization of existing ones are needed for food security and poverty alleviation in general and, in particular, for optimal utilization of irrigation water especially in the face of other water uses. Additionally, the present irrigation infrastructure only covers 30% of the potential irrigation service area identified for rice production and that most arable areas cannot be adequately fed by rainwater or sustained by groundwater supply especially in areas with swallow tubewells. Further discussions on the state of irrigation services in the country may be referred to Delos Reyes (2017).

### ***2.1.6 Flooding Issues and Concerns***

Every year, the Philippines experiences devastating water-related disasters such as floods, rainfall-triggered landslides, debris flow, and mudflow. Floods are technically pure water hazards in contrast to landslides, debris flows, and mudflows which carry with them solid materials such as sediments, boulders, and trees. In debris flows or mudflows, solid materials or sediment concentrations are more than 60% of the flows in contrast to flood flows which have less than 5% sediment concentration. Debris flow may fade into hyper-concentrated flows with solids or sediment concentration which ranges from 10 to 50%. Debris flows that develop from rainfall-induced landslides and massive slope failures or remobilized sediment materials in high-gradient rivers are the most disastrous debris flow. In rainfall-induced landslides and slope failures, as the slope material gets wet, its yield strength is reduced due to increase in water pore pressures, thus loosening and pushing particles apart. Once debris flow initiates, the sliding slope materials can continuously flow down-slope easily burying or carrying anything along the way for significant distances.

Among the major flood disasters in the past is the Central Luzon flooding of August 2004 affecting two million people with associated property damages of about 1.5 billion pesos and likewise the Mindoro Oriental flooding of December 2005 that isolated northern towns from the rest of the province for about 3 weeks. Both are considered the most destructive flood inundations in recent history. Major water-related disasters accompanied by landslides and debris flows (including floating logs) were as follows: debris flow disaster in Quezon and Aurora Provinces attributed to a series of four typhoons in November 2004 that killed over 2000 people; debris avalanche and mudflow in Guinsaugon, Leyte, in February 2006 that killed over 1000 people including school children when their school was buried; and rainfall-triggered mudflows from Mayon Volcano at the height of Typhoon Reming affecting major towns of Albay and killing about 500 people in December 2006 (Tabios 2008). Three other major devastating water-related disasters include the Ormoc City tragedy that killed more than 5000 people due to debris flow triggered by Typhoon Uring in November 1991 and in Camiguin Island where 200 died in the aftermath of Typhoon Nanang in November 2001. Close to Manila, the pyroclastic

materials or lahars from Mt. Pinatubo's eruption in 1991 produced several debris flow events over a span of 5 years toward the surrounding Santo Tomas River in Zambales, Pasig-Potrero River in Pampanga, O'Donnell River in Tarlac, and Porac-Gumain River in Bataan.

Admittedly, there is already a good amount of science and engineering technology for water-related disaster monitoring, prediction, mitigation, and management. For instance, watershed management is a very important component of flood disaster management. Rivers dynamically respond to watershed changes like changes in land use/cover. For example, if the forest cover is removed, the sponge effect of forest and/or ability of the watershed to infiltrate water is reduced that results in greater overland or surface runoff, thus increasing the rate of erosion and sedimentation from the watersheds. The resulting sediment erosion and deposition change the river topography or geometry and consequently change the flooding dynamics of the river basin especially at the downstream portion of the river. The natural dynamics of rivers is that rivers move away sediments during floods, while sediments are deposited during low flows. If this dynamics is altered such as building houses within the floodplains or river alterations due to dredging, then this alteration creates river instability that could change the river morphology affecting the flood conveyance capacity of the river. Likewise, one must properly plan the layouting of structures such as levees or bridges that could constrain the river system or change the flood dynamics of the river. Non-structural measures such as floodplain mapping and land use zoning are also worthwhile by basically mapping and identifying flood prone areas so that investments or developments in these areas can be avoided. Public awareness is also one important component in water-related disaster management to avoid indiscriminate government and private developments that could disrupt natural watershed processes. Finally, other adaptation measures with regard to water-related disasters in particular are early warning systems, education and awareness, response and recovery programs, coordination among agencies during the disaster, and also flood insurance.

### ***2.1.7 Design Level of Protection for Major Flood Control Projects***

On another issue related to flooding, the Department of Public Works and Highways' (DPWH) major flood control projects in the Philippines only provide design levels of protection ranging from 10-year to 30-year return period design flood with the exception of the Ormoc Project of 50-year as shown in Table 2.1. The flood design of Pasig-Marikina River including the Manggahan Floodway is only for 30-year return period flood. During Typhoon Ketsana in September 2009, the computed peak flow of  $5700 \text{ m}^3/\text{s}$  in Marikina River was associated to a return period flood way beyond 100-year (i.e., the 100-year flood is about  $3400 \text{ m}^3/\text{s}$ ). Thus, it is definitely worthwhile for the national and local government to rethink if

**Table 2.1** Flood control design level of protection in terms of return period and other pertinent information of major DPWH flood control projects

Name of River or Area	Return Period (years)	Design Discharge (m <sup>3</sup> /sec)	Catchment Area (km <sup>2</sup> )	Specific Discharge (m <sup>3</sup> /sec/km <sup>2</sup> )
Laoag	25	11,200	1,332	8.41
Agno	10	6,410	5,910	1.08
Pampanga Delta	20	3,800-4,300	-	-
KAMANAVA	30	450	18.5	24.3
Pasig-Marikina	30	2,900	529	5.5
Mangahan Floodway	30	2,400	-	-
Iloilo	20	1,000	412	2.4
Agusan	25	8,010	10,621	0.75
Ormoc	50	610	25.2	24.2

the 30-year return period design flood for the Pasig-Marikina River Basin is the only level of protection that they can provide the people (Tabios 2010, 2008).

In the case of the Lower Agno River Basin, the flood control design is based on a 10-year return period flood. The maximum outflow of 5361 m<sup>3</sup>/s from San Roque Dam during Typhoon Pepeng was a result of the 5547 m<sup>3</sup>/s reservoir inflow associated to an 80-year return period flood. During the August 25–30, 2004, Central Luzon flooding, the San Roque Dam peak inflow of 3029 m<sup>3</sup>/s that occurred in the afternoon of August 27 that year is associated to a 20-year return period flood. The 20-year or 80-year return period floods can happen again and even over and over again in Agno River Basin. Thus, in the same manner as the Pasig-Marikina River Basin, the national and local government should seriously rethink if the 10-year return period design flood is the only level of protection that can be provided to the communities in the lower Agno River Basin.

Note that a flood control project designed for a 10-year return period flood implies that 10 percent of the time, floods that can occur in a given location cannot be contained by that project in contrast to a flood control project designed for a 50-year or 100-year return period flood which implies that two (2) percent or one (1) percent of the time, respectively, such flood can be contained by the project. A flood control project designed to contain a 100-year return period flood significantly provides 10 times higher level of protection to communities compared to a 10-year return period flood design yet the project cost for the former is not necessarily 10 times bigger than the latter.

On a separate note, the national government through DPWH has ongoing efforts to revise the flood mitigation master plans to cope with potential impacts of climate

change, and together with this is the new policy to upgrade the design level of protection of major flood control projects to a 50-year return period design flood for major river basins with drainage areas of over 40 km<sup>2</sup> and 25-year return period design flood for rivers with less than 40 km<sup>2</sup> (Tabios et al. 2016). Note that this upgrade only refers to increasing the level of protection in terms of flood design return period based on historical flood frequency curves; otherwise it would be difficult to justify economically, a particular flood mitigation project based on a flood frequency curve contrived from some future climate change scenario. Ironically, with climate change, the 50-year return period design flood magnitude may be equivalent only to say, a 20-year return period flood. Or conversely, if the 50-year design flood of a river is 1000 m<sup>3</sup>/s from historical data, this 50-year flood may only be, say, 650 m<sup>3</sup>/s with future climate change.

### ***2.1.8 Environmental Problems and Conditions***

Increasing urbanization, industrialization, and inadequate sewerage and sanitation facilities are causing massive pollution to the country's water bodies. This effluent is in the form of raw sewage, detergents, fertilizer, heavy metals, chemical products, oils, and even solid waste. In a study made by World Bank and USAID on the Economic Impacts of Sanitation in the Philippines (World Bank 2008), it was reported that the country loses more than 77.8 billion pesos annually due to poor water and sanitation.

The Philippine Environment Monitor (World Bank 2007) reports that the biggest source of water pollution in the country is domestic wastes (48%), followed by agricultural (37%) and industrial (15%) waste. In Metro Manila alone, domestic waste accounts for 58% of the water pollution, and industrial wastes accounts for 37%. Untreated wastewater affects health, makes water unfit for human consumption and recreational use, and deteriorates overall quality of life.

With regard to the coastal environment, only 4–5% of coral reefs remain in excellent condition; thus 95% have been ruined or degraded due to marine or water pollution and other activities. Almost 70% of the country's mangrove forests have been converted to aquaculture, logged or reclaimed for other uses, or are obliterated due to saltwater intrusion after being deprived of freshwater supply due to upstream extraction (Melana et al. 2005).

As far as forest resources are concerned, there are currently 146 proclaimed watershed forest reserves covering a total area of 26,757 km<sup>2</sup> which constitute about 17% of the country's total classified forestland areas of 158,053 km<sup>2</sup> (FMB 2014). Forest cover loss in many watersheds in the country has been severe. The ratio of forest cover to irrigated and irrigable lands is generally quite low, and this could have serious implications on soil erosion and the availability and quality of water for domestic water supply and irrigation.

## 2.2 Water Governance in the Philippines

### 2.2.1 Current Water Governance and Institutional Arrangement

Water resources management in the Philippines is embodied in formal policies for its comprehensive development, utilization, conservation, and protection, notably in the Philippine Constitution, the Water Code, the Environmental Code, and, more recently, the Clean Water Act. Over time, water resources management has evolved into a complex one. To effectively implement these policies, water resources management functions were distributed among numerous government agencies. The Philippine Water Code under Presidential Decree (PD) 1067 of Dec 1976 already invoked integrated water resources management (IWRM) as stated that it is “based on rational concepts of integrated and multi-purpose management of water resources and sufficiently flexible to adequately meet future development and that the utilization, exploitation, development, conservation and protection of water resources shall be subject to the control and regulation of the government through the National Water Resources Council.” However, the implementing rules and regulations (IRR) of the Water Code which was crafted in June 1979 still recognized the legislated roles of many water-related agencies such as DENR, Department of Public Works and Highways (DPWH), National Irrigation Administration (NIA), National Power Corporation (NAPOCOR), Philippine Atmospheric, Geophysical and Astronomical Services Administration (PAGASA), Department of Interior and Local Government (DILG), Department of Health (DOH), local government units (LGU), and water districts (WD).

At a glance, Fig. 2.7 shows that there are more than 25 institutions, a combination of line agencies or departments and various offices under said line agencies share in the discharge of such function which covers policy making, regulation, coordination, water quality management and sanitation, watershed management, integrated area development, data collection, flood management, irrigation, hydropower, water supply, research and development, cloud seeding, and fisheries development. The main agency that has been given the basic mandate of overall management of water resources is the National Water Resources Board (NWRB). The mandate embraces the control, supervision, and regulation of the utilization, exploitation, development, and protection of water resources.

To better understand the complex roles and functions of the various water-related agencies shown in Fig. 2.7, Table 2.2 from Tabios and Vilaluna (2012) and likewise Rola et al. (2015) mapped out the current water management functions of the major water-related agencies based on their mandates. This table clearly shows that many of these agencies share and perform analogous functions under limited oversight and coordination that may either result in complementation of task or conflict among agencies. Each of the agencies performs functions with specific objectives, which can sometimes be in conflict with other agencies’ objectives. This kind of situation

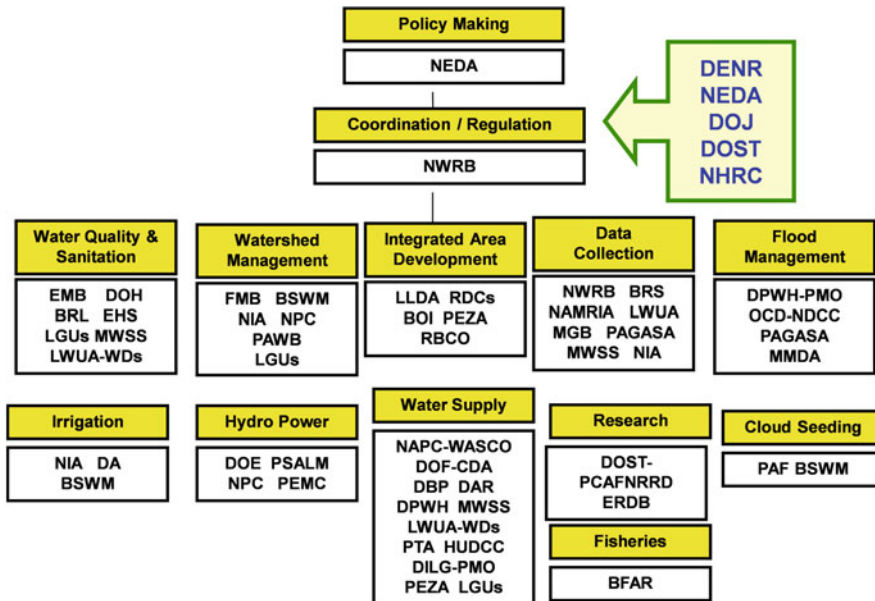


**Fig. 2.7** Water-related agencies in the Philippines and their functions

needs to be organized to effect clear, sustainable, more efficient, and effective water resources development and management.

As seen above, the National Water Resources Board (NWRB), the lead national government agency mandated by law to coordinate and regulate water resources management in the Philippines, is unfortunately ill-equipped to perform all its functions. With an annual budget of 52 million pesos and a staff complement of 88 filled-up positions (circa 2012), it is unable to perform much of the functions required to develop and manage the country's water resources.

The NWRB's current focus is mainly on policy and program coordination, resource regulation, and economic regulation. On policy and program coordination, the agency has difficulties orchestrating all the agencies engaged in water-related programs. The NWRB's data on water resource assessment are very much outdated and have never been updated since 1980. They currently do not have any capacities on scientific modeling and computerized decision support systems that will aid decision-makers and planners in the optimal management of the country's water resources.

With regard to legal instruments, the Philippines may have several existing laws that cover the proper implementation of water-related disaster management programs which were discussed in Tabios et al. (2018). One of the major laws related to water-related disasters is the National Disaster Risk Reduction and Management (DRRM) law which was passed by the Philippine Congress in May 2010. In relation to flood risk management, the law offers an institutional arrangement that distinguishes the role of DRRM councils at the national, regional, provincial, city,

**Table 2.2** Current roles and responsibilities of water-related agencies in the Philippines

	<i>Government agencies</i>																	
<i>Functional areas</i>	N W R B	L W U A	D E N R	L G U s	D P W H	D O H	N I A	P O C O R	A G A S A	M W S F	D O S	D I L G	D O E	M M D A	M M D A	D O T	L L D A	N E D A
Policy planning	●	●	●	●	●	●	●	●	●	●	●	●	●	●	●	●	●	
Data monitoring	●	●	●	●	●	●	●	●	●	●	●	●	●	●	●	●	●	
Scientific modeling									●									
Infrastructure and program development	●	●	●	●	●	●	●	●	●	●	●	●	●	●	●	●	●	
Operations of water facilities				●			●	●	●		●			●		●		
Regulatory functions	●	●	●	●	●	●					●		●	●	●		●	
Financing	●	●	●	●						●							●	
Public relations, capacity building, and IEC	●	●	●	●	●	●	●	●	●	●	●	●	●	●	●	●	●	
Local RBO development			●															

From Tabios and Vilaluna (2012)

**NWRB** National Water Resources Board, **LWUA** Local Water Utilities Administration, **DENR** Department of Environmental and Natural Resources, **LGUs** Local Government Units, **DPWH** Department of Public Works and Highways, **DOH** Department of Health, **NIA** National Irrigation Administration, **NAPOCOR** National Power Corporation, **PAGASA** Philippine Atmospheric, Geophysical and Astronomical Services Administration, **DOST** Department of Science and Technology, **DOF** Department of Finance, **MWSS** Metropolitan Waterworks and Sewerage System, **DILG** Department of Interior and Local Government, **DOE** Department of Energy, **MMDA** Metropolitan Manila Development Authority, **DOT** Department of Tourism, **LLDA** Laguna Lake Development Authority, **NEDA** National Economic Development Authority.

municipal, and barangay levels during emergencies, declaration of a state of calamity, and associated response and recovery. Laws related to the prevention and mitigation phase of disaster risk management are as follows: (i) the Forestry Code which includes provisions for soil erosion control and slope protection; (ii) the Water Code which includes guidelines on control of waters such as floods; and (iii) the National Integrated Protected Areas System (NIPAS) Act of 1992 which provides protection and management of environmentally sensitive areas such as watersheds. These latter laws also punishes activities harmful to the environment such as denudation of forest lands due to illegal logging as well as soil erosion caused by undesirable slash-and-burn farming practices which are identified as major causes of floods or water-related disasters.

On flood risk management in particular, the Department of Public Works and Highways (DPWH) is responsible for the planning, construction, operation, and maintenance of major flood control facilities and national drainage system (due to river flooding), while the local governments are responsible for the construction and maintenance of flood control and drainage facilities related to local drainage (due to street flooding). The local governments play a significant role in local flooding and drainage since they are responsible for issuance of permits in the flood control and drainage plans of residential subdivisions including industrial and commercial development projects which require close coordination with DPWH to properly convey local floodwaters to major rivers (i.e., the national drainage system).

On the early warning phase of water-related disaster management, the Philippine Atmospheric, Geophysical and Astronomical Services Administration (PAGASA) provides short-term rainfall forecasting or prediction which is useful for local flooding and river flooding forecasting. On the other hand, the Mining and Geosciences Bureau (MGB) of the Department of Environment and Natural Resources (DENR) is responsible for rainfall-triggered landslides or debris flow. However, MGB only provides long-term studies of vulnerability or potential areas for disaster, and they do not perform forecasting of rainfall-triggered landslides, debris flows, or mudflow hazards.

As concluded by Tabios et al. (2018), the above institutional framework has overlapping jurisdiction and authority which exist among various agencies, and it is not clear if such organizational redundancies and overlaps may have an effect on operation and maintenance functions. This requires a review and an assessment of the roles of various agencies especially on how they could coordinate for more effective planning and implementation of flood control plans and maintenance of infrastructures.

### **2.2.2 National Water Policy**

In response to the overlapping and fragmentary water resources' institutional framework in the Philippines, the national water policy of the Philippines is being revisited this time and spearheaded by the National Economic Development Authority (NEDA). This is a significant milestone to provide direction in the water resources management of the country in the coming years. The major points in this national water policy are as follows:

1. Coordinate the development and management of water resources in order to maximize economic and social welfare in an equitable manner without compromising the sustainability of vital ecosystems.
2. All departments, agencies, and instrumentalities of government involved in the utilization, development, conservation, protection and regulation of water

resources, and provision of water resource infrastructure, facilities, and service shall be guided by the principles of IWRM for the efficient, environmentally sustainable, and equitable management of water resources to enhance national socioeconomic welfare.

3. Resource management and development must be consistent with the principles of IWRM and emphasizes on participatory process involving planners, policymakers, and users including community members at all levels.
4. With regard to the resource allocation and utilization such that waters may be appropriated by the state, used, taken, or diverted from a natural source in the manner and for any purpose allowed by law and that when priority in time of appropriation from a certain source of supply cannot be determined, the order of preference in the use of the waters shall be as follows: domestic, municipal, irrigation, power generation, fisheries, livestock raising, industrial, commercial and recreational purposes, and in all its competing uses; water shall be recognized as having economic value and that pricing of raw water must reflect its true economic value.
5. On the institutional framework in particular, the proposal is to create an apex body to be named either National Water Resources Management Authority (NWRMA) or Department of Water Resources (DWR) in order to address the fragmented institutional setup of the water resources sector, strengthen, and ensure effective and efficient formulation, coordination, and implementation of policies, programs, and projects for sustainable management and utilization of the country's water resources and coordinated implementation of interventions pertaining to water supply, sanitation, irrigation, flood and drainage management, and watershed management.
6. In tandem with the creation of an apex body is the creation of Water Regulatory Commission (WRC) which is an independent regulatory body for water supply, sewerage, and sanitation in order to achieve a stable regulatory regime, eliminate conflicts of interest through the separation of economic and financial regulation and operation functions of agencies vested with these dual functions, and encourage investments especially from the private sector toward the immediate attainment of universal access to safe, adequate, affordable, and sustainable water supply, sewerage, and sanitation services.

The proposed creation of either National Water Resources Management Authority (NWRMA) or Department of Water Resources (DWR), an apex body, as well as the Water Regulatory Commission (WRC) is being pursued seriously by the current administration and being championed by NEDA. There were already bills submitted to the House of Representatives during previous congresses that proposed the creation of these water agencies, so it is hoped that these bills currently pending in Congress will be enacted into law. For the interested reader, Tabios and Vilaluna (2012) and Tabios et al. (2018) had extensively discussed the structure and implementation of the NWRMA and WRC in particular.

### ***2.2.3 Other Issues and Concerns on Water Governance in the Philippines***

#### **2.2.3.1 Implementation of IWRM Approach and Land Use Planning**

The Philippines recognizes the importance of IWRM principle as a mode of planning and management of watershed systems. However, as seen in the institutional structure of the country, comprehensive land use plans are formulated by local government units, and they only consider the nearby rural and urban watershed conditions. The problem is that land use planning and management in the communities are not properly coordinated with national government plans to ensure that regional land use and resource management activities are integrated in watershed management objectives.

#### **2.2.3.2 Structure of Decision-Making**

In the Philippines, most watershed management efforts are decided by the national government, so it depends on the priorities of the current administration, technical studies, and professional advice of either government personnel or consulting firms. In this case, watershed management is viewed as only a responsibility of the government. In IWRM, the decision-making involves the different players and actors (i.e., stakeholders or the entire community so to speak) in planning and management processes. Further discussion on this is given in Sect. 3.1, chapter on linking science, policy, and management decision with decision support systems.

#### **2.2.3.3 Water Resources Planning Approach**

In the Philippines, master plans of water resources projects are prepared by the government so that this is viewed by the community as an end product and that the implementation of the masterplan is the sole responsibility of the government. Ideally, master plans should be viewed only as a guide to water resources management actions so that plans can be revised and modified through actual, local experiences. In this sense, water resources plans are adaptive or work in progress and that the planning process is iterative and interactive. Section 12 of Chap. 12 discusses this iterative planning process through transdisciplinary approach to holistic flood risk management.

## References

- Delos Reyes MLF (2017) Modernisation strategy for national irrigation systems in the Philippines: Balanac and Sta. Maria River irrigation systems, PhD Thesis, Wageningen University and UNESCO-IHE, Institute for Water Education, Delft, The Netherlands, CRC Press/Balkema, 2301 EH Leiden, The Netherlands
- FMB (Forest Management Bureau) (2014) The Philippines forest statistics. FMB, Quezon City, pp 21–24
- JICA, (Japan International Cooperation Agency) (1998) Master plan study on water resources management in the Republic of the Philippines, Report to National Water Resources Board. Nippon Koei Ltd./Nippon Jugesuido Sekkei, Ltd, Tokyo
- Melana DM, Melana EE, Mapalo AM (2005) Mangroves management and development in the Philippines. Report of the Regional Technical Consultation for the Development of Code of Practice for Responsible Aquaculture in Mangrove Ecosystems, Tagbilaran, Bohol, Philippines 25–27 August 2004. Southeast Asian Fisheries Development Center (SEAFDEC)
- Rola AC, Pulhin JM, Tabios GQ III, Lizada JC, Dayo MHF (2015) Challenges of water governance in the Philippines. Philipp J Sci 144(2):197–208
- Rongavilla LS (2017) National water resources board and integrated water resources management, Presentation at Cavite Water Summit, Tagaytay City, November 9–10
- Tabios GQIII (2008) Recent water-related disaster in the Philippines. In: Proceedings of 2008 international symposium on hydrological environment. International Hydrologic Environment Society, Daegu, December 14–15
- Tabios GQIII (2010, December) Urban dimensions of flood management: case of Pasig-Marikina River Basin of Metro Manila, Philippines. J Hydrol Environ IHES 6(1):1–9
- Tabios GQ III, Villaluna RL (2012) Development of the implementation and operational plan for the National Water Resources Management Office (NWRMO), submitted to the Inter-Agency Committee on Water, Republic of the Philippines, November
- Tabios GQ III, Gaerlan NA, Hipolito DM (2016) Urban resilience to climate change: challenges and initiatives for Philippine urban setting. In: Proceedings of 4th national climate change: addressing climate risk for sustainable development. National Academy of Science and Technology, Tagaytay City, Philippines
- Tabios GQ III, Cruz RVO, David ME, Nguyen MR (2018) National and local initiatives in addressing water supply sustainability. In: Rola A, Pulhin J, Alcala Hall R (eds) Water policy in the Philippines global issues in water policy, vol 8. Springer, Cham, pp 209–231
- World Bank (2007) Philippines environment monitor 2006 (English). Washington, DC
- World Bank (2008) Economic impacts of sanitation in the Philippines: a five-country study conducted in Cambodia, Indonesia, Lao PDR, the Philippines, and Vietnam under the Economics of Sanitation Initiative (ESI) (Vol. 2): Main report (English). Water and Sanitation Program research report. Washington, DC

# Chapter 3

## Science and Art of Water Resources Modeling in the Philippines



**Abstract** This chapter begins with a discussion on linking science, policy, and management decisions with the decision support system (DSS). The DSS and its components are described, in which the heart of DSS are the models or modeling tools. Then, the distinction between optimization and simulation models as well as elements and features of these two types of models are presented. Sample optimization-simulation modeling problems are also presented to illustrate how different water resources planning, design, and management problem can be addressed. This chapter ends with a listing and brief background of the modeling studies and experiences presented in Chapters 4, 5, 6, 7, 8, 9, 10, and 11.

### 3.1 Linking Science, Policy, and Management Decisions with Decision Support System

In the last few years, integrated water resources management (IWRM) has been advanced and advocated toward effective planning, design, and operations as well as sustainable development of water resources systems. In 1992, the Rio Earth Summit forged a consensus stating that modern water resources management must be based on the following three fundamental principles known as the Dublin Principles:

- The ecological principle which argues that the river basin is the most logical unit for managing water resources holistically and sustainably and that both land and water should be managed together with much greater attention paid to the environment.
- The institutional principle, which argues that water resource management is best done when all the stakeholders participate.
- The instrument principle, which argues that water is a scarce resource as well as an economic and social good; thus, its allocation must be based on economic efficiency compatible with social equity considerations.

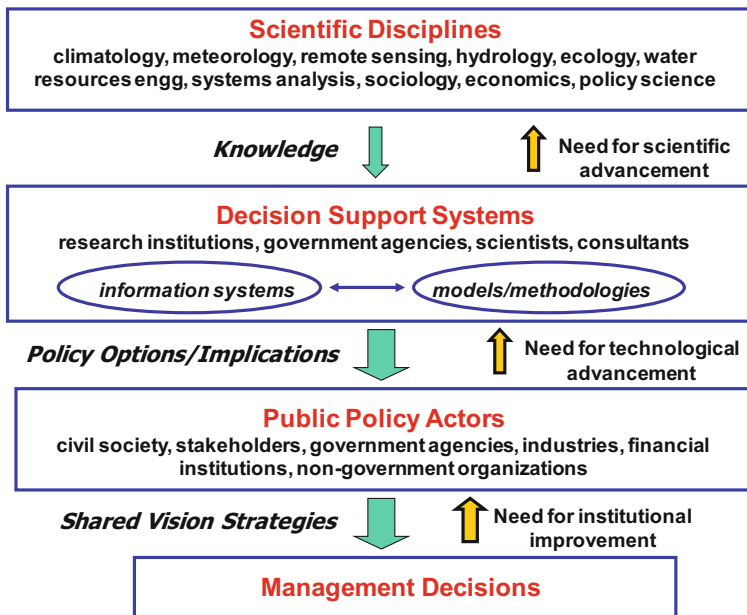


**Fig. 3.1** Linking science and public policy for effective integrated water resources management.  
(Adapted from Georgakakos 2004)

Integrated water resources management is indeed a complex process of formulating and implementing shared vision management strategies for sustainable water resources utilization with due consideration to all spatial and temporal interdependencies in the natural system and water uses. Also, IWRM must contend with changes in information, technology, natural processes, societal preferences, institutions, and policy actors.

Figure 3.1 was adopted from Georgakakos (2004) to link science and public policy toward an effective IWRM. It may be noted that the decision support system (DSS) which essentially evolves around models and modeling tools is an integral part of IWRM process facilitating the use of science and technology advances in public policy and management decisions. It brings together disciplines, people, and institutions necessary to address today's complex water resources problems. The DSS is designed to improve understanding of how the water resources system functions and how to evaluate alternative management options including their impacts or consequences and also building a *shared vision* to develop consensus for the sustainable development and utilization of the water resources. In this shared vision, the perspectives of the agronomists, ecologists, biologists, economists,

engineers, hydrologists, lawyers, sociologists, or political scientists are all considered and respected.

To emphasize, it can be advocated that IWRM entails a decision support system (DSS) which will link scientific disciplines (i.e., hydrology, ecology, sociology, economics, and policy science) and the policy actors (civil society, government, and business). When policy makers, planners, regulators, operators, and stakeholders sit together to make important water policies and management decisions, the DSS can be a very useful tool as a processor, integrator, and feedback control of knowledge and actions to policy options and decisions.

## 3.2 Models and Modeling Tools in Decision Support System

The heart of a decision support system (DSS) are models and modeling tools. In a decision support system (DSS), the models or modeling tools are composed of interactive computer programs that utilize analytical and numerical techniques such as spatial analysis, decision analysis, optimization, simulation, and project scheduling routines for developing solutions and strategies to help decision-makers formulate alternatives, analyze their impact, and select appropriate options for implementation. Figure 3.2 shows the components of a typical DSS taken from Loucks and van Beek (2017).

The DSS consists but is not limited to the following components:

- Measurement system or data acquisition system: This may include remote sensors or telemetered ground data.
- Information system or database management system: This includes GIS, spreadsheets, or knowledge-based expert system such as if-then-rules.
- Model system or model-based management system: This includes process models, planning and design models, and socioeconomic model.
- Analysis system: This includes statistical model, policy assessment models, and evaluation model.
- User-friendly interface: This is the link to the user which includes graphical interface or visualization tools.

The sophistication of the DSS lies in particular on the available tools or model in the model system. In particular, the components of the model system are as follows:

- Process/behavioral model: An example is a watershed model or a reservoir operation model. This model is used to describe and understand system behavior, to assess conditions whether they are desirable or undesirable, or to formulate objectives including control measures.

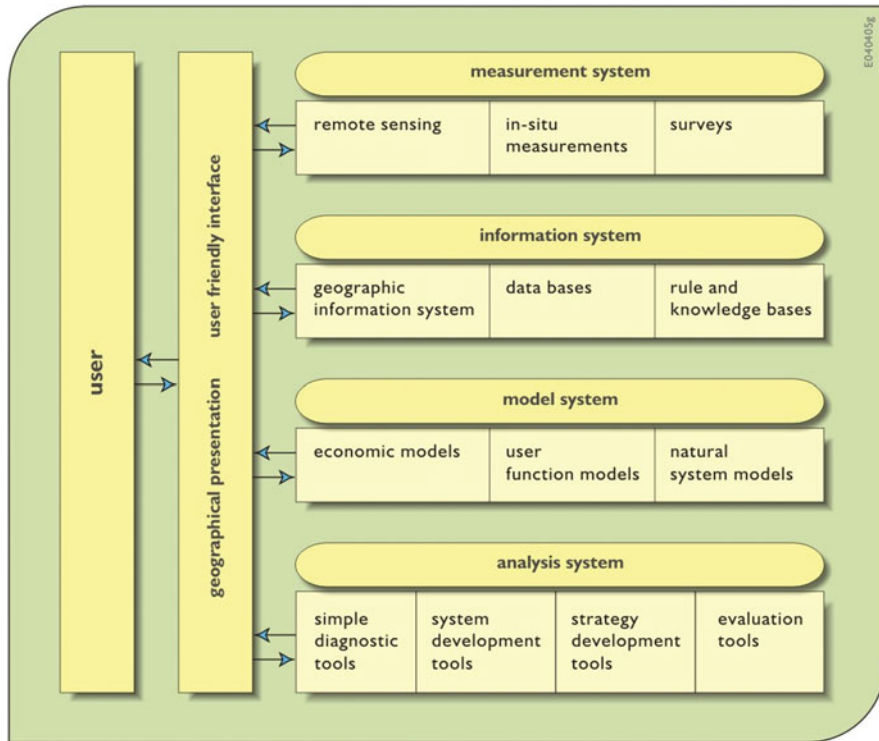


**Fig. 3.2** Components of an IWRM decision support system (DSS). (Taken from Loucks and van Beek 2017)

- Design/planning model: Example is an optimization model or a project scheduling model. This model is used to formulate and specify solution configurations and dimensions and to generate alternative plans and scenarios.
- Decision/evaluation model: Examples include input/output analysis model, conflict analysis model, and also an optimization model. This tool is used to assess impacts and effects of alternatives, to evaluate and rank solutions (optimal/suboptimal solutions), and to explain and communicate to decision-makers through appropriate graphical/visual method.

It may be noted that an essential feature of a DSS is a user-friendly and usually interactive interface that permits ease in data entry and manipulation, versatility, and generality of model, and the most important is its the graphical display and visualization capability.

### 3.3 Simulation and Optimization Models

In the model system of the decision support system (DSS), two types of models in particular can be classified as simulation and optimization models. Table 3.1 shows the general distinction between these two models. Water resources models may be formulated as a pure simulation model, an optimization model, or a combined optimization-simulation model. In the context of the decision support system discussed above, a simulation model is basically classified as process/behavioral model, while an optimization model is a design/planning model. The combined optimization-simulation model may likewise be a design/planning model or decision/evaluation model.

For the combined optimization-simulation model, the simulation model is usually embedded in the optimization model as shown in Box 3.1. Both models would interact by generating inputs to each other sequentially and/or iteratively. The results obtained from one model should converge with the other model to achieve the desired accuracy as the cycle of optimization-simulation process is repeated. When the optimal solution is obtained, the simulation model (which can accurately depict the operation of the entire water resources system) would use optimal operating policies generated from the optimization model.

**Table 3.1** Distinction between simulation model and optimization model

Simulation model	Optimization model
Physical system dynamics, that is, the various hydrologic and hydraulic processes of the water resources system are modeled in great detail	Physical system is modeled to fit into the framework or canonical form of the optimization model (i.e., linear programming method requires linear objective functions and constraints); thus, usually simplification is needed to fit to canonical form
Determines values of output variables (e.g., watershed outflows, lake levels) of physical system for given inputs (e.g., rainfall, irrigation water withdrawals)	Determines values of decision variables (e.g., river diversions, lake withdrawals) according to objective function subject to physical system, operational, contractual, and other constraints
Management questions are addressed by generating what-if simulation scenarios such as creating various combinations of location and amount of water withdrawals or combinations of gate openings for flood control; and usually an enormous number of combinations are needed for proper analysis	Management scenarios are generated internally in the optimization model, and best (optimal) management solutions are selected by maximizing or minimizing the objective function testing against constraint violations; a major constraint is the physical system constraint which may be defined by a full water resources system hydrologic and hydraulic model or essentially the simulation model (see Box 3.1)

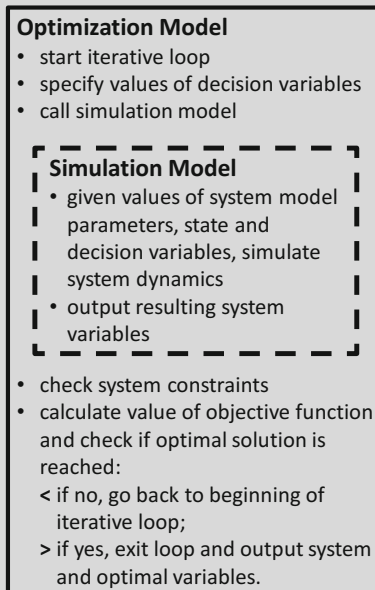
From a systems concept point of view, the components of water resources models such as system variables and other components are:

- Input variables (controllable and uncontrollable): rainfall, evaporation, tides, and physical system parameters.
- Output variables (desirable or undesirable): watershed outflows, flow velocities, and river stages.
- State variables (state of system): river stages, groundwater levels, lake or reservoir water levels, and water quality.
- Decision variables (controllable input or output): surface water diversions, groundwater pumping rates, and gate openings.
- System dynamics: watershed hydrology, river hydraulics, lake dynamics, and processes.
- Management/operating criteria: operating rules, objective functions, constraints, and contractual obligations.

### **3.4 Sample Water Resources Optimization-Simulation Modeling Problems**

Most water resources systems planning and management modeling problems are solved using combined optimization-simulation models. The typical simulation model module essentially consists of the hydrologic watershed model, describing the watershed surface and subsurface flows, and the river and/or lake hydraulic model, describing the river/lake dynamics such as flow velocities, flow directions, and water levels. On the other hand, the commonly used optimization model module is multidimensional, multistage, optimization method. Multidimensional refers to multiple decision variables, and multistage refers to multiple time intervals and/or space discretization.

Referring to Box 3.1, the solution process in a combined optimization-simulation model is to improve the objective function subject to some constraints by perturbing the state variables in an iterative process. At the start of the optimization, initial values of the state variable trajectories (e.g., time series of storage or flow variables) must be specified. Then, the iteration process is terminated when there is no further improvement or change in objective function between the current and previous iterations. In deterministic optimization, the future hydrologic inputs are assumed known (e.g., using historical data). In the case where the future hydrologic inputs are forecast values such as future watershed inflows or values with associated probabilities of occurrence, then this is referred to as stochastic optimization.

**Box 3.1 Combined Optimization-Simulation Model with Simulation Model Embedded in the Optimization Model**

The objective function and constraints of an optimization model can be any linear or nonlinear functions of system variables (e.g., domestic water supply production, irrigation water deliveries, artificial groundwater recharge, etc.). Generally, the objective function and constraints are based on physical, operational, environmental, economic, and political considerations. The art of optimization modeling essentially rests on the formulation of the objective functions and certain constraint functions which may require a multidisciplinary team of experts representing the various issues and concerns of planning and management of a water resources system which may encompass the physical and natural sciences and engineering to include social, economic, and political sciences.

In the optimization problem, the constraint functions may be formulated as hard constraints or soft constraints. At a given iteration stage or computational time interval, a possible solution which violates any real hard constraint will be immediately eliminated from the set of possible solutions. On the other hand, possible solutions that violate soft constraints are tolerated (or still considered in the iteration process), but a penalty term is imposed on the objective function in which the penalty function depends on the degree of violation. In the case that all possible solutions violate the hard or soft constraints, the solution with the least or minimum constraint violation may be selected; otherwise, the iteration process is terminated at that stage.

To appreciate the art of optimization-simulation modeling, here are some problem scenarios and the possible objective functions and constraints that can be specified in the model.

### 3.4.1 Determination of Water Supply Firm Yield

Determination of water supply firm yield on annual or monthly basis may be useful in water allocation in general or water use permit application in particular. It becomes an optimization problem especially when there are already existing, competing water resources users in the area. For instance, if a commercial/industrial or agricultural development in a township or region requires water to be diverted from the lake, a reservoir or a river that has already prior commitments (water rights allocated), the question is whether there is still additional water that can be derived from this resource, and by how much and how often, without adversely affecting the existing water users (i.e., users with prior water rights). An objective function in this case would be to maximize withdrawals with a penalty function if constraints are violated such that.

$$\text{Max } F = \sum_{m=1}^N b_m \cdot W_m - \sum_{k=1}^{NC} PNALTY_k \cdot CV_k \quad (3.1)$$

where  $W_m$  is the withdrawal rate at time  $m$ ,  $b_m$  is the benefit coefficient (e.g., price of water), and  $PNALTY_k$  is penalty coefficient or unit cost for violating a certain constraint with metric measure  $CV_k$  for  $k = 1, \dots, NC$  constraints.

A constraint may be to ensure that the minimum instream flow requirement (based on a certain water quality or an environmental criterion) is not below the actual river flows observed at a certain downstream point of the withdrawal point. Another type of constraint is a water demand constraint for a certain contractual agreement in which water is already committed to an existing water user. The constraint function to ensure that the minimum instream flow requirement  $Q_{instream}$  for some environmental purposes should not be below the actual river flow  $Q_{actual}$  would be:

$$CV_k = \max [Q_{instream} - Q_{actual}, 0.0] \quad (3.2)$$

Note that in Eq. (3.2),  $CV_k$  is positive only if there is a constraint violation, that is,  $Q_{actual}$  is less than  $Q_{instream}$ .

Constraints accounted for in the objective function as penalty terms are referred to as soft constraints since a possible solution resulting in this constraint violation is still considered (i.e., violation is tolerated but subject to penalty) in the solution process. This is in contrast to a violation of a hard constraint in which such possible

solution resulting in a hard constraint violation is immediately rejected and considered an infeasible solution in the optimization algorithm.

It is important to point out that the major set of constraints imposed in the optimization problem are the physical system constraints governed by the hydrology and hydraulics of the river, lake, and watersheds. This set of constraints is defined or computed in the hydrologic-hydraulic (watershed) simulation model, thus the essence of combined optimization-simulation method of the solution process. For instance, a tentative value (possible solution) of the withdrawal rate in the optimization model has to be tested through running the simulation model to check whether indeed such solution is a feasible solution or not. This is the reason why the optimization and simulation models undergo through an iterative and interactive solution process.

### **3.4.2 Allowable Groundwater Withdrawal Rate**

The problem of determining optimal groundwater withdrawal rate is similar to the problem of determining water supply firm yield from rivers or lakes. The objective function could likewise be maximizing firm water yield according to the amount of groundwater pumped similar in form to Eq. (3.1). Different set of constraints in addition to those in the surface water operations may be imposed when extracting groundwater. Constraints to prevent excessive groundwater pumping can be imposed. A specific constraint would be restricting or curtailing groundwater withdrawal so that the groundwater water table or piezometric head does not go down below a certain elevation. This particular constraint can be written as:

$$CV_k = \max [H_{crit} - H_{actual}, 0.0] \quad (3.3)$$

in which  $H_{actual}$ , the actual or prevailing groundwater head, is above the threshold or critical groundwater head  $H_{crit}$ .

If the above constraint is imposed as a hard constraint, a groundwater withdrawal rate for a given month currently being considered in the optimization algorithm which results in a groundwater head below a certain critical groundwater head would be eliminated immediately from the feasible set of solutions. This constraint may be imposed at several locations (observation wells) in the groundwater system modeled to account for the spatial variability of groundwater heads.

### **3.4.3 Optimal Cropping Patterns for Effective Water Use**

Another optimization problem would be to schedule and locate land parcels for optimal crop production. First, alternative parcels of land and alternative cropping seasons for various, potential crops to be produced will be predetermined. With these

alternative combinations of crops, land parcels, and cropping season schedules, the management model can be used on a pure simulation run to evaluate various combinations of scheduling cropping seasons (from planting to harvesting) and locating land parcels for the various crops. Then the best cropping pattern will be selected or prioritized according to crop production benefits and water use. However, this approach becomes tedious when a large number of combinations are to be evaluated. In this case, it would be better to use the management model in combined simulation-optimization mode to choose the best cropping pattern among the various alternatives. In the optimization problem, the state variables are essentially the predetermined combinations of crops, land parcels, and cropping schedules. The question of when (cropping schedule or season) to plant the crops would depend on the timing of rainfall and riverflows and the question of where (location of land parcels) to plant the crops would directly affect the infiltration properties and evapotranspiration requirements of the area planted.

In this optimization problem, a lot of information for a given decision policy (choice of crop) by the optimization algorithm are passed on to the hydrologic-hydraulic simulation of the optimization model. For a given type of crop, the infiltration rates in the sub-basin or overland flow plane the crop is to be planted would be modified accordingly. Also, the evapotranspiration requirements and interception properties in that parcel of land will be according to the type of crop chosen. Certain rules in the form of constraints would be imposed on where to get the additional water that may be diverted from the river or pumped from the groundwater to satisfy the crop water requirements.

### 3.5 Overview of Modeling Studies and Experiences

Chapters 4, 5, 6, 7, 8, 9, 10 and 11 present various modeling studies and experiences conducted by the author as independent researches or through commissioned work.

Chapter 4 presents surface and groundwater modeling for planning water supplies for future domestic and irrigation water demands as well as potential hydropower generation in both Pampanga River and Agno river basins. These two river basins are adjacent to each other and located in Central Luzon where they are relatively close to Metro Manila and other major metropolitan urban centers like San Fernando, Angeles, and Clark Air Base in the Pampanga River Basin and the cities of Tarlac, Rosales, and Dagupan in the Agno River Basin. These surface and groundwater modeling studies were commissioned studies by the Manila Water Company Incorporated (MWCI).

Chapter 5 discusses reservoir planning and operations studies with optimization-simulation models of the Angat Reservoir, the Upper Agno Reservoir, and the Agos Reservoir system. The Angat Reservoir studies started as an independent research done by the author out of fascination of the reservoir system but was later commissioned studies through the Philippine Institute of Development Studies (PIDS), a research arm of the National Economic and Development Authority (NEDA) to

examine the competing water uses of Angat Reservoir for domestic water supply, irrigation water use, and hydropower generation including flood control function. Subsequently, further studies of this Angat Reservoir as a subcontractor of a consulting firm were commissioned by MWCI. The study on Upper Agno Reservoir operations composed of the Ambuklao, Binga, and multipurpose San Roque Reservoir was commissioned by the National Water Resources Board (NWRB). As an aside, an optimization-simulation of the San Roque Dam flood operations during a major typhoon, Parma, in October 2009 that caused massive flooding in lower Agno River Basin was also conducted as an independent study by the author while acting as chair of an investigation committee of the Senate of the Philippines on this flood disaster. The reliability and project sequencing studies of alternative reservoir configurations of the Agos Reservoir system were commissioned by the Metropolitan Waterworks and Sewerage System (MWSS).

Chapter 6 presents the results of three studies. The first study discussed was commissioned by the National Irrigation Administration (NIA) to determine the reliability and cost-benefit efficiency of the Balog-Balog Reservoir system with single, high dam as opposed to a multiple dam system. The Balog-Balog single, high dam which was the project recommended in this NIA study is finally being built since the project was conceived and planned in 1986. The two other studies presented were commissioned by the National Power Corporation (NAPOCOR) on reservoir sedimentation studies in San Roque Reservoir in the Upper Agno River Basin for long-term sedimentation management and the other on sediment flushing operations in the Pulangi Hydropower Plant Reservoir in Bukidnon, Mindanao.

Chapter 7 presents the hydrodynamic and water quality modeling of Manila Bay with dissolved oxygen as index of the health of the bay and salinity intrusion modeling of Laguna Lake which is beneficial to fish farming but undesirable to domestic water use. The Manila Bay hydrodynamic and water quality study was commissioned by Manila Bay Coordinating Office (MBCO) of the Department of Environment and Natural Resources (DENR). The author has also done earlier independent study of the Manila Bay-Laguna Lake system through the Japan Society for the Promotion of Science (JSPS) Core University Program in collaboration with researchers from Tokyo Institute of Technology. The salinity intrusion modeling of Laguna Lake is an independent study in collaboration with other researchers.

Chapter 8 presents flood and dam-break modeling studies that included modeling the effect of moving storm in Pasac Delta flooding with stochastic space-time rainfall model and Marikina River Basin flood modeling during Typhoon Ketsana, both of which were results of independent studies by the author. Also presented is an assessment of alternative flood control mitigation plans for Cagayan de Oro River, commissioned by the Department of Public Works and Highways (DPWH). This particular study was done due to the devastating Typhoon Washi (locally called Typhoon Sendong) that occurred in Cagayan de Oro City in December 2011 so that the original flood mitigation master plan study of Cagayan de Oro River, completed in 2009, had to be revised. The independent studies on dam-break presented included a dam removal problem to validate the dam-break model with moveable

bed (i.e., sediment transport) followed by application of this model to an actual dam-break problem of Butas Dam of Cavite Province that occurred in late September 2006.

Chapter 9 presents the pipe network distribution modeling with optimization of the southwest portion of Metro Manila, commissioned by the Maynilad Water Services Incorporated (MWSI). MWSI when using the EPANET model then had difficulty calibrating this model for planning and operations of their pipe network, water distribution system (composed of thousands of nodes and links (junctions and pipelines) on the western part of Metro Manila, thus the motivation to incorporate an optimization model for automatic model calibration of EPANET. With the enhanced EPANET model, other model applications became possible such as for planning or layouting pipe networks, detection and surveillance of nonrevenue water, and normal pipe operations studies, aside from automatic model calibration.

Chapter 10 discusses climate change studies for reliability of the Upper Agno Reservoir system commissioned by NWRB, while Angat Reservoir climate change studies were done as an independent study by the author, which later on became a part of the commissioned study by MWCI. Both of these studies were part of the reliability studies conducted for these two reservoir systems that were presented in Chap. 5.

Finally, Chap. 11 presents modeling for environmental assessment studies that includes Subic Bay hydrodynamic and water quality modeling for developing an integrated coastal management plan, commissioned by the Ecology Center of the Subic Bay Metropolitan Authority (SBMA). The second study presented is the risk assessment of possible pollution of Novaliches Reservoir from leachate of Payatas dumpsite, commissioned by MWSS. The study on the risk of polluting the Novaliches Reservoir study was motivated by the concern of Metro Manila residents since the Payatas dumpsite is located near this water supply reservoir which is part of the chain of Angat-Ipo-Novaliches reservoir system that provides domestic water supply to the eastern side of Metro Manila's population.

## References

- Georgakakos AP (2004) Decision support systems for integrated water resources management with an application to the Nile Basin. IFAC-TC\_Environment, Venice
- Loucks DP, van Beek E (2017) Water resources systems planning and management: an introduction to methods, models and applications. Jointly published by Deltares and UNESCO-IHE, Springer Nature, Cham, Switzerland

# Chapter 4

## Surface and Groundwater Modeling for Water Utilization



**Abstract** This chapter presents surface and groundwater modeling and simulation studies of the Pampanga River Basin and Agno River Basin systems to assess the status and potential for additional water utilization for domestic water supply and hydropower generation. These two river basins are adjacent to each other and located in the Central Luzon where they are relatively close to Metro Manila and other major metropolitan urban centers like San Fernando, Angeles, and Clark in the Pampanga River Basin and the cities of Tarlac, Rosales, and Dagupan in the Agno River Basin. The simulation studies were conducted over 50 years of data to assess the availability and reliability of surface water and groundwater as domestic water supply sources at the major metropolitan urban centers of these two river basins as well as to identify potential locations for hydropower generation and determine the associated firm power yields.

### 4.1 Introduction

Surface and groundwater modeling and simulation studies were conducted for the two water resources systems, namely, (1) Pampanga River Basin and (2) Agno River Basin. The studies were conducted to assess the availability and reliability of surface and groundwater as water sources for the urban areas as well as identify location and determine potential hydropower generation for these two river basins. Both these studies were commissioned by the Manila Water Company Incorporated (MWCI) done by the author as principal investigator under the National Hydraulic Research Center (NHRC) of the University of the Philippines at Diliman, and most of the materials presented here may be referred to in the reports of National Hydraulic Research Center, NHRC (2011a) and NHRC (2011b), for Pampanga River Basin and Agno River Basin, respectively.

The surface water and groundwater modeling and simulation studies involved the following procedures:

1. Develop surface water and groundwater flow model of the area and conduct water balance studies through model simulation.

2. Assess and evaluate the availability and reliability of surface water and groundwater resources of the study area, for specified water demands projected over time.
3. Recommend possible surface water and groundwater sources to meet the future water demands in the basin as well as identify potential sites for hydropower generation.

For both river basins, the modeling and simulation studies utilized the same watershed and groundwater model described in the next section below.

#### 4.1.1 Watershed Model

The watershed model employed is a continuous-time, distributed model consisting of various components: rainfall input, evaporation, surface detention, infiltration, overland flow, channel flow, and most importantly, the soil moisture accounting model. This soil moisture accounting model is the Sacramento model originally developed by Burnash et al. (1973) at the Joint Federal-State River Forecast Center of the National Weather Service in Sacramento, California, hence the name Sacramento soil moisture model (see also Burnash 1985). This watershed model is essentially for modeling the natural surface water processes. A schematic representation of the surface water model and its interaction with the groundwater model is shown in Fig. 4.1. Detailed description of the Sacramento soil moisture accounting including brief descriptions of the flow routing model as well as the automatic model calibration with an optimization algorithm are given in Appendix A.

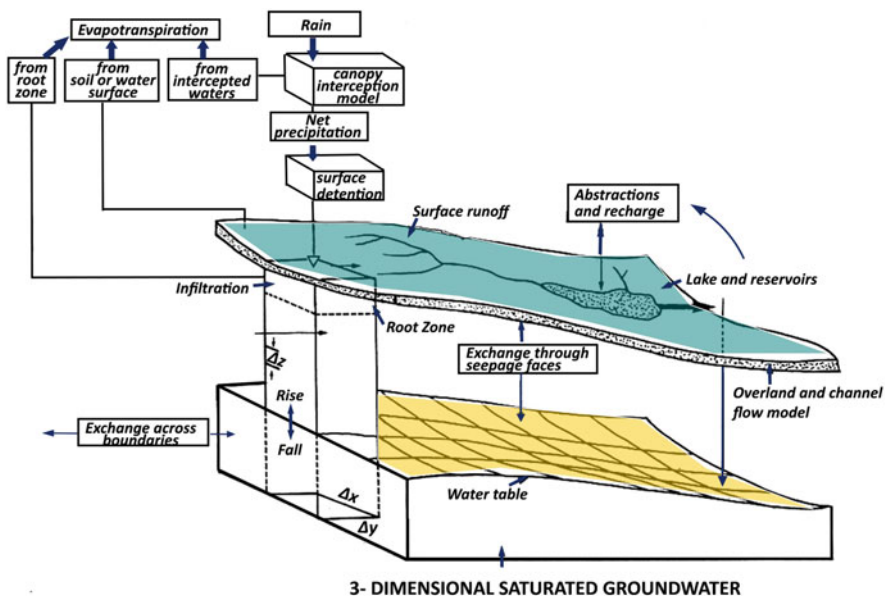
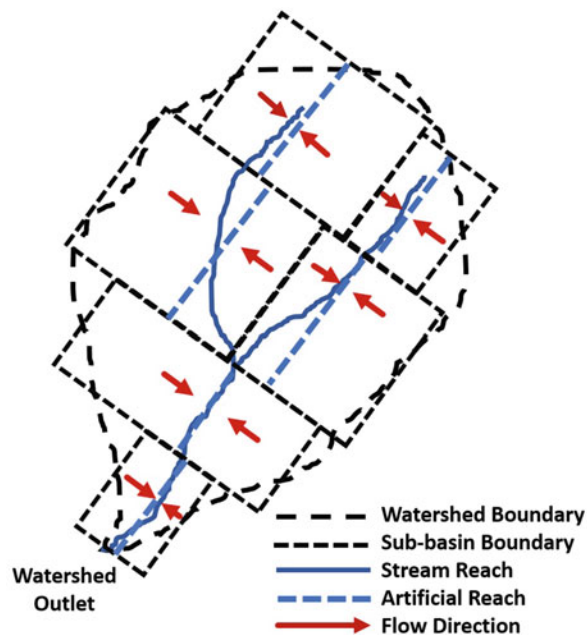


**Fig. 4.1** Schematic diagram of surface water and groundwater model used in this study

**Fig. 4.2** Watershed delineation into overland flow planes and river network. For each overland flow plane (rectangular area), the Sacramento soil-moisture accounting model which is schematically shown in Fig. 4.3 below is used



In employing this model in this study, the computer program of this watershed model developed by Tabios et al. (1986) was utilized which uses the Sacramento model for soil moisture accounting, and the outflows from each overland flow plane that include direct runoff, surface runoff, interflow, and subsurface flow (baseflow) are routed in the overland flow planes either using kinematic wave or unit hydrograph method; and the channel flow routing is either using kinematic wave or Muskingum method. In the option for automatic model calibration, the computer program includes calibration of selected model parameters using Rosenbrock optimization (Kuester and Mize 1973) by minimizing observed and computed outflows to arrive at the optimal model parameters.

In watershed modeling, the first major step is to delineate the watershed boundary and then the river network or topology and further delineate or partition the watershed system into overland flow planes as shown in Fig. 4.2. The delineation or watershed partitioning is based on basin topography, river network configuration, and slopes and considering as well the geology, soil types, vegetation, and land use.

The heart of the watershed model used here is the Sacramento soil moisture accounting model which is schematically shown in Fig. 4.3. For each overland flow plane in Fig. 4.2, there will be a unique set of Sacramento soil moisture model parameters although in actual cases, several overland flow planes may have the same set of model parameter values. Basically, for a given rainfall in each computation time interval, the upper and lower soil moisture contents of each sub-basin are updated, and then overland flows are routed at each overland flow plane in that sub-basin and into the channel or stream network of the basin from upstream to

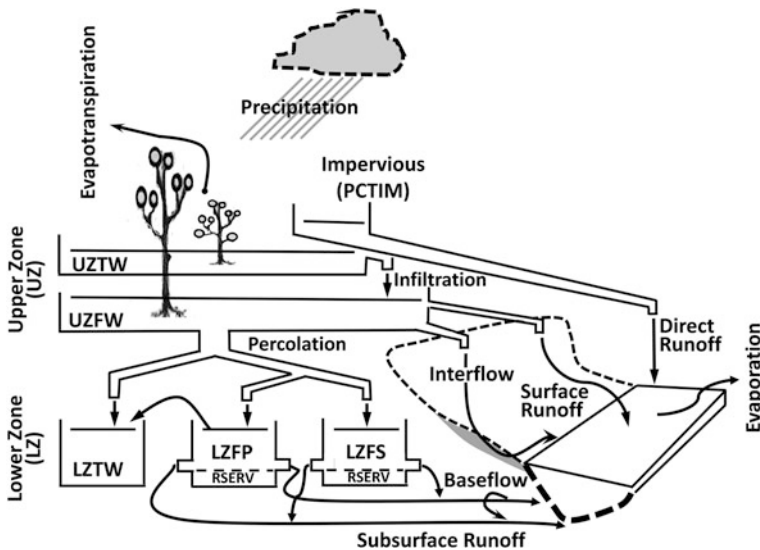


**Fig. 4.3** Schematic of the Sacramento soil-moisture accounting model and the model components representing different hydrologic processes

downstream. The rainfall data used in the model are long-term, historical (or forecasted) sequences of daily rainfall to calculate the long-term sequences of daily streamflows at the basin outlets.

#### 4.1.2 Groundwater Model

The groundwater model used is the MODFLOW model developed by McDonald and Harbaugh (1984) of the US Geological Survey which is a three-dimensional, saturated flow, finite-difference groundwater model. This model is used since it is computationally efficient for groundwater simulation over long periods of time (e.g., daily basis for several years). This model only simulates fully saturated groundwater flow so that the unsaturated groundwater flow processes are modeled in the watershed model. The spatial discretization of the groundwater aquifer in the MODFLOW model is given in Fig. 4.4.

The MODLOW solves the three-dimensional, saturated groundwater flow model given by:

$$S_c \frac{\partial h}{\partial t} = \frac{\partial}{\partial x} \left( K_{xx} \frac{\partial h}{\partial x} \right) + \frac{\partial}{\partial y} \left( K_{yy} \frac{\partial h}{\partial y} \right) + \frac{\partial}{\partial z} \left( K_{zz} \frac{\partial h}{\partial z} \right) + W \quad (4.1)$$

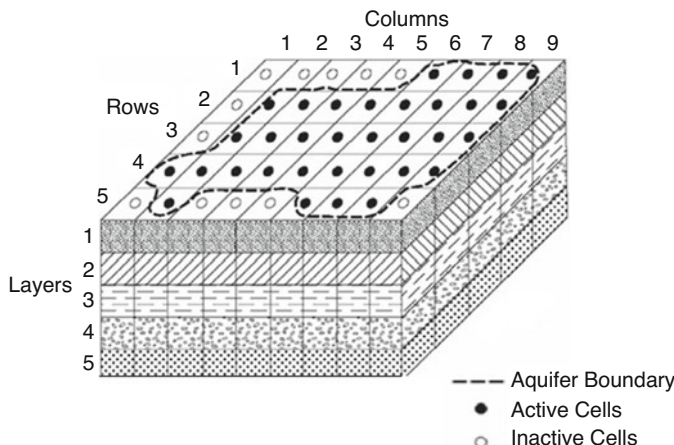


**Fig. 4.4** Spatial discretization of the groundwater aquifer in the 3-d, saturated groundwater flow, MODFLOW finite difference model. (From McDonald and Harbaugh 1984)

in which  $K_{xx}$ ,  $K_{yy}$ , and  $K_{zz}$  are the hydraulic conductivities in the  $x$ ,  $y$ , and  $z$  coordinate axes,  $h$  is the piezometric head,  $W$  is the volumetric flux representing sources and sinks,  $S_s$  is the specific storage, and  $t$  is the time.

The boundary conditions in the MODFLOW model include head boundaries for open water bodies such as lake or reservoir, sink/source term to account for rainfall and evaporation, river boundary to account for river stages and riverbed leakance, well boundary to account for pumping wells or recharge (with negative pumping rate), subsurface drain boundary, and other special boundaries such as flux boundary, no-flow or geologic fault boundary, and general head boundary.

In the modeling studies here, the groundwater recharge which is a major input to the groundwater model is calculated from the Sacramento soil moisture accounting (watershed) model which is the water that percolates deep into the groundwater system, that is, the portion of total baseflow that becomes inaccessible to surface channel flow. The reader may refer to details of this Sacramento model process in Appendix A.

The finite difference method is used in solving the groundwater equation in (4.1). Further details of the MODFLOW model maybe referred to the original computer model document by McDonald and Harbaugh (1984).

## 4.2 Pampanga River Basin

Pampanga River Basin covers an area of about  $10,710 \text{ km}^2$  as shown in Fig. 4.5. This area is bounded on the north by the portion of the Cordillera Mountains of Nueva Ecija and Nueva Vizcaya, on the west by the Sierra Madre Mountains along Aurora and Quezon, on the west side by Pangasinan, Tarlac, and Mt. Pinatubo mountain ranges of Zambales, and finally bounded on the south by Manila Bay along portions

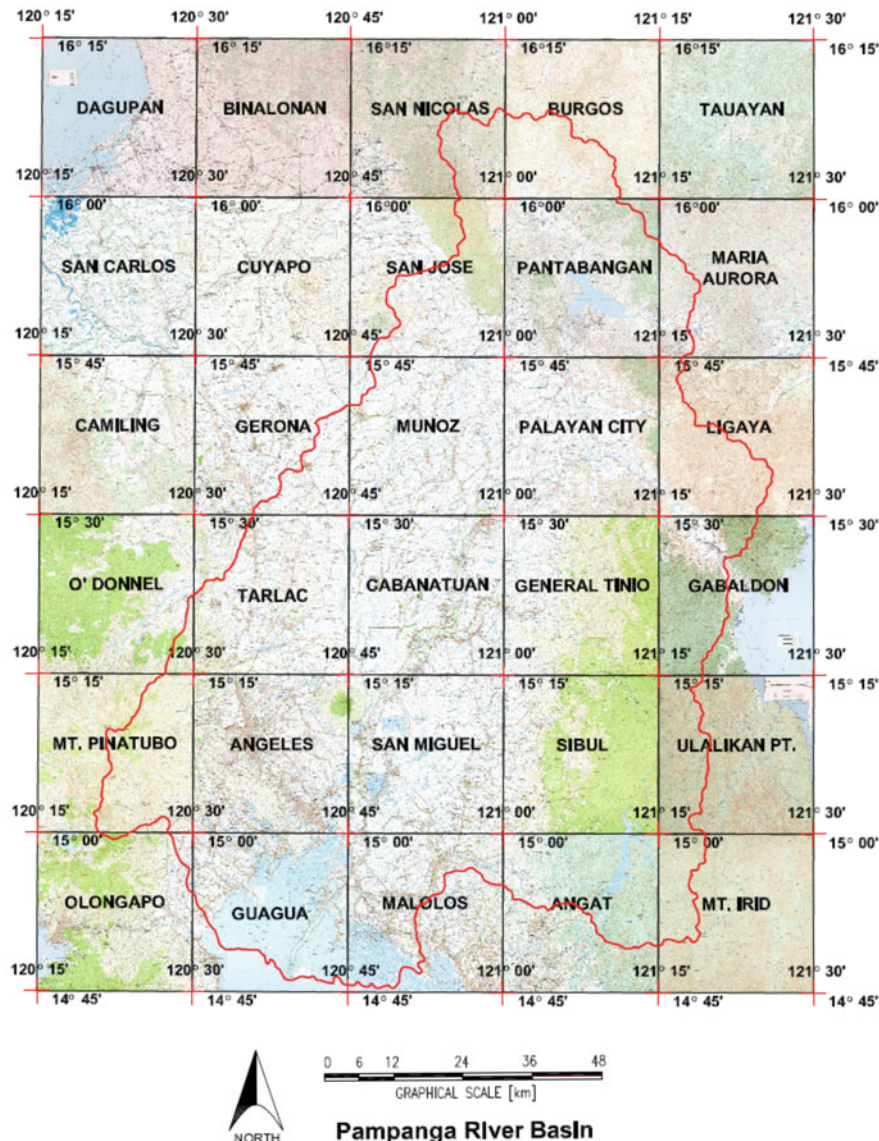


**Fig. 4.5** Assembly of 1:50,000 Scale NAMRIA topographic maps covering the entire Pampanga River Basin

of Bataan, Pampanga, and Bulacan. The entire river basin can be further divided into three major sub-basins, namely, (a) Pampanga River Basin with catchment area of 8,221 km<sup>2</sup>, (b) Guagua-Pasac River Basin with 1,366 km<sup>2</sup>, and (c) Angat River Basin with 1,123 km<sup>2</sup>.

#### 4.2.1 Watershed Delineation and Surface Water Modeling

With regard to the surface water resources in the area, Fig. 4.6 shows the river basin network indicating the sub-basin boundaries, river network, and major reservoirs. The two major reservoirs in this basin area are the Pantabangan Dam/Reservoir and Angat Dam/Reservoir. The Pantabangan Reservoir additionally derives water from the Casednan River (a tributary of Cagayan River) through the Casednan Diversion System. Likewise, Angat Reservoir derives additional water from Umiray River through the Umiray-Angat Diversion transbasin tunnel. Another major water conveyance system is from Angat Reservoir to Metro Manila through Ipo Dam, Ipo-Bicti Tunnel, and Bicti-Novaliches Aqueduct. For purposes of groundwater modeling, the groundwater aquifer boundary is basically the same as the Pampanga River Basin boundary shown in Fig. 4.6. This assumption is based on topographical and geological features of the river basin.

The entire Pampanga River Basin is divided into 11 major sub-basins, which are Pantabangan, Upper Pampanga, Coronel, Central Pampanga, Peñaranda, Talavera, Rio Chico Dela Pampanga, Lower Pampanga, Angat, Ipo-Bustos, and Guagua Basin Group. Moreover, each of these sub-basins is further subdivided into smaller sub-basin units in which together with other hydrologic elements represent the physical watershed in the surface water model. The three major river systems, namely, the (a) Pampanga, (b) Guagua-Pasac, and (c) Angat river basins are modeled separately in the surface water model. The Pampanga River system, which has the largest river network, is composed of 8 out of the 11 major sub-basins, while the Angat and Guagua-Pasac river basins contain only two and one major sub-basins, respectively. Table 4.1 summarizes the total drainage area and number of sub-basin units for the major sub-basins of the Pampanga River Basin. Note that the entire Pampanga-Angat-Guagua river system is divided into a total of 960 sub-basins so that as many as 960 streamflows can be calculated at each sub-basin outlet.

The main river of Pampanga River system stretches to 232 kilometers from the headwaters at Caraballo Mountains to Manila Bay. The main river, called Pampanga River, is fed by several tributaries in which the principal ones are the Peñaranda and Coronel rivers on the eastern side of the basin and the Rio Chico River from the western side. The basin is drained primarily through the Pampanga River as it exits to Manila Bay.

It may be noted that the Angat River joins the Pampanga River at Calumpit Bulacan via Bagbag River; however, Labangan Floodway acts as a cut-off channel that drains a small portion of Angat River flow directly to Manila Bay. The Guagua River Basin, on the other hand, is an allied system of rivers that drains the basin thru Pasig-Potrero, Porac-Gumain, Abacan, and Guagua-Pasac rivers into Manila Bay. The Guagua River Basin and Pampanga River Basin are actually two separate basins but connected through the Bebe-San Esteban Cut-off Channel, a man-made channel,

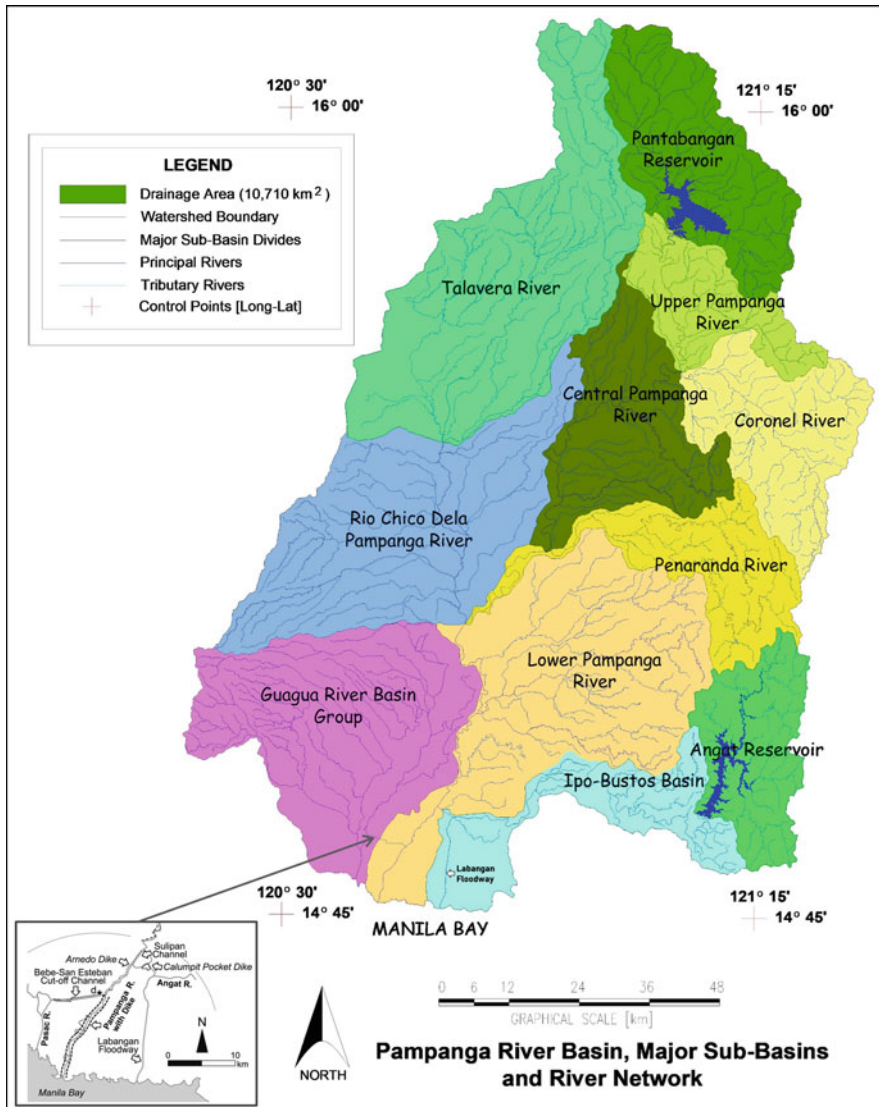


**Fig. 4.6** Major sub-basin delineations and river network of the Pampanga River Basin

in the town of Masantol. Before the Mt. Pinatubo eruption in 1991, excess floodwaters in Pampanga River flowed into the Guagua-Pasac River, but flow is reversed now due to lahar deposition in the Guagua-Pasac River side.

It is too lengthy to show details of all major sub-basins of the Pampanga River system so that only presented individually are Pantabangan and Lower Pampanga

**Table 4.1** Summary of drainage areas and number of sub-basin units for the major sub-basins of the Pampanga River system

Sub-Basin No.	River System	Sub-Basin Name	Major Rivers	Total Area (km <sup>2</sup> )	Total No. of Sub-basins
P-01	Pampanga	Pantabangan River Basin	Caragian River	845.8	126.0
P-02	Pampanga	Upper Pampanga River Basin	Pampanga River, Digmala River	436.1	80.0
P-03	Pampanga	Coronel River Basin	Coronel River	713.7	111.0
P-04	Pampanga	Central Pampanga River Basin	Pampanga River, Tambo Creek, Cabu Creek	801.1	82.0
P-05	Pampanga	Peñaranda River Basin	Peñaranda River, Sumacba River	607.4	61.0
P-06	Pampanga	Talavera River Basin	Talavera River, Casanova Creek	1,692.6	114.0
P-07	Pampanga	Rio Chico Dela Pampanga	Rio Chico Dela Pampanga River, Sacobia River	1,485.1	71.0
P-08	Pampanga	Lower Pampanga River Basin	Pampanga River, San Miguel River, Maasim River	1,640.0	93.0
P-09	Angat	Angat River Basin	Angat River, Catmun River	546.2	75.0
P-10	Angat	Ipo-Bustos River Basin	Angat River	576.6	48.0
P-11	Guagua/Pasac	Guagua River Basin Group	Abacan River, Pasig-Potero River, Porac River, Gumain River	1,365.7	99.0
			Total ----->	10,710.4	960

River Basins in Figs. 4.7 and 4.8, respectively. Each figure exhibits the major watershed boundary, sub-basin divides, river network, and the assigned number codes for identification of each sub-basin unit.

From these sub-basin delineations, geometry properties that are specified in the model such as the overland plane and the river lengths, widths, and slopes can be determined. Then, based on sub-basin delineations, the watershed model parameters such as interception, infiltration, and overland flow parameters can be obtained from soil type and land cover maps such as that shown in Fig. 4.9 for the Pampanga River Basin.

#### 4.2.2 *Groundwater Aquifer Characteristics and Groundwater Modeling*

From a geological perspective, the Pampanga River Basin is located within the Luzon Central Valley Basin bounded by the Sierra Madre mountain range on the east, the Caraballo mountain range acting as the northern boundary, while the Zambales mountain range as the western boundary. It is underlain by a thick pile of Tertiary sediments about 14 km thick at the center of the basin, tapering off at the east and west sides. These Tertiary sediments are covered by Recent Alluvium. Volcanic pyroclastic deposits which are products of volcanic activity from Mt. Pinatubo cover the older sedimentary sequence at the southwestern and

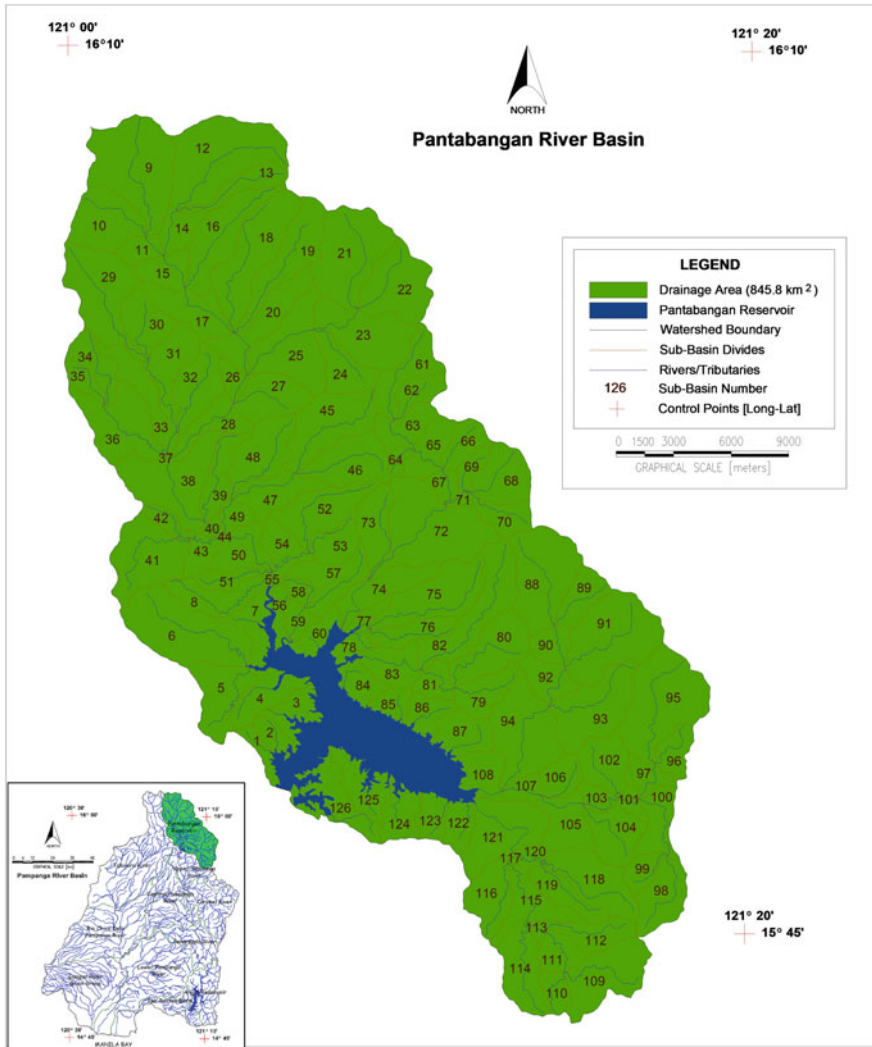


**Fig. 4.7** Sub-basin delineations of Pantabangan River Basin

southeastern periphery of the basin. Alluvial fan deposits also cover the older sedimentary sequence at the northern periphery of the basin.

The water-bearing formation tapped by the wells in the Pampanga River Basin generally consists of shallow aquifers and deep aquifers. The shallow aquifers are generally tapped by shallow wells at least 40 meters deep. These shallow aquifers consist of sand and gravel and interlayered with clays. These are generally related to the Recent Alluvium and Bamban Formation consisting of

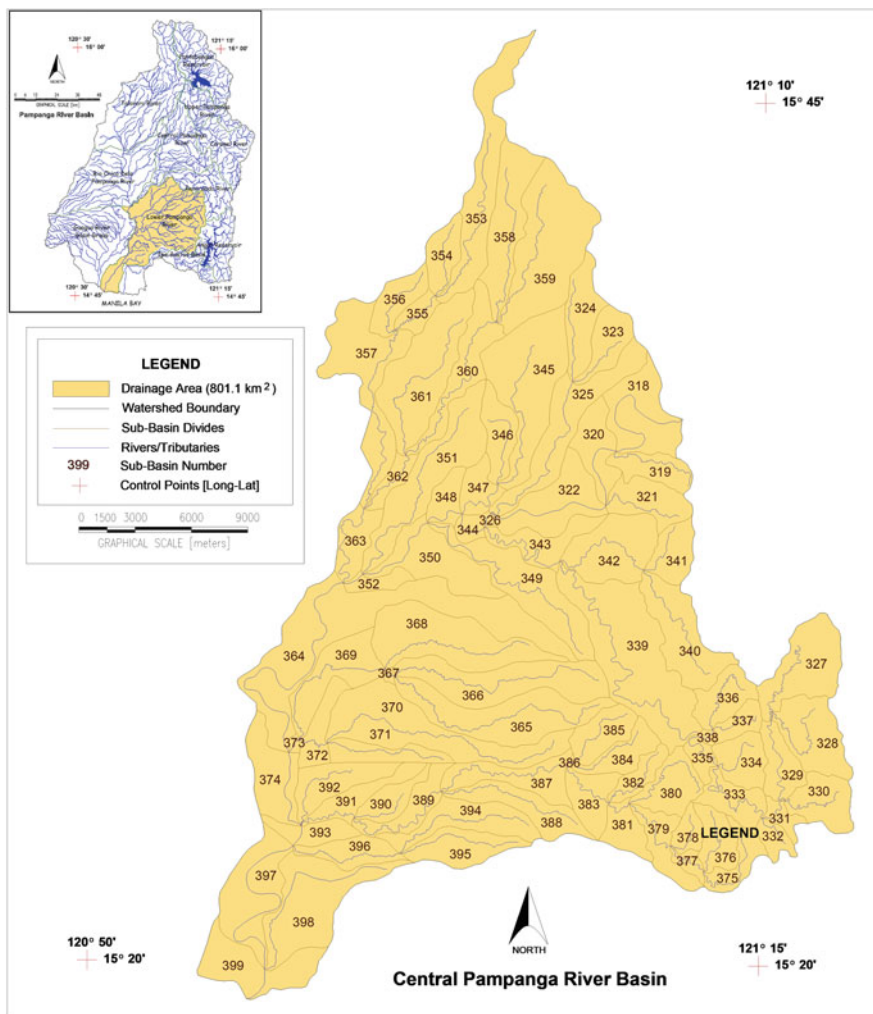


**Fig. 4.8** Sub-basin delineations of Lower Pampanga River Basin

tuffaceous sandstone and conglomerate. These shallow aquifers include unconfined, semi-confined, and locally confined aquifers.

The deep aquifers include the older sedimentary rocks more than 40–80 meters deep. These deep aquifers are part of the older sedimentary sequence Tarlac Formation (west side) and younger pyroclastic rocks of the Bamban Formation to the west and Tartaro Formation and Lambak to the east. The water-bearing layers consist of interbeds of porous and permeable sandstone and conglomerate members.

The subsurface configuration of aquifers and aquitards in the Pampanga River Basin generally assumes a shallow basin where the inflow comes from the periphery (Zambales/Pinatubo and Sierra Madre-Caraballo mountains) and converges at the

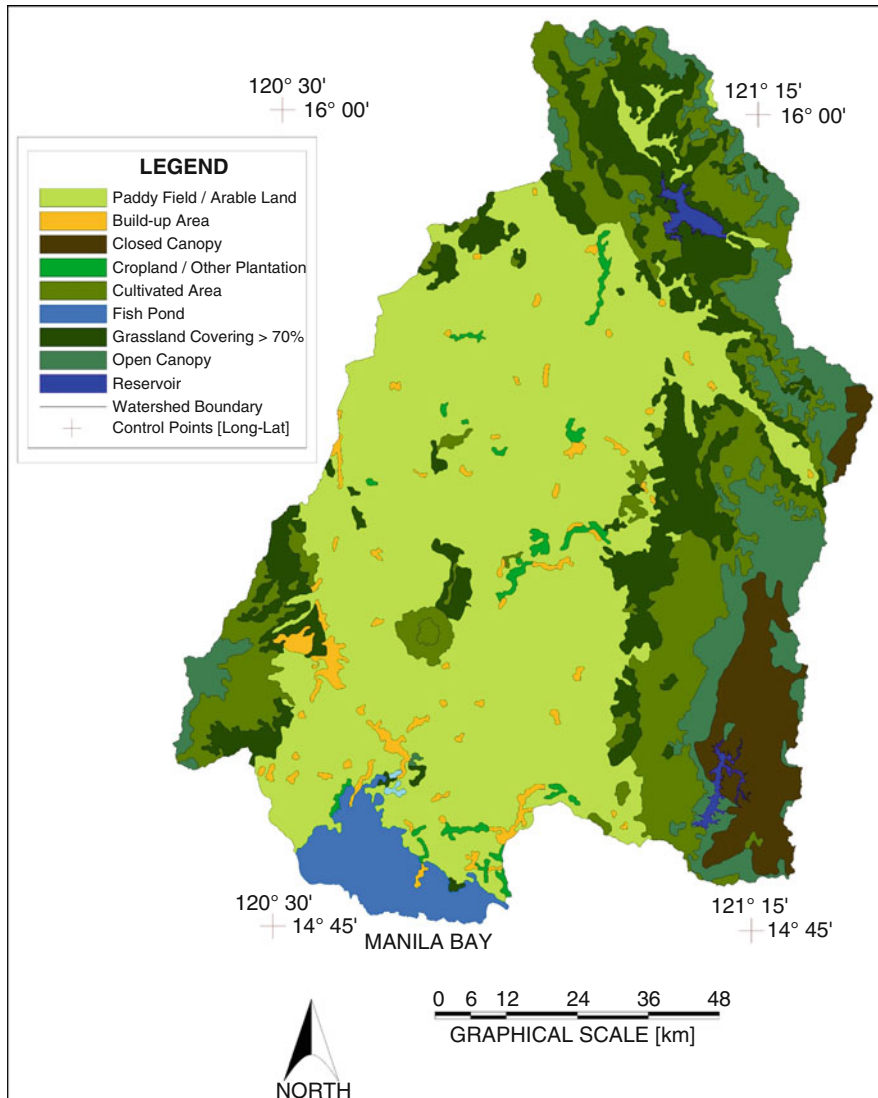


**Fig. 4.9** Land cover map of Pampanga River which is used to derive certain model parameters in the watershed model

center of the basin (Guimba, Pura, Concepcion, Gapan, and San Antonio in Nueva Ecija and Sta. Ana and Mexico in Pampanga). The aquifers in the central portion may be considered as having a relatively flat to gentle gradient following the flow of the Pampanga River.

To create the groundwater model geometry, a digital elevation map of the basin is needed as shown in Fig. 4.10 for the Pampanga River Basin. Based on this, the finite

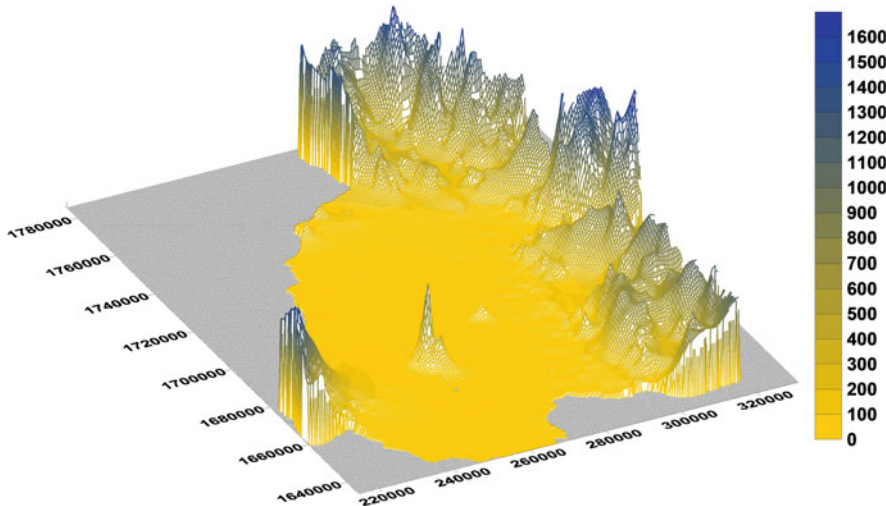


**Fig. 4.10** Digital elevation map of Pampanga River Basin

difference grid system is established consisting of  $1 \text{ km} \times 1 \text{ km}$  square grids to cover the rectangular area of 155 km (northing) by 121 km (easting) as shown in Fig. 4.11. In the rectangular area of  $155 \times 121$  grids, the number of active grids (within the basin boundary) is 11,046 grids. With a total of 16 layers (0 to  $-320$  m elevation with 20 m layer thickness) below zero ground elevation (at sea level), there will be roughly 176,736 grids below sea level. There is also a total of six layers (0 to 160 m elevations) which constitute additional grids in the model. Each of the grids represents specific geologic soil/material with associated groundwater properties such as porosity, hydraulic conductivity, specific yield, and storage coefficient. These properties are determined based on the geologic and groundwater aquifer characteristics.

With the groundwater model grid system, a major effort in groundwater modeling is the creation and rendering of the three-dimensional (3-d) geologic structure of the groundwater system based on the geologic data, lithology data from wells, and other hydrogeologic information. With the use of a computer software that employs three-dimensional spatial interpolation, this 3-d geologic structure is created based on lithologic data or core samples usually, available only at irregularly spaced locations (i.e., indicated by vertical, round columns) as shown in the sample computer-generated image in Fig. 4.12. This work is done by a geologist who is quite familiar with the geology of the area so that if there are portions in the 3-d geologic structure generated that do not appear reasonable, the geologist artificially and judiciously puts a contrived lithologic (core) data at certain locations until a reasonable 3-d geologic structure is created.

With the subsurface geology or soil structure rendering of the groundwater aquifer, a two-dimensional map of the groundwater properties (according to material codes) is created at the different layers of the groundwater aquifer. Figure 4.13 shows the map of the material codes for four selected layers at  $-100$  to  $-80$  m,  $-20$

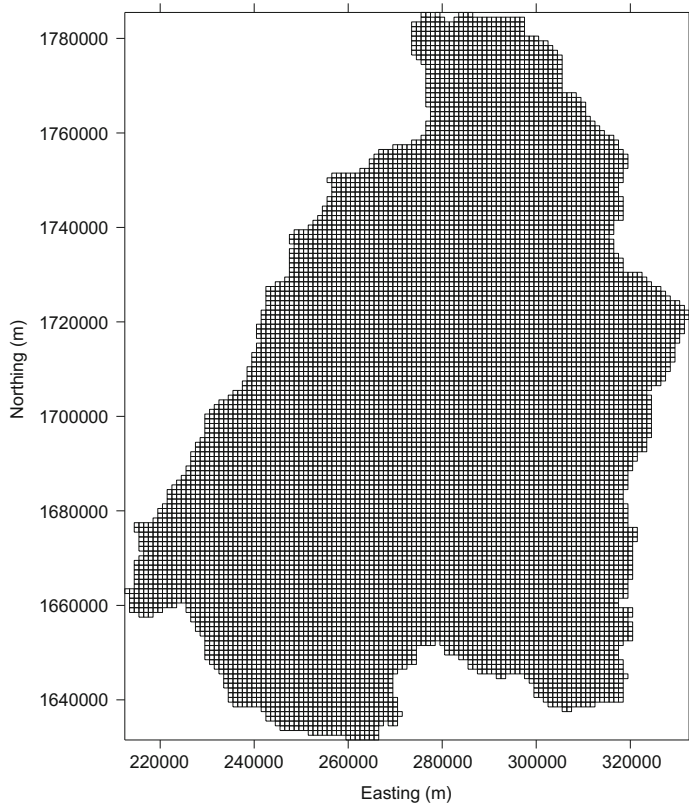


**Fig. 4.11** Finite-difference grid system of groundwater model of the Pampanga River Basin

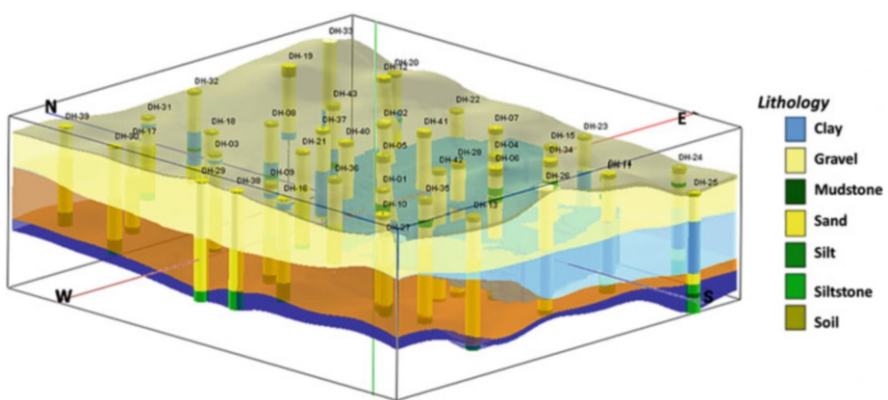


**Fig. 4.12** Sample three-dimensional rendering of the geologic structure of the groundwater system to create the geometry of the groundwater model

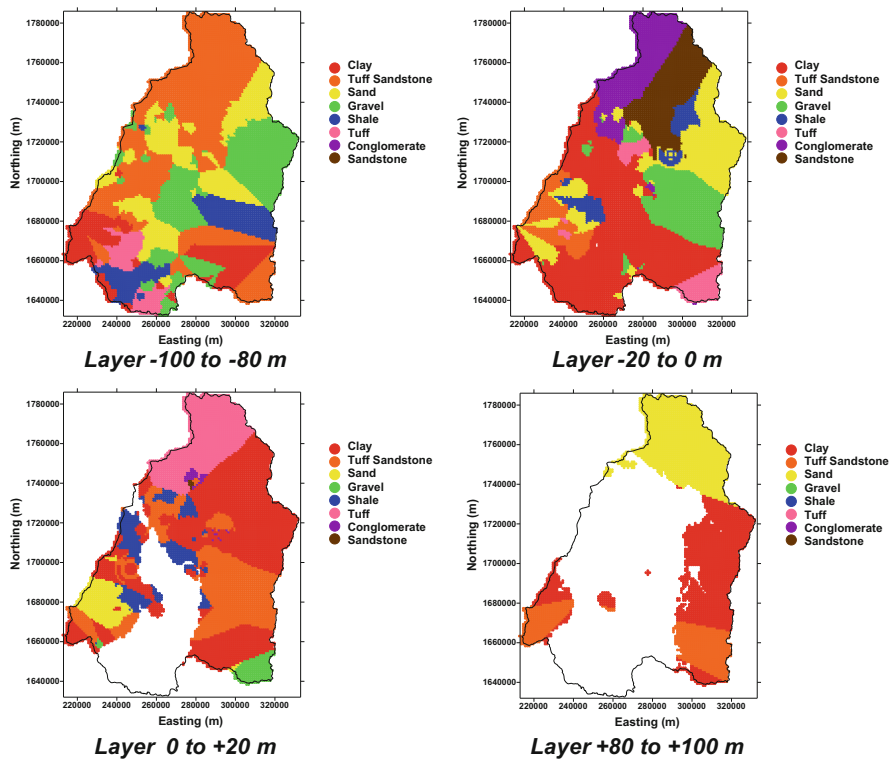


**Fig. 4.13** Map of groundwater material codes for layers  $-100$  to  $-80$  m,  $-20$  to  $0$  m,  $0$  to  $+20$ , and  $+80$  to  $+100$  m for the Pampanga River basin

to  $0$ ,  $0$  to  $+20$  m, and  $+80$  to  $+100$  m. These material code data constitute the major input to specify the three-dimensional (3-d) groundwater model geometry and properties. Table 4.2 shows the groundwater properties, namely, hydraulic conductivity, porosity, specific yield, and storage coefficient for each soil material which were taken from Bounding and Ginn (2004).

#### 4.2.3 Estimation of Surface Water and Groundwater Demands

The surface water and groundwater demands are the major bases for the reliability analysis of water resources in the study area. The water demands and uses are calculated in a stepwise manner. First is to estimate the existing demand based on available surface water and groundwater permits in the area. Then, this is validated by water use data from water districts or agencies responsible for water supply and distribution. Nonrevenue water is also estimated and added as part of existing water uses. Note that these water demands would have to be identified or associated to the

**Table 4.2** Groundwater properties of associated material codes. (From Boulding and Ginn 2004)

<i>Material</i>	<i>Hydraulic Conductivity (m/day)</i>	<i>Porosity</i>	<i>Specific Yield</i>	<i>Storage Coefficient</i>
Clay	0.00005	0.45	0.2	0.03
Tuffaceous Sandstone	5.02	0.25	0.12	0.05
Sand	50.0	0.325	0.3	0.05
Gravel	290.37	0.275	0.25	0.08
Shale	0.00005	0.05	0.05	0.01
Tuff	9.3	0.25	0.35	0.015
Conglomerate	14.79	0.105	0.2	0.05
Sandstone	10.0	0.105	0.15	0.05

various water sources (surface or groundwater sources). Then future water use/demands would have to be computed based on projected socioeconomic and demographic data.

The estimation of existing water demands and especially the projection of these demands into the future cannot be easily determined, since the accuracy of the computed future demands cannot be ascertained until actual water demand deliveries become known (i.e., observed or becomes historical). Oftentimes, simulation studies include sensitivity analysis according to variations of future demand projections.

In certain studies, the future groundwater demand projections are simply increasing the demand at the existing pumping locations. A realistic future demand will also expand in space thus the need to create plausible scenarios of spatial migration or expansion of groundwater pumping stations. Thus, the formulation of the simulation scenarios will not only be demand projections in time but also in space. The matching of when and where to divert or extract water from for a set of demand points or nodes is part of formulation of these simulation scenarios. The choices and matches of source-to-demand points can be aided by conducting a preliminary or initial assessment of surface water and groundwater availability from secondary data and employing a fail-fast criteria to narrow down possible sources of water for a given demand point based on water availability, distance from source to demand point, water quality, and other considerations. Surface water availability, for instance, can be based on available or neighboring flow duration curves to a potential surface water source. Data on groundwater availability may be obtained from previous studies or in fact can be based on groundwater amounts that remain to be allocated for water permits.

In summary, the estimation of the water demands and uses is done in a stepwise manner.

1. First, estimate the existing demand based on available surface water and groundwater permits in the area.
2. From these initial estimates, non-revenue water is estimated and superposed on this existing water uses.
3. These water demands are identified or associated to the various water sources (surface or groundwater sources).
4. Finally, future water use/demands are computed based on projected socioeconomic and demographic data.

The third step above requires the creation of water demand scenarios and development of source/demand matrix. This source/demand matrix is basically a list of candidate sources of water for delivery to multiple demand nodes for optimal water allocation.

For purposes of the simulation studies presented here, it is assumed that the bulk of the water demands are according to the amounts in the surface and groundwater water permits granted by the National Water Resources Board (NWRB) of the Philippines in the Pampanga River Basin with locations shown in Fig. 4.14. The specific amounts (in million liters per day, MLD) granted are shown in Fig. 4.15 for surface water permits and Fig. 4.16 for the groundwater permits. The amounts indicated in Fig. 4.16 are the sum of the groundwater water permit granted for domestic, agricultural, industrial, and commercial uses. It may be noted that generally, over 90% of groundwater permits granted are for domestic water supply. In the groundwater model runs, the demands are imposed which are increased every 5-year period for the total simulation of 70 years (2010 through 2080).

#### **4.2.4 Surface Water and Groundwater Model Simulation Studies**

The surface water and groundwater model simulation studies were conducted to investigate the availability and reliability of the water resources according to water uses/demands as well as potential nonconsumptive use of this water for hydropower generation prior to diversion for consumptive water use to domestic, commercial, or industrial purposes. The simulation studies were conducted on a daily time interval. The reliability analysis of the various surface water sources is based on dependable flow analysis (i.e., flow duration curves) and runs analysis of surplus and deficits at given demand or threshold levels. In the groundwater simulation, the resulting piezometric levels for existing and future water demands are basis for determining reliability and sustainability of the groundwater resources. These simulation results were then further analyzed to develop or match water source/demand matrix from a combination of surface water and groundwater supplies to the various demand points. For hydropower generation, the potential sites are identified based on the dependable flow analysis (i.e., flow duration curves) and net head (i.e., difference of

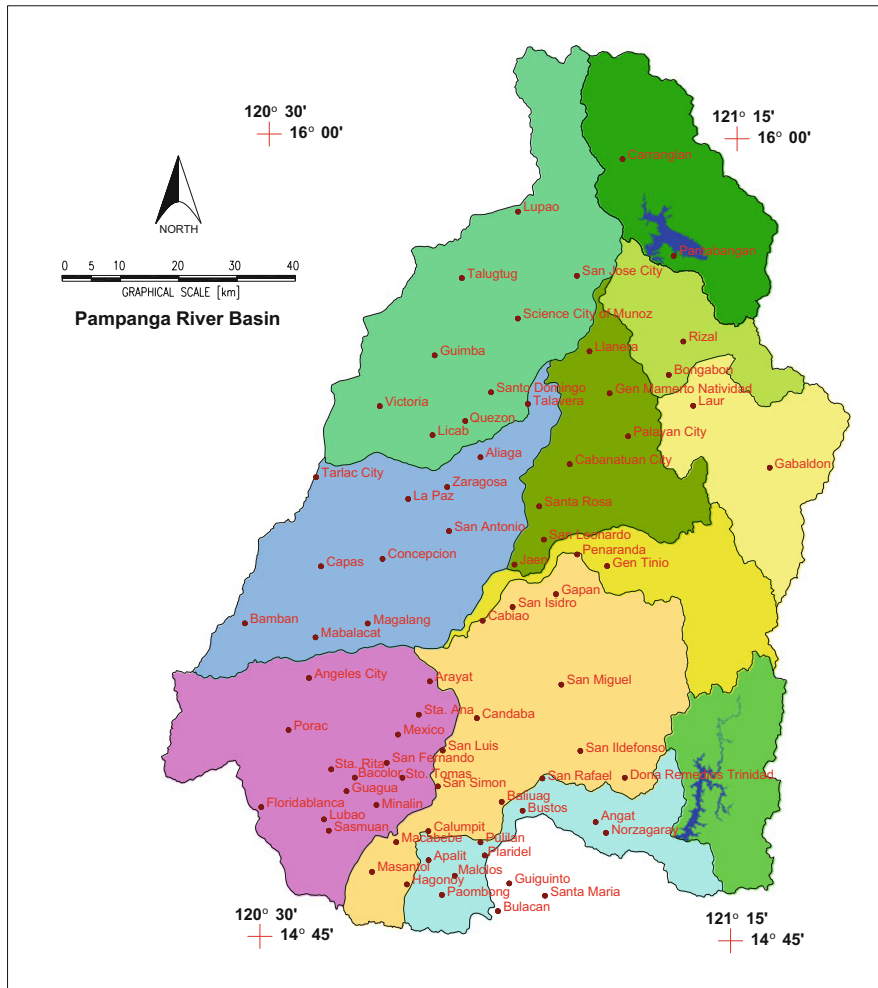


**Fig. 4.14** Locations in the Pampanga River Basin with existing surface water and groundwater permits issued by the National Water Resources Board (NWRB) of the Philippines

headrace which is elevation at water source diversion point and the tailrace which is elevation of hydropower plant site).

The rainfall data which is the major, driving input in the surface water model is using historical data from several gaging stations in the Pampanga River Basin. The available rainfall gaging stations and some pertinent information are given in Table 4.3. With the historical data, the point rainfall at several gaging points are spatially interpolated to account for the spatial variability of rainfall in the basin. A sample display of spatially interpolated rainfall over the basin at a particular 24-hour period (in mm) is shown in Fig. 4.17. The names and locations of the gaging stations used in the interpolation are also indicated. Note that as mentioned in Sect. 4.1.2, the

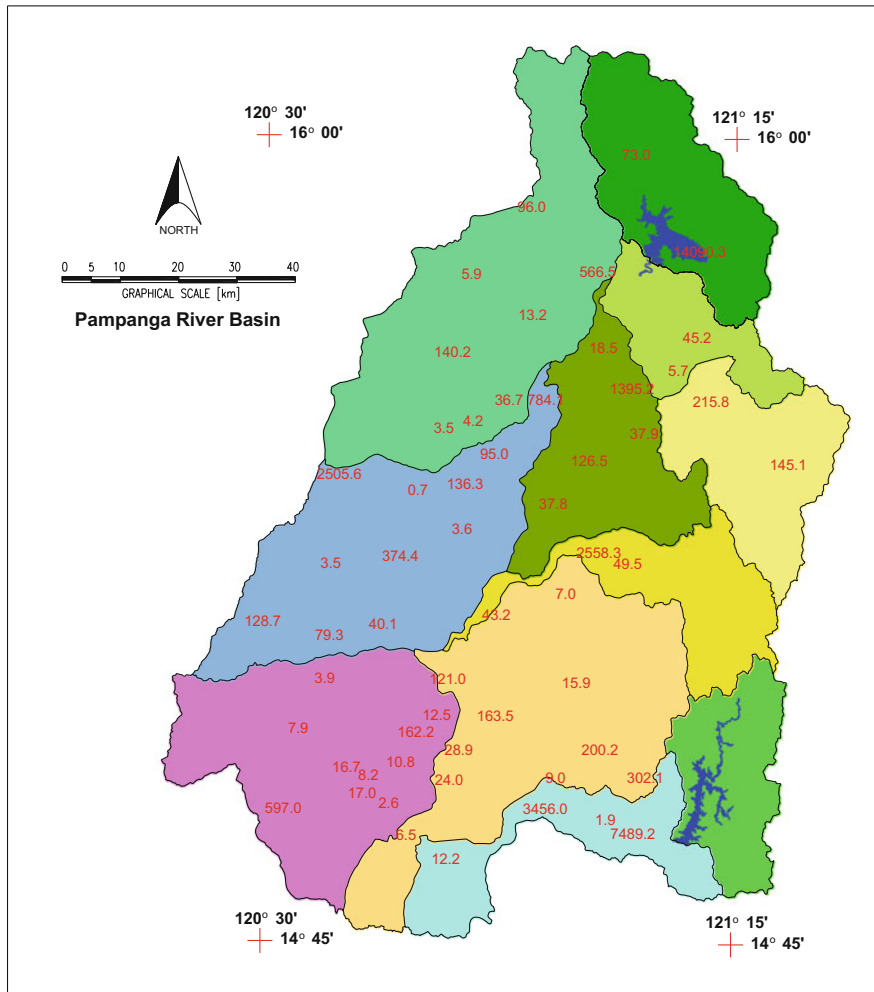


**Fig. 4.15** Amounts granted (in MLD) for surface water permits issued by NWRB in the Pampanga River Basin

groundwater recharge which is a major input in the groundwater model is calculated from the Sacramento soil moisture accounting (watershed) model which is the portion of total baseflow that becomes inaccessible to surface channel flow.

It will be too lengthy to show all the simulation results so only selected displays or tables of results are given here. Figure 4.18 shows long-term average daily flows of Talavera River Sub-basin, while Fig. 4.19 shows the long-term 80% dependable daily flows of Coronel River Sub-basin. These statistics were calculated based on long sequences of streamflow time series computed from the watershed model (i.e., 365 days over 50 years). In the Philippines, most water supply projects are designed (e.g., water diversion and treatment plant capacities) at 80% dependable daily flow

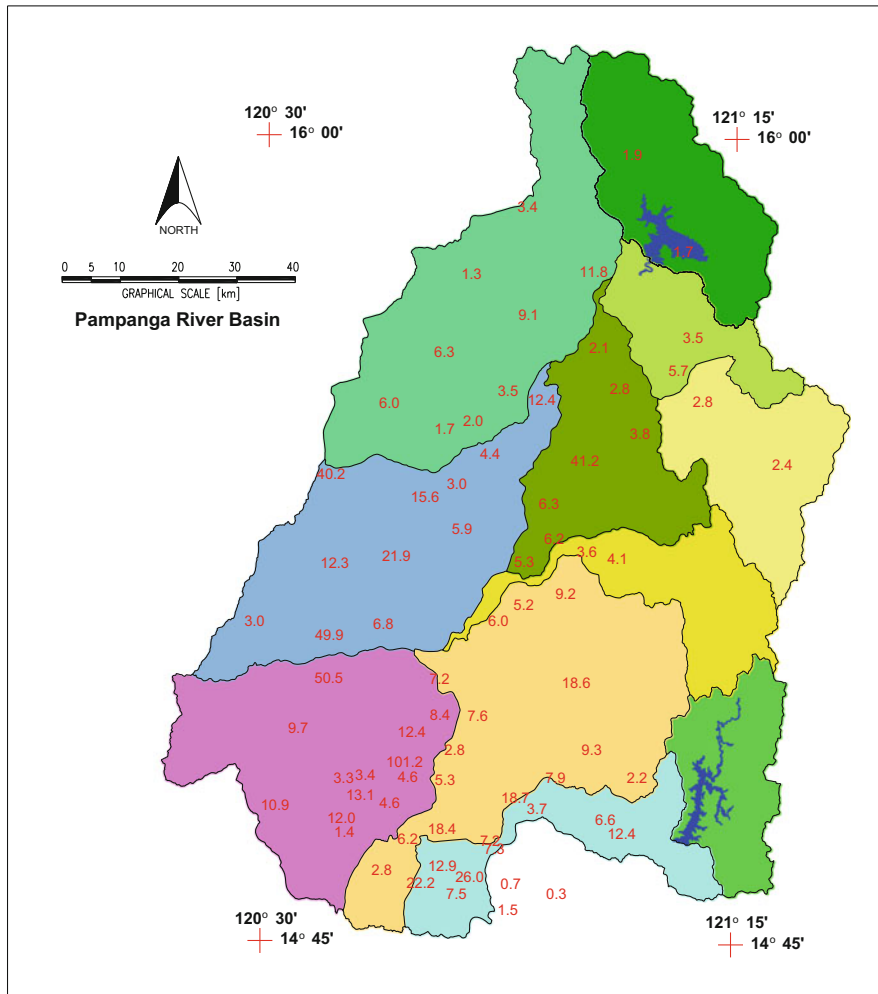


**Fig. 4.16** Amounts granted (in MLD) for groundwater permits issued by NWRB in the Pampanga River Basin

which means a reliability of getting streamflow in the river equal to or greater than that amount of observed flow eighty (80) percent-of-time or equivalently, about 290 days a year in the long term.

Before presenting results of runs analysis, it is worthwhile discussing this procedure. As shown in Fig. 4.20, for a given flow time series, assuming that the water demand or threshold level  $Q_0$  is imposed in the river, there will be periods when flows are greater or less than the water demand level. Surplus events are events when the flows for several successive days are above the demand level, while deficit events are events when the flows for several successive days are below the demand level. The surplus or deficit event has an associated duration and flow intensity (ratio of

**Table 4.3** Available rainfall data for Pampanga River Basin

Station <sup>a</sup>	Data source <sup>a</sup>	Type of data	Years of data	Remarks
CLSU, Munoz, Nueva Ecija	PAGASA	Daily	22	With missing data
Cabanatuan, Nueva Ecija	PAGASA	Monthly	45	With missing data
San Isidro, Nueva Ecija	PAGASA	Monthly	22	With missing data
DMIA, Angeles, Pampanga	CDC	Daily	10	Complete
Casiguran, Aurora	PAGASA	Monthly	48	Complete
Baler, Aurora	PAGASA	Monthly	45	With missing data
Iba, Zambales	PAGASA	Daily	43	With missing data
WLAC, San Marcelino Zambales	PAGASA	Daily	28	With missing data
Cubi Pt., Subic Bay, Zambales	PAGASA	Daily	10	With missing data
Hacienda Luisita, Tarlac	PAGASA	Monthly	20	With missing data
Mayantoc, Tarlac	PAGASA	Daily	19	With missing data
Angat dam, Angat, Bulacan	NAPOCOR	Monthly	40	With missing data

<sup>a</sup>CLSU, Central Luzon State University; DMIA, Diosdado Macapagal International Airport; PAGASA, Philippine Atmospheric, Geophysical and Astronomical Administration; NAPOCOR, National Power Corporation; CDC, Clark Development Corporation

volume of event and duration). With several years of daily flow data, several surplus or deficit events can be observed, and the calculated durations or flow intensities can be subjected to probability or statistical analysis such as calculation of their means, standard deviations, and skewness as well as their (empirical) cumulative distribution functions. The results of runs analysis such as analysis of deficits can be useful for planning for droughts or water shortages or the analysis of surpluses can be used for hydropower potential.

For Talavera River Sub-basin of Pampanga River Basin, the results of runs analysis with a demand or threshold level equal to the long-term mean daily flow are given in Figs. 4.21 and 4.22 for the average flow deficits (in  $\text{m}^3/\text{s}$ ) and number of days in deficit, respectively. At the outlet of Talavera River Sub-basin (going into Rio Chico River), the resulting average flow deficit was  $9.0 \text{ m}^3/\text{s}$ , and the average number of days in deficit was 32 days. In terms of average days in deficit, this implies that the flow demand equal to the long-term mean of  $44.2 \text{ m}^3/\text{s}$  at this outlet (see Fig. 4.18) if not satisfied would only last for a period of 32 days, on the average. Although not shown here, the 90% dependable flow computed at the outlet of Talavera River Sub-basin was  $11.2 \text{ m}^3/\text{s}$  (i.e., the river flow is equal to or greater

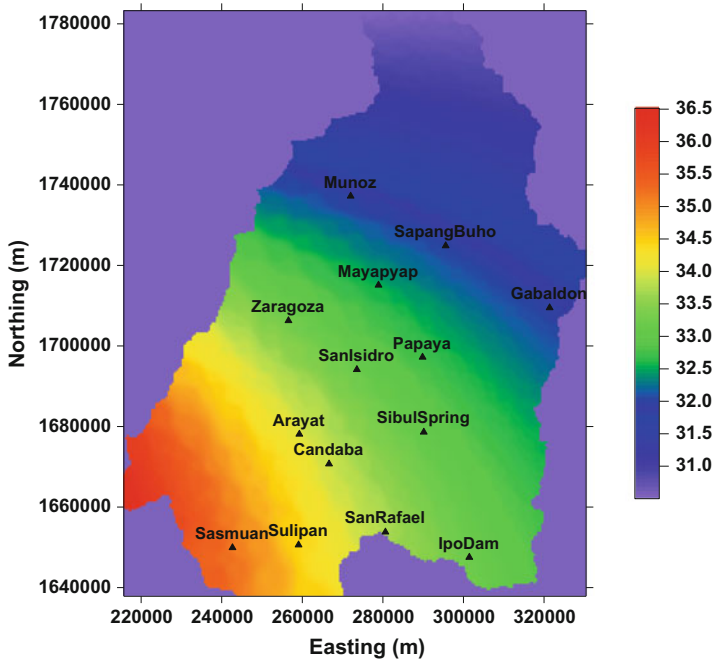


**Fig. 4.17** Spatially interpolated rainfall over the Pampanga River Basin for a particular 24-hour rainfall (in mm)

than that amount, 329 days or 90 percent-of-the-time in a year). The 90% dependable flow amount computed from frequency duration curve analysis may have some bearing on the average flow deficit in this case since the computed average days in deficit of 32 days is about 36 days (i.e., 365 minus 329 days).

The results of the groundwater model for the Pampanga River Basin are likewise too lengthy to show here. In summary, Fig. 4.23 shows the resulting piezometric (groundwater) heads at the end of year 2025 and 2050 starting in 2010 with groundwater pumping rates according to the existing NWRB water permit grants and increased every 5 years according to the population growth rate in the Pampanga River region. The important finding here is that it appears that there is ample groundwater resource in the entire Pampanga River Basin except for the areas around the Lower Pampanga River Basin and the downstream portions of Ipo-Bustos River Basin as indicated by the negative piezometric levels in these areas especially in 2050. This could be the result of inadequate groundwater recharge or excessive groundwater extraction or a combination thereof.

Another major result of this study is the identification of potential water sources for water supply as well as for hydropower generation. Table 4.4 shows the prospective service areas located within the sub-basins having water deficit which have to be supplied from the surplus of major potential rivers. The location of

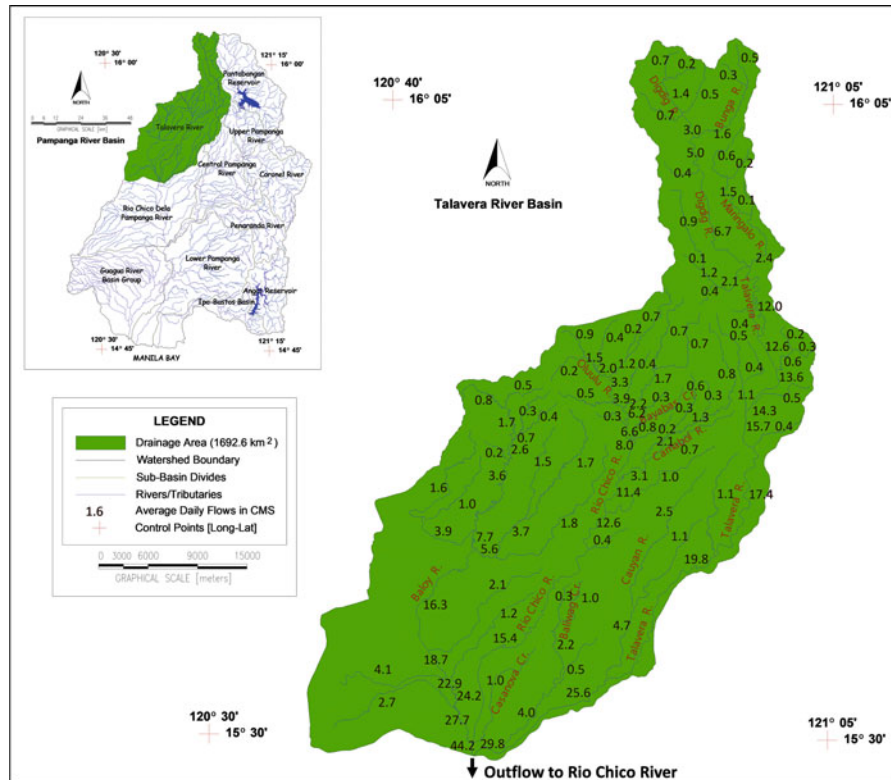


**Fig. 4.18** Long-term average daily flows ( $\text{m}^3/\text{s}$ ) of Talavera River Sub-basin

demand points (cities/municipalities) and possible abstraction points of major potential rivers within Pampanga River Basin is given in Fig. 4.24.

The Pampanga River Basin was also evaluated for potential hydropower generation based on dependable and reliable water flow and its location especially at some high elevation. Figure 4.25 shows the locations of these potential hydropower sites. Table 4.5 shows in particular more detail of the potential sites for hydropower generation with capacities of less than 5 megawatts (MW). These power plant capacities were calculated based on mean flows from these rivers. The calculated capacities based on 80% dependable flows are also shown in these tables.

### **4.3 Agno River Basin and Vicinity**

This section presents the modeling study of the Agno, Bued, Sinocalan-Mayruso, Alaminos-Bolinao, and Mabini-Dasol river basins to assess the availability and reliability of utilizing the surface and groundwater as water sources for the major cities and municipalities in Pangasinan Province and vicinity and also to identify

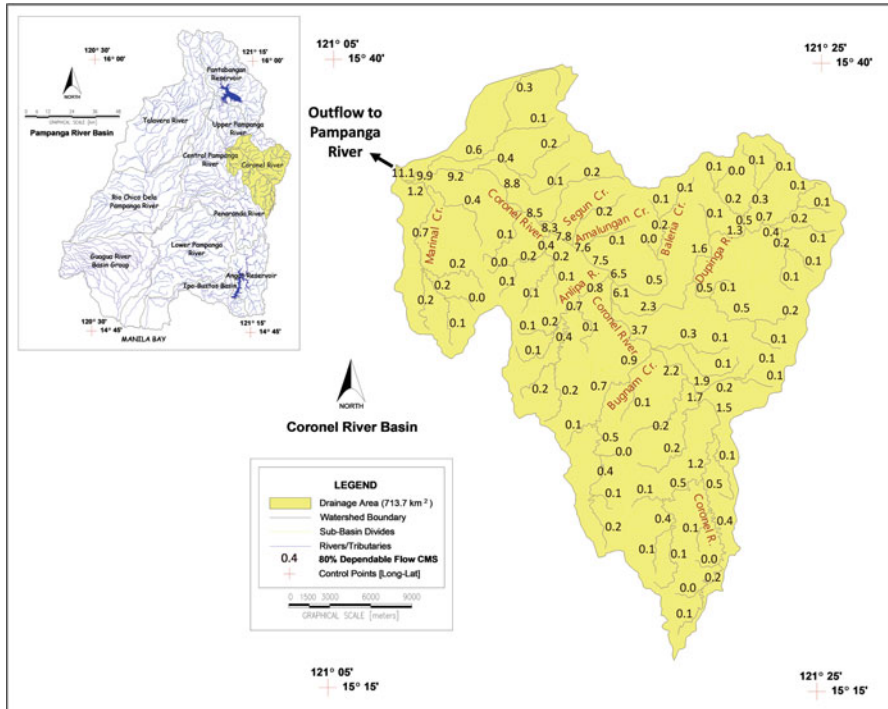


**Fig. 4.19** Long-term 80% dependable daily flows ( $\text{m}^3/\text{s}$ ) of Coronel River Sub-basin

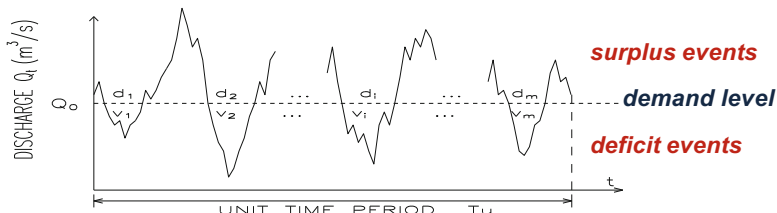


**Fig. 4.20** Schematic representation of water deficit events and surplus events below or above the demand levels, respectively

sites for potential hydropower generation. The same surface water and groundwater flow models as well as method of analyses are employed here as those for the Pampanga River Basin earlier.

The various river basins, Agno, Bued, Sinocalan-Mayruso, Alaminos-Bolinao, and Mabini-Dasol, are actually disjoint or separate basins. These basins cover the entire Pangasinan Province and portions of the surrounding provinces of Tarlac, Benguet, and Nueva Ecija and peripheries of Pampanga and Zambales. For brevity, all these river basins will simply be referred to as Agno River Basin or Agno-Pangasinan River Basin.

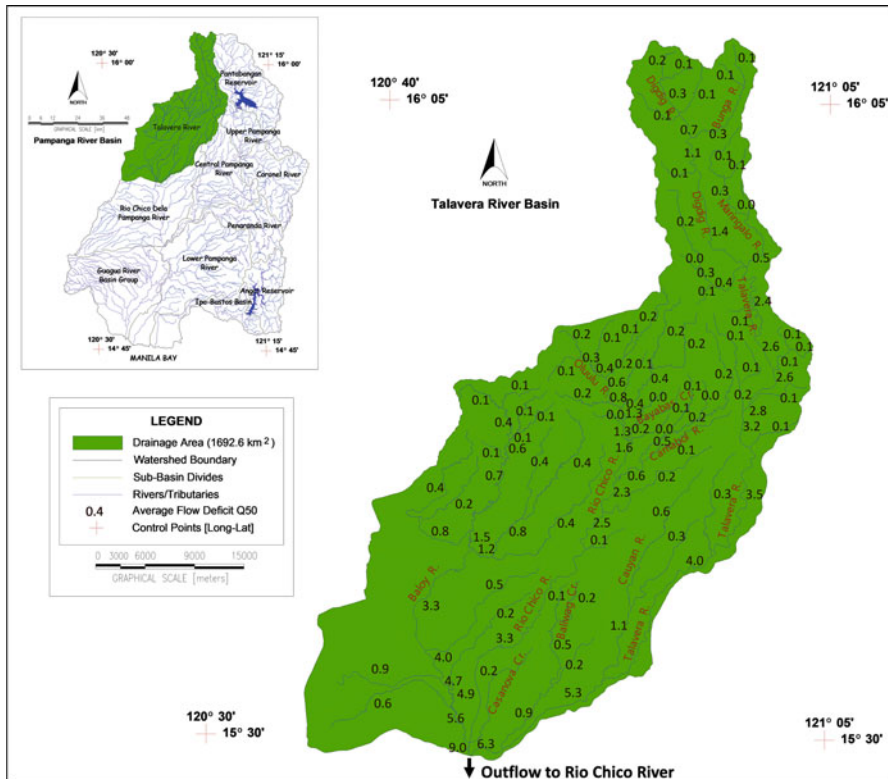


**Fig. 4.21** Average flow deficit ( $\text{m}^3/\text{s}$ ) for Talavera River Sub-basin by runs analysis at a demand level equal to mean daily flows ( $\text{m}^3/\text{s}$ )

Figure 4.26 shows the entire Agno River Basin which has a total area of 9202  $\text{km}^2$ . Figure 4.27 shows the river network and major rivers of Agno River Basin. The main Agno River system originates from Mt. Data in the north and traverses a north to south route passing through the Ambuklao Dam, the Binga Dam, and the San Roque Dam. Downstream of the San Roque Dam at San Manuel, the main channel forms a wide alluvial fan (the Agno River flood plain) from which several river tributaries spread out. This area is bounded on the north and northeast by the Cordillera Mountains of Benguet and Caraballo Mountains in Nueva Ecija, on the west by the Zambales mountain range and the Lingayen Gulf where the distributary rivers drain to, and on the south and southeast by Mt. Pinatubo and the Capas-to-Tarlac City diking system which serves as the divide between the Agno and Pampanga river basins.

With regard to the surface water resources in the area, there are three major reservoirs, namely, Ambuklao, Binga, and San Roque, in series along the main

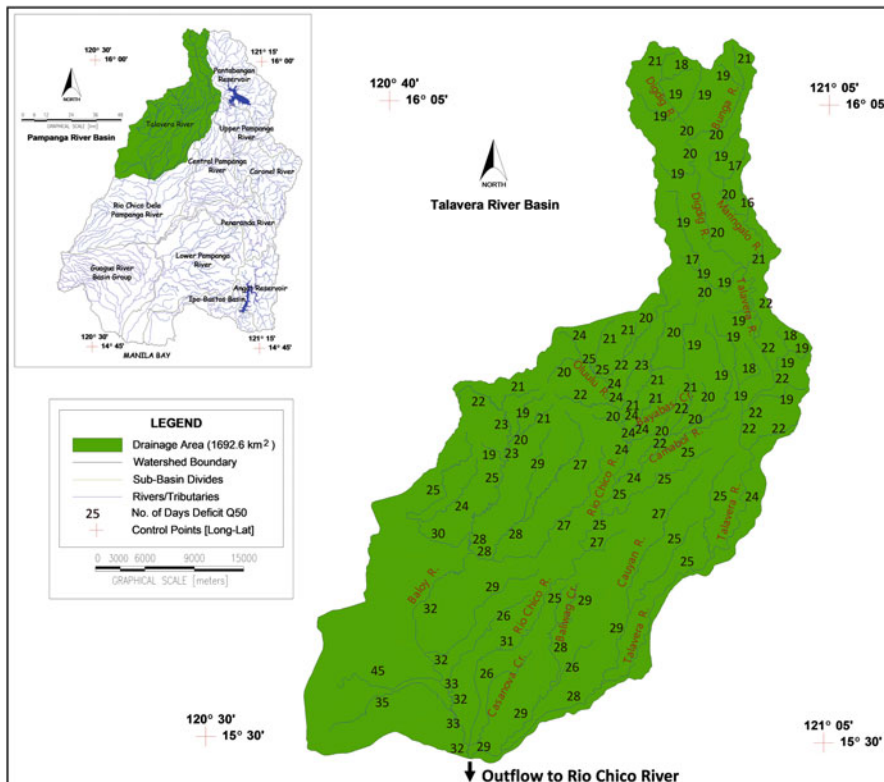


**Fig. 4.22** Average number of days in deficit for Talavera River Sub-basin by runs analysis at a demand level equal to mean daily flows (m<sup>3</sup>/s)

Upper Agno River. The Agno River downstream discharge is controlled by the San Roque Dam. An irrigation diversion weir diverts part of the outflow to the Agno River Integrated Irrigation Project (ARIIP) service area which is projected to cover 28,000 hectares. Recently approved for construction, the Balog-Balog Dam in Bulsa River, a tributary of Moriones River in Tarlac, is also under NIA. The Balog-Balog Dam study is presented in Sect. 6.1, Chap. 6.

With regard to the groundwater resources in the area, the groundwater aquifer system is the entire alluvial flood plain of the Agno River. The Recent Alluvium is partially consolidated to loose aggregate of sands, clays, and silts which were deposited by the periodic floods of Agno River. The underlying interlayers of these materials make up the sequence of aquifers and aquitards which is estimated to be more than 300 meters thick.

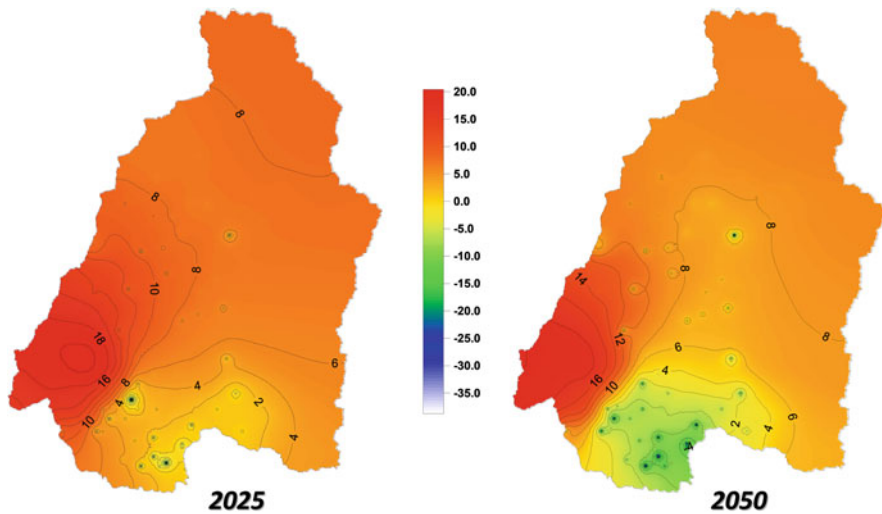


**Fig. 4.23** Simulated groundwater heads (in meters at mean sea level) of Pampanga River Basin at the end of year 2025 and 2050 starting in 2010 at extraction rates according to NWRB existing water permits and increased every 5 years based on population projection

**Table 4.4** Summary of prospective service areas located within the sub-basins having water deficit which have to be supplied from the surplus of major potential rivers

Sub-Basin (S.B.) Name	Possible Service Area to Adjacent Sub-Basins	Possible River Source	Surplus	Surplus	River Coordinates		Est. Dist. from Source (km)	Total Dem. 2025 (mld)	Total Dem. 2050 (mld)
			2025 (mld)	2050 (mld)	Longitude (deg. deg.)	Latitude (deg. deg.)			
Upper Pampanga	(1) Llanera	Digmalna River	112.9	109.2	121.12543	15.64371	11.9	22.3	24.7
	(2) Gen Mamerto Natividad	Pampanga River	505.4	498.5	121.12672	15.59711	8.3	1399.4	1401.3
Coronel	(1) Palayan City	Coronel River 2	588.9	582.9	121.12672	15.59711	8.5	43.0	44.9
	(2) Cabanatuan				121.12672	15.59711	19.1	189.4	221.3
	(3) Santa Rosa				121.12672	15.59711	27.8	46.3	49.6
Talavera	(1) Tarlac City	Rio Chico River 3	235.7	199.2	120.74942	15.48231	18.1	2561.1	2583.7
	(2) Aliaga	Talavera River 2	290.0	269.7	120.74942	15.48231	10.3	107.2	118.6
	(3) Zaragoza						5.5	142.8	147.8
	(4) La Paz						5.8	19.0	23.0
	(5) San Antonio						11.9	12.8	17.5
	(6) Concepcion						17.0	403.2	413.4
Lower Pampanga	(1) Apalit	San Miguel River 2	142.3	0.0	120.83561	15.08928	25.2	42.1	67.1
	(2) Minalin						22.0	8.9	11.5
	(3) Sasmuan						31.1	3.3	6.0
	(4) Lubao						30.7	21.6	35.7
	(5) Guagua						24.8	44.0	64.4
	(6) Paombong						30.5	11.4	17.2
	(7) Santo Tomas						15.5	9.9	17.6
	(8) Santa Ana						9.3	29.6	42.3

#### 4.3.1 Surface Water Modeling of Agno River Basin

Referring to Fig. 4.26, the entire Agno River Basin is subdivided into nine (9) major sub-basins, namely, Upper Agno, Central Agno, O'Donnell-Tarlac, Camiling, Lower Agno, Sinocalan-Mayruso, Bued, Alaminos-Bolinao, and Mabini-Dasol

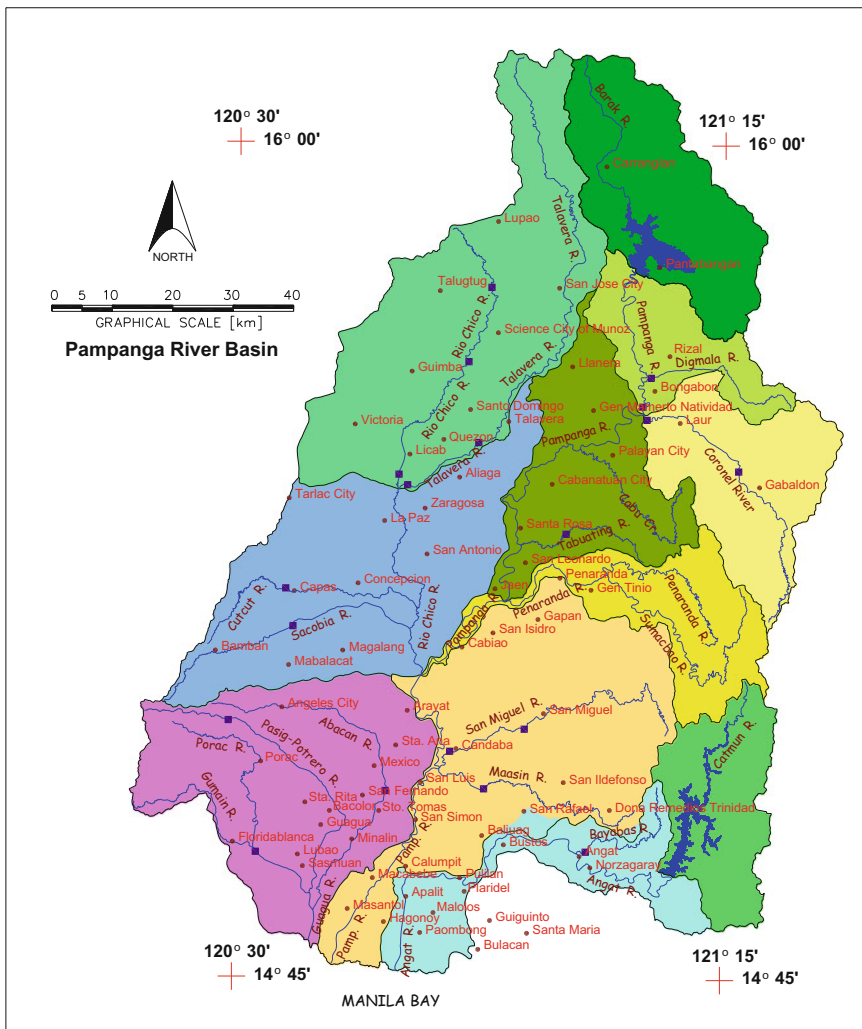


**Fig. 4.24** Location of demand points (cities/municipalities as indicated by round dots) and possible abstraction points of major potential rivers (as indicated by square dots) within Pampanga River Basin

basins. Each of these sub-basins is further subdivided into smaller sub-sub-basin units in which together with other hydrologic elements represent the physical watershed in the model.

Table 4.6 presents the summary of sub-basin number, sub-basin names, major rivers within the sub-basin area, corresponding drainage area, and the number of sub-basin units for the major sub-basins of the Agno River Basin. The entire river basin is divided into a total of 548 sub-basins so that as many as 548 riverflows or streamflows can be calculated in the watershed model.

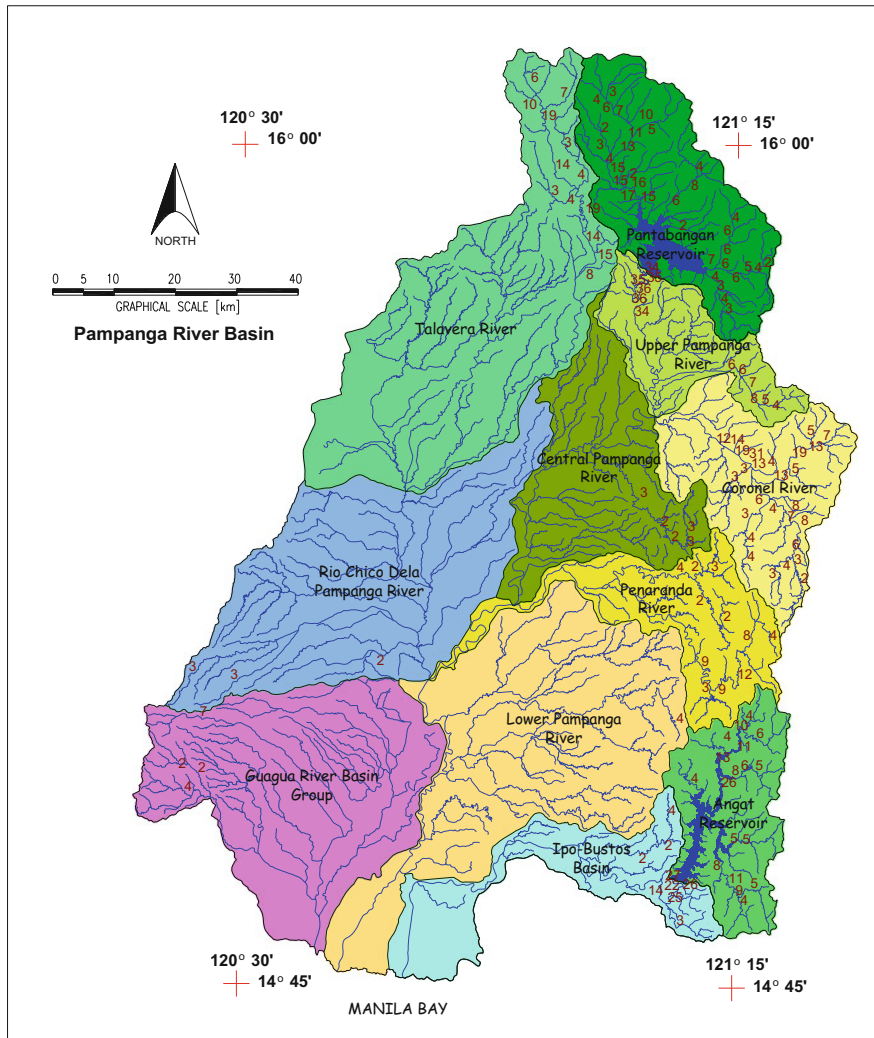


**Fig. 4.25** Potential hydropower sites and estimated capacity in megawatts (MW) within Pampanga River Basin

With the watershed delineated into sub-basins, the topology of the river network as well as model geometry such as overland flow planes and channel width, length, and slope can be obtained which is mainly based on the digital elevation data as shown in Fig. 4.28. Likewise, the watershed model parameters such as interception, infiltration, and overland flow parameters can be obtained from soil type and land cover maps such as that shown in Fig. 4.29 for the Agno-Pangasinan River Basin.

Rainfall data being a major input to the watershed model is given in Table 4.7 and accompanying Fig. 4.30 for the locations of gaging stations. Daily historical data

**Table 4.5** Potential hydropower sites and pertinent information with capacities of less than 5 MW based on mean river flows

Sub-Basin Name	SSB No.	River Name	Longitude Decimal Deg.	Latitude Decimal Deg.	Elevation	Q Average	Capacity, MW	Q 80%	Capacity, MW
Coronel	266	Dupinga R. Tributary	121.33576	15.51474	619	1.5	4.69	0.5	1.59
Pantabangan	103	Digoliat River	121.26151	15.81303	431	2.2	4.68	0.8	1.49
Angat	787	Macua River	121.26563	14.96286	500	1.9	4.67	0.7	1.48
Pantabangan	25	Deugurug River	121.11260	16.02283	383	2.5	4.63	0.9	1.47
Angat	748	Talagio River	121.18702	15.05375	634	1.4	4.44	0.5	1.45
Angat	801	Matulid River	121.26290	14.87223	680	1.3	4.43	0.5	1.38
Coronel	229	Coronel River	121.31009	15.45936	141	6.3	4.35	2.2	1.42
Upper Pampanga	178	Calaaanan River	121.30589	15.60794	683	1.3	4.36	0.5	1.34
Penaranda	402	Sumacbaao R. Tributary	121.30452	15.26669	799	1.1	4.29	0.4	1.36
Pantabangan	121	Cadaklan River	121.21382	15.79747	252	3.3	4.02	1.1	1.33
Penaranda	448	Peñaranda River	121.14534	15.35830	130	6.2	3.93	2.2	1.27
Ipo-Bustos	841	Balasbolas River	121.15266	15.00581	648	1.2	3.86	0.4	1.3

from 18 stations have varying period of records between 1950 and 2007 which is sufficient enough for the simulation studies conducted here. The rainfall for each sub-basin is obtained by interpolating rainfall from stations with available data on that day.

### 4.3.2 *Groundwater Modeling of Agno River Basin*

For the groundwater model, the finite difference grids or cells consist of 1 km x 1 km square grids to cover the rectangular area of 189 km (northing) by 129 km (easting) as shown in Fig. 4.31. The total number of active grids (within the basin boundary) is 9642 grids. With a total of 18 layers (-200 to 160 m elevation with 20-m layer thickness) below zero ground elevation (at sea level), there will be roughly 150,000 grids below sea level. Each of the grids represents specific geologic soil/material with associated groundwater properties such as hydraulic conductivity, porosity, specific yield, and storage coefficient. These properties are determined based on the geologic and groundwater aquifer characteristics.

The general hydrogeological configuration of the groundwater model is on the northern end of the Luzon Central Basin including the flood plain area of Pangasinan and Tarlac with the following boundaries: to the northwest by Lingayen Gulf, to the northeast and east by the Caraballo Mountains, to the southeast and south by the surface basin boundary extending from Tarlac to Pangasinan-Nueva Ecija, and to the west by the Zambales range. The estimated depth at the center is around 300 meters, while at the periphery is around 50 meters.

To define the three-dimensional (3-d) rendering of the subsurface geologic structure in the groundwater model, actual lithologic logs from 112 wells obtained from LWUA database and additionally 25 hypothetical lithologic data judiciously

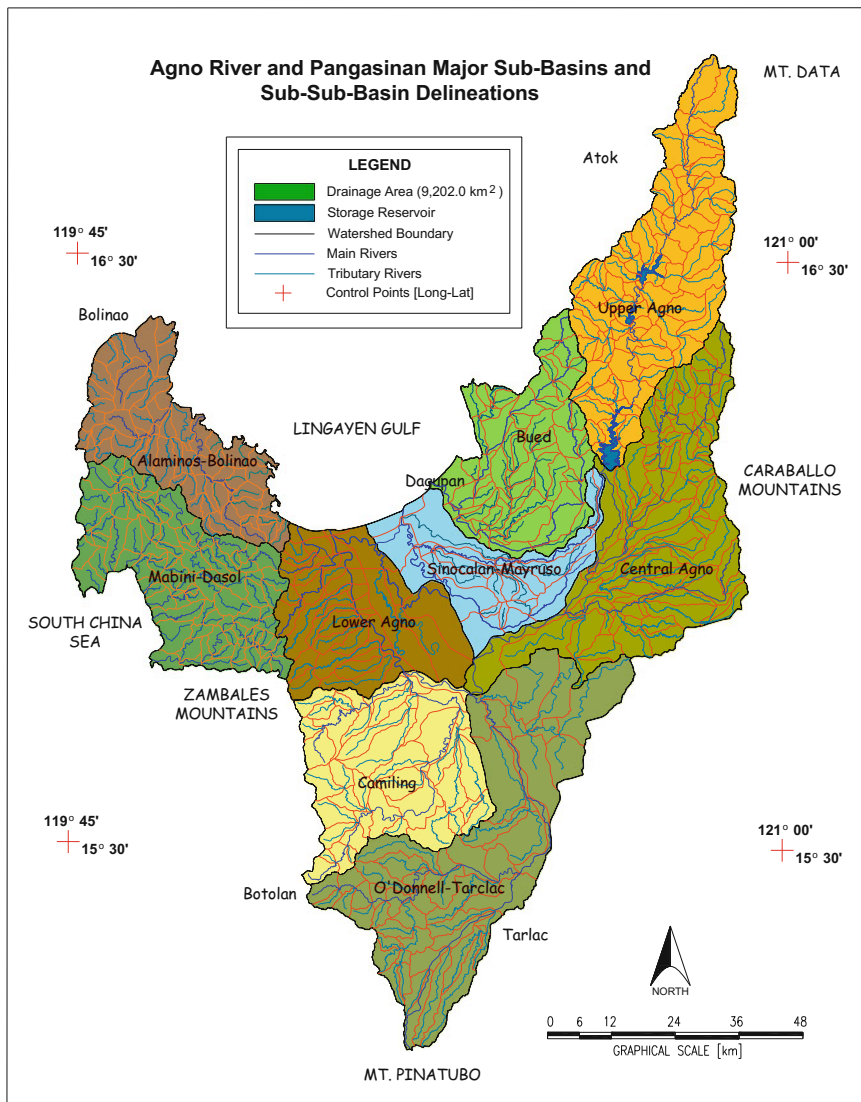


**Fig. 4.26** Map of Agno River Basin covering the entire Pangasinan Province and portions of Benguet, Tarlac, Pampanga, and Zambales. The watershed delineations into sub-basins are also indicated in the figure

located in the modeled area were contrived based on published geologic maps from the Mines and Geosciences Bureau and available literature.

With the 3-d subsurface geologic structure rendering of the groundwater aquifer, the specific groundwater properties (according to material codes) can be determined at the different layers of the groundwater aquifer. The material code data constitute

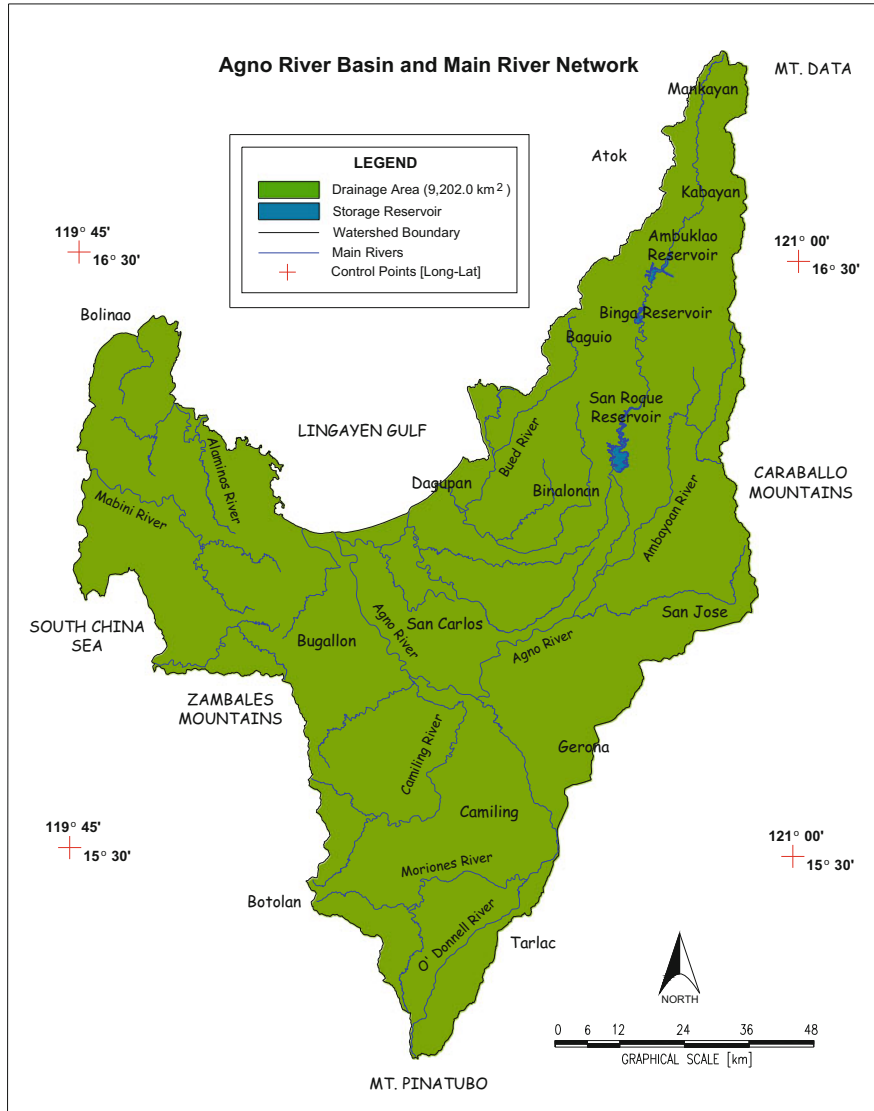


**Fig. 4.27** Major rivers and river network of Agno River Basin

the major input to specify the three-dimensional (3-d) groundwater model geometry and properties. Table 4.8 shows the groundwater properties specified in the model for each material code. Figure 4.32 shows the maps of material codes for layers 0 to +20, +60 to +80, +120 to +140, and +160 to +180. Likewise, Fig. 4.33 shows the maps of material codes for layers -40 to -20, -120 to -100, -240 to -220, and -320 to -300.

A major input into the groundwater model is groundwater recharge that deep percolates into the groundwater aquifer which is calculated from the watershed

**Table 4.6** Summary of drainage areas and number of sub-basin units for the major sub-basins of the Agno River Basin

Sub-Basin No.	Sub-Basin Name	Major Rivers and Tributaries	Area (km <sup>2</sup> )	Total No. of Sub-basins
A-01	Upper Agno River Basin	Agno River (Ambuklao, Binga, & San Roque Reservoir)	1,234.1	78
A-02	Central Agno River Basin	Agno River, Ambayoan River, Banila River	1,404.5	87
A-03	O'Donnell-Tarlac River Basin	O' Donnell River, Moriones River, Tarlac River	1,572.0	57
A-04	Camiling River Basin	Camiling River, Oro River	988.2	47
A-05	Lower Agno River Basin	Agno River, San Juan-Basing River	845.5	38
A-06	Sinocalan-Mayruso River Basin	Sinocalan-Mayruso River, Panto River, Ingaleria River	606.0	25
A-07	Bued River Basin	Bued River, Pantalan River, Amanduyan-Angalacan River	817.6	56
A-08	Alaminos-Bolinao River Basin Group	Alaminos River, Bani-Bawetwet River, Balingayan River	767.2	61
A-09	Mabini-Dasol River Basin Group	Mabini River, Dasol River, Uli River, Eguia River, Nayom River	966.9	99
		<b>Total -----&gt;</b>	<b>9,202.0</b>	<b>548</b>

model (see Sect. 4.1.2). Another major boundary condition to the groundwater model is the groundwater demand imposed as well as extractions or discharges. The groundwater demand is described in the next section.

### 4.3.3 Surface Water and Groundwater Demands

The surface water and groundwater demand data are the major bases for assessing the reliability of water resources in the study area. Figure 4.34 shows the location of existing surface and groundwater permits, while Figs. 4.35 and 4.36, respectively, show the amounts granted in the existing surface water and groundwater permits issued by NWRB, updated to 2010 which are the amounts imposed as water demands in the reliability studies. In the groundwater model simulations, the water demands (pumping rates) are projected and increase every 5 years based on the population growth rate starting from the 2010 groundwater extraction rates. Figure 4.37 shows the groundwater demands in year 2050. The groundwater demand is the sum of the domestic, agricultural, industrial, and commercial uses although generally, the domestic groundwater use is usually 90% or more of the total demand.

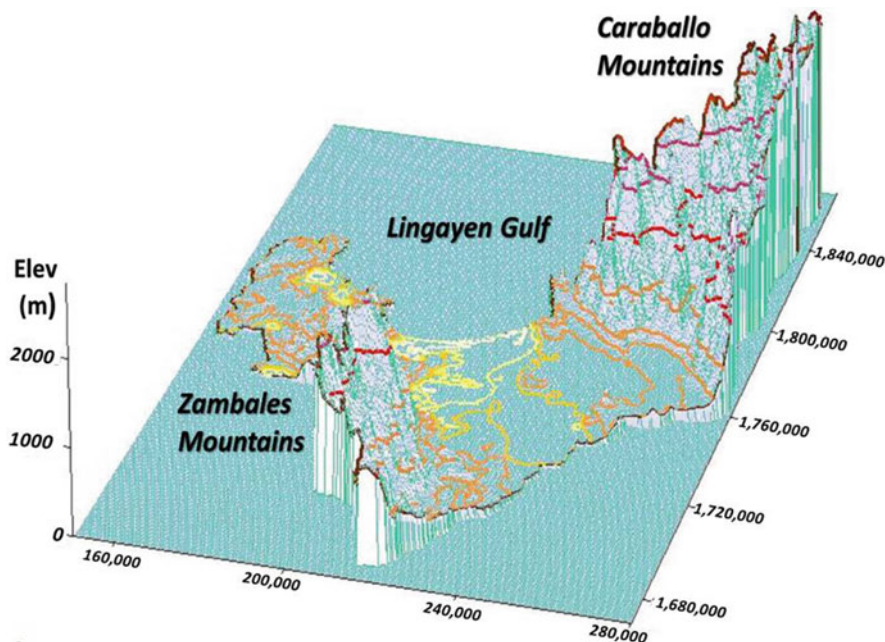


**Fig. 4.28** Digital elevation map of Agno River Basin

#### 4.3.4 Surface Water and Groundwater Model Simulation Studies

Presented below are the results of the surface water and groundwater model simulation studies to investigate the availability and reliability of the water resources of Agno River Basin for domestic, agricultural, and commercial water use and for potential (nonconsumptive) use of this water for hydropower generation. The reliability analysis conducted here is based on dependable flow analysis or flow duration curves and runs analysis for specific demand or threshold level as done for Pampanga River Basin in Sect. 4.2.4.

For brevity, only a few simulation results are shown here since it is too lengthy to show all of them. For instance, the long-term mean of daily flows is shown in Fig. 4.38 for the Lower Agno River Sub-basin. Likewise, from dependable flow analysis, Fig. 4.39 shows the 80% dependable flow of the Central Agno River.

Another useful result is from runs analysis as done in Pampanga River Basin earlier where deficit events are events when the flows for several successive days are below the specified demand level, while surplus events are when flows for successive days are above the demand level. The surplus or deficit event has an associated duration and flow intensity (ratio of volume of event and duration). Again, for brevity, Figs. 4.40 and 4.41 show the average flow deficits (in  $\text{m}^3/\text{s}$ ) and average number of days in deficit, respectively, for Lower Agno River Sub-basin at a demand

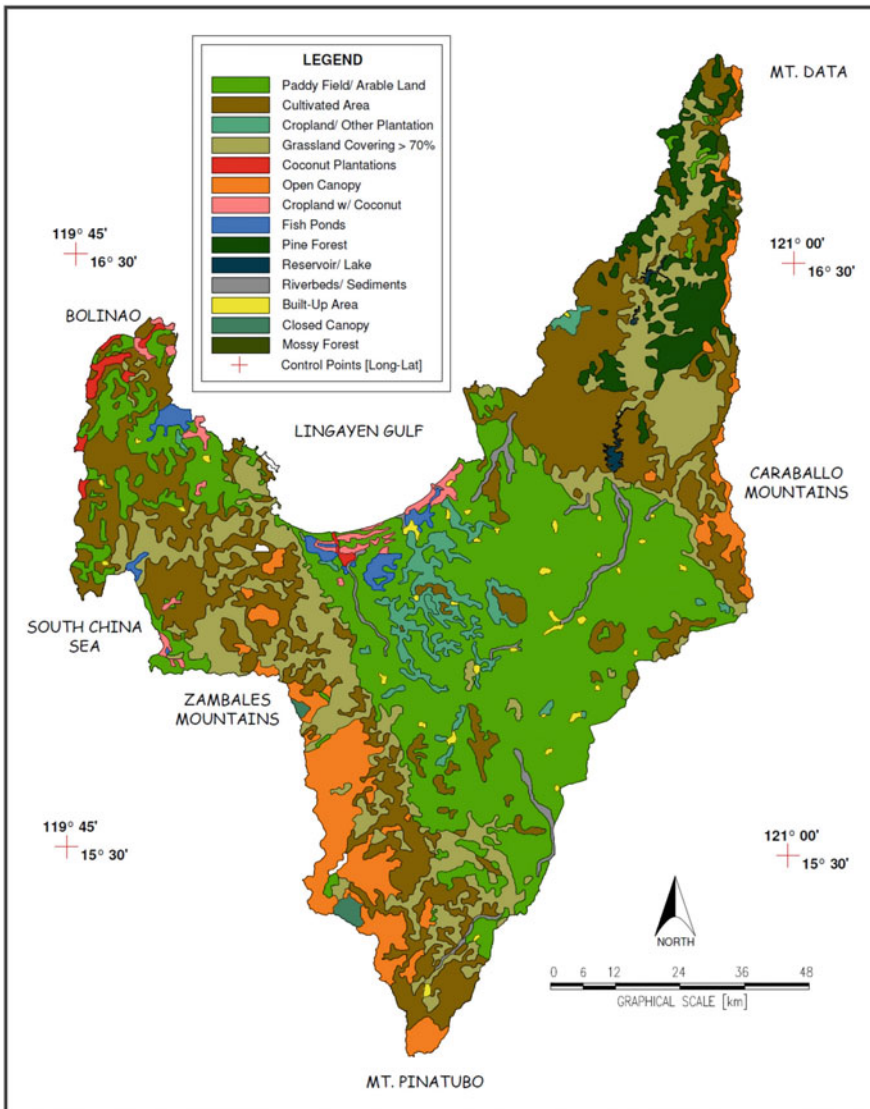


**Fig. 4.29** Land cover map of Agno River basin which is used to derive the model parameters in the watershed model

or truncation level equal to the long-term daily mean. Figures 4.42 and 4.43 show the average flow deficits and number of days in deficit, respectively, for the Central Agno River at a demand level equal to 80% dependable daily flow. In the case of Central Agno River Sub-basin, the resulting average flow and number of days in deficit at the outlet of the sub-basin (into Lower Agno Sub-basin) were  $5.3 \text{ m}^3/\text{sec}$

**Table 4.7** List of rainfall stations in Agno River Basin and vicinity

Station name	Location	Agency	Period of record		No. of years of complete data	Remarks
			From	To		
Ambuklao	Bokod, Benguet	PAGASA	1950	1996	47	Daily
Atok	Benguet	PAGASA	1950	1981	32	Daily
Baguio city	Benguet	PAGASA	1952	2000	49	Daily
Balatoc Mines	Ilogon, Benguet	PAGASA	1961	1996	36	Daily
Balungao	Pangasinan	PAGASA	1971	1997	27	Daily
Binalonan	Pangasinan	PAGASA	1972	1997	26	Daily
Bobok	Bokod, Benguet	PAGASA	1950	1996	47	Daily
Bulawon	Sta. Cruz, Zambales	PAGASA	1975	1996	22	Daily
BSU	La Trinidad, Benguet	PAGASA	1976	1995	20	Daily
CLSU	Munoz, Nueva Ecija	PAGASA	1974	1995	22	Daily
Dagupan city	Pangasinan	PAGASA	1961	2007	47	Daily
DMIA	Angeles, Pampanga	DMIA	1998	2007	10	Daily
Iba	Zambales	PAGASA	1961	1997	37	Daily
Mabini	Pangasinan	PAGASA	1968	1997	30	Daily
Masalep	Tubao, La Union	PAGASA	1966	1997	32	Daily
Mayantoc	Tarlac	PAGASA	1972	1990	19	Daily
Philex open pit	Benguet	PHILEX MINES	1989	2000	12	Daily
Philex Main camp	Benguet	PHILEX MINES	1989	2000	12	Daily

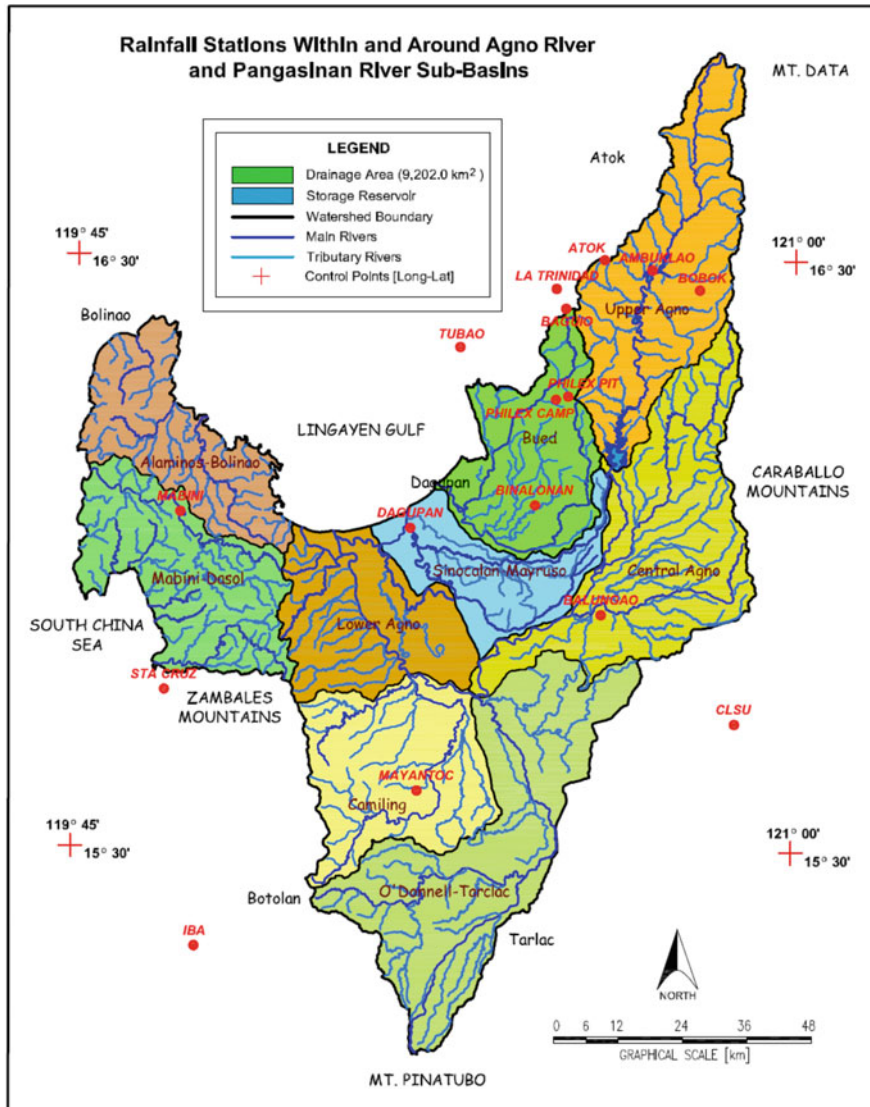


**Fig. 4.30** Location of rainfall stations (with round dots) within and around the Agno River Basin

and 28 days, respectively. Note that the demand level imposed in the runs analysis is the 80% dependable flow equal to  $35.7 \text{ m}^3/\text{s}$ .

The results of the groundwater model for the entire Agno River Basin are too huge to show here. However, the bottom line result can be summarized in Figs. 4.44 and 4.45 which show the resulting piezometric (groundwater) heads at the end of year 2025 and 2050, respectively. In these figures, the heads were obtained with imposed demand as shown including results with demands, 25% and 50% more than

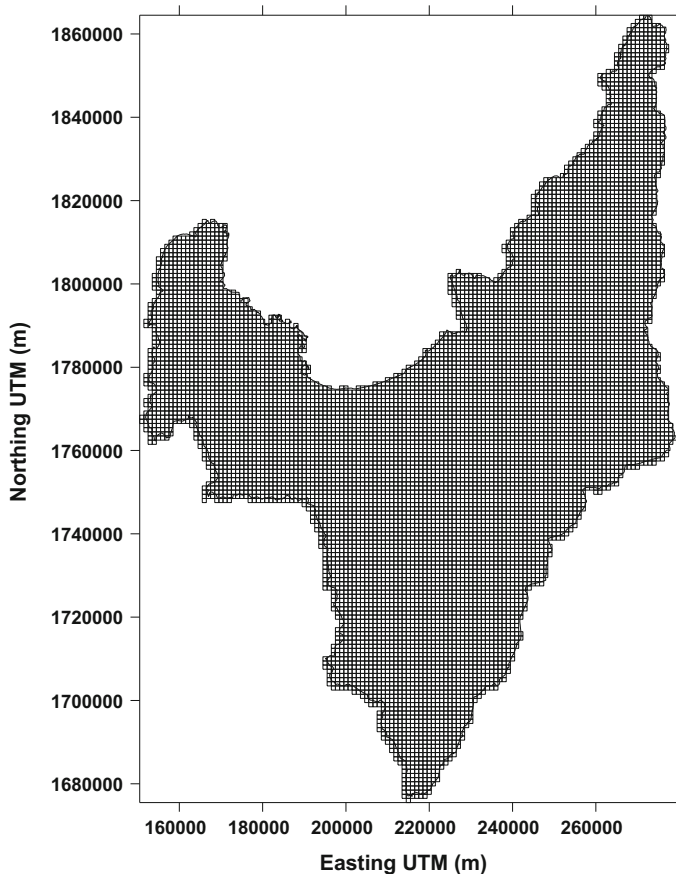


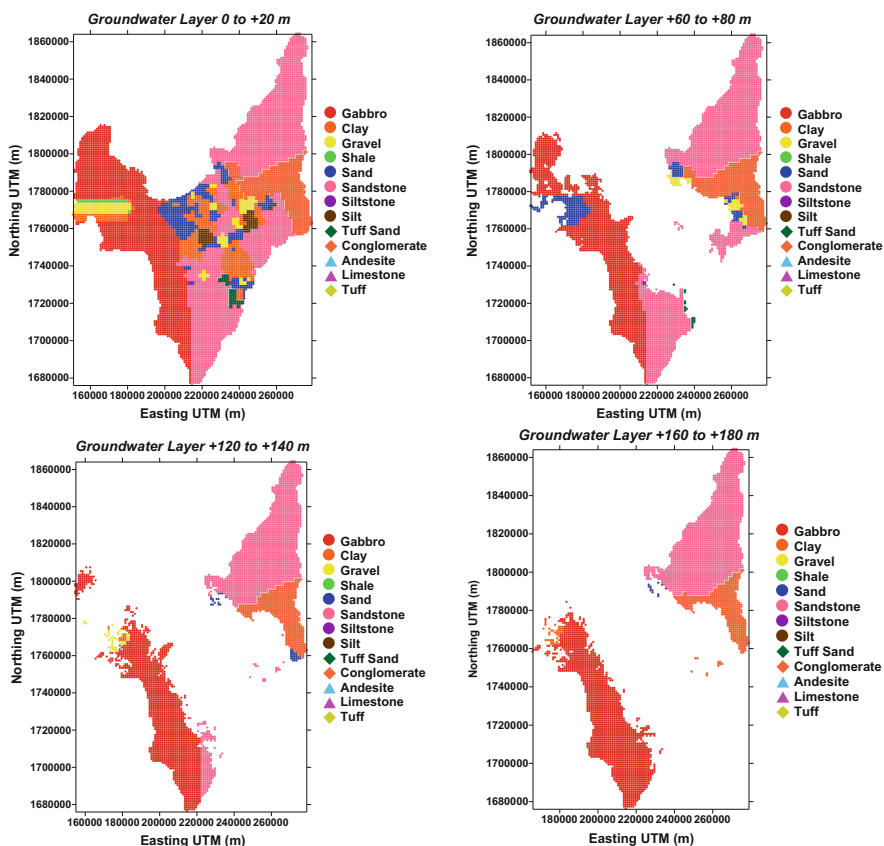
**Fig. 4.31** Finite difference grid system of Agno River Basin groundwater model

the projected demands. The cases with increased demands serve as sensitivity analysis runs to account for non-revenue water (NRW) or any uncertainty in the estimation of demands. The important finding here is that it appears that there is ample groundwater resource in the entire Agno River Basin except for a small portion in the middle of the basin where the groundwater levels of 2050 dropped 10 to 20 m below those of 2025. It may be noted that groundwater overextraction around the coastal zones of the Pangasinan peninsula such as in the lower portion of Agno River Basin (around outlet to Lingayen Gulf) may lead to saltwater intrusion problems.

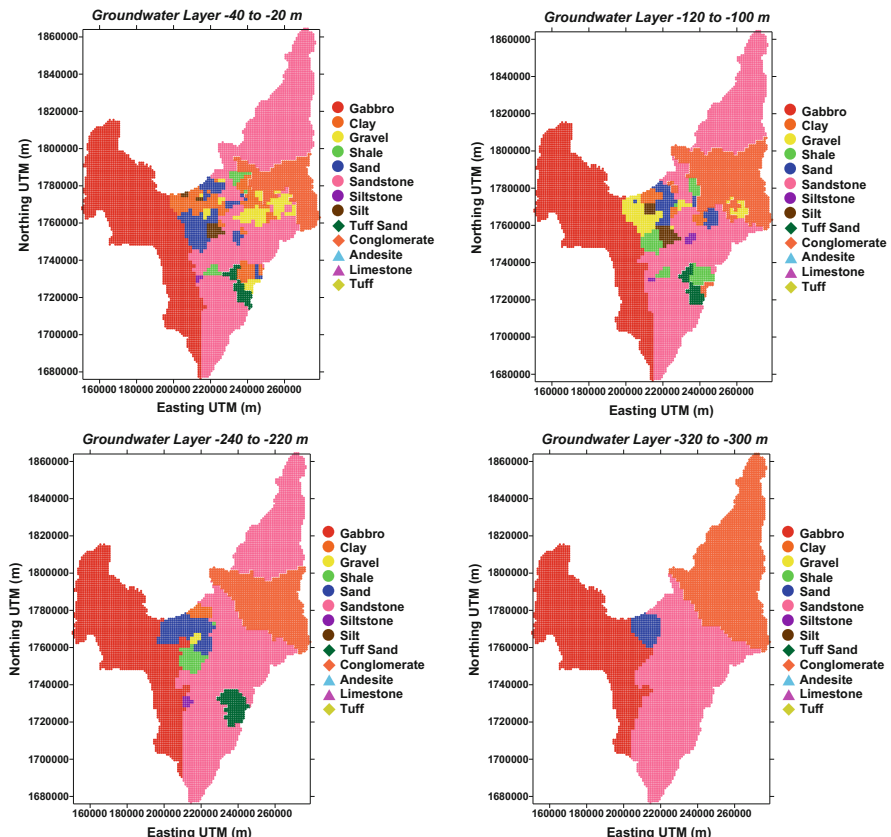
**Table 4.8** Groundwater properties for each material code used in the groundwater model

Material	Hydraulic Conductivity (m/day)	Porosity	Specific yield	Storage coefficient
Gabbro	0.0864	0.05	0.05	0.001
Clay	0.00005	0.45	0.2	0.03
Gravel	290.37	0.275	0.25	0.08
Shale	0.00005	0.05	0.05	0.01
Sand	50	0.325	0.3	0.05
Sandstone	10	0.105	0.15	0.05
Siltstone	0.000864	0.25	0.12	0.001
Silt	0.00864	0.4	0.18	0.00001
Tuffaceous sandstone	5.02	0.25	0.35	0.05
Conglomerate	14.79	0.105	0.2	0.05
Andesite	0.0864	0.05	0.01	0.001
Limestone	8.64	0.1	0.05	0.001
Tuff	9.3	0.25	0.35	0.015

Table values taken from Boulding and Ginn 2004



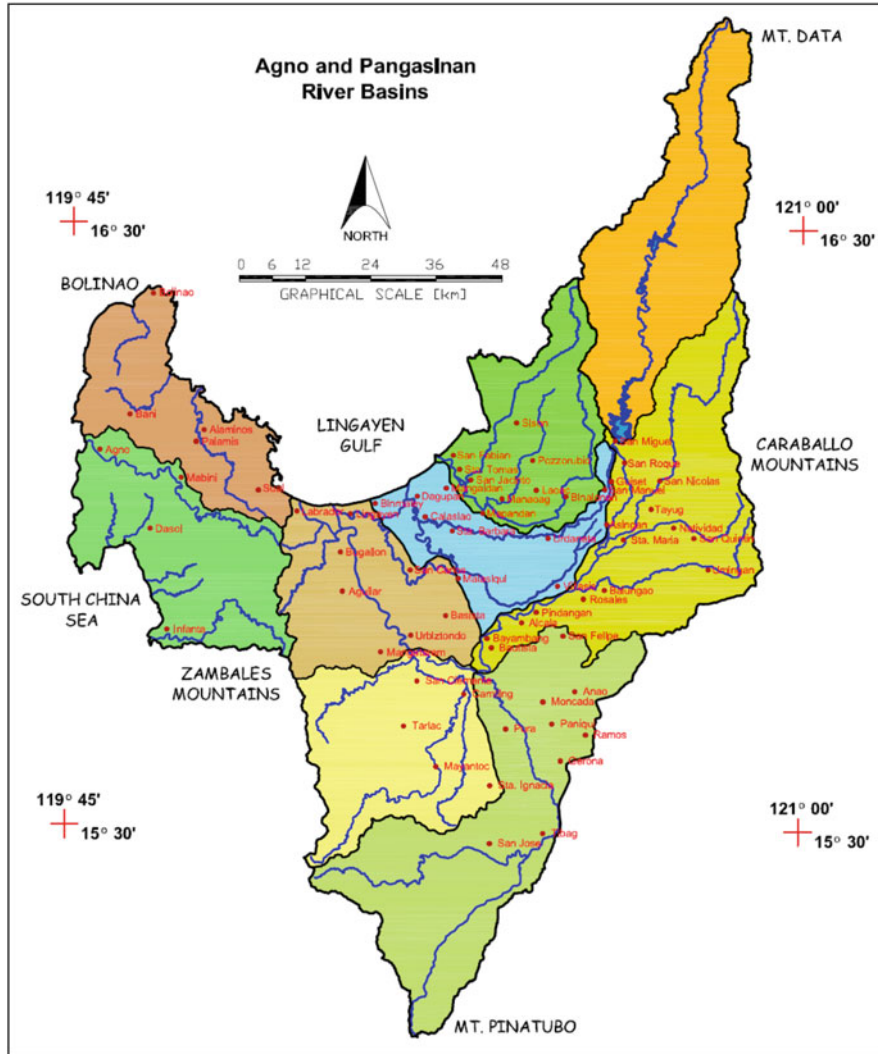
**Fig. 4.32** Maps of material codes for layers 0 to +20, +60 to +80, +120 to +140, and + 160 to +180



**Fig. 4.33** Maps of material codes for layers  $-40$  to  $-20$ ,  $-120$  to  $-100$ ,  $-240$  to  $-220$ , and  $-320$  to  $-300$

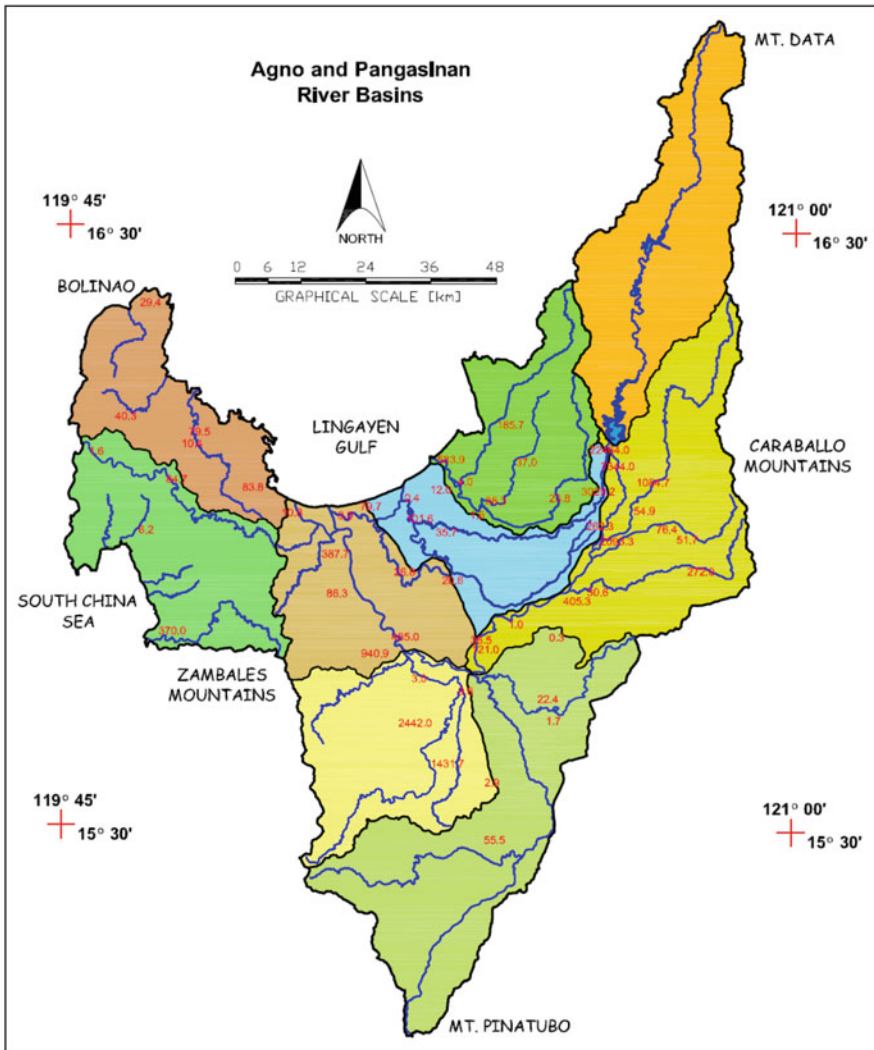
Finally, the simulation results can be used to identify and create a matrix of potential water sources for various water demand points (by cities or municipalities) as well as potential for hydropower generation.

Table 4.9 summarizes the assessment of surface water availability and projected surplus of major potential rivers within the potential sub-basins of Agno River Basin. This table specifically lists the water sources that may be potentially developed to provide the surface water demands of urban or suburban areas in the vicinity of these rivers.



**Fig. 4.34** Locations of municipalities/cities (indicated by round dots) with surface water and groundwater demands in the Agno River Basin

Tables 4.10 and 4.11 show the potential sites for hydropower generation with capacities of 5–7 MW and 10–15 MW, respectively. These power plant capacities were calculated based on mean flows as well as 80% dependable flows from these rivers.



**Fig. 4.35** Amounts granted (in MLD) in the existing surface water permits issued by NWRB

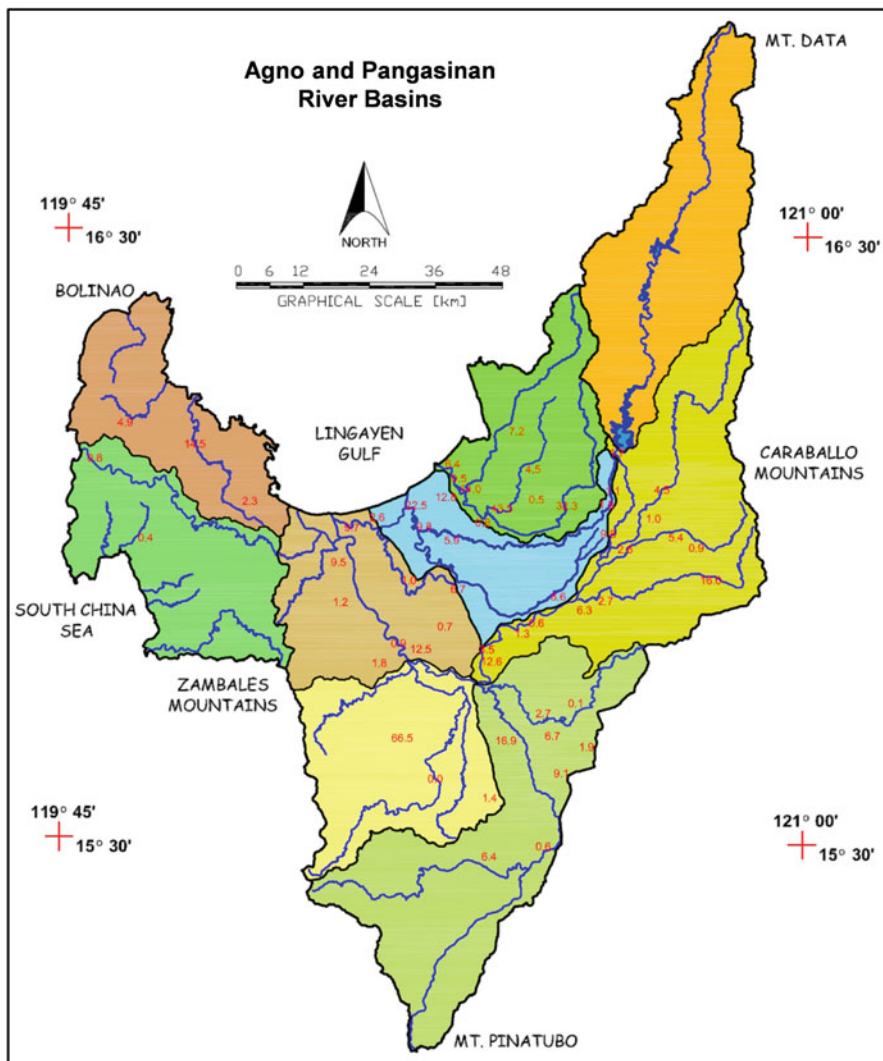


**Fig. 4.36** Amounts granted (in MLD) in the existing groundwater permits issued by NWWRB. (Data updated to 2010)

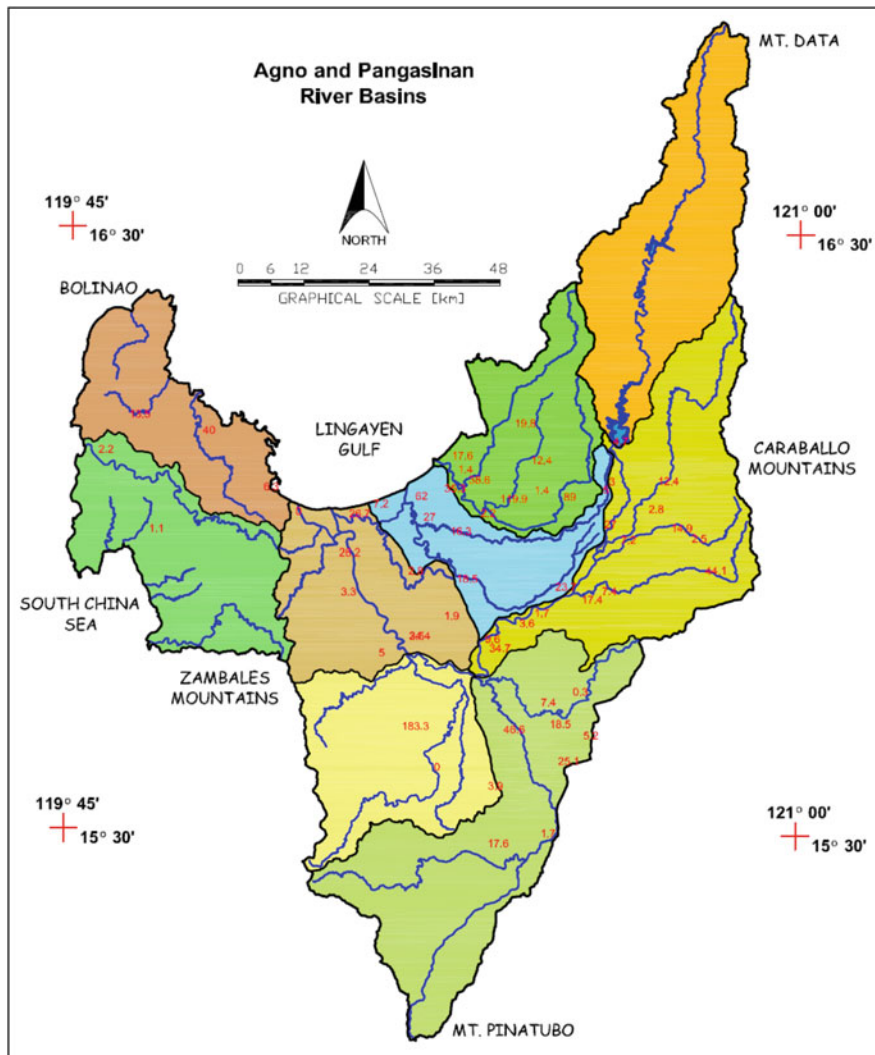


**Fig. 4.37** Projected groundwater demand (in MLD) for 2050 based on existing groundwater permits in 2010 and population projection

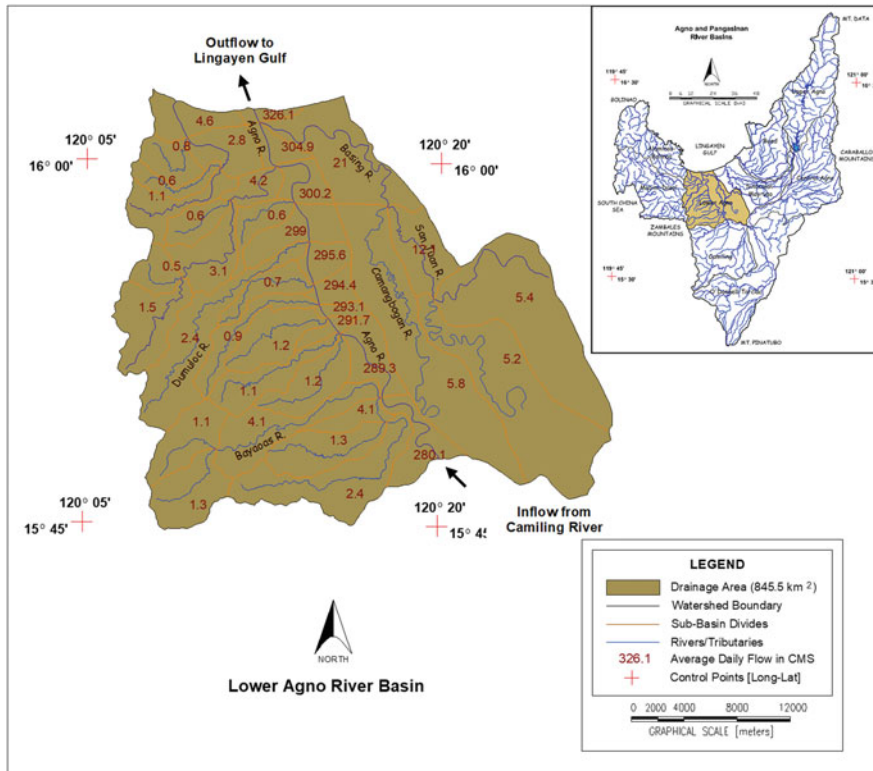


**Fig. 4.38** Long-term average daily river flows ( $\text{m}^3/\text{s}$ ) over the Lower Agno River Sub-basin

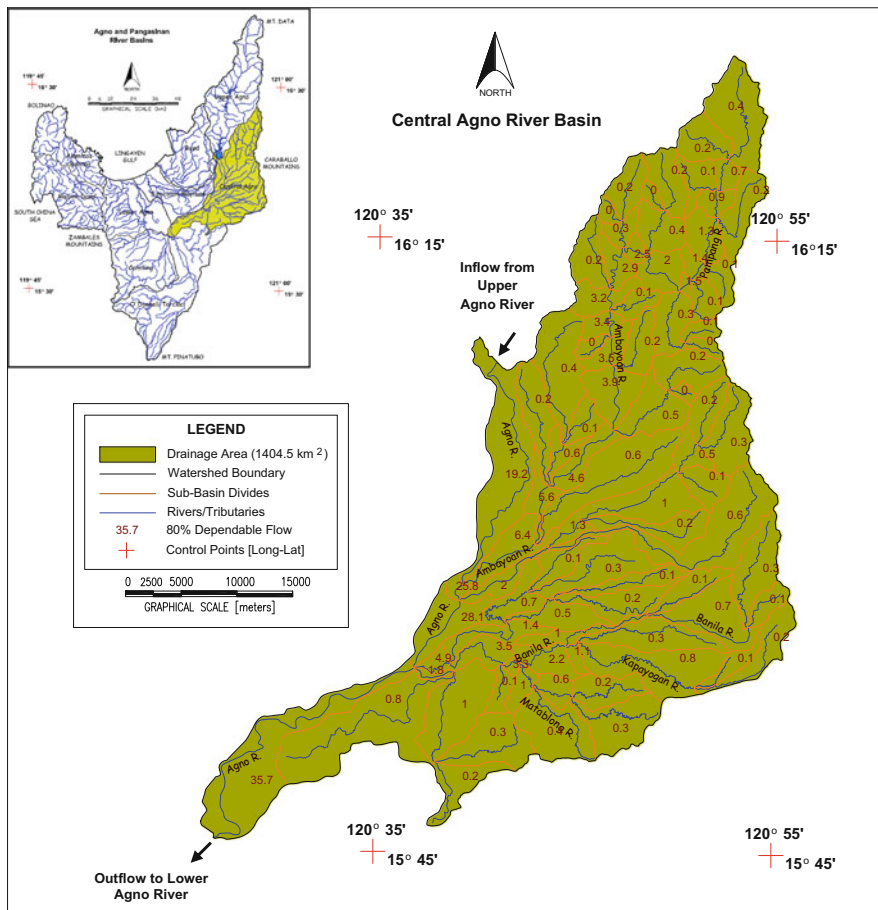


**Fig. 4.39** Long-term 80% dependable daily river flows (m<sup>3</sup>/s) over the Central Agno River Sub-basin

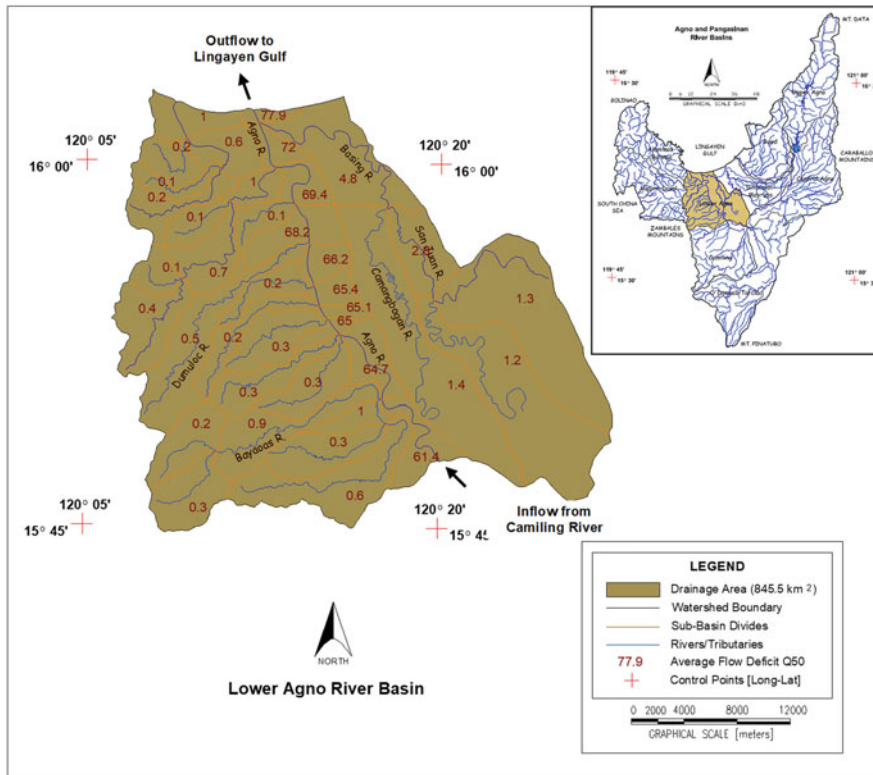


**Fig. 4.40** Average flow deficit ( $\text{m}^3/\text{s}$ ) of rivers in Lower Agno River Sub-basin by runs analysis at a demand level equal to the long-term daily mean

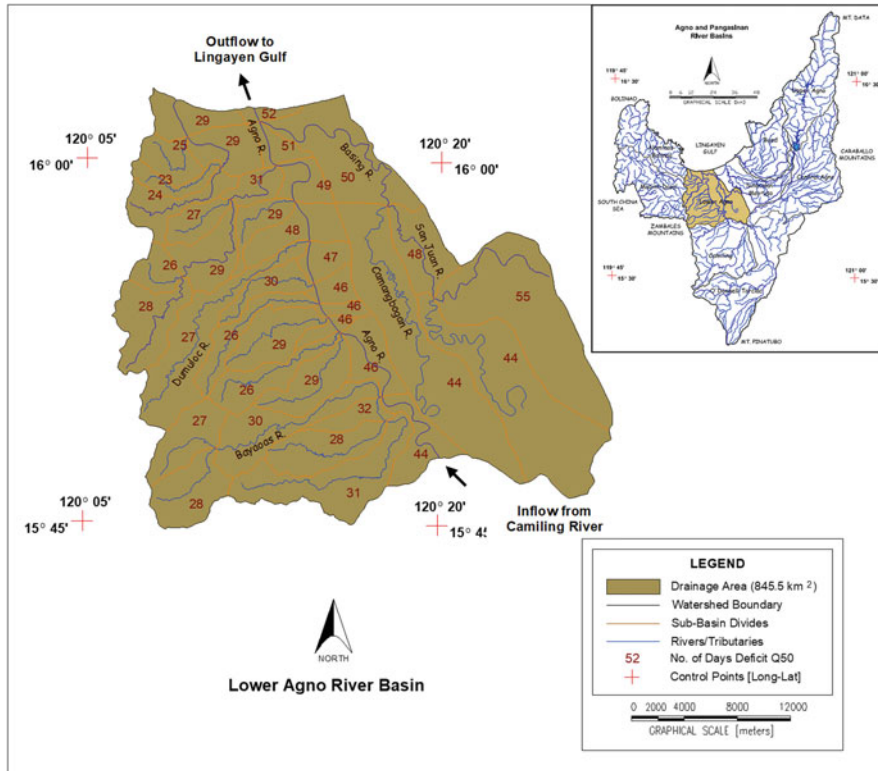


**Fig. 4.41** Average number of days in deficit for rivers in the Lower Agno River Sub-basin by runs analysis at a demand level equal to the long-term daily mean

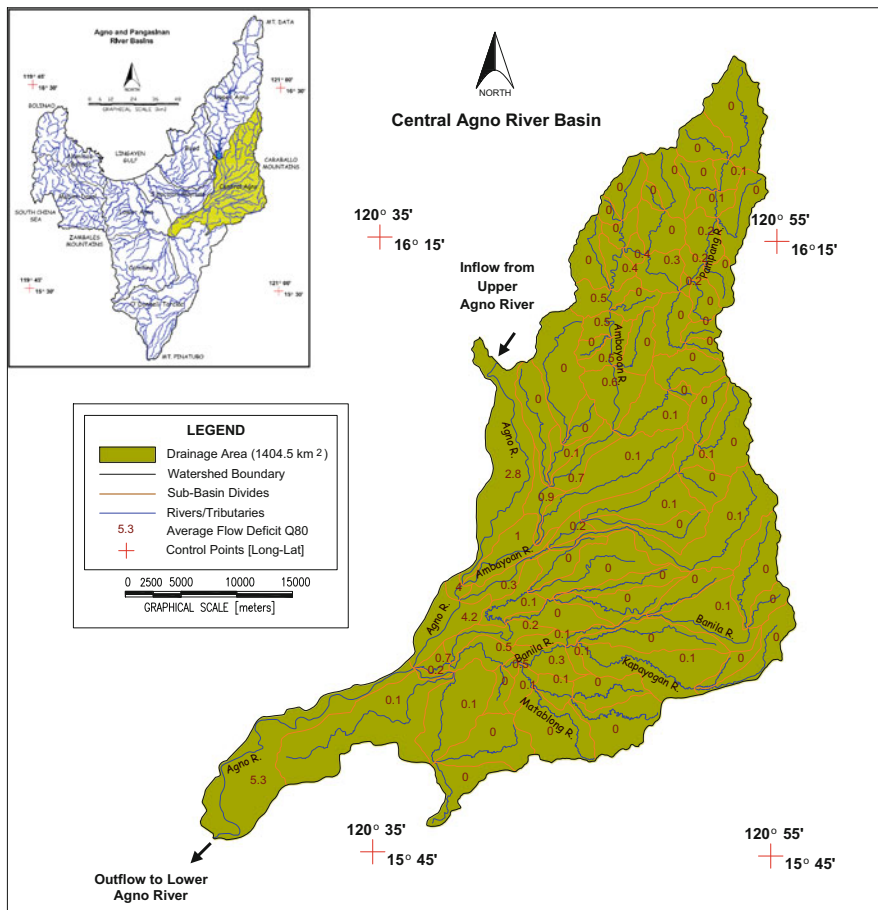


**Fig. 4.42** Average flow deficit ( $\text{m}^3/\text{s}$ ) for rivers in the Central Agno River Sub-basin by runs analysis at a demand level equal to the 80% dependable daily flow

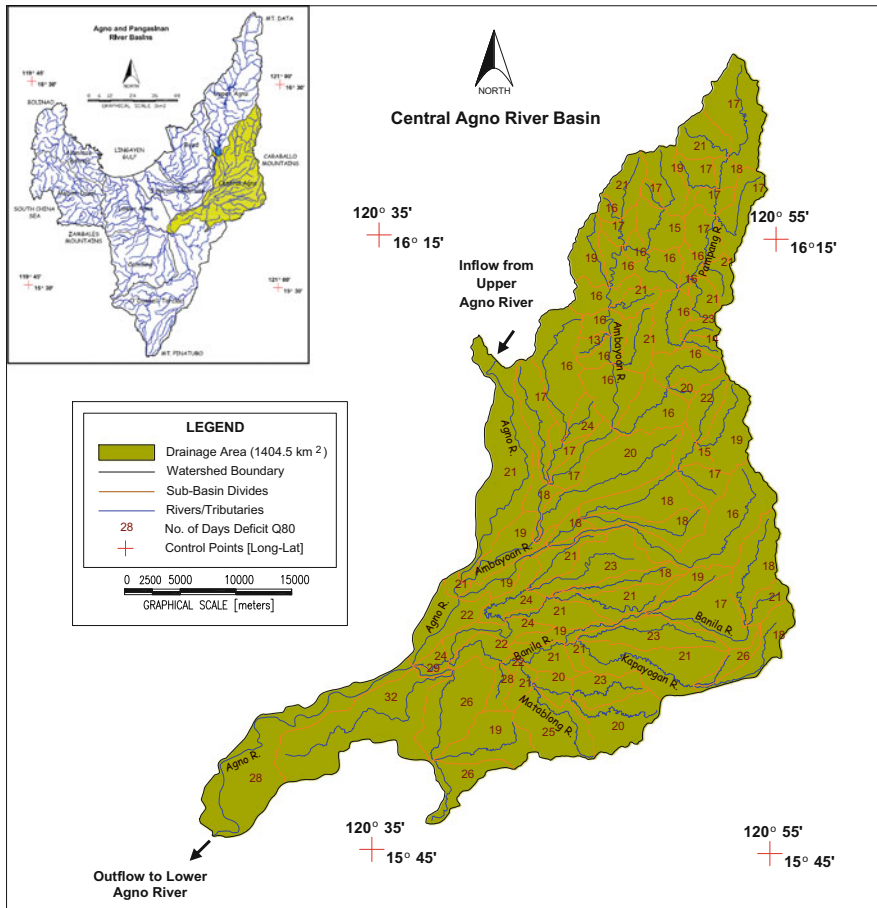


**Fig. 4.43** Average number of days in deficit for rivers in the Central Agno River Sub-basin by runs analysis at a demand level equal to the 80% dependable daily flow

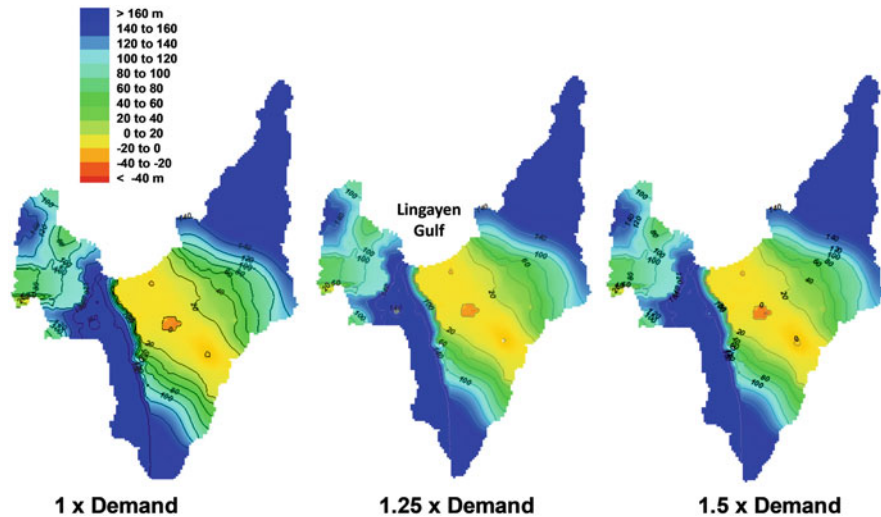


**Fig. 4.44** Groundwater heads in 2025 computed from the groundwater model with imposed base demands and the demands, 25% and 50% more than the base demand

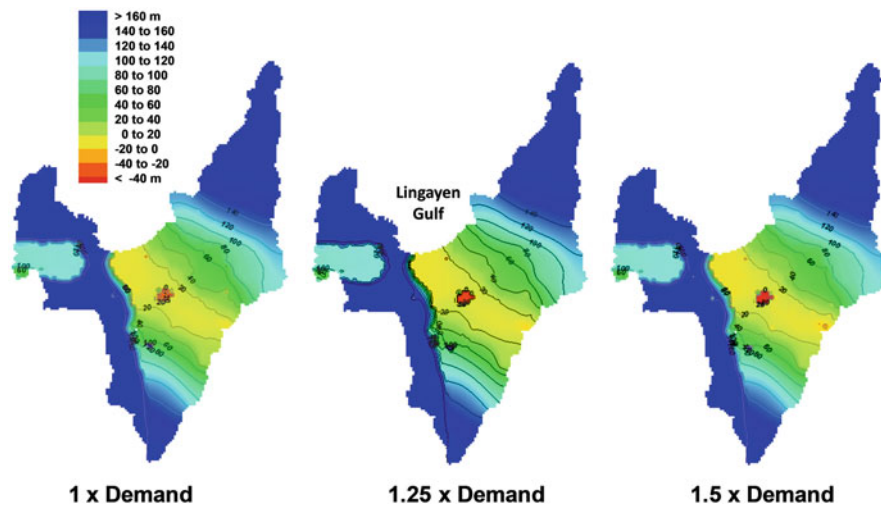


**Fig. 4.45** Groundwater heads in 2050 computed from the groundwater model with imposed base demands and the demands, 25% and 50% more than the base demand

**Table 4.9** Summary of assessment of surface water availability and projected surplus of major potential river sources within the potential sub-basins of Agno River Basin

Sub-Basin Name	Service Area Within the Sub-Basin	Possible River Source	River Coordinates		Est. Dist. from Source	80% S.W. Depend. F.	Existing SW Dem/Permit	Existing SW Available	Total Dem. 2025	Total Dem. 2050	Riv. Surplus 2025	Riv. Surplus 2050
			Longitude (dec. deg.)	Latitude (dec. deg.)	(km)	(mid)	(mid)	(mid)	(mid)	(mid)	(mid)	(mid)
O'Donnell-Tarlac	San Jose	Moriones River	120.5406	15.4560	6.5	725.8	55.5	670.3	66.5	73.2	658.2	650.9
	Tibag				5.7		0.0		1.0	1.7		
	Anao				8.4		0.0		0.1	0.1		
	Gerona				10.1		0.0		15.6	25.1		
	Moncada				2.6	527.0	22.4		26.9	29.7	468.0	446.7
	Paniqui				3.8		1.7		13.2	20.2		
	Ramos				10.4		0.0		3.2	5.2		
Sinocalan-Mayruso	Pura	Tarlac River	120.4715	15.7487	9.4	1745.3	0.0	1745.3	29.0	46.6	1716.3	1698.6
	Undaneta	Sinocalan River	120.6144	16.0030	1.0	190.1	485.0	0.0	506.4	519.5	0.0	0.0
	Bimaley	Ingaleria River	120.4515	15.9208	22.9		79.7	0.5	84.1	86.8	0.0	0.0
	Calasiao				14.7		101.6		118.3	128.6		
	Dagupan				18.4		0.4		38.8	62.3		
	Malaquique				3.9	250.8	20.6		32.1	39.2		
	Mangaldan				17.3		12.0		33.9	47.3		
	Sta. Barbara				9.7		35.7		45.8	52.0		
	Villasis				14.2		0.0		14.7	23.7		
Alaminos-Bolinao	Bani	Bani River	119.8865	16.1948	4.2		40.3	42.7	48.6	53.7	34.3	29.2
	Bolinao				20.7		29.4		29.4	29.4		
	Alaminos	Alaminos River	119.9808	16.1294	3.2		79.5	16.5	104.3	119.4	0.0	0.0
	Palamis				1.7	190.1	10.4		10.4	10.4		
	Sual				12.3		83.8		87.8	90.2		
Mabini-Dasol	Agno	Balingcaguin River	119.9476	16.0371	18.2		1.6	227.2	2.9	3.7	225.1	223.8
	Dasol				7.8	319.7	6.2		7.0	7.4		
	Mabini				4.6		84.7	0.0	84.7	84.7		
	Infanta	Nayom River	119.9352	15.8140	2.2	267.8	370.0		370.0	370.0	0.0	0.0
Camiling	San Carlos	Oro River	120.3316	15.7750	17.0		26.8	39.4	28.5	29.5	33.0	29.0
	Basisita				10.9		0.0		1.2	1.9		
	San Clemente				3.6	155.5	3.0		3.0	3.0		
	Urbiztondo				5.1		0.0		1.5	2.4		
	Aguilar				17.8		86.3		88.4	89.7		
Lower Agno	Labrador	Gueset Creek	120.2033	15.9766	8.7	95.0	10.8	83.3	10.9	10.9	66.6	56.4
	Lingayen				5.3		0.9		17.6	27.7		

**Table 4.10** Potential hydropower sites and pertinent information with capacities between 5 to 7 MW based on average daily flow (Q Average) and 80% (Q 80%) dependable daily flow

Sub-Basin Name	SSB No.	River Name	Longitude Decimal Deg.	Latitude Decimal Deg.	Elevation	Q Average	Capacity, MW	Q 80%	Capacity, MW	
Central Agno	82	Pampang River	120.8722	16.3053	1000		2.5	24.7	0.7	6.9
Upper Agno	44	Laboy River	120.6602	16.4520	1391		1.9	25.9	0.5	6.8
Camiling	232	Camiling River	120.2705	15.5470	500		5.1	24.9	1.3	6.4
Upper Agno	39	Oding Creek	120.8207	16.4197	1300		1.9	23.7	0.5	6.4
O'Donnell-Tarlac	202	Moriones River	120.4125	15.4676	100		22.5	22.1	6.3	6.2
Upper Agno	18	Batan River	120.7989	16.5845	1000		2.1	20.9	0.6	5.9
Upper Agno	26	Agisidan Creek	120.8494	16.4671	1200		1.8	20.7	0.5	5.9
O'Donnell-Tarlac	186	Moriones River	120.3259	15.4119	300		6.9	20.3	1.9	5.6
Central Agno	12	Pampang River	120.8841	16.6228	1900		1.0	19.1	0.3	5.6
Upper Agno	69	Albian Creek	120.6801	16.2695	800		2.6	20.0	0.7	5.5
Upper Agno	67	Albian Creek	120.6654	16.3099	1368		1.3	17.3	0.4	5.4
Upper Agno	8	Penetoan Creek	120.8615	16.6643	1800		1.1	18.7	0.3	5.3

**Table 4.11** Potential hydropower sites and pertinent information with capacities between 10 and 15 MW based on average daily flow (Q Average) and 80% (Q 80%) dependable daily flow

Sub-Basin Name	SSB No.	River Name	Longitude Decimal Deg.	Latitude Decimal Deg.	Elevation	Q Average	Capacity, MW	Q 80%	Capacity, MW
Central Agno	98	Pampang-Ambayoan River	120.7983	16.2419	600	9.3	54.6	2.5	14.7
Bued	337	Bued River	120.6102	16.3060	1200	4.3	51.1	1.2	14.1
Upper Agno	58	Ambalanga River	120.7064	16.3816	1000	4.9	48.1	1.4	13.7
Central Agno	106	Ambayoan River	120.7730	16.1801	400	12.7	49.7	3.4	13.3
Central Agno	104	Ambayoan River	120.7728	16.2001	400	12.0	47.0	3.2	12.6
Upper Agno	27	Bokod River	120.7989	16.4747	800	5.8	45.3	1.6	12.6
Central Agno	94	Pampang River	120.8189	16.2235	600	7.5	44.4	2.0	11.8
Upper Agno	38	Benneng River	120.7894	16.3859	900	4.6	41.0	1.3	11.5
Upper Agno	48	Laboy River	120.7186	16.4290	991	3.8	36.9	1.1	10.7
Bued	340	Bued River	120.5714	16.2849	600	6.3	37.0	1.8	10.6
O'Donnell-Tarlac	200	Moriones River	120.3897	15.4474	200	18.9	37.1	5.3	10.4
Central Agno	90	Pampang River	120.8408	16.2138	700	5.8	39.6	1.5	10.3
Central Agno	108	Ambayoan River	120.7796	16.1563	300	13.3	39.0	3.5	10.3

## References

- Boulding JR, Ginn JS (2004) Practical handbook of soil, vadose zone, and ground water contamination: assessment, prevention and remediation, 2nd edn. Lewis Publishers (CRC Press), Boca Raton
- Burnash RJC (1985) Real-time forecasting with the Sacramento watershed model. In: Proceedings of 14th annual hydrology days. Colorado State Univ., Fort Collins, pp 103–113
- Burnash RJC, Fernal RL, McGuire RA (1973) A generalized streamflow simulation system: conceptual modeling for digital computers, National Weather Service, California. Dept of Water Resources, Sacramento
- Kuester JL, Mize JH (1973) Optimization techniques with FORTRAN. McGraw Hill Book, Co., New York
- McDonald MG, Harbaugh AW (1984) A modular three-dimensional finite-difference ground-water flow model. U.S. geological survey, open-file report no. 83-875, Reston, VA, 528 p
- NHRC (National Hydraulic Research Center) (2011a) Hydro-geological assessment for the reliability of water supply Philippines: top metros (Pampanga), final report to Manila Water Company, Inc. (MWCI), May
- NHRC (National Hydraulic Research Center) (2011b) Surface water and groundwater resource evaluation for Pangasinan (Agno) river basin top metro area, final report to Manila Water Company, Inc. (MWCI), July
- Tabios GQ III, Obeysekera JTB, Salas JD (1986) National Weather Service model – PC version. Dept. of Civil Engineering, Colorado State University, Fort Collins

## Chapter 5

# Reservoir Planning and Operations Studies with Optimization-Simulation Models



**Abstract** This chapter discusses the application of combined optimization-simulation models for reservoir planning and operations studies to assess the ability and reliability of three reservoir systems to deliver water for domestic and/or irrigation water supply, hydropower generation, and possible flood control function. The three reservoir systems presented here are as follows: (1) Angat Reservoir which has a multipurpose function for domestic water supply to Metro Manila, irrigation water supply to Angat-Maasim area, hydropower generation for the Luzon electric power grid, and flood control for its downstream communities; (2) Upper Agno River Basin reservoir for hydropower generation for the Luzon power electric grid, irrigation water supply to Agno River Integrated Irrigation Project, and with significant sediment trapping storage for water quality control; and (3) proposed Agos Reservoir system as future water supply reservoir for Metro Manila. In the Agos Reservoir system, the Kaliwa Low Dam in particular has recently been approved by the national government to be constructed.

### 5.1 Angat Reservoir System

The Angat Reservoir is a multipurpose reservoir serving 90% of Metro Manila's domestic water supply needs under the Metropolitan Waterworks and Sewerage System (MWSS) and Bulacan's irrigation demand for about 25,000 hectares of riceland in the Angat-Maasim River Irrigation System (AMRIS) under the National Irrigation Administration (NIA) including hydropower generation and flood control. In view of its physical configuration and various water rights associated to its contractual water demands, the Angat Reservoir has competing water uses.

The watershed of the Angat Reservoir is the Angat River Basin (Fig. 5.1), which has a total drainage area of 546 km<sup>2</sup> upstream of the Angat Dam site located across a narrow gorge of the Angat River at Sitio Biniit, San Lorenzo, Bulacan. The Angat Dam is a rock-fill dam that is 131 m high with a road surface top at the dam crest and 630 m long that curves at a radius of 620 m. The reservoir has an active capacity of 865 million m<sup>3</sup> with absolute drawdown (dead storage) elevation at 158 m above

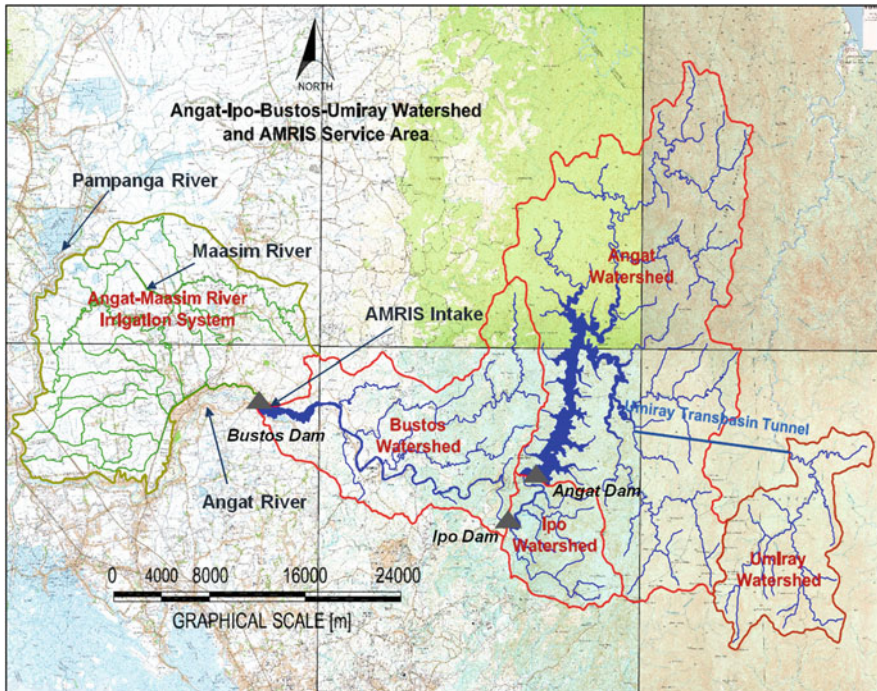


**Fig. 5.1** Watershed delineation and river network of the Angat-Ipo-Bustos-Umiray water resources system. (From Tabios and David 2014; Tabios 2018)

mean sea level (AMSL), spilling elevation at 217 m AMSL, design flood pool elevation at 219 m AMSL, and maximum (dam crest) elevation at 223.5 m AMSL.

Inflows to Angat Reservoir derived only from rainfall in the watersheds come at an annual average inflow of  $60 \text{ m}^3/\text{s}$ . Since 2001, however, inflow to the reservoir has been augmented by diverting water from the Umiray River watershed through the 13.1 km Umiray-Angat Transbasin Tunnel with carrying capacity of  $25 \text{ m}^3/\text{s}$ . The Umiray-Angat Transbasin Project is estimated to bring an average annual inflow of about  $9 \text{ m}^3/\text{s}$  to the Angat Reservoir. This brings a total of almost  $70 \text{ m}^3/\text{s}$  annual average inflow to this reservoir.

With regard to the physical configuration of the Angat Reservoir system as shown in Fig. 5.2, the main hydropower plant (HP) generation with a capacity of 200 megawatts (MW) is through releases to NIA for irrigation. The auxiliary HP generation with a capacity of 46 MW is through releases to MWSS for domestic water supply. However, twice as much power can be generated at the main HP compared with the auxiliary HP for the same flow discharge. For instance, at a reservoir elevation of 205 m, the head for power generation at the main HP is 187.5 m (i.e., 205 minus 17.5 m, tailwater elevation), while that for the auxiliary HP is 104 m (i.e., 205 minus 101 m, tailwater elevation).

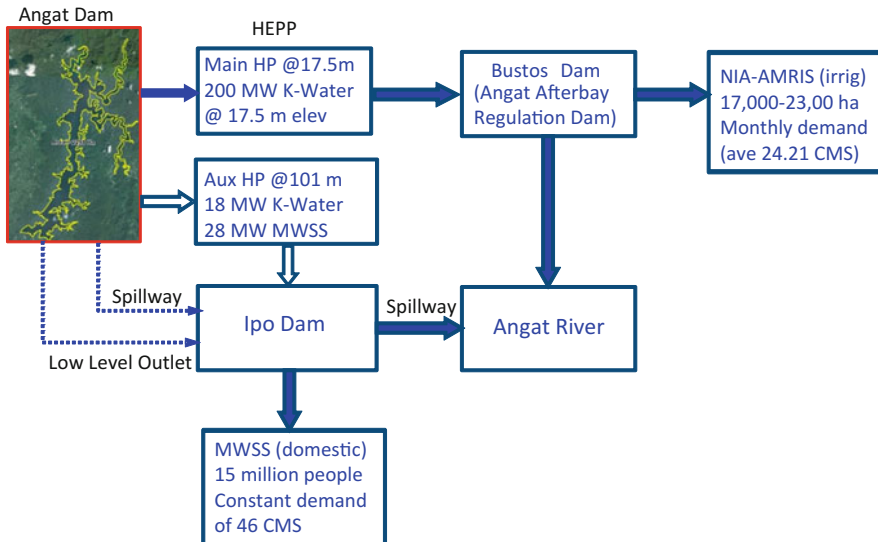


**Fig. 5.2** Physical components and water demand of the multipurpose Angat Multipurpose Reservoir System for domestic water supply, irrigation water supply, hydropower generation, and flood control. (From Tabios 2016, 2018)

With regard to NIA and MWSS water rights, originally, after Angat Dam was built in 1968, NIA had  $36 \text{ m}^3/\text{s}$  (CMS), while MWSS had 22 CMS, a total of 58 CMS, which is the amount equal to the water rights granted to the National Power Corporation to operate Angat Reservoir for its hydropower generation objectives provided that the MWSS (domestic water supply) and NIA (irrigation) water rights or allocations are satisfied on a long-term, average daily basis. The long-term average is emphasized here, because NIA has seasonal water requirements in contrast to MWSS, which is fixed on a daily basis. However, since the completion of the transbasin tunnel in 2000 to convey water from Umiray River to Angat Reservoir under the Umiray-Angat Transbasin Project (UATP), the water rights arrangement has evolved into the following: (i) MWSS water rights totaled to 46 CMS, which is the sum of the original 22 CMS plus 15 CMS referred to as conditional water rights from NIA plus 9 CMS from Umiray River; (ii) NIA-AMRIS water rights were reduced to 21 CMS, from the original 36 CMS less 15 CMS; and (iii) Bulacan bulk water rights is 3 CMS from Umiray River. The above water rights allocation is based on the long-term average inflows of the Angat and Umiray watersheds of 70 CMS.

In view of the above change in water allocation and priority, 200 MW capacity of the main HP of Angat is seldom reached, since NIA's allocation has been reduced to 21 CMS from its original 36 CMS. Also, in accordance with the Philippine Water Code, during water shortage conditions, the order of priority of water delivery from a multipurpose reservoir like Angat is to first satisfy domestic supply, followed by irrigation demand and hydropower that is incidentally generated.

### 5.1.1 Angat Reservoir Optimization-Simulation Model

Figure 5.3 shows the Angat Reservoir system with the Angat, Ipo, and Bustos watersheds and river network. For purposes of watershed modeling, the watershed system is delineated into 153 sub-basins according to basin topography, river network configuration, and slopes – considering as well the geology, soil types, vegetation, and land use. The watershed model with Sacramento soil moisture accounting model was employed in this study which is described in detail in Appendix A. This watershed model is a continuous-time, distributed model consisting of various components: rainfall input, evaporation, surface detention, infiltration, overland flow, and channel flow.

The daily rainfall record available in this study was from January 1974 to December 2012 for a total of 38 years of daily flows generated from the watershed

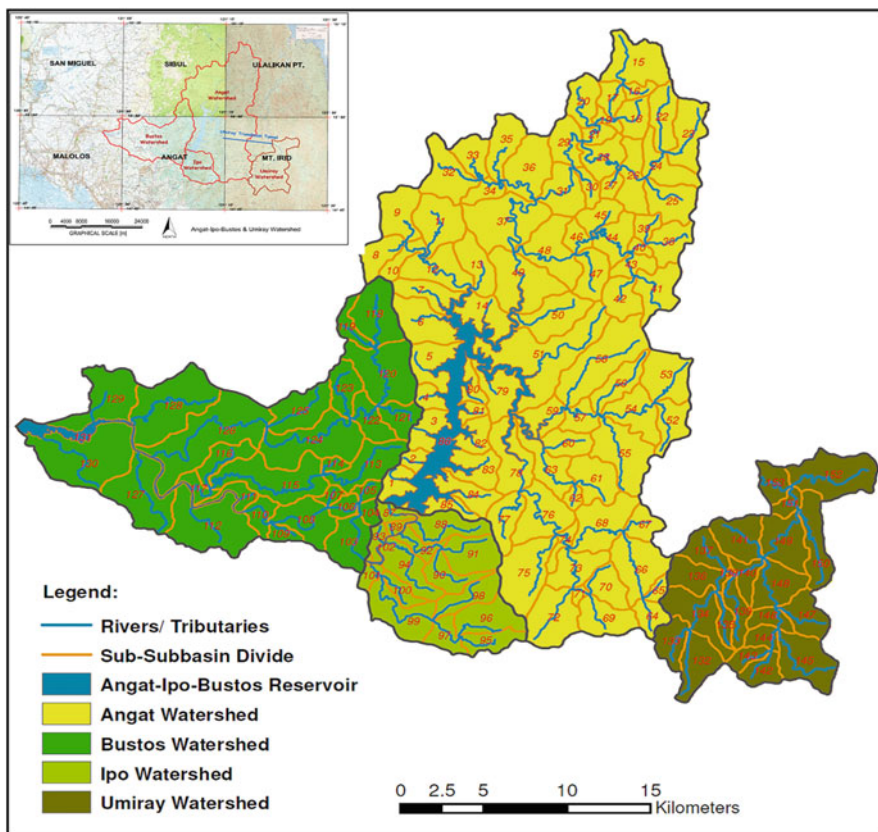


**Fig. 5.3** Watershed delineation and river network of the Angat-Ipo-Bustos-Umiray water resources system. The sub-basin numbers indicated in the figure are used in watershed modeling. (From Tabios 2016)

model to conduct the long-term simulations and reliability analysis of Angat Reservoir.

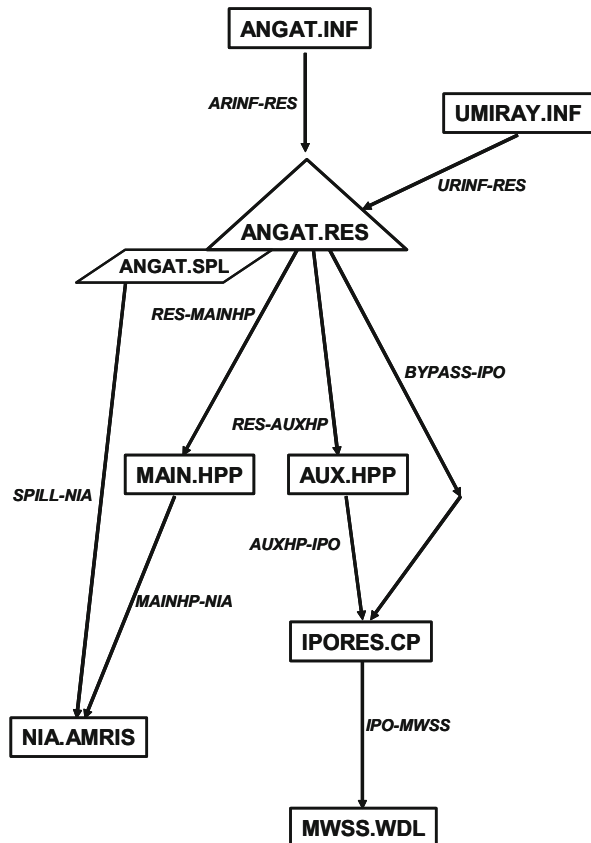
A combined optimization-simulation model was used here which is structured such that the simulation module involves the reservoir water balance computations, hydropower calculations, and other physical processes in reservoir operations, while the optimization module specifies the reservoir operating policies such as release schedules and gate openings. In some case, reservoir reliability studies are conducted by pure simulation that runs without optimization. For instance, in case of reservoir operations during normal conditions, the release rules can be specified *a priori* by employing *if-then rules*, such as given the reservoir inflow and the storage level (i.e., *if condition*), and then the releases can be calculated (i.e., *the outcome*). The resulting reservoir releases are then subjected to reliability analysis such as determining the dependable water yields through dependable flow analysis (i.e., flow duration curves). On the other hand, with combined simulation and optimization studies, the optimization model decides when and how much reservoir releases for a specified objective and constraint functions, and the simulation model calculates the resulting reservoir storages and other outflows including uncontrolled outflows for given reservoir inflows. Combined optimization-simulation is implemented in a recursive scheme where decisions are made in the optimization module and the bulk of the constraints especially systems constraints (e.g., reservoir water balance) are checked in the simulation module (Jacoby and Loucks 1972).

The WATPOW model originally developed by Tabios and Shen (1993) was used as the optimization-simulation model. This model may be used for pure simulation studies or for combined simulation optimization studies. There are three optimization procedures available in the WATPOW model, namely, (1) the constrained simplex algorithm by Box (1965) called COMPLEX, (2) incremental dynamic programming procedure, and (3) genetic algorithm. In this study, the COMPLEX optimization method is utilized since it is a fast and efficient method compared to the other techniques (Tabios 2010). The use of the COMPLEX algorithm in reservoir operations had been demonstrated by Ford et al. (1981). Further details of the WATPOW model especially the COMPLEX optimization algorithm are given in Appendix B.

Figure 5.4 shows the network representation of the Angat-Ipo-Bustos Reservoir system and components. The major physical components of this system include the inflow points, Angat River (ANGAT.INF) and Umiray River (UMIRAY.INF); the reservoirs, Angat (ANGAT.RES), Ipo (IPORES.CP), and Bustos (at NIA.AMRIS node); the main (MAIN.HPP) and auxiliary (AUX.HPP) hydropower plants; and the demands nodes, at NIA-AMRIS irrigation system for Bulacan (at NIA.AMRIS node) and MWSS of Metro Manila (at MWSS.WDL node).

The objective function of the optimization-simulation model is a weighted multi-objective to minimize water supply deficits (demand violations), maximize hydropower generation, and minimize spills. The constraints include capacities of release gates, storage volumes, operational constraints, and all other system constraints

**Fig. 5.4** Schematic of Angat-Ipo-Bustos Reservoir system indicating the nodes and links. (From Tabios 2008)



imposed implicitly in the simulation model. Specifically, the objective function to be maximized is given by (Tabios 2008):

$$F = p_{WS} \cdot \min [QWS_t - QWD_t, 0.0] + p_{IR} \cdot \min [QIR_t - QID_t, 0.0] - p_{SP} \cdot QSP_t + b_M EM_t + b_A EA_t \quad (5.1)$$

where  $QWS_t$  and  $QWD_t$  are MWSS water supply release (through the auxiliary HP) and MWSS water demand, respectively, at time  $t$  with penalty coefficient  $p_{WS}$ ;  $QIR_t$ , and  $QID_t$ , are the NIA-AMRIS irrigation release (through main HP) and irrigation demand, respectively, with penalty coefficient  $p_{IR}$ ;  $QSP_t$  is the reservoir spill with penalty coefficient  $p_{SP}$ ;  $EM_t$  is the energy generated at the main HP with benefit coefficient  $b_M$ ; and  $EA_t$  is the energy generated at the auxiliary HP with benefit coefficient  $b_A$ .

In the optimization algorithm, the anticipatory or hedging rule to account for future flow conditions is through a *moving planning horizon* or *window* of some extended period in time as done by Tabios (2008). For instance, for a 30-day

window, say in January 1 of the first year of historical data, the optimization-simulation run is performed for the next 30 days (from January 1 to January 30), and the resulting optimal release is for January 1 only. Then, proceed to January 2 for the 30-day window (from January 2 to January 31) to determine the optimal reservoir release for January 2. This procedure is continued until the end of the historical data, say December 2 of the last year of data, and then the optimal release for this date is based on the 30-day window from December 2 to December 31. Note that using the historical data in reservoir operations studies, perfect future inflow forecast is assumed. If this is done in real time, then actual inflow forecast should be made and entered as input into the model.

The major constraint function imposed in the Angat Reservoir operations study is the hard system constraint described by the reservoir water balance computations, maximum flow capacities of controlled releases, and the flood control storage requirement. Note that the water supply and irrigation demand violations as well as spillway flows are imposed as soft constraints incorporated in the objective function as penalty functions.

### **5.1.2 Optimization-Simulation Scenarios**

The optimization-simulation studies were conducted for two scenarios as follows: (a) existing case or conditions with 46 CMS MWSS demand and (b) with increased MWSS demand from 46 to 50 CMS. The first scenario, referred to as existing MWSS demand at 46 CMS, provides the MWSS domestic water supply demand at 46 CMS, while the NIA-AMRIS irrigation water demand varies from month-to-month. The second is referred to as scenario with increased MWSS demand at 50 CMS with the same monthly irrigation water demand for NIA-AMRIS imposed as done in the first scenario.

### **5.1.3 Results of Optimization-Simulation Studies**

Prior to the optimization-simulation studies, several trial runs were initially made to arrive at some reasonable values of the penalty and benefit coefficients in the objective function in Eq. (5.1). Ideally, the coefficients adapted in the equation should reflect the fact that domestic water supply has priority over irrigation water supply. However, in Eq. (5.1), the penalty coefficients used are:  $p_{WS} = p_{IR} = 20$ ,  $p_{SP} = 50$ , and the benefit coefficient  $b_M = b_A = 5.0$ .

The anticipatory or hedging rule is through a moving planning horizon scheme with a 30-day window. With 38 years of daily streamflow generated (January 1974 to December 2012) from the watershed model, the optimization-simulation model runs were conducted to determine the reservoir releases and associated hydropower generation. Then the flow duration curves (as the basis of reliability analysis) were

calculated on a monthly basis by pooling all the daily reservoir releases and hydropower generated by month. For the two optimization-simulation scenarios, the flow duration curves are given in Table 5.1 for Angat Reservoir releases to Ipo Dam and Bustos Dam, while Table 5.2 shows the power duration curves for the auxiliary and main hydropower plants. Note that HP generations are based on 10 hours a day of operation, so that the power generated (in MW) may be more than the actual installed capacities of these plants.

Comparing the results of scenario (a) with 46 CMS MWSS demand and scenario (b) with 50 CMS MWSS demand, generally, at higher MWSS water demand, the reliability (in terms of percent-of-time water deliveries) of the NIA-AMRIS water releases is lower. This is expected, since the MWSS water deliveries are given priority, especially during dry-year periods, when the Angat Reservoir elevations go below 180 m, an imposed operating rule in the model. At 46 CMS MWSS water demand, the reliability of water deliveries is 80 percent-of-time for the months of January and June through December but only 60 percent-of-time during the dry months of February through May. At 60 percent-of-time, it can be expected that the reservoir release to MWSS (through Ipo Dam) is greater than or equal to 46 CMS, 220 days a year, on the average and in the long term. At 50 CMS MWSS water demand, the reliability generally becomes lower but with only a relatively small decrease compared with the existing case with 46 CMS MWSS water demand, especially during the dry months of February to May, which is only expected with the 5.0 CMS increase in MWSS water demand. It may be mentioned that the 46 CMS, as natural Angat River flows at the Angat Reservoir damsite (assuming no reservoir), is only about 40 percent-of-time such that the natural river flows can be expected only to be equal to or greater than 46 CMS about 146 days a year. Obviously, the value of having the Angat Reservoir is to increase the reliability of the water availability for a particular water demand.

Finally, the competing water uses of the Angat Reservoir for domestic water supply and irrigation demand may actually be constrained due to the physical configuration of the system and also because of changes in increased water allocation and prioritization of domestic water supply over irrigation water supply in recent years. This has subsequently compromised hydropower generation, which may be unfavorable to the recent privatization of the hydropower asset. On the other hand, irrigation water demand has actually been reduced due to urbanization (conversion of rice fields to residential/commercial lands) as well as the seasonal flooding in the NIA-AMRIS area, thus leading to the transfer of 15 CMS of conditional water rights from NIA to MWSS due to unused NIA water rights (demand). But in any case, for Metro Manila, the increasing domestic water demand cannot be addressed by the Angat Reservoir alone, thus the need for a different water source for redundant water security purposes beyond the Angat Reservoir.

In Section 10.2, Chapter 10, optimization-simulation studies of Angat Reservoir with climate change and future reservoir sedimentation are also presented.

**Table 5.1** Angat Reservoir daily flow releases to Ipo Dam for MWSS domestic water supply and to Bustos Dam for NIA-AMRIS irrigation water for the two optimization-simulation model scenarios: (1) with MWSS demand of 46 CMS and (2) with MWSS demand of 50 CMS

Month	Percent of time	<i>Angat releases (CMS) to:</i>			
		<i>Ipo Dam</i>		<i>Bustos Dam</i>	
		46 CMS MWSS Dem	50 CMS MWSS Dem	46 CMS MWSS Dem	50 CMS MWSS Dem
Jan	80	46.00	47.36	36.00	34.42
	60	46.00	50.00	36.00	36.00
	40	46.00	50.00	45.98	49.85
Feb	80	<b>29.77</b>	<b>23.79</b>	<b>27.49</b>	<b>20.50</b>
	60	46.00	47.72	39.82	34.97
	40	46.00	50.00	39.86	39.86
Mar	80	<b>5.70</b>	<b>3.79</b>	<b>1.31</b>	<b>0.08</b>
	60	<b>36.70</b>	<b>30.51</b>	<b>22.07</b>	<b>15.50</b>
	40	46.00	50.00	31.00	31.00
Apr	80	<b>4.09</b>	<b>3.74</b>	<b>0.00</b>	<b>0.00</b>
	60	<b>19.43</b>	<b>12.80</b>	<b>0.00</b>	<b>0.00</b>
	40	46.00	50.00	15.50	15.50
May	80	<b>14.38</b>	<b>13.49</b>	0.00	0.00
	60	<b>46.00</b>	<b>50.00</b>	0.00	0.00
	40	46.00	50.00	0.00	0.00
Jun	80	46.00	50.00	27.90	27.90
	60	46.00	50.00	27.90	27.90
	40	46.00	50.00	27.90	27.90
July	80	46.00	50.00	28.00	28.00
	60	46.00	50.00	28.00	28.00
	40	46.00	50.00	28.00	28.00
Aug	80	46.00	50.00	25.00	25.00
	60	46.00	50.00	25.00	25.00
	40	46.00	50.00	25.00	25.00
Sep	80	46.00	50.00	22.73	22.73
	60	46.00	50.00	22.73	22.73
	40	46.00	50.00	22.73	22.73
Oct	80	46.00	50.00	13.00	13.00
	60	46.00	50.00	13.00	13.00
	40	46.00	50.00	13.00	13.00
Nov	80	46.00	50.00	17.57	17.57
	60	46.00	50.00	17.57	17.57
	40	46.00	50.00	17.57	17.57
Dec	80	46.00	50.00	36.00	36.00
	60	46.00	50.00	36.00	36.00
	40	46.00	50.00	45.99	49.99

Written in italic bold are cases that did not meet water demand

**Table 5.2** Auxiliary and main hydropower plant generation from Angat Reservoir daily flow releases for the two optimization-simulation model scenarios: (1) with MWSS demand of 46 CMS and (2) with MWSS demand of 50 CMS

Month	Percent of time	<i>Angat hydropower generation (MW)</i>			
		<i>Auxiliary hydropower plant</i>		<i>Main hydropower plant</i>	
		46 CMS MWSS Dem	50 CMS MWSS Dem	46 CMS MWSS Dem	50 CMS MWSS Dem
Jan	80	81.77	75.28	129.98	116.44
	60	91.79	95.21	146.78	140.71
	40	101.56	107.51	169.36	178.04
Feb	80	43.31	32.59	89.13	65.42
	60	79.17	74.44	137.13	117.75
	40	94.55	97.79	158.87	152.89
Mar	80	7.05	4.69	3.95	0.25
	60	50.89	40.21	70.04	50.85
	40	84.51	86.96	112.89	105.78
Apr	80	5.06	4.63	0.00	0.00
	60	24.04	15.84	0.00	0.00
	40	71.52	69.76	55.29	52.65
May	80	17.79	16.70	0.00	0.00
	60	58.31	62.58	0.00	0.00
	40	68.17	68.51	0.00	0.00
Jun	80	60.09	63.22	86.25	84.86
	60	68.52	70.26	93.41	89.17
	40	76.61	77.53	102.36	95.39
July	80	64.91	67.07	89.00	86.73
	60	76.76	79.61	100.26	96.28
	40	86.33	89.56	109.21	103.96
Aug	80	82.21	85.81	89.29	87.33
	60	89.55	93.88	94.11	92.18
	40	95.46	100.53	99.88	96.77
Sep	80	90.72	93.48	84.47	82.13
	60	95.69	100.12	88.06	86.69
	40	103.18	108.37	92.59	92.15
Oct	80	94.44	98.57	50.26	49.12
	60	101.26	105.60	52.54	51.64
	40	106.39	111.69	54.78	54.78
Nov	80	95.43	99.75	69.94	67.96
	60	103.40	108.13	73.47	72.27
	40	109.57	116.61	74.14	74.14
Dec	80	91.90	94.81	141.77	136.67
	60	100.12	105.31	151.74	148.81
	40	106.75	114.02	178.57	186.47

## 5.2 Angat Reservoir Monthly Allocation with Optimization-Simulation Model and Autoregressive Model to Forecast Inflows

In the actual operations of multipurpose Angat Reservoir, there is a technical working group (TWG) that decides on the monthly reservoir releases for domestic water supply and irrigation and the hydropower generation (i.e., implicitly since water supply releases pass through the turbines). The TWG is composed of personnel from MWSS (with MWCI and MWSI water concessionaires of Metro Manila) for domestic water supply use to Metro Manila, NIA for irrigation water use to AMRIS-Maasim, NAPOCOR for hydropower purposes, PAGASA for the climate outlook, and NWRB as chair. Basically, the TWG determines the domestic water supply and irrigation reservoir releases for the coming month (subject to the approval of the NWRB Board of Directors). Essentially the next month's reservoir release is determined based on storage rule curve over the next 6 months as planning horizon together with forecasts of monthly reservoir inflows.

With regard to the storage rule curves, they were developed based on historical hydrology and past experiences with the system. Unfortunately, these rule curves have not been updated for several years. Thus, this reservoir release policy is not adaptive and could be myopic since it only considers current reservoir levels and that any foresight or hedging is assumed to be captured in these end-of-month reservoir level targets. A more dynamic as well as anticipatory release policy can be developed for Angat Reservoir operations using an optimization-simulation model to determine the reservoir releases for say the next 6 months based on current reservoir levels and forecasted future inflows. Hedging or foresight in this case is accounted for by optimally determining reservoir releases to satisfy the various water demands over the 6-month window or planning horizon.

In making the monthly reservoir inflow forecast, there is an element of arbitrariness since the Angat Reservoir TWG does not use a parametric forecast model (e.g., autoregressive-moving average time series model of Box-Jenkins type) is used. Basically, inflows are forecasted as product of the long-term average monthly inflows of the reservoir and monthly factors (percentages that could be above or below the long-term average flows) provided by the PAGASA member of the TWG, based on the climate outlook and subsequent rainfall forecasts considering the Pacific Equatorial Index (i.e., El Nino, Neutral, or La Nina year). In some cases, the TWG members adjust the inflow forecasts based on their familiarity and experiences of the microclimate and local weather in the area.

In view of the above, this section presents another application of the optimization-simulation model for Angat Reservoir operations presented earlier and the use of a forecasting model using an autoregressive monthly time series model for monthly water allocation and operations studies as reported by Tabios (2008). A comparison of the performance of this reservoir operation with an optimization-simulation model and the existing rule curve including a proposed one is also presented using 58 years of historical Angat monthly inflow data. An application of this optimization-

simulation model for water allocation of Angat Reservoir with forecasted inflows is also presented here. It is strongly advocated and recommended that a dynamic, anticipatory reservoir operating strategy using an optimization-simulation model with reservoir inflow forecast methodology be used in actual, real-time reservoir operations instead of the rule curve-based reservoir operations procedure in Angat Reservoir.

### **5.2.1 Existing Release Policy Using Storage Rule Curve**

The existing Angat Reservoir release policy is based on the storage rule curve defined by the upper rule curve when the reservoir water level is at 212 m during the dry season (November to April) or 210 m during the wet season (May to October) and by a monthly varying lower rule curve with an ideally *minimum storage* equivalent to the reservoir level at 180 m. Based on these storage rule curves, the reservoir releases are made such that (1) when the water level is above the upper rule curve, all domestic water supply and irrigation water demands including instream river flow requirements are satisfied and power is generated at the capacity of the hydropower plants; (2) when the water level is between the upper and lower rule curves, all domestic water supply and irrigation water demands are satisfied; however, power generation is limited to the releases made for domestic water supply and irrigation water; and (3) when the water level is below the minimum lower rule curve, domestic water supply is satisfied first by whatever water is available in the reservoir, and that power generation is limited to the releases made through the auxiliary hydropower plants.

The monthly varying lower rule curve is designed for hedging purposes to avoid demand shortages or for some anticipated, more beneficial use of water in the future. Essentially, the lower storage rule curve are end-of-month target storages with the ideally minimum storage at the reservoir level of 180 m. As a policy, the monthly reservoir releases should not result in a reservoir storage below the desirable, end-of-month target storages. During critical periods (declared by PAGASA as dry or drought period), however, the reservoir storage is allowed to go below the *minimum* lower rule curve at 180 m down to the reservoir dead storage at elevation 160 m. Note that the upper rule curve is on monthly basis to relax or lower the flood control storage (elevation) requirement during the dry months of the year. Lately, there is a new storage rule curve (i.e., upper and target storages) proposed by the technical working group of Angat Reservoir to improve reservoir operations. Further discussion is needed to revise the minimum lower rule curve at 180 m in the light of the results given in Section 10.2.3, Chapter 10 on Angat Reservoir operations considering reservoir sedimentation.

### 5.2.2 *Reservoir Optimization-Simulation Model*

Reservoir reliability studies can be conducted by simulation studies alone. In the case of normal reservoir operations, for instance, the reservoir release rules must be specified a priori defined by *what-if-then* rules in the simulation model, so that given the long sequences of watershed inflows as input to the model, the reservoir releases can be calculated. The resulting reservoir releases are then subjected to statistical analysis to determine the reliability and dependability of the reservoir to satisfy its contractual water deliveries. On the other hand, with combined simulation and optimization studies, the optimization model decides amounts and timing of reservoir releases for a specified objective and constraint functions, and then the simulation model performs the reservoir water balance computations to determine the ending reservoir storages, the outflows including uncontrolled outflows for given reservoir inflows, and the calculation reverts to the optimization model to check if the objective function is satisfied and constraints are not violated.

In this section, the Angat optimization-simulation model presented in Section 5.1 was used here but for monthly (instead of daily) reservoir water allocation. The river and reservoir network system of Angat Reservoir were shown earlier in Fig. 5.4. Likewise, the objective function and constraints are the same as those described in Sect. 5.1.1. Presented below are two optimization-simulation runs with historical inflows and with forecasted inflows. In the case with forecasted inflows, the forecasting model is presented first followed by the optimization-simulation runs.

### 5.2.3 *Optimization-Simulation Runs with Historical Inflows*

For this optimization-simulation studies, several trial runs were made to arrive at some reasonable penalty and benefit coefficients in the objective function in Eq. (5.1). From these trials, four cases, referred to as OS1, OS2, OS3, and OS4, were selected in particular as shown in Table 5.3. In this study, the anticipatory or hedging operating rule is through the moving planning horizon scheme with a 6-month window. Note that a different set of penalty and benefit coefficients are used here from those in Sect. 5.1.3 which were used for daily optimization-simulation studies of Angat Reservoir.

**Table 5.3** Penalty coefficients for MWSS demand violations, NIA demand violations, reservoir spills, as well as hydropower generator benefit coefficient applied in the objective function for four optimization-simulation (OS) cases

Cases	Penalty coefficient for MWSS demand violations	Penalty coefficient for NIA demand violations	Penalty coefficient for spills	Hydropower generator benefit coefficient
OS1	100	10	10	4000
OS2	100	50	10	4000
OS3	100	100	10	4000
OS4	50	100	10	4000

**Table 5.4** Results of optimization-simulation runs (OS cases) for 58 years (1946–1963, 1968–2007) of historical data in terms of MWSS demand violations, NIA demand violations, and hydropower generation for various runs (cases). Also given are results for the pure simulation with existing rule curve-based (ERC case) and proposed rule curve-based (PRC case) operating procedures

Cases	MWSS demand violations		NIA demand violations		Overall monthly average surplus (TCM)		Annual energy generation GWH		
	Total months	Overall monthly average (TCM)	Total months	Overall monthly average (TCM)	MWSS	NIA	Aux HPP	Main HPP	Total
<b>Optimization-simulation cases</b>									
OS1	9	-28996	154	-51400	0	38131	326.1	300.9	626.9
OS2	9	-29411	166	-46649	0	36430	327.3	300.1	627.4
OS3	131	-32306	129	-25193	0	33800	313.5	318.5	632.0
OS4	180	-32170	48	-29302	0	30287	308.8	328.5	637.3
<b>Existing rule curve cases</b>									
ERC1	5	-21806	325	-44739	0	30573	332.1	226.9	559.0
ERC2	148	-32002	276	-39197	0	29110	317.0	251.0	568.0
<b>Proposed rule curve cases</b>									
PRC1	6	-22973	271	-43771	0	27511	327.3	236.4	563.7
PRC2	115	-34763	242	-38160	0	26464	315.9	256.4	572.3

The results of the optimization-simulation studies based on 58 years of monthly Angat River inflow (1946–1963 and 1968–2007) are summarized in Table 5.4. Umiray River inflows taken equal to the 12 monthly means so that these 12 values are recycled over the 58 years simulation period since only 5 years of historical data are available (2001–2005). Also shown are the results of reservoir operations based on existing rule curve as well as proposed rule curve procedures employed in the Angat Reservoir monthly water allocation to various uses. In the existing and proposed rule curve procedures, cases ERC1 and PRC1, the amount of MWSS reservoir release can be as large as possible to satisfy the MWSS demand and constrained only to reservoir dead storage elevation at 160 m, while the NIA release (after the MWSS demand is satisfied) is constrained such that the resulting end-of-month reservoir storage elevation does not go below the specified lower rule curve storage elevation for that month. In cases ERC2 and PRC2, both the MWSS and NIA reservoir releases are constrained such that the resulting end-of-month reservoir elevation does not go below the specified lower rule curve.

In Table 5.4, under optimization-simulation cases, case OS1 resulted in the least MWSS demand violations of 6 months with 152 NIA demand violations out of a total of 696 months optimization-simulation period. However, in case OS4 when the NIA demand was given more importance (i.e., the NIA and MWSS penalty coefficients are set to 100 and 50, respectively), it resulted in the least NIA demand violations of 43 months but with 186 months of MWSS demand violations. In terms of MWSS demand violations, the existing rule curve case ERC1 resulted in 5 months

demand violations, and the proposed rule curve case PRC1 resulted in 6 months demand violations, both of which are comparable to cases OS1 and OS2 with nine demand violations. On the other hand, the NIA demand violations in ERC1 and PRC1 cases resulted in 325 and 271 months in violations, respectively, which are twice as much as cases OS1 and OS2 with only 154 and 166 violations, respectively.

Another demand violation statistics is the resulting overall monthly average demand deficits. Case ERC1 resulted in the lowest MWSS average demand deficit of 21,806 TCM ( $1000\text{ m}^3$ ) with NIA average demand deficit of 44,739 TCM. These values may be compared to cases OS1 and OS2 with MWSS average demand deficits of 28,996 and 29,411 TCM, respectively, with corresponding NIA average demand deficits of 51,400 and 46,649 TCM, respectively. Note that a 31-day month, the MWSS demand is about 123,206 TCM or  $46\text{ m}^3/\text{s}$ , and largest NIA demand is 96,422 TCM. The average demand deficit statistics among the different cases may not be comparable since they are tied down to the absolute count or total number of months of demand violations.

In terms of hydropower generation, Table 5.4 shows that both the optimization-simulation cases OS1 and OS2 resulted in annual energy generation of about 627 GWH compared to the existing and proposed rule curve cases ERC1 and PRC1 of 559 and 563 GWH, respectively. Cases OS3 and OS4 resulted in even higher generation of 632 and 637 GWH, respectively, compared to all cases. The optimization-simulation cases OS1 and OS2 in particular resulted in about 65 GWH more energy generation annually compared to the existing and proposed rule curve cases ERC1 and PRC1. The existing and proposed rule curve cases ERC2 and PRC2 resulted in higher annual energy generation of 568 and 572 GWH, respectively, higher by about 10 GWH compared to cases ERC1 and PRC1.

Generally, these results show a significant improvement in Angat Reservoir water and power yields with the optimization-simulation model compared to the existing or proposed rule curve procedures.

#### 5.2.4 *Optimization-Simulation Runs with Forecasted Inflows*

With data only available up to the end of April 2008 (when this study was conducted by Tabios 2008), the optimization-simulation model including the existing and proposed rule curve schemes was used for 6-month ahead monthly water allocation of Angat Reservoir to various uses. In this case, the Angat River flows are forecasted flows from May to October 2008. As before, the Umiray River flows are recycled mean monthly flows based on 2001–2005 data. The first-order and second-order Box-Jenkins autoregressive models are tried as candidate models to be used in forecasting the Angat River inflows but not the Umiray River flows. These two models are formulated with seasonal (monthly) parameters, referred to as SAR(1) and SAR(2) as follows (Tabios 2008):

**SAR(1) model:**

$$Q_{y,m} = \bar{Q}_m + [\varphi_{1,m}(Q_{y,m-1} - \bar{Q}_{m-1})/S_{m-1} + \varepsilon_{y,m}]S_m \quad (5.2)$$

**SAR(2) model:**

$$Q_{y,m} = \bar{Q}_m + [\varphi_{1,m}(Q_{y,m-1} - \bar{Q}_{m-1})/S_{m-1} + \varphi_{2,m}(Q_{y,m-2} - \bar{Q}_{m-2})/S_{m-2} + \varepsilon_{y,m}]S_m \quad (5.3)$$

where  $Q_{y,m}$  is the monthly flow at year  $y$  and month  $m$  with associated mean  $\bar{Q}_m$  and standard deviation  $S_m = \sqrt{\text{Var}(Q_m)}$ ,  $\varphi_{1,m}$  and  $\varphi_{2,m}$  are first- and second-order autoregressive parameters, and  $\varepsilon_{y,m}$  is the error term. The model parameters are estimated via sequential parameter estimation method so that as new observations become available, the model parameters can be updated. With this sequential estimation technique, implementing the seasonal model for forecasting variables in real time is efficient.

In the sequential estimation method, the model parameters including the relevant statistics are estimated using the following equations. The seasonal AR(1) parameter is estimated as:

$$\varphi_{1,m} = \rho_{1,m} \quad (5.4)$$

with corresponding error term variance given by:

$$\text{Var}(\varepsilon_{y,m}) = [1 - \varphi_{1,m}^2]^2 \quad (5.5)$$

The seasonal AR(2) parameters are estimated as:

$$\varphi_{1,m} = (\rho_{1,m} - \rho_{1,m-1}\rho_{2,m})/(1 - \rho_{1,m-1}^2) \quad (5.6)$$

$$\varphi_{2,m} = (\rho_{2,m} - \rho_{1,m-1}\rho_{1,m})/(1 - \rho_{1,m-1}^2) \quad (5.7)$$

with corresponding error term variance given by:

$$\text{Var}(\varepsilon_{y,m}) = [1 - \varphi_{1,m}\rho_{1,m} - \varphi_{2,m-1}\rho_{2,m}]^2 \quad (5.8)$$

The autocorrelation functions are given by:

$$\rho_{1,m} = \text{Cov}(Q_{y,m}, Q_{y,m-1})/\sqrt{\text{Var}(Q_{y,m}) \cdot \text{Var}(Q_{y,m-1})} \quad (5.9)$$

$$\rho_{2,m} = \text{Cov}(Q_{y,m}, Q_{y,m-2})/\sqrt{\text{Var}(Q_{y,m}) \cdot \text{Var}(Q_{y,m-2})} \quad (5.10)$$

Finally, the sequential estimators of the mean, variance, and covariances are given by:

$$\bar{Q}_m^{(t)} = \frac{t-1}{t} \bar{Q}_m^{(t-1)} + \frac{1}{t} Q_{y,m}^{(t)} \quad (5.11)$$

$$Var(Q_{y,m})^{(t)} = \frac{t-1}{t} Var(Q_{y,m})^{(t-1)} + \frac{1}{t} [Q_{y,m}^{(t)} - \bar{Q}_m^{(t)}]^2 \quad (5.12)$$

$$\begin{aligned} Cov(Q_{y,m} Q_{y,m-1})^{(t)} &= \frac{t-1}{t} Cov(Q_{y,m} Q_{y,m-1})^{(t-1)} + \frac{1}{t} [Q_{y,m}^{(t)} - \bar{Q}_m^{(t)}] \\ &\cdot [Q_{y,m-1}^{(t)} - \bar{Q}_{m-1}^{(t)}] \end{aligned} \quad (5.13)$$

$$\begin{aligned} Cov(Q_{y,m} Q_{y,m-2})^{(t)} &= \frac{t-1}{t} Cov(Q_{y,m} Q_{y,m-2})^{(t-1)} + \frac{1}{t} [Q_{y,m}^{(t)} - \bar{Q}_m^{(t)}] \\ &\cdot [Q_{y,m-2}^{(t)} - \bar{Q}_{m-2}^{(t)}] \end{aligned} \quad (5.14)$$

The superscript  $(t)$  signifies the estimate of that particular statistic at that month  $m$  when the observed flow  $Q_{y,m}^{(t)}$  becomes available so that  $t$  is essentially the count of the total number of observed values at that concurrent month which is equal to the number of years of data.

Figure 5.5 shows the implementation of the SAR(1) and SAR(2) models in forecasting Angat inflows for 1997. Year 1997 is especially illustrated here since it is the start of a 2-year dry or low-flow year that is considered a severe El Nino episode. The topmost time series plot in Fig. 5.5 shows the 6-month ahead forecasts of March through August flows using the SAR(1) and SAR(2) models given only observed flows (information available) at the end of February 1997. The time series plot at the bottom of Fig. 5.5 shows the corresponding 6-month ahead forecasts given only information at the end of May 1997. It is demonstrated here that the forecasted inflows using the SAR(2) model are closer to the observed values compared to SAR(1) forecasts. The SAR(1) model forecasts consistently underestimate the observed values but relatively low values of observed inflows; the SAR(1) model forecasts somehow close in with the SAR(2) model forecasts. Details for selecting SAR(2) as the forecasting model based on forecast error analysis and performance are given in Tabios (2008).

With forecasted inflows, Table 5.5 shows the resulting hydropower generation and demand violations (or surplus) for the optimization-simulation cases OS1 and OS3 as well as using the existing and proposed rule curve cases ERC1 and PRC1. In terms of hydropower generation, the optimization-simulation cases OS1 and OS3 resulted in the same total of 597 GWH (308 from main hydropower plant plus 289 GWH from auxiliary hydropower plant) for this 10-month period compared to those of existing and proposed rule curve-based cases ERC1 and PRC1 of 488 GWH and 547 GWH, respectively. Both optimization-simulation cases OS1 and OS3 were about 110 and 50 GWH higher than the rule curve-based procedures ERC1 and PRC1, respectively. During the period from January through October 2008, there

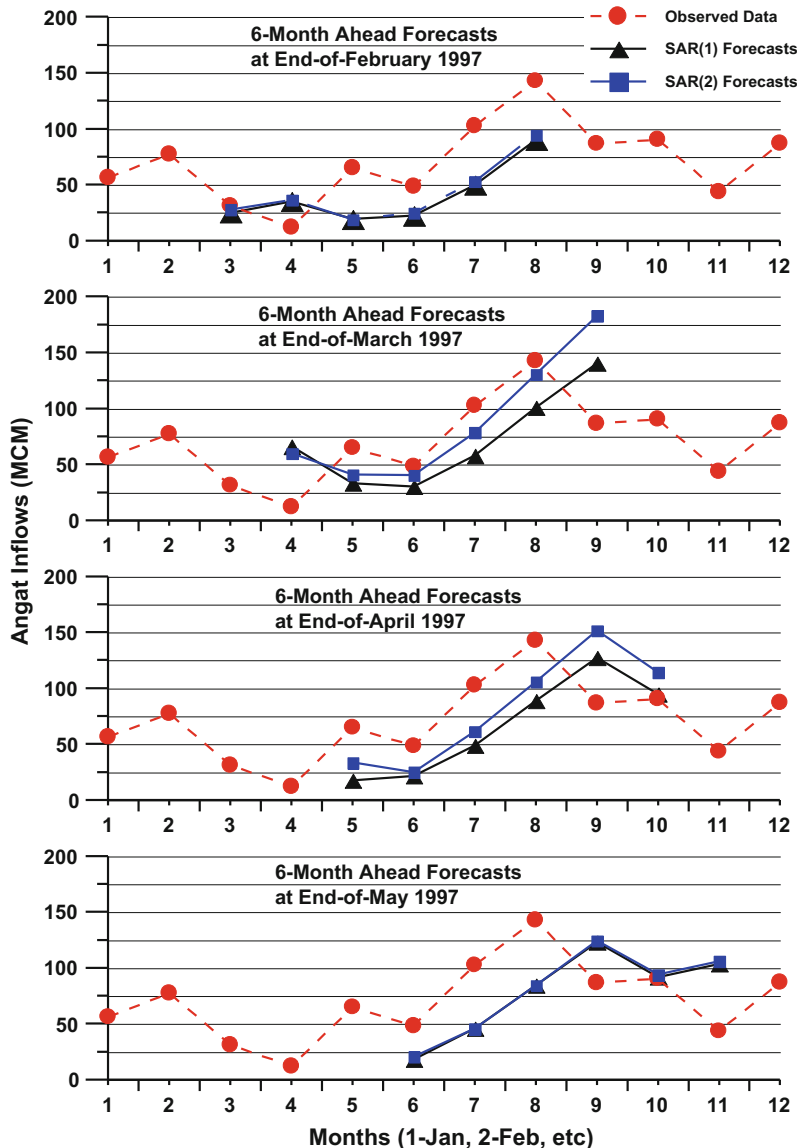


**Fig. 5.5** 6-month ahead forecasts using seasonal AR(1) and seasonal AR(2) models including observed data for year 1997

was no demand violation in any month in the four cases. However, there were surpluses (excess reservoir releases) for NIA irrigation through the main hydropower plants especially in cases OS1 and OS3 as shown in Table 5.5.

Finally, Fig. 5.6 shows the time series plots of reservoir elevations for 2008 for optimization-simulation cases OS1 and OS3 and for existing and proposed rule

**Table 5.5** Hydropower generation and demand violations (or surplus if positive values) for year 2008 for cases (i) OS1, (ii) OS3, (iii) existing rule curve ERC1, and (iv) proposed rule curve PRC1. Note that Angat River flows from January to April are observed data and those from May to October are forecasted inflows

Month	Auxiliary hydropower plant		Main hydropower plant		Demand violations (-) or surplus (+)	
	Power (MW)	Energy (GWH)	Power (MW)	Energy (GWH)	MWSS (TCM)	NIA (TCM)
<b>Optimization-simulation case 1 (OS1)</b>						
JAN	44.8	33.3	54.3	40.4	0	22399
FEB	44.8	30.1	53.6	36.0	0	9624
MAR	43.9	32.7	37.3	27.8	0	2
APR	42.4	30.5	18.1	13.1	0	0
MAY	41.4	30.8	0.0	0.0	0	0
JUN	40.4	29.1	31.5	22.7	0	4
JUL	40.1	29.8	31.4	23.4	0	0
AUG	41.3	30.8	28.7	21.4	0	9
SEP	42.7	30.7	26.8	19.3	0	0
OCT	41.6	31.0	114.7	85.4	0	231352
	Total	308.7		289.3		
<b>Optimization-simulation case 3 (OS3)</b>						
JAN	44.8	33.3	54.5	40.6	0	22929
FEB	44.8	30.1	53.7	36.1	0	9684
MAR	43.9	32.7	37.3	27.8	0	0
APR	42.4	30.5	18.2	13.1	0	1
MAY	41.4	30.8	0.0	0.0	0	0
JUN	40.4	29.1	31.5	22.7	0	2
JUL	40.1	29.8	31.4	23.4	0	0
AUG	41.3	30.8	28.7	21.4	0	2
SEP	42.7	30.7	26.8	19.3	0	1
OCT	41.6	31.0	114.7	85.4	0	231362
	Total	308.7		289.5		
<b>Existing rule curve case 1 (ERC1)</b>						
JAN	42.1	31.4	42.0	31.2	0	0
FEB	42.5	28.5	46.7	31.4	0	0
MAR	41.6	31.0	35.8	26.6	0	0
APR	40.0	28.8	17.4	12.5	0	0
MAY	38.9	29.0	0.0	0.0	0	0
JUN	37.8	27.2	29.9	21.5	0	0
JUL	37.5	27.9	29.8	22.2	0	0
AUG	38.9	28.9	27.4	20.4	0	0
SEP	40.4	29.1	25.6	18.5	0	0
OCT	41.6	30.9	15.0	11.2	0	0
	Total	292.7		195.5		

(continued)

**Table 5.5** (continued)

Month	Auxiliary hydropower plant		Main hydropower plant		Demand violations (-) or surplus (+)	
	Power (MW)	Energy (GWH)	Power (MW)	Energy (GWH)	MWSS (TCM)	NIA (TCM)
Proposed rule curve case 1 (PRC1)						
JAN	42.9	31.9	143.6	106.8	0	229147
FEB	41.0	27.5	45.4	30.5	0	0
MAR	40.1	29.8	34.7	25.8	0	0
APR	38.3	27.6	16.8	12.1	0	0
MAY	37.1	27.6	0.0	0.0	0	0
JUN	35.8	25.8	28.7	20.7	0	0
JUL	35.4	26.4	28.6	21.3	0	0
AUG	37.1	27.6	26.4	19.6	0	0
SEP	38.7	27.9	24.8	17.9	0	0
OCT	40.0	29.8	14.6	10.8	0	0
Total		281.8		265.5		

curve schemes ERC1 and PRC1. Superposed in the plots of OS1 and OS3 cases are the upper and lower rule curves of the existing and proposed rule curve schemes. In the cases of plots of reservoir elevations resulting from existing and proposed rule curve schemes, their associated upper and lower rule curves are also plotted. It is seen that in the OS1 and OS3 cases, the resulting reservoir storage elevations were high since the year started off at high reservoir levels. It may be noted that year 2008 was a fairly wet year thus the ample reservoir inflows that year.

### 5.3 Upper Agno River Basin Reservoir Operations Studies

The Upper Agno River Basin has three major cascading reservoirs, namely, Ambuklao, Binga, and San Roque reservoirs and the small Agno River Integrated Irrigation Project (ARIIP) re-regulation dam. Presented below is a combined optimization-simulation model that would enable to conduct watershed model streamflow simulation (as inflows to the reservoir) and optimization of reservoir operations according to the various objectives of the Upper Agno River reservoir system such as maximizing hydropower generation, minimizing irrigation demand (delivery) violations, and efficient operation of the reservoir for its flood control function especially in the San Roque Dam. Based on these optimization-simulation studies, develop reservoir operation rules that can be used as criteria or guidelines to operate the Upper Agno Reservoirs. Details of this study may be referred in the report of Woodfields (2017) in which the author is the principal investigator.

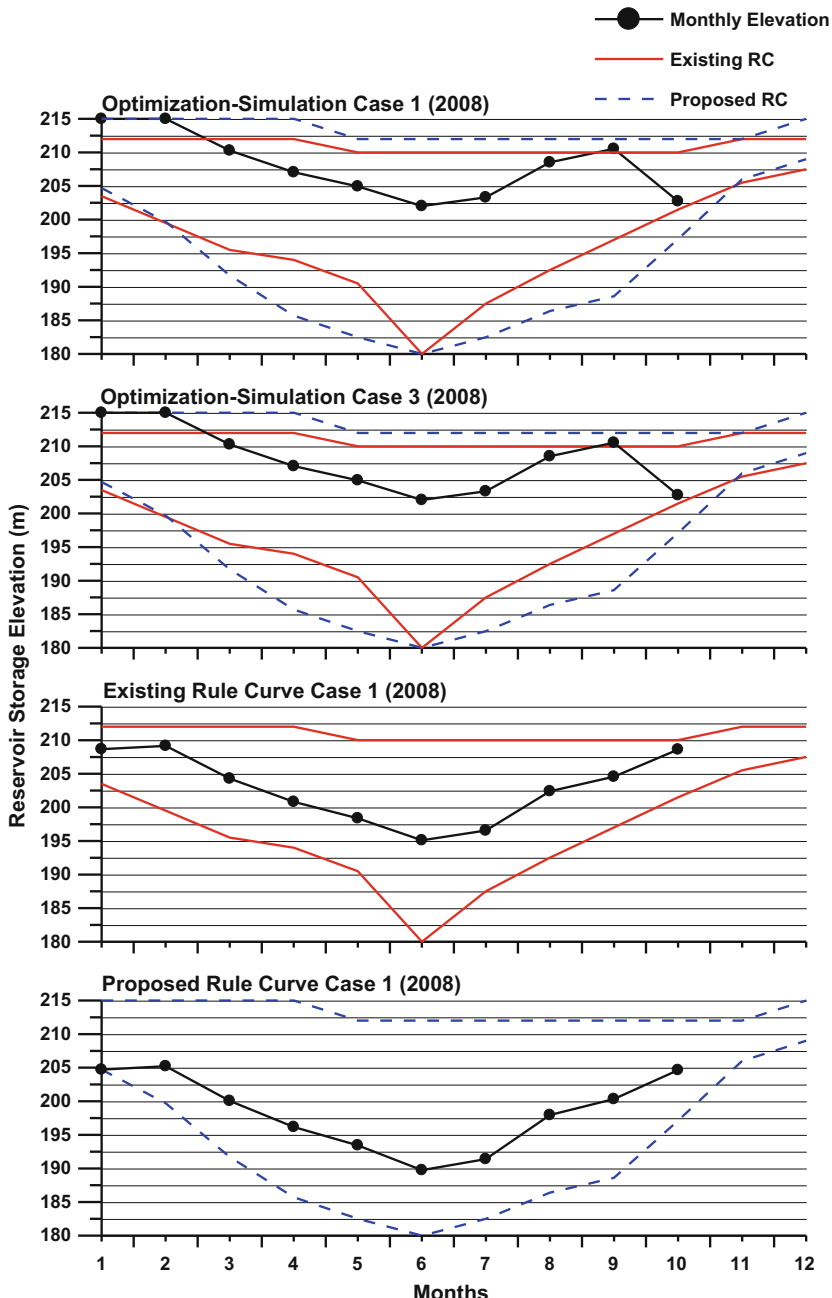


**Fig. 5.6** Monthly reservoir storages of cases: optimization-simulation cases OS1 and OS3, existing rule curve ERC1 case, and proposed rule curve PRC1 case in 2008 with forecasted Angat River inflows from May (month 4) to October. Envelope curves are upper and lower target storage elevations of existing and proposed rule curve operating procedures

As an aside, also presented below is an assessment of the adequacy of rainfall gaging stations in the Upper Agno River Basin and vicinity especially as input to the watershed model.

In Chapter 10, this optimization-simulation model is also used to assess the impacts of climate change in the hydrological regime and reservoir operations of the Upper Agno River Basin.

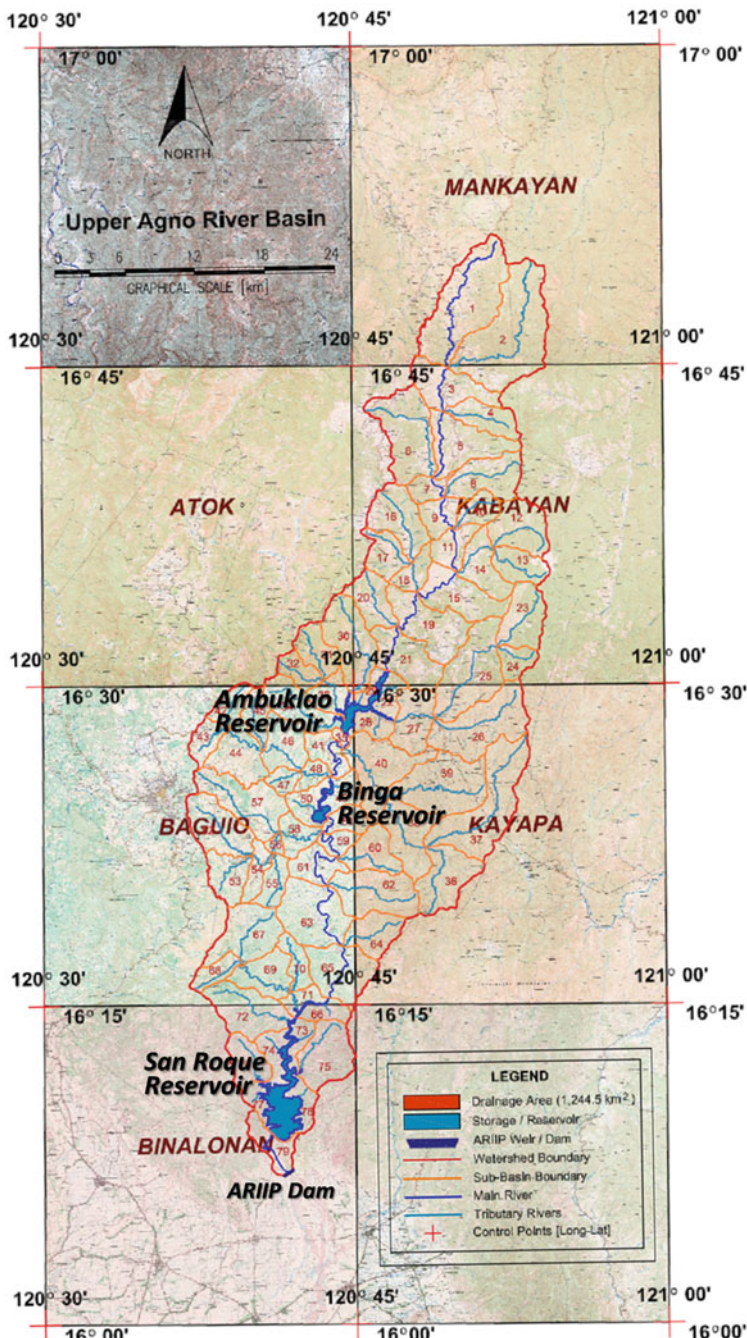
### ***5.3.1 Ambuklao, Binga, and San Roque Reservoirs of the Upper Agno River Basin***

Figure 5.7 shows a collage of 1:50,000 scale topographic maps from NAMRIA covering the Upper Agno River Basin. The river basin boundary shown in this figure for purposes of the reservoir operations studies has a total area of 1,225 km<sup>2</sup>. The river basin is bounded on the north by Mankayan of Benguet Province and runs south through Ambuklao, Binga, and San Roque reservoirs and finally ends on the south at the small re-regulation dam of NIA for the Agno River Integrated Irrigation Project (ARIIP) at San Manuel, Pangasinan.

San Roque Multipurpose Dam construction was completed in 2002 to provide flood control, water storage for irrigation and hydropower, and its unique function for water quality control by capturing sediments to minimize turbidity in its irrigation water releases. Its hydropower plant has a total installed capacity of 402 MW. Ancillary structures of the dam include the spillway, intake for power tunnel, and intake for low level outlet. The spillway is located at the right side of the dam; it is 110 m wide and controlled by six radial gates. The spillway chute is 484.83 m long (horizontal) and has a minimum elevation of 170.0 m at the bottom of a flip bucket located in the downstream end. The crest elevation of the spillway is 270.0 m. The maximum water operating level is 290.0 m, and its flood allocation storage is between 280 and 290 m. The flow is diverted toward the powerhouse by an 8.5 m diameter and 1.2-km-long power tunnel, located on the left side of the dam. The invert of the intake portal is located at elevation 206.5 m, while its downstream end is at elevation 87.85 m. The crown of the power tunnel at the dam face is at elevation 215.0 m. The low-level outlet is a smaller tunnel on the left side of the power tunnel. The axis of the low-level outlet, at elevation 202.75, is 8 m below that of the power tunnel.

Binga Dam is situated 50 km upstream of San Roque Dam and was constructed in 1959. The dam has an installed capacity of 100 MW. The dam has a height of 107 m and had an initial reservoir capacity of 87.4 million m<sup>3</sup>. The main features of Binga Dam are summarized below:

- Type of dam: Rock-fill dam
- Height of dam: 107.4 m
- Initial storage capacity: 87.4 million m<sup>3</sup>
- Max. water level: El. 579.5 m



**Fig. 5.7** Assembly of 1:50,000 scale NAMRIA topographic maps covering the Upper Agno River Basin. Also shown is the watershed delineation into sub-basins and the three (3) major reservoirs Ambuklao, Binga, and San Roque (in the order from north or upstream to south or downstream) and ARIIP Dam

- Min. water level: El. 555.0 m
- Dam crest: El. 586.0 m
- Spillway crest: El. 563.0 m
- Intake invert level: El. 540 m
- Tailrace invert: El. 410.5 m

Ambuklao Dam is located 36 km east of Baguio and 64 km upstream from San Roque dam. The dam and hydropower station were commissioned in 1956. The hydropower station has an installed capacity of 75 MW and was designed to supply power during peak demand. The main characteristics of the dam are as follows:

- Type of dam: Rock-fill with impervious core
- Height of dam: 129 m
- Initial storage capacity: 327 million m<sup>3</sup>
- Dam crest: El. 758.0 m
- High water level: El. 752.0 m
- Minimum level: El. 730.0 m
- Intake invert level: El. 686.0 m
- Base of dam: El 629.0 m

Ambuklao Reservoir has a length of approximately 10 km, with a top width varying between 300 and 700 m. The water levels at the reservoir pool are controlled by a gated spillway. The spillway crest is located at elevation 740.0 m, on top of which eight 12.5 m by 12.5 m tainter gates control water levels up to elevation 752.0 m.

### ***5.3.2 Assessment of Adequacy of Rainfall Sampling Network***

A map of the location of rainfall gaging stations in particular is shown in Fig. 5.8. These rainfall stations have at most 15 years of daily data ending in year 2015. There are 21 rainfall stations in the river basin and its vicinity with rainfall data available from 1950 to 2015 although certain stations have discontinuous and/or fragmentary data. In the watershed model, the input rainfall data are interpolated for each sub-basin from rainfall stations with concurrent (available) rainfall data at each day.

With the current configuration (number and location) of the rainfall gaging stations, the reliability of the sampling network can be assessed by geostatistical methods. The approach taken here is to map the root mean square error (RMSE) of spatial interpolation as basis for assessing the reliability of point estimation when rainfall data is transposed from the available rainfall gaging stations to any point in the watershed or river basin. Typically, areas in the basin which are far from the gaging stations will have a higher RMSE compared to areas near the gaging stations. On this basis, if the RMSE at certain points or region in the river basin become large and unacceptable, a new gaging station should be established in the vicinity of this high RMSE. While the minimum RMSE criterion is an important consideration in

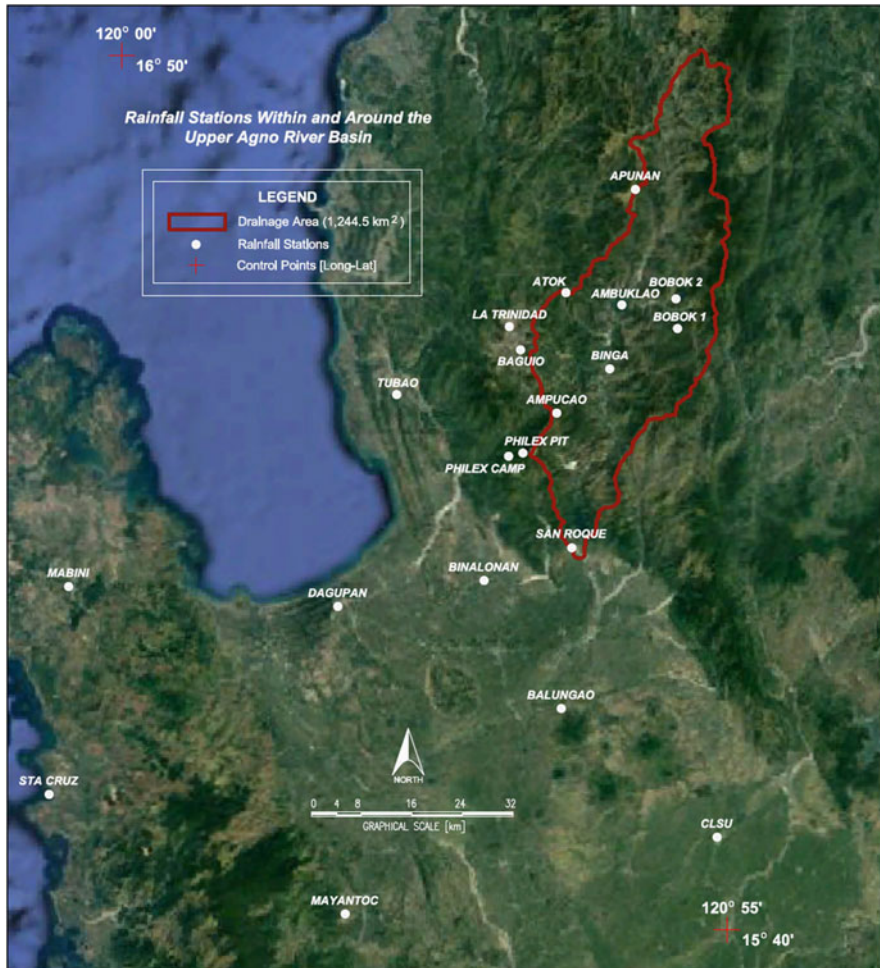


**Fig. 5.8** Location of rainfall gaging stations in the Upper Agno River Basin and vicinity

the design of a rainfall sampling network, other factors are considered such as cost, accessibility, and ease of maintenance and operations.

The RMSE calculation done here is based on optimal spatial interpolation technique (Tabios and Salas 1985) which is a minimum variance, unbiased estimator of the station weights used in the spatial interpolation. In other words, if rainfall is spatially interpolated or transposed in the river basin using optimal interpolation techniques, then this would be the corresponding RMSE. In optimal spatial interpolation, the first step is to model the spatial covariance or alternatively the spatial correlation function using the historical rainfall in the river basin. Essentially, the spatial correlation function describes the spatial characteristics of the rainfall field in say the Upper Agno River Basin in particular. Note that the spatial structure of the

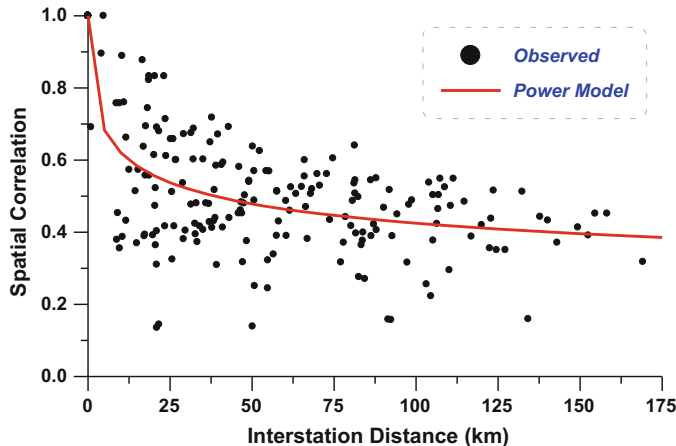


**Fig. 5.9** Observed and fitted power model of the spatial correlation function of the daily rainfall in the Upper Agno River Basin

rainfall process may vary depending on location, topographic effects, and other climatic and weather elements in the study area.

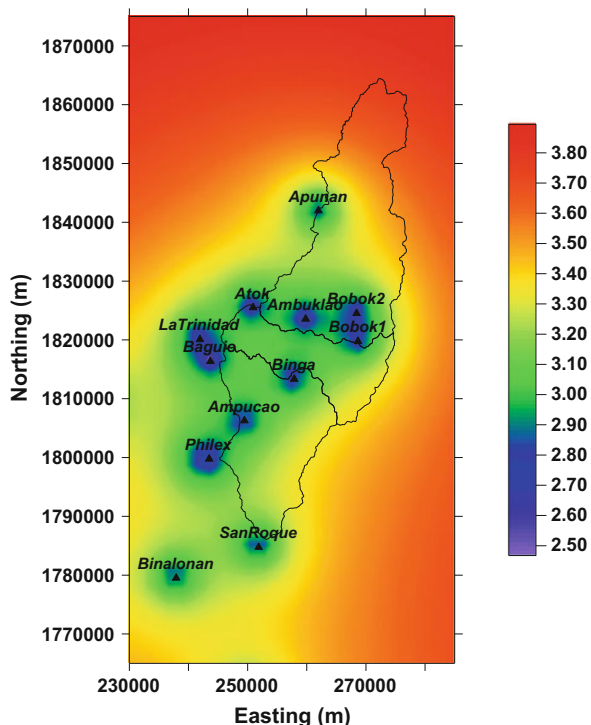
Figure 5.9 shows the observed spatial correlation coefficients plotted as a function of distance. There are 207 observed correlation coefficients which are calculated by pairing rainfall gaging stations in the study area. With 21 available gaging stations, as many as 231 pairs can be formed. However, since there are station pairs that have no concurrent daily rainfall data, the number of pairs is only 207 out of the theoretical 231 pairs.

To be able to calculate the spatial correlation between a gaging station and any point in the river basin, a spatial correlation model is fitted to the observed correlation which is also shown in Fig. 5.9. The fitted spatial correlation function is the power model written as:

$$\rho(D) = [2.4123D^{1.2634}]^{-0.1762} \quad (5.15)$$

With the spatial correlation model at hand, the optimal spatial interpolation technique is performed, and the map of the resulting RMSE in the vicinity of Upper Agno River Basin is given in Fig. 5.10. In this figure, the outline of the Upper Agno River Basin is shown as well as the location of existing stations within and outside the basin. There is a total of 21 gaging stations used in computing the map of RMSE, but only 12 are shown as indicated by the black triangles. As seen in this contour map, the RMSE are smallest around the existing gaging stations ranging from 2.5 to 2.8 (in mm of daily rainfall) RMSE. Within the basin boundary, only in the northeast portion above 184500 m northing and on the left of 26500 m easting are the RMSEs observed to be greater than 3.5 mm. Considering that the historical daily mean and standard deviation are 7.74 mm and 4.89 mm, respectively (calculated from 65 years

**Fig. 5.10** Contour map of root mean square errors of spatial interpolation of daily rainfall (in mm) in the Upper Agno River Basin and vicinity



of daily data), and that the RMSE or sampling error should not exceed the natural variability represented by the standard deviation of 4.89 mm, it can be concluded that the rainfall gaging network in this area is fairly adequate and reliable, since the RMSEs in the Agno River Basin are mostly below 3.5 mm.

In actual designing of a sampling network, the establishment or location of gaging stations is judiciously made through optimization techniques with multi-objective function such as minimizing MSE and cost at the same time considering road access as well as maintenance and operations considerations. If the rainfall gaging stations network is already established like in the Upper Agno River, redesigning the sampling network may include relocation and even discontinuing gaging stations due to cost considerations assuming that they provide redundant information.

For purposes of real-time monitoring especially during emergency operations (e.g., ongoing typhoon event), additional recording rainfall gaging stations (i.e., recording almost continuous-time data) may be installed in the Upper Agno River Basin. It may be noted that most rainfall stations in Upper Agno River Basin only collect data on a daily basis (non-recording stations) which is not appropriate for real-time reservoir operations during emergency operations that may require hourly or 15 min time interval rainfall. To design the optimal location and sampling frequency of a rainfall gaging network for flood forecasting, the spatial error analysis should be performed on short-time interval rainfall rather than on daily basis as done

here. On the other hand, nowadays, for real-time flood reservoir operations, ground rainfall observations and other remotely sensed data such as satellite and radar data can be combined to forecast basin rainfall as input to rainfall-runoff models to calculate the reservoir inflows as input to the flood operations model.

### **5.3.3 *Upper Agno River Watershed Model***

The watershed model employed here was the continuous-time, distributed watershed model built on the Sacramento soil moisture accounting model and described in Appendix A.

For the Upper Agno River Basin, Fig. 5.7 also shows the basin delineations in which the basin is divided into 3 sub-basins according to the watersheds associated to the major reservoirs, namely, the (a) Ambuklao, (b) Binga, (c) San Roque, and (d) ARIIP regulation dam. Each sub-basin is geometrically separate and is connected through the reservoirs from upstream to downstream. Pertinent information for each sub-basin is in Table 5.6.

For purposes of creating the model geometry, the Shuttle Radar Topography Mission (SRTM) – digital elevation model (DEM) – with 90m x 90 m resolution was used which is displayed in Fig. 5.11 as an elevation map. This elevation map can also be used to verify the manual and electronic delineations done for the watershed.

The values of the watershed model parameters such as interception, infiltration, and overland flow parameters may be obtained from slope map, soil type, and land

**Table 5.6** Summary of drainage areas and number of sub-basin units for the major sub-basins of the Upper Agno River System

Sub-Basin No.	Reservoir/ River System	Sub-Basin/ Watershed Name	Major Rivers and Tributaries	Total Area (km <sup>2</sup> )	No. of Sub-Basins
SB-01	Ambuklao Reservoir	Ambuklao Watershed	Agno River, Nalatang Mamasok River, Bokod River	607.8	34
SB-02	Binga Reservoir	Binga Watershed	Agno River, Benneng River, Laboy River	239.6	16
SB-03	San Roque Reservoir	San Roque Watershed	Agno River, Ambalanga River	365.8	28
SB-04	ARIIP Weir	ARIIP Catchment	Agno River, Tambo Creek, Cabu Creek	10.5	1
Res-01		Ambuklao Reservoir		4.6	
Res-02		Binga Reservoir		2.1	
Res-03		San Roque Reservoir		14.2	
			Total ---->	1,244.5	79

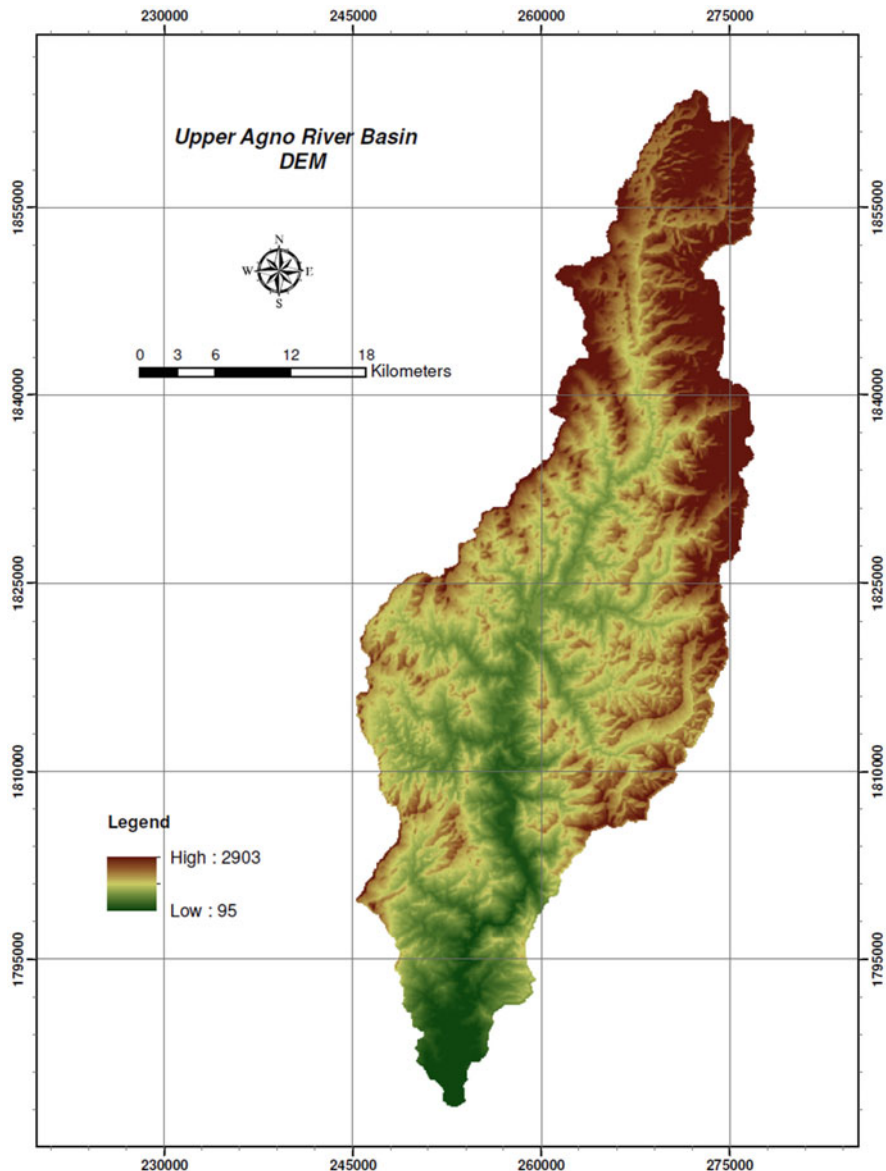


**Fig. 5.11** Digital elevation map of Upper Agno River Basin using SRTM data

use/cover maps. Figure 5.12 shows the slope map, and Fig. 5.13 shows the landcover/landuse map.

With this watershed model, streamflow simulations were conducted using daily rainfall data from 1950 to 2015 to calculate the watershed streamflows at the outlets of 79 sub-basins. The input rainfalls to the watershed model were interpolated

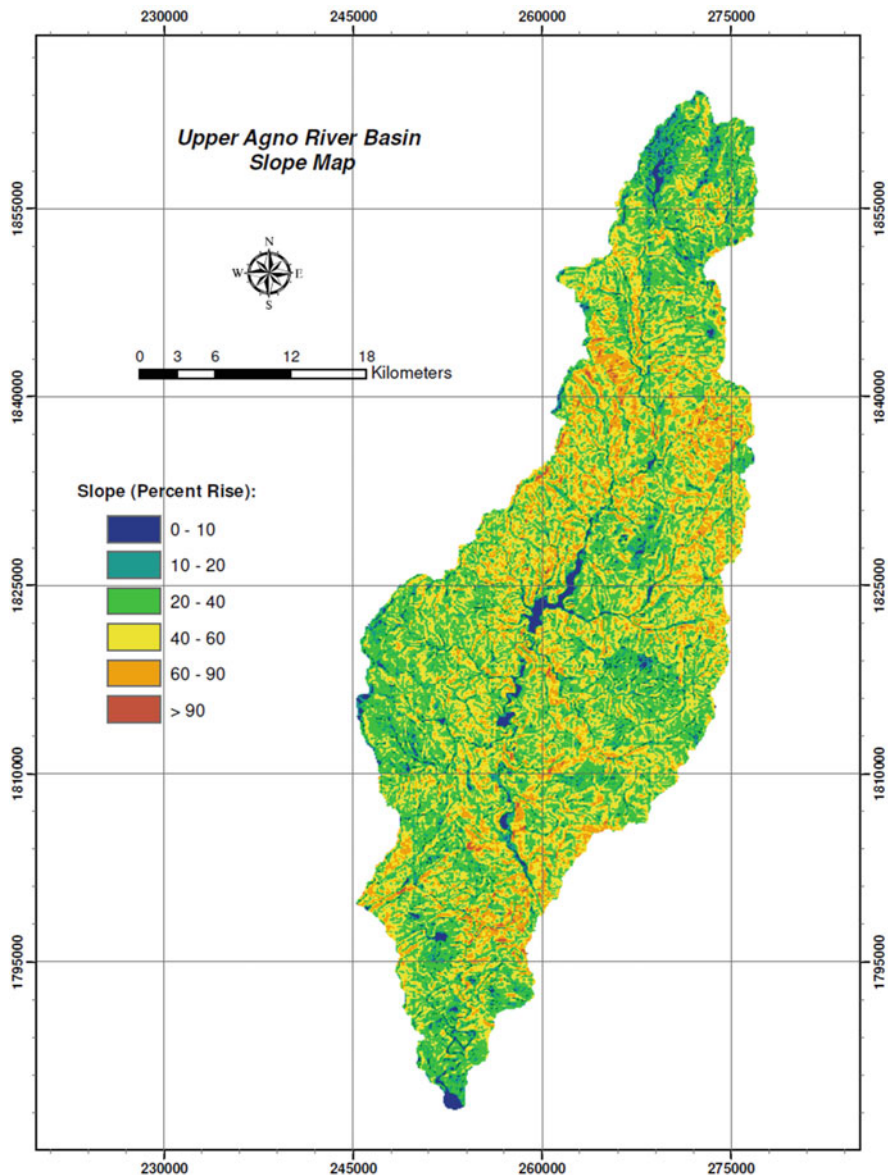


**Fig. 5.12** Slope map of Upper Agno River Basin derived from the digital elevation map

for each sub-basin from any of the 21 rainfall stations with concurrent (available) rainfall data at each day. Then, the reservoir inflows to each reservoir (Ambuklao, Binga, and San Roque) were summed up from the specific sub-basins flowing into that reservoir.

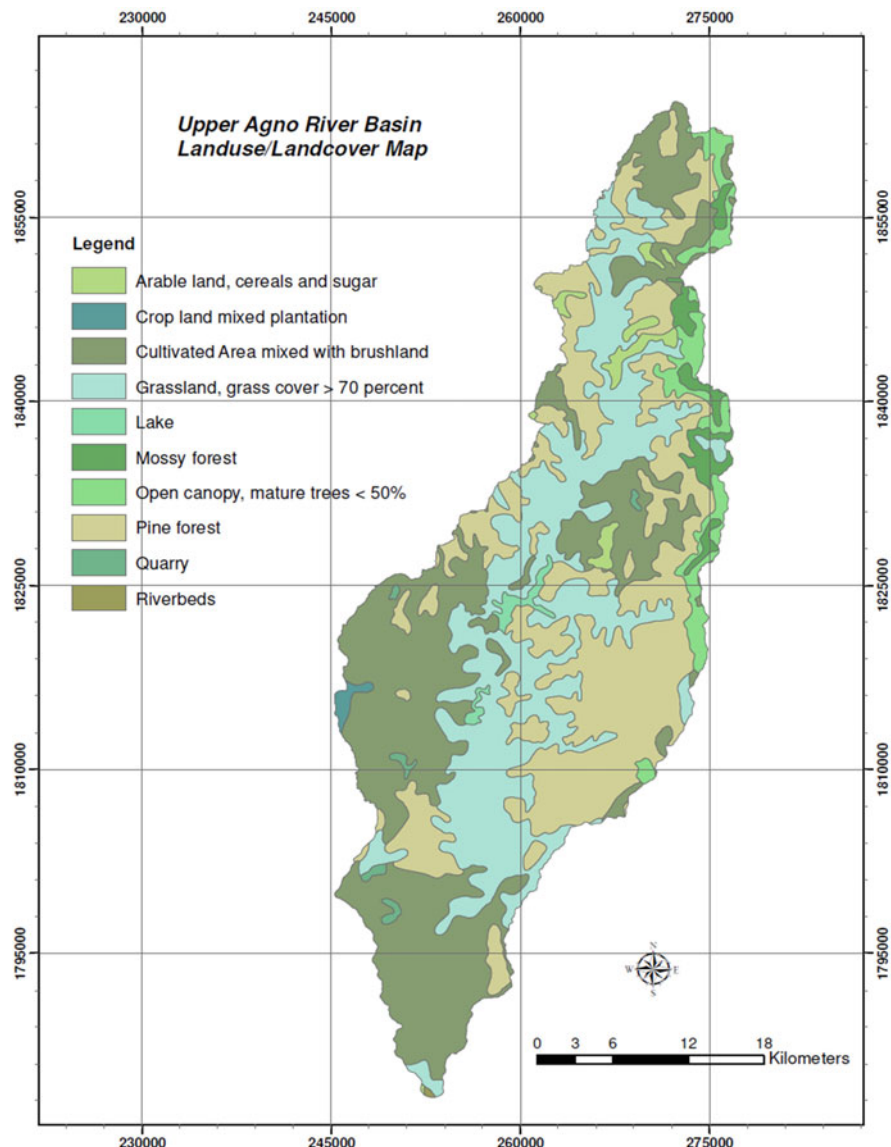


**Fig. 5.13** Landcover map of Upper Agno River Basin

#### 5.3.4 *Upper Agno Reservoir Optimization-Simulation Studies*

Since there are three reservoirs to be optimized, a multidimensional optimization formulation was implemented using the same WATPOW optimization-simulation model used in the Angat Reservoir study earlier. As before, the simulation module

contains the watershed and reservoir water balance computations which are embedded in the optimization module to decide the operating policies such as flow releases to irrigation and/or hydropower releases including spillway gate openings for specified objectives and constraints. The WATPOW model described in Appendix B was used with the COMPLEX optimization.

The objective function of the optimization-simulation model is a weighted, multi-objective function to minimize irrigation water supply deficits (demand violations), maximize hydropower generation, and minimize spills. The constraints include capacities of release gates, storage volumes, operational constraints, and all other system constraints imposed implicitly in the simulation model. The objective function to be maximized in particular is given by:

$$F = p_{IR} \min(QIR_t - QID_t, 0.0) - p_{SP}QSP_t + b_MHP_t + b_F(S_t + I_t) \quad (5.16)$$

where  $QIR_t$  and  $QID_t$  are the irrigation release and irrigation demand, respectively, with penalty coefficient  $p_{IR}$ ,  $QSP_t$  is the reservoir spill with penalty coefficient  $p_{SP}$ , and  $HP_t$  is the hydropower energy generated with benefit coefficient  $b_M$ . The quantity  $(S_t + I_t)$  with benefit coefficient  $b_F$  represents the future benefit function where  $S_t$  and  $I_t$  are the reservoir storage and total reservoir inflow, respectively. In the day-to-day reservoir operations (i.e., combined optimization-simulation run), this future benefit function accounts for hedging to avoid future water supply shortages so that the function balances between aggressively making releases to satisfy water demand in the short term against maximizing the amount of water stored plus inflow in the reservoir to ensure that future water deliveries are satisfied. The alternative hedging policy is to conduct the optimization through a multiple-day *moving planning horizon* or *window* so that the decision today is based on say, optimization with the objective function in Eq. (5.16) over a 15-day or 30-day period or window so that in this case, the future benefit function is no longer included in the objective function formulation. For long-term reservoir operations studies as done here, it is suggested that the *moving planning horizon* approach is used, while for real-time reservoir operations, the *future benefit function* term in Eq. (5.16) is included with a non-zero  $b_F$  coefficient.

The major constraint function imposed in reservoir optimization-simulation studies is the hard system constraint described by the reservoir water balance computations, maximum flow capacities of controlled releases, and the flood control allocation storage requirement. Other constraints inherent in the optimization method such as lower and/or upper values of decision variables as well as implicit constraints are also imposed. Note that the irrigation demand violations as well as spillway flows are imposed as soft constraints which are incorporated in the objective function as penalty functions.

### 5.3.5 Reservoir Storage-Elevation Curve over the Years

A major data needed in the reservoir operations model is the reservoir storage-elevation curve. Figures 5.14, 5.15, and 5.16 show the reservoir storage-elevation curves for Ambuklao, Binga, and San Roque reservoirs, respectively, and their associated table values. It may be noted in the time history of the storage-elevation curves, the reservoir filling-up starts at the deepest portions.

In the case where reservoir sedimentation is considered, estimates of the annual sediment inflow can be calculated from the change in reservoir storage-elevation curve over time. Similarly, if reservoir sedimentation is considered in the reservoir operations study, the reservoir storage-elevation curve can be modified or generated annually (for future simulation scenario) according to the sediment inflow derived from the different curves in time.

### 5.3.6 Results of Upper Agno Reservoir Optimization-Simulation Studies

The optimization-simulation runs were conducted on a daily basis for 65 years with reservoir inflows computed from the watershed model with historical rainfall from 1950 to 2015. Based on these results, reservoir release policies or operation rules can

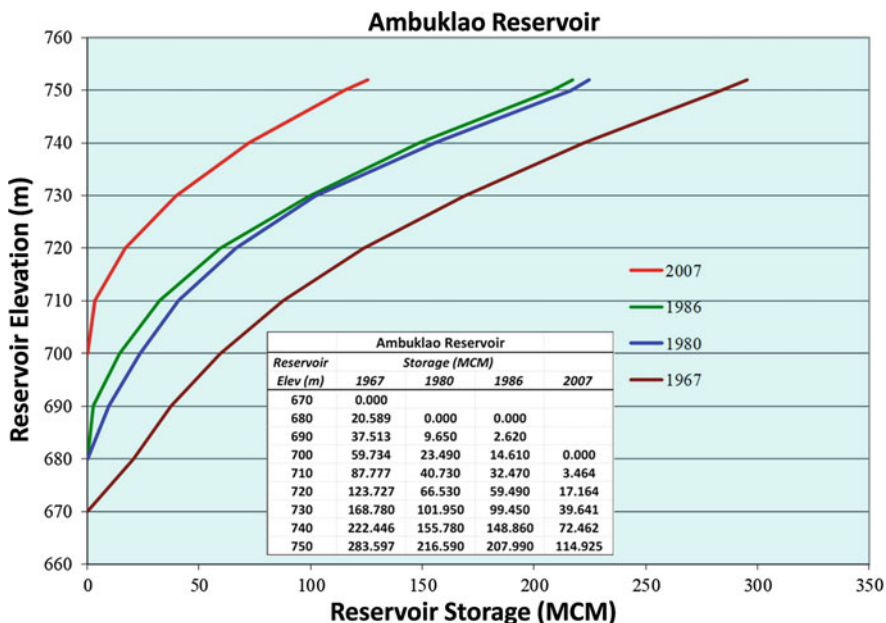


Fig. 5.14 Ambuklao Reservoir elevation-storage curve

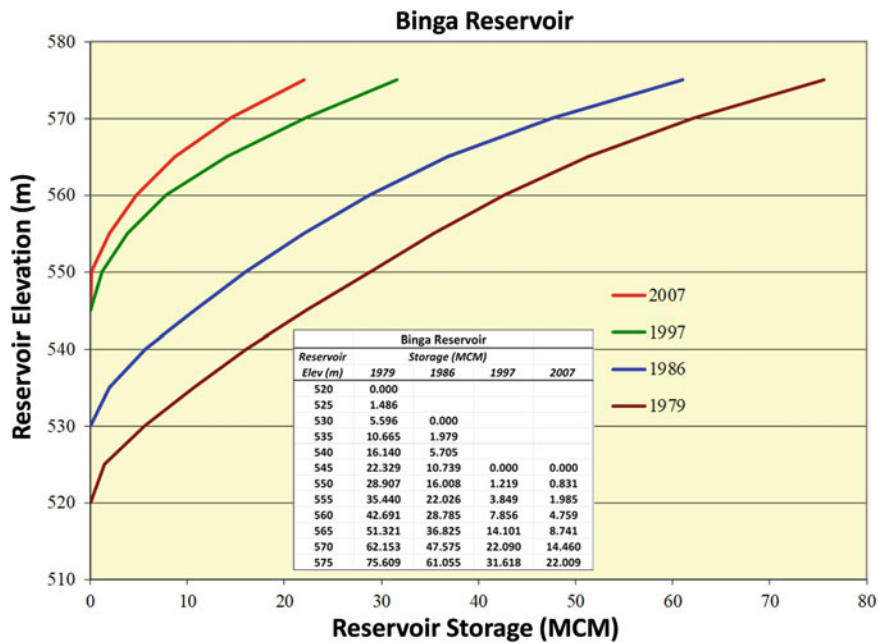


Fig. 5.15 Binga Reservoir elevation-storage curve

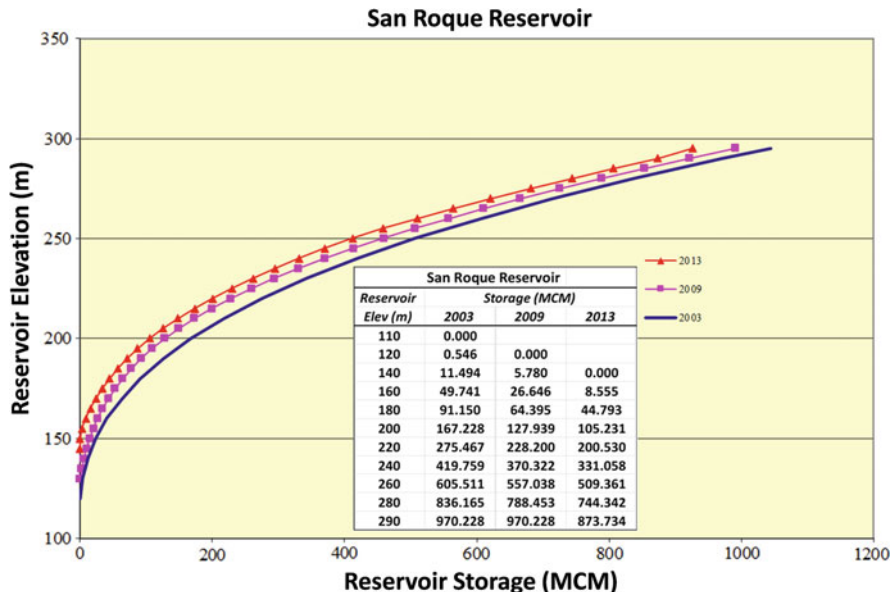


Fig. 5.16 San Roque Reservoir elevation-storage curve

**Table 5.7** Three (3) sets of target releases ( $\text{m}^3/\text{s}$ ) for Ambuklao, Binga, and San Roque reservoirs used in the optimization-simulation studies

Target releases	Ambuklao	Binga	San Roque
Set 1	25	25	60
Set 2	30	30	80
Set 3	30	35	70

be derived. The reservoir elevation-storage curves used were the latest available as shown in Figs. 5.14, 5.15, and 5.16 for Ambuklao, Binga, and San Roque reservoirs, respectively. Note that the spillway flows are uncontrolled releases.

In the optimization-simulation run, three (3) sets of reservoir target releases are given in Table 5.7 which essentially form the basis of operation rules developed here. The first set of target release is the most conservative compared to the second and third sets. The second set of target release is more aggressive than the third set. A conservative (or far-sighted) target release policy results in lower power generation in the short term due to fewer amounts of water releases, but it avoids severe water shortages in the future. On the other hand, an aggressive (or myopic) release policy results in higher power generation in the short term but tends to result in future water shortages. In the long term, too conservative release policy or too aggressive release policy both result in compromising the reliability of water delivery or power generation thus the need to determine an optimal target release policy. Reliability is defined here in terms of percent-of-time to deliver water or generate hydropower.

Tables 5.8, 5.9, and 5.10 show the results of optimization-simulation runs for the three (3) sets of target releases, respectively. In each of the tables, the reservoir end-of-month (EOM) elevations (in m); the inflows; releases and spills (in  $\text{m}^3/\text{s}$ ); hydropower generation (in MW) for Ambuklao, Binga, and San Roque reservoirs; and the final outflow (in  $\text{m}^3/\text{s}$ ) to ARIIP Reservoir are shown. Note that the hydropower was computed at fixed 10-hour operation for the reservoir flow release that day. In this case, the hydropower generated may be greater than the installed capacity, for instance, at San Roque Reservoir with installed capacity of 402 MW, it may be seen in Table 5.10 that say the hydropower generated could be over 550 MW at 20 or 10 percent-of-time dependability. In actual reservoir operations, when there is more than enough water that can be released during the day that result in hydropower generation beyond the installed capacity, the power generation can extend beyond 10 hours. For instance, hydropower generation for 10 hours at 550 MW will be revised to hydropower generation at only 402 MW installed capacity for 13.7 hours (calculated from  $550 \times 10/402$ ).

The values shown in these tables are in terms of *flow duration curves* on monthly basis at 90, 80, 50, 20, and 10 percent-of-time (or percentiles) of the daily variables (flows, EOM elevations, or hydropower) corresponding to 27, 24, 15, 6, and 3 days out of 30 days (for a 30-day month) that such variables can be greater or equal to the corresponding values in the table. For instance, the daily hydropower generated at Ambuklao Reservoir in March as shown in Table 5.8 at 80 percent-of-time means that the hydropower equal to or greater than 86.6 MW can be generated 24 days out

**Table 5.8** Reservoir end-of-month elevations (m); inflows, releases, and spills ( $m^3/s$ ); and hydropower generation (MW) for Ambuklao, Binga, and San Roque and outflow to ARIP Reservoir at 90, 80, 50, 20, and 10 percent-of-time on monthly basis for target release policy Set 1

Ambuklao Reservoir						Binga Reservoir						San Roque Reservoir						ARIP	
	EOM Elev	Inflow	Release	Power	Spill	EOM Elev	Inflow	Release	Power	Spill	EOM Elev	Inflow	Release	Power	Spill	Outflow			
<b>January</b>																			
90%	720.0	2.4	1.9	6.8	0.0	545.1	0.9	2.7	8.4	0.0	238.3	3.8	60.0	225.6	0.0	60.3			
80%	720.0	3.5	3.1	11.4	0.0	553.8	1.4	9.1	28.9	0.0	254.6	5.7	60.7	244.1	0.0	62.6			
50%	748.8	45.1	29.4	119.5	2.3	575.0	18.4	32.4	119.9	19.0	278.5	73.2	118.7	450.9	0.2	128.4			
20%	750.0	127.7	34.9	149.7	89.8	575.0	51.8	34.9	131.5	135.5	285.0	205.2	124.8	550.6	208.6	337.3			
10%	750.0	185.7	35.0	150.4	151.1	575.0	78.1	35.0	132.0	230.9	285.0	304.8	124.9	551.8	415.2	553.2			
<b>February</b>																			
90%	720.0	3.3	2.1	7.8	0.0	550.2	1.3	3.2	10.2	0.0	245.9	5.3	60.0	226.1	0.0	60.8			
80%	724.7	7.5	11.5	45.3	0.0	571.9	3.0	21.8	79.0	0.2	255.0	12.3	66.3	260.1	0.0	72.9			
50%	749.9	53.6	33.1	136.6	6.4	575.0	22.2	33.8	126.4	27.7	283.3	86.7	122.4	497.7	8.8	131.8			
20%	750.0	135.9	34.9	149.8	97.8	575.0	55.0	34.9	131.7	148.3	285.0	216.0	124.9	551.0	235.7	369.8			
10%	750.0	207.4	35.0	150.4	175.9	575.0	82.7	35.0	132.0	253.8	285.0	334.6	125.0	551.9	484.3	624.0			
<b>March</b>																			
90%	723.8	3.4	2.7	10.1	0.0	567.5	1.3	5.8	21.4	0.0	247.4	5.5	60.0	243.7	0.0	63.1			
80%	737.9	7.0	21.5	86.6	0.0	574.5	2.9	25.1	94.4	1.0	261.5	12.2	66.6	274.4	0.0	81.9			
50%	750.0	57.5	32.9	136.7	14.8	575.0	23.3	33.9	127.1	38.2	283.8	95.5	121.7	506.6	18.3	134.4			
20%	750.0	146.7	34.9	149.8	109.5	575.0	57.7	34.9	131.7	166.3	285.0	230.6	124.9	550.6	274.0	409.3			
10%	750.0	222.7	35.0	150.4	190.0	575.0	88.6	35.0	132.0	272.0	285.0	355.9	125.0	551.9	522.0	662.8			
<b>April</b>																			
90%	727.4	3.3	7.0	29.7	0.0	573.3	1.3	19.2	70.6	0.2	263.4	5.3	60.2	255.2	0.0	63.5			
80%	738.9	6.4	22.6	90.0	0.0	574.6	2.6	25.4	95.5	1.1	274.9	10.5	68.0	285.3	0.0	82.0			
50%	750.0	49.6	33.1	137.9	10.9	575.0	19.6	33.9	127.3	32.2	284.3	80.5	122.2	522.1	18.6	135.1			
20%	750.0	138.8	34.9	149.9	103.5	575.0	55.4	34.9	131.7	158.1	285.0	222.0	124.8	550.7	257.5	386.3			

	10%	750.0	212.0	35.0	150.4	177.9	575.0	84.6	35.0	132.0	267.1	285.0	339.7	125.0	551.9	486.8	627.3
<b>May</b>																	
90%	720.0	2.7	2.1	7.7	0.0	571.8	1.1	3.7	11.8	0.0	268.3	4.4	60.0	246.7	0.0	60.7	
80%	735.0	4.5	17.4	69.8	0.0	574.5	1.8	24.7	90.4	0.7	273.6	7.3	61.6	263.5	0.0	67.5	
50%	750.0	44.5	31.2	132.2	9.5	575.0	18.0	33.0	124.4	28.2	284.5	73.5	119.9	509.9	18.9	134.1	
20%	750.0	145.5	34.8	149.8	110.9	575.0	58.3	34.9	131.7	167.7	285.0	231.5	124.8	550.8	277.4	412.3	
10%	750.0	210.1	35.0	150.5	173.7	575.0	82.8	35.0	132.0	254.0	285.0	337.9	125.0	552.0	477.1	616.8	
<b>June</b>																	
90%	720.0	2.4	2.2	7.8	0.0	546.5	1.0	3.5	11.0	0.0	261.9	4.0	60.0	236.2	0.0	60.3	
80%	724.4	3.3	12.0	48.4	0.0	572.7	1.3	22.6	81.1	0.1	272.2	5.3	60.3	253.3	0.0	62.7	
50%	749.4	26.6	27.4	114.4	2.4	575.0	11.1	30.5	114.3	10.3	283.8	44.1	105.8	448.6	10.9	124.7	
20%	750.0	124.0	34.7	149.3	91.1	575.0	49.1	34.8	131.2	142.0	285.0	196.2	124.7	550.3	237.8	369.5	
10%	750.0	201.1	35.0	150.3	168.0	575.0	78.1	35.0	131.9	246.0	285.0	319.4	124.9	551.9	471.4	611.3	
<b>July</b>																	
90%	720.0	2.2	2.0	7.1	0.0	545.1	0.9	2.8	8.7	0.0	253.3	3.6	60.0	230.3	0.0	60.2	
80%	720.0	2.9	3.6	13.2	0.0	561.1	1.2	17.0	61.4	0.0	265.0	4.8	60.0	245.0	0.0	61.2	
50%	744.0	13.1	25.0	102.6	0.0	574.9	5.5	29.3	109.6	3.3	281.2	21.6	85.0	342.9	3.6	99.2	
20%	750.0	114.0	34.4	147.0	80.1	575.0	45.0	34.7	130.9	124.0	285.0	182.3	124.3	547.6	205.1	338.6	
10%	750.0	194.9	34.9	149.9	160.1	575.0	76.6	35.0	131.8	238.5	285.0	309.2	124.9	551.3	443.5	580.1	
<b>August</b>																	
90%	720.0	2.2	1.9	6.8	0.0	545.0	0.8	2.7	8.4	0.0	246.2	3.5	60.0	219.9	0.0	60.2	
80%	720.0	2.8	3.1	11.0	0.0	550.5	1.1	7.1	23.3	0.0	258.5	4.6	60.0	238.4	0.0	60.7	
50%	738.8	11.6	24.9	99.6	0.0	574.6	4.7	28.0	104.2	3.0	276.5	19.6	75.6	303.7	0.0	86.8	
20%	750.0	86.6	34.2	144.8	31.7	575.0	34.3	34.6	129.8	63.5	285.0	139.6	123.9	539.0	52.4	168.7	
10%	750.0	166.1	34.9	149.6	130.4	575.0	66.0	34.9	131.7	197.1	285.0	265.9	124.8	550.0	331.6	469.9	
<b>September</b>																	
90%	720.0	2.3	2.0	7.3	0.0	545.0	0.9	2.9	9.1	0.0	237.6	3.8	60.0	215.9	0.0	60.2	

(continued)

**Table 5.8** (continued)

Ambuklao Reservoir						Binga Reservoir						San Roque Reservoir								ARIIP	
	EOM Elev	Inflow	Release	Power	Spill	EOM Elev	Inflow	Release	Power	Spill	EOM Elev	Inflow	Release	Power	Spill						
80%	720.0	3.0	3.8	14.1	0.0	551.4	1.2	10.3	33.6	0.0	254.1	4.8	60.0	239.5	0.0	60.8					
50%	737.4	11.7	24.6	95.5	0.0	574.4	4.8	27.6	102.3	1.8	274.3	19.1	75.3	297.5	0.0	85.8					
20%	750.0	62.5	34.0	141.2	14.6	575.0	25.3	34.6	129.5	36.6	284.5	98.5	123.0	522.6	28.7	141.2					
10%	750.0	111.8	34.9	148.8	73.2	575.0	45.9	34.9	131.5	117.5	285.0	180.0	124.8	547.0	155.1	283.9					
October																					
90%	720.0	2.2	2.0	7.2	0.0	545.0	0.9	2.8	8.8	0.0	241.3	3.6	60.0	218.1	0.0	60.2					
80%	720.0	2.9	3.2	11.6	0.0	546.3	1.2	6.4	20.3	0.0	252.8	4.8	60.0	234.9	0.0	60.7					
50%	738.8	12.0	24.9	98.6	0.0	574.8	5.0	27.7	103.4	1.9	273.3	19.9	77.2	304.0	0.0	88.1					
20%	750.0	68.1	34.2	143.4	18.7	575.0	28.2	34.5	129.3	47.6	284.4	110.4	123.5	524.9	23.4	138.4					
10%	750.0	116.4	34.9	149.4	68.0	575.0	47.1	34.9	131.6	107.0	285.0	186.6	124.8	546.2	98.6	228.3					
November																					
90%	720.0	2.2	1.7	6.2	0.0	545.0	0.9	2.5	7.7	0.0	236.8	3.5	60.0	215.1	0.0	60.2					
80%	720.0	2.9	2.7	10.1	0.0	550.1	1.1	7.7	24.3	0.0	247.7	4.6	60.0	237.4	0.0	60.7					
50%	737.2	12.4	24.9	98.8	0.0	574.8	5.0	27.1	101.3	1.7	274.0	20.1	79.3	305.1	0.0	90.6					
20%	750.0	71.2	34.5	146.5	23.3	575.0	29.6	34.7	130.5	53.5	284.9	117.7	124.4	538.0	36.2	156.1					
10%	750.0	126.4	34.9	149.9	87.4	575.0	52.2	35.0	131.8	135.6	285.0	209.5	124.9	550.3	198.6	330.3					
December																					
90%	720.0	2.2	1.9	7.0	0.0	545.0	0.9	2.6	8.3	0.0	234.0	3.5	60.0	224.0	0.0	60.2					
80%	720.0	2.8	3.4	12.4	0.0	553.0	1.1	9.1	29.1	0.0	249.4	4.5	60.1	240.1	0.0	61.2					
50%	740.8	30.0	26.0	105.5	0.0	575.0	12.5	29.1	107.5	6.4	273.2	48.3	106.5	365.2	0.0	116.0					
20%	750.0	105.4	34.8	148.7	67.3	575.0	41.6	34.8	131.2	106.5	285.0	170.2	124.7	546.3	105.1	234.9					
10%	750.0	153.0	35.0	150.2	115.8	575.0	62.8	35.0	131.9	181.4	285.0	250.1	124.9	551.4	272.7	406.5					

**Table 5.9** Reservoir end-of-month elevations (m); inflows, releases, and spills ( $\text{m}^3/\text{s}$ ); and power generation (MW) for Ambuklao, Binga, and San Roque and outflow to ARJIP Reservoir at 90, 80, 50, 20, and 10 percent-of-time on monthly basis for target release policy Set 2

Ambuklao Reservoir				Binga Reservoir				San Roque Reservoir				ARJIP				
	EOM Elev	Inflow	Release	Spill	EOM Elev	Inflow	Release	Power	Spill	EOM Elev	Inflow	Release	Power	Spill	Outflow	
<b>January</b>																
90%	720.0	2.4	2.0	7.2	0.0	545.3	0.9	2.9	9.0	0.0	178.2	3.8	80.0	174.7	0.0	80.2
80%	720.0	3.5	4.2	15.3	0.0	550.2	1.4	9.2	28.8	0.0	204.9	5.7	83.4	254.4	0.0	84.9
50%	748.3	45.1	33.0	133.5	1.8	575.0	18.4	34.1	126.7	17.7	266.2	73.2	122.2	433.0	0.0	128.7
20%	750.0	127.7	34.9	150.0	83.9	575.0	51.8	34.9	131.8	131.8	285.0	205.2	124.9	550.2	177.9	309.9
10%	750.0	185.7	35.0	150.4	149.1	575.0	78.1	35.0	132.0	229.0	285.0	304.8	125.0	551.7	394.1	533.3
<b>February</b>																
90%	720.0	3.3	2.9	10.6	0.0	550.1	1.3	4.8	15.5	0.0	185.8	5.3	80.0	211.3	0.0	82.0
80%	723.0	7.5	21.1	84.6	0.0	568.4	3.0	29.8	105.0	0.2	213.1	12.3	93.0	268.8	0.0	98.2
50%	749.6	53.6	34.5	144.4	5.2	575.0	22.2	34.6	130.0	25.8	281.0	86.7	123.6	493.7	5.2	133.1
20%	750.0	135.9	35.0	150.1	93.9	575.0	55.0	35.0	131.9	144.2	285.0	216.0	124.9	550.9	209.6	341.8
10%	750.0	207.4	35.0	150.5	172.9	575.0	82.7	35.0	132.1	253.8	285.0	334.6	125.0	551.9	444.5	584.7
<b>March</b>																
90%	722.1	3.4	6.8	24.9	0.0	565.8	1.3	24.7	89.3	0.0	194.3	5.5	81.3	224.2	0.0	84.3
80%	735.5	7.0	27.6	108.9	0.0	573.8	2.9	31.1	116.4	1.1	233.1	12.2	96.7	327.6	0.0	105.5
50%	750.0	57.5	34.3	144.1	12.4	575.0	23.3	34.6	130.1	35.3	279.9	95.5	123.5	505.2	7.6	134.0
20%	750.0	146.7	34.9	150.1	107.6	575.0	57.7	35.0	131.9	163.7	285.0	220.6	124.9	550.6	249.4	382.7
10%	750.0	222.7	35.0	150.5	185.7	575.0	88.6	35.0	132.0	271.7	285.0	355.9	125.0	551.8	482.6	622.6
<b>April</b>																
90%	723.7	3.3	15.9	65.7	0.0	571.3	1.3	28.1	102.8	0.3	223.0	5.3	81.4	300.7	0.0	83.3
80%	736.7	6.4	28.3	111.2	0.0	574.3	2.6	31.6	117.8	1.7	258.2	10.5	93.9	344.2	0.0	100.3
50%	750.0	49.6	34.4	145.4	8.9	575.0	19.6	34.6	130.3	27.1	282.7	80.5	123.6	520.7	11.0	135.1
20%	750.0	138.8	35.0	150.1	101.8	575.0	55.4	35.0	131.9	154.8	285.0	222.0	124.9	550.8	234.9	369.7

(continued)

**Table 5.9** (continued)

Ambuklao Reservoir						Binga Reservoir						San Roque Reservoir								ARIIP	
	EOM Elev	Inflow	Release	Power	Spill	EOM Elev	Inflow	Release	Power	Spill	EOM Elev	Inflow	Release	Power	Spill						
10%	750.0	212.0	35.0	150.5	175.4	575.0	84.6	35.0	132.0	261.3	285.0	339.7	125.0	552.0	464.2	605.3					
<b>May</b>																					
90%	720.0	2.7	2.7	9.6	0.0	553.6	1.1	6.6	21.0	0.0	241.7	4.4	80.9	308.5	0.0	82.6					
80%	732.4	4.5	22.5	91.0	0.0	573.8	1.8	29.9	109.5	0.6	257.7	7.3	90.6	348.7	0.0	95.9					
50%	750.0	44.5	33.8	143.2	7.9	575.0	18.0	34.3	129.4	25.7	283.4	73.5	122.4	510.4	10.7	134.0					
20%	750.0	145.5	34.9	150.1	105.8	575.0	58.3	34.9	131.8	162.1	285.0	231.5	124.8	550.9	260.7	396.7					
10%	750.0	210.1	35.0	150.5	171.1	575.0	82.8	35.0	132.0	253.1	285.0	337.9	125.0	551.9	471.6	609.5					
<b>June</b>																					
90%	720.0	2.4	2.3	8.3	0.0	545.3	1.0	3.9	12.1	0.0	229.6	4.0	80.0	271.2	0.0	80.4					
80%	720.9	3.3	9.6	35.2	0.0	567.0	1.3	26.0	93.2	0.0	255.2	5.3	83.0	317.7	0.0	84.7					
50%	749.0	26.6	31.6	131.9	2.0	575.0	11.1	33.6	126.6	10.0	281.7	44.1	117.5	496.4	6.0	128.7					
20%	750.0	124.0	34.9	149.9	87.4	575.0	49.1	34.9	131.7	137.8	285.0	196.2	124.7	550.1	218.5	352.2					
10%	750.0	201.1	35.0	150.4	168.6	575.0	78.1	35.0	132.0	244.8	285.0	319.4	125.0	551.8	444.0	584.7					
<b>July</b>																					
90%	720.0	2.2	2.0	7.1	0.0	545.0	0.9	2.8	8.8	0.0	207.3	3.6	80.0	221.7	0.0	80.2					
80%	720.0	2.9	3.0	10.8	0.0	550.3	1.2	9.3	29.1	0.0	237.6	4.8	80.8	292.0	0.0	82.4					
50%	743.4	13.1	30.0	121.8	0.0	574.7	5.5	33.2	123.0	3.5	276.1	21.6	112.3	426.0	1.5	121.3					
20%	750.0	114.0	34.8	149.0	76.7	575.0	45.0	34.9	131.4	121.9	285.0	182.3	124.6	548.9	204.3	337.9					
10%	750.0	194.9	35.0	150.3	156.5	575.0	76.6	35.0	131.9	231.7	285.0	309.2	124.9	551.5	438.8	580.1					
<b>August</b>																					
90%	720.0	2.2	2.0	7.0	0.0	545.0	0.8	2.9	9.0	0.0	192.4	3.5	80.0	185.2	0.0	80.1					
80%	720.0	2.8	3.1	11.0	0.0	548.1	1.1	6.2	19.4	0.0	220.3	4.6	80.0	260.6	0.0	80.9					
50%	736.5	11.6	29.6	116.0	0.0	574.2	4.7	32.4	120.5	3.2	265.5	19.6	103.8	373.0	0.0	110.3					

	20%	750.0	86.6	34.8	148.0	27.4	575.0	34.3	34.9	131.4	62.5	285.0	139.6	124.4	541.8	43.6	159.2
	10%	750.0	166.1	35.0	150.0	128.0	575.0	66.0	35.0	132.0	193.5	285.0	265.9	124.9	550.7	327.5	464.6
September																	
90%	720.0	2.3	2.1	7.5	0.0	545.0	0.9	3.0	9.5	0.0	170.1	3.8	79.0	151.2	0.0	80.0	
80%	720.0	3.0	3.4	12.3	0.0	547.5	1.2	8.0	25.3	0.0	209.2	4.8	80.0	238.2	0.0	80.8	
50%	735.2	11.7	29.2	112.8	0.0	573.7	4.8	32.0	118.2	1.6	259.6	19.1	101.3	349.6	0.0	107.3	
20%	750.0	62.5	34.8	146.4	12.5	575.0	25.3	34.9	131.2	34.2	283.3	98.5	124.2	526.5	19.6	139.0	
10%	750.0	111.8	35.0	149.8	69.1	575.0	45.9	35.0	132.0	112.9	285.0	180.0	124.9	547.3	117.4	245.9	
October																	
90%	720.0	2.2	2.1	7.4	0.0	545.0	0.9	2.9	9.0	0.0	181.1	3.6	79.7	170.4	0.0	80.1	
80%	720.0	2.9	3.4	12.3	0.0	547.0	1.2	5.9	18.4	0.0	205.7	4.8	80.0	234.2	0.0	80.4	
50%	736.2	12.0	29.7	118.5	0.0	574.7	5.0	32.3	119.9	2.2	254.8	19.9	101.8	345.1	0.0	108.5	
20%	750.0	68.1	34.8	147.2	12.8	575.0	28.2	34.9	131.5	44.3	281.9	110.4	124.4	518.4	12.0	136.4	
10%	750.0	116.4	35.0	149.9	60.8	575.0	47.1	35.0	132.0	103.0	285.0	186.6	124.9	545.7	54.0	179.3	
November																	
90%	720.0	2.2	1.8	6.5	0.0	545.0	0.9	2.7	8.3	0.0	168.9	3.5	76.3	134.3	0.0	77.5	
80%	720.0	2.9	2.9	10.4	0.0	546.8	1.1	5.5	17.4	0.0	193.1	4.6	80.0	208.4	0.0	80.4	
50%	734.8	12.4	29.6	117.1	0.0	574.6	5.0	32.0	118.1	1.7	255.6	20.1	99.6	350.8	0.0	106.8	
20%	750.0	71.2	34.9	148.9	18.3	575.0	29.6	34.9	131.7	46.4	283.3	117.7	124.6	530.8	26.4	146.6	
10%	750.0	126.4	35.0	150.3	82.6	575.0	52.2	35.0	132.0	131.8	285.0	209.5	124.9	550.1	141.1	274.8	
December																	
90%	720.0	2.2	1.9	7.0	0.0	545.1	0.9	2.8	8.7	0.0	161.7	3.5	79.9	131.8	0.0	80.1	
80%	720.0	2.8	3.2	11.5	0.0	550.1	1.1	9.1	30.2	0.0	203.8	4.5	80.0	237.8	0.0	81.1	
50%	738.9	30.0	30.8	124.3	0.0	574.9	12.5	33.0	121.1	8.8	256.5	48.3	112.3	352.5	0.0	119.6	
20%	750.0	105.4	34.9	149.6	63.5	575.0	41.6	34.9	131.6	104.9	285.0	170.2	124.7	542.8	64.3	193.8	
10%	750.0	153.0	35.0	150.4	114.8	575.0	62.8	35.0	132.0	172.6	285.0	250.1	124.9	551.2	237.7	370.3	

**Table 5.10** Reservoir end-of-month elevations (m); inflows, releases, and spills ( $m^3/s$ ); and power generation (MW) for Ambuklao, Binga, and San Roque and outflow to ARIP Reservoir at 90, 80, 50, 20, and 10 percent-of-time on monthly basis for target release policy Set 3

Ambuklao Reservoir				Binga Reservoir				San Roque Reservoir				ARIP				
	EOM Elev	Inflow	Release	Spill	EOM Elev	Inflow	Release	Power	Spill	EOM Elev	Inflow	Release	Power	Spill	Outflow	
<b>January</b>																
90%	720.0	2.4	2.0	7.4	0.0	545.0	0.9	3.0	9.2	0.0	200.0	3.8	70.0	197.8	0.0	70.2
80%	720.0	3.5	3.8	14.1	0.0	550.1	1.4	7.4	22.9	0.0	223.2	5.7	75.1	260.1	0.0	76.8
50%	748.2	45.1	32.2	130.4	1.9	575.0	18.4	34.5	127.2	17.7	268.8	73.2	119.9	429.5	0.0	127.2
20%	750.0	127.7	34.9	149.8	86.0	575.0	51.8	35.0	131.8	131.8	285.0	205.2	124.8	549.9	183.7	315.6
10%	750.0	185.7	35.0	150.4	150.2	575.0	78.1	35.0	132.0	228.1	285.0	304.8	124.9	551.8	402.0	538.5
<b>February</b>																
90%	720.0	3.3	3.0	10.7	0.0	546.6	1.3	5.3	16.8	0.0	210.0	5.3	70.0	218.8	0.0	72.1
80%	722.9	7.5	18.7	73.6	0.0	565.8	3.0	30.8	112.9	0.1	227.3	12.3	83.7	279.1	0.0	89.8
50%	749.6	53.6	34.2	141.1	5.6	575.0	22.2	34.8	130.5	25.0	282.3	86.7	122.4	480.8	4.8	131.3
20%	750.0	135.9	34.9	150.0	95.3	575.0	55.0	35.0	131.9	145.3	285.0	216.0	124.9	550.6	212.3	345.2
10%	750.0	207.4	35.0	150.4	171.4	575.0	82.7	35.0	132.1	252.8	285.0	334.6	125.0	551.9	459.5	595.0
<b>March</b>																
90%	722.5	3.4	7.6	30.0	0.0	564.4	1.3	26.2	96.7	0.0	211.5	5.5	74.1	250.6	0.0	80.8
80%	736.1	7.0	26.4	108.5	0.0	573.0	2.9	33.0	121.5	1.5	242.5	12.2	90.6	322.4	0.0	100.7
50%	750.0	57.5	33.9	142.1	11.6	575.0	23.3	34.8	130.5	35.3	282.1	95.5	122.1	491.7	10.8	133.1
20%	750.0	146.7	34.9	149.9	109.0	575.0	57.7	35.0	131.9	163.6	285.0	230.6	124.8	550.1	251.1	386.8
10%	750.0	222.7	35.0	150.4	183.9	575.0	88.6	35.0	132.1	271.3	285.0	355.9	125.0	551.7	483.5	624.6
<b>April</b>																
90%	724.6	3.3	15.4	61.6	0.0	567.5	1.3	28.8	106.4	0.2	233.4	5.3	71.5	277.3	0.0	74.2
80%	736.5	6.4	27.6	109.6	0.0	573.4	2.6	33.1	122.4	1.9	264.0	10.5	86.6	325.0	0.0	96.1
50%	750.0	49.6	33.9	143.3	9.6	575.0	19.6	34.8	130.6	27.6	283.7	80.5	122.7	515.2	12.7	134.2
20%	750.0	138.8	34.9	150.1	101.4	575.0	55.4	35.0	131.9	155.3	285.0	222.0	124.9	551.0	245.7	381.0

	10%	750.0	212.0	35.0	150.5	175.2	575.0	84.6	35.0	132.1	263.0	285.0	339.7	125.0	551.9	475.5	618.3
<b>May</b>																	
90%	720.0	2.7	2.4	8.8	0.0	547.1	1.1	4.2	12.9	0.0	250.3	4.4	70.5	277.5	0.0	72.1	
80%	732.2	4.5	19.6	79.1	0.0	572.4	1.8	31.7	117.8	0.6	263.6	7.3	82.0	325.2	0.0	90.7	
50%	750.0	44.5	33.2	140.1	8.4	575.0	18.0	34.7	130.3	24.0	283.7	73.5	121.3	505.7	13.3	133.2	
20%	750.0	145.5	34.9	149.9	107.1	575.0	58.3	35.0	131.9	163.5	285.0	231.5	124.8	550.7	263.9	398.6	
10%	750.0	210.1	35.0	150.4	173.8	575.0	82.8	35.0	132.0	252.4	285.0	337.9	125.0	551.9	476.9	615.6	
<b>June</b>																	
90%	720.0	2.4	2.2	8.0	0.0	545.2	1.0	3.4	10.4	0.0	241.2	4.0	70.0	263.5	0.0	70.6	
80%	720.9	3.3	7.5	28.4	0.0	562.1	1.3	24.9	90.0	0.0	261.9	5.3	74.4	292.9	0.0	77.9	
50%	749.3	26.6	30.8	130.0	2.2	575.0	11.1	34.5	129.1	11.0	282.5	44.1	115.8	483.7	7.7	127.5	
20%	750.0	124.0	34.8	149.6	89.4	575.0	49.1	35.0	131.7	137.0	285.0	196.2	124.7	549.9	224.8	358.2	
10%	750.0	201.1	35.0	150.3	167.7	575.0	78.1	35.0	132.0	244.4	285.0	319.4	124.9	551.7	449.2	584.8	
<b>July</b>																	
90%	720.0	2.2	2.0	7.2	0.0	545.0	0.9	2.8	8.6	0.0	222.4	3.6	70.0	237.1	0.0	70.3	
80%	720.0	2.9	3.1	11.1	0.0	548.3	1.2	6.5	19.9	0.0	247.8	4.8	71.8	272.8	0.0	73.9	
50%	743.4	13.1	29.8	118.1	0.0	574.2	5.5	34.4	127.0	3.7	277.6	21.6	107.2	413.7	2.2	118.4	
20%	750.0	114.0	34.7	148.6	77.1	575.0	45.0	35.0	131.6	121.8	285.0	182.3	124.5	547.7	205.6	338.2	
10%	750.0	194.9	35.0	150.2	156.5	575.0	76.6	35.0	132.0	230.8	285.0	309.2	124.9	551.4	438.3	580.1	
<b>August</b>																	
90%	720.0	2.2	1.9	6.7	0.0	545.0	0.8	2.8	8.7	0.0	210.1	3.5	70.0	204.0	0.0	70.2	
80%	720.0	2.8	2.9	10.3	0.0	546.2	1.1	5.2	16.1	0.0	236.2	4.6	70.9	256.1	0.0	72.3	
50%	736.7	11.6	29.4	114.4	0.0	573.1	4.7	34.1	125.3	3.9	268.5	19.6	100.4	367.8	0.0	108.2	
20%	750.0	86.6	34.7	146.7	28.0	575.0	34.3	35.0	131.5	61.7	285.0	139.6	124.0	538.2	49.5	168.1	
10%	750.0	166.1	35.0	149.9	128.7	575.0	66.0	35.0	132.0	193.4	285.0	265.9	124.8	550.0	329.7	465.9	
<b>September</b>																	
90%	720.0	2.3	2.0	7.1	0.0	545.0	0.9	2.9	8.9	0.0	194.6	3.8	70.0	187.0	0.0	70.3	

(continued)

Table 5.10 (continued)

Ambuklao Reservoir						Binga Reservoir						San Roque Reservoir								ARIIP	
	EOM Elev	Inflow	Release	Power	Spill	EOM Elev	Inflow	Release	Power	Spill	EOM Elev	Inflow	Release	Power	Spill						
80%	720.0	3.0	3.1	11.2	0.0	546.1	1.2	6.3	19.6	0.0	221.5	4.8	70.6	245.8	0.0	72.3					
50%	734.7	11.7	28.7	110.8	0.0	572.8	4.8	34.1	123.6	1.7	264.8	19.1	100.3	339.3	0.0	107.4					
20%	750.0	62.5	34.6	144.5	12.6	575.0	25.3	35.0	131.3	34.4	283.7	98.5	123.7	525.9	22.4	140.1					
10%	750.0	111.8	35.0	149.3	70.2	575.0	45.9	35.0	132.0	112.6	285.0	180.0	124.8	545.5	126.9	253.3					
October																					
90%	720.0	2.2	2.0	7.3	0.0	545.0	0.9	2.9	9.1	0.0	195.9	3.6	70.0	194.0	0.0	70.2					
80%	720.0	2.9	3.2	11.7	0.0	546.2	1.2	5.1	16.0	0.0	216.7	4.8	70.3	243.0	0.0	71.7					
50%	736.6	12.0	29.5	114.7	0.0	574.1	5.0	34.0	124.6	2.7	261.9	19.9	100.8	343.0	0.0	110.0					
20%	750.0	68.1	34.7	145.7	15.4	575.0	28.2	35.0	131.7	44.8	283.0	110.4	124.0	518.4	15.0	136.0					
10%	750.0	116.4	35.0	149.6	62.5	575.0	47.1	35.0	132.0	104.3	285.0	186.6	124.8	544.4	65.1	190.1					
November																					
90%	720.0	2.2	1.8	6.6	0.0	545.0	0.9	2.7	8.3	0.0	190.3	3.5	70.0	184.5	0.0	70.2					
80%	720.0	2.9	2.8	10.2	0.0	545.7	1.1	4.8	14.9	0.0	213.4	4.6	70.1	226.9	0.0	71.0					
50%	735.0	12.4	29.5	114.5	0.0	573.6	5.0	34.3	125.0	2.2	260.6	20.1	101.5	335.7	0.0	109.4					
20%	750.0	71.2	34.8	148.1	18.9	575.0	29.6	35.0	131.7	46.4	284.2	117.7	124.5	532.2	27.0	147.4					
10%	750.0	126.4	35.0	150.2	82.8	575.0	52.2	35.0	132.0	132.0	285.0	209.5	124.9	549.6	167.5	287.8					
December																					
90%	720.0	2.2	2.0	7.1	0.0	545.0	0.9	2.8	8.7	0.0	187.2	3.5	70.0	179.8	0.0	70.2					
80%	720.0	2.8	3.2	11.9	0.0	547.5	1.1	6.4	19.7	0.0	217.8	4.5	70.5	237.9	0.0	71.9					
50%	739.3	30.0	30.0	120.6	0.0	574.6	12.5	34.3	124.5	8.5	261.3	48.3	109.5	347.9	0.0	116.6					
20%	750.0	105.4	34.9	149.2	64.9	575.0	41.6	35.0	131.7	104.2	285.0	170.2	124.6	543.6	69.7	200.1					
10%	750.0	153.0	35.0	150.4	115.0	575.0	62.8	35.0	132.0	173.4	285.0	250.1	124.9	551.1	247.8	384.9					

of 30 days in March. Likewise, hydropower equal to or greater than 136.7 MW (at 50 percent-of-time reliability) can be generated 15 days out of 30 days for the month of March.

It may be noted also in Tables 5.8, 5.9, and 5.10 that the outflow to ARIIP always satisfies the irrigation daily requirements (maximum of  $27 \text{ m}^3/\text{s}$ ) for all months at a reliability of 90 percent-of-time or even better. In fact, in almost all months, the average daily releases are as high as  $80 \text{ m}^3/\text{s}$  so in this case, ARIIP can even increase its irrigation service area to even twice the current service area.

One has to study carefully these tables to be able to compare across different target release policies. Generally, the results showed that among the three release policies, Set 2 provides higher hydropower generation compared to Set 1 (considered to be conservative release policy) or Set 3 (aggressive release policy). This implies that optimal reservoir releases should not be too conservative or too aggressive so that part of the study is to likewise seek for this best or optimal target release.

### **5.3.7 Optimization-Simulation of San Roque Dam Flood Operations During Typhoon Parma**

This is an aside on an optimization-simulation operations study of San Roque Dam during Typhoon Parma on October 2–10, 2009. This study was conducted by the author as chair of an investigation committee formed by the Senate of the Philippines as a result of the flood devastation brought about by this typhoon along the Agno River Basin, downstream of the San Roque Dam. Details of this investigation are contained in the report by Tabios et al. (2010).

#### **5.3.7.1 Typhoon Parma Track and Rainfall**

Typhoon Parma, locally called Pepeng in the Philippines as shown in Fig. 5.17, came in and out, in again, and finally out of Northern Luzon wreaking havoc especially in the Lower Agno River Basin of Pangasinan downstream of the San Roque Dam. Forecasting the track of Typhoon Parma was quite a challenge since at 2AM October 4 in 2009; Parma was heading out after hitting the San Roque Dam area the day before. But then, at 8AM on October 4, PAGASA (weather service agency of the Philippines) forecasted that it was coming back and only to reverse its forecast at 8PM on October 4 and 2PM on October 5 that Parma was heading out. In fact, at 10AM on October 6, PAGASA stated that there *is no major disturbance expected to affect the Agno River Basin within the next 24 hours* implying that Parma was not coming back. But barely 4 hours later, PAGASA announced at 2PM on October 6 that Parma was definitely coming back. The next day and especially on October 8–9, San Roque Dam had to make significant spillway releases before the dam was overtopped which caused the devastating flooding in the Lower Agno River Basin especially in the towns of San Manuel, Tayug, Rosales, Alcala, and Villasis in Pangasinan.

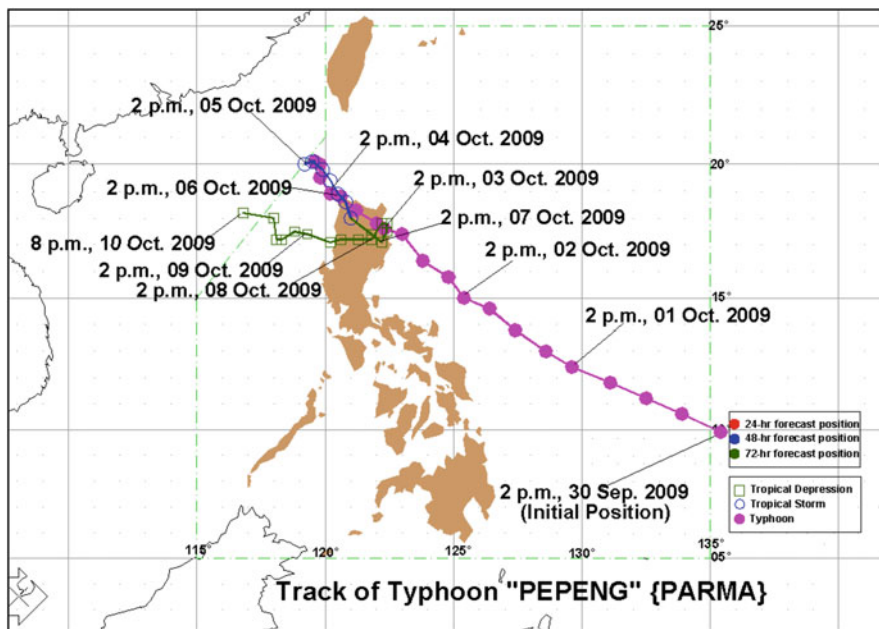


**Fig. 5.17** Tract of Typhoon Parma, locally called Pepeng during the period October 1–10, 2009 from PAGASA

Typhoon track forecasts provided useful information to reservoir flood operations, but it was definitely not enough for making crucial decisions under typhoon conditions and especially under critical states of the reservoir, like the San Roque reservoir levels during Typhoon Parma which was almost halfway to its maximum flood storage allocation and rising as early as October 5. Rainfall forecasts which could be used for river flow or runoff forecast associated to the typhoon could have been extremely useful for purposes of reservoir flood routing operations. However, PAGASA, for lack of the proper equipment or decision support system, did not provide rainfall forecasts.

### 5.3.7.2 Extent of Flooding in Pangasinan

The flooding in Pangasinan was not only from Agno River but also from Bued River (see Fig. 4.26, Sect. 4.3.1 of Chapter 4). The Bued River area (along Kennon Road and especially around Mt. Ampucao) was the major source of floodwaters that hit Dagupan City. The worst flooded area along the lower Agno River was the Carmen, Rosales, areas and generally downstream of San Roque Dam and upstream of Bayambang. An interesting observation here is that based on the observed time series of Agno River water elevations near Carmen Bridge (along MacArthur Highway), the peak water stage occurred at 12:24AM on October 9, 2009 which

was 3 hours earlier when the peak spillway release of San Roque Dam was made at 3AM on October 9, 2009. In fact, as early as 7:15AM on October 9, the water stage at Carmen Bridge was already rapidly rising; the significant spillway releases from San Roque starting at 11AM that day – beginning at  $2000 \text{ m}^3/\text{s}$  and going up to over  $5,000 \text{ m}^3/\text{s}$  – greatly exacerbated the situation. It may be noted that the flow travel time from San Roque Dam to Carmen area which is a distance of about 40 km along the Agno River was about 5.5–7.5 h assuming channel velocities of 1.5–2.0 m/s. The implication is that the peaking of water surface elevation of Agno River near Carmen Bridge must have been also a result of local inflows from Ambayoan, Viray, and Banila Rivers which are tributaries of Agno River upstream of Carmen area. In any case, part of these river floodwaters were coming from San Roque Reservoir since spillway releases above  $2,000 \text{ m}^3/\text{s}$  made around 12 noon, October 8 which must have already reached the Carmen, Rosales, area around 6PM that day.

### 5.3.7.3 San Roque Dam and Reservoir Operations

During Typhoon Parma, Ambuklao Dam was able to perform certain flood control function since it had attenuated the inflows of about  $3,500 \text{ m}^3/\text{s}$  during late evening of October 8 to become an outflow of about  $2,400 \text{ m}^3/\text{s}$ . However, Binga Dam has virtually no flood storage function since the inflows to the reservoir were almost equal to the outflows. San Roque Reservoir (see Fig. 5.18) was able to attenuate (or lessen) the flood peak of Agno River in the first passage of Typhoon Parma (i.e., October 3–4) and also in the second passage (October 7) but not in the third passage (October 8–9). In the third passage, the San Roque Reservoir was operated such that inflows were almost equal to the outflows as if the dam did not exist.

It is important to emphasize that during the period between October 5 and 7 with the reservoir already above 284 m (290 m is maximum operating level) and rising, the dam operators still made the decision not to spill/release from the reservoir. Two factors influencing the decision whether to release now or later are as follows: (1) spilling reservoir water at that instant would free more flood control storage space for future use (the already predicted return of Parma); the downside of such an action would be that it could exacerbate the flooding downstream of the dam; or 2) not spilling water would attenuate the flooding downstream of the dam; the downside of such an action would be that there would be very little flood control storage to attenuate any prospective flood inflow.

On hindsight, the dam operators actually waited too long to make significant pre-emptive releases during the period between October 5 and 7, 2009. It would have been perhaps too soon if it were done on October 5 which was one day after the first passage of the typhoon. On October 6, the press release made by PAGASA at 10AM that day stating that *with no major disturbance expected to affect the [Agno River] Basin within the next 24 hours, the present condition does not necessitate the operation of its spillways* would have directly influenced the dam operators not to make significant pre-emptive spillway release. However, with the typhoon track forecast bulletin issued by PAGASA 4 hours later at 2PM on October 6 indicating that Typhoon Parma was definitely coming back, this should have signaled the dam

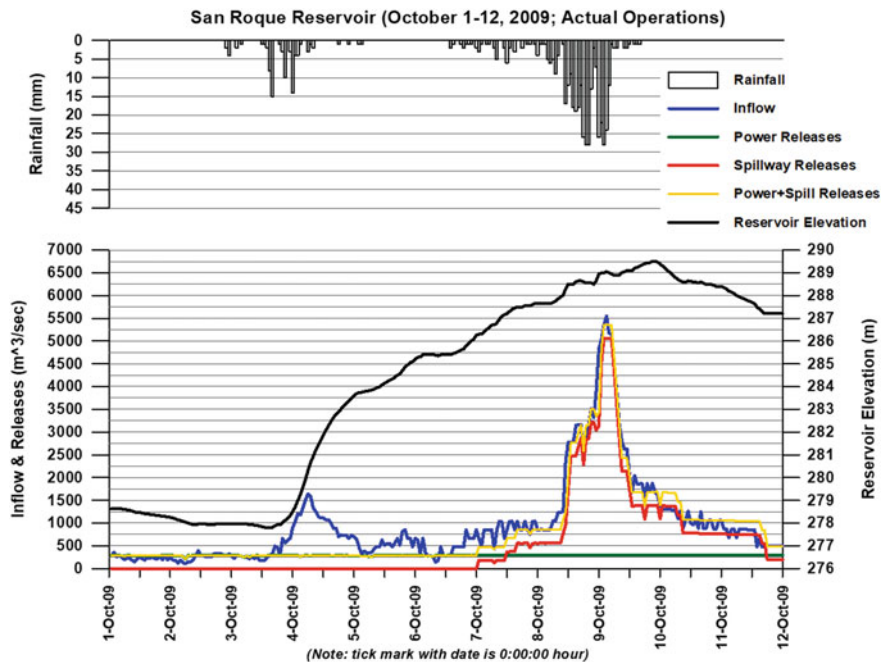


**Fig. 5.18** Time series plots of observed rainfall, reservoir levels, inflows, and spills of San Roque Dam during Typhoon Parma provided by NAPOCOR

operators to make significant pre-emptive spillway releases already. Yet they did not, but waited until 1AM on October 7, and even then released water at an insignificant rate of  $215 \text{ m}^3/\text{s}$  – increasing the rate at infinitesimal amounts – so that by 10AM of October 8, or almost 48 hours later, the release was still only at  $800 \text{ m}^3/\text{s}$ .

#### 5.3.7.4 Pre-emptive Reservoir Spillway Releases

What would have happened if the pre-emptive spillway releases had been made earlier and in greater amounts? An illustrative optimization-simulation study was conducted to find out. The optimization-simulation, WATPOW model (Tabios and Shen 1993), presented earlier was also used here. To validate the optimization-simulation model for San Roque Dam operations, the model was ran with given inflows, specified reservoir releases (power and spillway), and initial reservoir elevation on October 1, 2009 (12:00AM) up to October 12, 2009. Figure 5.19 shows time series of reservoir variables (inflows, outflows, and elevations including rainfall) computed by the WATPOW model which may be compared to the corresponding time series plots of the raw data in Fig. 5.18. It is seen here that the

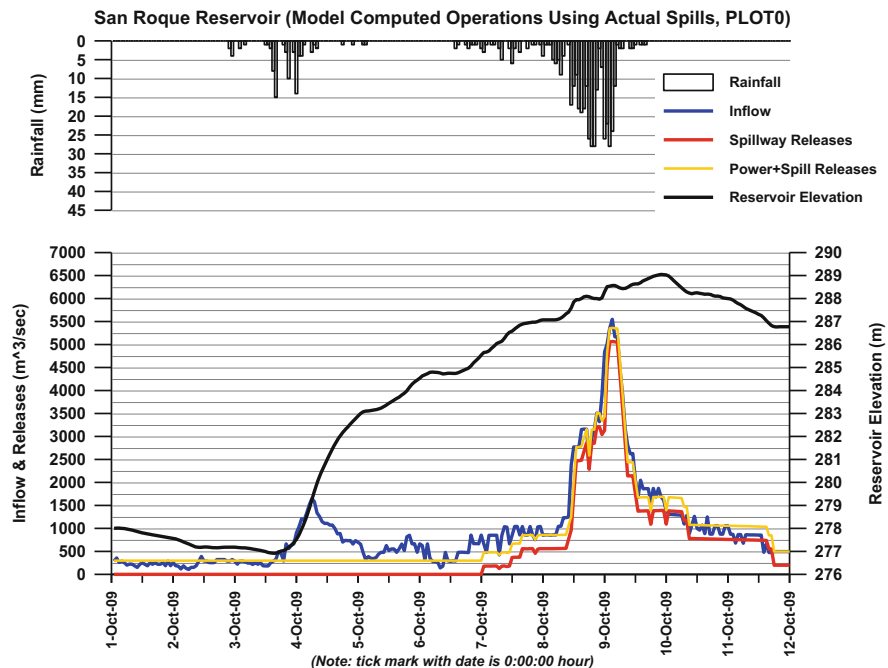


**Fig. 5.19** Time series plots of rainfall, inflows, power releases, spillway releases, power plus spillway releases, and reservoir elevations of San Roque Dam during Typhoon Parma computed from the optimization-simulation model

plots of reservoir elevations of raw data and model-calculated data are close to each other, thus validating the optimization-simulation model.

Using the optimization-simulation model, four reservoir operation cases (simulation scenarios) are ran below as follows:

- Case 1: Spills (pre-emptive releases) are made after 8AM October 5 and when the reservoir elevation (specified threshold elevation) is above 280 m.
- Case 2: Spills (pre-emptive releases) are made after 8AM October 5 and when the reservoir elevation is above 282 m.
- Case 3: Spills (pre-emptive releases) are made after 8AM October 6 and when the reservoir elevation is above 280 m.
- Case 4: Spills (pre-emptive releases) are made after 8AM October 6 and when the reservoir elevation is above 282 m.

In these optimization-simulation runs, the objective function is to minimize the maximum spillway releases (n.b., power or turbine releases are at maxima) starting at the specified pre-emptive release time (e.g., 8AM, October 5) provided that the reservoir elevation is above the specified threshold elevations (e.g., 280 m). The major constraint in the optimization model is the physical system constraint (i.e., reservoir hydrologic routing equation, reservoir storage-elevation relationship, and

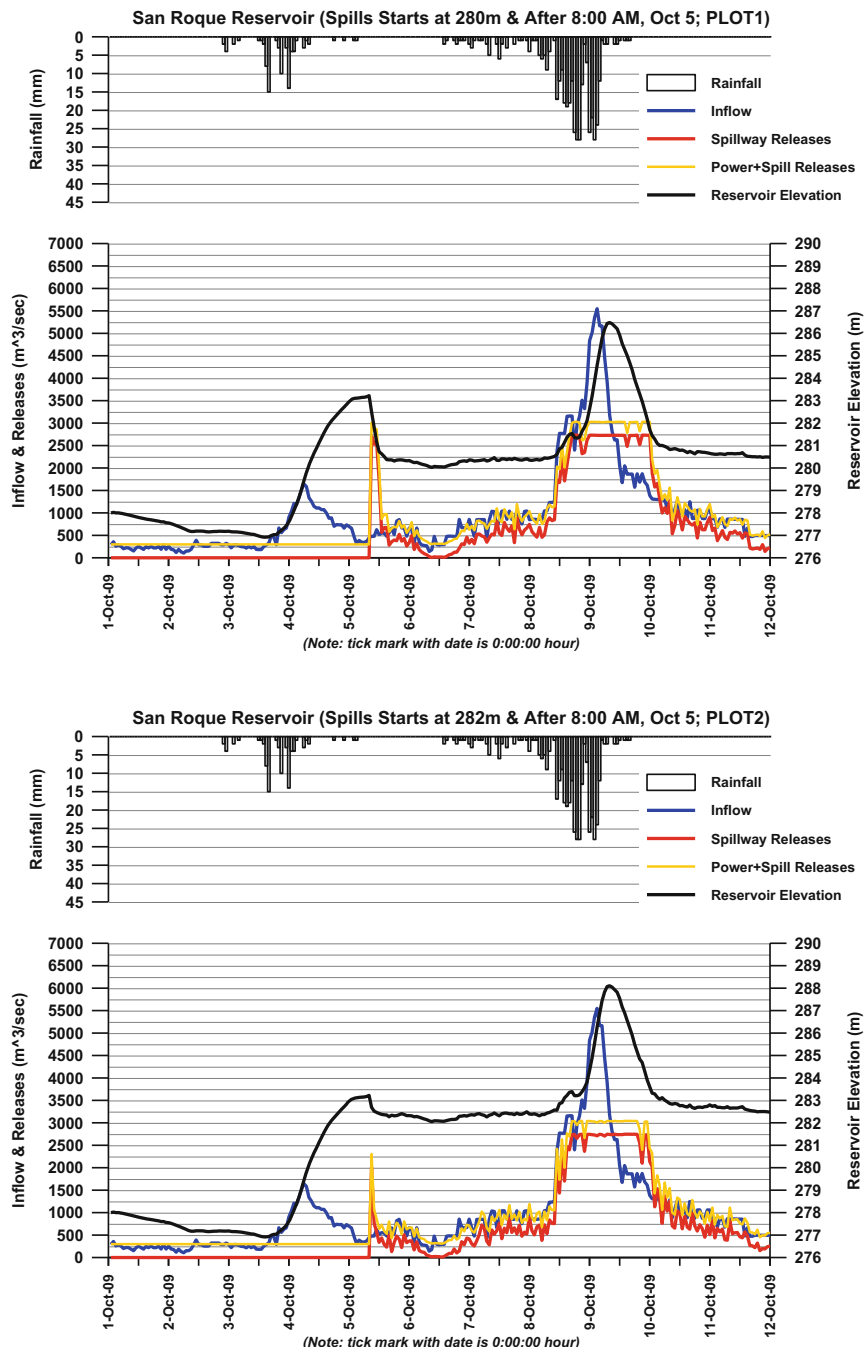
spillway rating curve) defined by the simulation model. For the case of 8AM, October 5, pre-emptive release time (simulation ending at midnight of October 12), the optimization model calculates (optimizes) a total of 161 hourly spillway flows, and for the case of 8AM, October 6, pre-emptive release time, a total of 137 hourly spillway flows. Note that these are considerable number of decision variables (hourly spillway flows) to calculate (optimize) if done manually thus the need for a mathematical, computerized optimization-simulation model especially in real-time operations.

Figure 5.20 shows the results of optimization-simulation model runs for Cases 1 (top figure) and 2 (bottom figure) while Fig. 5.21 for Cases 3 (top figure) and 4 (bottom figure). These two figures show the time series plots of rainfall, inflows, power releases, spillway releases, power plus spillway releases, and reservoir elevations of San Roque Dam using the optimization-simulation model. Tables 5.11 and 5.12 give the time and reservoir inflows, spills, outflows, and reservoir elevations at the occurrence of maximum outflows (spills plus power releases) and at the occurrence of maximum reservoir elevations, respectively, for the actual case (from October 1 to 12, 2009 flood data), Case 1, Case 2, Case 3, and Case 4.

It is seen in Figs. 5.20 and 5.21 that when the spillway prereleases (for Cases 1 through 4) were made at those particular times and threshold reservoir elevations, there was a spike of spillway release that almost reached as high as  $2,500 \text{ m}^3/\text{s}$  (except Case 2) to bring down the reservoir elevations to the threshold elevations. Referring to Table 5.13, the maximum spillway discharges reached about  $2,700 \text{ m}^3/\text{s}$  or a total reservoir outflow (spillway plus power releases) of about  $3,000 \text{ m}^3/\text{s}$  for the four optimization-simulation cases compared to the actual case of 5,101 and  $5,361 \text{ m}^3/\text{s}$ , respectively. Note that the power releases at those reservoir elevations were about  $260 \text{ m}^3/\text{s}$ . In Table 5.14, the maximum reservoir elevations reached 286.51 and 286.75 m for Cases 1 and 3, respectively, since early pre-emptive spillway releases were made as early as October 5 compared to the maximum reservoir elevations of 287.90 and 287.94 m for Cases 2 and 4, respectively. The actual case reached a maximum elevation of 289.50 m which was almost at the top elevation of the spillway gate of 289.6 m. Operating the reservoir at elevations of 288 m or higher is already at risky levels that could result in overtopping and possibly damaging the spillway structure even if water levels are still way below the dam crest elevation of 295 m. Of course, overtopping of the dam itself and especially resulting to a dam-break would be very catastrophic and damaging to the communities downstream of San Roque Dam since flood waves generated could be as high as tens of meters and spreading fifty (50) kilometers or so.

It should be emphasized that the illustrative optimization-simulation runs presented above considered only the flood control function of San Roque Reservoir and using perfect foresight or forecast since the actual inflows were used. Also, in actual reservoir operations under extreme flood conditions, the downstream flooding situations and inflow forecast errors should be factored in the reservoir operating strategies and decisions.

In any case, the results of these simulations show that early and significant pre-emptive spillway releases (rather than wait-till-the-last-minute attitude) would have alleviated flooding in Carmen-Rosales, Asingan, Sta. Maria, and Tayug (towns



**Fig. 5.20** Time series plots of rainfall, inflows, power releases, spillway releases, power plus spillway releases, and reservoir elevations of San Roque Dam using the optimization-simulation model. The top (Case 1) and bottom (Case 2) figures are plots when spillway releases are made after 8AM on October 5, 2009 when the reservoir elevations are above 280 m and 282 m, respectively

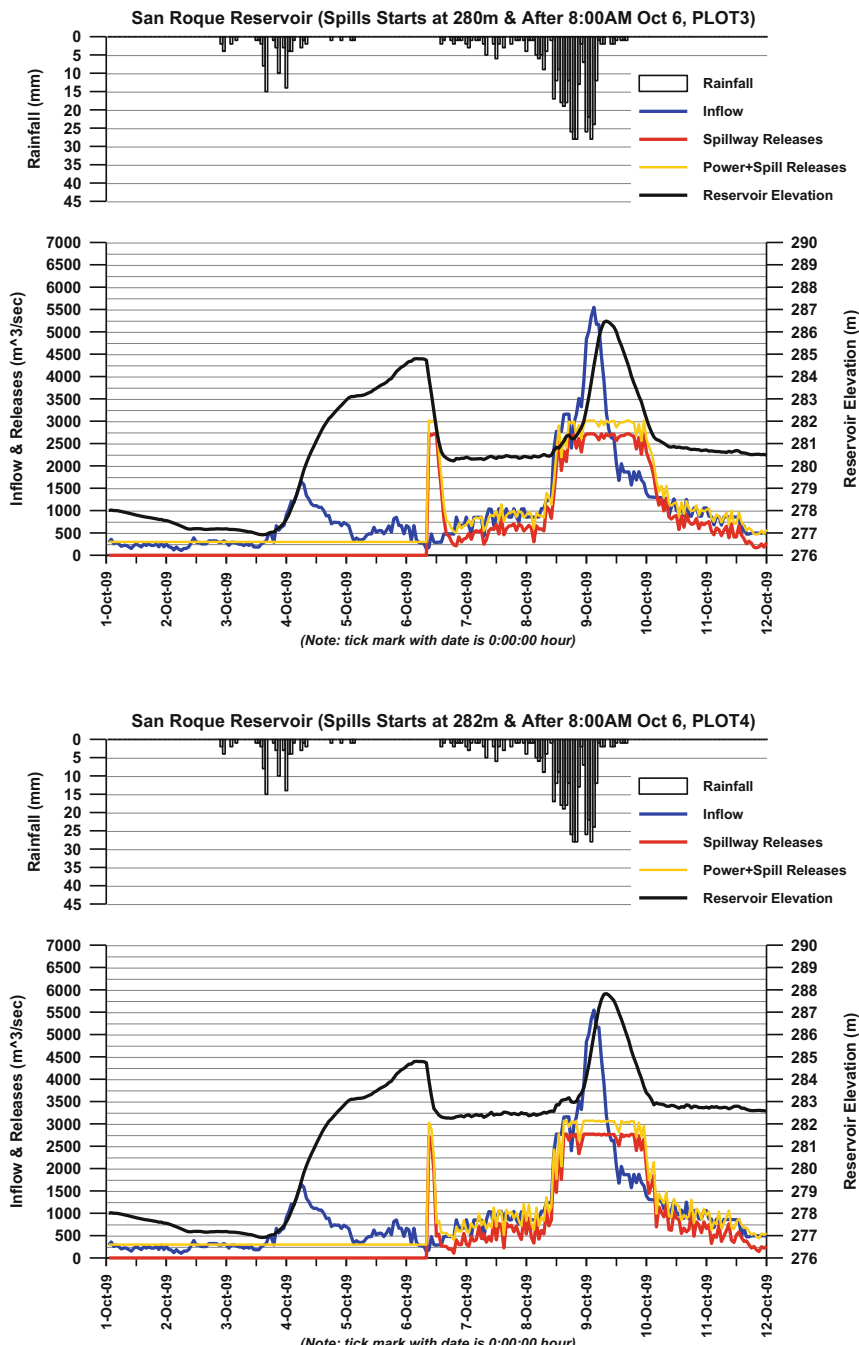


**Fig. 5.21** Time series plots of rainfall, inflows, power releases, spillway releases, power plus spillway releases, and reservoir elevations of San Roque Dam using the optimization-simulation model. The top (Case 3) and bottom (Case 4) figures are plots when spillway releases are made after 8AM on October 6, 2009 when the reservoir elevations are above 280 m and 282 m, respectively

**Table 5.11** Time and reservoir inflows, spills, outflows, and reservoir elevations at the occurrence of maximum outflows (spills plus power releases) for the actual case, Case 1, Case 2, Case 3, and Case 4

<i>Occurrence of Maximum Outflows (Spills + Releases)</i>					
Case	Time	Inflow (m <sup>3</sup> /s)	Spill (m <sup>3</sup> /s)	Outflow (m <sup>3</sup> /s)	Reservoir Elevation (m)
Actual	3AM, Oct 9	5547	5101	5361	289.05
Case 1	4 PM, Oct 8	3158	2724	2984	281.35
Case 2	5 PM, Oct 8	3156	2766	3026	283.15
Case 3	5 PM, Oct 8	3156	2670	2930	281.29
Case 4	8 PM, Oct 8	3148	2825	3085	283.04

**Table 5.12** Time and reservoir inflows, spills, outflows, and reservoir elevations at the occurrence of maximum reservoir elevations for the actual case, Case 1, Case 2, Case 3, and Case 4

<i>Occurrence of Maximum Reservoir Elevations</i>					
Case		Inflow (m <sup>3</sup> /s)	Spill (m <sup>3</sup> /s)	Outflow (m <sup>3</sup> /s)	Reservoir Elevation (m)
Actual	9 PM, Oct 9	1871	1424	1684	289.50
Case 1	8 AM, Oct 9	3180	2638	2898	286.51
Case 2	8 AM, Oct 9	3180	2753	3013	287.90
Case 3	8 AM, Oct 9	3180	2570	2830	286.75
Case 4	8 AM, Oct 9	3180	2806	3066	287.94

downstream of San Roque Dam) which can only be flooded if the discharge in Agno River is about 3,000 m<sup>3</sup>/s (see Tables 5.11 and 5.12) which is less than 3,000 m<sup>3</sup>/s indeed for optimized cases except for San Manuel which can be flooded even at 1,000 m<sup>3</sup>/s.

### 5.3.8 Some Discussions on Upper Agno Reservoir Operations

Based on the results of this optimization-simulation study in Sect. 5.3.6, the reservoir release policy should be based on the target release policy Set 2. In implementing this reservoir operating rules for real-time operation on daily basis, the recommendation is to implement this optimization-simulation model with the objective function and the benefit/penalty coefficients likewise to be refined and with a *moving planning horizon* or window of 15 to 30 days. In this case, forecast values of inflows must be provided. Essentially, this study recommends the use of *target reservoir release* operating rules in contrast to *target reservoir storage* operating rules as done in other reservoirs.

A more comprehensive way to develop reservoir operating rules for normal and emergency operations (under flood control conditions) requires further studies. In particular, the operation rules or protocol for multipurpose reservoirs, especially San Roque Dam as suggested by Tabios et al. (2010), must be three-tiered as follows:

1. A long-term reservoir operation rule which may be based on monthly or seasonal purposes such as hydropower generation and irrigation releases
2. A medium-term operation rule which is to fine tune the water allocation based on seasonal (monthly or weekly) outlook or forecast of weather or climatic conditions
3. A short-term (almost real-time) operation rule especially under emergency or flood control conditions which is based on dynamic, anticipatory, control-feedback flood operation model with rainfall-runoff forecasting model

It may be noted that the existing reservoir operations based on storage rule curve, for instance, at San Roque Dam, is a constant, all-year-round value of 280 m reservoir elevation. This constant-valued rule curve disregards long-term climate cycles, within-the-year seasonalities or, short-term, or near-future weather outlook such as an incoming typhoon or drought episode. Thus, the rationale for a three-tiered reservoir operating rule based on target release rule is to account for long-term beyond-the-year climate outlook (Equatorial Pacific-based El Nino versus La Nina years and including Indian Ocean index), seasonal variations (actual onset of wet and dry months) including seasonal outlook of medium-term climate or weather changes, and short- or near-term forecasts of incoming extreme weather or typhoon events.

The long-term reservoir operating rule should be developed considering the multipurpose objectives of the reservoir especially for San Roque Reservoir which include hydropower generation, irrigation water supply, and flood control function. This entails optimization-simulation studies to evaluate the long-term impacts of medium-term or short-term, seasonal occurrences of drought and typhoons or wet and dry years. For instance, the flood control function of the reservoir may entail large pre-emptive water releases that can compromise the long-term objectives of hydropower generation and irrigation purposes.

The medium-term reservoir operation rule is like the long-term operating rule curve but for fine tuning the long-term rule curves as a function of monthly or weekly weather outlook or forecast. These adjustments can likewise be developed based on optimization-simulation runs and a seasonal forecast model based on climatic/weather variables which must be developed as part of the procedure or protocol in implementing the medium-term rule curve adjustment.

The short-term, real-time flood operation rule would involve development of real-time optimization-simulation model of the reservoir as well as the peripheral models such as flood inundation model downstream of the reservoir, rainfall, and runoff forecasting model upstream of the reservoir. These models can then be tested for several optimization-simulation flood scenarios under different historical and future single-storm, multiple-storm, and catastrophic storm events. From these flood studies, specific protocols related to flood forecasting, flood warning including disaster management (evacuation, response, and recovery), strategies can also be developed.

The same models above should also be used in real-time reservoir operations given the forecasts of rainfall and runoff (inflows) to the reservoir. Note that in real-time operations, forecasting rainfall and subsequently runoff is necessary in order to implement the reservoir operations models in dynamic, anticipatory, and adaptive framework.

Finally, the above reservoir operating rules should be implemented through a computerized decision support system (DSS) together with a real-time data acquisition system (especially during emergency operations). Also, while the results and outputs of the computerized DSS provide operational and specific course of action, it should not replace the knowledge and judgment of dam operators in actual reservoir operations.

## **5.4 Proposed Agos Reservoir System Optimization-Simulation Studies for Reliability Analysis and Project Sequencing and Staging**

The Metropolitan Waterworks and Sewerage System (MWSS), in response to the increasing demand and deficit in water supply as projected at its service area, required the development of supplementary sources of water. Included in its priority list are the proposed Kaliwa Low Dam, Laiban Dam, Kanan Dam, and Agos Dam projects. These water sources, all situated within the Agos River Basin with Agos River the main stem fed by Kaliwa River and Kanan River, have already been proposed in the past, and several studies have already been conducted for this system. The development of these water sources includes dam and reservoir so that in addition to water supply purposes, hydropower generation is possible and even with some flood control function.

Most studies conducted in the past for this proposed water source were on a monthly basis which may not be adequate for reliability analysis of a water supply or hydropower project. Further, there are no sufficiently long daily stream flow records at the proposed sites to properly conduct reliability analysis. Since long term, daily rainfall data are available in the vicinity of the river basin, a continuous simulation watershed model is used to generate long sequences of streamflows at the various inflow points of the proposed reservoirs. Since this is envisioned to be a major, future water source for Metro Manila with an increasing water demand as time goes by, project sequencing or staging of the several alternative reservoir configurations and associated components is part of this study.

As in Angat Reservoir, a combined simulation-optimization reservoir operations studies (together with other components) with inflows generated from the watershed model were conducted to evaluate the availability and reliability of the alternative reservoir configurations to deliver water supply and hydropower generation. Then, from these results, a suggested project sequencing and staging of the various reservoir configurations is presented. Further details of this work may be referred to NHRC (2012) in which the author was the principal investigator.

### 5.4.1 Agos River Basin Watershed and River Network

Agos River Basin as shown in Fig. 5.22 embraces the four proposed water resource projects, namely, the Kaliwa Low Dam Project, Laiban Dam Project, Kanan Dam Project, and the Agos Dam Project. Figure 5.22 is the aggregation of six 1:50,000

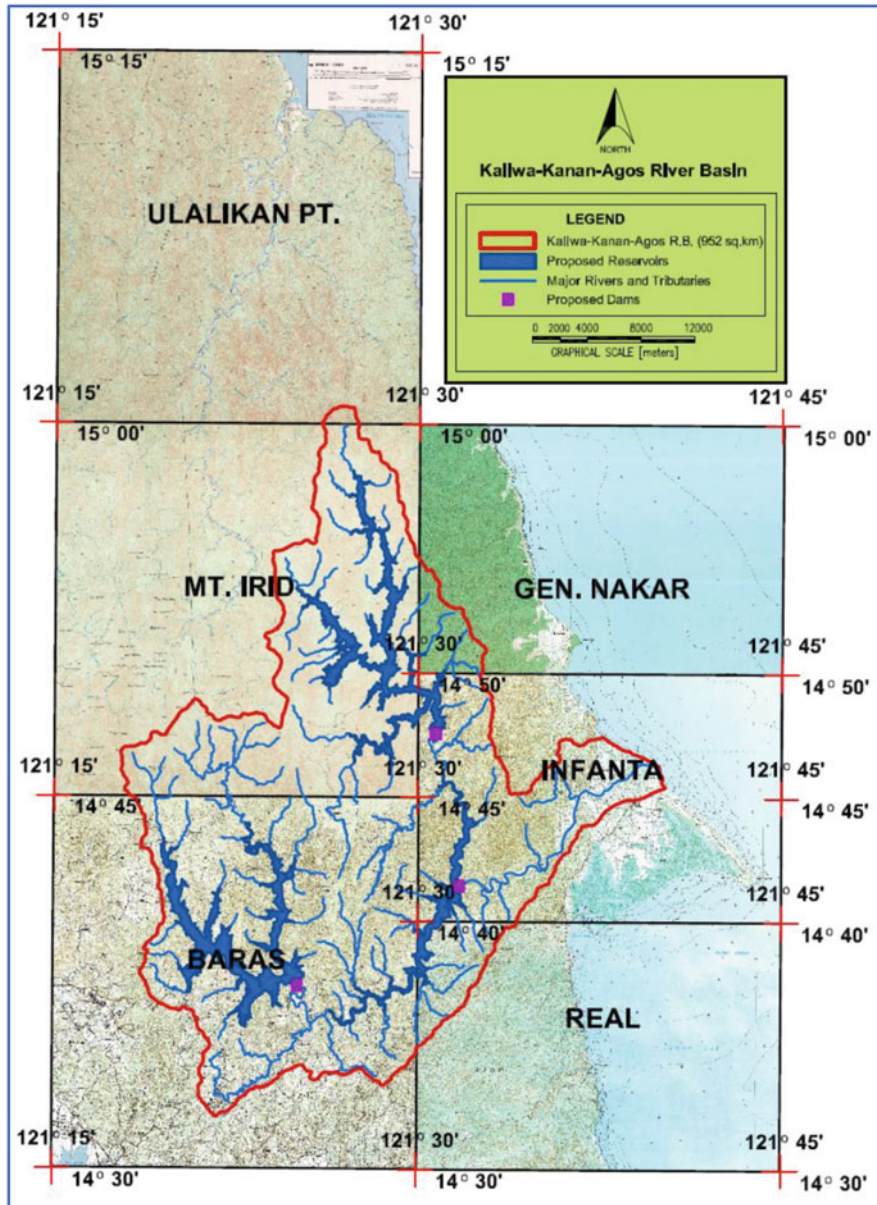


Fig. 5.22 Kaliwa-Kanan-Agos River System watershed boundary and river network

NAMRIA topographic maps of the towns of Ulalikan Point, Mt. Irid, Gen. Nakar, Infanta, Baras, and Real enclosing the watershed boundary of the Agos River Basin. The entire Agos River Basin is composed of approximately 952 sq. kilometers of watershed area including the catchment area of Agos River at Infanta, Quezon, downstream of the confluence of Kaliwa and Kanan Rivers. The combined catchment area of Kaliwa and Kanan Rivers alone is approximately 864 sq. kilometers. Agos River Basin lies on the northeast portion of Sierra Mountain Range, which runs along the coastline of the Pacific Ocean on eastern Luzon. The river system emanates from the headwaters of Kaliwa River from Mt. Irid and Mt. Calandang in the vicinity of northern Rizal as well as from the headwaters of Kanan River and moves downstream in eastern and southern direction, respectively, as they join downstream at Agos River before discharging to Polilio Strait.

#### **5.4.2 Alternative Water Resources System Configurations**

Nine (9) alternative water resources system configurations or schemes are considered here which consist of combinations of reservoirs and/or water conveyance (diversion) systems. The different configurations are briefly described and shown in Fig. 5.23 denoted by WRC1 through WRC9.

**Water Resource Configuration 1:** This scheme designated as WRC1 includes only the Kaliwa Low Dam (diversion with small storage potential) having an estimated reservoir capacity of around 57 MCM for a 53 m dam height based on its elevation-area-storage curve as shown in Fig. 5.24. The water conveyance from Kaliwa Low Dam to the water treatment facilities in Baras or Tanay before transferring water to Metro Manila is through the Kaliwa-Baras or Tanay Transfer Facilities as indicated by the dotted line and arrow on the lower, left-hand side of the figure which is applied to all configurations or schemes.

**Water Resource Configuration 2:** WRC2 is comprised of Laiban Dam (high dam) having an estimated reservoir capacity of around 980 MCM for a 103 m dam height (see storage-elevation curve in Fig. 5.25) in addition to the Kaliwa Low Dam. This scheme includes higher storage and can include hydropower generation in Laiban Dam. Laiban Dam releases are conveyed to Kaliwa Low Dam (downstream) since both are situated along Kaliwa River.

**Water Resource Configuration 3:** WRC3 is the same as WRC2 but with flow diversion from Kanan River to augment reservoir inflow to Laiban Dam through the Kanan-Laiban transbasin tunnel.

**Water Resource Configuration 4:** WRC4 is the same as WRC3 but includes the Kanan Dam (high dam) having an estimated reservoir capacity of around 682 MCM for a 141 m dam height. This scheme will have three storage reservoirs and can include hydropower generation at both Kanan Dam and Laiban Dam.

**Water Resource Configuration 5:** WRC5 is the same as WRC4 with the addition of Agos Dam which has an estimated reservoir capacity of around 476 MCM for a

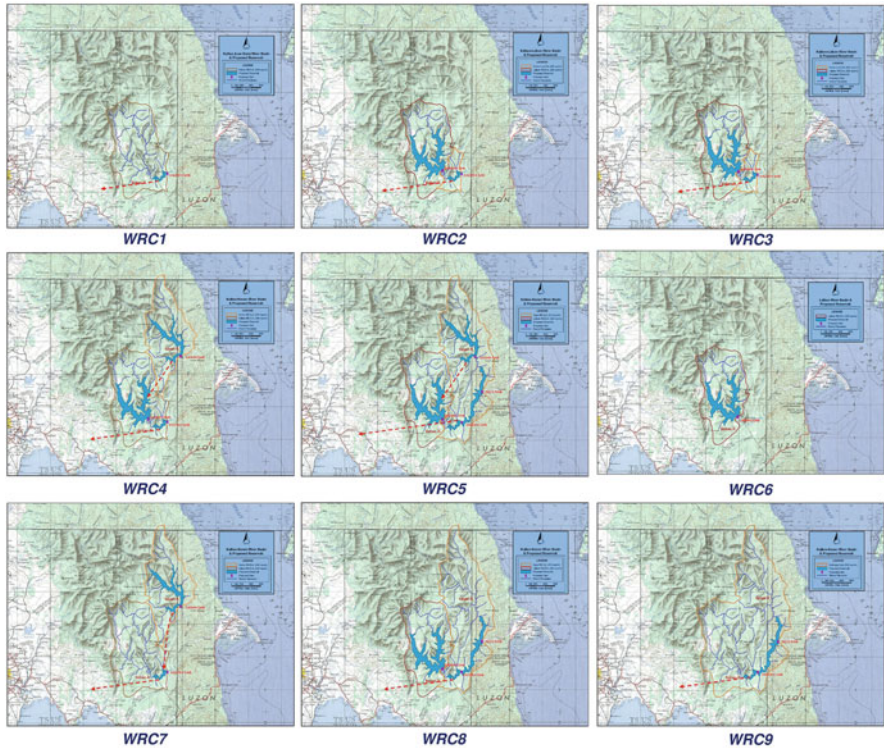


**Fig. 5.23** Nine (9) alternative water resources configurations or schemes denoted by WRC1 through WRC9 of the Agos River Basin composed of combinations of reservoirs and/or water conveyance systems

92 m dam height. In this case, the Kaliwa Low Dam being a low dam will be submerged, and its storage area becomes part of Agos Dam reservoir storage.

**Water Resource Configuration 6:** WRC6 is simply Laiban Dam which is the original scheme proposed in the late 1970s.

**Water Resource Configuration 7:** WRC7 comprises two reservoirs, the Kaliwa Low Dam and Kanan Dam with the water conveyance, the Kanan-Kaliwa Transfer Tunnel.

**Water Resource Configuration 8:** WRC7 comprises the Laiban Dam and Agos Dam with WRC in which Kaliwa Low Dam is also built. In the case, the Kaliwa Low Dam will be submerged, and its reservoir storage becomes part of this Agos Dam reservoir. Note that the conveyance system to the water treatment plant in Baras or Tanay will still emanate from the Kaliwa Low Dam location.

**Water Resource Configuration 9:** WRC9 simply comprises Agos Dam with the water conveyance to the treatment plant as in WRC8.

In the above Agos River water resource, the water conveyance or transfer facility from Kaliwa Low Dam location is approximately 21 km to the water treatment plant

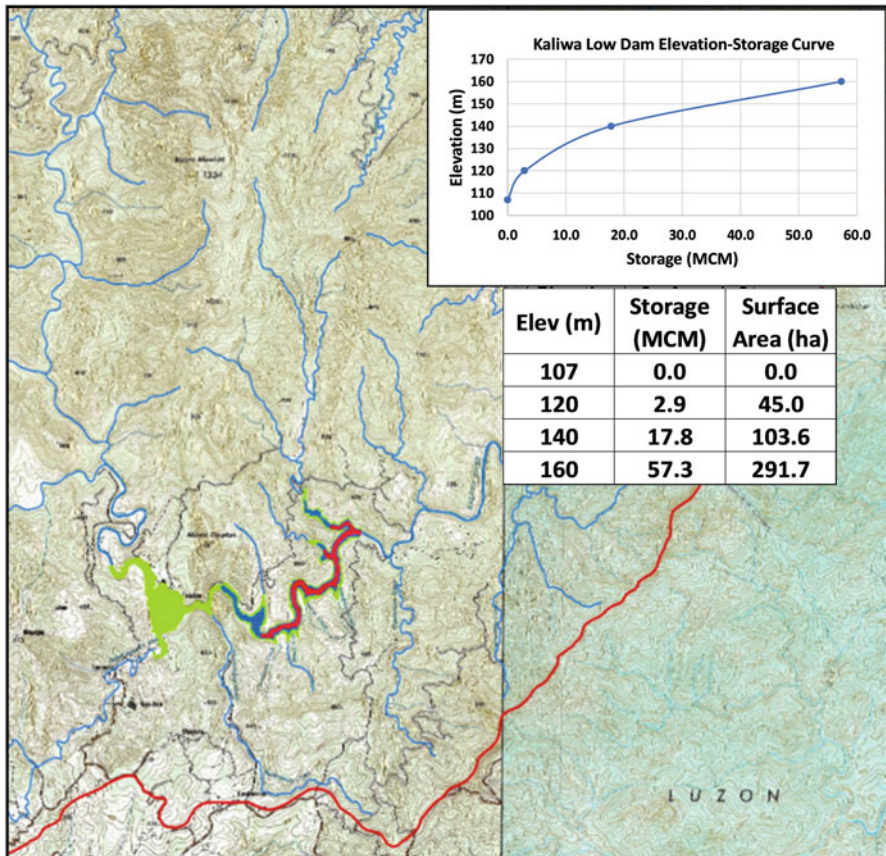


**Fig. 5.24** Elevation-area-storage data for the proposed Kaliwa Low Reservoir

in Baras or 22 km to Tanay. This may be comprised of three (3) 4.20 m diameter aqueducts with a capacity of  $22 \text{ m}^3/\text{s}$  each. It is envisioned that this will be constructed in two or three phases depending on the water source development and water supply requirement in Metro Manila. The proposed Kanan transbasin tunnel will be 22 km composed of two (2) 4.5 m diameter pipes with a capacity of  $25 \text{ m}^3/\text{s}$  each.

### 5.4.3 Agos River Basin Watershed Model

As in Angat and Upper Agno Reservoir studies, the watershed model employed was the Sacramento soil moisture accounting model described in Appendix A. This watershed model is essentially used to generate streamflows as inflows to the Agos River Basin reservoir operations studies conducted here.

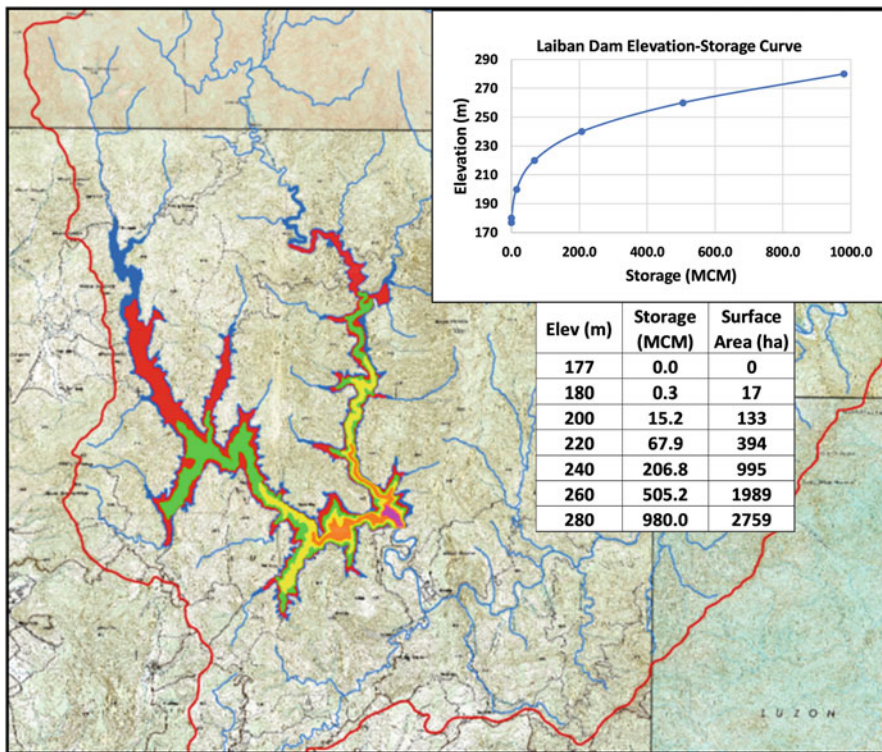


**Fig. 5.25** Elevation-area-storage data for the proposed Laiban Reservoir

For the development of the basin model, the Agos River Basin is delineated into several sub-basin units using the NAMRIA topographic maps and the 90 m by 90 m SRTM-DEM data, which resulted in 182 sub-basin units as shown in Fig. 5.26. From these sub-basin delineations, geometry properties that are specified in the model such as overland and river length, widths, and slopes were determined. Then, based on sub-basin delineations, the watershed model parameters such as interception, infiltration, and overland flow parameters were obtained from soil type and land use maps. Figure 5.27 exhibits the land cover map of the Agos River Basin. The land cover of the upper portion of the basin (around Kaliwa and Kanan Rivers before converging into Agos River) is predominantly woodland (closed and open canopies) with some percentage of cultivated area and grassland, while the downstream area which is outside of the water source project boundary is predominantly built up with a mixture of agricultural lands and riverbeds/terraces.

With regard to rainfall input to the watershed model, it is shown in Fig. 5.28 that only the Infanta rainfall station is situated within the Agos watershed which is on the eastern slope of Sierra Madre mountains (windward side relative to the Pacific Ocean). The other rainfall stations include Bosoboso, Mt. Oro and Mt. Campana (stations on the western slope of Sierra Madre), Tanay, Santa Maria, and Science

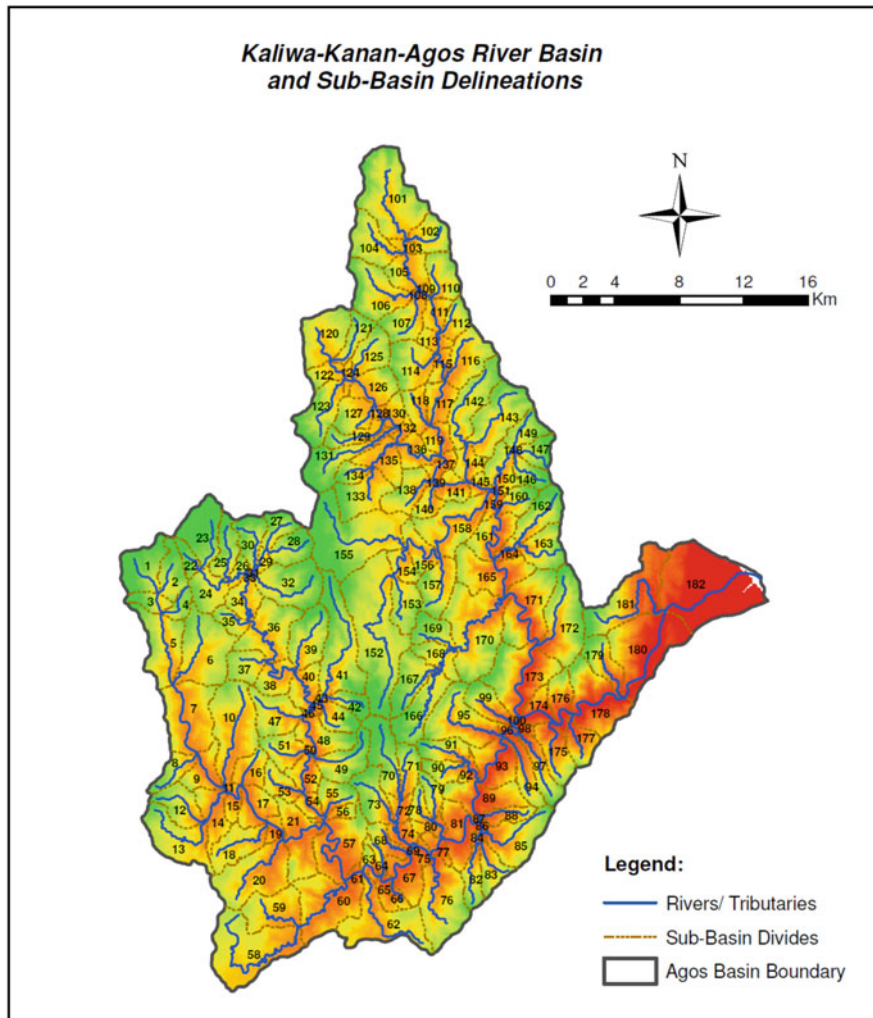


**Fig. 5.26** Watershed delineation of Agos River Basin resulting in 182 sub-basins for watershed modeling. The sub-basin numbers indicated are for purposes of watershed modeling

Garden, all of which are on the western slope of Sierra Madre (leeward side relative to Pacific Ocean). For the basin rainfall in the watershed model, daily rainfall data from the available stations were spatially interpolated to arrive at rainfall for each sub-basin in the modeled area. A total of 52 years of daily rainfall (1960–2011) were calculated for each sub-basin which is fairly long and adequate enough for purposes of reliability analysis of surface water resource and potential hydropower generation in the Agos River Basin.

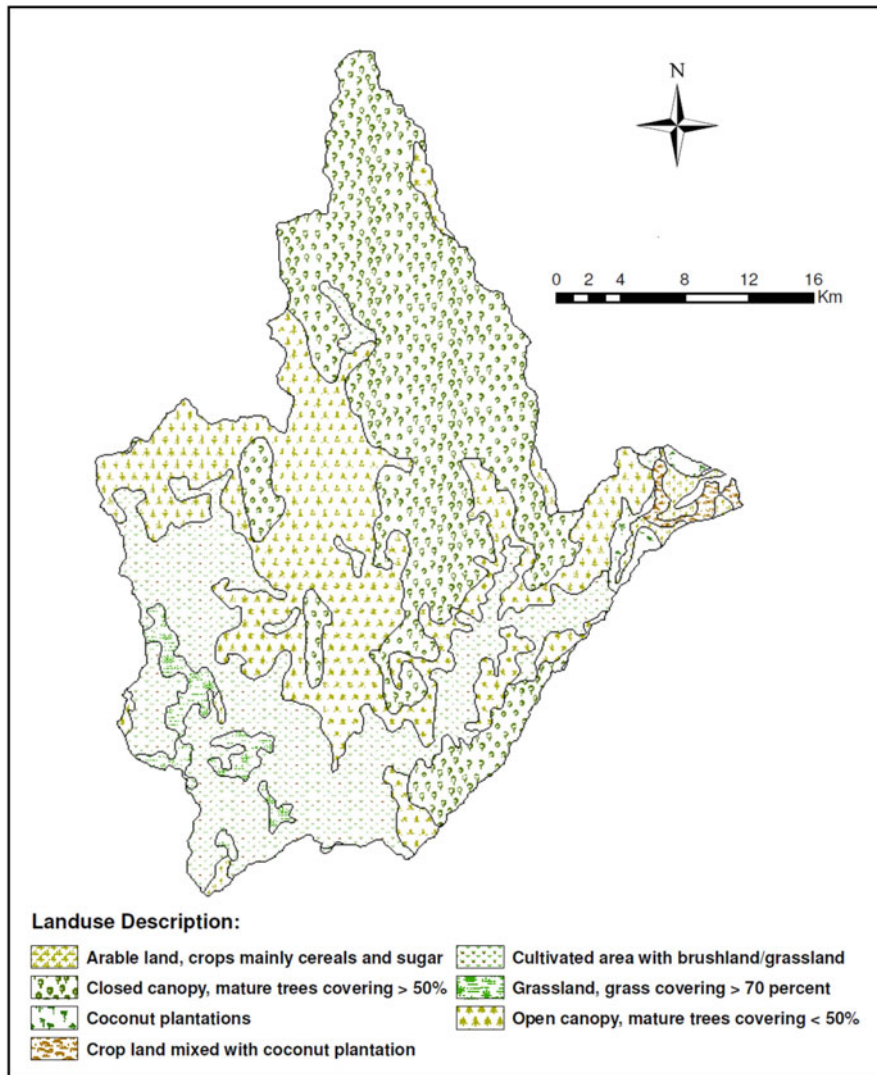


**Fig. 5.27** Land cover map of Agos River Basin

Table 5.13 presents the pertinent information of rainfall and climatological stations as well as the only streamflow gaging station in the Agos River Basin located at the downstream end of Agos River.

With the daily rainfall spatially interpolated for each sub-basin, the watershed model was used to generate the streamflows over 182 river points in the Agos River Basin which become the reservoir inflows to evaluate the performance of the alternative water resource configurations using combined optimization-simulation reservoir operations studies. For illustration purposes, Fig. 5.29 shows the time



**Fig. 5.28** Location of rainfall gaging stations in the Agos River Basin and vicinity

**Table 5.13** List of hydrometric stations within and near the Agos River Basin where hydrologic data have been gathered

Parameter	Station Name	Location	Agency	Latitude	Longitude	Period of Record From	To	No. of yrs. of operation	No. of years of complete data	Remarks
<b>Rainfall [mm]</b>										
	Angat	Angat, Bulacan	PAGASA	14° 54' 20"N	121° 09' 40"E	1961	2000	40	40	Monthly
	Bosoboso	Antipolo City, Rizal	PAGASA	14° 38' 00"N	121° 14' 00"E	1984	2006	23	23	Daily
	Infanta	Infanta, Quezon	PAGASA	14° 45' 00"N	121° 38' 48"E	1981	2006	26	26	20 yrs Monthly/ 6 yrs Daily
	Science Garden	Quezon City, MM	PAGASA	14° 38' 41"N	121° 02' 31"E	1961	2009	49	48	42 yrs Daily/ 7 yrs Hourly
	Sta. Maria	Macasipac, Sta. Maria, Laguna	PAGASA	14° 30' 00"N	121° 26' 18"E	1994	2007	14	7	Daily
	Tanay Radar	Tanay Rizal	PAGASA	14° 30' 00"N	121° 21' 00"E	1995	2005	11	10	Daily
	Bosoboso	Antipolo City, Rizal	EFCOS	14° 38' 24"N	121° 13' 23"E	2000	2009	10	8	Hourly/Daily
	Mt Campana	Antipolo City, Rizal	EFCOS	14° 40' 06"N	121° 17' 29"E	2003	2008	6	5	Hourly/Daily
	Mt. Oro	Rodriguez, Rizal	EFCOS	14° 45' 48"N	121° 09' 23"E	2000	2009	10	9	Hourly/Daily
<b>Pan Evaporation [mm]</b>										
	Science Garden	Quezon City, MM	PAGASA	14° 38' 41"N	121° 02' 31"E	1979	2003	25	21	Monthly
<b>Relative Humidity [%]</b>										
	Science Garden	Quezon City, MM	PAGASA	14° 38' 00"N	121° 14' 00"E	1961	2006	46	41	Monthly
	Infanta	Infanta, Quezon	PAGASA	14° 45' 00"N	121° 38' 48"E	1971	2000			Averages
<b>Mean Temperature [° C]</b>										
	Science Garden	Quezon City, MM	PAGASA	14° 38' 00"N	121° 14' 00"E	1961	2006	46	41	Monthly
	Infanta	Infanta, Quezon	PAGASA	14° 45' 00"N	121° 38' 48"E	1971	2000			Averages
<b>Wind Speed [m/s] and Direction</b>										
	Science Garden	Quezon City, MM	PAGASA	14° 38' 00"N	121° 14' 00"E	1961	2006	46	41	Monthly
	Infanta	Infanta, Quezon	PAGASA	14° 45' 00"N	121° 38' 48"E	1971	2000			Averages
<b>River Flows [m³/s]</b>										
	Agos River	Banugao, Infanta, Quezon	DPWH	14° 45' 15"N	121° 36' 45"E	1949	1985	37	21	Monthly

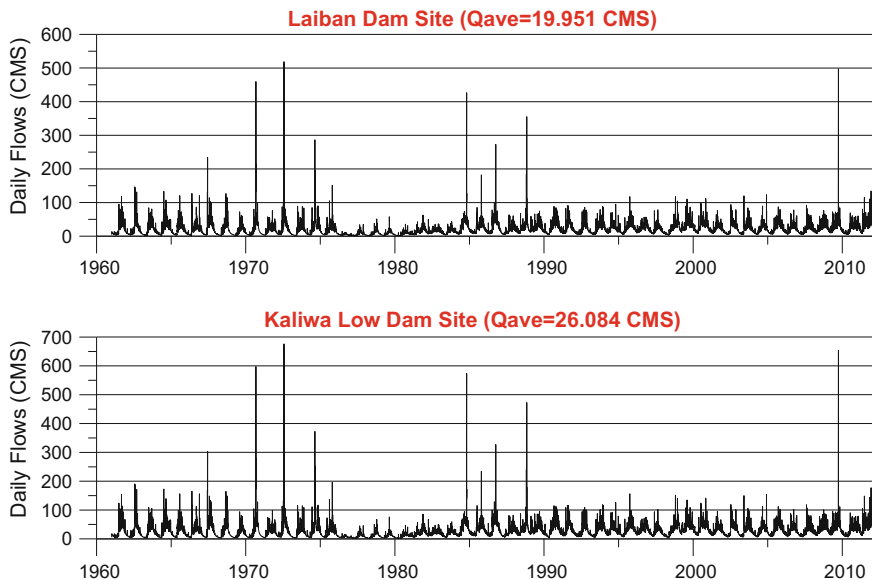


**Fig. 5.29** Time series plots of simulated daily flows from 1961 to 2011 at proposed Laiban Dam and Kaliwa Low Dam sites

series plots of daily streamflows calculated from the watershed models at the proposed Laiban Dam and Kaliwa Low Dam sites.

#### 5.4.4 *Results of Optimization-Simulation Studies of Proposed Agos River Reservoir System*

The optimization-simulation model used here is the same as that used in the Angat and Agno Reservoirs earlier. The objective function used in the optimization model is similar to the Upper Agno Reservoir which has penalty terms for domestic water supply demand violation and reservoir spills and benefit function for hydropower generation. Note that the amount of water demand is part of the quantity determined in this optimization-simulation runs and this is discussed below. Also, the optimization-simulation runs were conducted with 30-day window or moving horizon as an anticipatory release rule policy (in contrast to a myopic release rule policy) so that the decision for a given day was based on minimizing water delivery violations (according to target water delivery or flow demand), minimizing spills, and maximizing hydropower generation for the next 30 days assuming a perfect daily inflow forecast. This assumption of a perfect daily inflow forecast is applicable for long-term, reliability studies done here.

For the sake of brevity, only the results for the WRC1 (i.e., Kaliwa Low Dam alone) and WRC2 (i.e., Kaliwa Low Dam and Laiban Dam in tandem) configurations are discussed in detail below with regard to the results of reliability analysis. The recommended project sequencing and staging based on results of the optimization-simulation runs and reliability analyses for all alternative configurations (WRC1 through WRC9) are presented at the end of this section.

The mean daily flow of Kaliwa River at the proposed Kaliwa Low Dam site is 26.01 m<sup>3</sup>/sec (CMS), but its reliability (availability in percent-of-time) by flow duration analysis is only 40.27% or roughly 146 days a year, in the long term. Also, from flow duration analysis, if we divert or extract 15 CMS from this river at the location of the proposed Kaliwa Low Dam site, the reliability is only 64% of the time. Similarly, the mean flow of Kaliwa River at the proposed Laiban damsite is 19.21 CMS with a reliability of 40.08%, and likewise, if we divert 20 CMS from this river point, the reliability is only 38.1%. Thus, to increase the reliability of water supply from the Agos River Basin, there is the need for water infrastructures, reservoirs in this case, which are the essence of this study.

For the case where only Kaliwa Low Dam is built (WRC1 configuration), the results of the optimization-simulation and corresponding reliability analysis are summarized in Table 5.14 for three (3) different reservoir target releases (flow demand). The target release is desired release imposed in the optimization. It may be noted that as the target release is increased, the more aggressive the reservoir

**Table 5.14** Kaliwa Low Dam reliability analysis of **a** water supply deliveries and **b** hydropower generation for the WRC1 configuration (case with Kaliwa Low Dam only)

<b>a</b>	Target Release (CMS)	Water Supply Reliability (in MLD)		
		50%	80%	85%
	10	1930	864	864
	<b>15</b>	<b>1612</b>	<b>1294</b>	<b>924</b>
	20	1728	833	585

<b>b</b>	Target Release (CMS)	Power Reliability (MW)		
		40%	60%	80%
	10	32.52	15.96	8.70
	<b>15</b>	<b>30.20</b>	<b>17.62</b>	<b>9.32</b>
	20	25.86	17.94	4.91

releases are made but at the expense of lower reliability (ability to deliver water at higher reliability even at lower flows) because there is a tendency not to save or hedge into the future. On the other hand, too passive release rule results in lower firm water yield but has higher reliability especially at 85 percent-of-time. Thus, the optimum target release is 15 CMS. One could have further refined the optimal value of target release by analyzing for say 14.0 or 16.0 CMS. The resulting hydropower generation at optimal target release of 15 CMS is 30.20 MW and 17.62 MW at 60% and 40% reliability, respectively. Typically, the installed capacity is based on between 40% and 60% reliability.

For the WRC2 configuration with Kaliwa Low Dam and Laiban Dam in tandem, the results are given in Table 5.15. In this table, say 20/15 target release means that 20 CMS at Laiban Dam and 15 CMS at Kaliwa Low Dam. Upon examining these tables, the optimum target release is the 20/20 combination based on the argument that an aggressive reservoir release rule (high target release) will result in lower reliability, while too conservative release rule will result in lower firm water yield. Note that the releases at Laiban Dam go to Kaliwa Low Dam, so only the water supply reliability of Kaliwa Low Dam is meaningful as far as water deliveries to Metro Manila is concerned. The hydropower generated is separate for Laiban and Kaliwa Low Dams so that for the 20/20 target release at 40% and 60% reliabilities, the totals are 72.56 MW and 60.88 MW, respectively.

Again, as stated earlier in this section, the results for the water resource configurations (WRC3 through WRC9) for cases that included Kaliwa-Laiban-Kanan Diversion, Kaliwa-Laiban-Kanan Dam, Kaliwa-Laiban-Kanan-Agos, and so on are too lengthy to show here. Also, both WRC6 (case with Laiban Dam alone) and WRC9 (case with Agos Dam alone) configurations were not actually considered anymore since they are most likely going to be built as stand-alone dam or reservoir.

#### ***5.4.5 Recommended Project Sequencing and Staging of the Agos River Reservoir System***

A final, useful output of these optimization-simulation studies is the recommended project sequencing and staging of the various water resources configurations for the Agos River Basin reservoir system to meet the projected water demand of Metro Manila for the period 2005 to 2050. As discussed earlier, for a given project configuration, too aggressive water demand or delivery lowers the long-term water firm yield as well as hydropower generation since the reservoir elevation is frequently drawn down, thus resulting in smaller head for hydropower generation. On the other hand, too conservative (little) water demand decreases the firm water yield although at higher reliability but results in unnecessary reservoir spills. Thus, in actual reservoir operations, target water demands or deliveries must be properly set depending on prevailing weather and climate conditions to satisfy the long-term, reliable water supply and hydropower generation objectives.

**Table 5.15** Reliability analysis of **a** water supply deliveries at Kaliwa Low Dam, **b** hydropower generation at Kaliwa Low Dam, and **c** hydropower generation at Laiban Dam for WRC2 configuration (case with Laiban Dam and Kaliwa Low Dam in tandem)

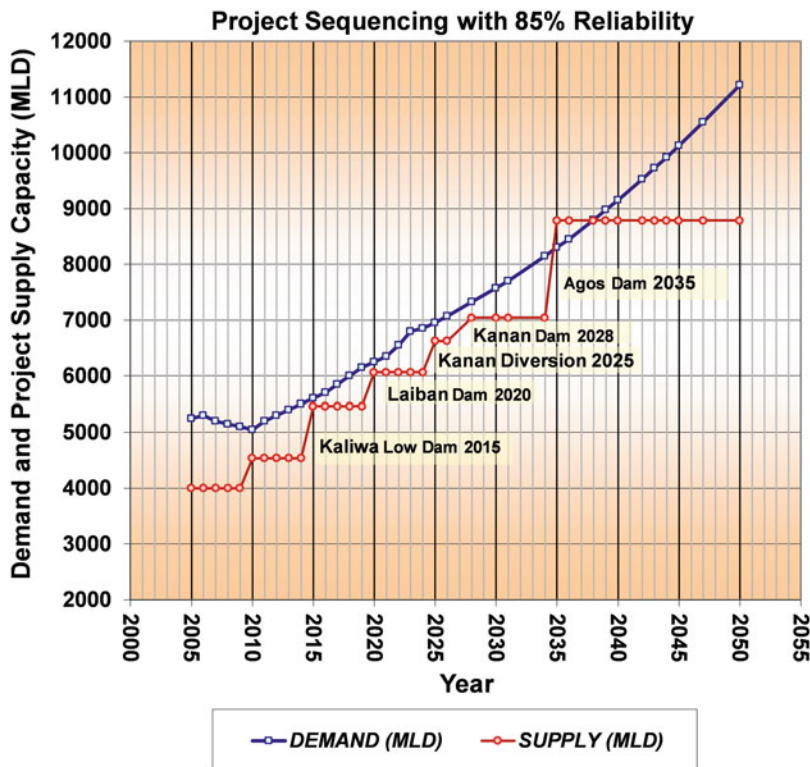
<b>a</b>	Target Release (CMS)	Water Supply Reliability (MLD)		
		50%	80%	85%
	20/15	2152	1296	260
	<b>20/20</b>	<b>1926</b>	<b>1655</b>	<b>1527</b>
	20/25	2263	1724	1385
	25/15	2335	1296	1251
	25/20	2119	1441	1141

<b>b</b>	Target Release (CMS)	Power Reliability (MW)		
		40%	60%	80%
	20/15	36.78	25.45	15.50
	<b>20/20</b>	<b>30.46</b>	<b>26.33</b>	<b>22.20</b>
	20/25	34.70	30.56	16.53
	25/15	38.75	27.58	15.69
	25/20	34.95	26.27	16.11

<b>c</b>	Target Release (CMS)	Power Reliability (MW)		
		40%	60%	80%
	20/15	40.39	23.90	8.90
	<b>20/20</b>	<b>42.10</b>	<b>34.55</b>	<b>17.68</b>
	20/25	40.88	29.43	14.60
	25/15	37.02	21.76	7.89
	25/20	41.35	25.05	8.76



**Fig. 5.30** Recommended project sequencing and staging at 85% reliability of the projected Metro Manila water demand for years 2012–2060

For the projected water demand of Metro Manila extending up to year 2050, Fig. 5.30 shows the best water resources project sequencing and staging selected based on optimal water supply and hydropower generation at 85% reliability. In this sequence, the Kaliwa Low Dam will provide 924 MLD at a target year of 2015, and similarly, the Laiban Dam will provide an additional 603 MLD (difference of 1,527 and 924 MLD) which is drawn at Kaliwa Low Dam with a completion date in 2020. Kanan Diversion will provide 563 MLD at the target year of 2025, while Kanan Dam development will also provide an additional 416 MLD by 2028. Agos Dam will have a target year of 2035 to provide an additional 1,743 MLD. The total additional water supply up to year 2035 at 85% reliability is 4,249 MLD.

As far as the water needs of Metro Manila is concerned, the operations of multipurpose Angat Reservoir as the only major source of water supply of Metro Manila and irrigation water use for Bulacan farmers compete with each other, and this is further complicated by its physical configuration in relation to its hydropower plant (owned privately by K-Water and SMC). With increasing water demand, reservoir sedimentation, and even climate change, Metro Manila can no longer

solely rely on Angat Reservoir thus the need to seriously consider the use of Agos River Basin as an alternative, additional water source starting with the proposed Kaliwa Low Dam which can definitely augment the water supply for Metro Manila, and it also serves as a redundant system for water security in case Angat Reservoir cannot fully deliver water. In fact, even with the addition of the Kaliwa-Kanan-Agos reservoir system, other water sources will still need to be developed from elsewhere to meet Metro Manila's water needs (see Fig. 5.30).

## References

- Box MJ (1965) A new method of constrained optimization and a comparison with other methods. *Computer Journal* 8(1):42–52
- Ford DT, Garland R, Sullivan C (1981) Operation policy analysis: Sam Rayburn reservoir. *Jour. of Water Resources Planning and Management*, ASCE 107(WR2):339–350
- Jacoby HD, Loucks DP (1972) Combined use of optimization and simulation models in river basin planning. *Water Resources Research* 8(6):1401–1414
- NHRC (National Hydraulic Research Center) (2012) Hydrological study, reliability and sustainability analysis for the new water supply source project: Kaliwa-Kanan-Agos River System, Final Report to Metropolitan Waterworks and Sewerage System (MWSS), August.
- Tabios GQ III (2008) Angat Reservoir monthly operations using an optimization-simulation model with seasonal autoregressive model to forecast inflows. *Philippine Engineering Journal XXIX* (1):13446–13469
- Tabios GQ III (2010) Comparison of COMPLEX and genetic algorithms for optimal monthly releases of the multi-purpose Angat Reservoir. In: Proceedings of the UP-ICE centennial conference on harmonizing infrastructure with the environment and the 3rd ASEAN Civil and Environmental Conference, EDSA Shangri-La Hotel, Metro Manila, November 11–12.
- Tabios GQ III (2016) Competing water uses of Angat multipurpose reservoir with increased domestic water demand under future reservoir sedimentation and climate change. In: Banta SJ (ed) Water in agriculture: status, challenges, and opportunities. Published by The Asia Rice Foundation, College, Laguna, pp 73–90
- Tabios GQ III (2018) Multiple and integrated water resource utilization. In: Rola A, Pulhin J, Alcala HR (eds) Water policy in the Philippines global issues in water policy, vol 8. Springer, Cham, pp 163–184
- Tabios GQ III, David CC (2014) Appraisal of methodology in estimating irrigable areas and processes of evaluating feasibility of NIA irrigation projects, Policy Notes, No. 2014–13. Philippine Institute of Development Studies, Makati
- Tabios GQ III, Salas JD (1985) A comparative analysis of techniques of spatial interpolation of precipitation. *Water Resources Bulletin*, AWRA 21(3):365–379
- Tabios GQ III, Shen HW (1993) WATPOW (water and power) simulation-optimization model: Program documentation and user's manual, Document submitted to the electric resource planning. Pacific, Gas and Electric Company, San Francisco
- Tabios GQ III, Monsod SC, Arcilla C, Momo RS, Rabonza GJ, Salazar CS, Chiu MS, Nilo PD, Ordona PM, Loyzaga MA, Connell WB (2010) San Roque Dam during typhoon Pepeng of October 2009, Report of Investigating Committee Created under Department Order DO2009-10-0015 of Secretary Angelo T. Reyes, Department of Energy, Republic of the Philippines
- Woodfields (Woodfields Consultants, Inc.) (2017) Climate-resilient management of the dams and reservoirs in the Upper Agno River Basin Project, Report submitted to National Water Resources Board, June.

# Chapter 6

## Reservoir Sedimentation Studies



**Abstract** The Balog-Balog Reservoir was conceptualized in 1986 as a single, high dam that would supply irrigation water supply to the Balog-Balog River irrigation system of Tarlac. However, the proposal remained on the drawing board until an unsolicited proposal to construct a multiple dam system composed of nine reservoirs with small dams was submitted to the government in 2012. This chapter presents the Balog-Balog Reservoir study with single, high dam versus this multiple dam system. In the context of reservoir sedimentation, it is expected that the single, high dam would have a longer life compared to the low dams. The San Roque Reservoir study is also presented in this chapter to assess the reservoir life with reservoir sedimentation. This study was a requisite of a loan package agreement that after its completion in 2002, every 5 years a reservoir operations and sediment management study would be conducted. Finally, the sediment flushing operations study in Pulangi Reservoir is discussed in this chapter. Pulangi Reservoir is the only major reservoir in the Philippines with a sediment flushing facility but was never activated since its completion in 1985 until after the study on sediment flushing was conducted in 2005. For both San Roque and Pulangi Reservoir sedimentation management studies, a two-dimensional hydraulic model of flow and sediment transport was employed to conduct the study.

### 6.1 Balog-Balog Reservoir Reliability and Cost-Benefit Analysis of a Single, High Dam Versus a Multiple Dam System

The Balog-Balog Irrigation System as shown in Fig. 6.1 consists of Phase I which covers an irrigation service area of 12,475 ha, while Phase 2 covers an area of 21,935 ha, thus a total area of 34,410 ha. Historically, in 1976, the irrigated area reached 12,904 ha which reduced to about 10,000 ha in 1989 but drastically reduced to less than 1000 ha after the Mt. Pinatubo eruption in 1991 although it has gradually recovered over the years to as high as 4600 ha annual irrigated area. To fully rehabilitate the Balog-Balog Irrigation System, NIA proposed the construction of Balog-Balog Multipurpose Dam Project (BBMP), which has a single, high dam as

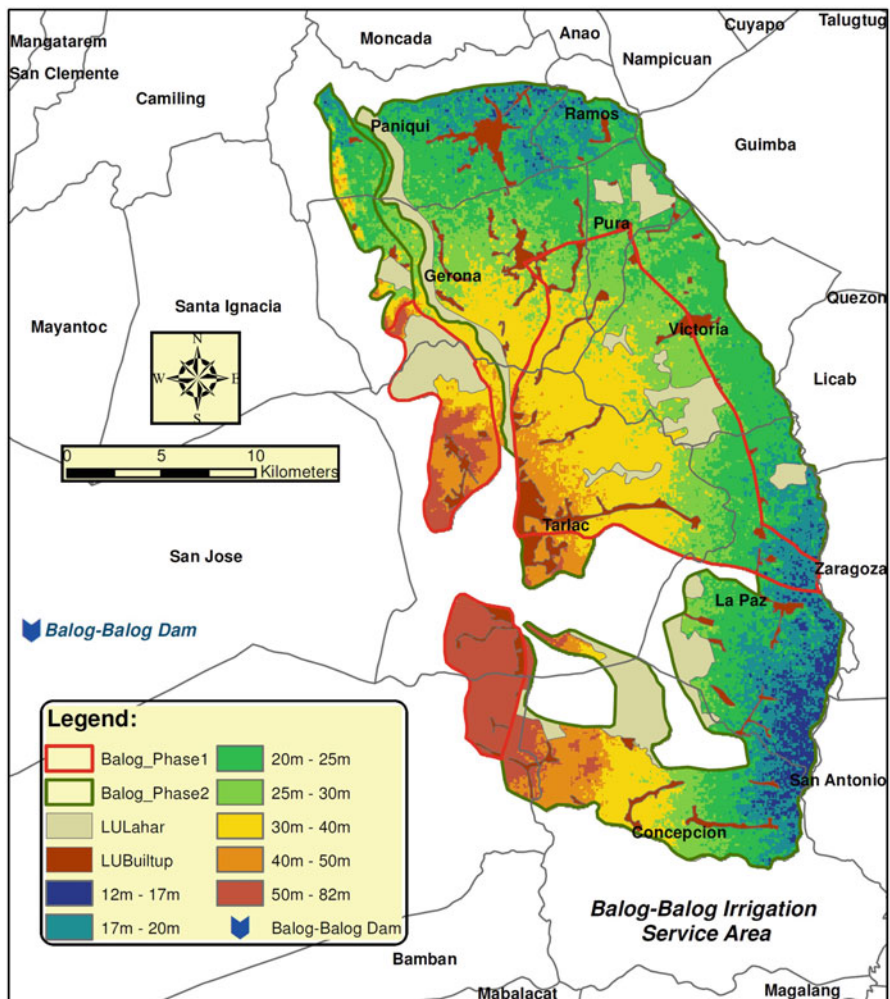


**Fig. 6.1** Map of Balog-Balog irrigation system service area

source of irrigation water. In 2012, a joint venture company through an unsolicited proposal (TWEDCO 2012) submitted the Balog-Balog multiple dam system (BBMDS) which consists of a series or cascade of nine low dams in the Bulsa River and O'Donnell River watersheds as an alternative to BBMP proposed by NIA.

This modeling study was conducted to compare the proposed BBMP and the proposed BBMDS that would supply water to the Balog-Balog Irrigation System in terms of their reliability and likely benefits and consequent costs. The reliability analysis in particular assessed the ability of these proposed reservoir systems to

deliver irrigation water supply, potential for hydropower generation, extent of reservoir life with sedimentation, and possible flood control function. Details of this study are reported in NHRC (2015) in which the author is the principal investigator.

### ***6.1.1 Balog-Balog Multipurpose Project with Single, High Dam***

The construction of the Balog-Balog Multipurpose Project (BBMP) which consists of a single, high dam was proposed by the National Irrigation Administration (NIA) of the Philippines in 1986 and had been the subject of several studies by NIAConsult (2010, 2011, 2012) as the major, alternative source of water for the Balog-Balog Irrigation System. The need to build the multipurpose dam became more urgent when the Armenia Dam at O' Donnell River and Tarlac Diversion Dam at Tarlac River were decommissioned after being buried by lahar or pyroclastic materials when Mt. Pinatubo erupted in 1991. The Armenia Dam served the irrigation areas of San Miguel-O'Donnell River Irrigation System (SMORIS), while the Tarlac Diversion Dam served the irrigation areas of Tarlac River Irrigation System (TARRIS), which both composed the Balog-Balog Irrigation System.

The location of the proposed BBMP is shown in Fig. 6.2. The major data required in the reliability analysis is the reservoir elevation-storage curve shown in Fig. 6.2, which was developed from SRTM digital terrain data with 90 m × 90 m spatial resolution. For purposes of the optimization-simulation modeling studies, the major reservoir and dam specifications are (1) dam height at 95 m; (2) spillway elevation at 245 m; (3) storage capacity of 570.2 MCM at 245 m; and (4) minimum storage elevation at 150 m. The elevation datum used here was the NAMRIA datum which is 0.0 m at mean sea level (MSL). Note that in actual dam construction, there is a freeboard such that the dam height is higher than 95 m with the spillway crest elevation at 245 m and appropriate width to contain the design spillway flow.

### ***6.1.2 Balog-Balog Multiple Dam System***

The Balog-Balog multiple dam systems (BBMDS) as proposed (TWEDCO 2012) would require the construction of nine (9) dams at the locations denoted by S1 through S9 in Fig. 6.3. The reservoir elevation-storage curves for each reservoir are also shown in Fig. 6.3, and pertinent reservoir specifications are given in Table 6.1.

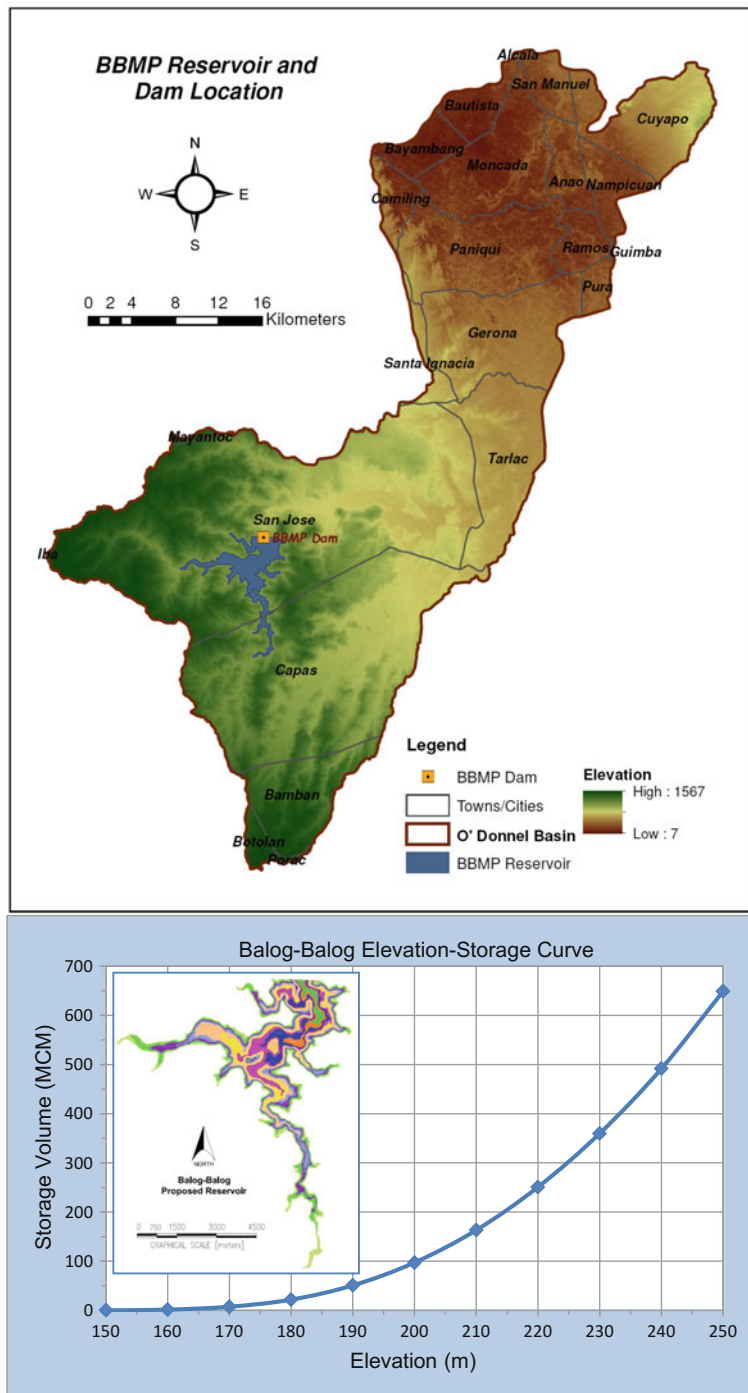


**Fig. 6.2** Location of Balog-Balog multipurpose project (BBMP) with single, high dam, and its reservoir elevation-storage curve

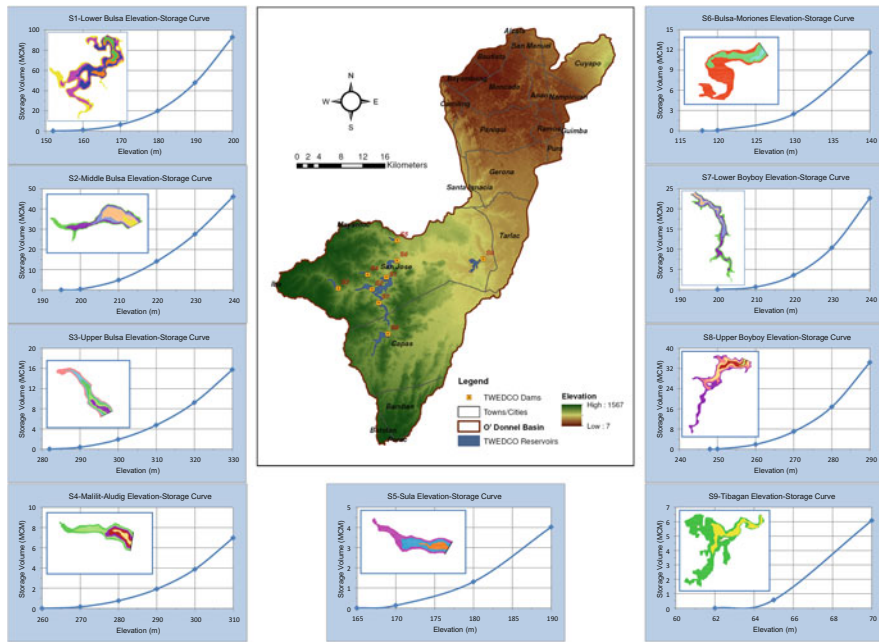


**Fig. 6.3** Location of the nine Balog-Balog multiple dam systems (BBMDS) denoted by S1 through S9 and their corresponding reservoir elevation-storage curves

**Table 6.1** Specifications of the nine reservoirs of Balog-Balog multiple dam system (BBMDS)

Reservoir	Dam height (m)	Dam elevation (m)	Dam base elevation (m)	Maximum storage (MCM)
S1	48	200	152	93.09
S2	45	240	195	46.22
S3	48	330	282	15.81
S4	50	310	260	7.09
S5	25	190	165	4.02
S6	22	140	118	11.63
S7	40	240	200	22.67
S8	42	290	248	34.42
S9	8	70	62	6.08

### 6.1.3 Reservoir Optimization-Simulation Model and Watershed Modeling

For purposes of comparing the performance of the two reservoir systems – single, high dam (BBMP) and multiple dam system (BBMDS) – an optimization-simulation model was used to simulate the watershed/reservoir operations in which the watershed model represents the physical processes involved in the watershed system and

reservoir water balance, while the optimization model will decide the operating policies such as flow releases for specified objectives and constraints. The same watershed model and optimization algorithm are used as in Chap. 5.

In the optimization model using complex nonlinear optimization method (Box 1965), the objective function is weighted, multi-objective function to minimize irrigation water supply deficits (demand violations), maximize hydropower generation, and minimize spills. The constraints include capacities of release gates, storage volumes, operational constraints, and all other system constraints imposed implicitly in the simulation model.

The continuous-time, distributed watershed model with Sacramento soil moisture accounting was used with input daily rainfall spatially interpolated in each sub-basin of the watershed. Figure 6.4 shows the O'Donnell River Basin watershed subdivided into 57 sub-basins. This figure also indicated the locations of the reservoirs. It may be noted that 28 sub-basins are associated to the proposed BBMDS while only 21 sub-basins are associated to BBMP. To specify the model geometry and some parameters in the watershed model, the elevation map and land use map of O'Donnell River Basin were used as shown in Figs. 6.5 and 6.6.

#### ***6.1.4 Comparison of Balog-Balog Multipurpose Project (BBMP) with Single, High Dam, Versus Balog-Balog Multiple Dam System (BBMDS)***

The interest in reliability analysis is to evaluate the ability of the two proposed reservoir systems to provide irrigation water to Balog-Balog Irrigation System with a targeted irrigation service area of 34,000 ha. Assuming that the maximum water requirement is  $1.2 \text{ m}^3/\text{s}$  per 1000 ha, then the total water requirement is about  $40.0 \text{ m}^3/\text{s}$  for 34,000 ha. The question here is at what level of reliability the amount of  $40 \text{ m}^3/\text{s}$  can be delivered in terms of percent of time per year, in the long term. A secondary interest is the reliability of generating hydropower.

For both single, high dam (BBMP) and multiple dam system (BBMDS), the results of reliability analyses from the optimization runs are shown in Tables 6.2 and 6.3 at the S1 and S9 locations, respectively. Note that the BBMP Dam and the S1 reservoir are both located at S1 location (see Fig. 6.3). At S9 location, only the S9 reservoir of BBMDS is positioned, but it is a good location in the river to compare the reliability analysis for both BBMP and BBMDS.

It is seen that the BBMP provided more reliable irrigation water deliveries and hydropower generation compared to BBMDS. At the S1 location, assuming that the water requirement is  $1.2 \text{ m}^3/\text{s}$  per 1000 ha, then as much as 21,027 ha could be irrigated by BBMP compared to only 17,783 ha in the BBMDS scheme on year-round basis. In both instances, areas irrigated were larger compared to 12,281 ha in areas dependent on natural flows (i.e., without a reservoir). During the dry season,

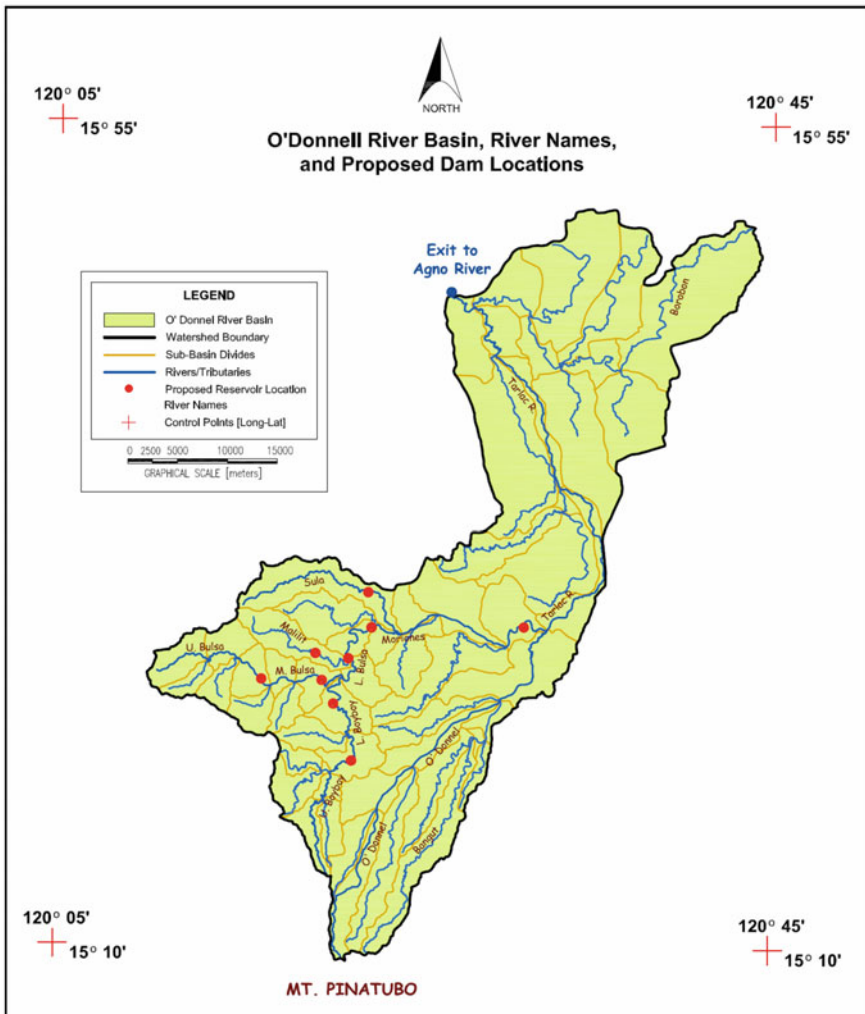


**Fig. 6.4** Map of the study area showing the watershed delineation and the locations of the proposed reservoirs

BBMP could irrigate as much as 11,534 ha as against BBMDS' 2337 ha and 1679 ha without a reservoir (i.e., from natural flows only). During the wet season, all three, BBMP, BBMDS, and without a reservoir (natural flows only), could irrigate as much as 26,000 ha.

At location S9, the irrigation water deliveries were higher, likewise in the areas that could be irrigated. In any case, at both locations S1 and S9, the BBMP resulted in higher irrigation water deliveries compared to BBMDS. Definitely, the reservoirs are needed to increase the reliability of irrigation water supply upon comparing the

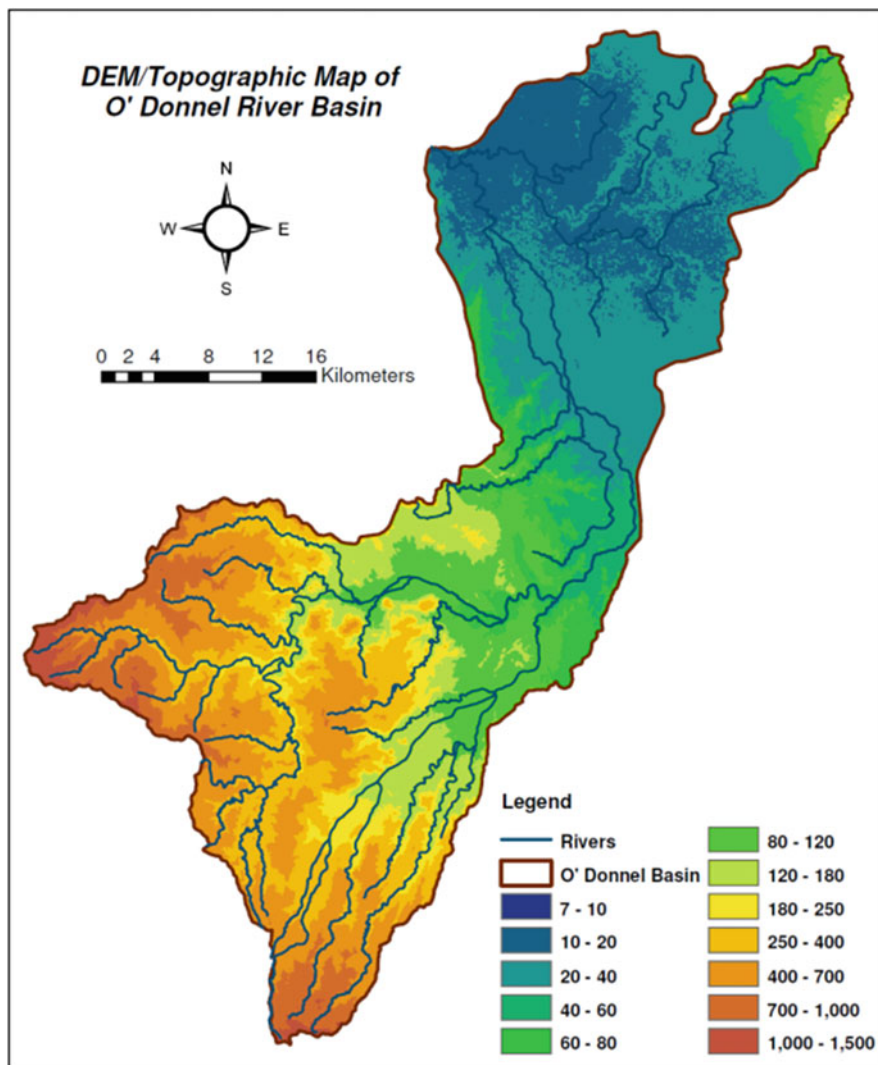


**Fig. 6.5** Digital elevation map of the study area

higher reliability (percent-of-time) and corresponding larger water volumes (irrigation water deliveries) with either BBMP or BBMDS schemes compared to the case without a reservoir.

The reliability analysis of irrigation water deliveries was also performed considering reservoir sedimentation. Based on observation and assessment of several watersheds with reservoirs in the Philippines, the annual sediment inflow at these reservoirs is  $3500 \text{ m}^3$  per  $\text{km}^2$ . In the reservoir optimization-simulation model, the

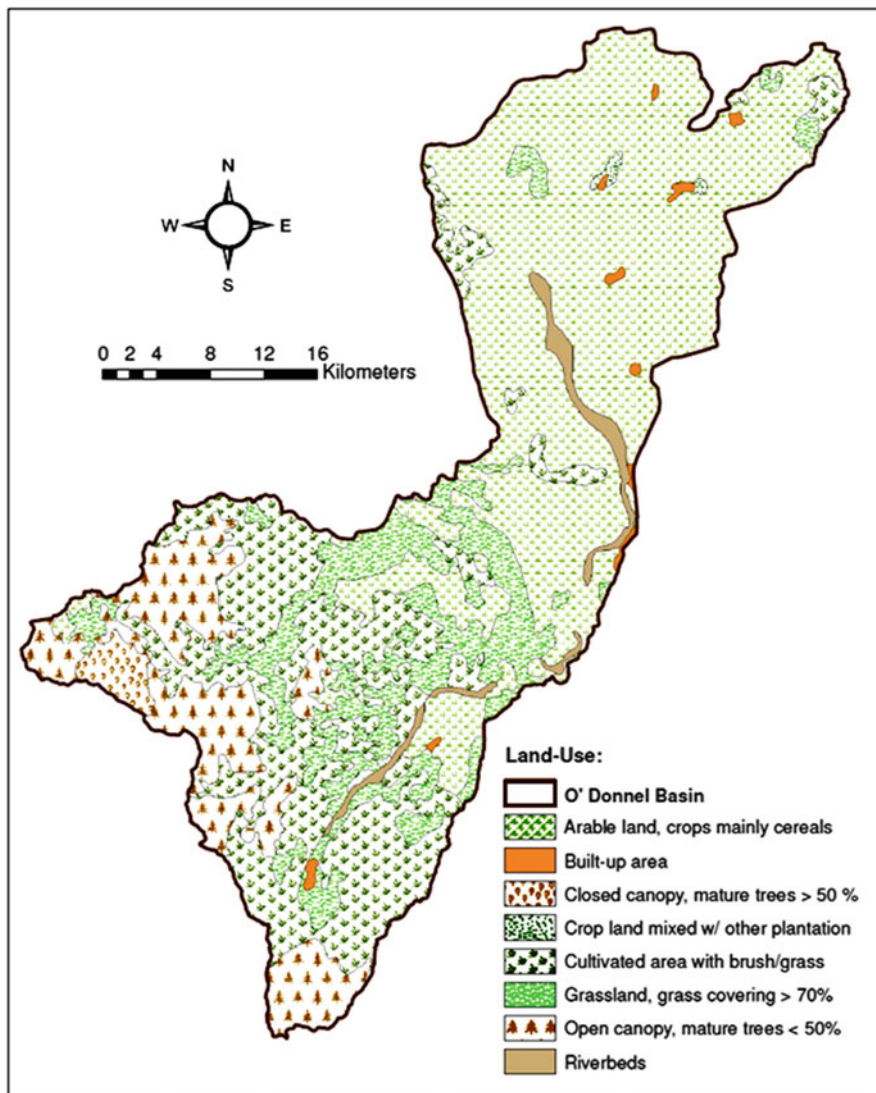


**Fig. 6.6** Land cover map of the study area

reservoir sedimentation was accounted for by modifying the reservoir elevation-storage curves for say after 25 years sedimentation or 50 years sedimentation. This approach is normally employed as done by Shen and Tabios (1992). Table 6.4 shows the number of years that the BBMP and BBMDS reservoirs will be half-filled and fully filled. Note that four (4) BBMDS reservoirs, namely, S3, S4, S5, and S9, would be half-filled in less than 40 years and it would take 321 years for BBMP to be half-filled.

**Table 6.2** Comparison of irrigation water deliveries ( $m^3/s$ ) of BBMP and BBMDS (six reservoirs) including lower Bulsa River natural flows for the case with no sedimentation at S1 location

No reservoir sedimentation at S1 location	All year-round			Dry season (Dec-Apr)			Wet season (May-Sept)		
	Natural	BBMP	BBMDS	Natural	BBMP	BBMDS	Natural	BBMP	BBMDS
Q90 (330/140 days) <sup>a</sup>	0.96	0.96	0.55	0.77	0.77	0.14	6.86	7.51	4.60
Q80 (290/125 days)	1.35	1.93	1.18	0.96	0.96	0.52	19.08	18.02	16.95
Q60 (220/95 days)	3.76	24.00	6.48	1.25	1.64	1.08	40.00	40.00	39.71
Q40 (145/60 days)	13.40	40.00	38.80	1.73	6.26	2.21	40.00	40.00	39.99
Q20 (70/30 days)	36.53	40.00	40.00	3.86	40.00	6.82	40.00	40.00	40.00
EV(Q) <sup>b</sup>	14.74	25.23	21.32	2.01	13.84	2.80	31.89	31.83	31.17
Area irrigated (ha) <sup>c</sup>	12,281	21,027	17,763	1679	11,534	2337	26,576	26,525	25,977

<sup>a</sup>Q90 (330/140 days) signifies 90% of time observed flow equal or greater than Q90 ( $m^3/s$ ) 330 days over the year or 140 days over the 5-month period

<sup>b</sup>EV(Q) is expected value of Q integrated over Q20 through Q90

<sup>c</sup>Area irrigated assuming 1.2  $m^3/s$  per 1000 ha calculated based on EV(Q) values

**Table 6.3** Comparison of flow duration curves of daily irrigation water deliveries ( $\text{m}^3/\text{s}$ ) of BBMP system and BBMDS (nine reservoirs) for the case with no reservoir sedimentation at S9 location

No reservoir sedimentation at S9 location

	All year-round		Dry season (Dec–Apr)		Wet season (May–Sept)	
	BBMP	BBMDS	BBMP	BBMDS	BBMP	BBMDS
Q90 (330/140 days) <sup>a</sup>	1.93	0.43	1.45	0.00	14.55	29.75
Q80 (290/125 days)	3.93	3.98	1.83	0.8	33.01	37.81
Q60 (220/95 days)	34.95	26.61	3.18	3.02	40.00	39.89
Q40 (145/60 days)	40.00	39.76	13.59	8.58	40.00	39.99
Q20 (70/30 days)	40.00	39.99	40.00	23.54	40.00	40.00
EV(Q) <sup>b</sup>	27.87	25.94	15.85	9.39	35.13	38.11
Area irrigated (ha) <sup>c</sup>	23,223	21,614	13,205	7828	29,279	31,758

<sup>a</sup>Q90 (330/140 days) signifies that the observed flow  $\geq$ Q90 ( $\text{m}^3/\text{s}$ ), 90% of the time or 330 days a year or 140 days over the 5-month period

<sup>b</sup>EV(Q) is expected value of Q integrated over Q20 through Q90

<sup>c</sup>Area irrigated assuming 1.2  $\text{m}^3/\text{s}$  per 1000 ha calculated based on EV(Q) values

**Table 6.4** Reservoir life computations due to sedimentation with a sediment inflow of  $3500 \text{ m}^3/\text{year}/\text{km}^2$  for BBMP and BBMDS reservoirs

	Drainage area ( $\text{km}^2$ )	Annual sediment inflows (MCM)	Starting storage (MCM)	Half-filled storage (MCM)	Year to half-filled reservoir	Years to fully filled reservoir
BBMP single, high dam	289.31	1,013	648.97	324.49	321	641
BBMDS dams	S1	36.43	0.128	93.09	46.54	366
	S2	48.74	0.171	46.10	23.05	136
	S3	67.34	0.236	15.77	7.89	34
	S4	24.65	0.086	6.98	3.49	41
	S5	41.62	0.146	4.02	2.01	14
	S6	10.36	0.036	11.63	5.81	161
	S7	42.91	0.150	22.67	11.33	76
	S8	69.23	0.242	34.42	17.21	72
	S9	182.27	0.638	6.08	3.04	5
						10

For the case with reservoir sedimentation after 50 years, the results are shown in Table 6.5. It is seen here that BBMP still resulted in higher irrigation water deliveries and thus higher irrigated areas compared to BBMDS at S1 location.

With regard to potential hydropower generation as shown in Table 6.6, generally BBMP (with 1 hydropower plant) versus BBMDS multiple reservoir system (with five hydropower plants located at S1, S2, S3, S4, and S5) resulted in higher hydropower generation and subsequently higher annual revenue assuming the selling price of electricity is 3 pesos per kW-h, for base year condition, after 25 years sedimentation and after 50 years sedimentation. Note that the hydropower

**Table 6.5** Comparison of flow duration curves of daily irrigation water deliveries ( $\text{m}^3/\text{s}$ ) of BBMP system and BBMDS (six reservoirs) for the case with 50 years reservoir sedimentation at S1 location

After 50 years with reservoir sedimentation						
	All year-round		Dry season (Dec–Apr)		Wet season (May–Sept)	
	BBMP	BBMDS	BBMP	BBMDS	BBMP	BBMDS
Q90 (330/140 days) <sup>a</sup>	1.06	1.06	0.77	0.00	7.511	5.737
Q80 (290/125 days)	1.93	1.93	0.96	0.08	18.02	18.14
Q60 (220/95 days)	21.03	20.24	1.64	0.83	40.00	39.78
Q40 (145/60 days)	40.00	40.00	6.27	1.98	40.00	40.00
Q20 (70/30 days)	40.00	40.00	40.00	5.52	40.00	40.00
EV(Q) <sup>b</sup>	24.65	20.42	13.84	2.23	31.83	31.54
Area irrigated (ha) <sup>c</sup>	20,545	20,414	11,534	1858	26,525	26,280

<sup>a</sup>Q90 (330/140 days) signifies that the observed flow  $\geq Q90$  ( $\text{m}^3/\text{s}$ ), 90% of the time or 330 days a year or 140 days over the 5-month period

<sup>b</sup>EV(Q) is expected value of Q integrated over Q20 through Q90

<sup>c</sup>Area irrigated assuming 1.2  $\text{m}^3/\text{s}$  per 1000 ha calculated based on EV(Q) values

**Table 6.6** Hydropower generation (in MW) at BBMP (one hydropower plant) versus BBMDS project (five hydropower plants located at S1, S2, S3, S4, and S5)

	Hydropower generation in MW for 10 h daily operations					
	No sedimentation		After 25 years sedimentation		After 50 years sedimentation	
	BBMP	BBMDS	BBMP	BBMDS	BBMP	BBMDS
Q90 (330 days) <sup>a</sup>	0.00	1.24	0.78	1.79	0.99	1.91
Q80 (290 days)	0.00	3.65	1.42	4.77	1.81	5.09
Q60 (220 days)	1.59	7.01	16.94	9.98	20.19	10.53
Q40 (145 days)	38.46	22.99	43.28	32.85	47.64	34.25
Q20 (70 days)	60.38	60.32	62.65	64.37	64.75	65.09
EV(Q) <sup>b</sup>	26.13	24.83	31.17	28.86	33.41	29.53
GW-h/year	95.36	90.63	113.76	105.35	121.94	107.79
Annual revenue in million pesos at 3 pesos per KW-h	286	272	341	316	366	323

<sup>a</sup>Q90 (330 days) signifies that the observed flow  $\geq Q90$  ( $\text{m}^3/\text{s}$ ), 90% of the time or 330 days a year

<sup>b</sup>EV(Q) is expected value of Q integrated over Q20 through Q90. Also KW, MW, and GW for kilo-, mega-, and gigawatts

generation is higher as sediment accumulate since reservoirs during these periods will be operating at higher reservoir elevations but the tailhead elevations of hydropower plants are assumed the same during construction (i.e., same with base case).

As far as cost of dams is concerned, BBMP dam costs 3.99 billion pesos compared to BBMDS's nine small dams total cost of 5.08 billion pesos (2015 prices). BBMDS scheme results in higher costs because there are more clay core and rock-fill materials needed to build the nine dams compared to BBMP single dam and noting that the clay core is more expensive than the rock-fill materials.

**Table 6.7** Estimates of benefit/cost (B/C) ratio, net present value (NPV), and economic internal rate of return (EIRR) for BBMP and BBMDS for base case and after 25 years and after 50 years with sedimentation. [Irrigation benefits for rice, sugarcane, corn, potato, eggplant, tomato, string beans, and ampalaya (bitter gourd) but excludes hydropower]

Indicator	Base case		Base case plus higher investment and 20% less irrigation benefits		Case with 25 years reservoir sedimentation		Case with 50 years reservoir sedimentation	
	BBMP	BBMDS	BBMP	BBMDS	BBMP	BBMDS	BBMP	BBMDS
B/C ratio	2.77	1.67	1.84	1.12	2.73	1.19	2.71	1.16
NPV at 15% (million pesos)	6128	2972	3514	612	5991	819	5921	703
EIRR	27	20	21	16	27	17	27	16

From results of economic analysis given in Table 6.7, assuming benefits from growing 13 crops, the benefit/cost (B/C) ratios, net present values (NPV), and economic internal rate of return (EIRR) for all BBMP were all higher compared to those for BBMDS. The EIRRs while all above 15%, the estimates for BBMDS were nearer the cutoff at 16–17%, even for the worst scenario (with reservoir sedimentation). Similarly, although the NPVs were positive in both instances, those for BBMDS were smaller compared to those for BBMP. The same is true for B/C ratios which were all above 1.0 but were much higher with those for BBMP. The above analysis reveals that while both projects appear to be economically viable based on the three (3) economic indicators, the BBMP produces better numbers. Going for more conservative estimates of benefits, with only two crops assumed to benefit from the project, the results obtained showed a dismal picture for BBMDS. BBMP, in consistently producing good outcomes, makes a better choice as BBMDS proposal becomes unviable based on all three measures, B/C ratio, NPV, and EIRR.

With regard to the reservoir backwater inundated areas, the communities and estimated number of households that could be inundated at full reservoir capacity were 330 households for BBMP dam against 448 households for the 9 BBMDS dams. With these estimates of the number of households affected, corresponding resettlement costs can be calculated.

Finally, with regard to flood benefits, Fig. 6.7 shows the flood frequency curves of uncontrolled flows at S9 location for both BBMP and BBMDS. It is seen here that BBMP reduced the natural annual maxima daily flow (equivalent to 50-year return period flow) from about 3600 m<sup>3</sup>/s to about 1950 m<sup>3</sup>/s (a difference of 1650 m<sup>3</sup>/s) while BBMDS scheme only reduced this natural 50-year return period daily flow to 3200 m<sup>3</sup>/s (or a difference of 400 m<sup>3</sup>/s). In this case, the resulting flood inundated areas and corresponding average flood depth were lowest with BBMP compared to BBMDS and case without the reservoir under natural river flows (NHRC 2015; Tabios 2018). The BBMDS scheme and without reservoir case (under natural river flows) resulted in the same flood inundated areas, but the flood inundated depths were lower for BBMDS.

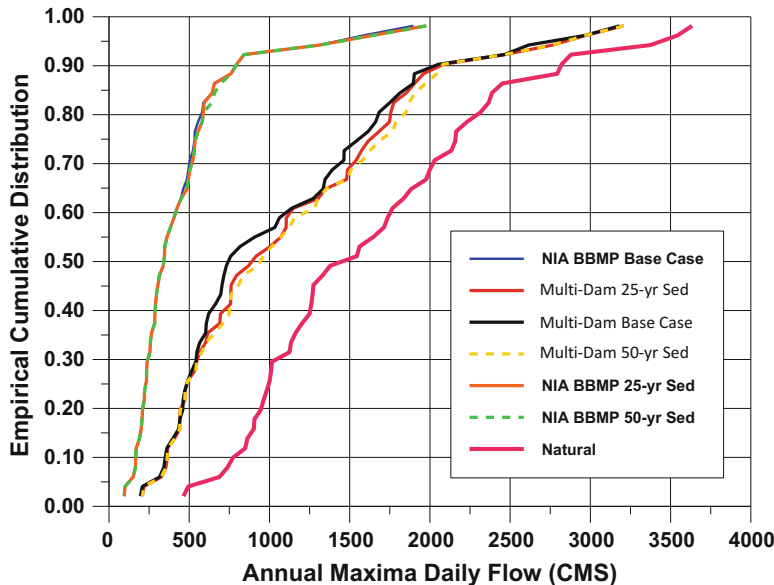


**Fig. 6.7** Flood frequency curves of uncontrolled flows (in  $\text{m}^3/\text{s}$  or CMS) at S9 location for both Balog-Balog single, high dam, multipurpose project (BBMP) and multi-dam (BBMDS) including natural flow (without dam project)

As a final remark, it is seen in the results that the proposed Balog-Balog dam projects, either the single, high dam (BBMP) or the multiple dam system (BBMDS), would not be able to provide adequate irrigation water supply if the target irrigation service area was 34,000 ha since the BBMP could only irrigate an average of 23,000 ha (BBMDS can irrigate a much smaller area) for two cropping seasons (13,000 ha during dry season and 29,000 ha during wet season); thus an alternative irrigation water source is needed. For this reason, it is critical to explore and examine in more detail how the Rio Chico River and Talavera river basins (see Fig. 6.8) can be used to augment the Balog-Balog Irrigation System considering that the Balog-Balog irrigation service areas extend to those two rivers. Note that Rio Chico River and Talavera river basins drain into the Pampanga River Basin (see Sect. 4.2, Chap. 4), while the Tarlac-O'Donnell River Basin drains into the Agno River Basin (see Sect. 4.3, Chap. 4).

## 6.2 San Roque Reservoir Sedimentation and Operations Study Using a Two-Dimensional Hydraulic Model

The San Roque Reservoir is a multipurpose reservoir for hydropower generation, irrigation water supply, and flood control. The reservoir is located in the Lower Agno River of Pangasinan, Philippines, and its dam construction was completed in

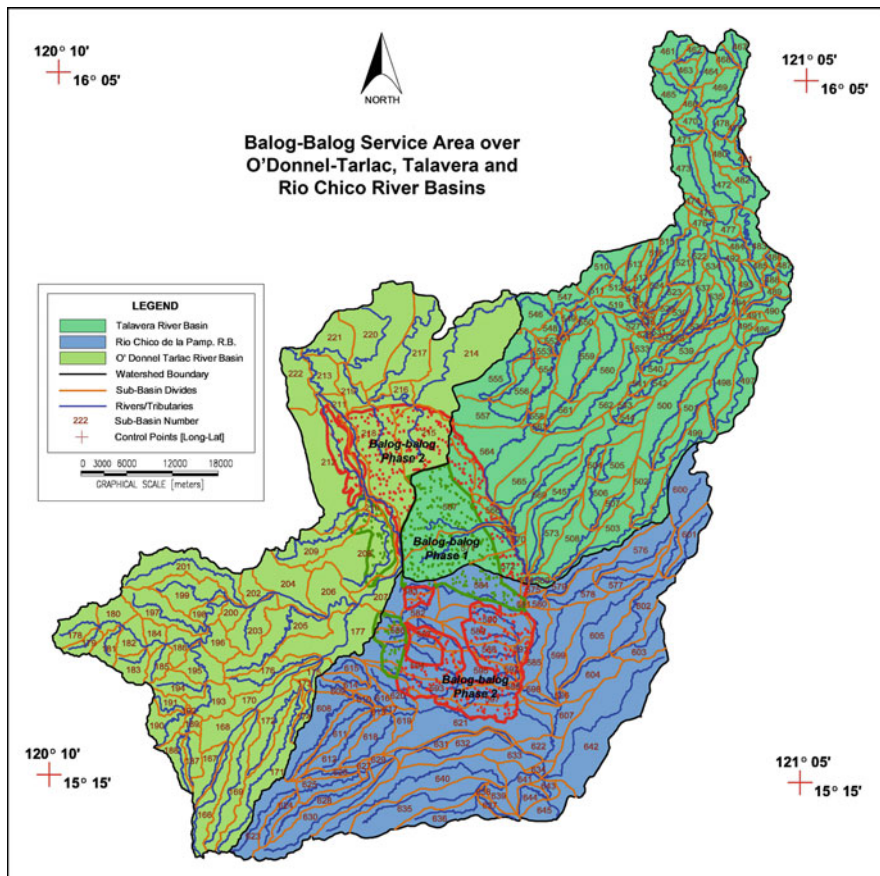


**Fig. 6.8** Map showing the Balog-Balog Irrigation System service area traversing three major watersheds, namely, O'Donnell, Rio Chico, and Talavera river basins

2002. The maximum storage capacity of the reservoir is about 840 MCM (million m<sup>3</sup>), and its hydropower plant has a maximum operating capacity of 402 MW. Figure 6.9 below shows the location of the reservoir. A major concern regarding reservoirs in general and specifically San Roque Reservoir is sedimentation. At the upper end of the Lower Agno River is Binga Reservoir, built in 1959. Its storage volume is largely reduced by sedimentation; thus its outflows contain significant amounts of sediments into San Roque Reservoir. The watersheds around Agno River likewise contribute to reservoir sedimentation; thus it is necessary that proper sediment control measures are imposed to minimize watershed sediment yields.

The impact of reservoir sedimentation on water yield and hydropower generation of San Roque Reservoir was investigated. A two-dimensional (2-d) reservoir and river hydraulic model was used which had been enhanced to function as a reservoir operations model for San Roque Reservoir. The sediment inflows into the reservoir

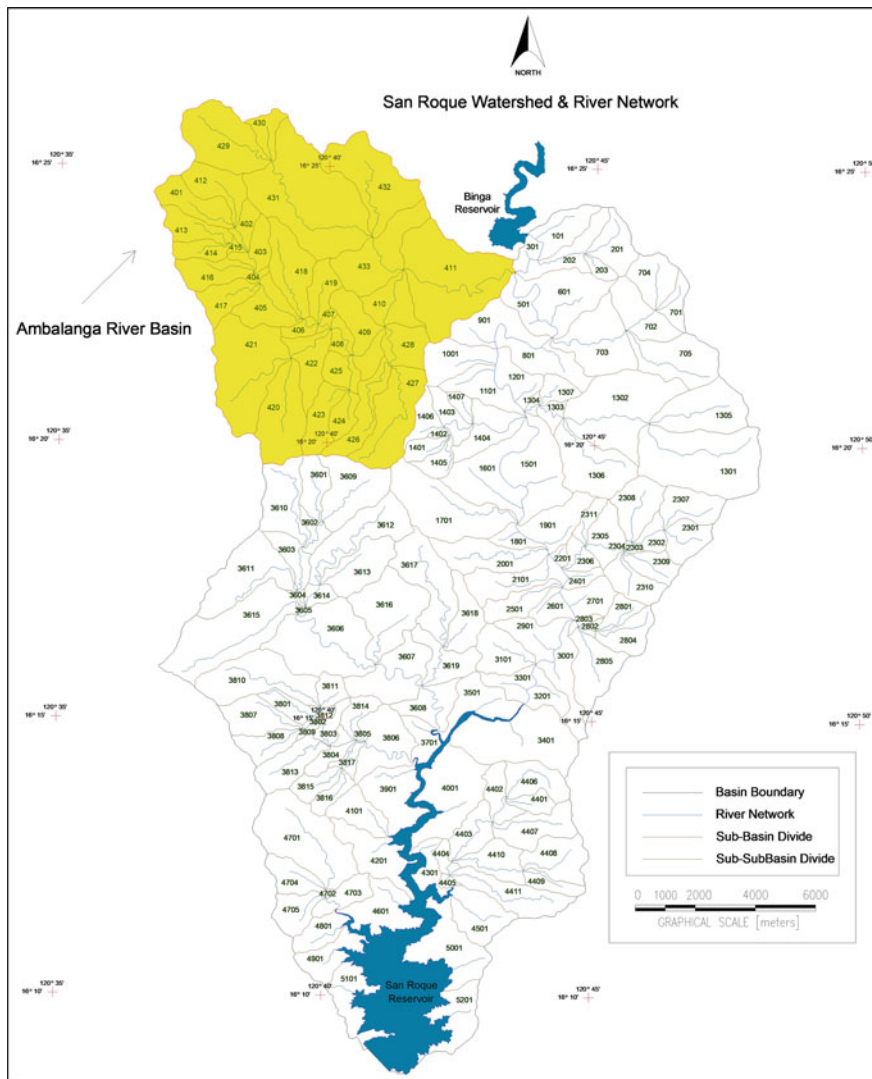


**Fig. 6.9** San Roque Reservoir and watersheds. Also indicated is the Ambalanga watershed

consist of outflow from Binga Reservoir and sediment inflows from surrounding watersheds. The local sediment inflows were estimated using a physically based watershed sediment yield model with long-term rainfall sequences generated by a continuous-time, stochastic model. This study is reported in the papers by Tabios et al. (2007a, b) and also in the NHRC (2007) report.

### 6.2.1 Two-Dimensional Flow and Sediment Hydraulic Model

In this study, the two-dimensional (2-d) flow and sediment transport hydraulic model was specifically enhanced to be able to assess the impact of sedimentation on the reservoir operations and especially hydropower generation. In particular, certain model components were added such as reservoir release rules, gated spillway operations, and hydropower energy calculations in the 2-d hydraulic model. In essence, this 2-d hydraulic model can be utilized as a reservoir operations model as well.

The 2-d hydraulic model is based on the finite volume method (FVM) formulation. This model is based on an earlier work by Zhao et al. (1994) and later Tabios (2007). The governing equations of the 2-d model are (1) mass conservation equation of water-sediment mixture; (2) momentum conservation equations in the  $x$ - and  $y$ -directions; (3) suspended sediment conservation equation; (4) bed load conservation equation; and (5) sediment-laden flow density equation.

The mass conservation equation is written as:

$$\frac{\partial(\rho_m h)}{\partial t} + \frac{\partial(\rho_m h u)}{\partial x} + \frac{\partial(\rho_m h v)}{\partial y} = \rho_{xx} q_{xx} \quad (6.1)$$

where  $h(x,y,t)$  is flow depth;  $u(x,y,t)$  is depth-averaged velocity in  $x$ -direction;  $v(x,y,t)$  is depth-averaged velocity in  $y$ -direction;  $\rho_m(x,y,t)$  is the water-sediment mixture density,  $q_{xx}(x,y,t)$  is external inflow or source term; and  $\rho_{xx}(x,y,t)$  is density of external flow. The momentum equation in the  $x$ -direction is written as:

$$\begin{aligned} & \frac{\partial(\rho_m h u)}{\partial t} + \frac{\partial(\rho_m h u^2 + \rho_m g \frac{h}{2})}{\partial x} + \frac{\partial(\rho_m h u v)}{\partial y} \\ &= \rho_m g h (S_{ox} - S_{fx}) + \frac{\partial(h \tau_{xx})}{\partial x} + \frac{\partial(h \tau_{xy})}{\partial y} \end{aligned} \quad (6.2)$$

In the  $y$ -direction:

$$\begin{aligned} & \frac{\partial(\rho_m h v)}{\partial t} + \frac{\partial(\rho_m h u v)}{\partial x} + \frac{\partial(\rho_m h v^2 + \rho_m g \frac{h}{2})}{\partial y} \\ &= \rho_m g h (S_{oy} - S_{fy}) + \frac{\partial(h \tau_{yx})}{\partial x} + \frac{\partial(h \tau_{yy})}{\partial y} \end{aligned} \quad (6.3)$$

where  $S_{ox}(x,y,t), S_{oy}(x,y,t)$  are bed slopes in  $x$ - and  $y$ -directions;  $S_{fx}(x,y,t), S_{fy}(x,y,t)$  are friction slopes in  $x$ - and  $y$ -directions;  $\tau_{xx}(x,y,t), \tau_{yy}(x,y,t)$  are normal stresses in  $x$ - and  $y$ -directions;  $\tau_{yx}(x,y,t), \tau_{xy}(x,y,t)$  are lateral stresses in  $x$ - and  $y$ -directions; and  $g$  is acceleration due to gravity. Appropriate equations are needed to define the friction

slope such as the use of the Manning's equation and likewise for the normal and lateral shear stresses.

The suspended sediment conservation equation is given by:

$$\frac{\partial hC}{\partial t} + \frac{\partial huC}{\partial x} + \frac{\partial hvC}{\partial y} = \frac{\partial}{\partial x} \left( D_x h \frac{\partial C}{\partial x} \right) + \frac{\partial}{\partial y} \left( D_y h \frac{\partial C}{\partial y} \right) - \alpha_o \omega (C - C_b) \quad (6.4)$$

where  $C(x,y,t)$  is the depth-averaged suspended sediment concentration by volume;  $D_x(x,y,t)$ ,  $D_y(x,y,t)$  are sediment mixing coefficients in the  $x$ - and  $y$ - directions;  $\omega$  is the particle settling velocity;  $C_b(x,y,t)$  is the equilibrium suspended sediment concentration; and  $\alpha_o$  is the non-equilibrium adaptation parameter that is an empirical coefficient.

In the suspended sediment conservation equation, the effective depth should be  $(h - \delta)$  in which  $\delta$  is the thickness of the bed load zone, where  $\delta$  is usually taken equal to 2–3 times the grain diameter of the sediment material transported. However, since flow depth is so many orders of magnitude greater than  $\delta$ , it is usually assumed that  $(h - \delta) \cong h$ .

The bed load conservation equation in the bed load zone can be written as:

$$\frac{\partial z}{\partial t} + \frac{1}{1-p} \left[ \alpha_0 \omega (C_b - C) + \frac{\partial q_{bx}}{\partial x} + \frac{\partial q_{by}}{\partial y} + \frac{\partial (\delta c_b)}{\partial t} \right] = 0 \quad (6.5)$$

where  $z(x,y,t)$  is the bed elevation;  $q_{bx}(x,y,t)$ ,  $q_{by}(x,y,t)$  are the bed load transport rates in the  $x$ - and  $y$ -directions;  $p$  is the porosity;  $c_b$  is the average bed load concentration at bed load zone; and  $\delta$  is the thickness of the bed load zone. The above formulation is referred to as a non-equilibrium transport model (Wu 2004).

The total flowing mixture mass per unit volume is the sum of sediment and water mass as:

$$\rho_m = C\rho_s + (1 - C)\rho_w \quad (6.6)$$

where  $\rho_m(x,y,t)$  is the mixture density;  $\rho_s$  is the sediment density; and  $\rho_f$  is the fluid density.

In the finite volume method (FVM), the mass and momentum equations in Eqs. (6.1) to (6.3) are solved coupled with the suspended load conservation equation in Eq. (6.4). Then, the bed load transport rate is calculated using an appropriate equation (e.g., Duboys bed load equation [see Garde and Raju 1985]) and applied to the bed load conservation equation in Eq. (6.5) which essentially calculates the bed change or deformation. The mass, momentum, and suspended sediment fluxes of the conservation equations are calculated for each side of a finite volume by a Riemann problem solution (Zhao et al. 1996) which involves approximating the fluxes by the characteristic solution of the governing equations. In the model formulation above, the river sediments are treated as non-cohesive materials and also assuming one, uniform sediment size.

The major boundary conditions imposed in the model are the following: (1) upstream flow and sediment discharges from Binga Reservoir; (2) the flows and sediment yields from watersheds along the entire stretch of Agno River between San Roque Dam to the toe of Binga Dam; (3) gated spillway at San Roque Dam; and (4) controlled reservoir releases for power and irrigation from San Roque. The spillway equations used in the model were provided by San Roque Power Corporation. Rainfall, evaporation, and bed leakage in the San Roque Reservoir are assumed small and not considered in the model.

### **6.2.2 Watershed Flow and Sediment Yield Modeling**

The KINEROS2 model was developed by Woolhiser et al. (1990) of the Agricultural Research Service, US Department of Agriculture, which is a physically based model to simulate the following watershed processes: (1) interception; (2) infiltration; (3) surface runoff; and (4) erosion from overland flow planes and channels. In this model, the flow routing is by kinematic wave equation through rectangular overland flow planes and trapezoidal channels. The soil erosion from overland flow planes is due to splash erosion caused by raindrop energy and hydraulic or rill erosion caused by flowing water. The finite difference method is used to solve the overland flow, channel flow, erosion, and sediment transport equations. For details of this model, the reader is referred to Woolhiser et al. (1990).

In KINEROS2, the overland flow and channel flow equations are based on kinematic wave routing. In particular, the continuity equation is written as:

$$\frac{\partial A}{\partial t} + \frac{\partial Q}{\partial x} = q_L \quad (6.7)$$

Under kinematic wave assumption, the momentum equation simplifies to:

$$S_0 = S_f \quad (6.8)$$

in which  $Q$  is discharge,  $A$  is the flow area,  $q_L$  is lateral inflow,  $S_0$  is bed slope, and  $S_L$  is friction slope. With Eq. (6.8), the continuity Eq. (6.7) can be written homogeneous in  $Q$  or  $A$  by substituting the equation:

$$Q = \alpha A^\beta \quad (6.9)$$

Using the Manning's  $\alpha = S_0^{1/2} P^{-2/3} / n$  equation:  $\beta = 5/3$  and for a rectangular channel.

The erosion and sediment transport in overland flow plane and channel are described as follows. The sediment continuity equation in the overland flow plane is given by:

$$\frac{\partial A C}{\partial t} + \frac{\partial Q C}{\partial x} - e_s(x, t) - e_h(x, t) = q(x, t) \quad (6.10)$$

where  $Q$  is discharge,  $C$  is sediment concentration,  $A$  is flow area,  $e_s$  is splash erosion rate,  $e_h$  is hydraulic erosion, and  $q$  is lateral sediment inflow.

The splash erosion term is written as:

$$e_s = c_f e^{-c_h h r^2} \quad (6.11)$$

in which  $r$  is rainfall,  $h$  is water depth,  $c_f$  is a constant related to soil and surface properties, and  $c_h$  is a coefficient representing the damping effectiveness of surface water.

The hydraulic erosion (deposition if  $C > C_m$ ) term is the rate of exchange of sediment between flowing water and soil over which it flows.

$$e_h = c_g (C_m - C) A \quad (6.12)$$

where  $C_m$  is concentration at equilibrium transport capacity (i.e., calculated using modified Engelund-Hansen equation) and  $c_g$  is a coefficient.

The major data requirement for the watershed modeling is the watershed geometry and topology as well as watershed physical characteristics such as overland flow and channel characteristics, soil and vegetal cover, infiltration, and subsurface flow characteristics. The watershed geometry is shown in Fig. 6.9. The watershed system bounded by Binga Dam and San Roque Dam with a drainage area of about  $366 \text{ km}^2$  is divided into 164 subwatersheds with 52 inflow points (subwatershed outlets) to the San Roque Reservoir and Agno River. In the watershed model, the surface and subsurface flow parameters like retention storage, Manning's roughness coefficient, effective capillary drive, vertical hydraulic conductivity, porosity, and residual water content were estimated from the soil and land use maps.

Another important data are watershed sediment data and characteristics. A uniform, single sediment size of 0.2 mm is used to represent the sediment yield from the watersheds. It is found that the watershed sediment yield is not so sensitive to the size of sediment used since the sediments observed in the Agno River and San Roque Reservoir are mostly silt and sand fractions.

For illustration, Fig. 6.10 shows the simulation run using KINEROS2 model for Ambalanga watershed (located in upper left-hand side of the San Roque watershed shown in Fig. 6.9). In particular, Fig. 6.10 shows the time series plots of rainfall, resulting discharges, and sediment yield at the 29th year of simulation.

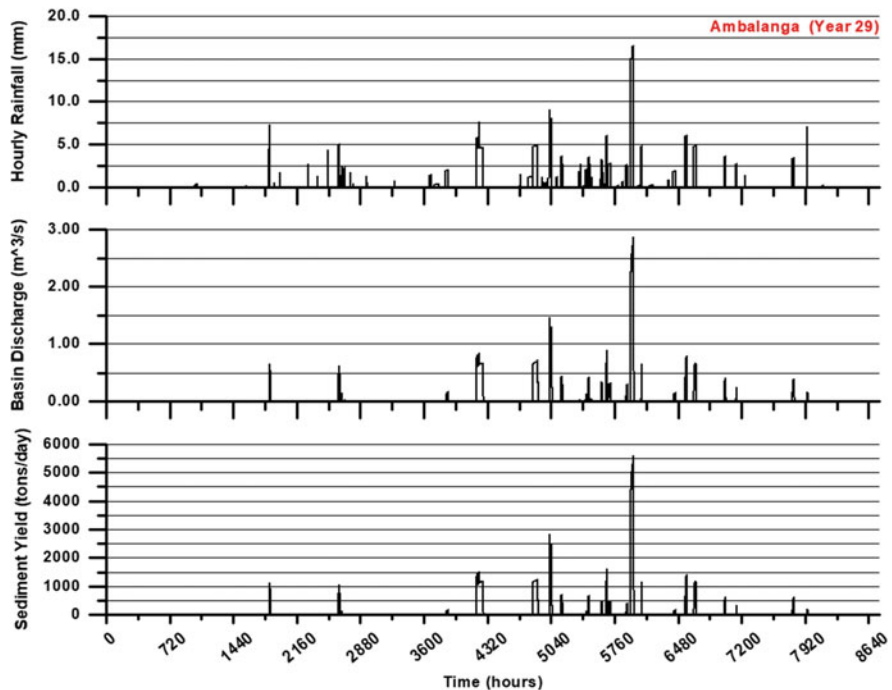


**Fig. 6.10** Time series plots of simulation of rainfall input, watershed flows, and sediment yield for Ambalanga sub-basin on 29th year of simulation

### 6.2.3 Stochastic Rainfall Modeling

For purposes of this study, 70 years of hourly rainfall data were used. Generation of long-term rainfall sequences was accomplished using a stochastic rainfall model. The rainfall was modeled as a point rainfall in continuous time using two alternative stochastic model formulations, namely, the Poisson rectangular pulse (PRP) model and the Neyman-Scott white noise (NSWN) model (Waymire et al. 1984; Obeysekera et al. 1987). In the PRP model, the occurrence of rainfall events is characterized by a Poisson process. Associated with each event are the intensity and duration, which are assumed to be independent and exponentially distributed. In the NSWN model, the arrival of storms is characterized likewise by the Poisson process. Associated with each storm are a random number of rainfall bursts, each of which produces an instantaneous rainfall with magnitude independent from one burst to another. The rainfall magnitude is assumed to be exponentially distributed. Also, the time of occurrence of bursts relative to the storm origin is exponentially distributed.

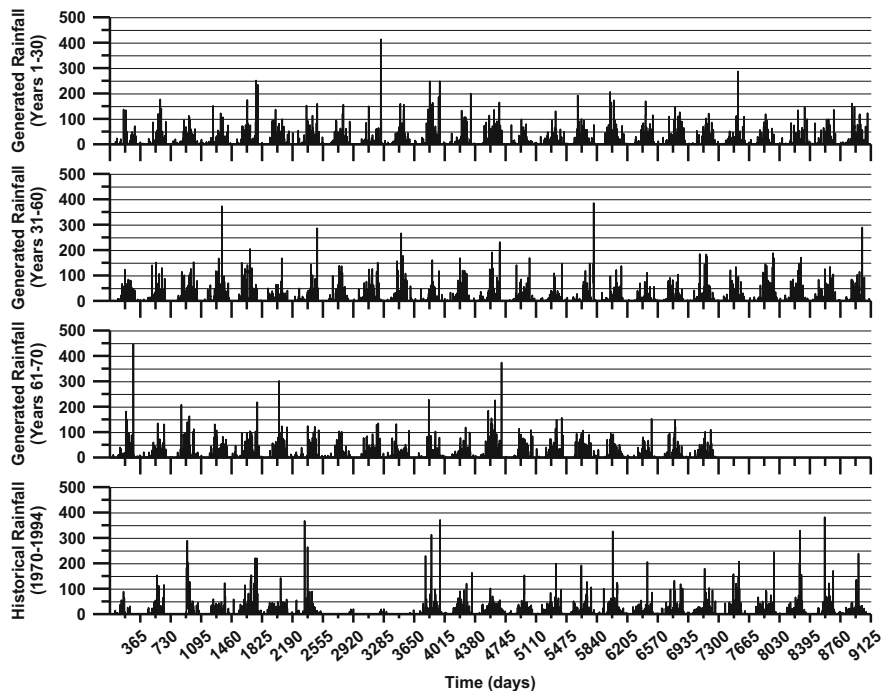


**Fig. 6.11** Time series plots of stochastically generated rainfall aggregated on a daily basis using the Poisson rectangular pulse model for 70 years (first three plots) and the historical daily rainfall data at Binga Dam (bottom plot)

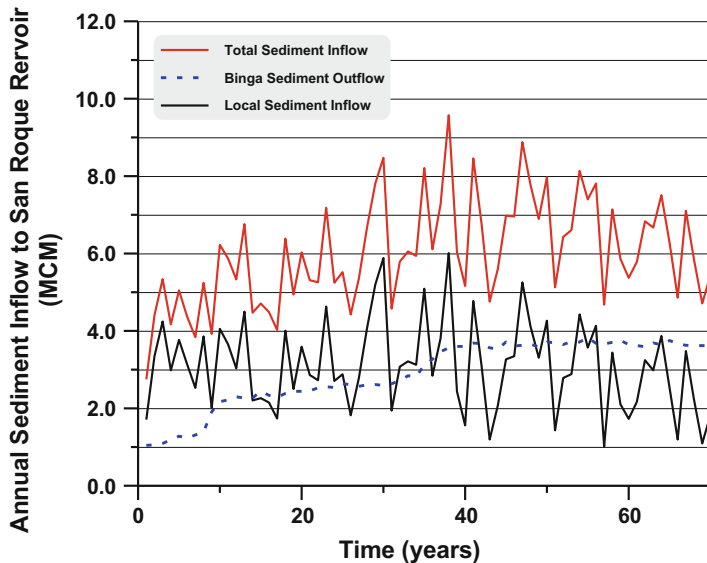
In this study, the Binga Reservoir rainfall data collected at the damsite was used to represent the areal rainfall of each subwatershed due to the proximity of this gaging station to the study area as well as its length of record (1961–1997) available for fitting the rainfall model. Using daily rainfall record, the Poisson rectangular pulse model was found to be the best fitting model to the Binga rainfall. The stochastic model was fitted with monthly varying parameters by method of moments based on daily rainfall means, variances, and covariances. Note that the rainfall model formulation, which is a continuous-time, continuous-variable, stochastic model, has model parameters that are applicable at any level of aggregation of the data (i.e., minute, hourly, or daily time intervals).

Figure 6.11 shows the stochastically generated rainfall data for 70 years plotted on a daily basis using the fitted Poisson rectangular pulse model. The actual rainfall generated is continuous in time, but these were aggregated on a daily basis for plotting purposes and to be comparable to the historical daily rainfall of Binga in Fig. 6.11. In the watershed model, the rainfall used was aggregated on an hourly basis.

### 6.2.4 Reservoir Simulation Scenarios

Three simulation scenarios are presented here to investigate the impact of reservoir sedimentation on water yield and hydropower generation, namely, (i) Case 1, (ii) Case 2, and (iii) Case 3. Cases 1 and 3 adopt an aggressive reservoir release rule policy where releases are non-zero even when the reservoir level is below the lower rule curve. The lower rule curve is a target or desirable storage developed for a particular reservoir according to its flood control and water conservation objectives. Case 2 adopts a conservative release rule so that zero or no release is made when the reservoir level is below the lower rule curve. Case 3 differs from Case 1 in that its so called non-equilibrium adaptation parameter in the sediment conservation equations (see Eq. 6.4) is set higher to artificially increase sediment deposition in the reservoir.

A total of 70 years of hourly rainfall were generated to calculate the watershed flows and sediment yields. The Binga outflows and sediment load were provided in this study by Northwest Hydraulic Consultants (NHC 2008). The total sediment inflow to San Roque Reservoir is 420.9 MCM (million cubic meters) in 70 years in which 204.2 MCM is from Binga Reservoir and 216.7 MCM is from the surrounding watersheds. The time series plots of the sediment inflows on an annual basis are given in Fig. 6.12.



**Fig. 6.12** Time series plots of annual sediment inflow to San Roque Reservoir

### 6.2.5 Results of Reservoir Flow-Sediment Simulations

Table 6.8 shows the remaining reservoir capacities and total sediment deposited in the reservoir for the end of periods of 0, 25, 50, and 70 years at 280 m reservoir levels. The percentages of sediment deposited for a total sediment inflow of 420.9 MCM in 70 years are 80.5, 80.3, and 92.0% for Cases 1, 2, and 3, respectively. Table 6.9 shows the total water yield, total energy generation (in gigawatt-hours or GWH), and sediment load of power releases in 70 years for Cases 1, 2, and 3. Note that the power is calculated based on 85% turbine operating efficiency. Case 2 resulted in the highest hydropower generation followed by Case 1 and Case 3. Case 1 resulted in highest water yield. Case 2 yielded higher hydropower generation because of higher reservoir levels, despite that Case 1 had higher water yield.

For discussions here, only selective results are given below. For Case 3 only, the change in bed elevations from year 0 (start of simulation) to the end of 25 and 70 years is given in Fig. 6.13. Generally, the sediment deposition in the reservoir area was widespread in the first 10 years of simulation, and after 30–40 years, the sedimentation tended to be in areas only along the banks of old, submerged river. Consequently, there was less deposition in areas along the main channel path of this old, submerged river. Generally, the amounts of sediment deposited were significantly large at the various parts of the reservoir compared to the amounts eroded, which were relatively small, and at very limited portions in the reservoir area. Similar deposition patterns could be observed in Cases 1 and 2.

The time series plots of reservoir inflows, reservoir levels, and spillway releases for Cases 1 and 2 are given in Figs. 6.14 and 6.15, respectively. With regard to the type of reservoir release policy, it is shown here that Case 1 resulted in fewer spills than Case 2. This is because the release policy in Case 2 is conservative compared to

**Table 6.8** San Roque Reservoir capacities and sediment deposited (in MCM) for Cases 1, 2, and 3

Years in simulation	Case 1		Case 2		Case 3	
	Reservoir capacity (MCM)	Sediment deposited (MCM)	Reservoir capacity (MCM)	Sediment deposited (MCM)	Reservoir capacity (MCM)	Sediment deposited (MCM)
0	840.4	0.0	840.4	0.0	840.4	0.0
25	679.6	160.8	680.1	160.3	656.0	181.9
50	567.7	272.7	571.7	268.7	529.2	309.2
70	501.4	339.0	502.4	338.0	460.9	387.4

**Table 6.9** Total water yield (in MCM), total energy generation (in GWH), and sediment load of power releases (in MCM) in 70 years for Cases 1, 2, and 3

	Case 1	Case 2	Case 3
Total water yield (MCM)	417,324	416,523	402,021
Total energy generation (GWH)	104,840	106,319	97,246
Power release sediment load (MCM)	35.46	40.12	4.71

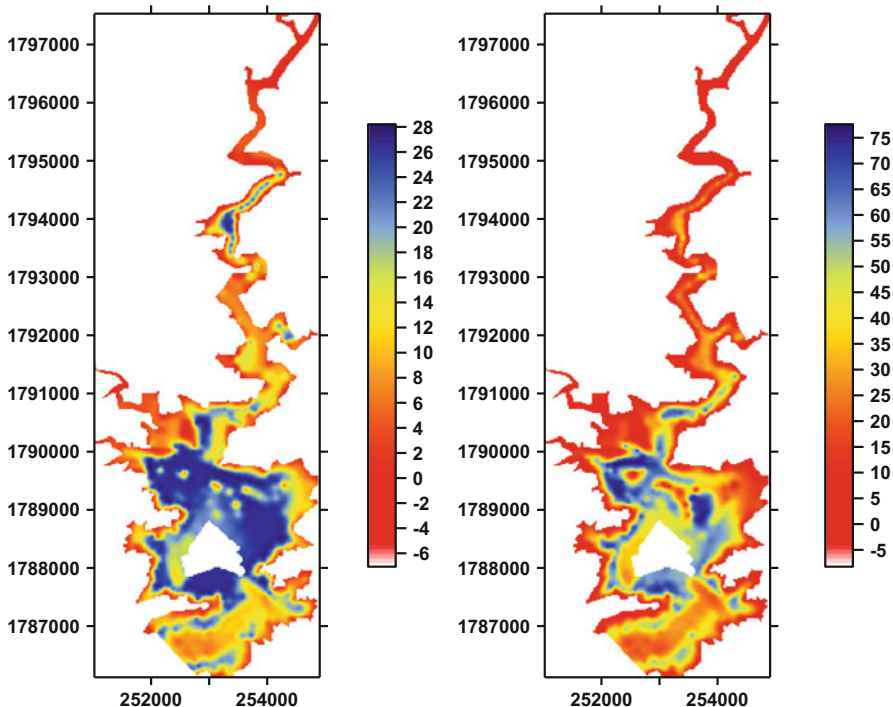


**Fig. 6.13** Change in bed elevations for Case 3 from year 0 to end of years 25 (left) and 70 (right). Positive values indicate sediment deposition

Case 1 that is aggressive. In other words, while Case 2 adopted a conservative or anticipatory release policy and saved or hedged water for the future, it ended up in more frequent spills. On the other hand, Case 2 with conservative release rule resulted in higher total energy generated over 70 years compared to Case 1 and Case 3. This can be attributed to the ability of Case 2 to sustain higher power releases all months of the year by hedging into the future (i.e., the latter months of the year) so there is enough water in storage to make releases when inflows are waning after the wet months of the year and since the reservoir water levels remain high thus the higher operating heads in hydropower generation.

The time series plots of power releases, energy generated, and power release sediment load (sediment carried in the power releases) for Cases 1 and 3 are given in Figs. 6.16 and 6.17, respectively. With regard to the impact of sediment deposition on reservoir operations and especially hydropower generation, it is noted that the reservoir levels near the dam as well as the power releases were significantly lower in Case 3 due to more sediment deposition in the reservoir. This is especially observed when sediment deposition in the San Roque Reservoir reduced its capacity to 529 MCM (at 280 m water level) which happened around year 50. Thus, in the 70 years simulation, Case 3 resulted in lower total energy generated than Cases 1 and 2.

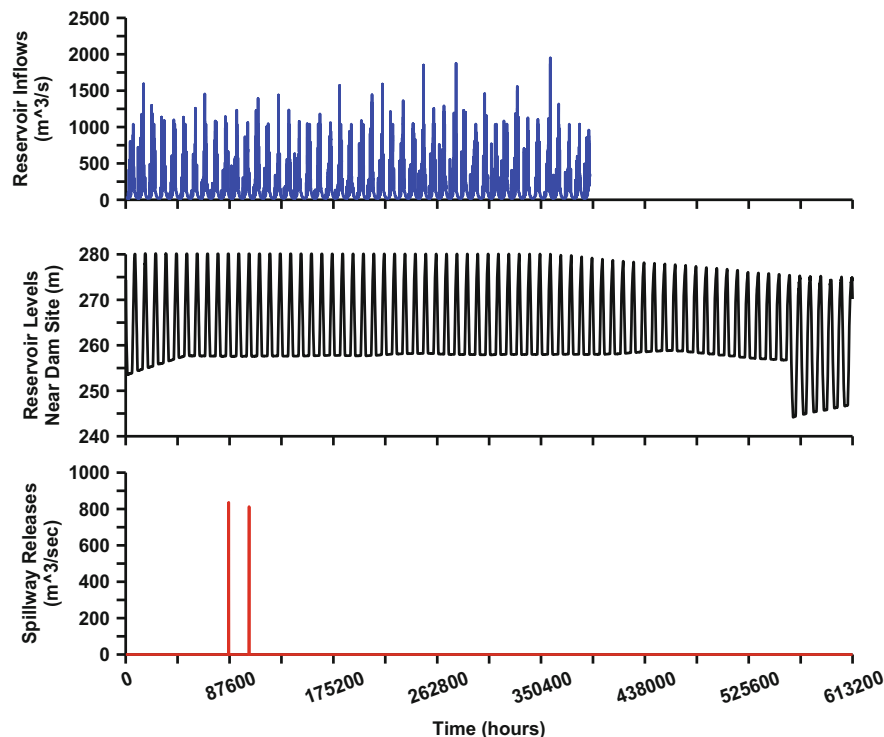


**Fig. 6.14** Time series plots of reservoir inflows, levels and spills for Case 1

### 6.2.6 Some Highlights of San Roque Flow-Sediment Modeling and Simulation Studies

One of the highlights of this study is the use of a 2-d hydraulic model for flow and sediment transport which has been enhanced as a reservoir operations model to assess the impact of sedimentation on water yield and hydropower generation of San Roque Reservoir. In this case, certain model components were added in the 2-d hydraulic model such as reservoir release rules based on current operating policies, use of specific spillway equations, and hydropower energy calculations for San Roque Reservoir. This model in particular can be utilized as a long-term reservoir operations model as well and can even be adopted as a real-time reservoir operations model for normal and/or emergency operations.

With regard to the simulation results, it was seen that there were differences in water yield and hydropower generation depending on the type of reservoir release policy adopted as well as the reservoir sedimentation or deposition that is inevitable in San Roque Reservoir. The conservative or anticipatory release policy resulted in more spills compared to an aggressive release rule. However, the conservative

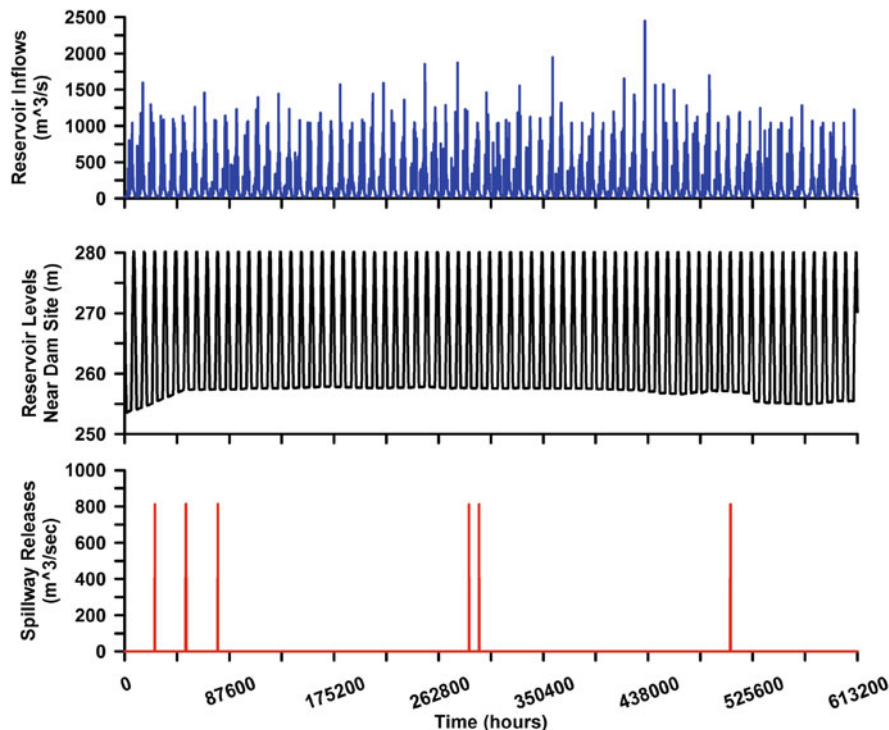


**Fig. 6.15** Time series plots of reservoir inflows, levels, and spills for Case 2

release rule resulted in higher hydropower generation in the long term since it could sustain power releases and maintain higher reservoir levels all months of the year by hedging into the future (i.e., the latter months of the year) so there was enough water in storage to make releases when inflows were waning after the wet months of the year. On the impact of high sediment deposition on reservoir operations as illustrated by Case 3 in particular, it is noted that the reservoir levels near the dam as well as the power releases were significantly lower because of lesser storage capacity, lower water levels, and consequently smaller hydropower operating heads. Considering all the three simulation cases however, it can be concluded that the effect of sediment accumulation in the San Roque Reservoir over the next 70 years has relatively no drastic, negative impact on the reservoir operations including its hydropower generating capacity according to the sediment inflow scenarios used in this study.

Finally, this 2-d reservoir and river hydraulic model together with the watershed model can be used to conduct further simulation studies for purposes of improving and optimizing the reservoir operations of San Roque. The reservoir operations studies may be useful to maximize reservoir yields for water supply purposes or hydropower generation or effective emergency reservoir operation for flood control purposes.

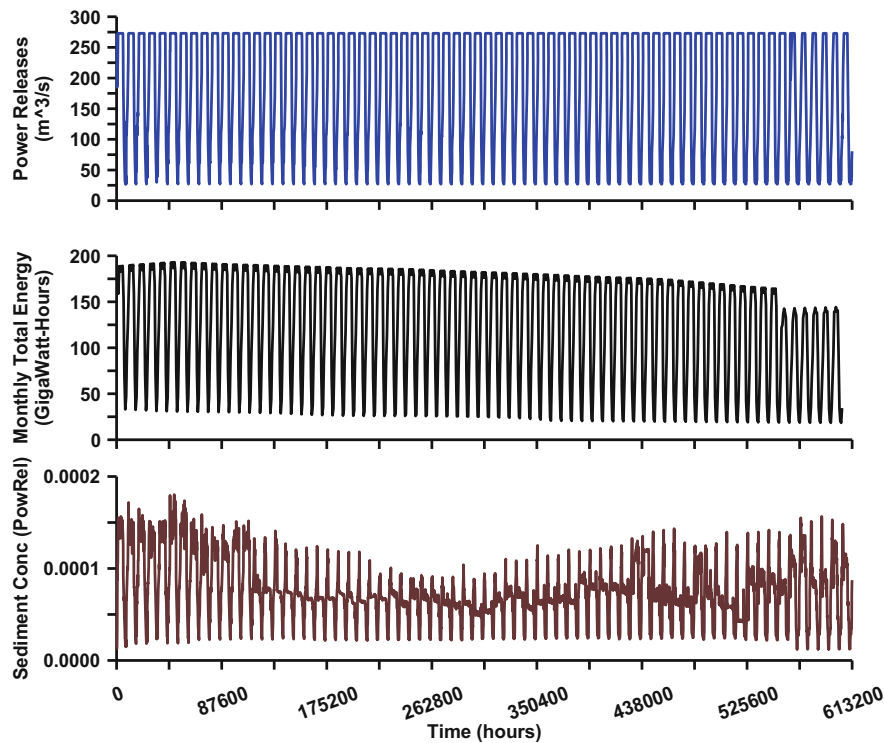


**Fig. 6.16** Time series plots of reservoir releases, energy generation, and power release sediment load for Case 1

### 6.3 Pulangi Reservoir Sediment Flushing Studies with Two-Dimensional Hydraulic Model

The Pulangi Reservoir is located in Maramag, Bukidnon, as shown in Fig. 6.18 from a collage of 1:50,000 scale NAMRIA maps covering the entire Pulangi River Basin system which has a drainage area of  $3114.6 \text{ km}^2$ . The reservoir has experienced accelerated sedimentation; thus it is in danger of filling up with sediments unless drastic engineering intervention measures are employed. In particular, the original storage capacity of Pulangi reservoir in 1985 of about 67 MCM has been reduced to 47 MCM due to sediment accumulation (year 2002 estimates of CMA 2002). This translates to a reduction in reservoir capacity by as much as 30%.

In 2004–2005, a sediment study was conducted by Tabios (2005) for the National Power Corporation (NAPOCOR) to investigate the feasibility of various engineering measures and reservoir operations to control sedimentation in Pulangi Reservoir. That study involved estimation of reservoir inflows and sediment into Pulangi reservoir as input to a two-dimensional reservoir, hydraulic flow-sediment model, and simulation studies to investigate and assess the effectiveness and impacts of the

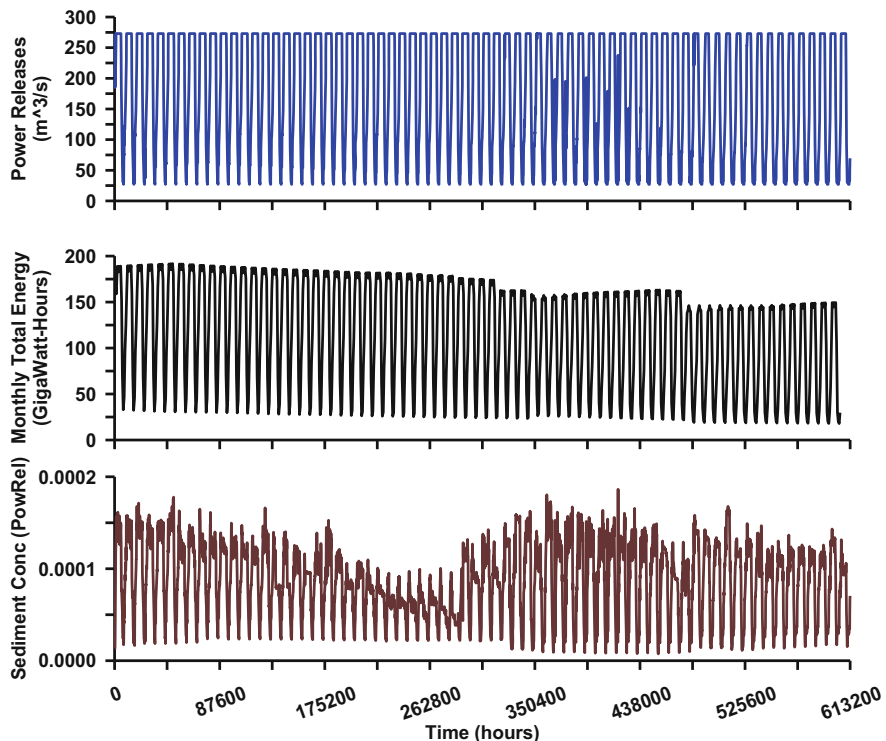


**Fig. 6.17** Time series plots of reservoir releases, energy generation and power release sediment load for Case 3

alternative engineering measures and reservoir operation strategies to control sedimentation. The major conclusion in this 2004–2005 study is that reservoir sediment flushing operation is the most economical, long-term sediment control strategy. However, initially and perhaps occasionally in the future, dredging operations are needed. Other conclusions include the following: periodic sediment flushing removes at the least the incoming annual sediment inflow of 1.4 MCM, thus extending the viable operating life of the reservoir, improves the quality of water, and prevents sediment-laden flow to go through turbines since they are flushed out at the main dam, and an additional 46.5 GWH per annum during summer is realized due to turbine water quality.

In 2008, the Pulangi Reservoir dredging project was implemented based on recommendations from Tabios (2005) by dredging as much as 400,000 cubic meters of deposited sediments in the vicinity of the damsite, designed especially to clean the area around the sediment flushing sluiceway. The specific dredging scheme is to create a fan-shaped area starting from sluiceway that widens while sloping upstream into a fan. This resulted in a huge amount of savings for NAPOCOR, who initially

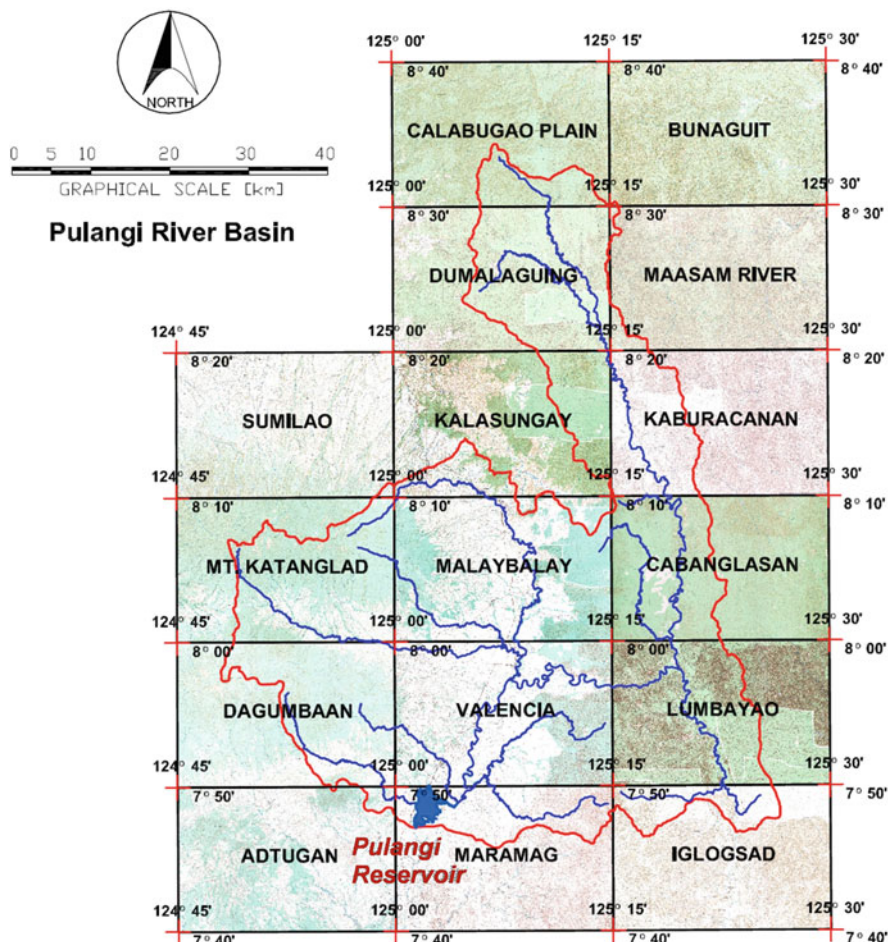


**Fig. 6.18** Pulangi River Basin and location of Pulangi Reservoir in Maramag, Bukidnon, at the southern part in the map created from a collage of 16, 1:50,000 scale NAMRIA maps

set aside 2 billion pesos for dredging based on the evaluation of a private contractor but ended up spending only 212 million pesos (2008 prices).

A highlight of the dredging project was that the area around the sluiceway was cleaned and, in fact, the sluiceway was successfully tested for sediment flushing operations for about 20 h in September 2007 which removed an estimated  $9000\text{ m}^3$  of sediments. In the study of Tabios (2005), it was computed, for instance, that about  $36,000\text{ m}^3$  could be removed over 48 h of continuous flow flushing operations. If one extrapolates the actual sediments removed in 48 h instead of only 20 h, perhaps, the sediments removed could be as high as  $25,000\text{ m}^3$  or even more since retrogressive erosion becomes faster once sediment remobilization has occurred. In any case, this

actual sediment flushing operation is a very good indication that sediment flushing operations indeed work and should be done regularly to prevent significant accumulation or redeposition of sediments in the vicinity of the sluiceway.

In 2010, another study was commissioned by NAPOCOR conducted by Tabios (2011) to revisit the Pulangi Reservoir with the main objective to develop reservoir sediment flushing operation rules (as part of dam operations). The approach was to conduct simulation studies using the two-dimensional (2-d) reservoir flow-sediment model to assess the effectiveness and impacts of the various reservoir sediment flushing operation rules and strategies (schedules and schemes) depending on hydrologic and hydraulic conditions as well as reservoir conditions recognizing the trade-off of long-term sediment management objectives (to prolong the life of the reservoir) and short-term hydropower operation objectives. The reader may refer to Tabios (2011) for details of the study presented below. The papers of Tabios and Mondoñedo (2005) and Tabios (2013) also described the works on Pulangi Reservoir flushing studies in 2005 and 2011, respectively.

### ***6.3.1 Reservoir Sedimentation and Sediment Flushing Operations***

It may be worthwhile to provide a discussion at this point on reservoir sedimentation and sediment flushing operations. The inflowing sediment could settle longitudinally along the reservoir as flow velocity and transport capacity diminish, and a deltaic or wedge-shaped deposit could be formed. Regarding the geometric shape of reservoir, the shape and size of delta along the thalweg depend on the amount of incoming sediment-water discharge and the operation of reservoir.

In most of the storage reservoirs operating with relatively high-water level for long duration, the deltaic deposit could be formed and is typically divided into four parts: the topset, foreset, tail reach, and front reach as shown in Fig. 6.19. In general, the topset bed containing coarser materials has a milder slope than that of the original riverbed. Finer sediments such as wash loads predominate downstream of topset deposits. For the gorge-shaped reservoir with comparatively small storage or in the case of operating drawdown flushing regularly, sediment-laden flows could arrive at front reach quickly and result in a wedge-shaped deposit. With wedge-shaped deposit, a flushing cone could be formed in the vicinity of the sluice gate.

Prolonging the life of this reservoir would require proper sediment management and control. The control of reservoir sedimentation may be accomplished by: (1) controlling the sediment yield from watersheds into reservoirs by erosion control and sediment traps; (2) mechanical removal of sediment by dredging; and (3) reservoir operations by letting high sediment-laden inflows pass through the reservoir (desilting sluiceway) with minimized deposition or flushing out previously deposited sediments (Fan 1985; Fan and Morris 1992; Morris and Fan 2009). In reservoir

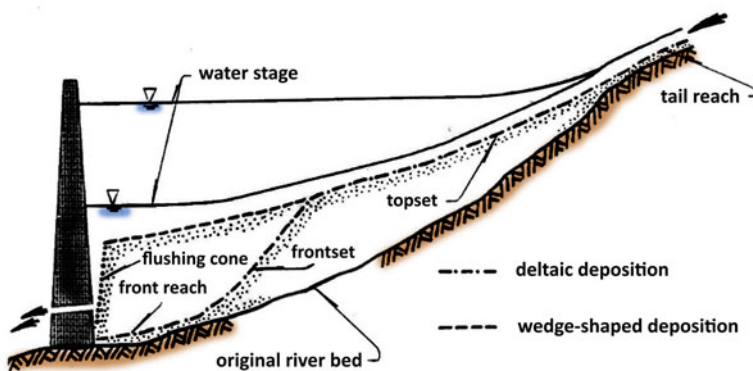


**Fig. 6.19** Schematic sketch of depositional patterns in the longitudinal direction. (From Fan and Morris 1992)

sediment flushing studies in particular, two types of flushing operations are employed, local flushing and drawdown flushing which are described below.

**Local Flushing** For a reservoir with wedge-shaped sediment deposit, a cone-shaped scour hole could be formed as a flushing cone through flushing operation at relatively high reservoir water level. This occurs at the vicinity of the outlet/intake works without lowering the water stage. Compared with the erosion scale of drawdown flushing, the flushing cone is of small-scale erosion. It is crucially important for the protection of hydraulic structures and turbines in powerhouse because of the abrasion. For practical design purposes, the formation of the flushing cone formation is to reduce the sediment concentration around the entrance of the intake.

**Drawdown Flushing** When the water surface level of reservoir drops to near or below the apex point of delta, a retrogressive erosion could occur (Chien 1985). Fan and Morris (1992) classified the hydraulic control of sediments into four categories: sediment routing during floods, drawdown flushing, emptying and flushing, and venting density current. The first three methods require substantial or full drawing down of reservoir water level. Thus, these first three methods are called “drawdown flushing” regime similar to open channel flow with minimum backwater effect during flushing. Related to the outlet structure design, the sediment can be flushed in the pressurized (as in submerged pipe flow) or free (free water surface as weir flow) flow condition (Wu 1989). The latter must be operated in the process of emptying the reservoir. In drawdown flushing, retrogressive erosion of delta will result in sluicing sediments effectively. Figures 6.20 and 6.21 illustrate the sketch of drawdown flushing operations for a deltaic and wedge-shaped depositional pattern, respectively.

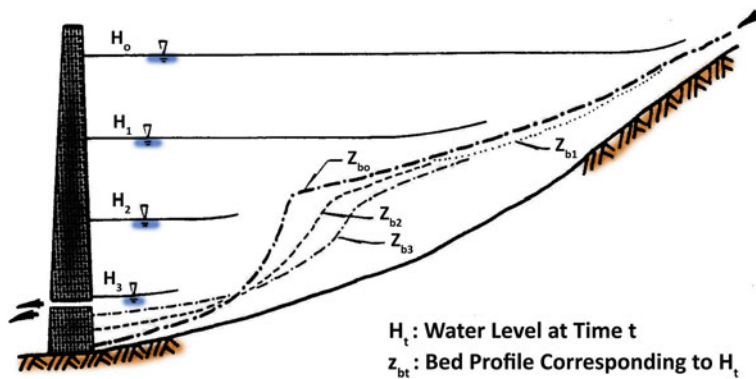


**Fig. 6.20** Schematic diagram of flushing processes with deltaic deposition during drawdown flushing. (From Fan and Morris 1992)

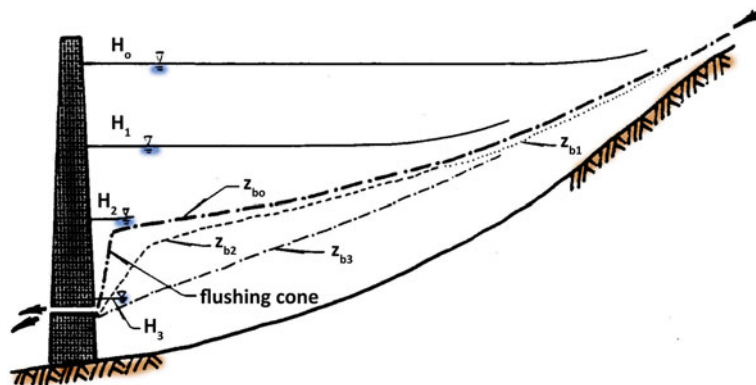


**Fig. 6.21** Schematic diagram of flushing processes with wedge-shaped deposition during drawdown flushing. (From Fan and Morris 1992)

### 6.3.2 Pulangi Reservoir Modeling for Sediment Flushing Operations

The two-dimensional (2-d) reservoir flow-sediment model presented in Sect. 6.2.1 was also utilized in the reservoir sediment flushing study here. To reiterate, this model is based on an earlier work by Zhao et al. (1994) and consequently Tabios (2007), and the governing equations of the 2-d model are (1) mass conservation equation of water-sediment mixture; (2) momentum conservation equations in the  $x$ - and  $y$ -directions; (3) suspended sediment conservation; (4) bed load conservation equation; and (5) sediment-laden flow density equation. As done for San Roque Reservoir operations, this 2-d hydraulic model was enhanced so it could be utilized for reservoir operations to account for hydropower generation, spillway operations, and sediment flushing operations aside from being mainly a flow and sediment transport model.

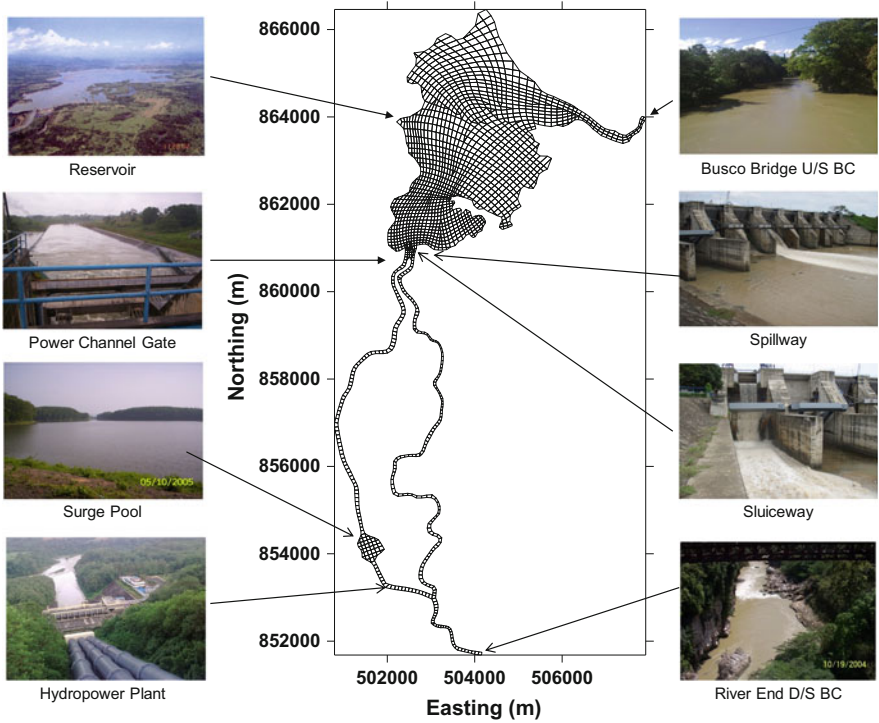


**Fig. 6.22** Pulangi Reservoir 2-d model geometry and associated hydraulic structures and hydro-power components

Shown in Fig. 6.22 is the finite volume grid system of the Pulangi Reservoir and associated hydraulic structures and hydropower components. Shown in particular are the following: (1) main pondage of Pulangi Reservoir bounded upstream by the inflowing river link at Busco Bridge and downstream end of the damssite; (2) power channel, surge pool, and hydropower plant penstock/outlet; and (3) old river system from damssite extending to about 1 km downstream of confluence of hydropower plant tailrace. The 1 km downstream stretch of the river is needed to assess the impact of river sediments flushed downstream. A closer view of the finite volume mesh in the main Pulangi Reservoir is shown in Fig. 6.23.

The major boundary conditions imposed in the 2-d hydraulic model are the following: (1) upstream flow and sediment discharges from the upper Pulangi Reservoir area; (2) the flows and sediment yields around the lower Pulangi Reservoir area; (3) gated spillway at Pulangi Dam; (4) controlled reservoir sluiceway releases for sediment flushing; and (5) intake structure to power channel. Evaporation and bed leakage in the reservoir are assumed small and negligible.

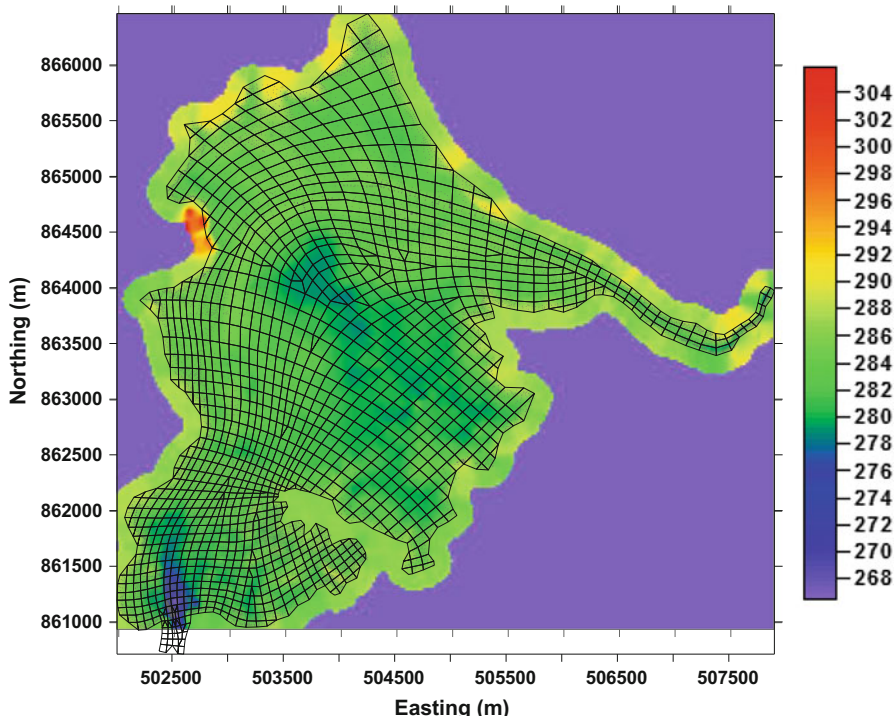


**Fig. 6.23** Pulangi Reservoir finite volume grid system superposed on the bathymetry data provided by NAPOCOR, Pulangi Office, last November 2010

### 6.3.3 Reservoir Inflow and Sediment Discharge Rating Curve

There are available historical daily streamflow data at Busco Bridge (around the mouth of Pulangi HP IV reservoir) from 1956 to 1973 before the reservoir was built in 1985. This streamflow data represent the natural inflows into the reservoir. Historical daily data of reservoir inflows are available from 1995 to 2003 that were back-calculated from the observed reservoir elevations and observed reservoir outflows such as power channel and spillway flows. The above historical daily flow data were utilized as input to the reservoir sediment flushing simulations studies.

For the sediment-discharge rating curve, Duque (2004) as well as Paguntalan (2003) gave estimates of sediment yields from surrounding watersheds in upper Pulangi River as well as Manupali River. These data however are incomplete to allow proper data transposition from these watersheds as sediment inflow to the Pulangi Reservoir system. The alternative is to estimate the reservoir sediment inflows based on bathymetric changes in Pulangi HP IV Reservoir. Between 1985 and 1992, Paguntalan (2003) stated that the reservoir capacity was reduced from 70.371 MCM (at 285 m reservoir elevation) to about 62.74 MCM, thus essentially decreasing the reservoir capacity by 7.63 MCM, over the 7-year period, resulting in

an average annual reservoir inflow of 1.1327 MCM. Another estimate of the sediment inflow into the reservoir was provided by the CMA (2002) showing that reservoir capacity of 70 MCM in 1985 was reduced to 47 MCM in 2002 which corresponds to a sediment inflow of about 1.38 MCM per year. A more recent estimate can be obtained from the bathymetric survey data collected by NAPOCOR last November 2010 resulting in a reservoir capacity of 38.3 MCM at 285 m reservoir elevation from 47 MCM in year 2002 (over an 8-year period), which corresponds to an annual sediment inflow of 1.1 MCM.

### **6.3.4 *Simulation Scenarios and Results of Sediment Flushing Studies***

#### **6.3.4.1 *Sediment Flushing Simulation Scenarios***

Before presenting the simulation scenarios, some considerations are discussed with respect to the historical operations and conditions. Given in Table 6.10 below are the historical conditions based on actual reservoir operations from January 1995 to December 2003. This table shows average reservoir inflows and number of days on monthly basis when the reservoir was spilling. As a fundamental reservoir operation rule, the reservoir flushing operations should be conducted when both the reservoir level and inflows are high. For the Pulangi Reservoir, the spilling elevation is at 285 m (i.e., it is unsafe to let the reservoir level go above this level). In Table 6.10, the average inflows under spilling condition range from 200 to 270 m<sup>3</sup>/s with a minimum of 125 m<sup>3</sup>/s and maximum of 360 m<sup>3</sup>/s. The average number of days per month where spilling occurred is about 8 days for most months except for about 5 days only during the months of November, December, and March. But during wet years (above average flows), the number of spilling days are in the high range of 20–25 days. During the months of April, May, August, September, and October, the spilling conditions are in the high range of 20 days or so and almost 300 m<sup>3</sup>/s of inflows. These particular spilling periods can be taken advantaged of so that instead of spilling, reservoir sediment flushing can be conducted through sluicing the excess flows.

It may be noted that the Pulangi Reservoir is effectively operated between 280 and 285 m elevation due to some operational constraints; thus the operational storage of the reservoir is only about 17.5 MCM. At full hydropower generation of 275 m<sup>3</sup>/s, the effective storage of 17.5 MCM can be drained in approximately 17.7 h since as much as 1.0 MCM (i.e., 275 m<sup>3</sup>/s × 3600 s) can be drawn from the reservoir every hour. In other words, the Pulangi Reservoir is essentially a runoff-the-river hydropower plant.

Based on the above considerations, two (2) simulation scenarios were conducted, (1) for 48-h simulation runs and (2) for 1-year simulation run. The 48-h simulation runs were carried out to investigate the reservoir operations and sediment flushing performance for purposes of calculating the sediment rating curves at the sluiceway

**Table 6.10** Historical average daily inflows and number of day under spilling conditions of Pulangi Reservoir HP IV based on 1995–2003 data

Year		Jan	Feb	Mar	Apr	May	Jun	Jul	Aug	Sep	Oct	Nov	Dec
1995	Inflow	360	0	360	0	0	0	178	230	283	262	263	246
	Days	5	0	3	0	0	0	10	15	20	23	2	12
1996	Inflow	214	208	0	312	200	194	280	250	186	163	260	185
	Days	6	9	0	4	10	14	5	4	4	1	2	1
1997	Inflow	0	301	219	0	0	0	304	0	280	245	293	0
	Days	0	5	6	0	0	0	6	0	4	11	4	0
1998	Inflow	0	0	0	0	0	0	0	0	0	0	0	0
	Days	0	0	0	0	0	0	0	0	0	0	0	0
1999	Inflow	313	264	211	197	135	209	193	196	125	0	184	160
	Days	10	6	3	25	27	8	14	4	15	0	6	10
2000	Inflow	228	228	170	0	0	263	217	186	0	260	253	0
	Days	13	14	18	0	0	13	7	19	0	12	8	0
2001	Inflow	0	280	0	0	219	0	0	204	0	0	0	0
	Days	0	3	0	0	10	0	0	9	0	0	0	0
2002	Inflow	252	225	0	0	0	270	197	221	0	207	0	0
	Days	10	4	0	0	0	12	2	3	0	2	0	0
2003	Inflow	0	278	108	0	0	143	227	184	208	220	188	250
	Days	0	1	1	0	0	8	14	20	16	20	7	10
<b>Min<sup>a</sup></b>	Inflow	214	208	108	197	135	143	178	184	125	163	184	160
	Days	5	1	1	4	10	8	2	3	4	1	2	1
<b>Max<sup>a</sup></b>	Inflow	360	301	360	312	219	270	304	250	283	262	293	250
	Days	13	14	18	25	27	14	14	20	20	23	8	12
<b>Ave<sup>a</sup></b>	Inflow	273	185	148	102	184	187	213	217	119	178	192	118
	Days	9	7	5	6	7	9	8	9	8	8	4	5

<sup>a</sup>Min, max, and ave are minima, maxima, and averages, respectively, on monthly basis

to form part of the sediment flushing operations procedure as well as to investigate the resulting reservoir elevations, hydropower generated, sediment concentrations, and power channel and spillway outflows. The 1-year simulation run was done to investigate details of spatial and temporal variation of the sediment movement (erosion and deposition) in the reservoir and especially to address issues of long-term sediment management especially to determine if further maintenance dredging is needed or not or if dredging is needed at all.

**48-h Simulation Runs** This simulation scenario is for various reservoir inflows sustained for 48 h at 100, 150, 200, 250, and 300 m<sup>3</sup>/s; different sediment sluice gate openings (commencing 24 h after start of simulation) set at 0.2, 0.5, 1.0, 1.5, and 2.0 m; power channel outflows equal to 275 m<sup>3</sup>/s; and the initial storage level is 284.5 m.

**1-Year Simulation Run** In this case, the historical inflow data for year 1965 were used which was a normal year from the Pulangi Reservoir historical data. In this simulation, sediment flushing operation is triggered and continues for 12 h when the reservoir inflow is above 150 m<sup>3</sup>/s and the reservoir water surface elevation is equal to or greater than 284 m. The rationale for this operating policy is that before water spills, it is released through the sluiceway instead of allowing water to spill through the spillway. For year 1965, there were a total of fifty-seven (57) 12-h flushing operations experienced.

**Table 6.11** Estimates (including high and low) of sediments flushed for 12-h flushing operations at various sustained reservoir inflows and sluice gate openings

Reservoir inflows (m <sup>3</sup> /s)	Sluice gate opening (m)	Sluice discharge ((m <sup>3</sup> /s) h)	Estimated sediments flushed (m <sup>3</sup> for 12 h)	Low estimate of sediments flushed (m <sup>3</sup> for 12 h)	High estimate of sediments flushed (m <sup>3</sup> for 12 h)
100	0.2	141	11,469	10,773	12,164
	0.5	273	21,758	20,217	23,299
	1.0	446	30,104	26,496	33,712
	1.5	593	38,392	33,714	43,070
	2.0	723	46,076	40,224	51,927
150	0.2	141	11,513	10,825	12,200
	0.5	273	17,574	15,134	20,014
	1.0	447	28,514	24,792	32,236
	1.5	593	38,661	33,935	43,387
	2.0	724	46,843	41,071	52,614
200	0.2	142	9027	7773	10,282
	0.5	273	21,114	19,641	22,588
	1.0	447	28,625	24,988	32,261
	1.5	595	38,816	34,092	43,541
	2.0	727	46,823	40,836	52,810
250	0.2	142	5970	3708	8231
	0.5	273	21,243	19,792	22,694
	1.0	447	29,600	26,241	32,959
	1.5	594	38,412	33,649	43,176
	2.0	726	47,147	41,286	53,007
300	0.2	142	5802	3829	7776
	0.5	273	20,655	19,109	22,201
	1.0	448	29,899	26,687	33,112
	1.5	597	38,946	34,279	43,613
	2.0	729	47,315	41,180	53,449

### 6.3.4.2 Discussion of Simulation Results

For 48-h simulation runs, Table 6.11 summarizes the results for the various scenarios particularly showing the amount of sediment flushed for the continuous 12-h flushing operations. Upon examination, Table 6.11 shows that generally, as the sluiceway gate opening increases, the amount of sediment flushed increases about the same in magnitude for inflows ranging from 100 to 300 m<sup>3</sup>/s. However, it may be noted that there was a decrease in sediments flushed for increasing inflow at the sluiceway gate opening of 0.2 m. This was due to the storage elevation of the reservoir which was initially at 284.5 m. It was already around spilling conditions so that at the inflow of 200 m<sup>3</sup>/s or higher (compared to at 100 m<sup>3</sup>/s inflow), the spills (through the spillways) increased resulting in decreased sluiceway outflow, thus the decrease in sediments flowing out of the sluiceway. This indicates that the maximum

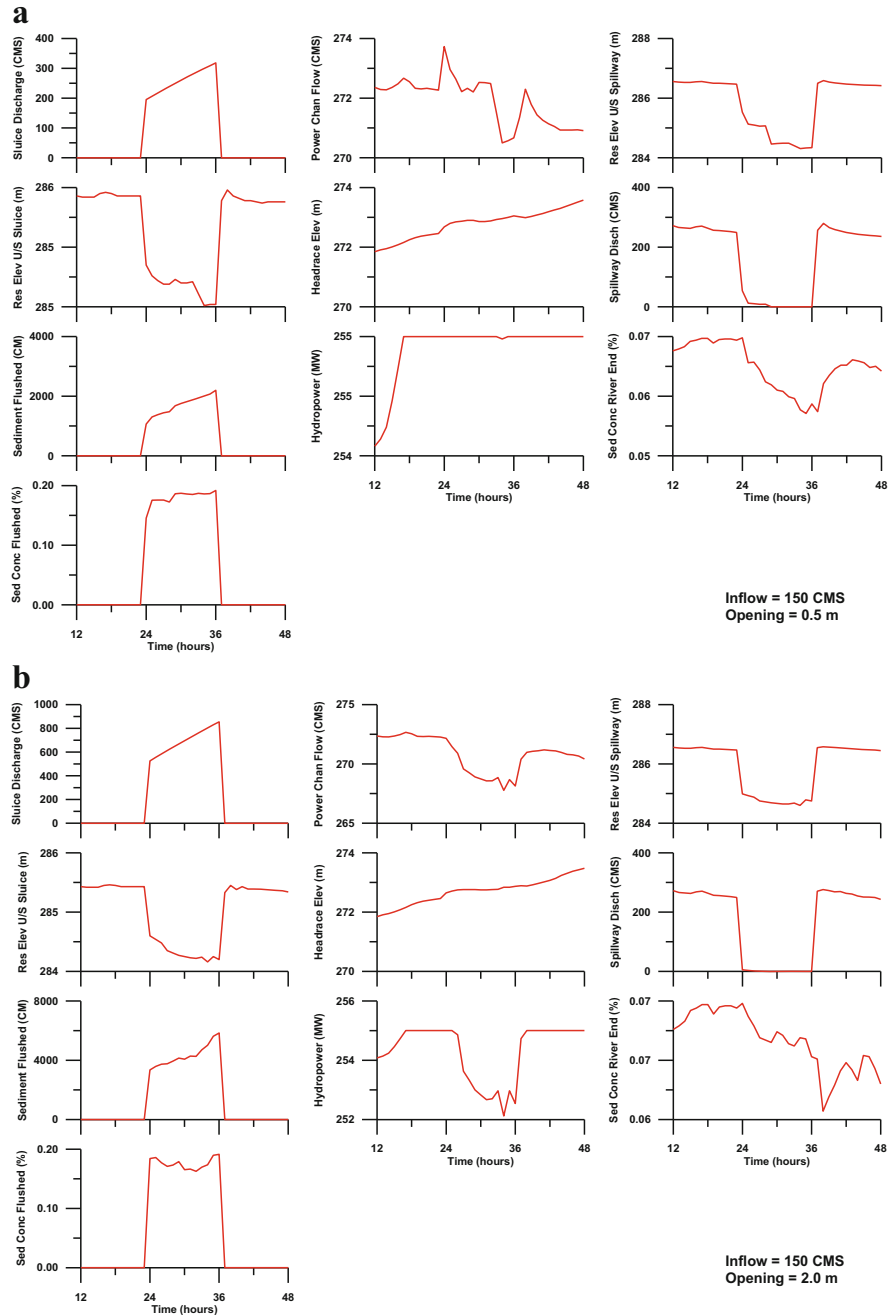
(optimal) amounts of sediments flushed occurred when the reservoir inflows were in the range of 150–200 m<sup>3</sup>/s. Sediment flushing operations can also be done for continuous 24-h flushing operations although the results are no longer shown here. But, basically, the amounts of sediments flushed for 24-h operations are about twice as much compared to those for 12-h flushing operations.

On specific amounts of sediments flushed, the range of sediments flushed were 11,000 to 40,000 m<sup>3</sup> for gate openings from 0.2 to 2.0 m at inflow of 100 m<sup>3</sup>/s over a 12-h period. At inflows greater than 200 m<sup>3</sup>/s, the sediments sluiced were 20,000–45,000 m<sup>3</sup> for gate openings from 0.5 to 2.0 m over the 12-h period. The results here are consistent with the flushing operations conducted at Pulangi Reservoir sometime in September 2009 where over 15-h flushing, as much as 18,000 m<sup>3</sup> of sediments were flushed.

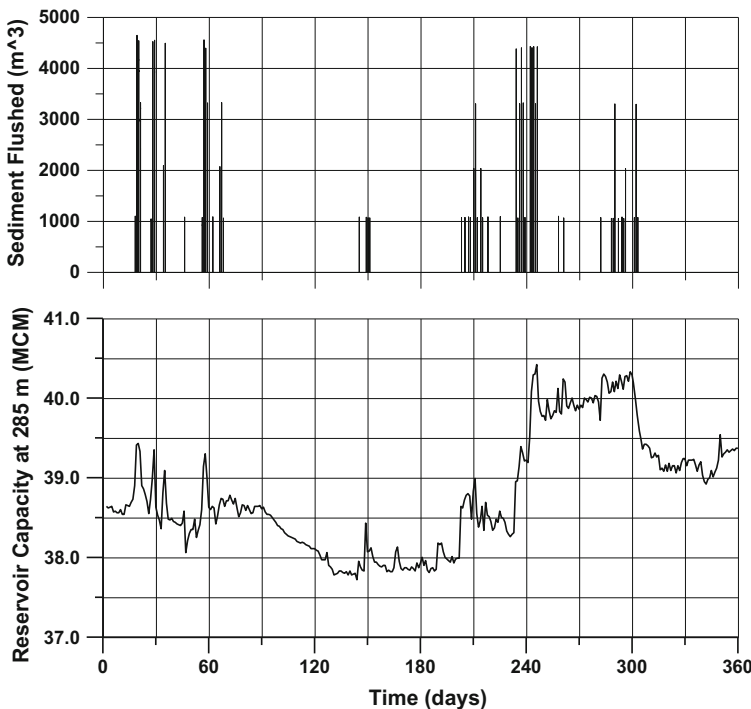
The implications of the above results indicate that at 12-h sediment flushing operations and at gate openings of 1.0–1.5 m, the sediments flushed can reach as much as 20,000 m<sup>3</sup>. Referring to Table 6.10 earlier, that historically except for the months of March, April, November, and December, the average is about 9 days for 8 months a year, number of days when Pulangi Reservoir is under spilling conditions. If a 12-h sediment flushing operation was conducted in a typical hydrological year during the wet months of May through September and December for a total of 60 days (6 months × 10 days), as much as 1.2 million m<sup>3</sup> of sediments could be flushed out a year. To reiterate, this can be conducted when reservoir storage levels are around 284.5 m and that the inflows are 170 m<sup>3</sup>/s and above. However, during wet hydrologic years, several more sediment flushing operational days can be conducted which could be as many as 90 days (6 months × 15 days) for 12-h flushing operations, thus resulting in at least 1.8 million m<sup>3</sup> of sediments flushed out.

Figure 6.24 shows the time series of flows, water elevations, sediment flushed, sediment concentrations, and power generated at pertinent locations in the Pulangi Reservoir system at inflow of 150 m<sup>3</sup>/s and sluiceway gate openings of 0.5 and 2.0 m. It will be too lengthy to show the results at inflows 100, 200, 250, and 300 m<sup>3</sup>/s and for all different sluiceway gate openings, but the results are typical of what are shown in Fig. 6.24. Generally, the plots of reservoir elevations, power channel flow, spillway discharge, and hydropower generation dipped (decreased) during the periods when sediment flushing operations were ongoing. It may be noted that during flushing operations, the hydropower generated dipped by only about 2 MW of the 252–255 MW range of hydropower normal operating power generated, which implies that power generation is not compromised during sediment flushing operations. Also, at reservoir inflows of 250 m<sup>3</sup>/s or more, the hydropower generated was almost 255 MW. Of interest in sediment flushing is the resulting water quality downstream which is quite acceptable considering that the sediment concentrations during flushing operations are only around 0.07% (volume of sediment over volume of water).

*For the 1-year simulation study*, the time series of the sediment flushed and associated reservoir capacity are given in Fig. 6.25. The simulation run started in January 1 of year 1965 of historical data for 360 days. A total of fifty-seven (57) 12-h sediment flushing operations resulted by imposing the operating rule such that when



**Fig. 6.24** Time series of plots of flows ( $\text{m}^3/\text{s}$ ), water elevations (m), sediment flushed ( $\text{m}^3$ ), sediment concentrations (%), and hydropower (MW) generated at pertinent locations in the Pulangi Reservoir system at inflow of  $150 \text{ m}^3/\text{s}$  and gate opening of (a) 0.5 m and (b) 2.0 m



**Fig. 6.25** Time series plots of sediments flushed (in cubic meters) and reservoir capacity (in million cubic meters) for 360-day simulation run with fifty-seven (57) 12-h flushing operations

the reservoir inflow is above  $200 \text{ m}^3/\text{s}$  and the reservoir water surface elevation is equal to or greater than 284.5 m high, the 12-h flushing operations commence. Specifically, the sediment flushing operation protocol is as follows:

- When the inflow is greater than  $200 \text{ m}^3/\text{s}$  but less than  $300 \text{ m}^3/\text{s}$  and the reservoir elevation is above 284.5 m, commence flushing operation after 10 h by initiating the sluice gate opening from 0 to 0.25 m in 30 min, then 0.5 m gate opening for 12 h, and then initiate gate closing from 0.5 to 0 m in 15 min.
- When the inflow is greater than  $300 \text{ m}^3/\text{s}$  but less than  $400 \text{ m}^3/\text{s}$  and the reservoir elevation is above 284.5 m, do as above, but the sequence of gate opening is 0 to 0.5 m in 30 min, then 1.0 m for 12 h, and gate closing from 1.0 to 0 m in 15 min.
- When the inflow is greater than  $400 \text{ m}^3/\text{s}$  and the reservoir elevation is above 284.5 m, do as above, but the sequence of gate opening is 0–0.75 m in 30 min, then 1.5 m for 12 h, and gate closing from 1.5 to 0 m in 15 min.

As shown in Fig. 6.25, the reservoir capacity started at around 38.5 MCM and approached around 37.7 MCM during the March–April dry months of the year and started increasing reaching about 40 MCM during the wet months of July through October but finally settling back to 39.3 MCM at the end of the year. A net sediment

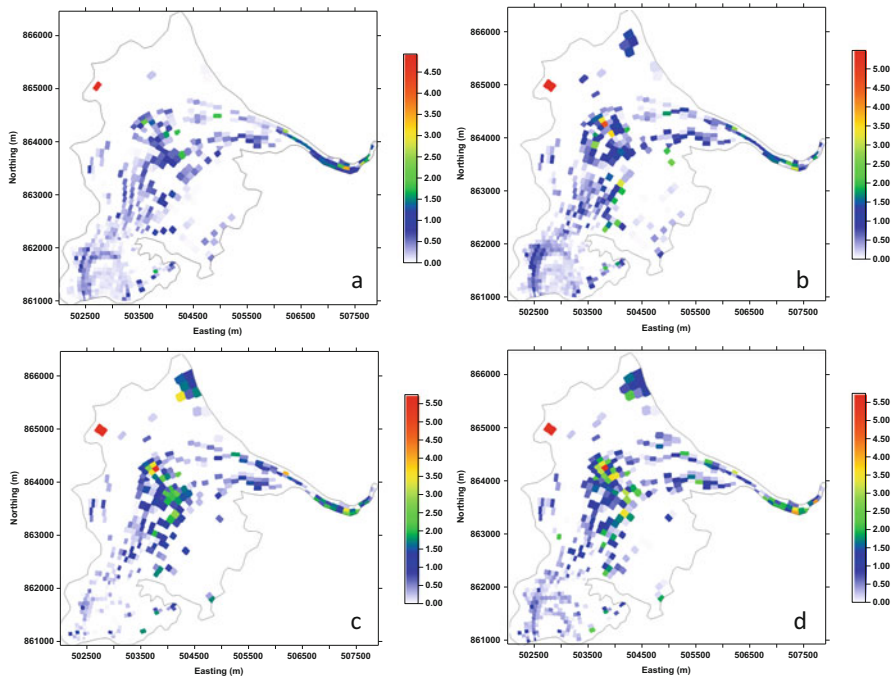


**Fig. 6.26** Areas in the reservoir with net bed deposition (in m) from (a) days 30 to 90, (b) days 30 to 180, (c) days 30 to 240, and (d) days 30 to 360

volume of about 0.8 MCM was removed (flushed out) from the reservoir during the 360-day simulation period.

Figure 6.26 shows spatial plots of the areas of net bed deposition from day 30 to 90, day 30 to 180, day 30 to 240, and day 30 to 360. In contrast, Figure 6.27 shows the spatial plots of net bed erosion in the reservoir for the periods day 30 to 90, day 30 to 180, day 30 to 240, and day 30 to 360. One must closely examine these figures to discern areas of deposition and erosion especially during the period around April (day 90) to August (day 210) when there is net bed deposition. After this period, the regime of net bed erosion dominates. The results in Figs. 6.26 and 6.27 reinforced the time history when the first half of the year was characterized by net deposition upon comparing the net bed deposition and net bed erosion for the periods 30–90 and 30–180 days in contrast to the dominant net bed erosion in the second half of the year.

From the above results, a significant portion of the reservoir area underwent cycles of sediment deposition and erosion. However, in the area in the upper left-hand quadrant of the reservoir (see Figs. 6.26 and 6.27) above 864500 Northing and between 503000 and 504500 Easting, a large sandbar is located, and there was practically no sediment movement. Flow velocities slow down when approaching

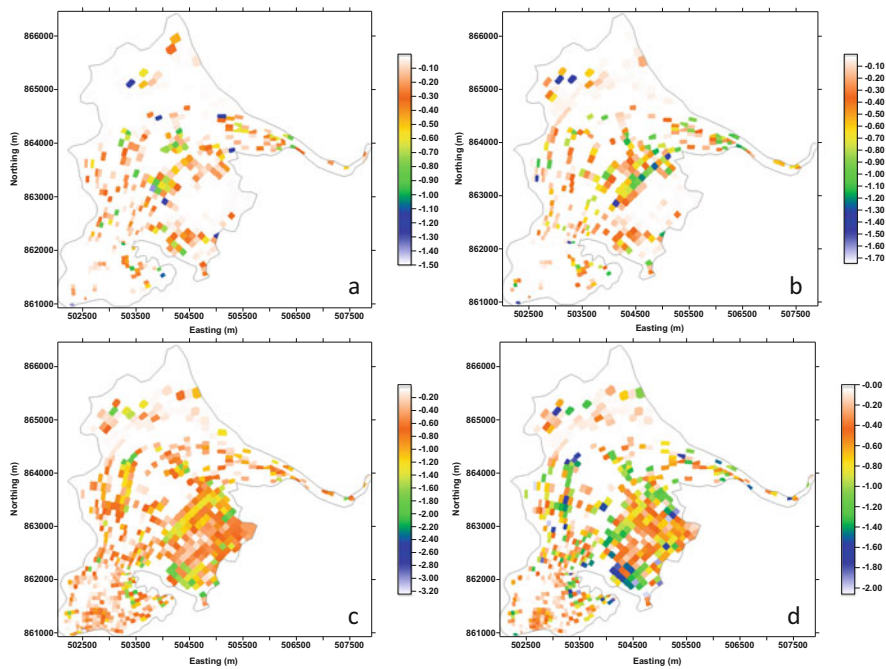


**Fig. 6.27** Areas in the reservoir with net bed erosion (in m) from **(a)** days 30 to 90, **(b)** days 30 to 180, **(c)** days 30 to 240, and **(d)** days 30 to 360

this sandbar, and this flow deceleration caused flowing sediments to collect around the sandbar, consequently further expanding or enlarging it.

There were areas in the reservoir where sediments could not be removed by sediment flushing operations. This condition impedes or causes certain reservoir and hydropower operational problems. When this happens, surgical or selective maintenance dredging may be applied in this particular area. The strategy in selective maintenance dredging is to remove the sediments by mechanical means (preferably by suction). The extracted deposit is discarded in areas in the reservoir where there is a fairly active sediment transport or movement, thus ensuring that it will be flushed out eventually. This practice prevents dumping of removed sediments elsewhere outside the reservoir.

## References

- Box MJ (1965) A new method of constrained optimization and a comparison with other methods. *Comput J* 8(1):42–52  
 Chien N (1985) Lecture notes of the training course on reservoir sedimentation. Series of Pub. IRTCES, Beijing, China

- CMA (CMA Geoservices & Construction Corporation) (2002) Final report on the engineering preparatory works for the dredging/desilting of Pulangi IV HE plant complex, Maramag, Bukidnon, Philippines, vol 1: main report, August
- Duque C (2004) A Catchment approach of monitoring soil erosion: on-site and off-site impacts, Professorial Chair Lecture in soil fertility and soil conservation, Central Mindanao University, Musuan, Bukidnon, September 22
- Fan J (1985) Methods of preserving reservoir capacity. In: Bruk S (ed) *Methods of computing sedimentation in lakes and reservoirs*. UNESCO, Paris, pp 65–164
- Fan J, Morris GL (1992) Reservoir sedimentation II: reservoir desiltation and long-term storage capacity. *J Hydraul Eng ASCE* 118(3):370–384
- Garde RJ, Raju KGR (1985) Mechanics of sediment transportation and alluvial stream problems, 2nd edn. Halsted Press Book/Wiley, New York
- Morris GL, Fan J (2009) Reservoir sedimentation handbook. McGraw Hill, New York, p 784
- NHC (Northwest Hydraulic Consultants) (2008, April) Reservoir sedimentation/backwater effect study and sediment management plan. Final Report to San Roque Power Corp and National Power Corp, North Vancouver, BC, 111 p
- NHRC (National Hydraulic Research Center) (2007) Reservoir sedimentation study and management plan of San Roque Multi-purpose Reservoir (LSRQFS-0405), Final Report to National Power Corporation (NAPOCOR), September
- NHRC (National Hydraulic Research Center) (2015) Reliability and project cost analyses of NIA's proposed Balog-Balog Multipurpose Dam Project and TWEDCO's proposed Balog-Balog Multiple Dam Project, Final report to National Irrigation Administration (NIA), May
- NIA Consult, Inc. (2010) Updating of the feasibility study for the Balog-Balog Multipurpose Project, Phase II (BBMP-II). Report to National Irrigation Administration, Quezon City, May
- NIA Consult, Inc. (2011) Updated proposal for the Balog-Balog Multipurpose Project. Report to National Irrigation Administration, Quezon City, August
- NIA Consult, Inc. (2012) Final report for Balog-Balog Multipurpose Project Phase II, Technical assistance for the detailed engineering design. Report to National Irrigation Administration, Quezon City, June
- Obeysekera JTB, Tabios GQ III, Salas JD (1987) On parameter estimation of temporal rainfall models. *Water Resour Res* 23:1837–1850
- Paguntalan RB (2003) Water resources utilization in the Upper Pulangi River Basin, Bukidnon, Philippines. Ph. dissertation, Institute of Graduate Studies, Central Luzon State University, Science City of Munoz, Nueva Ecija, Philippines
- Shen HW, Tabios GQ III (1992) Risk assessment of reservoir sedimentation accumulation. In: Kou JT, Lin GF (eds) *Proceedings of the sixth IAHR international symposium on stochastic hydraulics*, Taipei, May 18–20, pp 139–146
- Tabios GQ III (2005) Sedimentation and control study of Pulangi Hydropower Plant IV, Report submitted to National Power Corporation, Quezon City, Philippines, June
- Tabios GQ III (2007) Reservoir sedimentation and operations study using a two-dimensional hydraulic model. *J Hydrol Environ IHES* 3(1):41–50
- Tabios GQ III (2011) Formulation of sediment control and reservoir management plan for Pulangi IV hydroelectric plant (MinP10Z235Sh), Report submitted to National Power Corporation (NAPOCOR), March
- Tabios GQ III (2013) Sediment flushing operations of Pulangi Hydropower Plant IV Reservoir, Philippines. In: Fukuoka S, Nakagawa H, Sumi T, Zhang H (eds) *Advances in river sediment research*. ISBN:9781138000629. CRC Press/Taylor & Francis Group
- Tabios GQ III (2018) Reliability and cost-benefit analysis of Balog-Balog multipurpose Dam and Balog-Balog multiple Dam Project. *DLSU Bus Econ Rev* 26(1):39–50
- Tabios GQ III, Mondoñedo CJ (2005) Two-dimensional hydraulic model for reservoir sediment flushing studies. In: *Proceedings of XXXI International Association of Hydraulic Engineering and Research (IAHR) Congress*, COEX, Seoul, Korea, September 11–16, Paper C09-7

- Tabios GQ III, Valdes TT, Delgado VM Jr (2007a) Watershed sediment yield study of Lower Agno River Basin in Benguet-Pangasinan, Philippines. In: Proceedings of the international conference on Hydrology and Water Resources Management for Hazard Reduction and Sustainable Development (HRSD 2007), UNESCO-International Hydrology Program, Manila, Philippines, November 19–23
- Tabios GQ III, Delgado VM Jr, Valdes TT (2007b) Impact of reservoir sedimentation on water yield and hydropower generation in San Roque Reservoir, Pangasinan, Philippines. In Proceedings of international conference on Hydrology and Water Resources Management for Hazard Reduction and Sustainable Development (HRSD 2007), UNESCO-International Hydrology Program, Makati City, Philippines, November 19–23
- TWEDCO (Tarlac Water and Electric Development Company) (2012) Tarlac Mini Dams Project: A proposal based on JVG IRR for a multiple run mini dams irrigation and run of the river power system along Bulsa River, TWEDCO, Manila
- Waymire E, Gupta VK, Rodriguez-Iturbe I (1984) A spectral theory of rainfall intensity at the meso- $\beta$  scale. *Water Resour Res* 20:1453–1465
- Woolhiser DA, Smith RE, Goodrich DC (1990) KINEROS, A kinematic runoff and erosion model: documentation and user manual. U.S. Department of Agriculture, Agricultural Research Service, ARS-77, 130 p
- Wu CM (1989) Hydraulic properties of reservoir distilling. In: Proceedings of the XXIII Congress of the IAHR, Ottawa, Canada, pp B587–B593
- Wu W (2004) Depth-averaged two-dimensional numerical modelling of unsteady flow and nonuniform sediment transport in open channels. *J Hydraul Eng ASCE* 130(10):1013–1024
- Zhao DH, Shen HW, Tabios III GQ, Lai JS, Tan WY (1994) Finite volume two-dimensional unsteady-flow model for river basins. *J Hydraul Eng ASCE*, July, pp 863–883
- Zhao DH, Shen HW, Lai JS, Tabios III GQ (1996) Approximate Riemann solvers in FVM for 2D hydraulic shock wave modeling. *J Hydraul Eng ASCE*, pp 692–702

# Chapter 7

## Hydrodynamic and Water Quality Modeling for Bays and Lakes



**Abstract** This chapter presents the hydrodynamic and water quality modeling of the Manila Bay-Laguna Lake system. Laguna Lake is a freshwater, inland, and multipurpose lake for fisheries, domestic water supply, flood control (as temporary flood storage of Metro Manila), and hydropower generation. Manila Bay is a major water body surrounding major cities of Metro Manila and the neighboring provinces of Pampanga, Bulacan, Bataan, and Cavite. It is connected to Laguna Lake through Pasig River. The specific modeling study presented is dissolved oxygen in Manila Bay as an index of the health of the bay and salinity intrusion into Laguna Lake which is beneficial to fish farming but undesirable to domestic water supply use.

### 7.1 Introduction

Manila Bay by itself is a major habitat for diverse aquatic life, where significant amount of marine fish is sourced. Its physical structure allows easy ingress and egress to and from Metro Manila through its channel and for ports and coastal aquaculture to be built along the shorelines. Laguna Lake, on the other hand, is an inland lake; it is a multipurpose water resources system suitable for the fishing industry, water source for domestic water supply and irrigation, hydropower generation with the Caliraya pumped-storage system, as well as for navigation and transport.

In the past decade or so, there has been a growing concern on degradation of the environmental quality of the Manila Bay-Laguna Lake system due to rapid expansion of economic activities and population growth in Metro Manila area and its neighboring cities and provinces. For these reasons, the Bay-Lake system has virtually become a sink to urban waste and pollution, and any further environmental degradation would be detrimental to natural aquatic resources and would certainly jeopardize the fishing industry.

The first study presented below is the hydrodynamic and water quality modeling of Manila Bay which focuses on dissolved oxygen as an index of the health of the bay. This study was conducted by NHRC (2015) which was headed by the author for the Manila Bay Coordinating Office (MBCO) of the Department of Environment

and Natural Resources (DENR). The second study is modeling of salinity intrusion into Laguna Lake being connected to Manila Bay coastal waters.

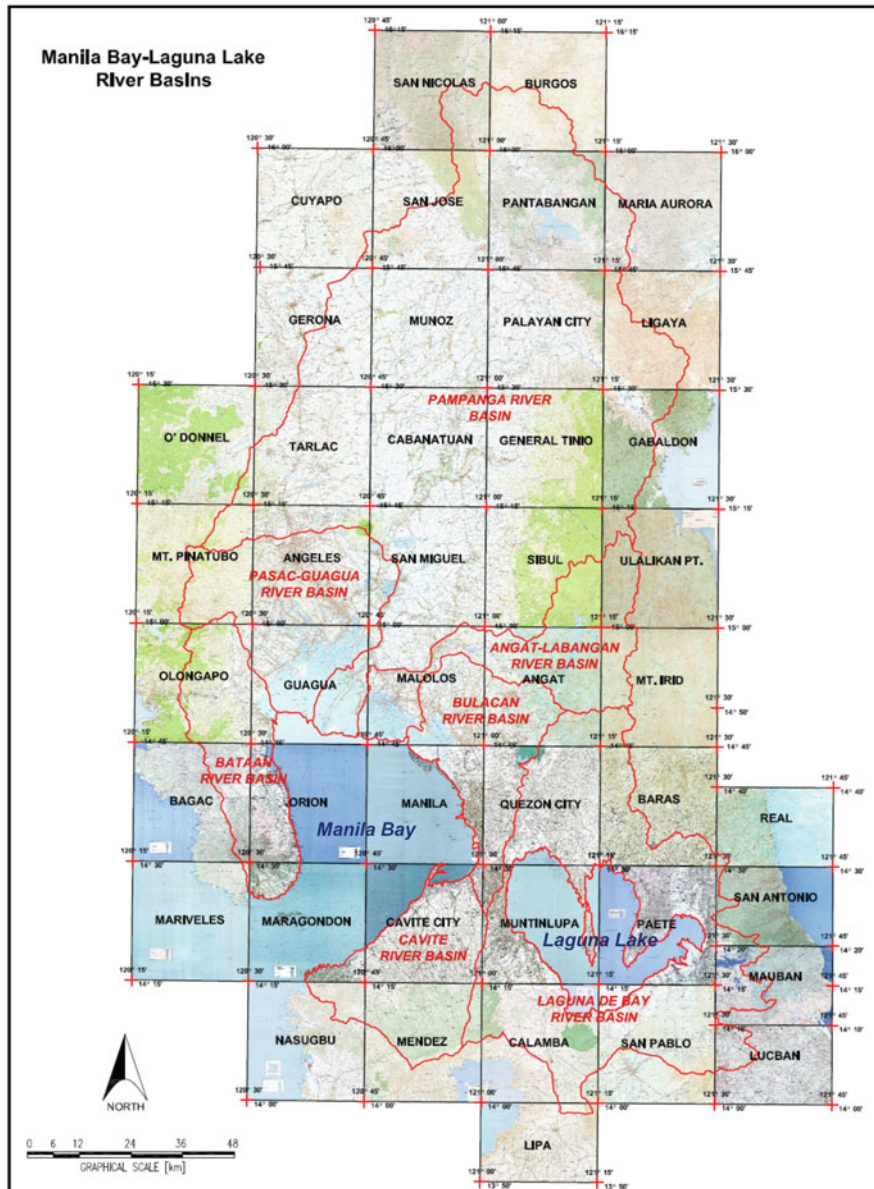
## 7.2 Manila Bay-Laguna Lake and Watershed System

Figure 7.1 shows the location and physical configuration of the Manila Bay-Laguna Lake system and its surrounding watersheds (Bataan, Pasac-Guagua, Pampanga, Angat-Labangan, Bulacan, Laguna de Bay, and Cavite river basins). This figure was assembled from forty four (44) 1:50,000 scale NAMRIA topographic maps.

Manila Bay has an estimated surface area of 1800 km<sup>2</sup> with a coastline of approximately 190 km. It has an average depth of 25 m and is approximately 52 km long, with widths varying from 19 km at its mouth to 56 m inside the bay. The estimated storage capacity of the bay based on the above morphometry is 45 billion cubic meters. The mouth is divided into a South Channel and a North Channel by Corregidor Island and the Caballo Islands, which reduce the net width of the entrance to only about 10 km. Slightly less than 4 km wide, the North Channel (between Bataan and Corregidor Island) has a maximum depth of 71 m, whereas the South Channel, somewhat less than 6 km wide, is no more than 47 m deep.

The southern part of Manila Bay opens to the China Sea, while its northern end is fed by the lahar sediment-laden freshwater discharges from the Pasac Delta and the larger flow discharges from the Pampanga River Basin, which is the largest tributary basin. The eastern part of Manila Bay receives the combined rural and urban river flows from the coastal towns of Bulacan on the north, Bataan on the west, and Cavite on the south as well as urban and polluted runoff from the Metro Manila rivers, including the Pasig River which is the outlet of Laguna Lake (or Laguna de Bay). Manila Bay receives watershed inflows from approximately 17,000 km<sup>2</sup> of drainage area. The two major basins are Pampanga River Basin including the Pasac Delta which has a catchment area of about 10,700 km<sup>2</sup> and Pasig River Basin including Marikina River Basin and Laguna Lake watersheds which have a catchment area of about 3900 km<sup>2</sup>.

Laguna Lake is a large inland body which interacts with Manila Bay through Pasig River and receives significant freshwater inflows of varying water quality from the urban and rural watersheds of the surrounding lakeshore towns. Laguna Lake has an approximate total surface area of 934 km<sup>2</sup> (at 11.5 m lake level). The lake has more or less the shape of a maple leaf with four distinct lobes, referred to as, West Bay, Central Bay, East Bay, and South Bay delineated by a total shoreline length of 285 km. The lake's average depth from mean lake level is 2.5 m with the deepest located in Diablo Pass at 18 m. The estimated storage capacities of the lake are 2.227 billion m<sup>3</sup> and 4.108 billion m<sup>3</sup>, when the lake water levels are at 10.5 m and 12.5 m, respectively. Note that the Department of Public Works and Highways (DPWH) datum which is used in water-related maps around Metro Manila has an assigned value of 10.47 m at mean sea level (MSL) so that when the Laguna Lake level is at 12.5 m, it means that the lake is 2.03 m above MSL.



**Fig. 7.1** Manila Bay-Laguna Lake system and surrounding watersheds

Three major factors affecting the Manila Bay circulation pattern are (Tabios 2003) (1) discharges from surrounding watersheds, (2) tidal forcing from China Sea, and (3) wind stresses. Other factors that affect the bay circulation patterns include dynamic balance of salinity and freshwater which gives rise to varying

density-driven currents, as well as seasonal temperature effects which affect stratification and thus gravitational circulation patterns.

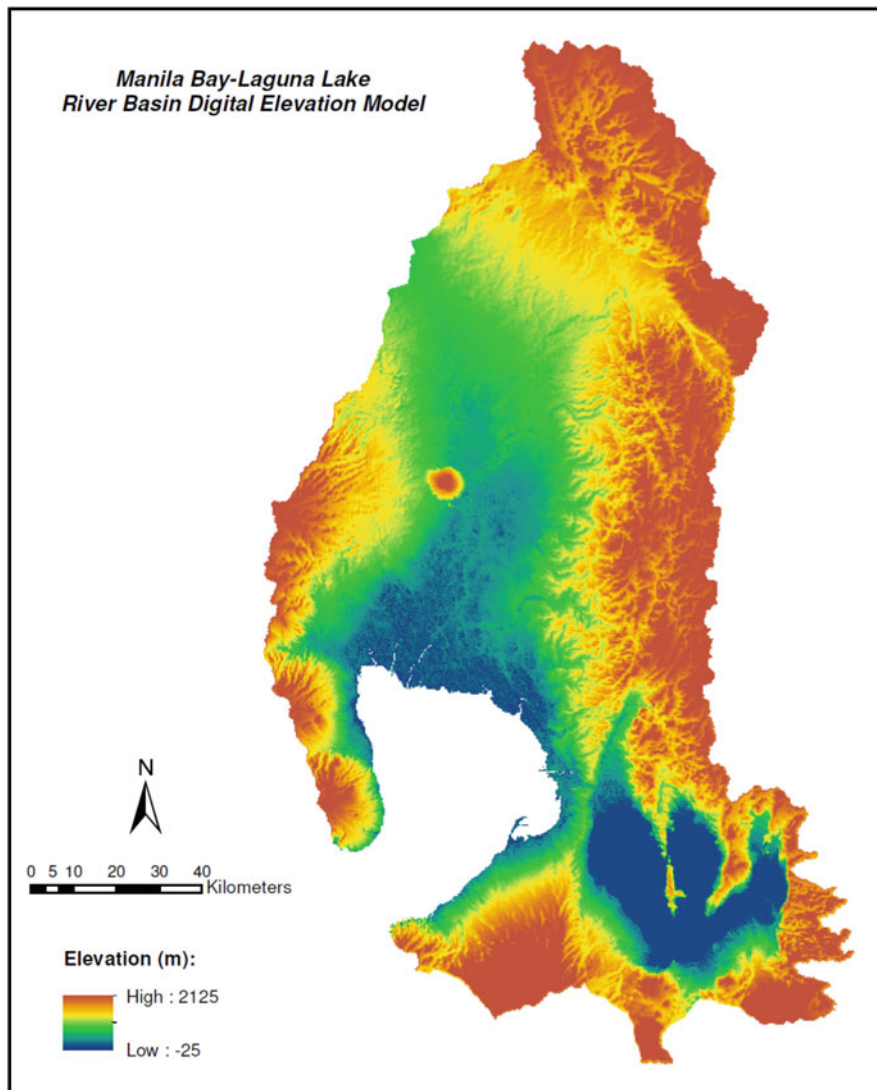
As with Manila Bay, Laguna Lake circulation patterns are affected by three major factors including discharges from watershed inflows, tidal forcing from Manila Bay through Pasig River, and wind forcing. Additionally, the presence of structures for fishing industries called fish pens and fish cages can somehow influence flow patterns especially the fish pens with fences driven all the way down the water. Also, bottom friction (bed shear stress) being a shallow lake (3–6 meters deep), occurrence of high turbidity, and the occasional proliferation of water hyacinths can significantly affect lake circulation.

Figure 7.2 shows the elevation map of Manila Bay-Laguna Lake system generated from NASA-SRTM digital elevation with 90 m x 90 m resolution. The elevation map is used to generate the slope map and to aid in delineating the watershed and sub-basin boundaries which are essential in developing the watershed model data. From these sub-basin delineations, the watershed model parameters such as interception, infiltration, and overland flow parameters can be obtained from soil type and land use maps. Figure 7.3 shows the land use/cover map of covering the Manila Bay-Laguna Lake and surrounding river basins.

### 7.3 Brief Observation on Manila Bay-Laguna Lake Hydrodynamics

It would be worthwhile looking at some field data on the Manila Bay-Laguna Lake system for a broad picture of its hydrodynamic and water quality status. These data were obtained during a 2-day survey on October 12–13, 2001, under the JSPS Core University Research Project entitled Integrated Manila Bay-Laguna Lake and Surrounding Watersheds Environmental Study (IMSWES) in which this author was involved (Tamura et al. 2003). The IMSWES effort was a collaboration between the University of the Philippines and Tokyo Institute of Technology and certain Japanese universities to develop an information base related to the hydrodynamics and transport characteristics of Manila Bay.

In semi-enclosed bays like Manila Bay, the tidal signal offshore dominates the circulation patterns except in shallow areas adjacent to the coasts where wind forcing may be more dominant. The overall tide offshore at the mouth of the bay (around Corregidor Island and Ternate, Cavite) is significantly lower than the observed tide level inside the Bay at Limay, Bataan. Tidal wave crests and troughs seem to increasingly propagate as it moves toward the inner portion of the bay. This phenomenon may have been induced by shoaling effect due to the gentle slope of the inner bay. Lifting due to the large volume of freshwater input is also probable as major sources of watershed discharge are mostly located inside the bay. There is a slight increase in the amplitudes of the tidal components toward the head of the bay and into the shallow area as a result. Nevertheless, given the relatively narrow mouth



**Fig. 7.2** Elevation map of Manila Bay-Laguna Lake Basins generated from NASA-STRM digital elevation data

of Manila Bay, tidal advection is expected to be weak so that water residence time inside is expected to be longer. Efficient flushing of material out of the Bay therefore will be unlikely if the tidal advection scale is less than the distance toward the bay mouth. Long-term monitoring statistics (NAMRIA, Tide and Current Tables) indicate a diurnal and mean tidal range of 0.93 m and 0.44 m, respectively, for Manila Bay.

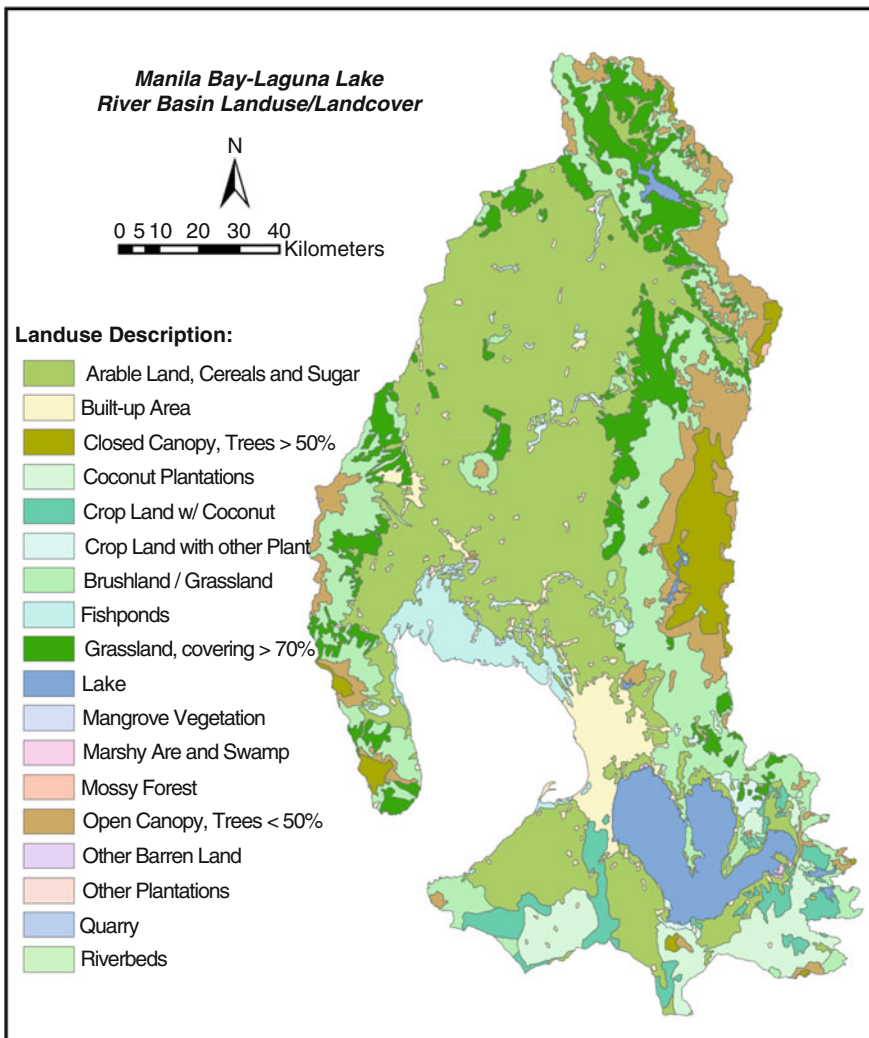


**Fig. 7.3** Land use/cover map of Manila Bay-Laguna Lake watershed system

As shown in Fig. 7.4, the velocity distribution clearly indicates current movement in the east-southeast direction near surface and west-northwest near bottom during ebb tide. Current magnitudes range between 8 and 20 cm/s (in m/s in Fig. 7.4) near surface and between 0 and 12 cm/s near bottom. During flood tide observations on the other hand, velocity profiles depict current movement in the south-southwest direction near surface and east-northeast near bottom. Velocities vary between the same range of values (8–20 cm/s and 0–12 cm/s) near surface and near bottom, respectively. Flow separation is evident in the observed current profiles for both ebb and flood tides. This can be expected in a typical estuarine flow

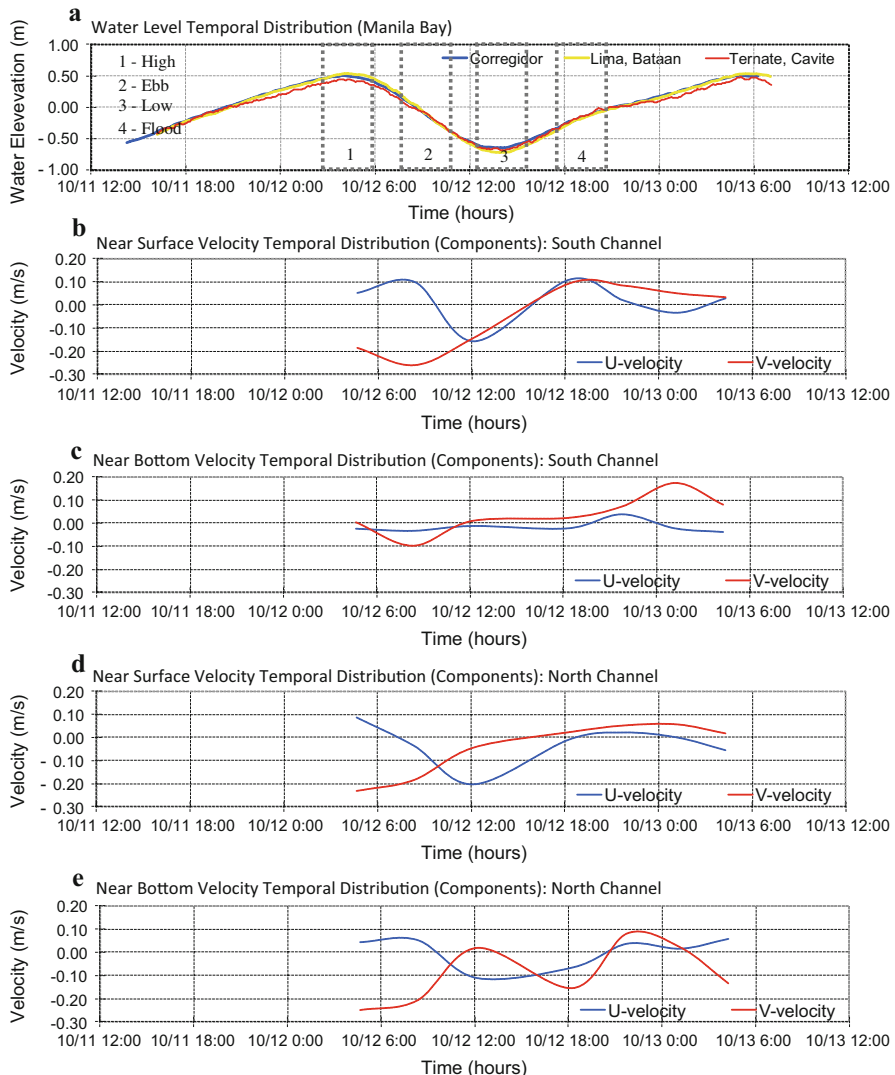


**Fig. 7.4** Temporal distribution of hydrodynamic condition: (a) water elevation; (b) near surface velocity at South Channel (U northing and V easting components); (c) near bottom velocity at South Channel; (d) near surface velocity at North Channel; and (e) near bottom velocity at North Channel. (Data from IMSWES, October 11–12, 2001)

circulation where flows are stratified with a flooding freshwater plume on top of saline bottom water. The freshwater plume is driven to flow out more during the ebb tide. In contrast, the flux changes direction to onshore during flood tide with a relatively weaker magnitude. Nevertheless, the fact remains that there is a clear

delineation in the current vector field observed between near surface and near bottom water mass.

## 7.4 Manila Bay-Laguna Lake Modeling

A short discussion for choosing the models is now in order. Manila Bay is considered a deep water body so that a three-dimensional (3-d) treatment of its hydrodynamics is necessary. The salinity and temperature gradient or stratification inherent in deep waters such as Manila Bay give rise to secondary currents that create vertical motions superposed on horizontal motions driven by tidal forcing from China Sea, lateral inflows from the watersheds, and wind forcing. Although the 3-d model can be computationally time-consuming, it is important to properly capture the bay's hydrodynamics using a 3-d model. With regard to the water quality model, it is decided that the two-dimensional treatment of the water quality process is adequate since only near-shore coastal areas that are relatively shallow water bodies are of primary importance. Water quality movement in shallow waters is normally well-mixed so that two-dimensional, horizontal treatment is adequate.

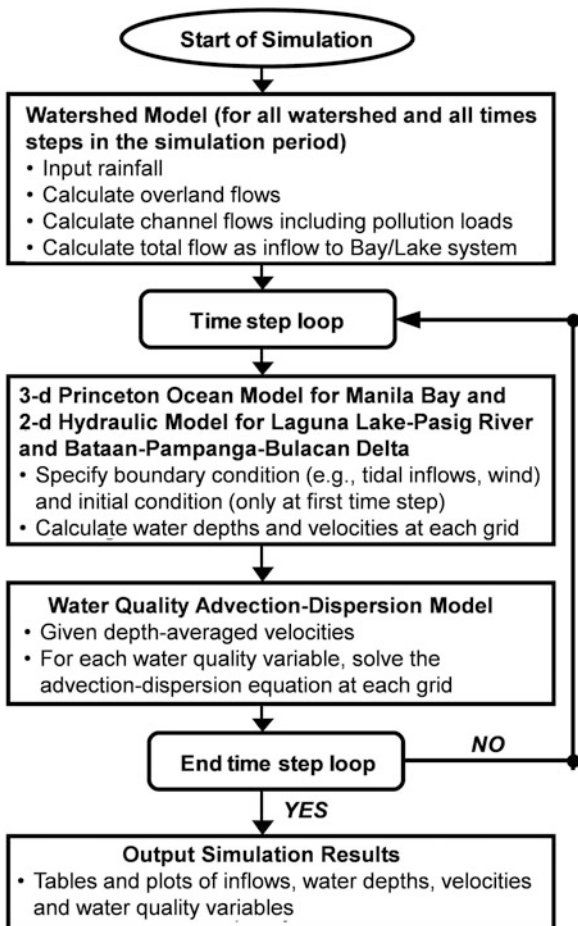
The Manila Bay-Laguna Lake model as shown in the flowchart of Fig. 7.5 has three parts: (1) a watershed model to generate the inflows to the Bay-Lake system; (2) a hydrodynamic/hydraulic model to calculate water depths and velocities; and (3) advection-dispersion model to describe the movement and evolution of water quality constituents (e.g., dissolved oxygen, suspended solids, sediments, and fecal coliform). The computed velocities from the hydrodynamic/hydraulic model are the major driving variables in the advection-dispersion model. In this study, the models used were the 3-d Princeton hydrodynamic ocean model for Manila Bay, 2-d finite volume hydraulic model for Laguna Lake and around the Bataan-Pampanga-Bulacan Delta (ponds/wetlands), and advection-dispersion model for the Bay-Lake system water quality processes. An application of this Manila Bay-Laguna Lake model has been done by NHRC (2015) with the author as principal investigator based on some earlier works on the hydrodynamic and hydraulic modeling of the Manila Bay-Laguna Lake system by Tabios et al. (2000a).

The major factors or variables affecting the hydrodynamics/hydraulics/transport processes in the Bay-Lake system are the following:

- River inflows from surrounding watersheds
- Tidal forcing from China Sea
- Wind forcing
- Rainfall
- Density-driven currents due to salinity-freshwater balance and stratification due to temperature effects
- Nutrient and pollution loading

The modeling tool developed here considers the above factors or variables so that one can either control, manage, or account those factors to properly manage the environmental quality of the Bay/Lake system.

**Fig. 7.5** Program flowchart of Manila Bay-Laguna Lake hydrodynamic and water quality model



#### 7.4.1 Watershed Model of Manila Bay-Laguna Lake System

As mentioned above, the major inputs to the Bay-Lake model are the watershed inflows from surrounding watersheds. These inflows are calculated using a continuous simulation watershed model using the Sacramento soil moisture accounting model with appropriate overland and channel flow routing models. The components of the hydrologic process considered in the model are rainfall, infiltration, excess rainfall, and retention storage, soil moisture storage in the root zone, evapotranspiration, interflow storage, interflow discharge, groundwater recharge flow, stream-aquifer return flow, overland flow, and channel flow. Being a continuous simulation watershed model, the soil moisture accounting scheme essentially tracks the state of moisture of the watershed that generates streamflow (i.e., interflow or/and

groundwater recession flow) during periods of no rainfall. The Sacramento soil moisture accounting model including the flow routing model is described in Appendix A.

### 7.4.2 Hydrodynamic Model of Manila Bay

The Princeton Ocean Model (POM) developed by Blumberg and Mellor (1983, 1987) is adopted here to model the hydrodynamics of Manila Bay. Details of this model may be referred to Blumberg and Mellor (1987) and Mellor (2004). In this model, the three-dimensional (3d) hydrodynamic equation of conservation of mass and momentum are given by:

*Continuity equation:*

$$\frac{\partial \eta}{\partial t} + \frac{\partial D u}{\partial x} + \frac{\partial D v}{\partial y} + \frac{\partial \omega}{\partial \sigma} = 0 \quad (7.1)$$

*Momentum equation in the x-direction:*

$$\begin{aligned} \frac{\partial u D}{\partial t} + \frac{\partial u^2 D}{\partial x} + \frac{\partial u v D}{\partial y} + \frac{\partial u \omega}{\partial \sigma} - \varphi v D + g D \frac{\partial \eta}{\partial x} \\ + \frac{g D^2}{\rho} \int_{\sigma}^0 \left[ \frac{\partial \rho'}{\partial x} - \frac{\sigma'}{D} \frac{\partial D}{\partial x} \frac{\partial \rho'}{\partial \sigma'} \right] d \sigma' \\ = \frac{\partial}{\partial \sigma} \left[ \frac{K_M}{D} \frac{\partial u}{\partial \sigma} \right] + \frac{\partial}{\partial x} (H \tau_{xx}) + \frac{\partial}{\partial y} (H \tau_{xy}) \end{aligned} \quad (7.2)$$

*Momentum equation in the y-direction:*

$$\begin{aligned} \frac{\partial v D}{\partial t} + \frac{\partial v^2 D}{\partial y} + \frac{\partial u v D}{\partial x} + \frac{\partial v \omega}{\partial \sigma} \\ + \varphi u D + g D \frac{\partial \eta}{\partial y} + \frac{g D^2}{\rho} \int_{\sigma}^0 \left[ \frac{\partial \rho'}{\partial y} - \frac{\sigma'}{D} \frac{\partial D}{\partial y} \frac{\partial \rho'}{\partial \sigma'} \right] d \sigma' \\ = \frac{\partial}{\partial \sigma} \left[ \frac{K_M}{D} \frac{\partial v}{\partial \sigma} \right] + \frac{\partial}{\partial y} (H \tau_{yy}) + \frac{\partial}{\partial x} (H \tau_{yx}) \end{aligned} \quad (7.3)$$

where  $D = H + \eta$  = water depth

$H$  = bottom elevation

$\eta$  = water surface elevation

$u$  = velocity component in  $x$ -direction

$v$  = velocity components  $y$ -direction

$g$  = gravitational acceleration

$\varphi$  = Coriolis parameter

$\rho$  = density of water (in particular  $\rho'$  varies with  $\sigma'$ )

$K_M$  = vertical kinematic viscosity

The model used here employs a *dual-sigma* coordinate system where the computation is divided between the upper layer and the lower layer by a horizontal sigma interface. This is especially, computationally advantageous when appreciable density stratification exists in the upper layer since errors could arise in the diffusion and pressure gradient terms when the coordinate transformation must also account for deformation due to abrupt changes in bottom topography. The sigma transformation is employed to achieve more accurate approximation of the surface and especially bottom boundaries (Nadaoka et al. 2000). The sigma coordinate transformation is defined as:

$$\sigma = \frac{z - \eta}{H + \eta} \quad (7.4)$$

Essentially,  $\sigma$  ranges from  $\sigma = 0$  at  $z = \eta$  to  $\sigma = -1$  at  $z = -H$ .

The velocity component  $\omega$  is actually the transformed vertical velocity normal to sigma surfaces. In Cartesian coordinates, the velocity  $w$  in the  $z$ -direction is given by:

$$w = \omega + \sigma \frac{\partial D}{\partial t} + \frac{\partial \eta}{\partial t} + u \left( \sigma \frac{\partial D}{\partial x} + \frac{\partial \eta}{\partial x} \right) + v \left( \sigma \frac{\partial D}{\partial y} + \frac{\partial \eta}{\partial y} \right) \quad (7.5)$$

In the momentum Eqs. (7.2) and (7.3), the last two terms are the horizontal viscosity and diffusion terms. In particular, the turbulent shear stress variables  $\tau_{xx}$ ,  $\tau_{xy}$ ,  $\tau_{yx}$ , and  $\tau_{yy}$  in which  $\tau_{xy}$ , for instance, is the shear stress in the  $x$ -direction on a plane perpendicular to the  $y$ -direction are defined as follows:

$$\tau_{xx} = 2A_M \frac{\partial u}{\partial x}; \quad \tau_{xy} = \tau_{yx} = A_M \left( \frac{\partial u}{\partial y} + \frac{\partial v}{\partial x} \right); \quad \tau_{yy} = 2A_M \frac{\partial v}{\partial y} \quad (7.6)$$

where  $A_M$  is the diffusion coefficient which is defined based on Smagorinsky diffusivity for horizontal diffusion.

The vertical kinematic viscosity  $K_M$  in the momentum equation above and the vertical diffusivity  $K_H$  in the turbulence equations below are important parameters describing the surface and bottom mixing layer in the ocean. These two parameters are defined as a function of the turbulence kinetic energy  $q^2$  and the turbulence

length scale  $\varsigma$  based on the second-order turbulence closure model. The turbulence model in terms of these two quantities are as follows.

(1) Turbulence kinetic energy  $q^2$  is:

$$\begin{aligned} \frac{\partial q^2 D}{\partial t} + \frac{\partial u q^2 D}{\partial x} + \frac{\partial v q^2 D}{\partial y} + \frac{\partial \omega q^2}{\partial \sigma} \\ = \frac{\partial}{\partial \sigma} \left[ \frac{K_q}{D} \frac{\partial q^2}{\partial \sigma} \right] + \frac{2K_M}{D} \left[ \left( \frac{\partial u}{\partial \sigma} \right)^2 + \left( \frac{\partial v}{\partial \sigma} \right)^2 \right] \\ + \frac{2g}{\rho} K_H \frac{\partial \bar{\rho}}{\partial \sigma} - \frac{2D q^3}{B_1 \varsigma} + \frac{\partial}{\partial x} \left( H A_H \frac{\partial q^2}{\partial x} \right) + \frac{\partial}{\partial y} \left( H A_H \frac{\partial q^2}{\partial y} \right) \end{aligned} \quad (7.7)$$

(2) Product  $q^2 \varsigma$  is given by:

$$\begin{aligned} \frac{\partial q^2 \varsigma D}{\partial t} + \frac{\partial u q^2 \varsigma D}{\partial x} + \frac{\partial v q^2 \varsigma D}{\partial y} + \frac{\partial \omega q^2 \varsigma}{\partial \sigma} = \frac{\partial}{\partial \sigma} \left[ \frac{K_q}{D} \frac{\partial q^2 \varsigma}{\partial \sigma} \right] \\ + E_1 \varsigma \left\{ \frac{K_M}{D} \left[ \left( \frac{\partial u}{\partial \sigma} \right)^2 + \left( \frac{\partial v}{\partial \sigma} \right)^2 \right] + E_3 \frac{g}{\rho} K_H \frac{\partial \bar{\rho}}{\partial \sigma} \right\} \\ - \frac{D q^3}{B_1} \left( 1 + E_2 \frac{\varsigma}{kL} \right) + \frac{\partial}{\partial x} \left( H A_H \frac{\partial q^2 \varsigma}{\partial x} \right) + \frac{\partial}{\partial y} \left( H A_H \frac{\partial q^2 \varsigma}{\partial y} \right) \end{aligned} \quad (7.8)$$

where  $L^{-I} = (\eta - z)^{-I} + (H - z)^{-I}$

$$\partial \bar{\rho} / \partial \sigma = \partial \rho / \partial \sigma - c_s^{-2} \partial p / \partial \sigma$$

$k$  = von Karman constant usually taken equal to 0.4

$c_s$  = speed of sound

$p$  = pressure

$A_H$  = horizontal heat diffusivity taken as a product of turbulence Prandtl number and  $A_M$

$A_M$  = horizontal kinematic viscosity

$K_H$  = vertical diffusivity

$K_q$  = mixing coefficient

$E_1, E_2, E_3$ , and  $B_1$  = model parameters.

Note that in the above Eqs. (7.7) and (7.8), the variable  $K_q$  is also defined as a function of  $q^2$  and  $\varsigma$  as with the variables  $K_M$  and  $K_H$ .

Earlier application of the above model to Manila Bay has been made by Tabios et al. (2000a).

### 7.4.3 Hydraulic Model of Laguna Lake and Bataan-Pampanga-Bulacan Coastal Areas

The 2-d flood hydraulic model used in this study is based on the finite volume method (FVM) formulation. The governing equations of the 2-d model include the mass conservation equation of water-sediment mixture and the momentum conservation equations in the  $x$ - and  $y$ -directions.

The mass conservation equation is written as:

$$\frac{\partial(\rho_m h)}{\partial t} + \frac{\partial(\rho_m hu)}{\partial x} + \frac{\partial(\rho_m hv)}{\partial y} = \rho_{xx} q_{xx} \quad (7.9)$$

where  $h(x,y,t)$  is flow depth,  $u(x,y,t)$  is depth-averaged velocity in  $x$ -direction,  $v(x,y,t)$  is depth-averaged velocity in  $y$ -direction,  $\rho_m(x,y,t)$  is the mixture density (in case it's not pure water),  $q_{xx}(x,y,t)$  external inflow or source term, and  $\rho_{xx}(x,y,t)$  is density of external flow.

The momentum equation in the  $x$ -direction is written as:

$$\begin{aligned} \frac{\partial(\rho_m hu)}{\partial t} + \frac{\partial \left( \rho_m hu^2 + \rho_m g \frac{h}{2} \right)}{\partial x} + \frac{\partial(\rho_m huv)}{\partial y} \\ = \rho_m gh (S_{ox} - S_{fx}) + \frac{\partial(h\tau_{xx})}{\partial x} + \frac{\partial(h\tau_{xy})}{\partial y} \end{aligned} \quad (7.10)$$

In the  $y$ -direction:

$$\begin{aligned} \frac{\partial(\rho_m hv)}{\partial t} + \frac{\partial(\rho_m huv)}{\partial x} + \frac{\partial \left( \rho_m hv^2 + \rho_m g \frac{h}{2} \right)}{\partial y} \\ = \rho_m gh (S_{oy} - S_{fy}) + \frac{\partial(h\tau_{yx})}{\partial x} + \frac{\partial(h\tau_{yy})}{\partial y} \end{aligned} \quad (7.11)$$

where  $S_{ox}(x,y,t)$ ,  $S_{oy}(x,y,t)$  are bed slopes in  $x$ - and  $y$ -directions,  $S_{fx}(x,y,t)$  and  $S_{fy}(x,y,t)$  are friction slopes in  $x$ - and  $y$ -directions,  $\tau_{xx}(x,y,t)$  and  $\tau_{yy}(x,y,t)$  normal stresses in  $x$ - and  $y$ -directions,  $\tau_{yx}(x,y,t)$  and  $\tau_{xy}(x,y,t)$  are lateral stresses in  $x$ - and  $y$ -directions, and  $g$  is acceleration due to gravity. Appropriate equations are needed to define the friction slope such as the use of the Manning's equation and likewise for the normal and lateral shear stresses. A more complete formulation of the momentum equations is given in Appendix C that includes Coriolis effect, surface stresses and density driven current.

In the finite volume method (FVM), the mass and momentum equations in Eqs. (7.9), (7.10), and (7.11) are solved simultaneously. The mass and momentum

fluxes are calculated for each side of a finite volume by a Riemann problem solution which involves approximating the fluxes by the characteristic solution of the governing equations (Zhao et al. 1996).

#### **7.4.4 Advection-Dispersion Water Quality Model of Manila Bay and Laguna Lake**

For the water quality model, a two-dimensional formulation is used instead of a three-dimensional formulation. The water quality equations used here were adopted from HEC-RAS model of the US Army Corps of Engineers (USACE 2008) which were written in one-dimensional form but reformulated here in two-dimensional form. The water quality model is solved by finite difference method so that for each finite difference cell, the depth-averaged advection-dispersion equation with reactions and waste load terms for various water quality constituents is given by:

$$\frac{\partial C}{\partial t} = \frac{\partial}{\partial x} \left( D_x \frac{\partial C}{\partial x} - U_x C \right) + \frac{\partial}{\partial y} \left( D_y \frac{\partial C}{\partial y} - U_y C \right) + \text{Source/Sink} \quad (7.12)$$

where  $C$  = concentration of a particular water quality constituent

$D_x, D_y$  = dispersion coefficients in the x- and y-directions

$U_x, U_y$  = depth-averaged velocities

$t$  = time.

The specific water quality constituents included in the model are as follows:

1. Dissolved oxygen (DO).
2. Organic nitrogen (OrgN).
3. Inorganic nitrogen ammonium ( $\text{NH}_4$ ).
4. Inorganic nitrogen nitrite ( $\text{NO}_3$ ).
5. Inorganic nitrogen nitrate ( $\text{NO}_2$ ).
6. Organic phosphorus (OrgP).
7. Inorganic phosphorus orthophosphate ( $\text{PO}_4$ ).
8. Algae (A).
9. Carbonaceous biological oxygen demand (CBOD).

Figure 7.6 which was taken from HEC-RAS User's Manual of USACE (2008) shows the schematic of the water quality model which evolves around the dissolved oxygen process. Basically, water quality variables interact with each other such that at the start, dissolved oxygen (DO) is affected by the amount of organic matter present, photosynthesis which is parameterized by algae, ammonia ( $\text{NH}_3$ ) and nitrate ( $\text{NO}_2$ ) oxidation, benthic animals, and zooplankton, among others. The various variables could be source/sink terms in the model and evolve around the DO process.

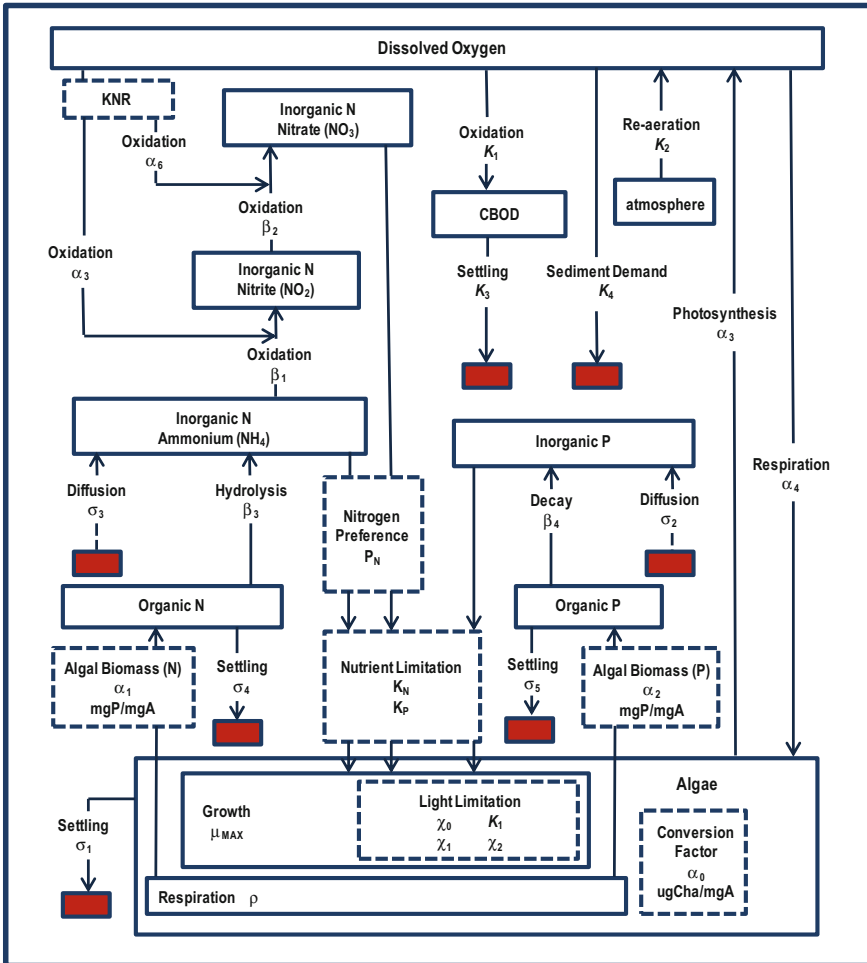


**Fig. 7.6** Schematic of dissolved oxygen model and its interactions with other chemicals and other sink/source terms or processes. (Taken from HEC-RAS User's Manual, USACE 2008)

In any case, for purposes of fisheries, of interest would be the water quality variables DO and chlorides and perhaps the population of benthic animals and zooplankton.

In Eq. (7.12), the *source/sink* term defines the interaction or causal effects among the various water quality constituents. These terms are given below for each of the water quality constituents listed above. In certain cases, the source/sink term may be water quality inflows from surrounding watersheds which could be carrying desirable or undesirable substances that are part of the water quality processes of the bay. These water quality inflows treated as model boundary conditions must be also properly accounted.

### Dissolved Oxygen (DO)

For dissolved oxygen, the source/sink term in Eq. (7.12) is given by:

$$DO_{Source/Sink} = K_1^*(DO_{Sat} - DO) + A(\alpha_3\mu^* - \alpha_4\rho^*) - K_1^*CBOD - K_4^*/d - \alpha_5\beta_1^*NH4 - \alpha_6\beta_2^*NO2 \quad (7.13)$$

where  $DO$  = dissolved oxygen concentration

$DO_{Sat}$  = saturation  $DO$  as a function of water temperature

$A$  = algal biomass concentration

$CBOD$  = carbonaceous biological oxygen demand

$NH4$  = ammonium nitrogen concentration.

$NO2$  = nitrite nitrogen concentration.

$K_1^*$  =  $CBOD$  deoxygenation rate

$K_2^*$  = reaeration transfer rate

$K_4^*$  = sediment oxygen demand rate

$\alpha_3$  = oxygen production per unit algal growth

$\alpha_4$  = oxygen uptake per unit algae respiration

$\alpha_5$  = oxygen uptake per unit  $NH4$  oxidized

$\alpha_6$  = oxygen uptake per unit  $NO2$  oxidized

$\beta_1^*$  = rate of oxidation of ammonium to nitrite

$\beta_2^*$  = rate of oxidation of nitrite to nitrate

$\mu^*$  = local algal growth rate

$\rho^*$  = local algal respiration rate

$d$  = average channel depth.

### Organic Nitrogen (OrgN)

The source/sink term for organic nitrogen in Eq. (7.12) is given by:

$$OrgN_{Source/Sink} = \alpha_1\rho^*A - \beta_3^*OrgN - \alpha_4^*OrgN \quad (7.14)$$

where

$\alpha_1$  = fraction of algal biomass that is nitrogen

$\beta_3^*$  = rate of hydrolysis of organic nitrogen to ammonium nitrogen

$\alpha_4^*$  = rate of settling of organic nitrogen

### Inorganic Nitrogen Ammonium (NH4)

The source/sink term for nitrogen ammonium in Eq. (7.12) is given by:

$$NH4_{Source/Sink} = \beta_3^*OrgN + \sigma_3^*/d - \beta_1^*\left(1 - \exp^{-KNR/DO_{Sat}}\right)NH4 - F_1\alpha_1\mu A \quad (7.15)$$

where  $\alpha_3^*$  = rate of benthos source of ammonium

$KNR$  = first order nitrification inhabitation coefficient

$F_1$  = fraction algal uptake from ammonia

**Inorganic Nitrogen Nitrite (NO<sub>2</sub>)**

The source/sink term for nitrogen nitrite in Eq. (7.12) is given by:

$$\begin{aligned} NO_2_{Source/Sink} = & \beta_1^* \left( 1 - \exp^{KNR/DO_{SAT}} \right) NH4 \\ & - \beta_2^* \left( 1 - \exp^{-KNR/DO_{Sat}} \right) NO_2 \end{aligned} \quad (7.16)$$

**Inorganic Nitrogen Nitrate (NO<sub>3</sub>)**

The source/sink term for nitrogen nitrate in Eq. (7.12) is given by:

$$NO_3_{Source/Sink} = \beta_2^* \left( 1 - \exp^{-KNR/DO_{Sat}} \right) NO_2 - (1 - F_1) \alpha_1 \mu A \quad (7.17)$$

**Organic Phosphorus (OrgP)**

The source/sink term for organic phosphorus in Eq. (7.12) is given by:

$$OrgP_{Source/Sink} = \alpha_2 \rho^* A - \beta_4^* OrgP - \alpha_5^* OrgP \quad (7.18)$$

where

$\alpha_2$  = fraction of algal biomass that is phosphorus

$\beta_4^*$  = rate of oxidation of organic phosphorus to inorganic phosphorus.

**Inorganic Phosphorus Orthophosphate (PO<sub>4</sub>)**

The source/sink term for inorganic phosphorus in Eq. (7.12) is given by:

$$PO_4_{Source/Sink} = \beta_4^* OrgP + \alpha_2^* / d - \alpha_2 \mu A \quad (7.19)$$

where  $\alpha_2^*$  = benthos source rate of orthophosphate.

**Algae (A)**

The source/sink term for organic nitrogen Eq. (7.12) is given by:

$$A_{Source/Sink} = A \mu^* - A \rho^* - \frac{\sigma_1^*}{d} A \quad (7.20)$$

where  $\sigma_1^*$  = rate algal settling.

**Carbonaceous Biological Oxygen Demand (CBOD)**

The source/sink term for CBOD in Eq. (7.12) is given by:

$$CBOD_{Source/Sink} = -K_1^* CBOD - K_3^* CBOD \quad (7.21)$$

Note that in Eqs. (7.14), (7.15), (7.16), (7.17), (7.18), (7.19), (7.20), (7.21), certain coefficients or variables have already been defined in Eq. (7.13) or in equations previous to them.

For further details of the water quality variables and especially model parameters, the HEC-RAS User's Manual of the US Army Corps of Engineers (USACE 2008) may be consulted.

## 7.5 Watershed Modeling and Streamflow Simulation

The first major task in watershed modeling is the delineation of the watershed boundary. This basin delineation is done for the Pampanga River Basin, Laguna Lake Basin, and the watersheds of Bataan and Cavite Provinces. The watershed model system for the entire modeled area is shown in Fig. 7.7. Table 7.1 gives the summary of the drainage area and number of sub-basin in this modeled area. From these sub-basin delineations, geometry properties that are specified in the model such as overland and river length, widths, and slopes can be determined. Based on sub-basin delineations, the watershed model parameters such as interception, infiltration, and overland flow parameters can be obtained from soil type and land use maps.

With the watershed model, streamflow simulations can be conducted as input to the Manila Bay-Laguna Lake system. Table 7.2 presents the rainfall stations within and around Manila Bay-Laguna Lake watersheds with the accompanying Fig. 7.8 showing the locations of these gaging stations. Some of these gaging stations also have pan evaporation data such as in Science Garden in Quezon City, CLSU Muñoz in Nueva Ecija, UPLB in Laguna, and Hacienda Luisita in Tarlac. There are 35 rainfall stations with historical daily rainfall from which the basin rainfall is obtained by spatial interpolation. Although some rainfall stations may have fragmentary or discontinuous data, as long as there is one gaging station with recorded data for that day, the basin rainfall can still be calculated. With this, the daily rainfall data from 1972 to 2012 were used to calculate the streamflows at 2066 river points.

Typical time series plots of these simulated streamflows are shown in Fig. 7.9 for two sub-basins. Note that only daily data from 1988 to 2003 are shown here since it is too tight to plot data for more than 15 years. In any case, these plots show typical daily time series pattern of river flows. Based on this simulated daily streamflows, daily flow statistics can be calculated such as the average daily flows over 40 years data (1972–2012) as shown in Figs. 7.10, 7.11, 7.12 and 7.13 for the Pampanga-Bulacan, Bataan, Laguna, and Manila-Cavite sub-basins, respectively.

For purposes of the Manila Bay-Laguna Lake water quality modeling, the watershed inflows can be computed for certain time period or epochs such as episodic storms of short duration, intense storm events of long duration, and medium intense events like the *Habagat* (southwest monsoons). On the other hand, over long periods in months or years, the watershed inflows calculated here can be used to assess the long-term water quality processes of Manila Bay-Laguna Lake system.

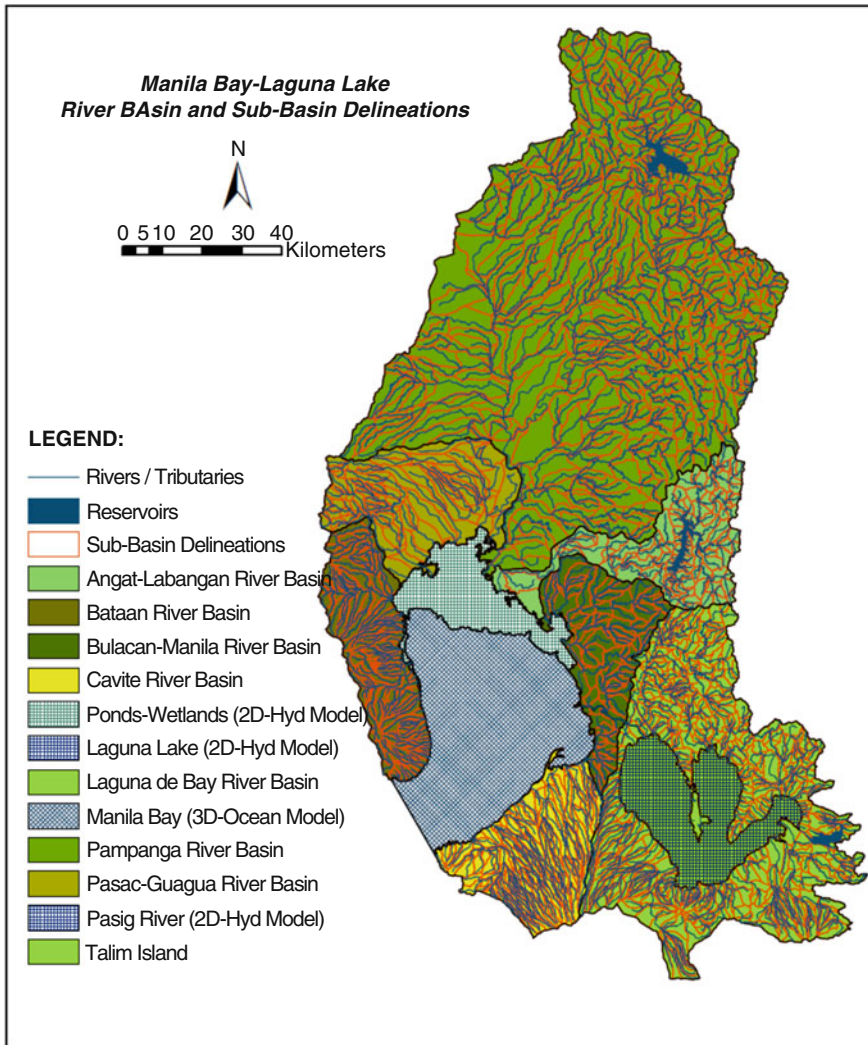


**Fig. 7.7** Major sub-basin delineations of the Bataan, Pampanga (including Guagua), Bulacan, Manila-Cavite, and Laguna River Basins. Also indicated are areas handled by 2-d hydraulic model and 3-d Princeton Ocean Model

## 7.6 Manila Bay Hydrodynamic and Water Quality Modeling and Simulations

The area modeled by the 3-d Princeton Ocean Model shown in Fig. 7.7 was the Manila Bay, while the 2-d hydraulic model covered Laguna Lake and Pasig River as well as portions of the Bataan-Pampanga-Bulacan Delta on the southern part

**Table 7.1** Summary of drainage areas and number of sub-basin units of the modeled area

Sub-Basin No.	River System	Sub-Basin Name	Major Rivers	Total Area (km <sup>2</sup> )	No. of Sub-Subbasins
SB-01	Pampanga	Pantabangan River Basin	Caragian River	845.8	126
SB-02	Pampanga	Upper Pampanga River Basin	Pampanga River, Digmala River	436.1	80
SB-03	Pampanga	Coronel River Basin	Coronel River	713.7	111
SB-04	Pampanga	Central Pampanga River Basin	Pampanga River, Tambo Creek, Cabu Creek	801.1	82
SB-05	Pampanga	Peñaranda River Basin	Peñaranda River, Sumacba River	607.4	61
SB-06	Pampanga	Talavera River Basin	Talavera River, Casanova Creek	1,692.6	114
SB-07	Pampanga	Rio Chico Dela Pampanga	Rio Chico Dela Pampanga River, Sacobia River	1,485.1	71
SB-08	Pampanga	Lower Pampanga River Basin	Pampanga River, San Miguel River, Maasim River	1,640.0	93
SB-09	Angat	Angat River Basin	Angat River, Catmun River	546.2	75
SB-10	Angat	Ipo-Bustos River Basin	Angat River	576.6	48
SB-11	Guagua/Pasac	Guagua Basin Group	Abacan River, Pasig-Potrero River, Porac River, Gumain River	1,365.7	99
SB-12	Bataan	Bataan Basin Group	Culaman River, Orani River, San Juan River, Talisay River	996.1	226
SB-13	Bulacan	Bulacan Basin Group	Balagtas River, Sta. Maria-Bocae River, Marilao-Meycauayan River	631.5	68
SB-14	Manila	Manila Basin Group	Tulahan-Malabon River, Pasig River, Paranaque-Las Pinas River	348.4	61
SB-15	Laguna	Laguna Lake Basin Group	Marikina, Binan, Sta. Rosa, San Cristobal, San Juan, Sta. Cruz, Pagsanjan, Sta. Maria Rivers	2,950.1	593
SB-16	Cavite	Cavite Basin Group	Imus-Zapote, San Juan, Canas, Timalan, Balsahan-Alemang, Maragondon Rivers	1,028.6	158
Total ----->				16,665.1	2066
<i>Lake and Reservoir Areas (areas not included above)</i>					
				38.5	
				24.4	
				874.2	

Pampanga River Basin (area north of Manila Bay). Figure 7.14, in particular, shows Manila Bay modeled area which is spatially discretized into 16 (sigma-delta) layers over 11,967 horizontal, orthogonal grids of size 400 m x 400 m each. The bathymetric map of Manila Bay is also superposed in this figure. The 2-d model geometry together with the elevation map of Bataan-Pampanga-Bulacan Delta which is a flatland/wetland area is shown in Fig. 7.15 consisting of 4927 irregular grids or finite elements. Finally, Fig. 7.16 shows the 2-d model geometry and bathymetric of Laguna Lake with Pasig River (not totally shown) which is composed of 3572 finite elements. In Laguna Lake, finite elements were manually created to follow the river alignment, the location of fish and hydraulic structures, as well as other land features.

**Table 7.2** List of rainfall gaging stations within and around the Manila Bay-Laguna Lake River Basins and pertinent information of these stations

Station name	Location	Agency	Latitude	Longitude	Length of record	Data
<b>Rainfall (mm)</b>						
Ambulong	Ambulong, Tanauan, Batangas	PAGASA	14° 05' 30"	121° 03' 18"	40	Daily
Amadeo	Maitim, Amadeo, Cavite	PAGASA	14° 10' 18"	120° 57' 00"	25	Daily
Bacoor	Mabolo E.S., Bacoor, Cavite	PAGASA	14° 27' 00"	120° 56' 00"	35	Daily
Nasugbu	Wawa, Nasugbu, Batangas	PAGASA	14° 05' 06"	120° 37' 19"	33	Daily
NAIA	Pasay City, MM	PAGASA	14° 31' 00"	121° 01' 00"	40	Daily
Sangley point	Cavite City, Cavite	PAGASA	14° 29' 54"	120° 54' 54"	26	Daily
Tagaytay city	Tagaytay City, Cavite	PAGASA	14° 07' 18"	120° 58' 00"	16	Daily
UPLB	Los Baños, Laguna	PAGASA	14° 10' 00"	121° 15' 00"	24	Daily
Tayabas	Tayabas, Quezon	PAGASA	14° 01' 42"	121° 35' 18"	29	Daily
Infanta	Infanta, Quezon	PAGASA	14° 45' 00"	121° 38' 48"	30	Daily
Baler	Baler, Aurora	PAGASA	15° 45' 00"	121° 38' 08"	45	Daily
Angat	Angat, Bulacan	PAGASA	14° 54' 20"	121° 09' 40"	40	Daily
Bosoboso	Antipolo City, Rizal	EFCOS	14° 38' 00"	121° 14' 00"	23	Hourly/daily
Science garden	Quezon City, MM	EFCOS	14° 38' 41"	121° 02' 31"	49	Hourly/daily
Sta. Maria	Macasipac, Sta. Maria, Laguna	PAGASA	14° 30' 00"	121° 26' 18"	14	Daily
Tanay radar	Tanay, Rizal	PAGASA	14° 30' 00"	121° 21' 00"	11	Daily
Mt. Campana	Antipolo city, Rizal	EFCOS	14° 40' 06"	121° 17' 29"	6	Hourly/daily
Mt. Oro	Rodriguez, Rizal	EFCOS	14° 45' 48"	121° 09' 23"	10	Hourly/daily
Morong	Morong, Bataan	PAGASA	14° 41' 00"	120° 16' 00"	6	Daily
Pilar	Pilar, Bataan	PAGASA	14° 40' 38"	120° 33' 50"	6	Daily
Mayantoc	Mayantoc, Tarlac	PAGASA	15° 36' 00"	120° 21' 00"	19	Daily

(continued)

**Table 7.2** (continued)

Station name	Location	Agency	Latitude	Longitude	Length of record	Data
Balungao	Balungao, Pangasinan	PAGASA	15° 54' 00"	120° 40' 00"	27	Daily
Muñoz	Sci. City of Muñoz	PAGASA	15° 42' 18"	120° 52' 21"	39	Hourly/daily
Sapang Buho	Palayan city	PAGASA	15° 35' 45"	121° 05' 36"	39	Hourly/daily
Mayapyap	Mayapyap, Cabanatuan	PAGASA	15° 30' 21"	120° 56' 20"	39	Hourly/daily
Gabaldon	Gabaldon, Cabanatuan	PAGASA	15° 27' 30"	121° 20' 06"	39	Hourly/daily
Zaragoza	Zaragoza, Pangasinan	PAGASA	15° 25' 27"	120° 43' 54"	39	Hourly/daily
Papaya	Papaya, general Tinio	PAGASA	15° 20' 43"	121° 02' 32"	39	Hourly/daily
San Isidro	San Isidro, Nueva Ecija	PAGASA	15° 18' 58"	120° 53' 27"	39	Hourly/daily
Arayat	Arayat, Pampanga	PAGASA	15° 10' 11"	120° 45' 34"	39	Hourly/daily
Candaba	Candaba, Pampanga	PAGASA	15° 06' 13"	120° 49' 43"	39	Hourly/daily
Sibul spring	Sibul, San Miguel, Bulacan	PAGASA	15° 10' 38"	121° 02' 48"	39	Hourly/daily
Sasmuan	Sasmuan, Pampanga	PAGASA	14° 54' 49"	120° 36' 29"	39	Hourly/daily
Sulipan	Sulipan, Apalit, Pampanga	PAGASA	14° 55' 17"	120° 45' 37"	39	Hourly/daily
Ipo dam	Norzagaray, Bulacan	PAGASA	14° 53' 49"	121° 09' 15"	39	Hourly/daily
San Rafael	San Rafael, Bulacan	PAGASA	14° 57' 07"	120° 57' 37"	39	Hourly/daily

The hydrodynamic and water quality model simulations presented below are only for Manila Bay. Since running the 3-d Princeton Ocean Model requires tremendous computer time, the simulation was conducted for a period of 6 months on a daily basis for a particular, typical year selected from the historical data with the overall period 1972–2012.

For real-world water quality model simulation of Manila Bay, the surface water sink/source terms as well as pollution loadings and associated flow discharge as input or boundary conditions to Manila Bay-Laguna Lake models must be properly quantified. Unfortunately, this is always an issue because there are not enough data collected, not even secondary data especially pollution loading that can be imposed as boundary conditions in the model. On the other hand, when there are government monitoring efforts that collect pollution data, the associated flow discharge is not

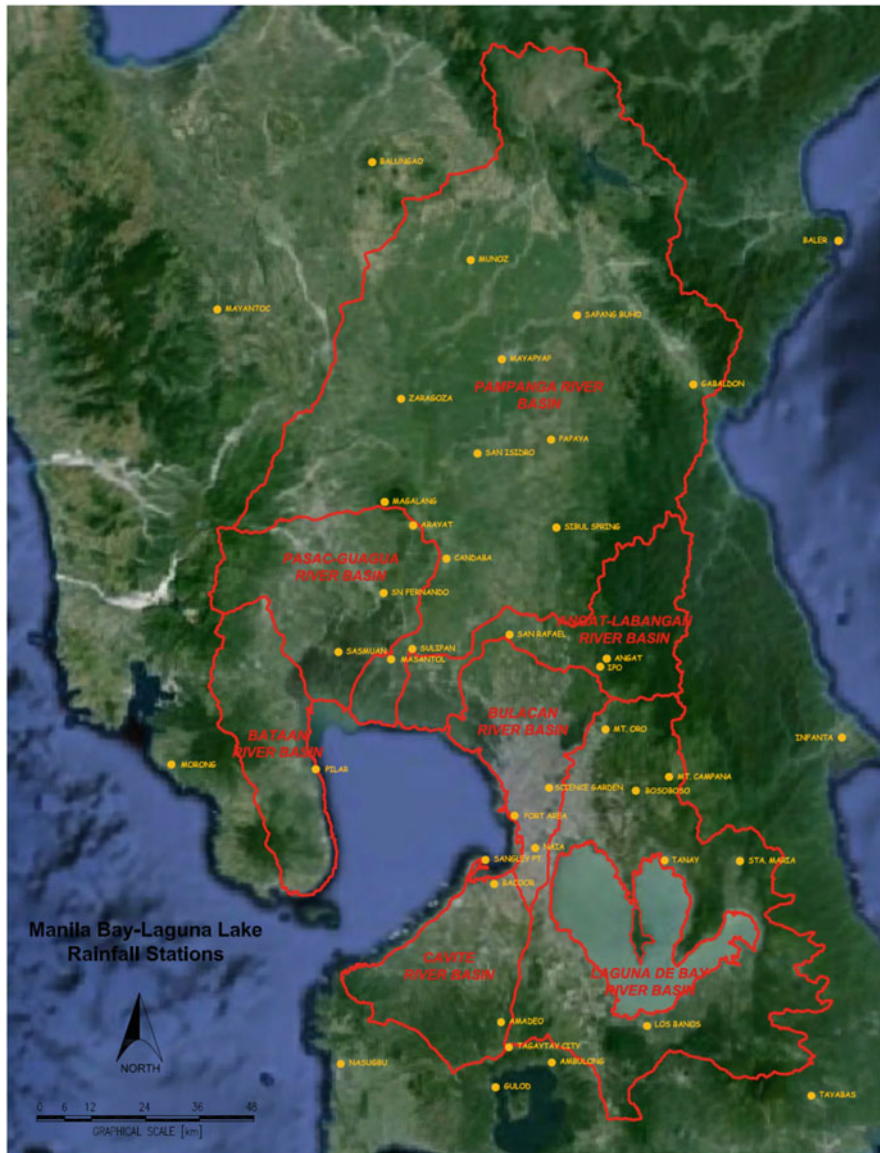


**Fig. 7.8** Location of rainfall gaging stations within and around Manila Bay-Laguna Lake watersheds

collected at the time of sampling. In view of this, the water quality model simulations conducted and presented here are at best illustrative only and may only provide indicative information or inferences, so they may not be sufficient to develop strategies to manage the environmental quality of the Manila Bay-Laguna Lake

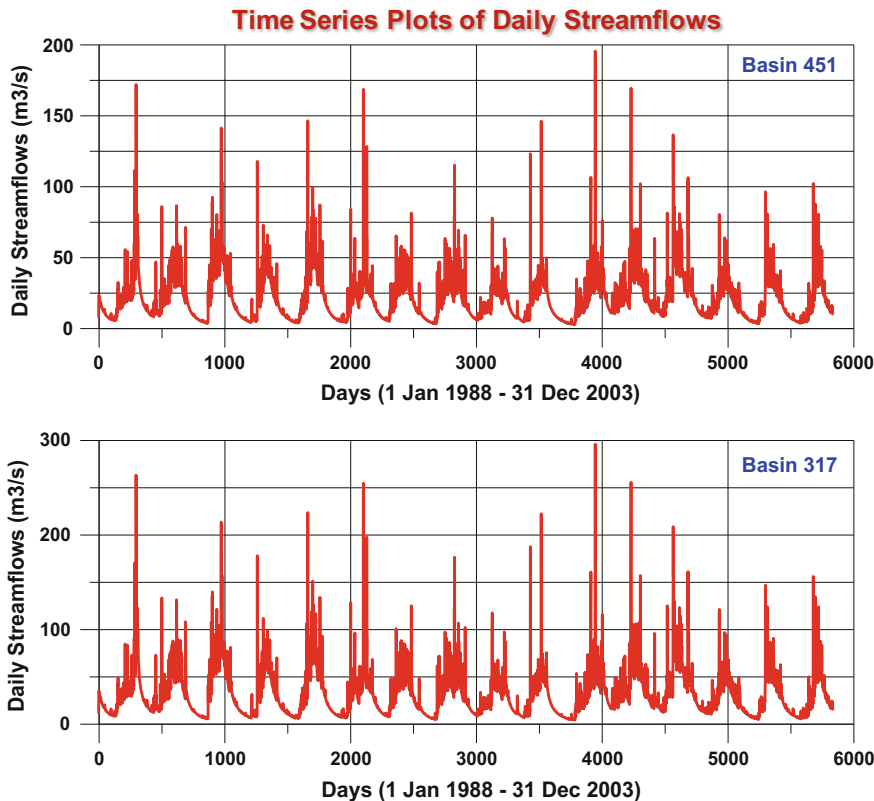


**Fig. 7.9** Sample time series plots of daily flows calculated from the watershed modeling of two sub-basins in the Pampanga River Basin

system. The Manila Bay water quality simulations presented herein were based on pollution loadings derived from regression analysis of secondary pollution data as a function of river discharges.

From a water quality sampling survey conducted by the Marine Science Institute of the University of the Philippines at Imus River in Cavite and Orion River in Bataan at their mouths in Manila Bay, BOD (biological oxygen demand) and DO (dissolved oxygen) data and associated river flows were obtained. These BOD and DO data were then plotted as a function of river flows ( $Q$ ) as shown in Figs. 7.17 and 7.18 for Imus and Orion, respectively. These plots generally show that due to dilution effects, BOD decreases with increasing discharge which is consistent in the case of Imus and Orion Rivers, while DO increases with discharge as exhibited clearly in Orion River. Other data are available from Laguna Lake Development Authority (LLDA) which are annual BOD, DO, nitrate, and phosphate with associated annual streamflow data. Unfortunately, these data are on an annual basis which

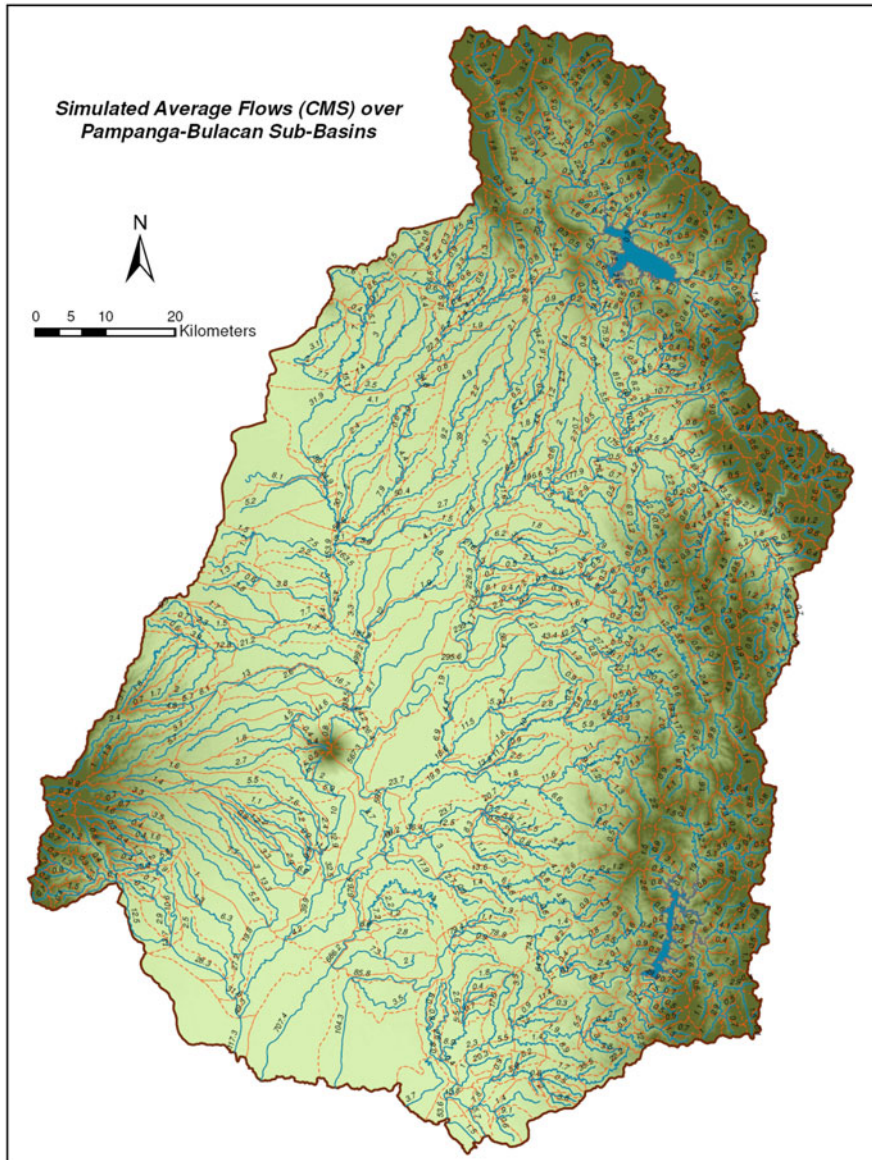


**Fig. 7.10** Average daily flows ( $\text{m}^3/\text{s}$ ) in the Pampanga River Basin calculated from the watershed model simulation using rainfall data from 1972 to 2012

is not useful for the purposes of this study since model simulations are conducted on a daily basis.

In the absence of a complete pollution data that can be used here, pollution loadings imposed in the water quality simulation were estimated as follows. Based

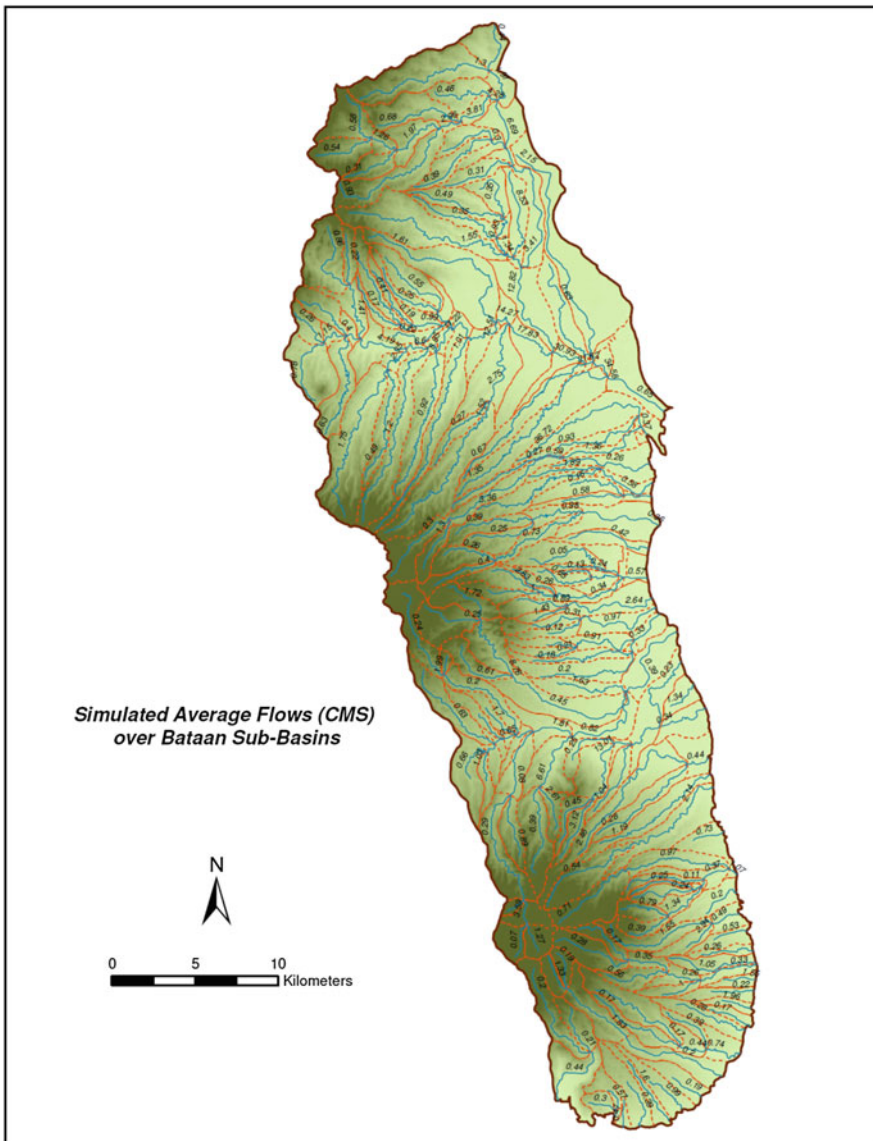


**Fig. 7.11** Average daily flows ( $\text{m}^3/\text{s}$ ) in the Bataan sub-basins calculated from the watershed model simulation using rainfall data from 1972 to 2012

on the very limited observed daily data of BOD and phosphate loadings, regression equations of BOD and phosphate loadings were developed as a function of population and flow discharges at the 28 river points outflowing to Manila Bay as shown in Fig. 7.19. Likewise, the map of population data is displayed in Fig. 7.20. The population and flow statistics are shown in Table 7.3. Using these regression

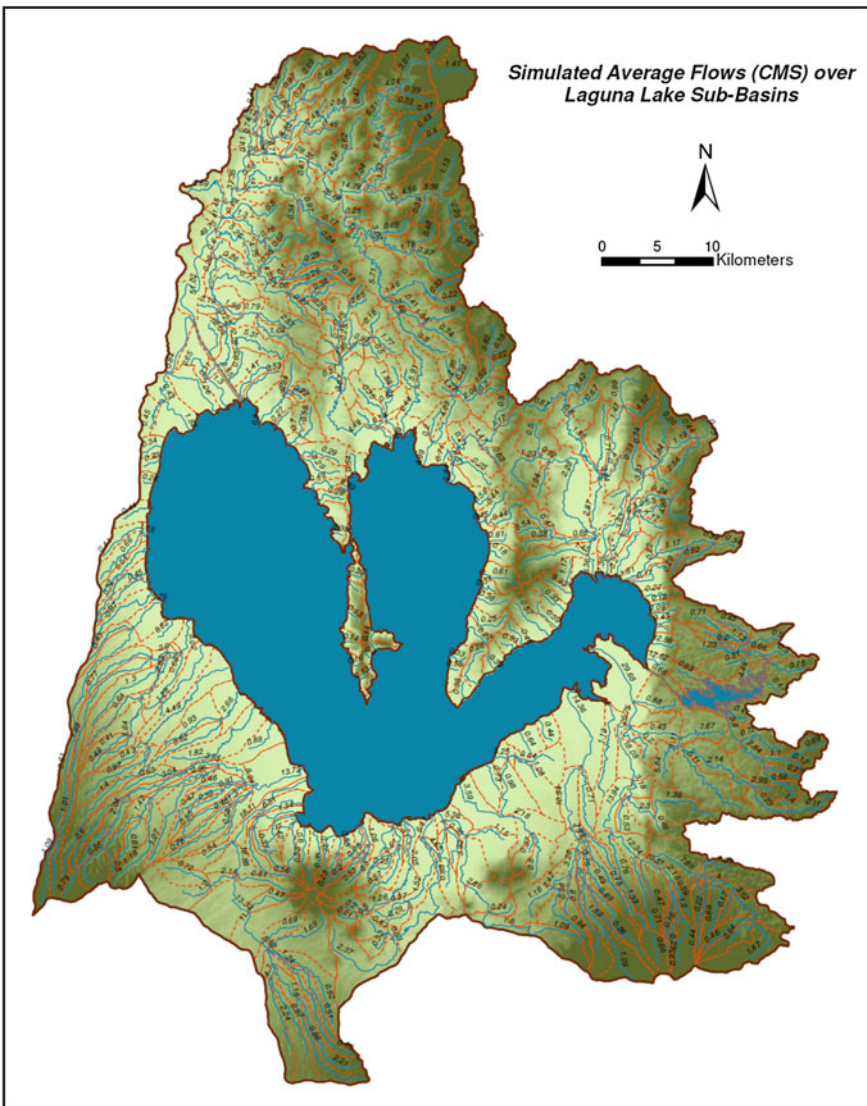


**Fig. 7.12** Average daily flows ( $\text{m}^3/\text{s}$ ) in the Laguna River Basin calculated from the watershed model simulation using rainfall data from 1972 to 2012

equations, the time series of BOD and phosphate can be generated or derived given the streamflows generated from the watershed model as well as the population in the city or town associated to that river which can be used as river water quality loadings (i.e., BOD and phosphate) into Manila Bay. For instance, Figs. 7.21 and 7.22 show time series of calculated BOD and phosphate loadings for Pampanga, and Limay Rivers, respectively.

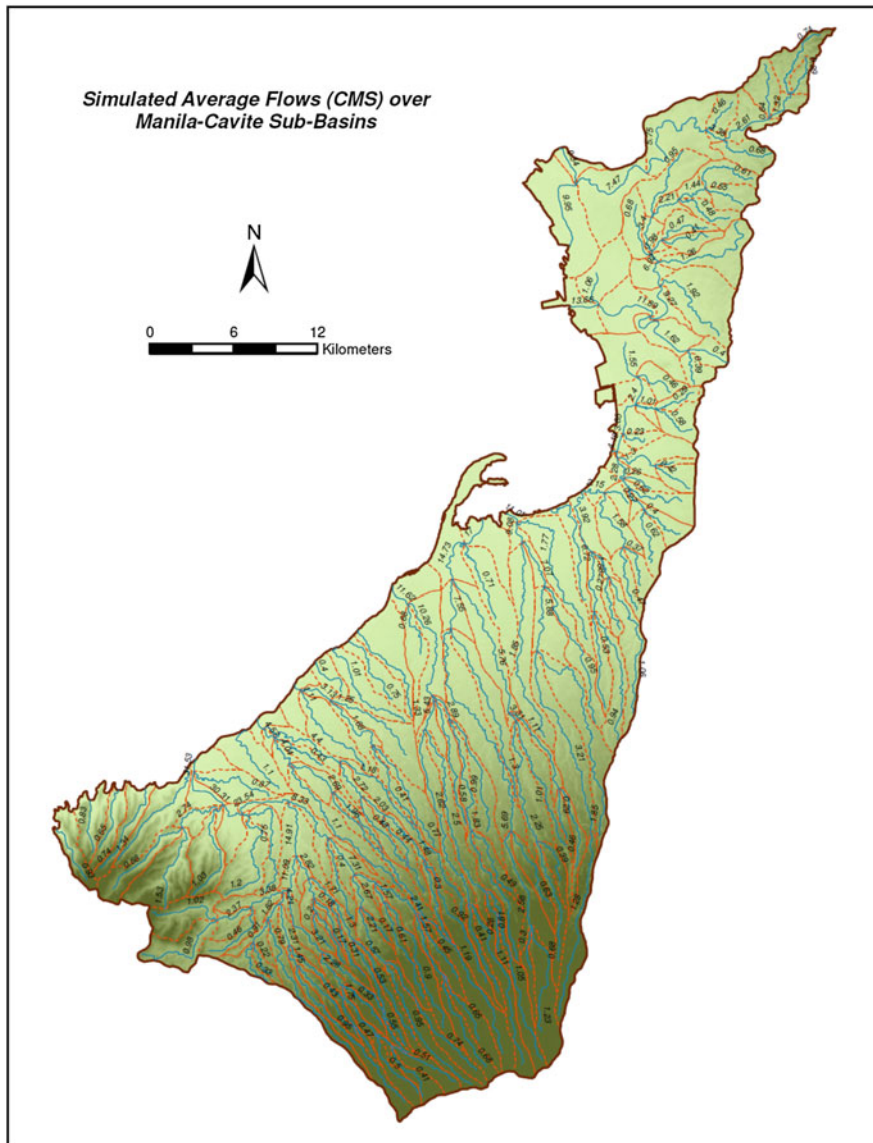


**Fig. 7.13** Average daily flows ( $\text{m}^3/\text{s}$ ) in the Manila-Cavite sub-basins calculated from the watershed model simulation using rainfall data from 1972 to 2012

In using BOD and phosphate, the Manila Bay water quality model simulations were conducted with three (3) water quality constituents only, namely, DO, BOD, and phosphate. The resulting map showing dissolved oxygen (DO) concentrations is displayed in Fig. 7.23 over a period of 8 days or 196 hours. Qualitatively, the results

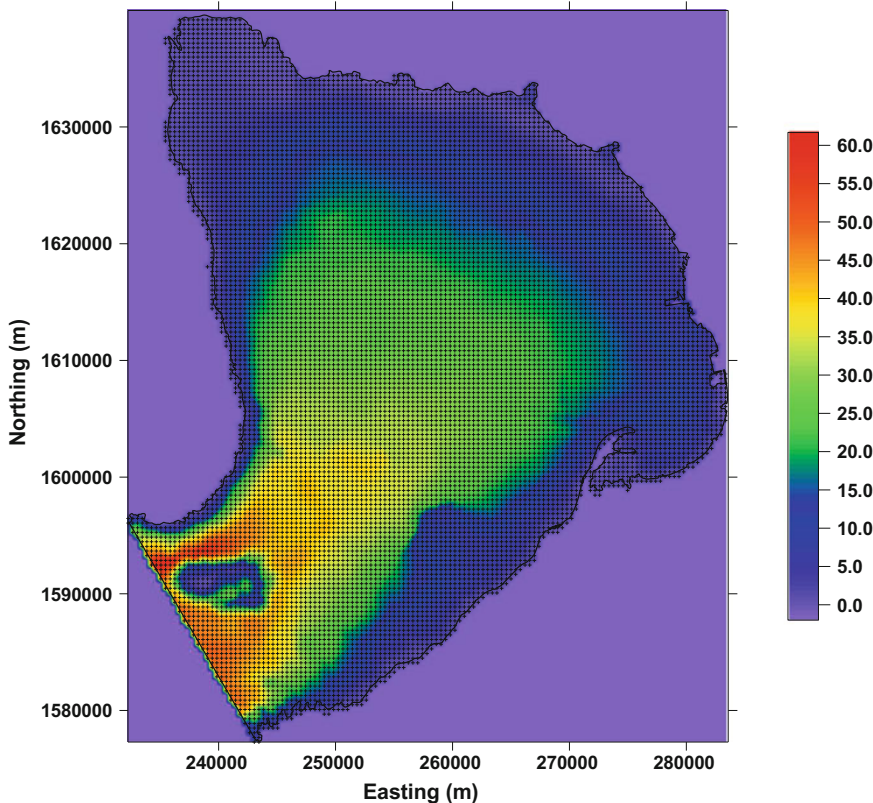


**Fig. 7.14** Finite difference grid of Manila Bay consisting of 16 (sigma-delta) layers of 11,996 square grids of size 400 m x 400 m each together with bathymetric map

here show certain resemblance to the spatial distribution of the contour plots of water quality data samplings conducted by IMSWES (Tamura et al. 2003).

A brief remark at this point is in order. The optimal and sustainable use of the Bay-Lake system requires proper understanding of the physical and environmental processes that govern the system. Managing the environmental quality of the Manila Bay-Laguna Lake can be greatly aided using mathematical models that describe the hydrology of the watersheds, the hydrodynamics and hydraulics of the Bay-Lake system, and the transport of nutrients, salinity, sediments, or contaminants from the watersheds to the Bay-Lake system.

For real-world water quality model simulation of Manila Bay, the surface water sink/source terms as well as pollution loadings as input or boundary conditions to Manila Bay-Laguna Lake models must be properly quantified. Unfortunately, this is an issue in the Philippines since there are no appropriate data, even secondary data on pollution loading or sink/source are not available. There is dearth of data from ongoing efforts and studies related to Manila Bay-Laguna Lake system such as those done by certain government agencies, like the Bureau of Soil and Water

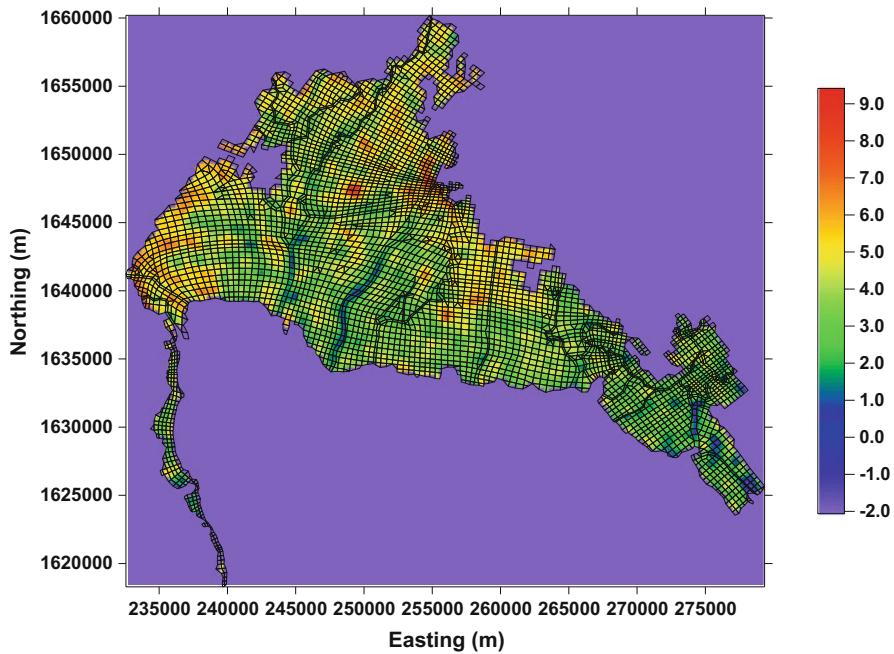


**Fig. 7.15** Detailed 2-d model geometry and elevation map of Bataan-Pampanga-Bulacan Delta consisting of 4927 finite elements

Management (BSWM) and Laguna Lake Development Authority (LLDA) and the University of the Philippines-Marine Science Institute (UP-MSI). Thus, the water quality model simulations presented here are at best only for illustrative purpose, so it may not be sufficient for purposes of developing management strategies to manage the environmental quality of the Manila Bay-Laguna Lake system.

## 7.7 Laguna Lake 2-d Coupled Lake Flow-Salinity Modeling

Laguna Lake has various uses such as fisheries, domestic and irrigation water supply, flood control, hydropower generation, and navigation. Two competing uses are the fish production in the lake and extraction of lake water for domestic water supply. The fishing industry prefers saline water from Manila Bay through Pasig River. On the other hand, the water supply concessionaires would prefer minimal salinity into the lake. This is one major motivation in developing this lake flow-salinity model for Laguna Lake as a tool to possibly resolve such conflicting uses.

Saltwater from Manila Bay is allowed to enter the lake through the Pasig-Napindan River. This practice greatly benefits the fishing industry as the saline

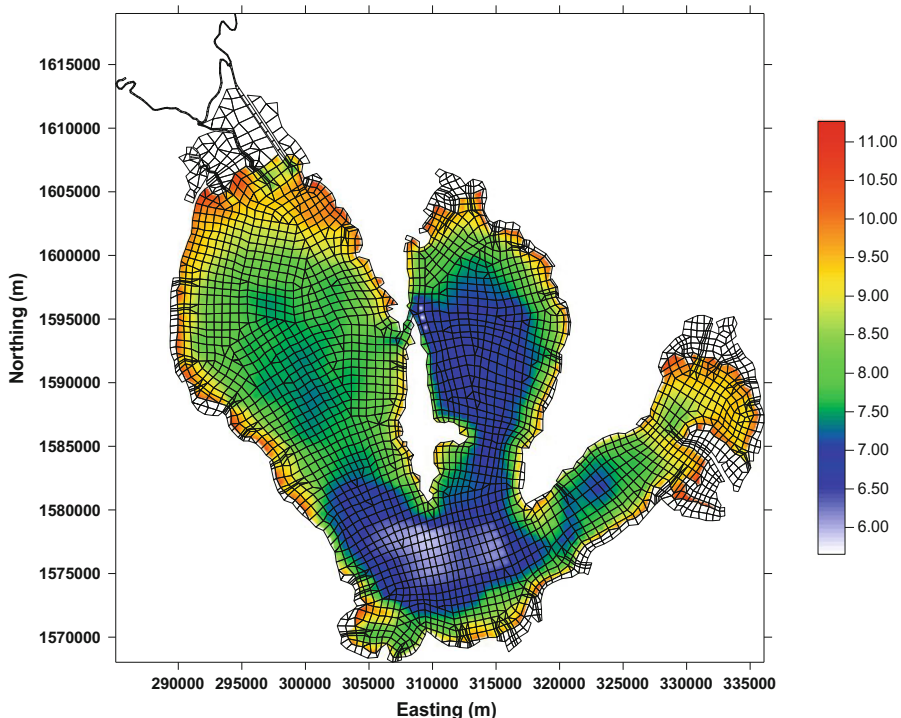


**Fig. 7.16** Detailed 2-d model geometry and bathymetric map of Laguna Lake-Pasig River composed of 3572 finite elements

water tends to clean the lake from turbidity especially after the wet season. It is also believed that saltwater from Manila Bay is laden with nutrients such as diatoms (greenish in color, nutritious to fish) that add to the sustenance of fish grown in the lake. On the other hand, lake water withdrawal for domestic water supply requires a certain salinity standard that consequently affects the quality of water for optimum growth and survival of the fish raised in the lake. Thus, the push and pull between the two conflicting interests and uses.

The question is how to properly manage saltwater entering or exiting the lake through Pasig River which can be controlled by the Napindan Hydraulic Control Structure (HCS) to arrive at a win-win solution to two conflicting interest: fisheries versus domestic water supply. Specifically, salinity levels of 2 to 6 ppt (parts per thousand) in the lake are desirable for fish production. However, treatment of water for domestic water use could become too expensive if the raw water has a salinity greater than 0.3 ppt.

In this particular application, the two-dimensional (2-d) hydraulic model utilizes the shallow water equation (SWE) to describe the mass and momentum conservation laws of the lake flow dynamics, while salinity transport is described using an advection-dispersion equation (ADE). The shallow water equations and advection-

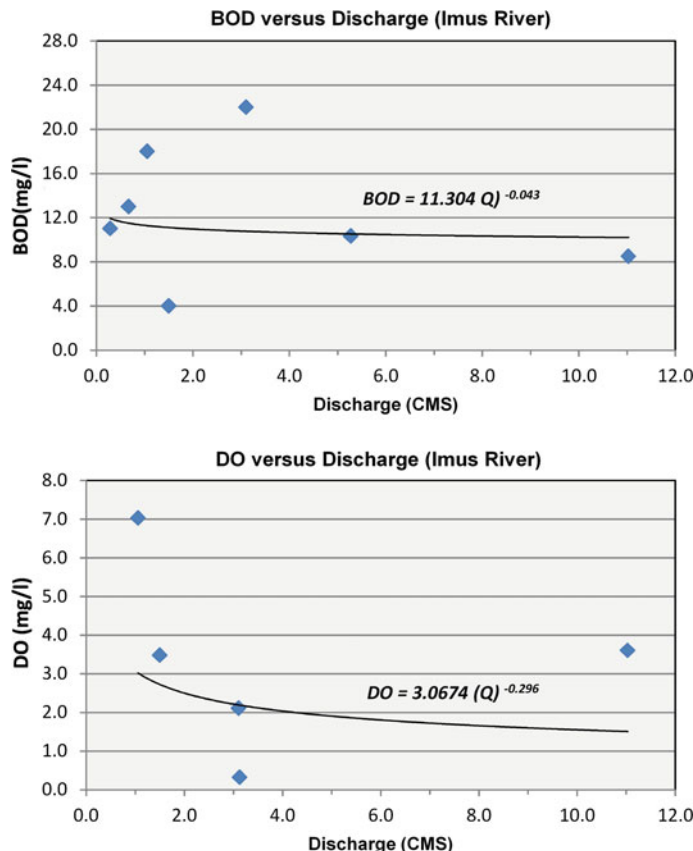


**Fig. 7.17** Plot of BOD and DO loadings versus discharge of Imus River

dispersion equation are solved as coupled systems of equations using the finite volume method (FVM).

The major motivation for solving the shallow water equations and advection-dispersion equation as coupled system of equations is that the salinity interact with flow and thus affecting the flow velocities and water stage. Specifically, when salinity concentrations are high, baroclinic effects become important which is directly incorporated as a term in the momentum equations (Smith and Cheng 1987). The details of this model and finite volume method of solution as coupled flow and salinity model are given in Appendix C. An application of this model was done by Tabios et al. (1995) for salinity variations in the San Francisco Bay/Delta area and by Qi et al. (1997) for modeling river-estuarine flow dynamics and industrial effluent transport.

In running the Laguna Lake model, the boundary conditions include watershed inflows at over 40 points surrounding the lake, tidal forcing with a specified salinity concentration at San Juan station in Pasig River, gate operation at Rosario weir

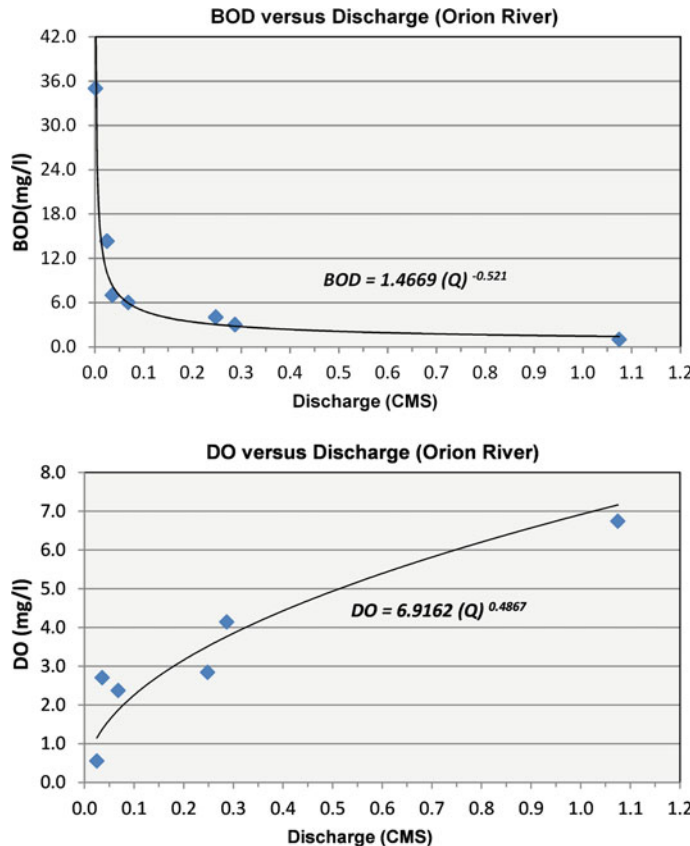


**Fig. 7.18** Plot of BOD and DO loadings versus discharge of Orion River

structure at the north end of Manggahan floodway, and the hydraulic control structure and navigation channel at the Napindan channel. It may be noted that the boundary conditions are applied at the interface of an element. The normal flux at an interface with a specified boundary condition is calculated based on the equation specific to that boundary condition (e.g., weir equation is used for a weir structure) instead of using the shallow water equation.

The flow and salinity simulation presented is for a typical dry season condition, around the months of March and April where lake salinity is high. In the model, a tidal inflow is specified at San Juan station in Pasig River which has a salinity of 7.5 ppt (parts per thousand) and the watershed inflows which are relatively low at this time of the year. Figure 7.24 shows a typical vector plot of lake velocities simulated. It may be noted in this figure that the location of the fish cages are indicated by round symbols and the fish cages are indicated by square symbols. Currently, over 140 km<sup>2</sup> of the 934 km<sup>2</sup> (at 11.5 m level) of the lake area are occupied by fish structures (i.e., fish pens and fish cages). The fish pens are

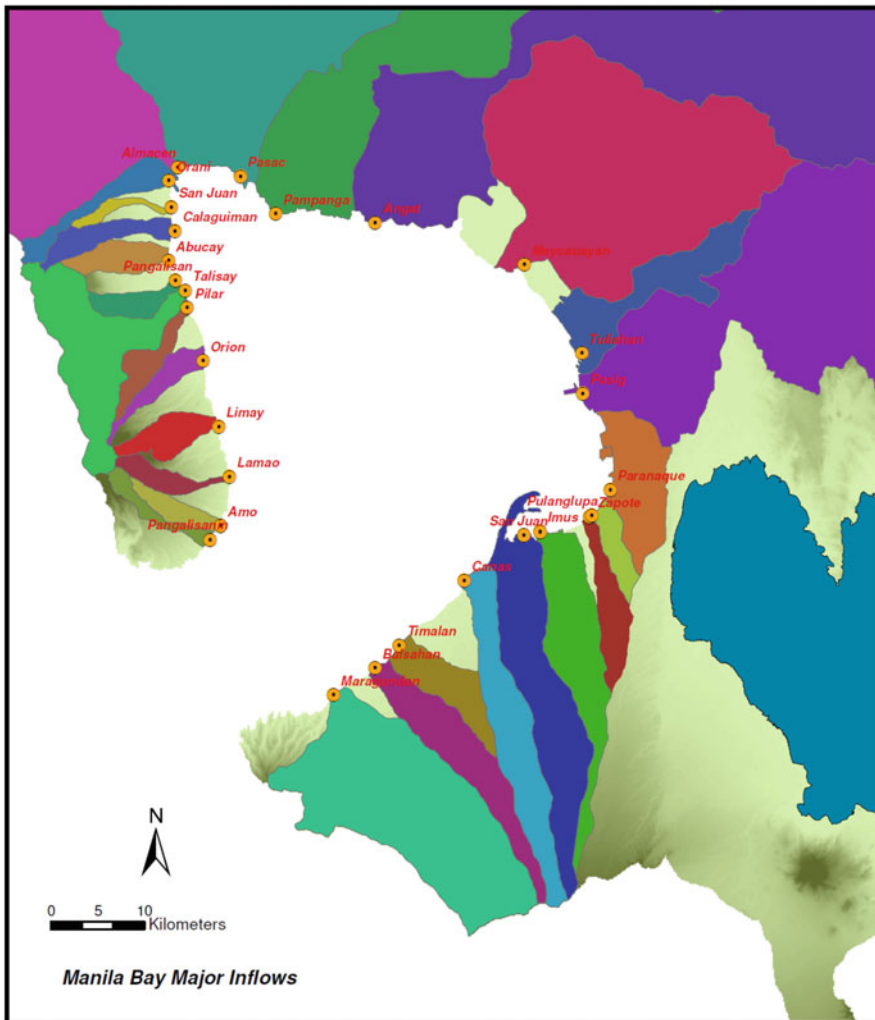


**Fig. 7.19** Locations of rivers with outflows to Manila Bay

enclosures (fences) that penetrate into the lake bed, while the fish cages are fishnets hanging from the top down to about half of the lake depth.

Figure 7.25 shows the resulting salinity movement after 10, 30, 57, and 96 h. At the onset of simulation, the salinity advanced from Pasig River through Napindan channel such that at the tenth hour of simulation, the salinity concentration of 6.0 ppt appeared at the Napindan channel outlet to the lake (upper left hand corner of the

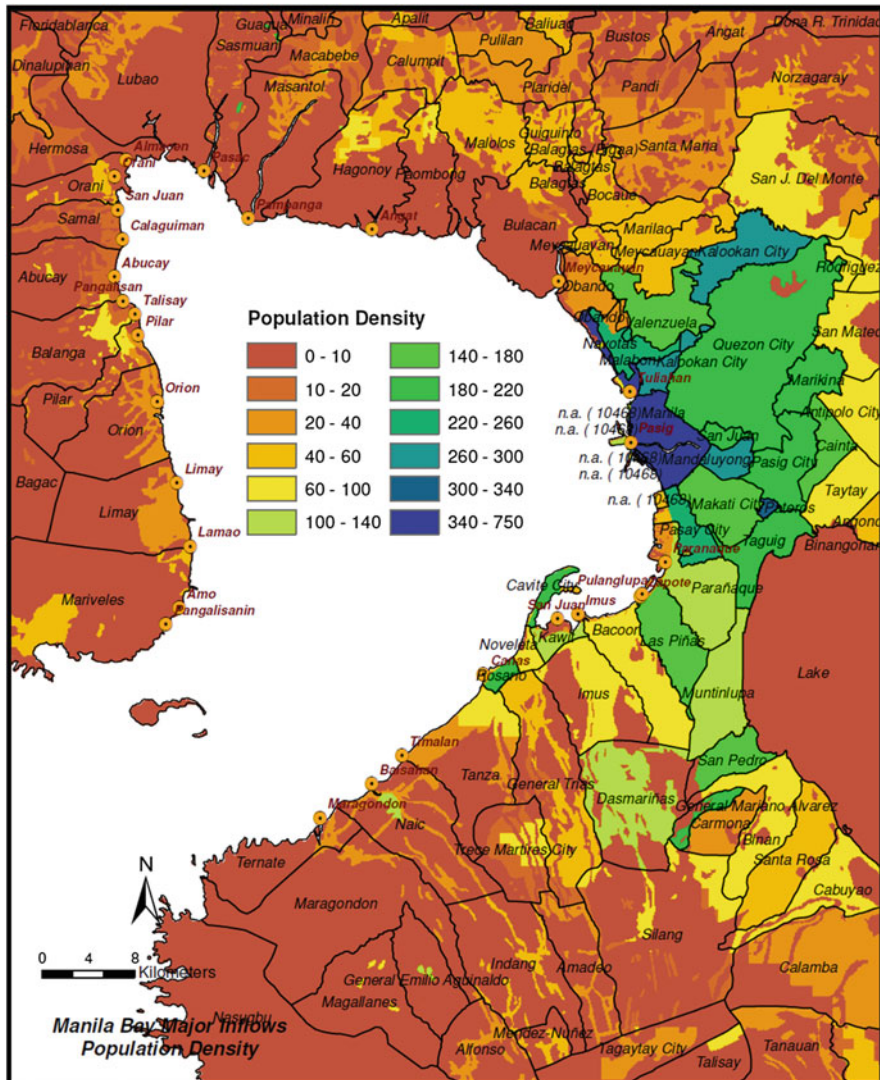


Fig. 7.20 Population density map of the study area

figure) while the rest of the lake had from 1.0 to 3.0 ppt salinity concentration. At hour 57, salinities of 8.0 were shown on the central part of Laguna Lake through the Diablo Pass. The salinity front could advance deep into the south part of Laguna Lake after 4 days (96 h) which happens especially in April and possibly hovers in that area up to mid-May.

**Table 7.3** List of rivers around Manila Bay with derived BOD and phosphate loadings

Inflow No.	Basin	Town /city	River name	SB code	X-coord (m)	Y-coord (m)	Accum DA. (m <sup>2</sup> )	Qave (m <sup>3</sup> /s)	Qmax (m <sup>3</sup> /s)	Qmin (m <sup>3</sup> /s)	Available data (sampling)	Ave population density**
1	Cavite	Las Piñas	Zapote River	1007	278854.2	1600244.8	42.1	3.92	189.9	0.082	DO, BOD	105.5
2	Cavite	Bacoor	Imus River	1018	275698.6	1599922.1	118.3	11.01	532.0	0.229	DO, BOD	71.0
3	Cavite	Kawit	San Juan River	1037	273930.4	1593514.7	174.9	17.00	687.8	0.357	-	42.6
4	Cavite	Rosario	Cañas River	1054	267540.4	1594704.1	119.1	11.62	457.7	0.245	-	59.6
5	Cavite	Tanza	Timalan River	1065	260534.0	1587671.1	50.1	4.72	197.4	0.102	-	5.1
6	Cavite	Naic	Balsahan River	1083	257931.3	1585251.9	96.3	9.26	363.1	0.199	-	13.2
7	Cavite	Ternate	Maragondon River	1153	253498.7	1582315.3	327.2	31.53	1187.1	0.679	-	4.0
8	Manila	Malabon	Tullahan River	1825	280158.2	1619115.8	75.2	9.95	381.5	0.203	-	217.7
9	Manila	Manila	Pasig River	1848	280237.0	1614747.6	610.9	52.05	1941.6	1.064	DO, BOD, NO <sub>3</sub> , PO <sub>4</sub>	256.8
10	Manila	Paranaque	Paranaque River	1869	283200.9	1604373.3	85.0	7.80	520.9	0.159	-	162.5
11	Manila	Las Piñas	Pulanglupa River	1874	281213.5	1601629.2	23.3	2.15	123.1	0.045	-	139.5
12	Bulacan	Bulacan	Meycauayan River	1879	274001.5	1628653.1	569.5	53.56	2058.9	1.155	DO, BOD	48.2
13	Pampanga	Hagonoy	Angat River	861	257947.8	1633153.3	1122.9	104.33	3700.7	2.203	-	7.7
14	Pampanga	Masantol	Pampanga River	738	247280.2	1634114.0	8221.8	707.40	22360.9	17.889	DO, BOD	2.5
15	Pampanga	Sasmuan	Pasac River	960	243481.0	16338203.6	1365.7	117.28	4353.2	2.974	-	1.3

16	Bataan	Hermosa	Almacen River	3224	236774.5	1639119.5	417.2	36.72	1397.0	0.888	-	8.3
17	Bataan	Orani	Orani River	3226	235772.4	1637717.3	37.7	3.36	132.7	0.079	-	10.3
18	Bataan	Samal	San Juan River	3088	236064.7	1634836.2	10.5	0.93	37.0	0.022	-	8.3
19	Bataan	Samal	Calaguinan River	3098	236476.5	1632247.8	31.8	2.83	111.8	0.067	-	4.4
20	Bataan	Abucay	Abucay River	3112	235775.7	1629061.3	29.7	2.64	105.2	0.062	-	4.7
21	Bataan	Balanga	Pangalisan River	3125	236516.2	1626948.5	21.5	1.93	76.6	0.045	-	13.3
22	Bataan	Balanga	Talisay River	3156	237549.9	1625847.8	144.0	13.01	514.2	0.303	-	13.9
23	Bataan	Pilar	Pilar River	3163	237795.0	1624036.6	27.2	2.46	98.7	0.057	-	9.3
24	Bataan	Orion	Orion River	3168	239453.3	1618274.2	23.6	2.14	86.1	0.049	DO, BOD	6.7
25	Bataan	Limay	Duata-Limay River	3184	241152.1	1611210.3	32.2	2.94	119.3	0.067	-	2.6
26	Bataan	Limay	Lanaao River	3198	242310.6	1605778.4	21.3	1.96	79.9	0.044	-	1.5
27	Bataan	Mariveles	Amo River	3208	241360.6	1600481.8	19.9	1.83	73.4	0.041	-	0.7
28	Bataan	Mariveles	Pangalisan River	3212	240218.3	1599032.0	17.4	1.60	64.2	0.036	-	0.9

Note: \*\*Average population density in person per 90 m x 90 m grid (consider areas from basin outlet to 10 km upstream)

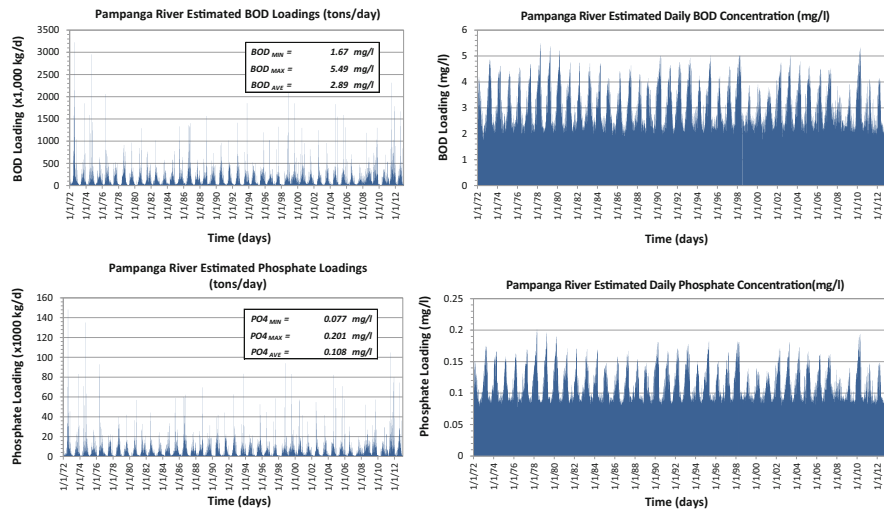


Fig. 7.21 Time series plots of derived BOD and phosphate loadings of Pampanga River

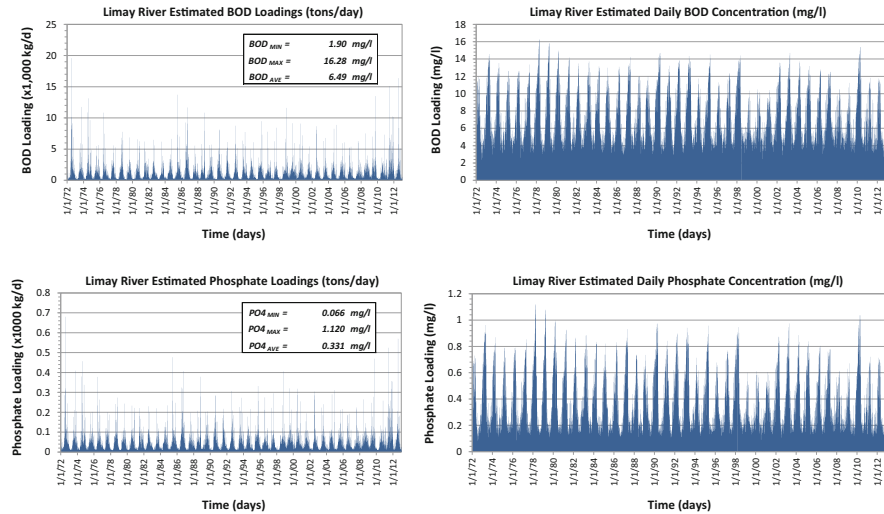
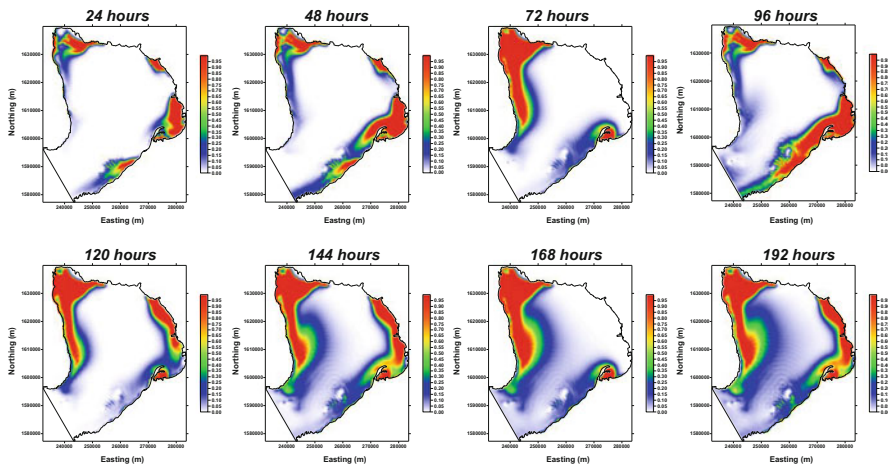


Fig. 7.22 Time series plots of derived BOD and phosphate loadings of Limay River

## 7.8 Other Water Quality Issues on Laguna Lake

Two issues, lake pollution and lake use zoning, which greatly affect water quality management of Laguna Lake for fishery sector are worth discussing here.



**Fig. 7.23** Simulated dissolved oxygen concentrations around Manila Bay using the derived BOD and phosphate loadings using the water quality model with components DO, BOD, and phosphate

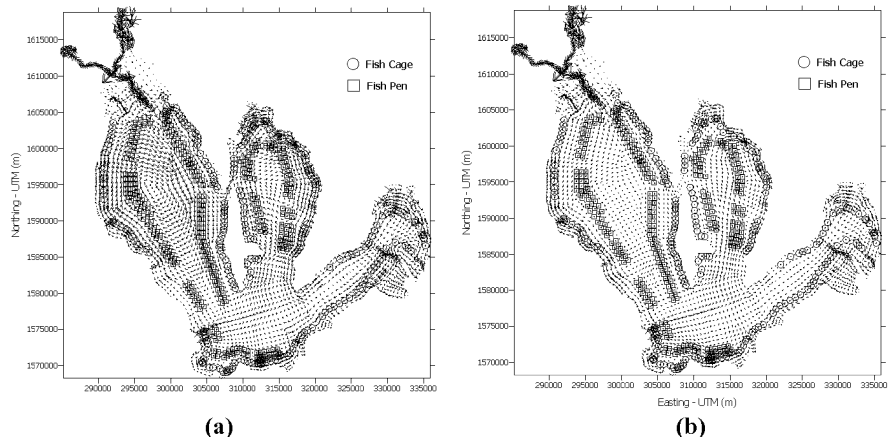


**Fig. 7.24** Typical vector plot of lake velocities (a) with spatially varying wind field and (b) with uniform wind field (taken from Tabios et al. 2000b)

### 7.8.1 Lake Pollution Control and Effects on Fisheries

All kinds of pollutants are dumped into the lake including heavy metals and toxic chemicals that disrupt the endocrine system. Catalan (2000) stated that there is an alarming amount of contaminated fish caught in the lake confirming reports from fishermen about tailless fish, fish that are blind or with crooked spine or skin cancer. There are also reports on the ill effects of pollutants on the people living around the

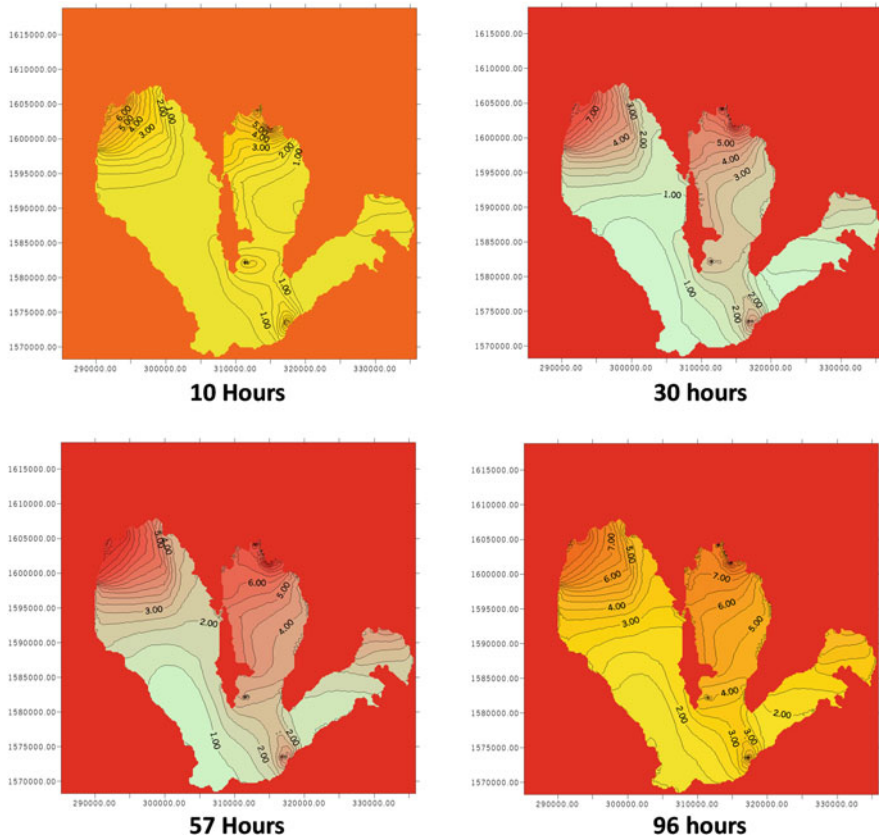


**Fig. 7.25** Salinity concentration around Laguna Lake 10, 30, 57, and 96 hours from start of simulation which is typical during the dry month of April when the freshwater inflows are low and the lake can have significant saline intrusion from Manila Bay

lakeshore and regularly consume fish caught in the lake who gave birth to babies with deformity and/or immune or mental deficiencies.

The degree of lake pollution from industrial effluents or domestic waste around the lake varies within the year due to the seasonality of dilution effects of freshwater inflows from watersheds around the lake, including rainfall. The lake is at its worst condition during the dry season when lake inflows and rainfall are low, thus reducing pollutant dilution. To properly manage and control lake pollution, the Laguna Lake Development Authority (LLDA) must constantly monitor lake water quality to be able to detect sources (including timing and spatial extent) of pollution. Only then can appropriate actions be taken against these polluters, if man-made through imposition of penalties or closure of pollution sources or if natural through proper treatment and rehabilitation.

### 7.8.2 *Optimal Lake Use Zoning*

Fisheries is a big industry in Laguna Lake. A major portion of the lake is devoted to fisheries, from commercial fish production with the use of fish pens and fish cage structures to individual, subsistence fishing. LLDA derives significant revenue from rental fees paid by owners of fish pens and fish cages for use of the lake. The question here is how much of the lake area should be allocated to commercial fish production and where to locate the fish pens/cages without affecting the water quality dynamics and health of the lake. In 1995, the total area of the lake covered with fish pens and cages was about 15,140 hectares (ha). In 1999, the area occupied by these fish structures was reduced to 11,160 ha (in which the fish pens occupied about 6160 ha, while fish cages occupied about 5000 ha) when a strong typhoon destroyed fish structures in 1997. During these two periods, the water quality in the lake in terms of the BOD (biochemical oxygen demand) was about 12.5 mg/l in 1996 and about 10.4 mg/l, an improvement, in 1999 (Catalan 2000). This indicates that there may be an optimal number of hectares in Laguna Lake to be devoted to commercial fish farming. The incident of fish kills in nearby Taal Lake may be didactic in this case. The fish kills were attributed to low levels of dissolved oxygen to sustain fish population.

Depletion of dissolved oxygen may have been caused by fish overcrowding or poor aeration of the water body. Poor aeration may have been due to limited water circulation. Thus, there must be some limit in either the number of fish population per unit area or the area for fisheries production that enhances lake circulation and ensures adequate water aeration. Perhaps, a better design for that would not affect lake circulation.

The optimal lake use zoning problem can be a very interesting problem that can best be solved with an interdisciplinary or transdisciplinary effort. The question of how much area and how many cropping seasons a year of fish production entails balancing of the economic objectives of fish pen/cages owners and the livelihood and subsistence of local fisherfolks without compromising ecological integrity and sustainability of the lake resource.

## References

- Blumberg AF, Mellor GL (1983) Diagnostic and prognostic numerical circulation of the South Atlantic Bight. *J Geophys Res* 88:4579–4592
- Blumberg, A.F. and G.L. Mellor. (1987) A description of a three-dimensional coastal ocean circulation model, Proceedings of three-dimensional coastal ocean models, Vol. 4, N. Heaps, pp. 208, American Geophysical Union, Washington, DC
- Catalan Z (2000) Laguna Lake – Biological Environments. In Proceedings of integrated Manila Bay/Laguna Lake and Surround Watershed Environment Study, Japan Society for the Promotion of Science, Nov. 23–24
- Mellor GL (2004) User's guide for a three-dimensional, primitive equation, numerical ocean model. Program in Atmospheric and Oceanic Sciences, Princeton University, Princeton, New Jersey, 56 p

- Nadaoka K, Yoshino T, Nihei Y (2000) Dual-sigma coordinate system for improvement of coastal ocean model. *J Hydraul, Coastal Environ Eng JSCE* 656/II-52:183–192
- NHRC (National Hydraulic Research Center) (2015) Development of analysis and modeling tools as part of decision-support system for managing the environmental quality of Manila Bay/Laguna Lake watershed system, report submitted to Manila Bay Coordinating Office (MBCO), Department of Environment and Natural Resources (DENR), Quezon City, December
- Qi C, Zhao DH, Tabios GQ III, Shen HW (1997) 2d Coupled Water Quality Model for Industrial Effluent Transport, ASCE Int'l. In: Water Resources conference, Tennessee, USA
- Smith LH, Cheng RL (1987) Tidal and tidally averaged circulation characteristics of Suisun Bay, California. *Water Resour Res* 23(1):143–155
- Tabios GQ III (2003) Modeling imperatives of Manila Bay/Laguna Lake system. In: Proceedings of symposium on environmental issues related to infrastructure development. Japan Society for the Promotion of Science-Philippine Department of Science and Technology, Makati City., August 8–9, pp 43–52
- Tabios GQ III, Shen HW, Zhao DH (1995) Analysis of salinity variations in the San Francisco Bay/Delta, paper presented at the HYDRA 2000. International Association for Hydraulic Research XXVI Congress, London., Sept, pp 11–15
- Tabios GQ III, Nadaoka K, Hanada G (2000a) Manila Bay/Laguna Lake linked ocean circulation/ lake hydraulic model, unpublished report submitted to the Core University program (1998–2008). Japan Society for the Promotion of Science (JSPS), Tokyo Institute of Technology, Tokyo, Japan
- Tabios GQ III, Nadaoka K, Kanda M (2000b) Laguna Lake 2d model with spatially and temporally varying wind stresses from an atmospheric model. In: Proceedings of 3rd regional symposium on infrastructure development in civil engineering, Tokyo, Japan, December, pp 253–262
- Tamura, H., K. Nadaoka, E. Paringit, F. Sirigan, G.Q. Tabios III, C. Villanoy, A. Blanco, J. Kubota and H. Yagi. (2003). Field survey on hydrodynamics and water quality in Manila Bay and Laguna Lake, *In* Proceedings of the symposium on environmental issues related to infrastructure development, Japan Society for the Promotion of Science (JSPS), Philippine Department of Science and Technology, Makati City., August 8–9, (pp. 81–94)
- USACE (U.S. Army Corps of Engineers) (2008) HEC-RAS: river analysis system, user's manual, version 4.0. Hydrologic Engineering Center, Davis, March
- Zhao DH, Shen HW, Lai JS, Tabios GQ III (1996a) Approximate Riemann Solvers in FVM for 2D hydraulic shock wave modeling. *J Hydraul Eng ASCE* 122(12):692–702

# Chapter 8

## Flood and Dam-Break Modeling Studies



**Abstract** This chapter presents four modeling studies as follows: (1) space-time, stochastic rainfall modeling to evaluate the effect of moving storm on flooding in the Pasac Delta, Pampanga, using an unsteady, channel network model; (2) flood modeling of Marikina River Basin during Typhoon Ketsana in September 2009; (3) assessment of alternative flood control mitigation plans for Cagayan de Oro River with 2-d flood hydraulic model; and (4) dam-break model studies of Butas Dam of Cavite Province with 2-d flow and sediment model. The Pasac Delta experiences severe and prolonged flooding annually, yet people continue to live there for fishpond farming and rice production. The Marikina River which joins the Pasig River before draining into Manila Bay is along the major cities of Metro Manila that experiences major floods, thus the importance of proper flood studies for its flood risk management. The Cagayan de Oro River Basin goes through Cagayan de Oro City, a major urban center in Mindanao, and its flood mitigation plan underwent revision after the devastating floods brought by Typhoon Washi in December 2011. Butas Dam when it broke in September 2006 was blamed for properties sliding into the river caused by river bank collapse due to deeply incised riverbed that propagated upstream of the dam.

### 8.1 Influence of Storm Rainfall Movement in Pasac Delta Flooding

The Pasac Delta in Pampanga, Philippines, regularly experiences severe and prolonged flooding, yet people endure and continue to live on the land due to the area's great potential for fishpond farming and rice production from where many get their livelihood. Pasac Delta is situated in an area that has been geologically formed by the deposition of sediment brought down from four major watersheds of Pasig-Potrero, Porac-Gumain, Abacan-San Fernando-Guagua, and Pampanga Rivers through several millennia of flood cycles. In the delta, slopes are very flat, and waterways are interconnected in a network, and it is affected by the fluctuating tide levels of Manila Bay resulting in complex flow interactions and reversals in flow direction in many channels. The 1991 eruption of Mt. Pinatubo had dramatically

increased the delivery of volcanic sediments into the delta. The resulting sediment deposition has altered the topographic landscape, clogged channels, and brought persistent flooding in many towns of Pampanga.

This section presents a study to investigate the influence of storm rainfall movement in the flooding of Pasac Delta. This work is contained in the paper by Tabios (2003a), and related works are in Tabios et al. (1986) and Tabios (2006, 2007a). In this study, a one-dimensional, unsteady flow, network model based on the St. Venant equations was used to describe the Pasac Delta hydraulics. Then various storm rainfall fields, stochastically generated using a Neyman-Scott process, space-time rainfall model at different speeds and directions, were imposed as rainfall input at the various sub-reaches in the flow network. For the different rainfall field generated, the Pasac Delta flooding levels in terms of velocities, discharges, and water stages were investigated.

One of the earliest studies recognizing the influence of storm movement on surface runoff was Maksimov (1964) who showed that the rainstorm movement altered peak discharge. Yen and Chow (1968) using laboratory simulators showed that storms moving in the same speed and direction of streamflow produce higher peaks and steeper limbs as opposed to storms moving upstream. Surkan (1974) likewise performed a simulation study on the effect of storm movement on streamflow using a distributed mathematical model calibrated for natural catchments in Nebraska. One of the highlights of Surkan's results is that both average and peak flows dramatically reach maximum levels when the velocity vector (i.e., both speed and direction) of the moving storm coincides with that of the average channel flow. This condition is called resonance effects such that the largest peak flows occur when the stream velocity vectors coincide with the storm kinematics. Niemczynowicz (1984) determined the influence of storm direction, intensity, velocity, and duration on the runoff hydrograph and peak discharge on a conceptual watershed and a real watershed in the City of Lund in Sweden. Analytical studies conducted by Singh (1997) show that a storm moving downstream produces a higher peak than a storm moving upstream. The time to peak is longer for downstream moving storms than for upstream moving storms. Likewise, of the storms moving downstream at different velocities, the storm moving at the velocity of flow produces the highest peak. Furthermore, the areal coverage – the extent and location of the watershed area covered by the storm – plays a critical role in flood generation.

### ***8.1.1 One-Dimensional, Unsteady Flow, Network Modeling of Pasac Delta***

The Pasac Delta consists of an intricate network of river channels over a flat, swampland. On the basis of the size and shape of river channels and the topography of the area, it is best to model the river system using a one-dimensional network model in contrast to a full two-dimensional model. As shown in Fig. 8.1, the Pasac

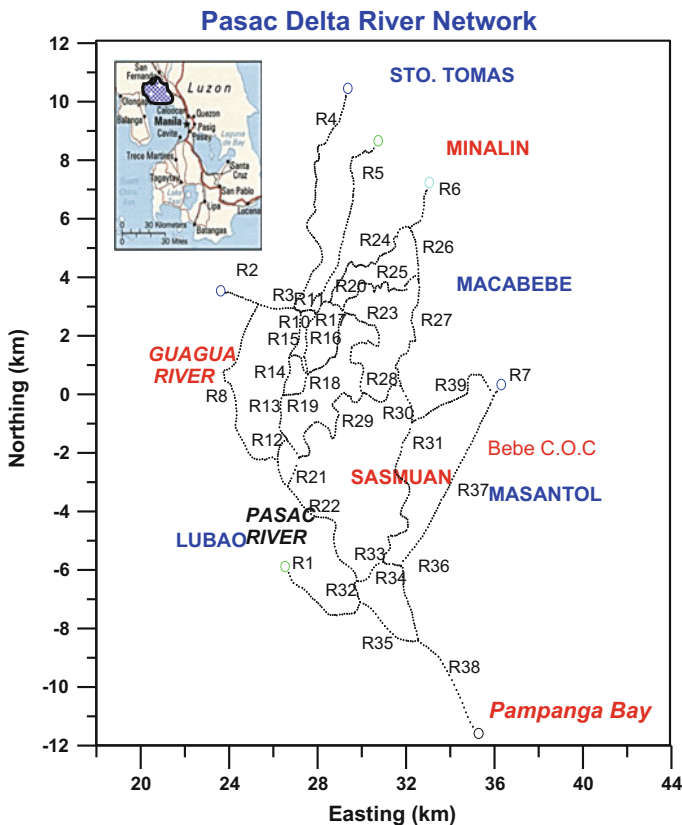


**Fig. 8.1** Pasac Delta network located northwest of Manila. [The river reaches are denoted by the letter R (e.g., R38 is reach 38).]

Delta consists of an intricate network of about 40 river channels over a flat swamp-land which is fed by 7 major rivers on the north and affected by the fluctuating tides of Manila Bay on the south resulting in complex flow interactions and reversals in flow directions in many channels.

For this purpose, the UNET model of the US Army Corps of Engineers (USACE 1995) was used. UNET is a one-dimensional, unsteady flow model through a network of open channels. The model is a quasi, two-dimensional model in that the network of channels is represented by interconnected one-dimensional channel reaches and each reach is composed of several cross sections with distinct main channel flow and floodplain area. Several external and internal boundary conditions can be specified in the model, including flow and stage hydrographs; gated and uncontrolled spillways; bridges, culvert, and levee systems; and off-channel storage and overbank storage areas.

The governing equations of the UNET model are the continuity equation and momentum equations. The continuity equation written for the channel and the floodplain are:

$$\frac{\partial Q_c}{\partial x_c} + \frac{\partial A_c}{\partial t} = q_f \quad (8.1)$$

$$\frac{\partial Q_f}{\partial x_f} + \frac{\partial A_f}{\partial t} + \frac{\partial S}{\partial t} = q_c + q_L \quad (8.2)$$

where  $x$  is the distance along the channel,  $t$  is for time,  $Q$  is flow,  $A$  is cross-sectional area,  $S$  is off-channel storage,  $q_L$  is lateral inflow per unit distance,  $q_c$  and  $q_f$  are the exchange of water between the channel and the floodplain, and the subscripts  $c$  and  $f$  refer to the channel and floodplain, respectively.

The momentum equations for the channel and for the floodplain are:

$$\frac{\partial Q_c}{\partial t} + \frac{\partial (V_c Q_c)}{\partial x_c} + gA_c \left( \frac{\partial z}{\partial x_c} + S_{fc} \right) = M_f \quad (8.3)$$

$$\frac{\partial Q_f}{\partial t} + \frac{\partial (V_f Q_f)}{\partial x_f} + gA_f \left( \frac{\partial z}{\partial x_f} + S_{ff} \right) = M_c \quad (8.4)$$

where  $M_c$  and  $M_f$  are the momentum flux per unit distance exchanged between the channel and floodplain, respectively.

The continuity and momentum equations above are nonlinear, and they are solved by an implicit finite difference scheme in UNET. To avoid stability and convergence problems in the numerical solution, the equations are linearized using the Preissmann technique as described by Liggett and Cunge (1975).

The major boundary conditions in the Pasac Delta flow model are (1) storm rainfall that falls directly into the channels; (2) inflows from contributing watersheds; and (3) downstream water stage due to tidal forcing from Pampanga Bay. In the flow model, the storm rainfall is added as a source term in the continuity equation. It is assumed that rainfall into the watersheds (contributing to Pasac Delta) do not reach the delta area within the 30 h simulation period conducted here so that storm rainfall-to-runoff from watersheds is not considered. Thus, the inflow discharge hydrographs based on a 3-year return period design hydrograph of the area (USACE 1994) is assumed not to vary with the prevailing storm rainfall event. At the downstream end of the network, namely, reach 38, a tidal water stage boundary condition is specified. The tidal water stages were taken equal to the tide data of North Harbor, Manila (NAMRIA 1995). An important model parameter that needs to be mentioned is the Manning's roughness coefficient. These roughness coefficients are taken equal to 0.025 in the main channels and 0.1 in the floodplains.

### 8.1.2 Stochastic, Space-Time Rainfall Modeling of Moving Storm

The storm rainfall is generated using the stochastic, space-time rainfall model based on Neyman-Scott process. This model was developed by Gupta and Waymire (1979) and subsequently improved by Waymire et al. (1984). In this model, the storm systems referred to as rainbands arrive as a Poisson process with mean parameter  $\lambda_M$ . The location of the rainband is relative to some fixed spatial origin at the ground with specified centroid [ $X_M$  and  $Y_M$  in rectangular coordinates]. A rainband contains a distinct number of cluster potential regions (CPR) and that the centroids of these CPR constitute a spatial Poisson process with parameter  $\rho_L$  relative to the fixed spatial origin of the rainband. Associated to each CPR are raincells that are randomly born in time and located relative to the centroid of the CPR. The number of raincells associated to a CPR is random variable  $\nu$  which is assigned a Poisson distribution with mean rate  $E[\nu]$ . Raincells within a moving rainband are born in time and space according to the probability density function:

$$f_{T,X,Y}(\tau, x, y) = f_T^1(\tau) f_X^2\{x - [x_c + u_x(\tau - t)]\} \cdot f_Y^2\{y - [y_c + u_Y(\tau - t)]\} \quad \text{for } \tau > t - \Delta c \quad (8.5)$$

where  $t$  is the time of arrival of the rainband,  $\tau$  is the time of birth of a raincell,  $(x, y)$  is the location of raincells at birth,  $(x_c, y_c)$  is the centroid of the CPR,  $(u_x, u_y)$  is the rainband velocity relative to the fixed spatial origin on the ground, and  $\Delta c$  is a specified mean raincell duration. In Eq. (8.5),  $f^1\{\cdot\}$  and  $f^2\{\cdot\}$  can take the following form:

$$f_T^1(\tau) = \beta e^{-\beta(\tau-t)} e^{-\beta\Delta c} \quad (8.6)$$

$$f_W^2(w) = \frac{1}{\sigma_w \sqrt{2\pi}} \exp\left[-\frac{w^2}{2\sigma_w^2}\right] \quad (8.7)$$

in which  $\beta$  is the cellular birth rate and  $\sigma_w$  is the cluster spread factor.

Associated to each raincell is its rainfall intensity from a cell of age  $\delta$  and at a radius  $r$  from the cell center assumed to be of the form:

$$i(\delta, r) = i_0 e^{-\alpha\delta} e^{-r^2/2D^2} \quad \text{for } \delta \geq 0 \text{ and } r = 0 \quad (8.8)$$

where  $i_0$  is the rainfall intensity at the cell center at the time of its birth,  $\alpha$  is an attenuation coefficient in time, and  $D$  is an attenuation coefficient in space. Eq. (8.8) takes rainfall intensity to be spatially symmetric around the cell center and its intensity exponentially decays in time.

To obtain the rainfall depth  $R_i(x_0, y_0)$  at some fixed time interval,  $(i - 1)\Delta T$  to  $i\Delta T$ , and at some point in the ground located at  $[x_0, y_0]$ , Eq. (8.8) can be integrated such that:

$$R_i(x_0, y_0) = i_0 \int_{(i-1)\Delta T}^{i\Delta T} e^{-\alpha\delta - r^2(\cdot)/2D^2} d\delta \quad (8.9)$$

in which:

$$\begin{aligned} r^2(\cdot) &= (x - x_0)^2(y - y_0)^2 + [2u_x(x - x_0) + 2u_y(y - y_0)]\delta \\ &\quad + (u_x^2 + u_y^2)\delta^2 \end{aligned} \quad (8.10)$$

The rainfall data used to estimate the parameters of the space-time model are daily rainfall from storms during the typhoon months of July, August and September in the Philippines. Storm rainfall data from 1984 to 1992 are available at five rainfall stations in the vicinity of Pasac Delta area. The parameters of the space-time rainfall model were estimated by method of moments except for the mean parameter  $\lambda_M$  of the rainband arrivals and the mean cell duration  $\Delta c$  which were estimated directly from the data. The Newton-Raphson nonlinear least squares method was used to solve the moment equations (Waymire et al. 1984), based on the station means, variances, and covariances between stations. Table 8.1 below shows the parameters of the space-time rainfall model.

For purposes of this study, four storm directions were investigated which are storms coming from (1) northeast, (2) east, (3) southeast, and (4) south directions. These were parameterized in the rainfall model through the spatial origin of the rainband as well as the storm speeds ( $u_x, u_y$ ). The effect of varying storm speeds was also investigated in this study for storm speeds of 10, 20, 30 and 40 kph (km/h). In all cases investigated here, the vertical and horizontal extent of rainbands was taken equal to 100 km thus representing a synoptic storm with spatial scale of about 10,000 km<sup>2</sup>.

**Table 8.1** Space-time rainfall model parameters for the Pasac Delta network

Parameter	Value
Mean rate of storm arrivals, $\lambda_M$	0.255 h <sup>-1</sup>
Mean number of CPR, $\rho_L$	0.4654 CPR/km <sup>2</sup>
Mean number of cell per CPR, $E[\nu]$	1.7844 cells/CPR
Cluster spread factor, $\sigma_x$ and $\sigma_y$	0.7278 km
Mean raincell birth rate, $\beta$	1.9569 h <sup>-1</sup>
Attenuation of rain lifespan, $\alpha$	1.5862 h <sup>-1</sup>
Attenuation of rain spatial extent, D	4.1902 km
Rain intensity, $i_0$	31.196 mm/h
Mean rainfall duration, $\Delta c$	0.7 h

### ***8.1.3 Results of Pasac Delta Flooding with Moving Storm***

Figures 8.2, 8.3, and 8.4 show the resulting water stages (m), velocities (m/s), and discharges ( $\text{m}^3/\text{s}$ ) for storms coming from the northeast, east, southeast, and south directions. These plots show that the storm from south direction resulted in highest water stages, velocities, and discharges, followed by the storm from northeast direction, then the storm from east direction. The storm from southeast direction resulted in the lowest values. An explanation for the higher water stages for the storm coming from the south is that flow from north (upstream) toward the south (downstream) was held up in the delta due to the faster rise in the water stage at the downstream end. For the storm coming from the northeast direction, the higher water stages may be partly explained as due to resonance effects which happen when the speed of storm approaches average channel velocities and storm direction is in the direction of effective channel flow orientation (Surkan 1974).

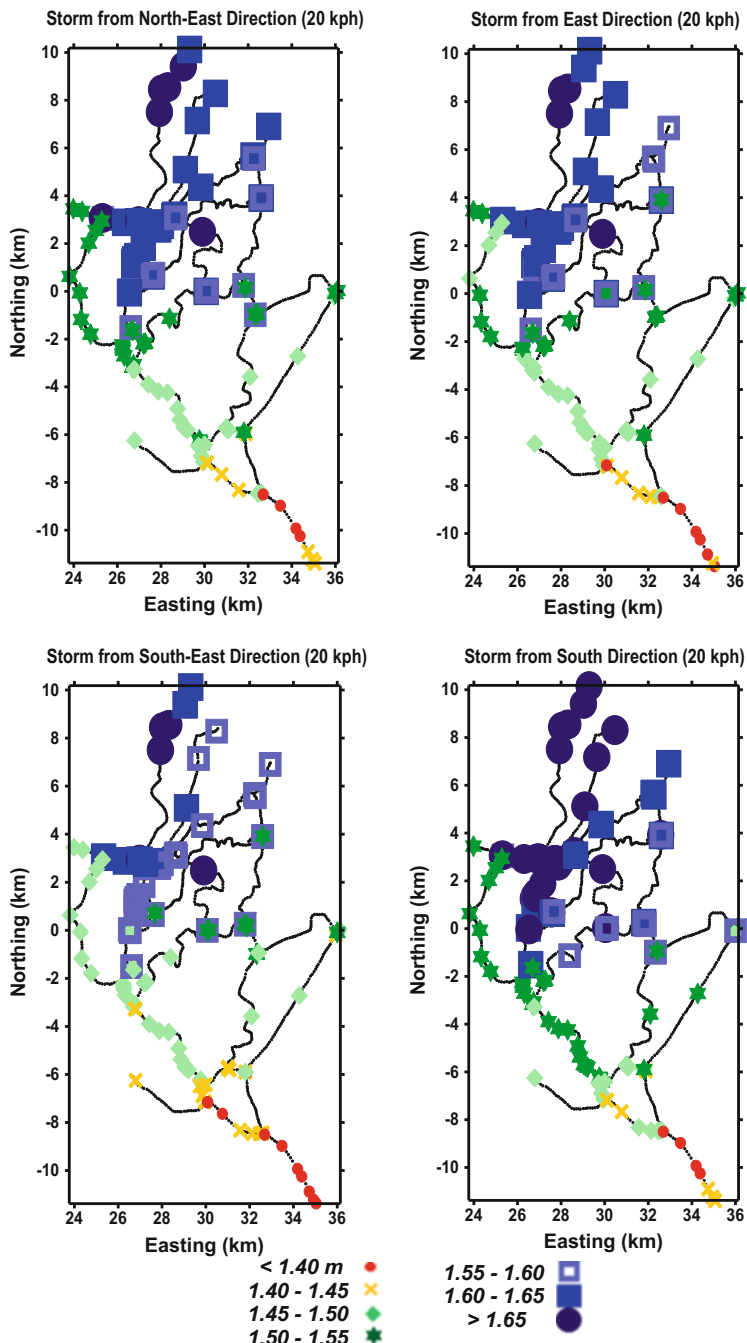
Figure 8.5 shows the resulting water stages for varying speeds of 10, 20, 30, and 40 kph (km/h) of the storm from south direction. The storm with the speed of 40 kph resulted in the highest stages. This is somewhat an anomaly since it is expected that a slow-moving storm can dump more rain in the area than a faster-moving storm.

Figure 8.6 shows the time series plots of water stages, velocities, and discharges at two selected river cross sections in the network. These cross sections were at the Guagua River (Reach 8, Sect. 3 km) and Pasac River (Reach 22, Sect. 3.4 km). The time series plots are only for storms coming from the northeast, east, and south directions. It is clearly shown here that the storm from south direction resulted in higher flow variables, followed by those from northeast storm and then those from east storm.

Finally, Fig. 8.7 shows the empirical cumulative distribution functions (CDF) of water stages, velocities, and discharges for the three storm directions (northeast, east, and south) and at the two selected cross sections (Guagua River and Pasac River). These empirical CDF were obtained from 50 traces of stochastically generated storm rainfall. It is seen that while the storm from south direction resulted in higher flow variables in general, the storm from east direction resulted in higher values at lower probability values.

### ***8.1.4 Brief Remarks on Pasac Delta Flooding with Moving Storm***

It is shown in this study that there are differences in flooding conditions in the Pasac Delta for the different directions and speeds of the storm rainfall movement. The results show that the dynamic characteristics of the storm such as its speed and direction are far too important to be neglected. Thus, in order to properly assess and evaluate alternative flood mitigation plans in the Pasac Delta, the influence of storm movement must be seriously considered. In general, it is still a common practice in flood estimation to use a design storm obtained from point rainfall values projected



**Fig. 8.2** Maximum water stages (m) resulting from storms coming from (1) northeast, (2) east, (3) southeast, and (4) south directions (all storms at speed of 20 kph)

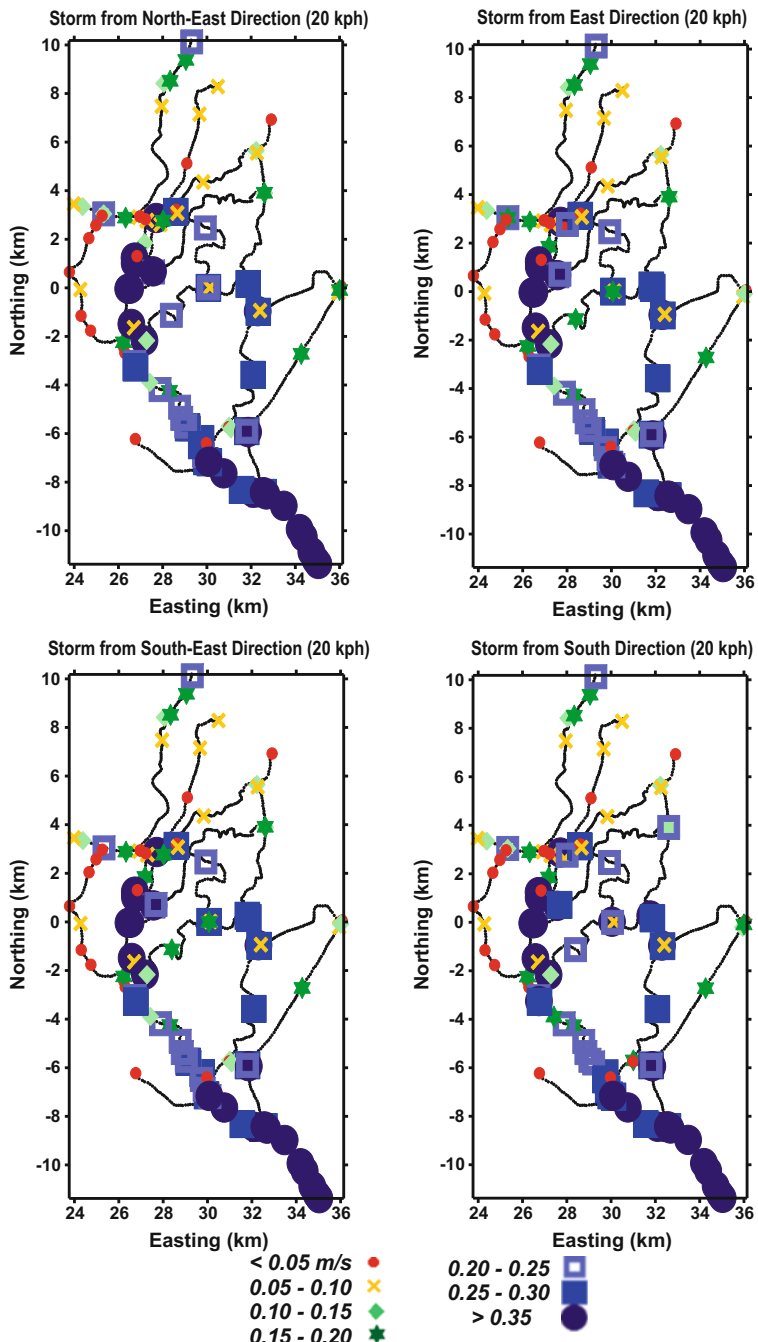


**Fig. 8.3** Maximum flow velocities (m/s) resulting from storms coming from (1) northeast, (2) east, (3) southeast, and (4) south directions (all storms at speed of 20 kph)

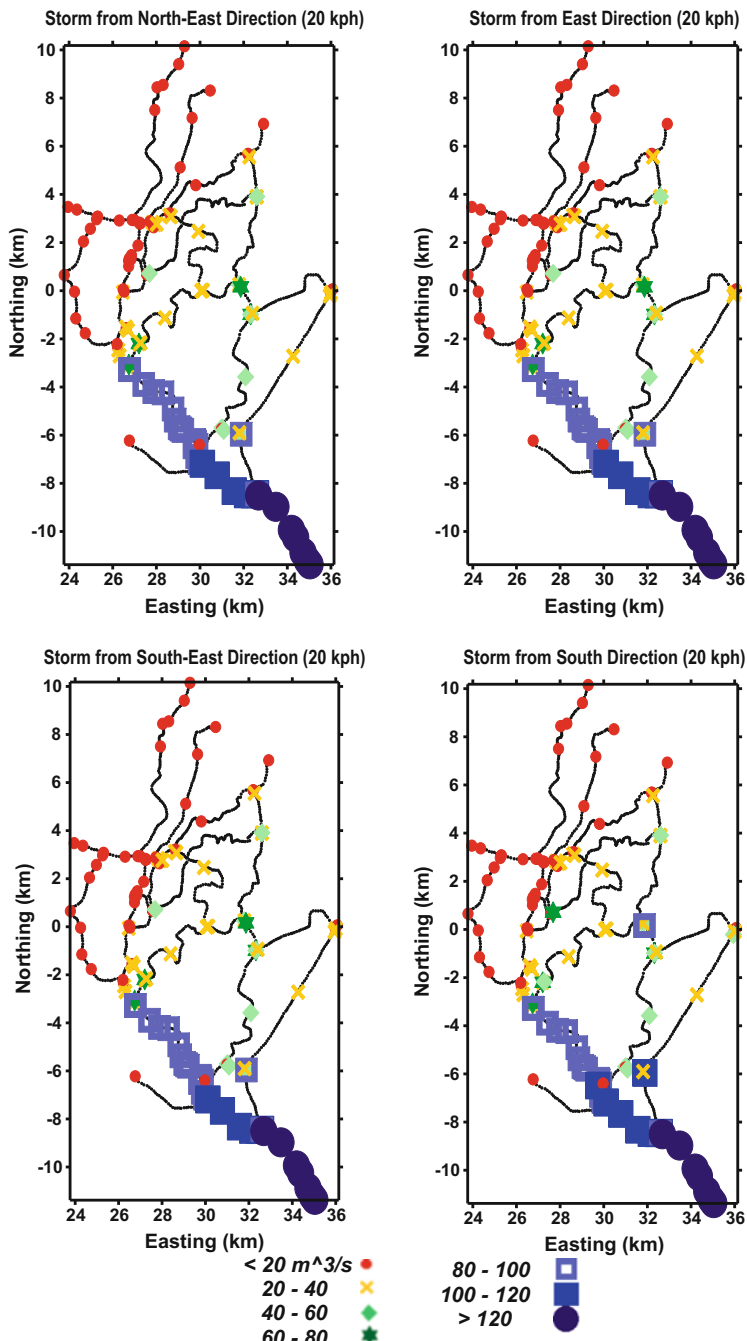


**Fig. 8.4** Maximum discharges ( $\text{m}^3/\text{s}$ ) resulting from storms coming from (1) northeast, (2) east, (3) southeast, and (4) south directions (storms at speed of 20 kph)

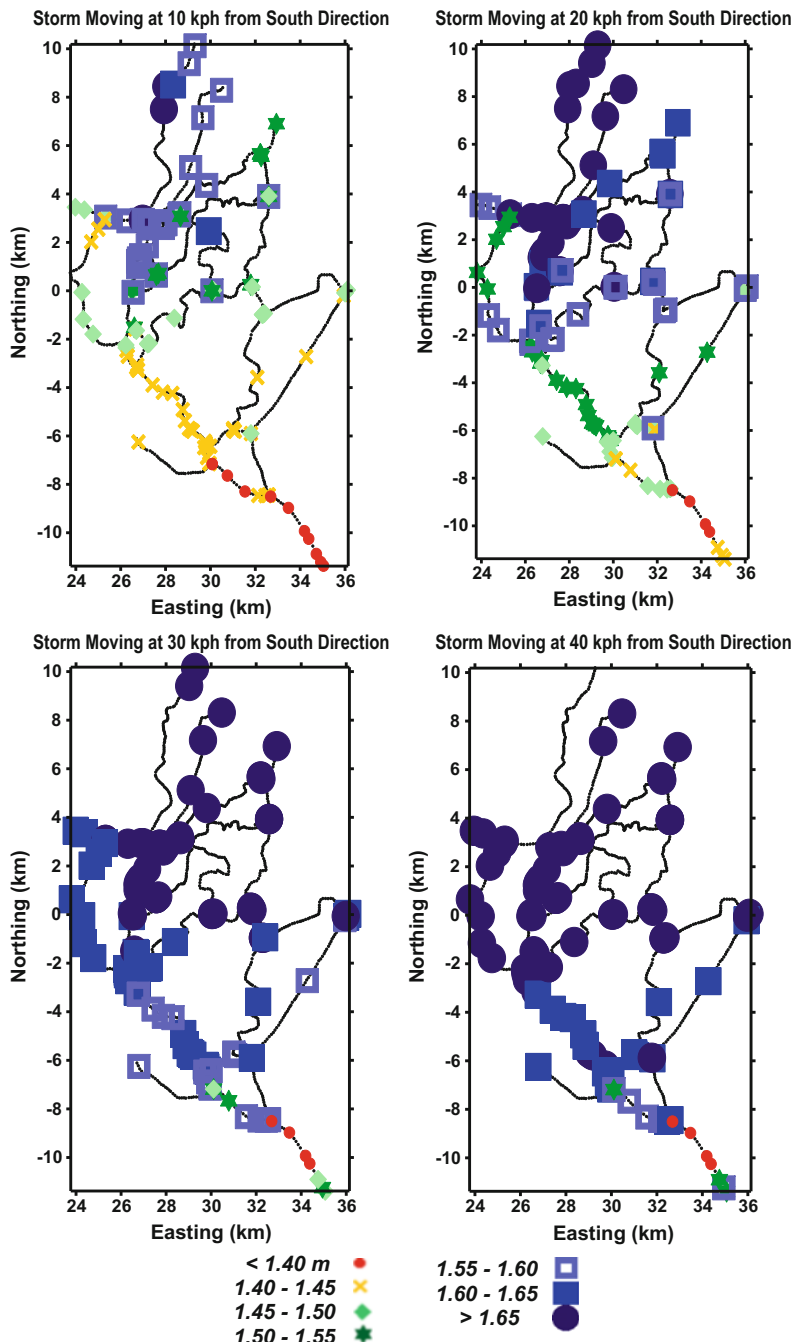


**Fig. 8.5** Maximum water surface elevations (m) resulting from storms coming from the south direction at speeds of (1) 10 kph, (2) 20 kph, (3) 30 kph, and (4) 40 kph

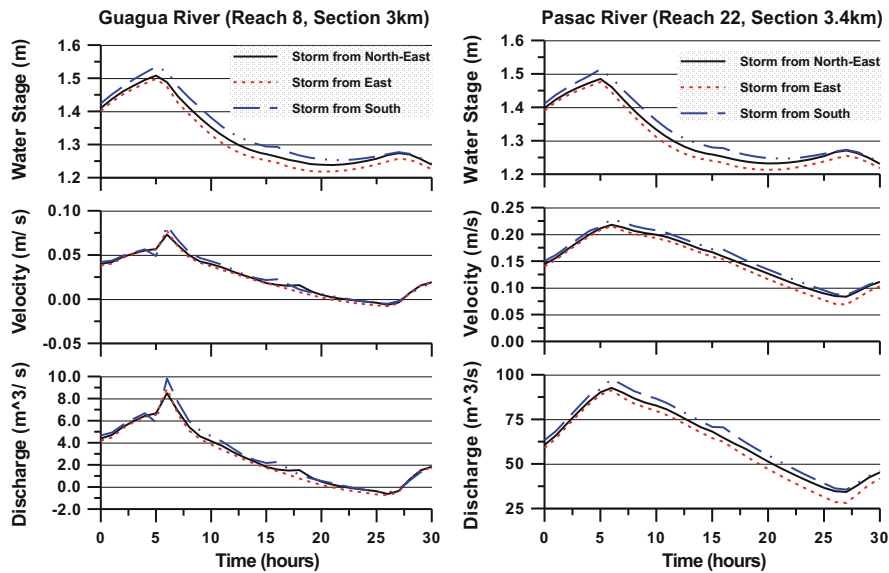


**Fig. 8.6** Time series plots of water stages (m), velocities (m/s), and discharges ( $\text{m}^3/\text{s}$ ) at Guagua River (Reach 8, Sect 3 km) and Pasac River (Reach 22, Sect 3.4 km) for storms coming from northeast, east, and south directions (all moving at 20 kph)

over an area and ignores the effect of storm movement. As seen in this study, it is highly suggested that flood studies should take into account the influence of storm direction as well as speed.

## 8.2 Flood Modeling of Marikina River Basin During Typhoon Ketsana in September 2009

Metro Manila has several highly urbanized river basins, and the Pasig-Marikina River Basin in particular is the major one that runs through a large portion of Metro Manila as shown in Fig. 8.8. The Marikina River Basin with a drainage area of 529 sq. km is located northeast of Metro Manila and joins the Pasig River. The Pasig River Basin is a highly urbanized river basin (with a drainage area of 702 sq. km.) and drains directly to Manila Bay. Nearby is the Laguna de Bay (Laguna Lake) Basin which is an extensive and urbanizing lake region southeast of Metro Manila. The total lake basin area is 3229 sq. km composed of 21 tributary sub-basins (2300 sq. km) and a lake area (929 sq. km). Laguna Lake is connected to the Pasig-Marikina River through the Napindan River and Manggahan Floodway (built in 1985) to serve as temporary storage of floodwaters from these two rivers. The flood-prone areas in Metro Manila including the Pasig-Marikina River Basin area are shown in Fig. 8.9.

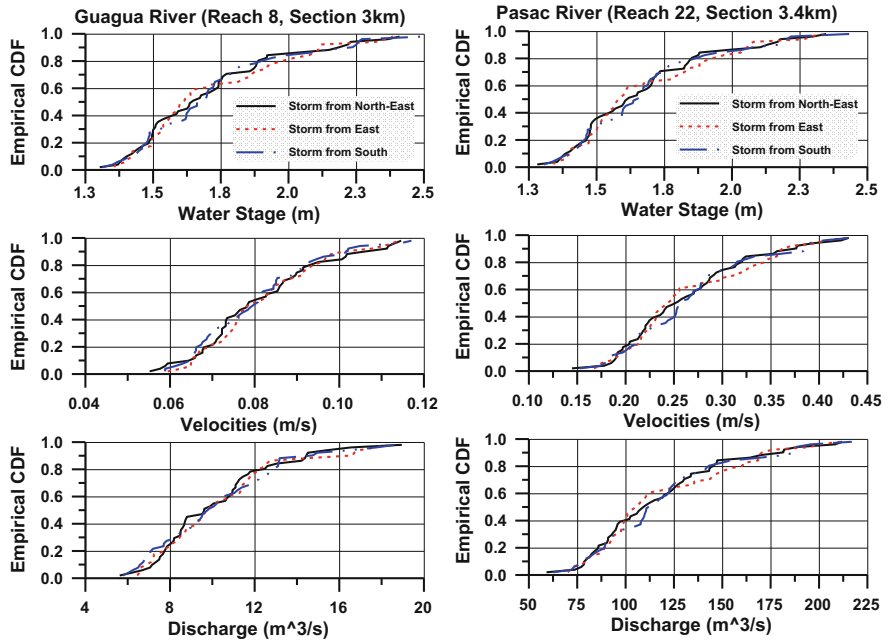


**Fig. 8.7** Empirical cumulative distribution functions (CDF) of water stages (m), velocities (m/s), and discharges ( $\text{m}^3/\text{s}$ ) at Guagua River (Reach 8, Sect 3 km) and Pasac River (Reach 22, Sect 3.4 km) based on 50 traces of stochastic generated storms coming from northeast, east, and south directions (all moving at 20 kph)

Metro Manila experiences severe flooding hazards due to meteorological events such as typhoons from the Pacific Ocean that occur between August to November or the southwest monsoons from the Indian Ocean around June to September. During Tropical Storm (TS) Ketsana on September 26, 2009, Metro Manila was severely flooded that time and again, necessitating reassessment of its flood management schemes and especially its major flood control infrastructure (Tabios 2015).

In particular, Tropical Storm (TS) Ketsana, locally called Typhoon Ondoy in the Philippines, went through the heart of Metro Manila on September 26, 2009. Figure 8.10 shows the typhoon path starting at 8 AM September 24 through 8 AM September 28. The eye of the typhoon went through Metro Manila around 8 AM in the morning of September 26 and quickly exited in about 4 h.

In the Metro Manila area and especially in the Marikina River Basin, there are several rainfall recording stations, and during TS Ketsana, the hourly time series of rainfall at five (5) stations from 8:00 h (8 AM) to 16:00 h (4 PM) are shown in Fig. 8.11. With these hourly point rainfalls, Fig. 8.12 shows the spatially interpolated hourly rainfall fields from 8 AM to 2 PM by multiquadric interpolation (Tabios and Salas 1985). At the Science Garden rainfall station, a total 350 mm of rainfall was recorded in 6 h that day.

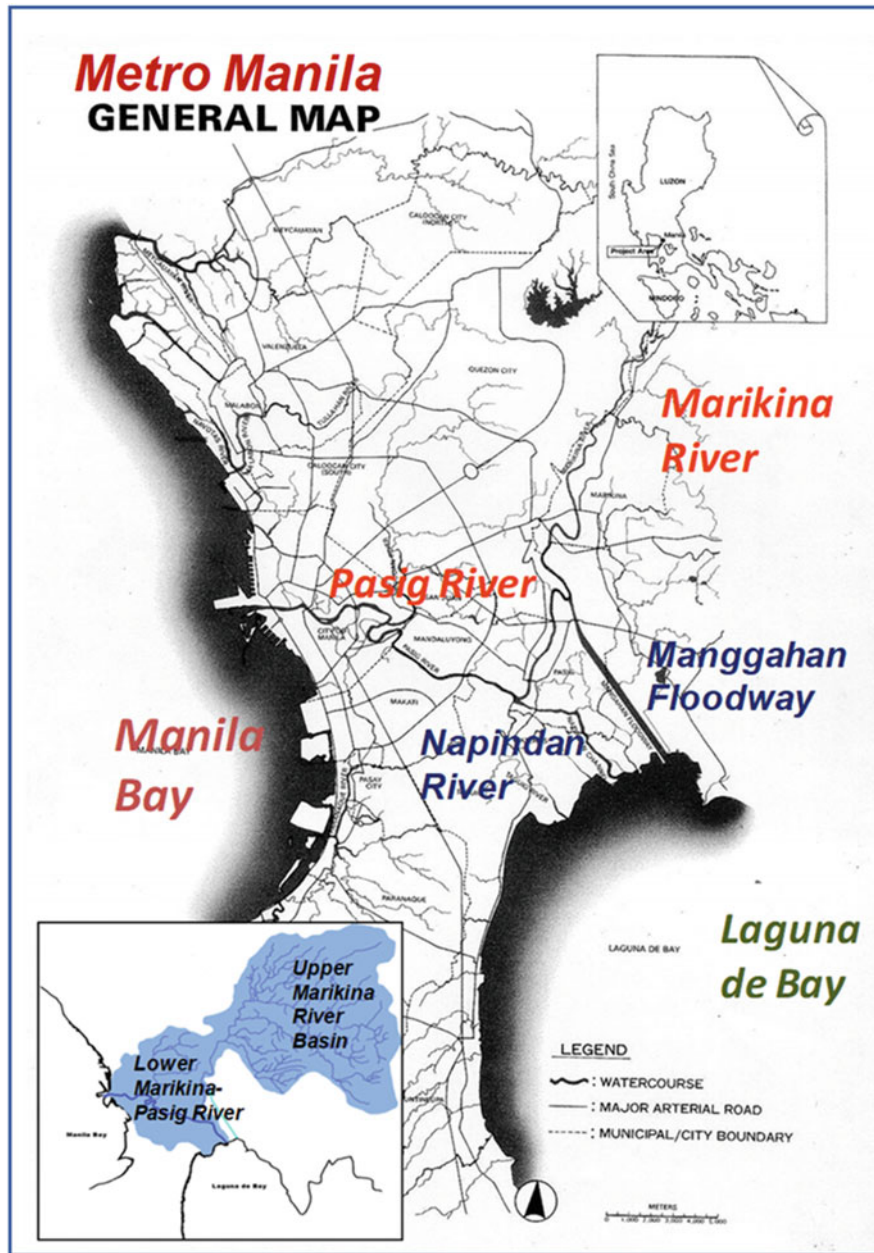


**Fig. 8.8** Map of Metro Manila showing Pasig-Marikina River system with Manggahan Floodway, Laguna de Bay (Laguna Lake), and Napindan River

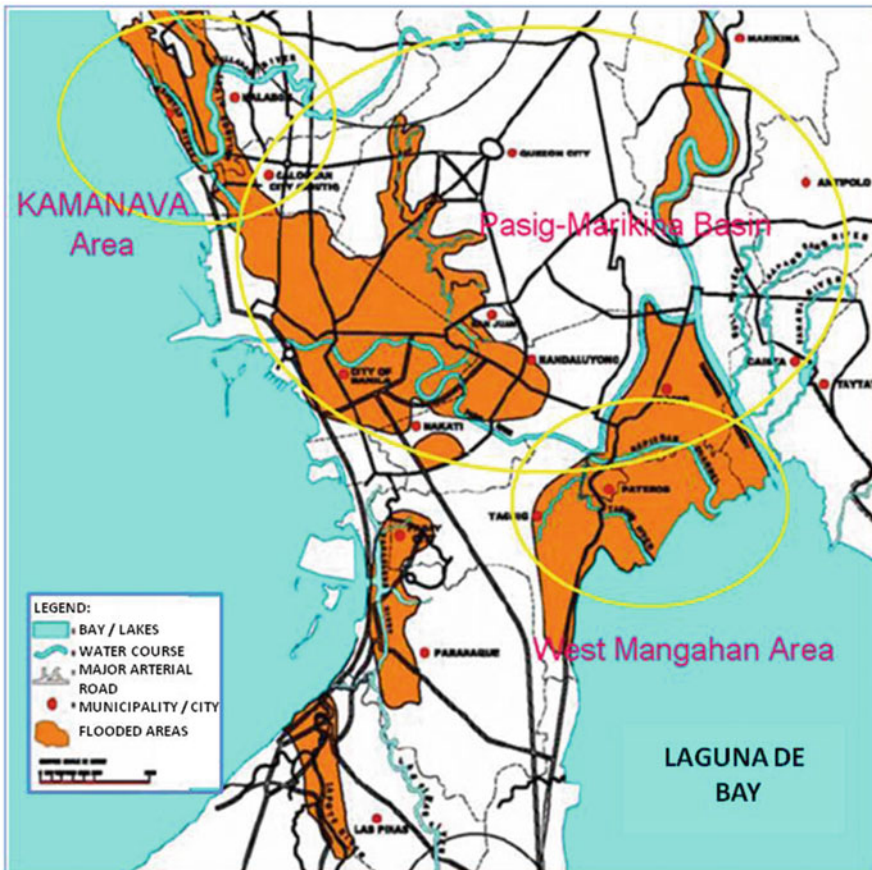


**Fig. 8.9** Major flood-prone areas in Metro Manila (JICA Report)

In Laguna Lake, several towns were flooded for over 3 or 4 months after this storm event because of the severely restricted Napindan channel outlet to efficiently evacuate the floodwaters from Marikina River that were temporarily stored in the lake into Manila Bay. Figure 8.13 shows Laguna Lake levels at its Angono station during TS Ketsana where Laguna Lake level rose in 1 day (on September 26) from about 12.7 m to 13.75 m and took over 3 months for the lake level to go down to around 12.5 m, the level when towns around the lake are free from floodings.

### 8.2.1 Pasig-Marikina River Basin Flood Calculations

For purposes of quantifying the extent of flooding in the Pasig-Marikina River during TS Ketsana, the unsteady flow, network hydraulic model HEC-RAS described in Sect. 8.1.1 was used here. Figure 8.14 shows the Pasig-Marikina

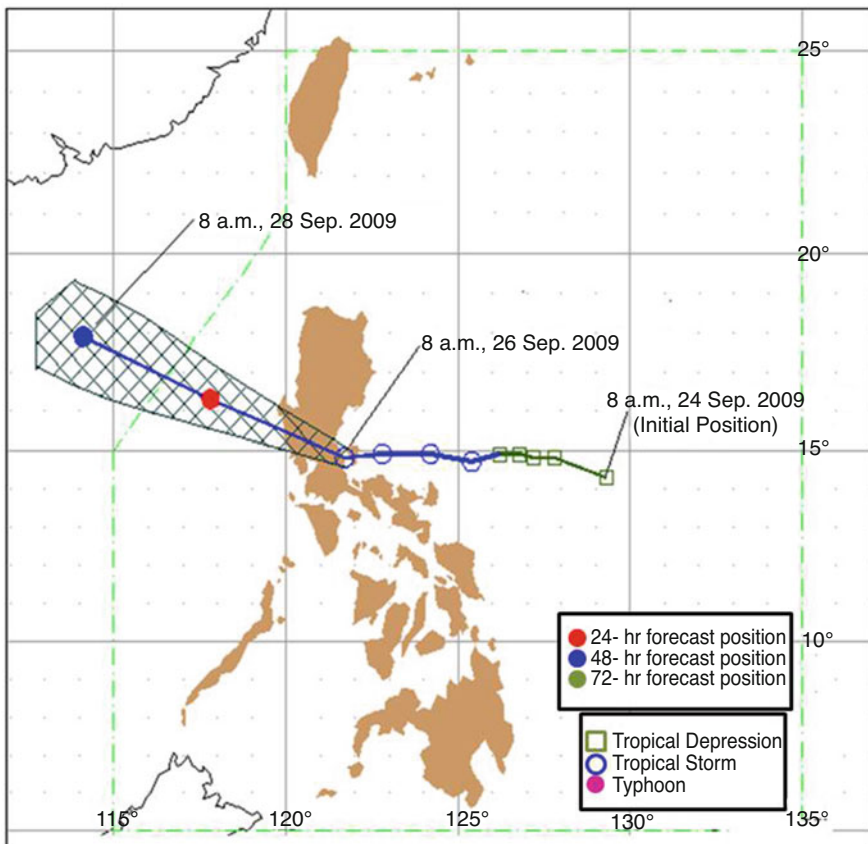


**Fig. 8.10** Path of Tropical Storm (TS) Ketsana (international name) locally called in the Philippines as Typhoon Ondoy passing through Metro Manila on September 26, 2009

River system where the flood calculation was done over the area covered by model geometry mesh (main channel and floodplain areas). The flood model geometry is composed of 312 cross sections to define the main river and floodplain channels. The watershed inflow as input to the flood model, which is mainly emanating from the Marikina River Basin, is calculated using the SWATC<sub>H</sub> watershed model. In Fig. 8.14, the Marikina River Basin is delineated into 127 sub-basins.

The SWATC<sub>H</sub> model is a physically based, continuous simulation watershed model. Originally developed by Morel-Seytoux and Alhassoun (1987) and likewise described in Morel-Seytoux et al. (1999). SWATC<sub>H</sub> models surface and subsurface flows in a soil-aquifer-stream system. The model components representing various hydrologic processes are rainfall, infiltration, excess rainfall, interception and retention storage, soil moisture storage in the root zone, evapotranspiration, interflow storage, interflow discharge, groundwater recharge flow, stream-aquifer return flow,

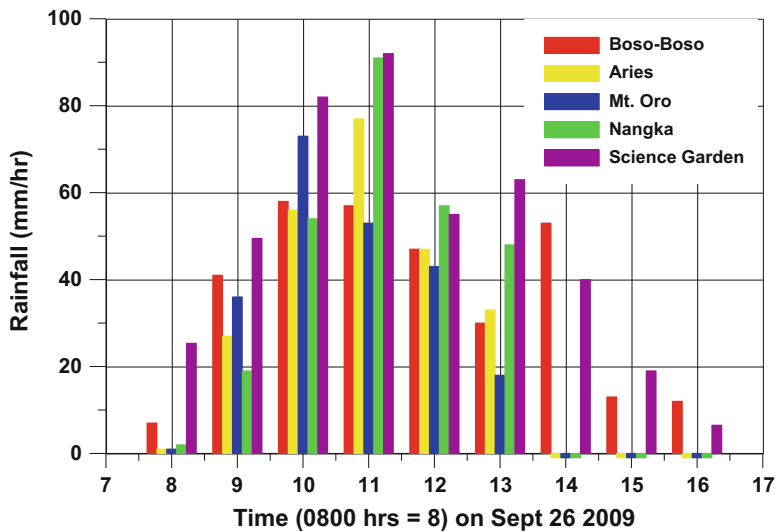


**Fig. 8.11** Hourly rainfall (mm/h) during TS Ketsana at five gaging stations around Marikina River Basin

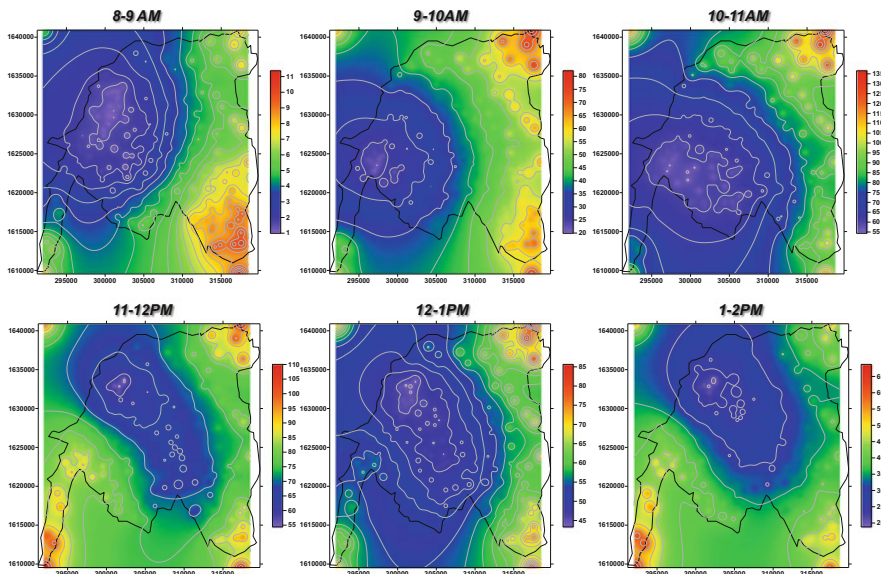


**Fig. 8.12** TS Ketsana's hourly rainfall fields (in mm) by multiquadric spatial interpolation from 8 AM to 2 PM on September 26, 2009

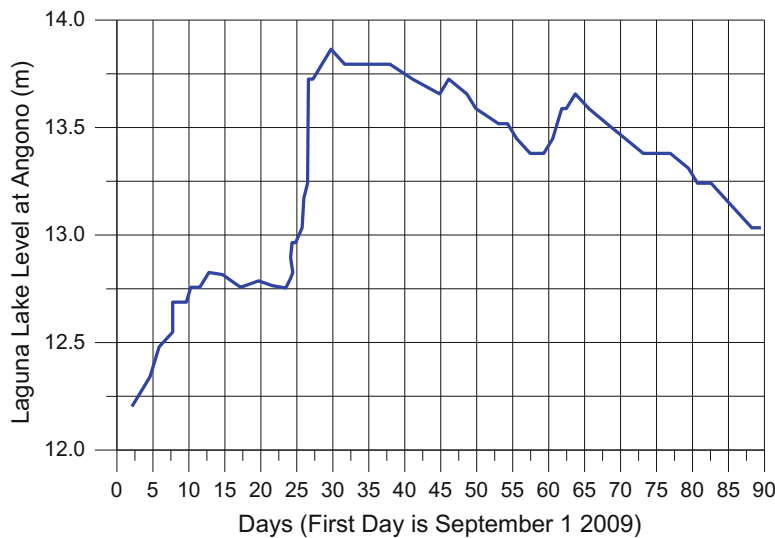


**Fig. 8.13** Laguna Lake levels at Angono station during TS Ketsana

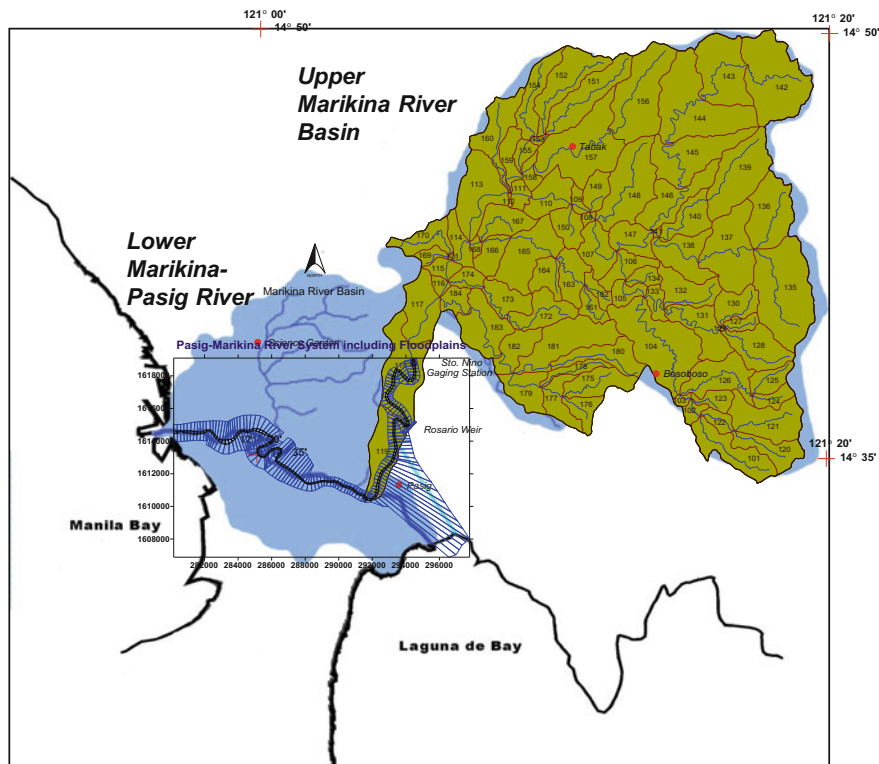


**Fig. 8.14** Pasig-Marikina River Basin with the unsteady flow, network model geometry (mesh area)

overland flow, and channel flow. Details of the SWATCH model components and hydrologic/hydraulic equations used are given in Appendix D.

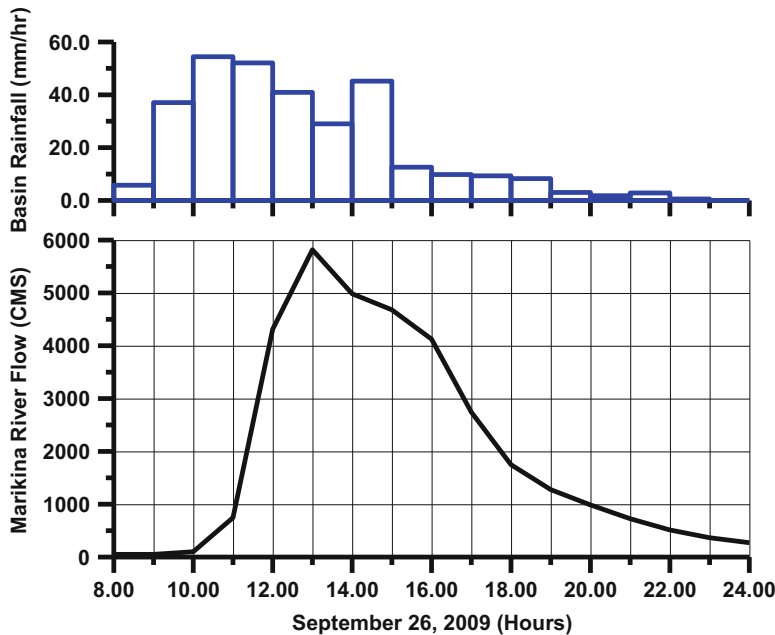
Given the rainfall fields on an hourly basis in Fig. 8.12, the flood hydrograph calculated from SWATCH model is shown in Fig. 8.15. Also shown in this figure is the average basin (composite) rainfall hyetograph during this period. As seen here, the peak inflow calculated was about  $5600 \text{ m}^3/\text{s}$ . With this inflowing flood hydrograph at Sto. Niño Bridge station, the Pasig-Marikina River flood model was run from 8 AM to 12 midnight on September 26, 2009.

Figure 8.16 shows the maximum river stages (elevations in m, DPWH datum) plotted along the alignment of the Pasig-Marikina River from Sto. Niño Bridge in Marikina City to its outflow in Manila Bay, a distance of about 34 km. These river stages are superposed on the left overbank and right overbank ground elevations looking downstream. In areas where the river stage was higher than overbank ground elevation, the river water spilled over the floodplain and also into the city's residential and commercial areas.

One validation of the computed flood stages is based on some pictures taken after the flood as shown in Fig. 8.17 at around SM Mall (km 31 in Fig. 8.16a) where flood heights above the overbank ground elevation reached as high as 8 m. The extent of flood inundation is also displayed in Fig. 8.18 which is the area between Marikina City and Pasig City near Rosario Weir (km 34 to km 27 in Fig. 8.16). Definitely, TS Ketsana has brought large-scale, massive flooding in these areas.

### ***8.2.2 Suggestions for Holistic Flood Management in Pasig-Marikina River System***

In the Pasig-Marikina River system, although meteorological events such as TS Ketsana can bring severe storms and floodings that the local drainage system could not handle, other factors could have worsened the flooding situation such as hydrological or river management factors and also human factors associated with urbanization (Tabios 2010, 2015). These other factors include reduction of river capacities because of sedimentation of soils eroded from forest denudation; dumping of solid waste in the river and encroachment of river banks especially by illegal settlers; poor land use planning or implementation of it that allow legal or illegal settlements in flood-prone areas; and obliteration of pervious areas due to urbanization thus virtually no opportunity for rainwater infiltration into the ground. Other factors include insufficient design level of protection of flood infrastructure, lack of maintenance of drainage system for de-clogging drains or desilting river channels, and fragmented and lack of coordination among flood agencies.



**Fig. 8.15** Marikina River Basin hourly flood hydrograph as upstream inflow ( $\text{m}^3/\text{s}$ ) of the Pasig-Marikina River flood model and associated average (composite) basin rainfall (mm/h) during TS Ketsana

As mentioned earlier, TS Ketsana on September 26, 2009, brought severe flooding in Metro Manila that time and, again, necessitated reassessment of its flood management schemes and especially its major flood control infrastructures. For the Pasig-Marikina River system, specific suggestions toward holistic flood management by a combination of structural and nonstructural measures are as follows.

### 8.2.2.1 Structural Measures

These include (1) retrofit flood infrastructure to provide a higher level of protection to people since flood control projects in Metro Manila or Pasig-Marikina River system in particular are designed based on 30-year or 40-year return period while the flood during TS Ketsana is associated to over a 100-year return period storm; (2) implementing proper local flood drainage design standards especially in housing subdivisions as some of them do not have an outlet to the main drainage systems; and (3) improving flood control plans with optimal combination of flood walls or dikes, small flood detention ponds, pumping stations, and sediment detention structures (especially in Upper Marikina River). But perhaps, an ultimate structural measure is to divert the floodwaters of Marikina River at a certain point upstream that covers

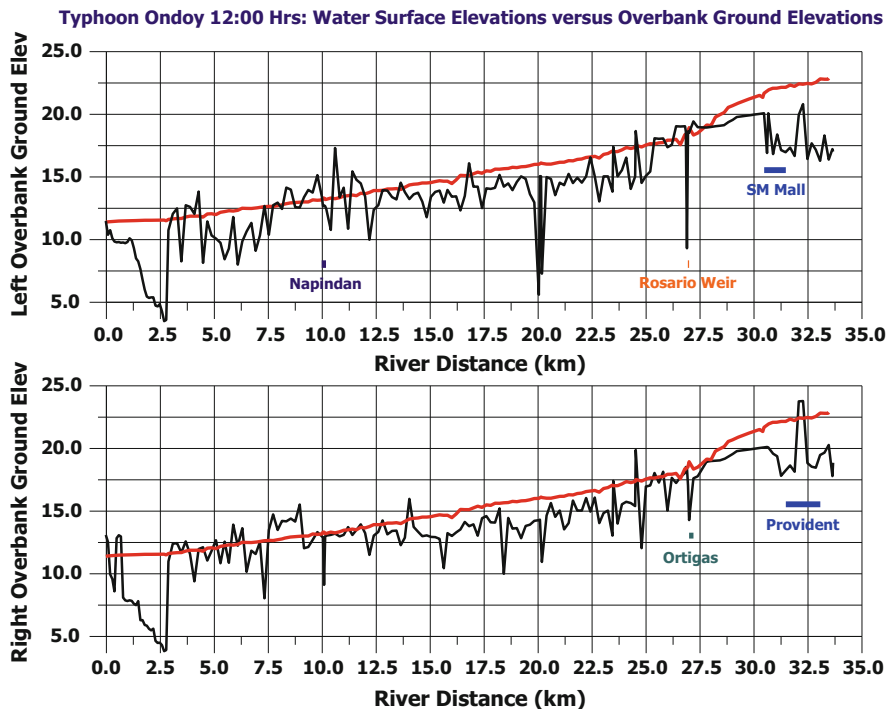


**Fig. 8.16** Maximum river stages (m) along the alignment Pasig-Marikina River from Sto. Niño Bridge (km 34) to Manila Bay (km 0) superposed on (a) left and (b) right river overbank ground elevations

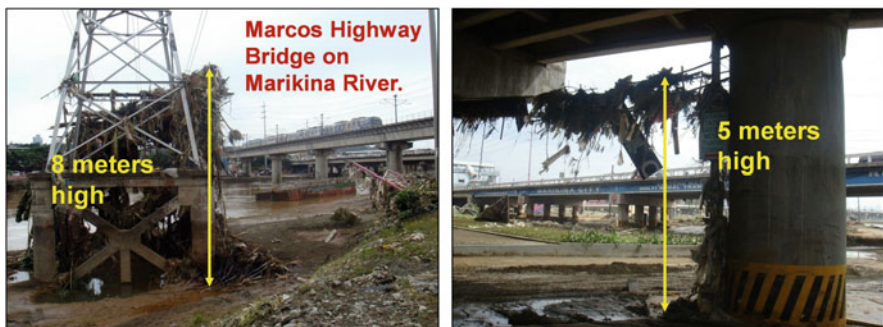


**Fig. 8.17** Pictures taken a day after the TS Ketsana at Marcos Highway Bridge near SM Mall (km 31 in Fig. 8.16) where flood heights above the overbank ground elevation reached as high as 8 m

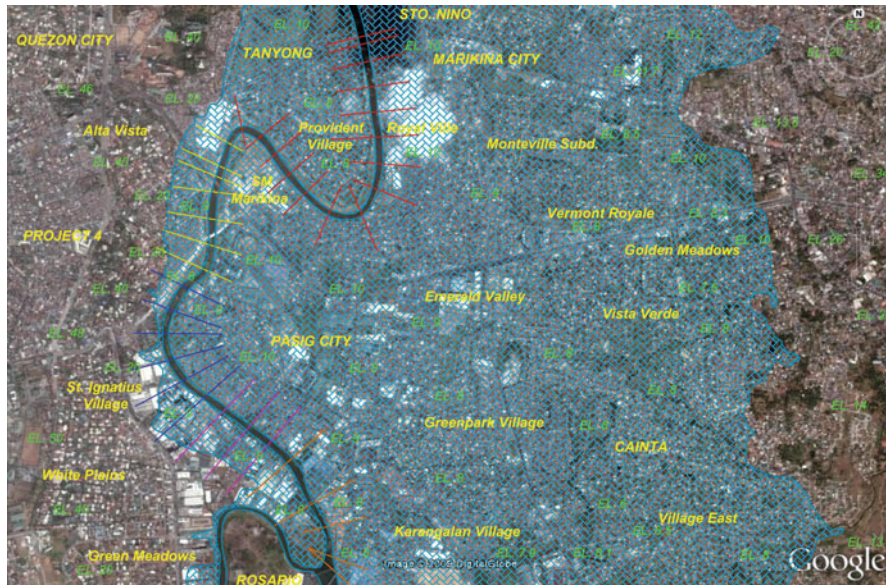


**Fig. 8.18** Flood inundation map along Marikina River between Marikina City and Pasig City near Rosario Weir (km 34 to km 27 in Fig. 8.16)

half of its drainage area of  $529 \text{ km}^2$  by building a tunnel through Sierra Madre mountain range into Agos River. Note that Marikina River is on the western slope of Sierra Madre and runs to Manila Bay while Agos River is on the eastern slope of Sierra Madre and runs to the Pacific Ocean.

### 8.2.2.2 Nonstructural Measures

These include (1) real-time rainfall prediction and flood forecasting system to provide early warning system and proper flood evacuation procedures; (2) flood studies that consider future land use changes especially due to urbanization, extreme events and fluctuations due to climate change, and river basin flow and sedimentation; and (3) proper land use planning and floodplain zoning to avoid residential or commercial developments in flood-prone areas and also construction of infrastructure in river floodplains.

### **8.3 Assessment of Alternative Flood Control Plans for Cagayan de Oro River**

In response to the devastation of the Cagayan de Oro River Basin brought about by Typhoon Washi (locally known as Typhoon Sendong) in December 2011, the Japan International Cooperation Agency (JICA [2014](#)) in March 2014 reviewed and updated a previous flood mitigation masterplan for Cagayan de Oro River Basin conducted in June 2011. However, this 2014 review of the flood mitigation plan was met with resistance from the people, particularly from land developers like the Paseo Del Rio (PDR) and Torre de Oro (TDO). At the time JICA was doing the review, PDR had ongoing commercial/residential project complex along the Cagayan de Oro River. In response to this, the Department of Public Works and Highways (DPWH) commissioned the National Hydraulic Research Center of the University of the Philippines (UP-NHRC) to conduct a review and value engineering study of the flood risk management project for Cagayan de Oro City. UP-NHRC served as a third party to provide an independent review of the flood mitigation plan. An important task of UP-NHRC was to engage the stakeholders that included land developers, PDR and TDO, City Mayor's Office, Mindanao Development Authority, and DPWH, among others, to meetings and consultations in order to inform and get their inputs.

UP-NHRC formulated alternative flood mitigation plans and conducted flood simulations based on the alternative flood plans. The results were presented to the stakeholders for comments on the performance of the alternative flood plans according to the objectives of the project and the stakeholders' concern. Agreements were reached to revise and further refine the proposed plans. Subsequently, flood simulations were redone and presented again in another round of public consultation until consensus was reached among proponents and stakeholders.

Presented here is the review and value engineering study of the Cagayan de Oro River masterplan by comparing the original flood mitigation plans and the alternative plans that were formulated in the course of this study by taking into consideration the issues and concerns raised by the stakeholders during public consultations. Then flood simulation studies were conducted to evaluate the performance of the alternative plans based on technical and economic criteria. Additionally, the flood design parameters were re-examined considering the recent typhoon data as well as the physical conditions in the Cagayan de Oro River Basin. This study was conducted by the author as principal investigator and reported in NHRC ([2016](#)) and also in the paper by Tabios ([2017](#)).

### ***8.3.1 Watershed and Flood Inundation Modeling of the Cagayan de Oro River Basin***

In the flood simulation studies to evaluate the alternative flood mitigation plans, the lower portion of Cagayan de Oro River Basin around the Cagayan de Oro City was modeled using a two-dimensional (2-d) flood inundation model with inflow flood hydrograph calculated from the watershed model of the entire Cagayan de Oro River Basin. In particular, the watershed model (with Sacramento soil-moisture accounting) was used which is described in Sect. 4.1, Chap. 4 (see also Appendix A), and the 2-d flood inundation model used is 2-d hydraulic model based on finite volume formulation described in Sect. 6.2.1, Chap. 6, with only the flow component (without sediment transport).

Figure 8.19 shows the Cagayan de Oro River Basin with a drainage area of 1370 km<sup>2</sup>. The headwaters of the Cagayan de Oro River is at Kalatungan mountain ranges in Bukidnon, southwest of the basin, and the river runs north and drains into Macajalar Bay in Cagayan de Oro City.

In the watershed model, the Cagayan de Oro River Basin is delineated into 68 sub-basins as shown in Fig. 8.20. From this, the topology of the river network, the overland flow planes, and channel geometry are determined to specify the input model geometry. An important data for this purpose is the topographic data as shown in Fig. 8.21. Likewise, to get the various model parameters such as interception, infiltration, and overland flow parameters, an important data is the land use and soil type. Figure 8.22 shows the land use/cover map of Cagayan de Oro River Basin.

The major data in this 2-d flood inundation model is the geometry data in finite element grid representation as shown in Fig. 8.23 which is composed of 6092 elements and 6158 nodes. With this model geometry data, the alternative flood mitigation plans or scenarios can be created and discussed in Sect. 8.3.3 below.

### ***8.3.2 Storm Rainfall and Computed Inflow Flood Hydrograph***

For purposes of the flood simulations conducted here, it was decided that the inflow flood hydrograph computed from the watershed model with rainfall hyetograph associated to Typhoon Washi (TS Washi) of December 16–17, 2011, from the JICA (2014) study should be used. However, for purposes of comparison and discussions, flood hydrographs associated to 10-year and 50-year return period, 24-h duration rainfalls at Lumbia Airport from its rainfall-intensity-duration curve (RIDF) were also used. The Lumbia Airport rainfall station is located about 10 km south of Cagayan de Oro City as indicated in Fig. 8.19.

During TS Washi, the total rainfall recorded at Lumbia Airport station was 179 mm from 8 AM December 16 to 8 AM on December 17, 2011 (i.e., meteorologic data of the Philippines), while the 6-h total rainfalls recorded at the height of the typhoon when it traversed Cagayan de Oro City were 72 mm from 8 PM to 2 AM

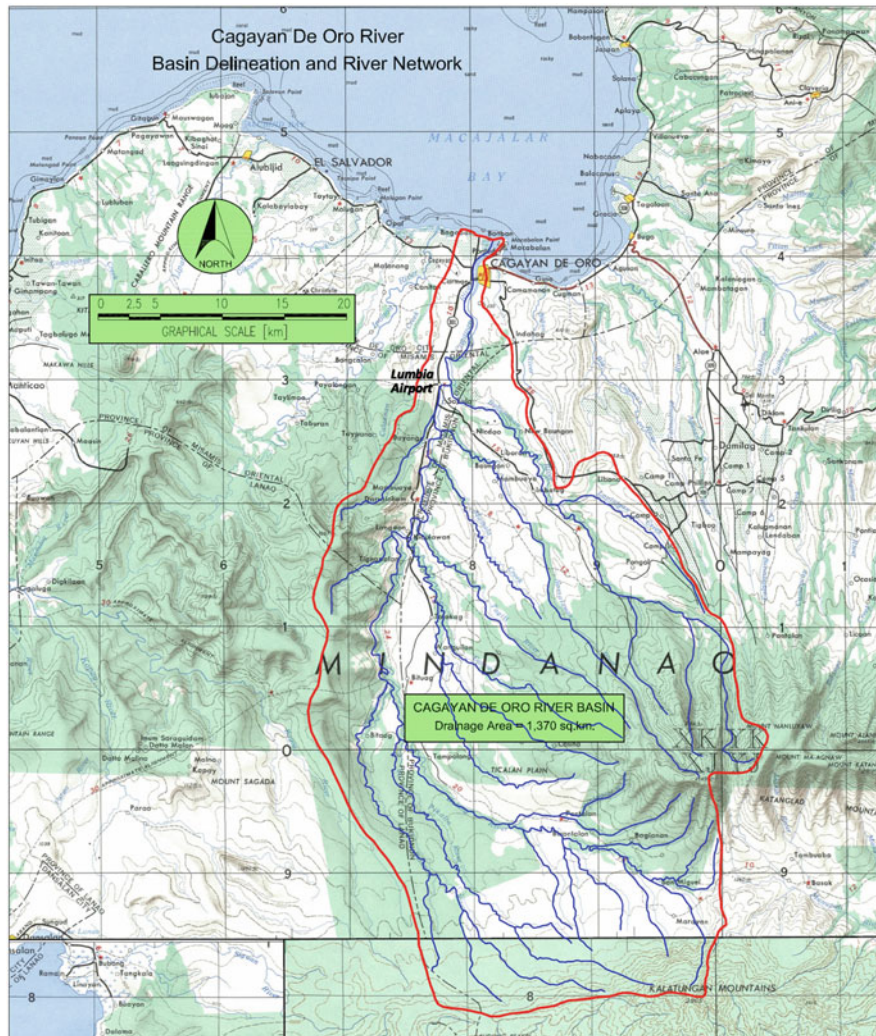


**Fig. 8.19** Watershed boundary and river network of the Cagayan de Oro River Basin

(starting December 16) and 97 mm from 2 AM to 8 AM (ending December 17). Referring to the rainfall total-duration-frequency curve in Table 8.2, the 24-h rainfall totals at Lumbia Airport were 156, 181.6, and 215 mm corresponding to the 10-year, 20-year, and 50-year, respectively, while the 6-h rainfall totals of 104.8 and 119.9 mm correspond to 5-year and 10-year return period storms, respectively. It shows here that the TS Washi rainfall with respect to Lumbia Airport station is associated to a 20-year return period storm for the 24-h rainfall total, while it is between 2-year and 5-year return period storm for the 6-h rainfall total.

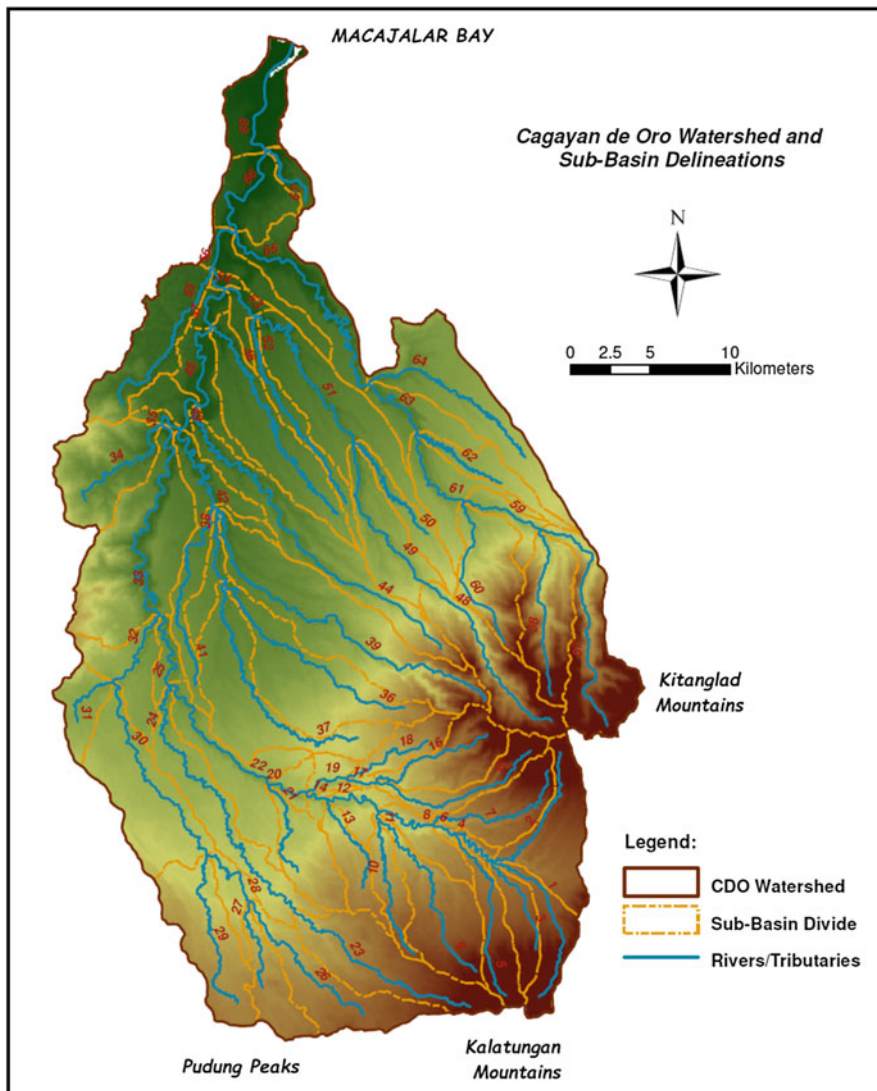


**Fig. 8.20** Cagayan de Oro River Basin delineation for a total of 68 sub-basins

In the JICA (2014) study, the 24-h rainfall total associated to TS Washi was only 130.9 mm as shown in Table 8.3. Since the flood simulation study presented here was commissioned by the Department of Public Works (DPWH) of the Philippines, it was decided that the same design storm rainfall from the JICA (2014) study should be used. In any case, a rationale for using this storm rainfall total of 130.9 mm considers the areal reduction factor based on guidelines by WMO (1982) where the 24-h point rainfall total (at a gaging station) is reduced by a factor of about 0.87 for a

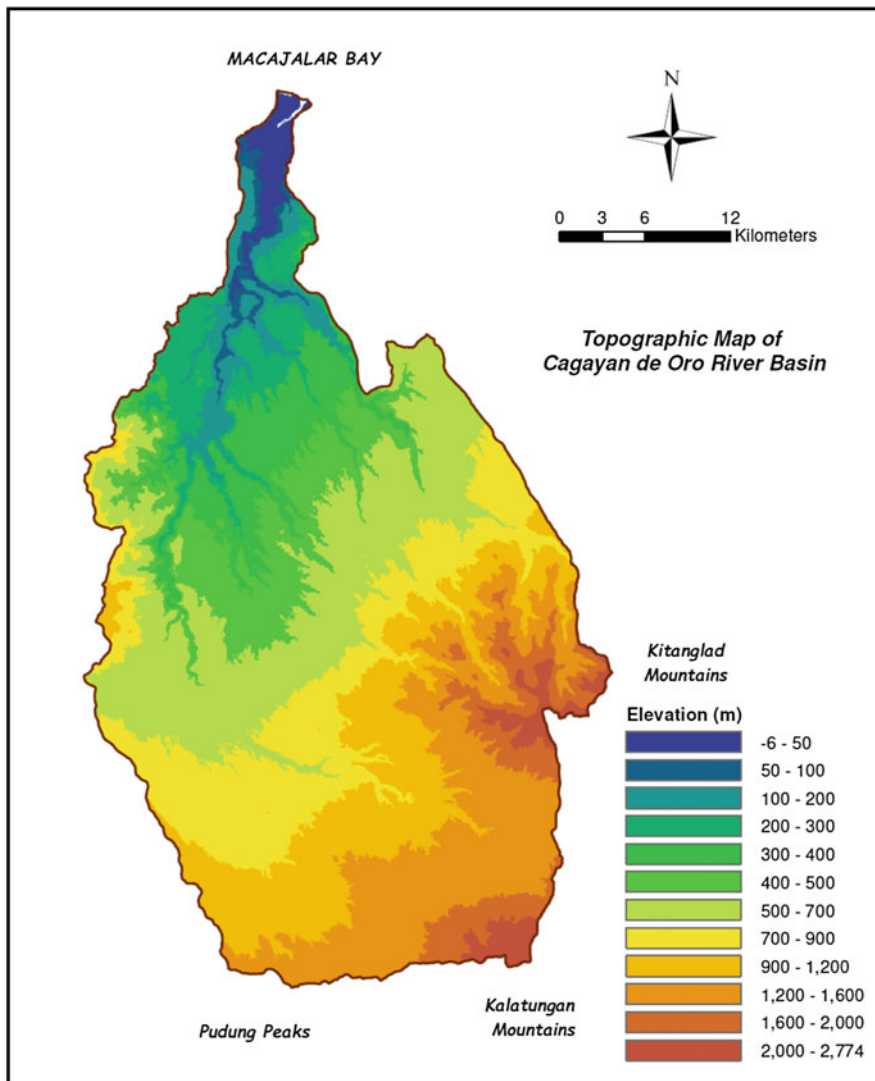
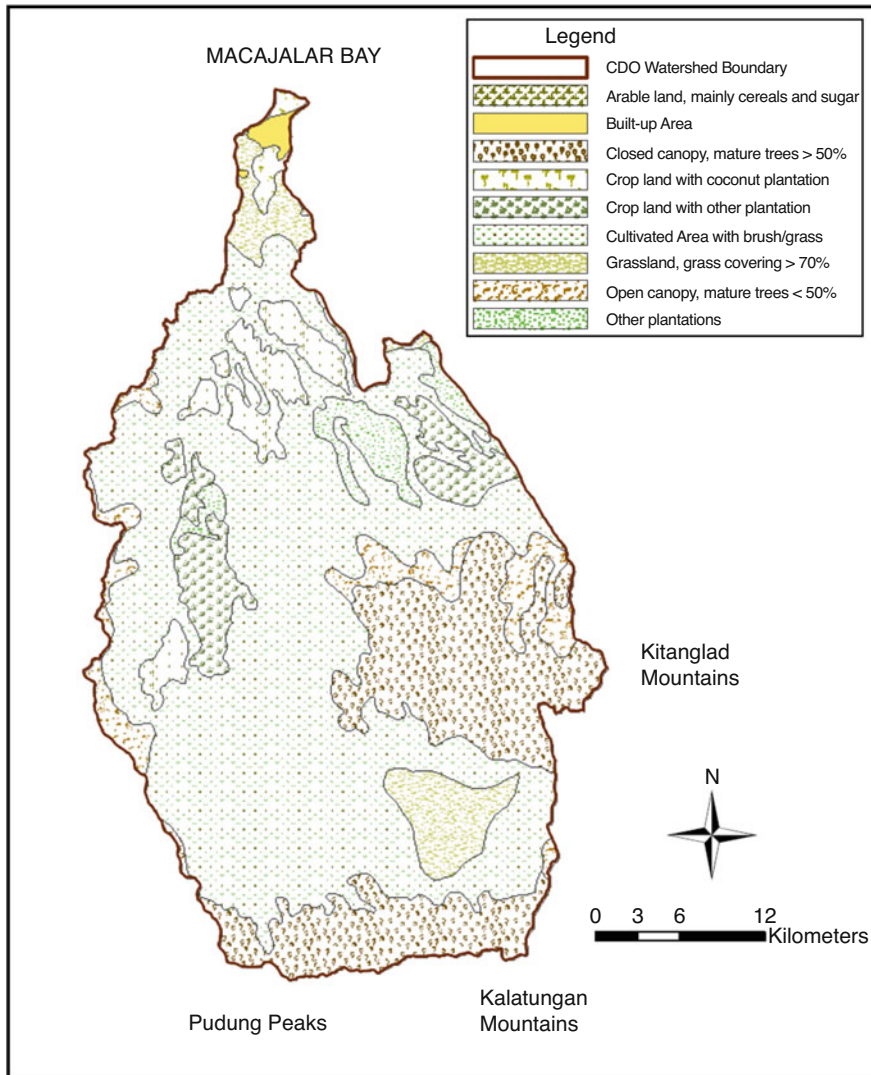


Fig. 8.21 Cagayan de Oro River Basin topographic map

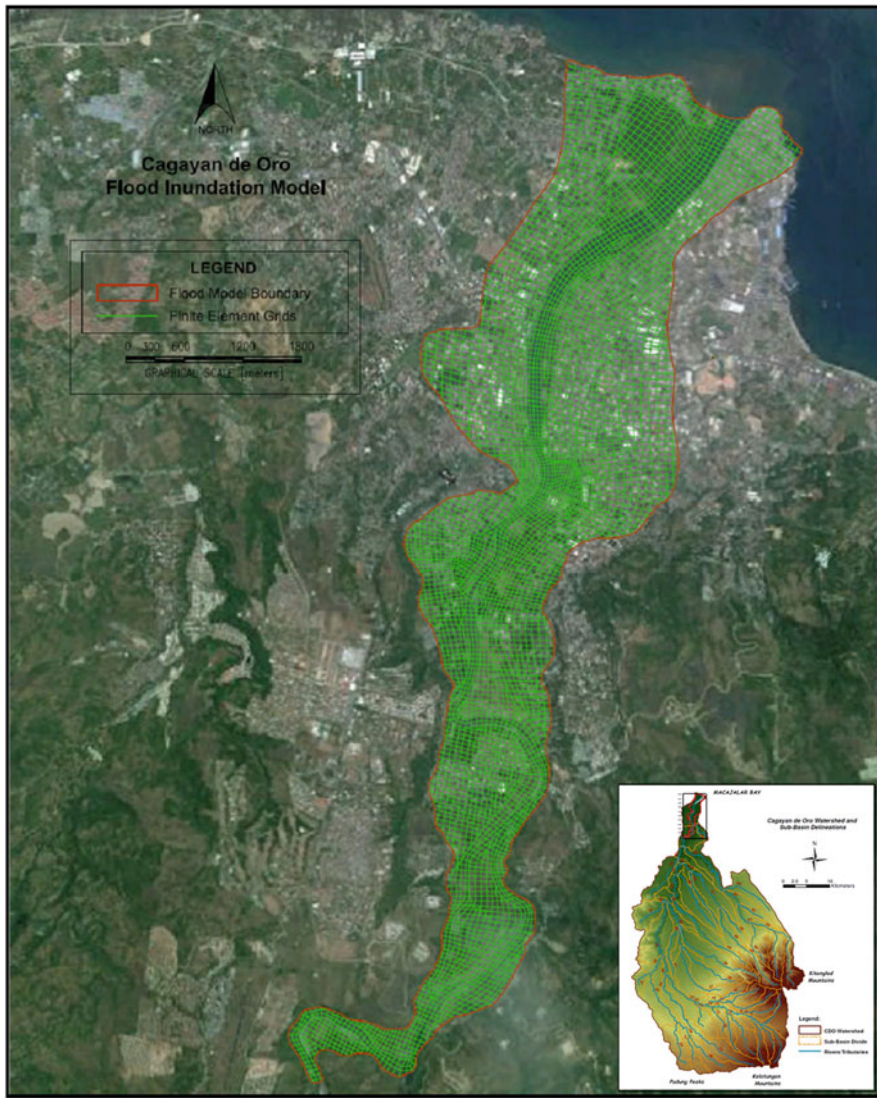
1000 km<sup>2</sup> basin when translated to basin rainfall. In this case, the 10-year return period rainfall total of 156 mm at Lumbia Airport is about 131 mm with the 0.87 areal reduction factor.

Table 8.3 shows the rainfall hyetograph of TS Washi (Typhoon Sendong) in the JICA (2014) study as well as the rainfall hyetographs of the 10-year and 50-year return period, 24-h rainfall totals at Lumbia Airport derived with the same time distribution of the JICA (2014) rainfall hyetograph. Note that in this table, hour



**Fig. 8.22** Land use/cover map of Cagayan de Oro River Basin

(time) 1 corresponds to 8 AM–9 AM of December 16, 2011, so that the peak rainfall occurred around hour 16 which was about 12 AM–1 AM of December 17, 2011. With this rainfall hyetographs, the corresponding inflow flood hydrographs at the location slightly upstream of Pelaez Bridge as well as those at the outlet of Sub-basin 67 were calculated using the watershed model presented here. Also included was the inflow flood hydrograph computed in the JICA (2014) study. It may be noted that the peak flow of Cagayan de Oro River at Pelaez Bridge computed in the JICA (2014)



**Fig. 8.23** Finite element grid representation composed of 6092 elements and 6158 nodes of the 2-d flood inundation model covering the lower portion of Cagayan de Oro River Basin. Shown in the inset is the location of the 2-d model geometry relative to the river basin

study was  $4924 \text{ m}^3/\text{s}$  in contrast to the peak flow of  $5715 \text{ m}^3/\text{s}$  computed from the watershed model here using the rainfall hyetograph from the JICA (2014) study.

The  $4924 \text{ m}^3/\text{s}$  peak flow in the JICA (2014) study may be qualified or justified based on the Rational Equation where peak flow  $Q_{\text{peak}} = \text{CIA}$  in which the runoff coefficient C is taken equal to 0.255, rainfall intensity I = 52 mm (see Table 8.3) and

**Table 8.2** Rainfall-duration-frequency Curve Lumbia Airport based on 26 years of data from PAGASA. Note: rainfall total (mm), duration (mins or h), and frequency or return period T (years)

T (yrs)	10 min	20 min	30 min	1 h	2 h	3 h	6 h	12 h	24 h
<b>2</b>	22.3	32.5	42.0	56.6	68.1	74.1	82.1	85.1	88.8
<b>5</b>	27.1	39.9	52.7	74.0	91.5	96.5	104.8	110.4	129.2
<b>10</b>	30.2	44.9	59.8	85.4	107.1	111.4	119.9	127.1	156.0
<b>15</b>	32.0	47.6	63.8	91.9	115.8	119.7	128.4	136.5	171.1
<b>20</b>	33.3	49.6	66.6	96.4	122.0	125.6	134.4	143.1	181.6
<b>25</b>	34.2	51.1	68.7	99.9	126.7	130.1	139.0	148.2	189.8
<b>50</b>	37.2	55.7	75.4	110.7	141.3	144.0	153.1	163.9	214.8
<b>100</b>	40.2	60.3	82.0	121.3	155.7	157.8	167.2	179.4	239.7

**Table 8.3** Rainfall hyetographs (mm) corresponding inflow flood hydrographs ( $\text{m}^3/\text{s}$ ). The peak rainfall and peak runoff are highlighted below, and the time 1 corresponds to 8 AM–9 AM, December 16, 2011

Time (hr)	JICA Sendong Rainfall (24-hr total = 130.9 mm)	10-Yr Rainfall from Lumbia RIDF (24-hr total = 156 mm)	50-Yr Rainfall from Lumbia RIDF (24-hr total = 215 mm)	JICA Sendong Flood Hydrograph at Pelaez Bridge	Derived JICA Sendong Hydrograph at Subbasin 67	Inflow Flood Hydrograph near Pelaez Bridge from Watershed Model			Inflow Flood Hydrograph at Subbasin 67 from Watershed Model		
						JICA Sendong Rainfall	10-yr Lumbia Rainfall	50-yr Lumbia Rainfall	JICA Sendong Rainfall	10-yr Lumbia Rainfall	50-yr Lumbia Rainfall
1	0.59	0.48	0.64	131.73	0.64	106.97	107.15	107.63	0.42	0.42	0.42
2	0.39	0.46	0.64	131.73	0.64	115.97	116.21	116.84	1.12	1.13	1.16
3	0.39	0.46	0.64	131.73	0.64	140.03	140.46	141.68	1.42	1.45	1.54
4	0.39	0.46	0.64	131.73	0.64	182.76	183.67	186.26	1.45	1.50	1.63
5	0.39	0.46	0.64	131.74	0.64	232.70	234.47	239.55	1.45	1.51	1.66
6	0.39	0.46	0.64	131.75	0.64	273.19	276.21	284.96	1.43	1.50	1.66
7	0.82	0.98	1.35	131.82	0.64	298.71	303.32	316.63	1.40	1.47	1.64
8	0.82	0.98	1.35	132.04	0.65	311.81	318.50	337.45	1.44	1.53	1.76
9	1.18	1.41	1.94	134.03	0.65	317.21	326.68	352.88	1.51	1.63	1.93
10	1.18	1.41	1.94	155.71	0.76	320.35	333.59	370.13	1.64	1.81	2.21
11	1.44	1.72	2.36	194.28	0.95	325.39	343.86	394.30	1.76	1.96	2.45
12	2.08	2.48	3.42	301.58	1.47	335.17	346.40	428.62	1.90	2.13	2.68
13	2.02	2.46	4.06	597.93	4.93	353.00	367.40	474.62	2.20	2.51	3.10
14	6.73	6.83	9.41	1060.63	5.18	385.77	434.11	564.67	2.62	3.17	4.36
15	12.58	14.99	20.66	1868.81	9.20	459.38	537.70	754.92	4.32	5.27	7.27
16	52.00	61.95	65.38	3121.92	15.26	699.91	878.56	1387.66	9.24	11.13	15.60
17	22.36	26.64	36.71	4326.58	21.14	2804.74	3803.41	6490.99	37.59	45.46	64.22
18	8.01	9.54	13.15	4924.51	24.07	5715.15	7209.49	10673.19	27.13	31.81	42.68
19	4.19	4.99	6.88	4556.73	22.27	5522.53	6605.18	9028.74	13.04	15.08	19.78
20	2.85	3.40	4.68	3787.47	18.51	4004.80	4615.24	5935.71	6.84	7.90	10.37
21	1.76	2.10	2.89	3063.28	14.97	2756.88	3094.04	3817.23	4.52	5.21	6.88
22	1.45	1.73	2.38	2473.08	12.09	1960.43	2163.13	2616.83	3.39	3.89	5.09
23	1.21	1.44	1.99	2010.56	9.83	1472.05	1612.75	1936.88	2.59	2.94	3.98
24	0.90	1.07	1.48	1651.91	8.98	1164.26	1278.24	1520.50	2.27	2.59	3.10
25	0.60	1.07	1.48	1278.36	6.74	905.40	1051.64	1263.49	2.02	2.30	2.94
26	0.90	1.07	1.48	1164.82	5.69	815.66	896.21	1080.46	1.85	2.10	2.69
27	0.46	0.55	0.76	997.60	4.88	711.36	782.56	949.52	1.74	1.99	2.57
28	0.46	0.55	0.76	865.23	4.23	631.27	696.90	848.59	1.57	1.78	2.28
29	0.46	0.55	0.76	759.27	3.71	566.85	626.63	765.16	1.41	1.60	2.02
30	0.46	0.55	0.76	673.53	3.29	513.33	567.86	694.19	1.31	1.47	1.86
31	0.46	0.55	0.76	603.43	2.95	468.30	518.33	634.18	1.23	1.39	1.77
32	0.46	0.55	0.76	545.54	2.67	430.39	476.74	584.21	1.17	1.33	1.70
33	0.46	0.55	0.76	497.30	2.43	398.58	442.02	543.08	1.13	1.28	1.65

drainage area  $A = 1335 \text{ km}^2$  (at the location slightly upstream of Pelaez Bridge) so that  $Q_{\text{peak}} = 0.255 \times 52 \times 1335 \times 1000/3600 = 4924 \text{ m}^3/\text{s}$ . However, for the same rainfall intensity and drainage area, but with a runoff coefficient of 0.3, the resulting  $Q_{\text{peak}} = 5794 \text{ m}^3/\text{s}$ , which is closer to what was obtained using the watershed model. For the 10-year and 50-year return period storms, the peak flows from the watershed model are 7209 and 10,673  $\text{m}^3/\text{s}$ , respectively.

The computed flood hydrographs at the outlet of Sub-basin 67 are also given in Table 8.3 which is another inflow boundary condition in the 2-d flood inundation

model. The corresponding JICA hydrograph at Sub-basin 67 has been derived based on the ratio of Sub-basin 67 and flood hydrographs computed from the watershed model.

### **8.3.3 Alternative Flood Mitigation Plans for the Cagayan de Oro River**

A total of eight flood simulation scenarios or flood mitigation plans were evaluated in this study. These different scenarios or plans were the outcome of consultation meetings with various stakeholders and especially DPWH of Cagayan de Oro City. The eight flood simulation scenarios are given in Fig. 8.24, and each is briefly described below.

*Scenario 1 – Existing Condition (Present Flood Control Structures).* This scenario simulates the existing river hydraulic condition of the Cagayan de Oro River with the present DPWH hydraulic structures.

*Scenario 2 – Existing and Urgent/Ongoing Flood Control Projects.* Scenario 2 simulates the existing river hydraulic condition of the Cagayan de Oro River with the present and urgent/ongoing DPWH flood control projects.

*Scenario 3A – JICA Proposed Long-Term Flood Mitigation Project (With Baby Dikes).* This scenario simulates the proposed JICA long-term structural flood mitigation project for the Cagayan de Oro River together with the existing and urgent/ongoing DPWH flood control projects. In particular, there is a retarding basin at Torre de Oro and Paseo del Rio development and therefore these areas are on the river side. There is also a dike across the City Hall indicated referred to as baby dike with a crest elevation of 5 m.

*Scenario 3B – JICA Proposed Long-Term Flood Mitigation Project (Without Baby Dikes).* This scenario is basically the same as Scenario 3A but with no baby dikes across the City Hall.

*Scenario 4 – Modified JICA-DPWH Proposed Structural Flood Mitigation Project as in Scenario 3B with Realigned Dike Around Torre de Oro and Paseo del Rio Area.* This scenario simulates the proposed JICA long-term structural flood mitigation project for the Cagayan de Oro River with the existing and urgent/ongoing DPWH flood control projects with some modification in the floodwall alignment around the proposed Torre de Oro-Paseo del Rio retarding basin. In this case, Torre de Oro and Paseo del Rio areas are protected by the proposed floodwall and therefore on the land side of the dike in contrast to Scenario 3B.

*Scenario 5 – Modified JICA-DPWH Proposed Structural Flood Mitigation Project as in Scenario 3B with Realigned Dike Around Torre de Oro and Paseo del Rio Area with Instream Detention Basin 1.* Scenario 5 is the same as Scenario 4 but includes an instream detention Basin 1 located on the left bank upstream of Cagayan de Oro City area.

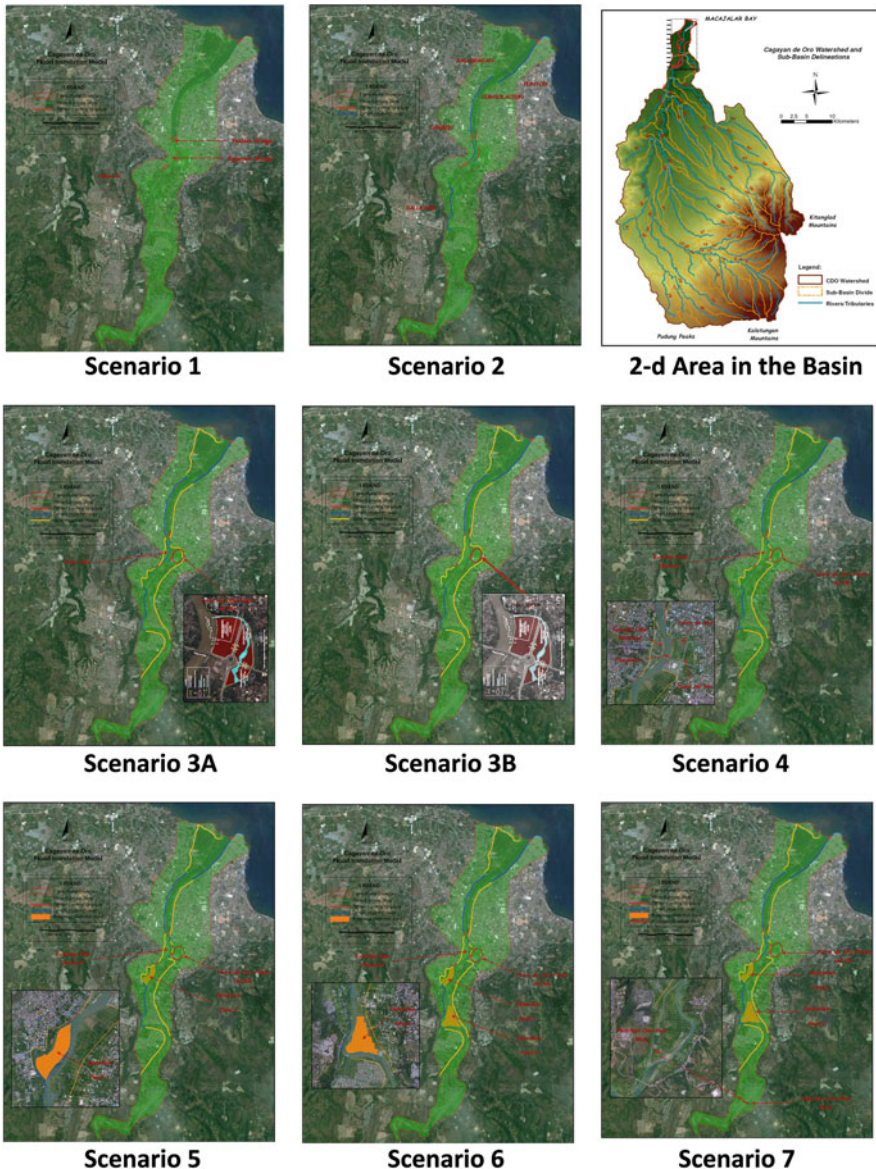


**Fig. 8.24** Eight flood mitigations plans or scenarios for Cagayan de Oro River Basin

*Scenario 6 – Modified JICA-DPWH Proposed Structural Flood Mitigation Project as in Scenario 3B with Realigned Dike Around Torre de Oro and Paseo del Rio Area with Instream Detention Basins 1 and 2. Scenario 6 is the same as Scenario 4 but includes two instream detention ponds, Basin 1 and Basin 2, upstream of the city area.*

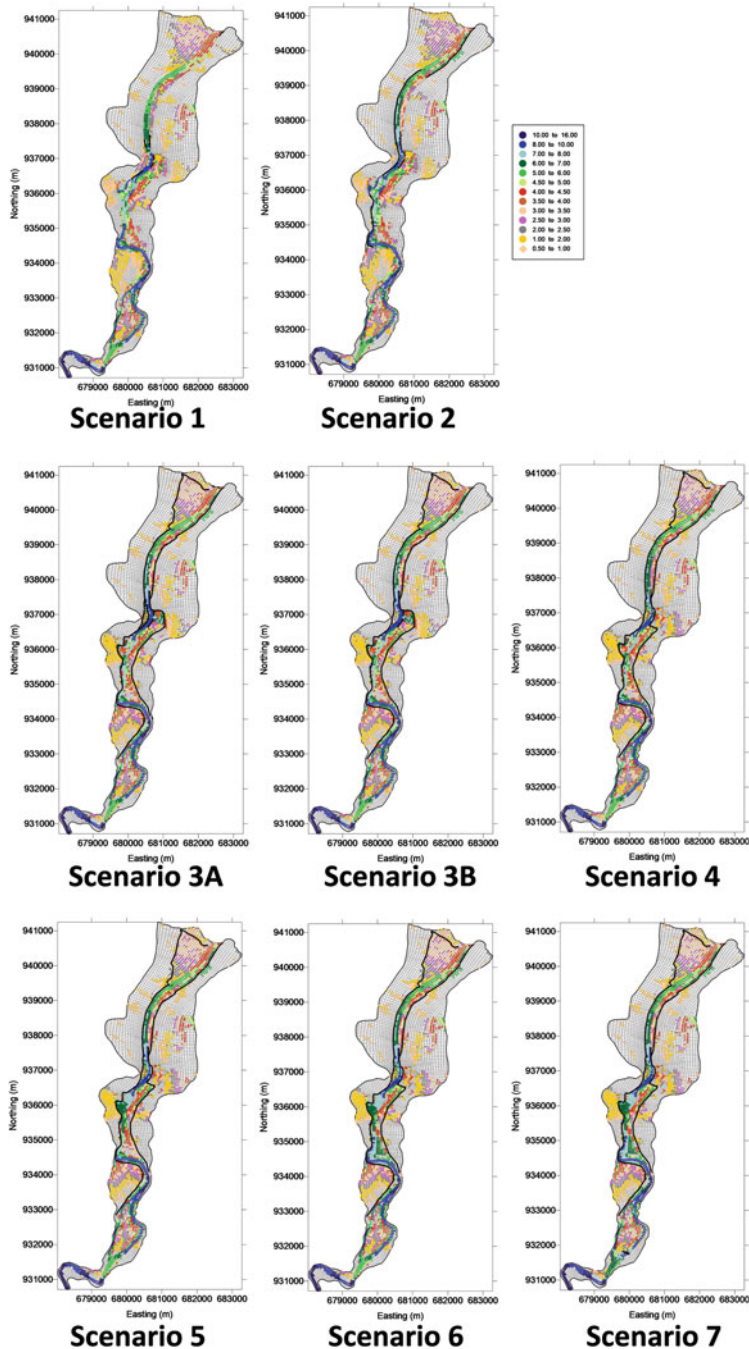
*Scenario 7 – Modified JICA-DPWH Proposed Structural Flood Mitigation Project as in Scenario 3B with Realigned Dike Around Torre de Oro and Paseo del Rio Area, with Instream Detention Basins 1 and 2 and a River Flood Storage with Overflow Weir Downstream of Pelaez Bridge.* Scenario 7 is the same as Scenario 6 but includes a river flood storage inside the river by constructing an overflow weir located downstream of Pelaez Bridge. Originally, there was a low weir upstream of Pelaez Bridge which was destroyed during TS Washi but may also be reconstructed to create river flood storage.

### **8.3.4 Results of Flood Simulations of the Alternative Flood Mitigation Plans**

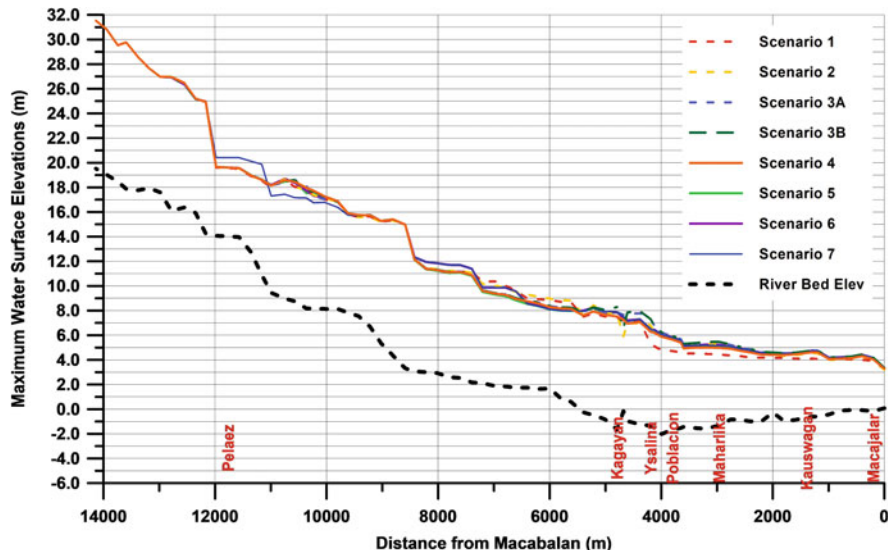
As stated earlier, the flood simulations here were only for TS Washi rainfall with inflow flood hydrograph, upstream boundary condition at Pelaez Bridge which was computed using the watershed model (i.e., with peak flow of  $5715 \text{ m}^3/\text{s}$ ) including the inflow hydrograph at Sub-basin 67. Also, the downstream boundary condition is tidal water level at Macajalar Bay (mouth of Cagayan de Oro River) during the typhoon. The flood simulations were carried out for a period of 33 h on an hourly basis.

Figure 8.25 shows the maximum water depths (m) over the simulation period of 33 h for the 8 simulation scenarios or cases. In this figure, the maximum water depths are plotted by *class posting* at every grid cell whereby different colors represent the different ranges of depths as indicated in the legend. It is seen here that Scenarios 1 and 2 had relatively larger spatial extent of flooding compared to the other scenarios. Upon comparison with Scenarios 3A, 3B, and 4 through 7 for cases with more dikes in place, the spatial extent of the flood inundations was reduced compared to Scenarios 1 and 2. Comparing among Scenarios 3A, 3B, and 4 through 7, it seems that there were only slight differences in the magnitude and spatial extent of flooding among them. Even between Scenarios 3A and 3B, there seems to be very slight differences between them.

Another way to compare the different plans or scenarios is to examine the plots of the profiles of maximum water surface elevations. Figure 8.26 shows the maximum water surface profiles which was averaged from 2 to 3 elements or grids (transverse-wise) at that location. It is seen here that Scenario 1 resulted in lowest water surface elevations compared to the other scenarios at around Ysalina Bridge (at distance 4.2 km from Macajalar Bay) because the floodwaters spread into the floodplain in these areas since there were no dikes, compared to the other cases where the floodwaters were confined by the diking system. On the other hand, comparison of the water surface elevations among Scenarios 3A, 3B, and 4 through 7 shows that Scenario 4 followed by Scenarios 5, 6, and 7 results in lower water surface elevations



**Fig. 8.25** Class posting of maximum water depths (m) for the eight flood simulation scenarios. Note that only depths of greater than 0.5 m are posted



**Fig. 8.26** Profiles of maximum river stage water surface elevations along the center line of the Cagayan de Oro River for the eight flood simulation scenarios

compared to the other cases and in particular Scenario 3A. The reason for this is that in Scenario 3A, the existing (ongoing project) baby dike segment constructed around the Ysalina (Carmen) Bridge/COA Building area (across City Hall) was retained (although it was opened at the upper and lower end of the dike segment) in contrast to Scenarios 3B and 4 through 7 in which that particular segment of the dike was removed. In any case, overall, it can be concluded that the differences in water surface profiles among Scenarios 3A, 3B, and 4 through 7 are not that significant.

### 8.3.5 Remarks on Cagayan de Oro River Flood Mitigation Simulations

As stated earlier, the flood simulation study was commissioned by DPWH, and the recommendations of the study have been actually implemented in Cagayan de Oro River Basin. To reiterate, the results of flood simulations showed that there were only slight differences among the different flood plans/configurations. Scenarios 4 and 5 resulted in relatively smaller flood inundation levels compared to Scenarios 3B and 3A. It was noted that while Scenarios 1 and 2 resulted in lower flood water stages or elevations along the Cagayan de Oro River downstream of Ysalina Bridge compared to the other cases, the lower water stages were due to the spreading of floodwaters in the floodplain thus the greater spatial extent of flooding in that area.

In this project, cost analysis as well as economic analysis were also done, but the results are no longer shown here and may be referred to NHRC ([2015](#)) report. In terms of costs, Cases 4 (lowest) and 3B (2nd lowest) have the least combined construction and dredging costs compared to the other cases based on resulting economic internal rates of return (EIRR), B/C ratios, and net present values including sensitivity analyses, all projects are viable, and overall, Scenario 4 appears to be the best option economically followed by Scenario 3B.

Thus, overall, it is concluded that Scenarios 3B and 4 are equally competitive based on flood level reductions and project costs. Note that Case 4 proposed to realign the dike around the Paseo del Rio and Torre de Oro developments so that they would be in the inland side of the dike in contrast to Scenario 3B where these two developments would be on the river side of the dike.

## **8.4 Dam-Break Model Studies of a Dam Removal Problem and Butas Dam of Cavite Province with Flow and Sediment Movement**

In a dam-break or levee failure, a shock wave is generated and propagates upstream and/or downstream from the point of failure in the reservoir or channel system. Shock waves are also observed in sudden opening or closing of sluice gates in reservoirs or channels. The dam-break problem in particular is even more complicated due to the rapid and abrupt changes in bed elevations as a result of massive scour or erosion in the vicinity of the dam. Thus, models for dam-break problems must be able to capture shock waves, rapidly varying and discontinuous flows, as well as wetting and drying flow boundaries. Also, it must include a sediment transport component to handle bed changes or movement due to scour and deposition.

One of the earliest dam-break model was developed by Fread and Lewis ([1998](#)) of the US National Weather Service (NWS) called FLDWAV which is a one-dimensional, unsteady flow model that could simulate the failure of dams caused by overtopping or piping failure and flood inundation mapping, among other applications. The FLDWAV model replaced the older dam-break model of NWS called DAMBRK and DWOPER for dam-break and unsteady flow dynamic-routing model using the 1-d (one-dimensional) St. Venant equations to route the flow downstream the river valley. These NWS dam-break models were very widely used and are still in general distribution. Another early dam-break model for 2-d (two-dimensional) dam-break and floodplain studies was presented by Hromadka and Yen ([1987](#)) of the US Geological Survey referred to as the diffusion hydrodynamic model (DHM). The DHM is based on the non-inertial form of the St. Venant equations.

In the past decade or so, several papers had been devoted in refining the use and numerical solution of the St. Venant equations to accurately capture shock wave and

discontinuities associated to dam-break modeling. Fennema and Chaudry (1987) introduced an artificial dissipation terms in order to remove the oscillations around discontinuities in solving the St. Venant equations for 1-d and 2-d dam-break problems which consist of a set of hyperbolic, nonlinear equations that yields a discontinuous solution. Applications of these schemes for 1-d dam-break problems have been presented by Alcrudo et al. (1992) and Sanders (2001). Zhao et al. (1996) applied three approximate Riemann solvers, namely, the flux vector splitting (FVS) and Roe and Osher (Osher and Solomone 1982) schemes to solve hydraulic shock wave problems in the framework of finite volume method (FVM).

In the dam-break models above, the reservoir and/or downstream riverbeds are assumed fixed or immobile; thus only the water flows are calculated. There are several mobile bed, open-channel flow models (e.g., HEC-6 of US Army Corps of Engineers 1993 or HEC2SR of Simons et al. 1984), but modeling of dam-break problems with mobile bed is not very common and is lacking in the literature. However, mobile bed, dam-break models have been of interest lately not only for dam-break studies but for dam removal (or dam-break by design) problems. Removal of dam by design is done for reasons of economics or safety or for ecological restoration or rehabilitation purposes. Two recent papers on dam removal modeling and model application had been presented by Cui et al. (2006a, 2006b) using a 1-d backwater flow model with quasi-normal assumption and Exner (sediment continuity) equation for cohesive or non-cohesive sediment transport.

Presented here are two dam-break studies by Tabios (2008) using a two-dimensional flow and sediment, hydraulic (2-d) model. The use of this model here differs from traditional dam-break models which treat the bed as immobile or fixed. Details of this 2-d hydraulic model were given in Sect. 6.2.1 in Chap. 6 (also in Tabios 2007b). Two dam-break problems are presented below to illustrate the application of this 2-d model. The first is for a dam removal problem (i.e., dam-break by design) in a rectangular reservoir using experimental data, and the second problem simulates the dam-break of Butas Dam in Cavite, Philippines, that occurred during a typhoon event in September, 2006.

### 8.4.1 *Dam Removal Problem in a Rectangular Reservoir*

The simulation of this rectangular reservoir dam-break problem is motivated by the dam removal problem posed by Cui et al. (2006a, 2006b) as shown in Fig. 8.27 with exaggerated vertical scale. In this figure, the reservoir is relatively filled with sediments with a steep slope facing downstream before the removal of the dam. After the removal of the dam, the reservoir sediment can quickly erode, move down rapidly, and subsequently deposit downstream.

For the specific dam-break simulation conducted here, Fig. 8.28 shows the finite volume grid of the straight, rectangular modeled area which is represented by 3000 grids. The color scale is for the bed elevation. The modeled area is 450 m long and 60 m wide. The left and right overbanks are 10 m wide each so that the main

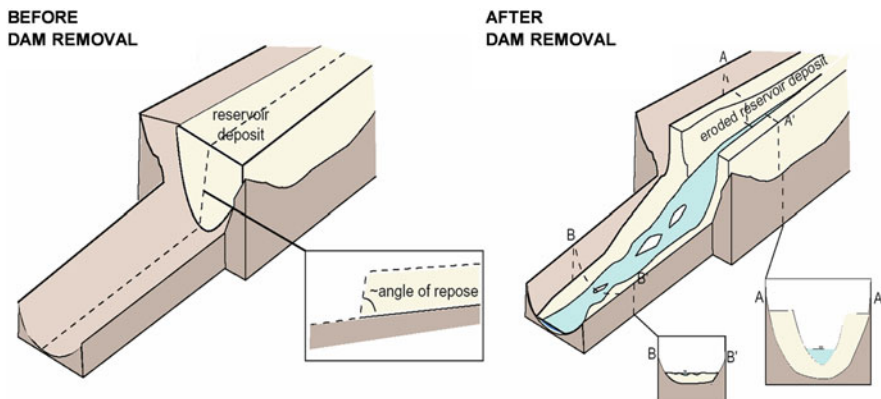


**Fig. 8.27** Sediment-filled reservoir before and after removal of dam by design or accident. (Taken from Cui et al. 2006b)

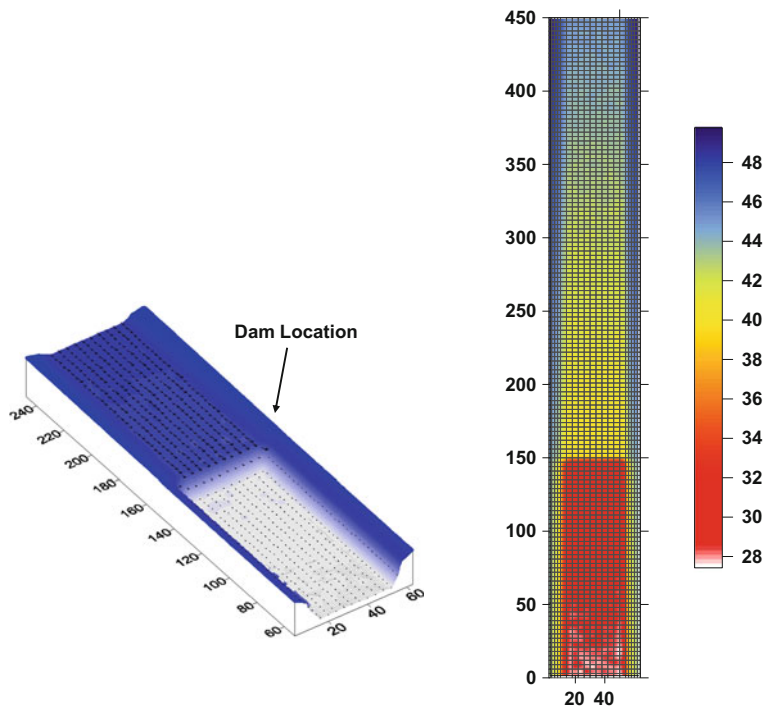


**Fig. 8.28** Dam removal problem in a rectangular reservoir in plan view (right figure) and perspective partially showing the reservoir (left figure). The finite volume mesh is 450 m by 60 m composed of 3000 elements, and the 13-m-high dam is located at vertical ordinate 150 m in the figure. The color/grayscale scale is bed elevation in meters

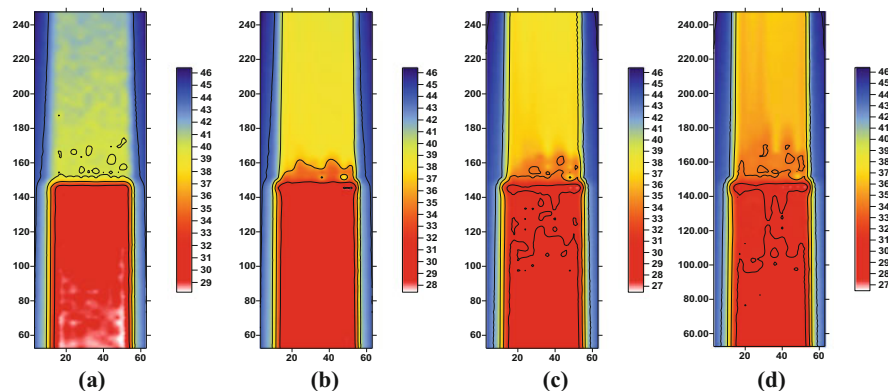


**Fig. 8.29** Bed elevations (m) at time steps (a) –10, (b) 10, (c) 30, and (d) 60 min from time of dam-break of the rectangular reservoir. The color scale is for bed elevations

reservoir width is 40 m. The bed elevation of the reservoir is 45 m at the upstream end (at vertical ordinate 450 m) and slopes to about 40 m at the downstream end (at ordinate 150 m) over the distance of 300 m. The overbank elevations are 5 m higher than the reservoir bed elevations. After this point (dam location), the bed elevation immediately drops to 35 m and slopes to 28 m at the downstream end over the remaining distance of 150 m. The dam which is 13 m high from its base at elevation 35 m is positioned at vertical ordinate 150 m. In the simulation study, the dam is removed after 1 h of simulation over a 1-minute period and the model continues running for another 2 h. This problem is similar to the laboratory dam-break experiment of Cantelli and Parker (2004). The figures below only show the results around the modeled area between vertical ordinates 50 and 250 m.

Figure 8.29 shows the bed elevations at time – 10, 10, 30, and 60 min after dam-break. Figure 8.30 shows the change in bed elevations (current minus original bed elevations so that negative values imply erosion) at 10, 30, 60, and 120 min after dam-break. The color scales in Figs. 8.29 and 8.30 are for bed elevations and differences in bed elevations, respectively. It is observed here that in the first 30 min of simulation, abrupt and massive erosion of as high as 5 m deep propagated upstream from the dams site. Downstream from dams site, noticeable sediment deposition occurs about 30 min after dam-break with accumulation of as much as 2 m high after 120 min simulation. The results of the simulation here may be compared to the experimental results of Cantelli and Parker (2004).

#### 8.4.2 Dam-Break Simulation of Butas Dam of Cavite in September 2006

The dam-break study simulated the dam-break of Butas Dam near General Trias City in Cavite, Philippines, that occurred during a typhoon event in late September 2006

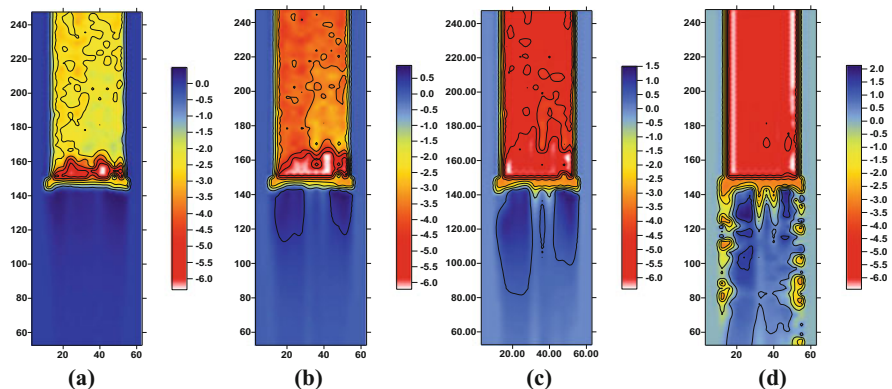


**Fig. 8.30** Difference between bed elevations (m) and original bed elevations at time steps (a) 10, (b) 30, (c) 60, and (d) 120 min from time of dam-break of the rectangular reservoir. The color scale is for differences in bed elevations, and a negative value indicates scour

that killed about 20 people. Figure 8.31 shows pictures from Butas damsite 2 weeks after the dam-break event. In particular, Fig. 8.31a shows the remains of the concrete dam (looking downstream), while Fig. 8.31b shows the channel (looking upstream from dams site) that was incised in the reservoir from the original bed elevation filled with 5 m depth of sediments. These pictures although taken 2 weeks after the dam-break event show the massive movement of sediments from the Butas Dam reservoir which were eroded after about 1.5 h (from eyewitness accounts) during the said event and may be compared to the results presented here 1.5 h into the model simulation period.

For the dam-break simulation study, the dam configuration is shown in Fig. 8.32. The finite volume grid representation is also shown in Fig. 8.32 which is composed of 1140 irregular grids. The dam height is about 9 m from its base at 90 m elevation. Since dam construction, over 5 m of sediments have deposited in the reservoir from its original riverbed elevation of 90 m; thus the reservoir bed elevation before the dam-break was about 95 m. Downstream of the dam, the bed elevation is about 90 m sloping to almost 80 m at the downstream end of the modeled area (lower left-hand side of Fig. 8.6). The simulation run was for 3 h, and the dam was removed within 5 min that commenced 1 h into the model run.

Figure 8.33 also shows the velocity vectors 10 min after dam-break plotted over the image river channel and bank geometry. This figure however only shows qualitatively the results of dam-break simulation. Figure 8.34 shows the bed elevations at time 0, 10, 20, 40, 60, and 120 min after dam-break. Figure 8.35 shows the differences in bed elevations (current minus original bed elevations) at 10, 30, 60, and 90 min after the dam-break. The color scales in Figs. 8.34 and 8.35 are for bed elevations and differences in bed elevations, respectively. Within 10 min after dam-break, as high as 2.8 m of sediment was eroded, that propagated about a distance of 100 m upstream of the dam. After 60 min, the total depth eroded was



(a)

(b)

**Fig. 8.31** Pictures taken at Butas Dam on October 9, 2006, about 2 weeks after the dam-break in which (a) looking downstream into the dam that broke and (b) looking upstream from the damsite

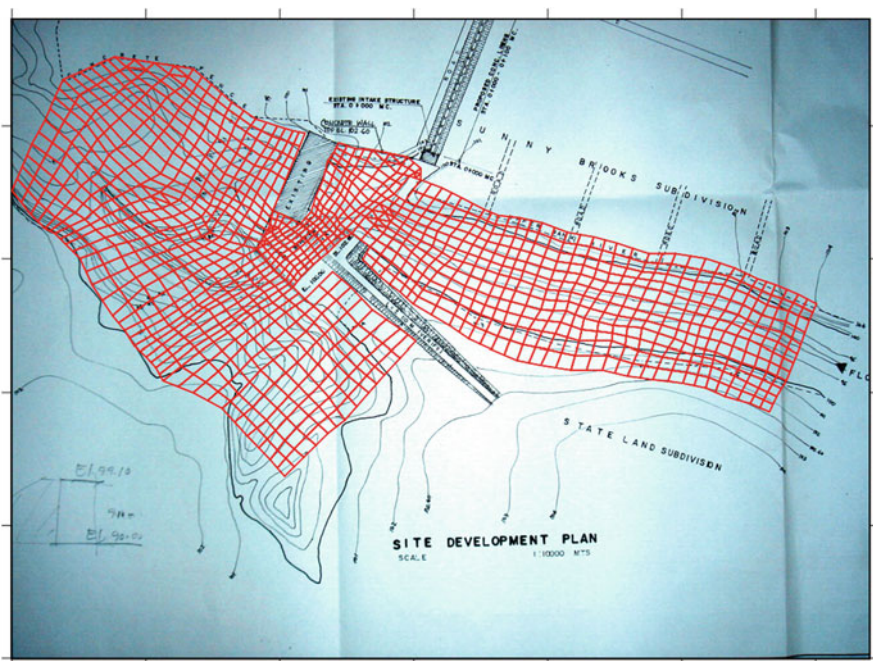


**Fig. 8.32** Plan view of dam configuration and the finite volume grid representation composed of 1140 irregular grids

**Fig. 8.33** Velocity vectors 10 min after dam-break plotted over the image of river channel and bank geometry. Note that dam is approximately located at ordinates  $x = 1250$  m (long side) and  $y = 1780$  m (short side)

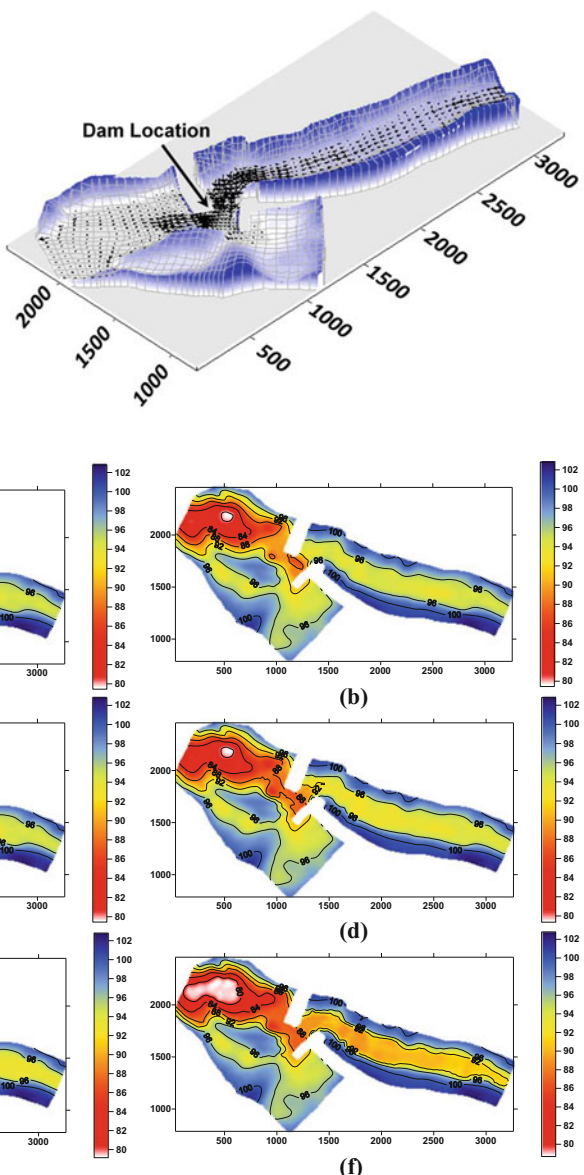


**Fig. 8.34** Bed elevations (m) at time steps (a) 0, (b) 10, (c) 20, (d) 40, (e) 60, and (f) 120 min from time of dam-break of Butas Dam. The color scale is for bed elevations

about 5 m which propagated up to a distance of 300 m upstream. At 90 min, the total depth of erosion upstream of the dam was 5 m and tapered to about 3 m over the entire length of about 2000 m. About 2 m of sediment was eroded immediately downstream of the dam, and about 0.5 m of sediment was deposited far downstream

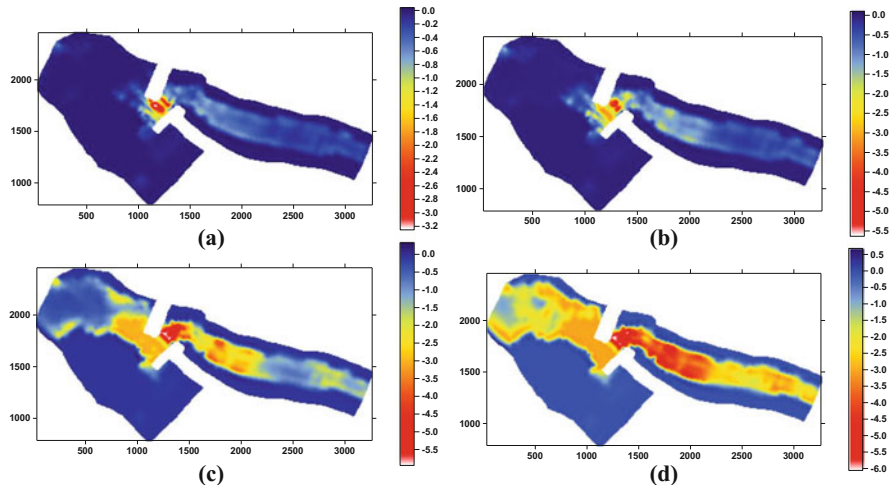


**Fig. 8.35** Differences between bed elevations (m) and original bed elevations at time steps **(a)** 10, **(b)** 30, **(c)** 60, and **(d)** 90 min from time of dam-break of Butas Dam. The color scale is for differences in bed elevations, and a negative value indicates scour

of the dam after 90 min simulation. As mentioned earlier, the results after 90 min simulation may be compared to the pictures in Fig. 8.31 which is about the same bed elevations about 1.5 h after the dam-break event.

## References

- Alcrudo F, Garcia-Navarro P, Sapiro JM (1992) Flux difference splitting for 1-d open channel flow equations. *Int J Numer Methods Fluids* 14:1009–1018
- Cantelli CP, Parker G (2004) Experiments on upstream-migrating erosional, narrowing and widening of an incisional channel caused by dam removal. *Water Resour Res* 40(3):W03304
- Cui Y, Parker G, Braudrick C, Dietrich WE, Cluer B (2006a) Dam removal express assessment models (DREAM). Part 1: model development and validation. *J Hydraul Res* 44(3):291–307
- Cui Y, Braudrick C, Dietrich WE, Cluer B, Parker G (2006b) Dam removal express assessment models (DREAM). Part 2: sample runs/sensitivity tests. *J Hydraul Res* 44(3):308–323
- Fennema RJ, Chaudry MH (1987) Simulation of one-dimensional dam-break flows. *J Hydraul Res IAHR* 25(1):25–51
- Fread DL, Lewis JM (1998) FLDWAV: a generalized flood routing model. In: Proceedings of national conference on hydraulic engineering. ACE, Colorado Springs
- Gupta VK, Waymire EC (1979) A stochastic kinematic study of subsynoptic space-time rainfall. *Water Resour Res* 15(3):637–644
- Hromadka TV, Yen CC (1987) A diffusion hydrodynamic model, U.S. geological survey water resources investigations report 87-4137. U.S. Government Printing Office, Washington, DC
- JICA (Japan International Cooperation Agency) (2014) Preparatory survey for flood risk management project for Cagayan de Oro River (FRIMP-CDOR), report submitted to Department of Public Works and Highways. Manila Office, Nippon Koei, Company, Ltd, Tokyo

- Liggett JA, Cunge JA (1975) Chapter 4: numerical methods of solution of the unsteady flow equations. In: Mahmood K, Yevjevich V (eds) Unsteady flow in open channels, vol 1. Water Resources Publ, Fort Collins
- Maksimov VA (1964) Computing runoff produced by a heavy rainstorm with a moving center. *Soviet Hydrol* 5:510–513
- Morel-Seytoux HJ, Alhassoun SA (1987) A multi-process watershed model for simulation surface and subsurface flows in a soil-aquifer-stream hydrologic system, report. No. 87.3. HYDROWAR Publications, Atherton
- Morel-Seytoux HJ, Alhassoun SA, Tabios GQ III, Liongson LQ, Rojas DS Jr (1999) SWATCH – a distributed hydrologic watershed model. In: Proceedings of 19th annual hydrology days. American Geophysical Union, Colorado State University, Fort Collins. August 16–20
- NAMRIA (National Mapping and Resource Information Authority) (1995) Tide and current tables, Philippines: 1995, Dept. of Environment and Natural Resources, Fort Andres Bonifacio, Makati, Metro Manila
- Niemczynowcz J (1984) Investigation of the influence of rainfall movement on runoff hydrograph: Part II. Simulations of real catchments in the City of Land. *Nord Hydrol* 15:71–84
- NHRC (National Hydraulic Research Center) (2015) Reliability and project cost analyses of NIA's proposed Balog-Balog Multipurpose Dam Project and TWEDCO's proposed Balog-Balog Multiple Dam Project, Final report to National Irrigation Administration (NIA), May
- NHRC (National Hydraulic Research Center) (2016) Review and value engineering study of the flood risk management project for Cagayan de Oro River, Final Report to Department of Public Works and Highways (DPWH), Manila, August
- Osher S, Solomone F (1982) Upwind difference schemes for hyperbolic systems of conservation laws. *Math Comput Simul* 38:339–374
- Sanders B (2001) High-resolution and non-oscillatory solution of the St. Venant equations in non-rectangular and non-prismatic channels. *J Hydraul Res* 39(3):321–330
- Simons DB, Li R-M, Cotton GK (1984) Mathematical model for estimating scour through bridge crossings. In: Proceedings of 2nd bridge engineering conference, transportation research record no. 950, vol 2. Federal Highway Administration, Washington, DC, pp 244–251
- Singh VP (1997) Effect of spatial and temporal variability in rainfall and watershed characteristics on streamflow hydrograph. *Hydrol Process* 11:1649–1669
- Surkan AJ (1974) Simulation of storm velocity effects of flow from distributed channel network. *Water Resour Res* 10(6):1149–1160
- Tabios GQ III (2003a) Influence of storm movement in Pasac delta flooding, In: Takara K, Kojima T (eds) Proceedings of international symposium on managing water resources under climatic extremes and natural disasters, Sigatoka, Fiji, (International Hydrological Programme, IHP-VI Technical Document in Hydrology, Focal Area 4.4), October 27–28, pp. 257–266
- Tabios GQ III (2003b) Modeling imperatives of Manila Bay/Laguna Lake System. In: Proceedings of symposium on environmental issues related to infrastructure development. Japan Society for the Promotion of Science-Philippine Department of Science and Technology, Makati City, August 8–9, pp 43–52
- Tabios GQ III (2006) Effect of moving storm rainfall on soil erosion and sediment transport from watersheds. In: Proceedings of international symposium on managing water supply for growing demand held in Bangkok, Thailand, IHP, Technical Document in Hydrology, no. 6. UNESCO Office, Jakarta, October 16–20
- Tabios GQ III (2007a) Influence of storm rainfall movement on watershed sediment yield. *J Hydrol Environ IHES* 3(1):31–40
- Tabios GQ III (2007b) Reservoir sedimentation and operations study using a two-dimensional hydraulic model. *J Hydrol Environ IHES* 3(1):41–50
- Tabios GQ III (2008) Two-dimensional hydraulic model with mobile bed for dam-break problems. *J Hydrol Environ IHES* 4(1):17–25
- Tabios GQ III (2010) Urban dimensions of Flord management case of Pasig-Marikina River Basin of Metro Manila, Philippines. *J Hydrol Environ IHES* 6(1):1–9

- Tabios GQ III (2015) Chapter 6: Urban Flord management issues and challenges: case of Pasig. Marikina River Basin in Metro Manila. In: Vojinoric Z, Huang J (eds) Flord risk: the holistic perspective, moving beyond integrated urban Flord management. IWA publishing, Netherlands
- Tabios GQ III (2017). Alternative flood mitigation plans for Cagayan De Oro River. In: Soriano RS, Tabios GQ III (eds) Proceedings of UNESCO-JASTIP joint symposium on intra-regional water security and disaster management, Quezon City, Metro Manila, November 13–16, pp 52–53
- Tabios GQ III, Salas JD (1985) A comparative analysis of techniques of spatial interpolation of precipitation. *Water Resour Bull AWRA* 21(3):365–379
- Tabios GQ III, Obeysekera JTB, Shen HW (1986). The influence of storm movement on hydrographs through space time rainfall generation and hydraulic routing, Paper presented at AGU Fall Meeting, San Francisco, California, December 8–12. Abstract published in EOS, Vol. 67, No. 44, November 4, 1986, p. 930.d to the Electric Resource Planning, Pacific, Gas and Electric Company, San Francisco, California, January
- USACE (U.S. Army Corps of Engineers) (1993) HEC-6 generalized computer program: scour and deposition in rivers and reservoirs, User's manual. Hydrologic Engineering Center, Davis
- USACE (U.S. Army Corps of Engineers) (1994) Mt. Pinatubo recovery action plan, supplemental data, Volume 1, General Data, USACE, Portland District, USA
- USACE (U.S. Army Corps of Engineers) (1995) UNET: one-dimensional unsteady flow through a full network of open channels, User's manual. In: Hydrologic engineering center. Davis, California
- Waymire E, Gupta VK, Rodriguez-Iturbe I (1984) A spectral theory of rainfall intensity at the meso- $\beta$  scale. *Water Resour Res* 20(10):1453–1465
- WMO (World Meteorological Organization) (1982) Manual for Determination of Probable Maximum Precipitation, Geneva, Switzerland
- Yen BC, Chow VT (1968) A study of surface runoff due to moving rainstorms. Hydraulic engineering series no. 17. Department of Civil Engineering, University of Illinois, Urbana, p 112
- Zhao DH, Shen HW, Lai JS, Tabios GQ III (1996) Approximate Riemann solvers in FVM for 2D hydraulic shock wave modeling. *J Hydraul Eng ASCE* 122(12):692–702

# Chapter 9

## Pipe Network Distribution Modeling with Optimization



**Abstract** This chapter presents an enhancement of the EPANET pipe network, hydraulic model by incorporating the COMPLEX optimization algorithm which is a constrained, nonlinear optimization algorithm. The entire EPANET model is embedded inside the COMPLEX optimization algorithm so that in the iterative solution process, COMPLEX specifies values of the decision variables and then evaluated in EPANET by pure simulation until reasonable values of the decision variables are optimal. The enhanced model can be utilized for purposes of automatic model calibration of parameters, layout (plan) pipe network to minimize pipe costs, detection, and surveillance of non-revenue water due to pilferage and leakage as well as optimal operations of pipe network to satisfy volume and pressure requirements. Sample application of the enhanced model to a service area of MWSI's west zone water concession south of Manila is presented in this paper to illustrate capability of the model for automatic model calibration.

### 9.1 Introduction

The EPANET model developed by the US Environmental Protection Agency (Rossman 2000) has been used by the Maynilad Water Services (MWSI) for the west zone water concession of Metro Manila as pure simulation model. To enhance the EPANET model capability, the COMPLEX optimization algorithm has been incorporated into this model which is a constrained, nonlinear optimization algorithm using a sequential search technique. This enhanced EPANET with optimization can be used for the following purposes: (1) ease in calibration of pipe network hydraulic model; (2) detection, surveillance, and quantification of non-revenue water due to pipe leakage or pilferage; (3) planning and expansion studies of pipe network distribution system by optimal layout of pipes and sizing of pipe; and (4) normal pipe operations such as optimizing booster pump operations or valve throttling scheduling to satisfy flow and pressure requirements. A sample application of the enhanced model is presented below for model calibration to a portion of the pipe distribution network of MWSI located south of Manila. Details of this work are reported in NHRC (2009) as well as in the paper by Tabios (2010).

## 9.2 Description of EPANET Model

The EPANET model performs extended period hydraulic simulation of a water distribution network composed of pipes, nodes or junctions, pumps, control valves, delivery or demand points, and storage tanks or reservoirs as shown in Fig. 9.1. In actual pipe operations, monitoring is important through flow and pressure gaging points (GP). Also, pilferage and leakage in a water distribution cannot be avoided, and these are considered as non-revenue water (NRW). Typical time series plots of main water use NRW pilferage and leakage as well as pressure at a node is shown in Fig. 9.2.

As described by Rossman (2000), EPANET solves the flow continuity and headloss equations characterizing the hydraulic state of the pipe network at a given point in time using a gradient or Newton-type node-loop method. Specifically, for a pipe network of  $N$  junction nodes, the flow-headloss in a pipe between nodes  $i$  and  $j$  is given by:

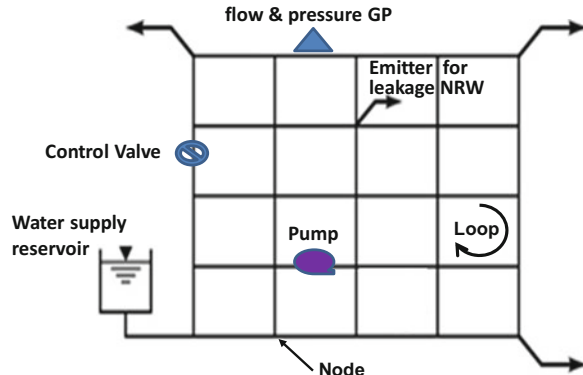
$$H_i - H_j = h_{ij} = rQ_{ij}^2 + mQ_{ij}^2 \quad (9.1)$$

where  $H$  = nodal head,  $h$  = headloss,  $r$  = resistance coefficient,  $Q$  = flow rate,  $n$  = flow exponent, and  $m$  = minor loss coefficient. The value of the resistance coefficient depends on the type of friction headloss formula used. For pumps, the headloss (negative of the head gain) can be represented by a power law of the form:

$$h_{ij} = -\omega^2 [h_0 - r(Q_{ij}/\omega)^n] \quad (9.2)$$

where  $h_0$  is the shutoff head for the pump,  $\omega$  is a relative speed setting, and  $r$  and  $n$  are the pump curve coefficients. The second set of equations that must be satisfied is the flow continuity around all nodes:

**Fig. 9.1** Typical water distribution pipe network



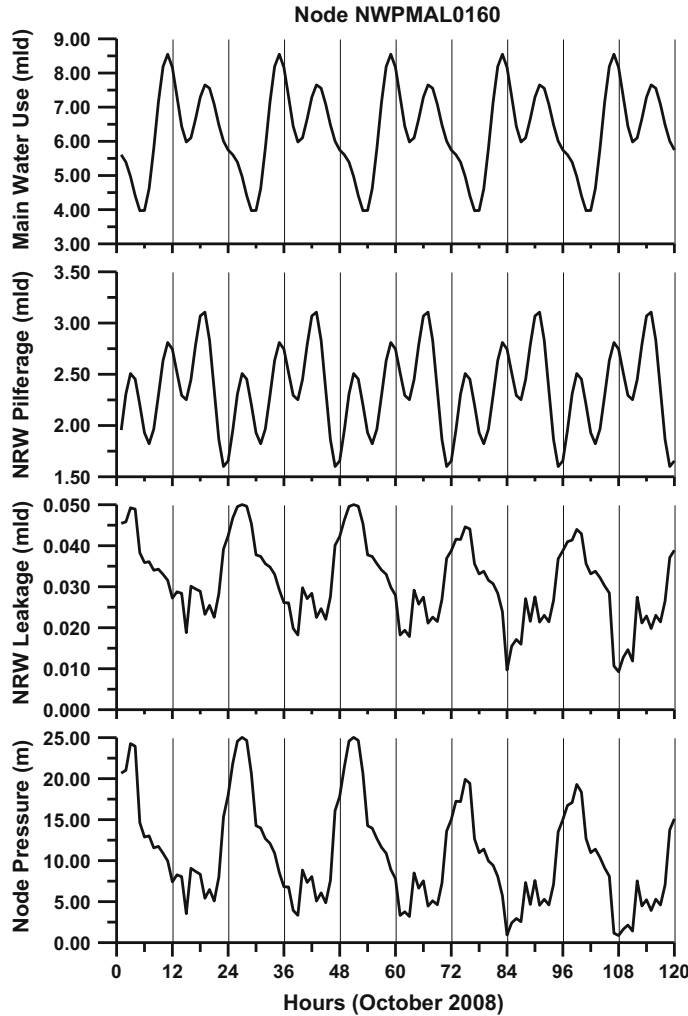


**Fig. 9.2** Typical time series plot of hourly main water use and non-revenue water (NRW) pilferage and leakage water (in million liters per day, mld) as well as hourly pressure head (in m) at a node

$$\sum_j Q_{ij} - D_i = 0 \quad \text{for } i = 1, \dots, N \quad (9.3)$$

where  $D_i$  is the flow demand at node  $i$  and, by convention, flow into a node is positive. For a set of known heads at the fixed grade nodes, we seek a solution for all heads  $H_i$  and flows  $Q_{ij}$  that satisfy Eqs. (9.1) and (9.3).

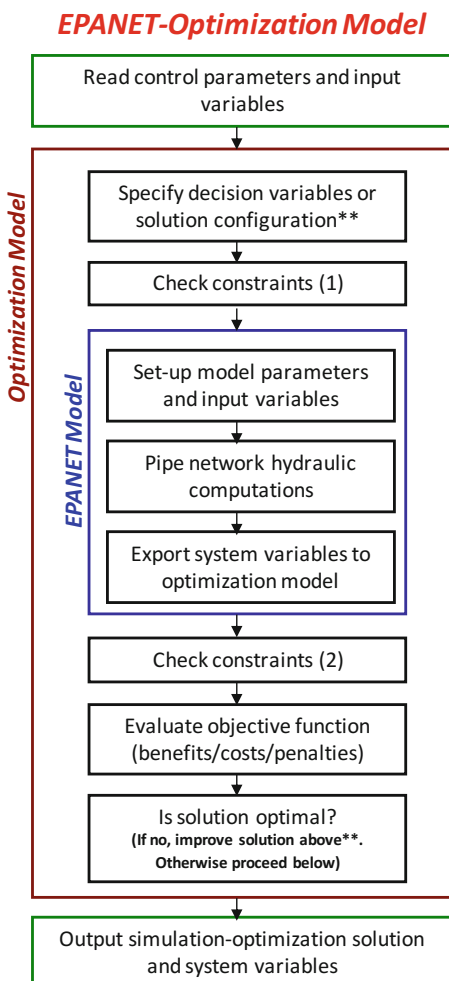
The EPANET model is a pure simulation model. To enhance the capability of the EPANET model, an optimization model is incorporated here.

### 9.3 Enhancement of EPANET with COMPLEX Optimization

Essentially the enhanced model consists of the COMPLEX optimization model to decide the values of the decision variables (i.e., parameters to be optimized) based on specified objective function or performance function and constraints; and the EPANET model performs the hydraulic computations of the pipe network to be able to calculate the objective or performance function and check against the constraints. A flow chart of the enhanced EPANET with optimization is shown in Fig. 9.3.

The constrained simplex algorithm called COMPLEX due to Box (1965) is a nonlinear optimization algorithm using a sequential search technique. To initiate the

**Fig. 9.3** Flowchart of EPANET-Optimization model



search technique, a set of alternative feasible solutions are randomly generated based on the constraints on the decision variables. The technique tends to find the global solution due to the fact that the initial set of solutions are randomly scattered throughout the feasible region of the optimization problem. No derivatives are required in the technique, and the technique is generally applicable in solving optimization problems with nonlinear objective function and nonlinear equality and inequality constraints. The COMPLEX algorithm is described in Appendix C.

Referring to Box 9.1, the decision variables of the optimization model in the enhanced EPANET include base demand parameters, time series patterns, emitter parameter, pipe roughness, pipe diameter, open/close switches of pipe, and control valve settings. For model calibration in particular, the most important model parameters and variables to be adjusted or calibrated are base demand parameters and water use time series patterns as well as roughness coefficients. The control valve settings also need to be calibrated. The base demand parameters and time patterns represent the primary water uses in a given node and at the same node; the unknown NRW due to pilferage is represented by a separate set of base demand parameters and water use time patterns. The presence of NRW due to leakage at that same node is represented by an emitter which is a function of pressure and thus the emitter coefficient also needs calibration.

With regard to the objective and constraint functions, the optimization algorithm operates by evaluating the objective function also called the fitness or performance function of the water distribution system for each alternative or potential solution consisting of values for the set of model parameters to be calibrated.

The fitness or performance of the system is determined by comparing how well the simulated flows and pressures resulting from how one alternative or candidate solution matches the measured values. Without an optimization algorithm, this will entail several model simulation runs to simulate a variety of demand conditions, including the operating conditions for minimum, maximum, and average demands. At each measurement point and for each steady-state run, the differences between simulated and observed data (head and/or flow) are calculated, and the objective function (an overall error value for the network) is computed.

Objective functions can be formulated in different ways to achieve different goals. Usually, a squared error or root mean square error criterion is adopted. Different weighings between head and flow measurements can also be incorporated within the objective function. A multi-objective (i.e., dual-objective) function by flow balance calibration and hydraulic gradient calibration can be formulated. Flow balance calibration is by minimizing the differences of actual and model calculated water delivery volumes, while hydraulic gradient calibration is by minimizing the differences of actual and model calculated hydraulic gradients (sum of potential, kinetic, and pressure gradients).

The major constraint function is the overall system constraint which is defined by the EPANET model. Other operational, environmental, and contractual constraints can also be included, but these constraints must be programmed in the enhanced EPANET computer program.

**Box 9.1 Objective Functions and Decision Variables of the EPANET-Optimization Model**

Objective function (minimize sum of mean square differences of the following):

1. Observed and calculated GP flows.
2. Observed and calculated GP pressures.
3. Observed BV (billed volume) and calculated primary water use.
4. Cost as function of pipe diameters.
5. Cost as function of open/close pipes.

Decision variables (parameters to be optimized):

1. Base demand parameter (multiplier) of primary water use and pilferage (NRW).
2. Time patterns of primary water use and pilferage (NRW), also pump speed schedule.
3. Emitter parameter of emitter equation to represent leakage (NRW).
4. Pipe roughness.
5. Pipe diameter.
6. Switches to open/close pipes.
7. Control valve settings.

## 9.4 Enhanced Model Capabilities

Referring to Table 9.1, four specific capabilities of the enhanced EPANET model worth discussing here are for (1) automatic model calibration; (2) detection, surveillance, and quantification of non-revenue water; (3) planning studies; and (4) normal operations.

**Automatic Model Calibration** Without an automatic calibration technique, the calibration process is by trial and error, manual process where the analyst or modeler supplies the estimates, for instance of pipe roughness or loss coefficients, then runs the model and compares model predicted variables to the observed variables. This process is conducted iteratively, through adjusting the model parameters manually until a satisfactory match is obtained between the computed and observed values. With an automatic calibration technique through an optimization model, the model parameters will be adjusted automatically by the optimization algorithm with the objective that a satisfactory agreement of computed and observed variables is attained.

**Detection and Surveillance for Non-revenue Water** The model can also be used for detection and surveillance of non-revenue water (NRW) especially NRW due to pilferage including quantifying the NRW which is assumed to be an unknown variable. The optimization problem in this case is to locate and quantify the unknown

**Table 9.1** Capabilities of enhanced EPANET with optimization model

	Automatic model calibration	Planning studies	Detection and surveillance model for non-revenue water	Normal operations
Purpose	Calibration of EPANET model parameters	Planning for expansion or rehabilitation of existing pipe network	Locating and quantifying NRW	Answer “what, how much, and when” to open valves instead of “what if questions” in pure simulation
Decision variables	Pipe roughness, loss coefficients, NRW parameters	On/off pipelines to find optimal layout and sizing	On/off pipelines to locate NRW and quantifying pilferage NRW	Schedule and volume of valve openings and also pump operations
Objective function	Minimize difference between observed and computed flows and pressures	Minimize cost for alternative pipe network configuration and penalty for flow and pressure violations	Minimize difference between observed and computed flows and pressures	Minimize penalty for flow and pressure violations
Constraints <sup>a</sup>	Bounds of model parameters	Pipe sizes and physical layout restrictions	Flow limitations	Physical system constraints from EPANET model
Outputs	Calibrated model with proper system parameters, time series patterns or Fourier functions of water demands, and NRW due to pilferage, emitter parameters of NRW due to leakage.	Minimum cost layout of pipe network and pipe sizes	Location of possible NRW especially due to pilferage and also the time series pattern or Fourier function of NRW	Schedules of valve operations (time of opening and closing) as well as volume of opening. Also, pump operation schedules

<sup>a</sup>All optimization problems are subject to physical system constraints dictated by EPANET model

NRW in the pipe network given the actual water deliveries and pressure heads. The objective function or convergence criterion in the optimization-simulation model is attained when the model duplicates the observed flow volumes and pressure heads. It may be noted that NRW due to leakage may be characterized or quantified as a function of pressure, but its location may be unknown, so finding its location is similar to switching *on or off* the pipes in the optimization problem for planning and pipe expansion studies.

**Planning Studies** For planning purposes such as expansion or rehabilitation of existing pipe network, the model can be used for optimal (i.e., economically and technically) layouting of new pipe network and the use of other components such as

reservoirs and pumping station. In this case, the optimization may be cost minimization for alternative pipe network/layout configuration and dimensions provided that water delivery and pressure requirements are satisfied. In the optimization model, overspecified pipe network configuration will be laid out, and the decision variables in the optimization model is simply to switch *on or off* pipe components that minimize costs and yet satisfy the flow and pressure requirements.

**Normal Operations** For purposes of normal water delivery operations, the enhanced EPANET model can be used as a pure simulation model. This application is purely to answer “what if” questions such as what would be the flow and pressure distribution at certain points in the pipe network given that a set of valves will be throttled and by how many turns. On the other hand, if “what to do” or “how much to open” questions are asked, then the optimization capability of the model is utilized. For instance, the question that may be asked is “how big and what is the schedule” of a set of valves in a certain service area such that the flow and pressure requirements are satisfied. In this case, the optimization problem would be a scheduling problem to determine the timing/sequencing at various locations of pumping stations and gate/valve nodes satisfying the water costumer flow volume and pressure requirements.

## 9.5 Application of EPANET-Optimization Model for Model Calibration

The sample application presented here is for calibration of model parameters and forcing functions around the water distribution area south of Manila as schematically shown in Fig. 9.4. The pipe network consists of 369 junction nodes, 382 pipe links, 2 reservoirs, 4 pumping stations, 61 control valves, and 418 demand nodes (primary water use and suspected pilferage). The objective function in the optimization is to minimize differences of observed and computed flows and pressures at gaging points. A total of 2874 decision variables are optimized as follows: (1) 180 base demand parameters, (2) 99 by 24 h water use time patterns, and (3) 318 pipe roughness coefficients. The constraints are the upper and lower bounds of decision variables, and most importantly, system constraints defined by the EPANET model.

Figures 9.5 and 9.6 show the time series plots of the observed flows and computed flows with optimization including the case of pure simulation at the gaging points designated as 22SMA-L008 and 22SMA-L007, respectively. Figures 9.7 and 9.8 show the time series plots of the observed pressures and computed pressures with optimization including the case of pure simulation at the gaging points designated as 22SMA-4P-4Q and 22SMA-1G, respectively.

These runs illustrate that different results can be obtained in the optimization runs depending on the specific objective function used. As shown in Figs. 9.5 and 9.6, with an objective based on minimizing the square of differences of observed and computed flows only, or both flows and pressures, the observed flows are well captured or reproduced compared to the case based on pressures alone. The pure

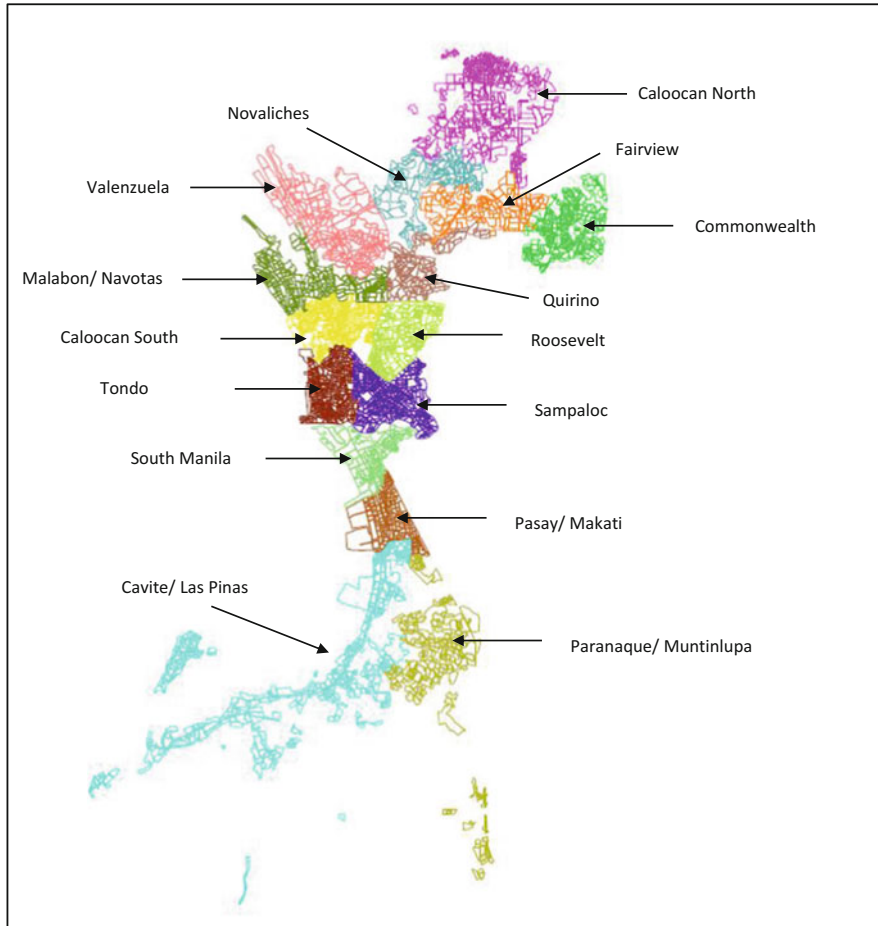


**Fig. 9.4** Water distribution concession area of Maynilad Water Service Incorporated (MWSI) which is on the west zone of Metro Manila

simulation runs are definitely not able to match the observed flows. In the case of the pressures as shown in Figs. 9.7 and 9.8, the objective function based on pressures only as well as both flow and pressures satisfactorily captures the observed pressures compared to the flow only objective function and pure simulation cases.

## 9.6 Brief Final Remarks

A number of water distribution network problems can be cast as optimization problems. This work developed an enhanced EPANET pipe network hydraulic model with an optimization model. Sample application of the enhanced EPANET

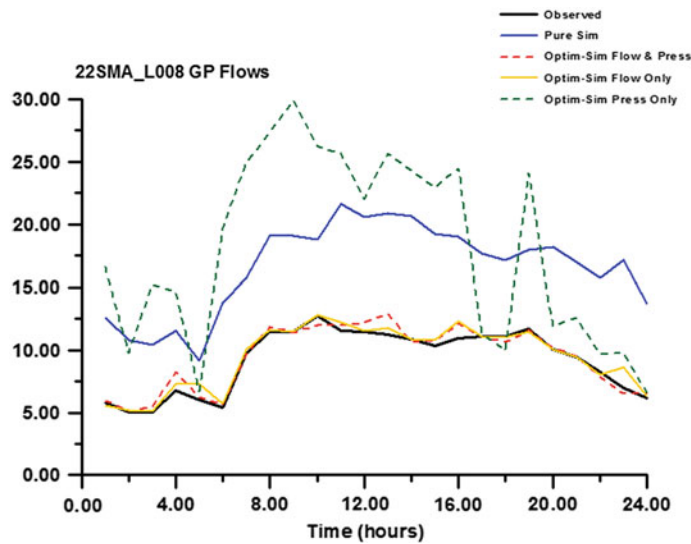


**Fig. 9.5** Time series plots of observed flows and computed flows with optimization including pure simulation for gaging station 22SMA-L008

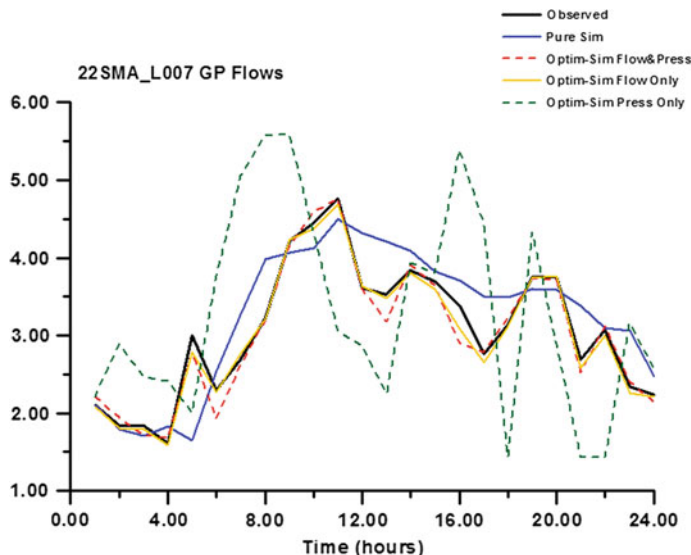


**Fig. 9.6** Time series plots of observed flows and computed flows with optimization including pure simulation for gaging station 22SMA-L007

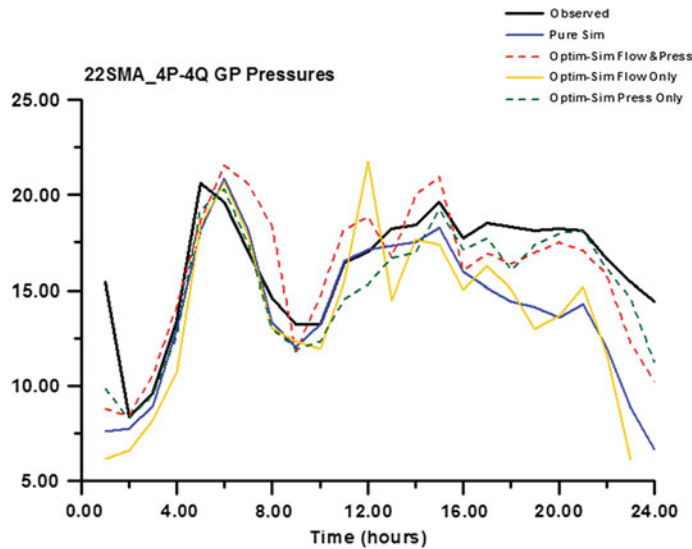


**Fig. 9.7** Time series plots of observed pressures and computed pressures with optimization including pure simulation for gaging station 22SMA-4P-4Q

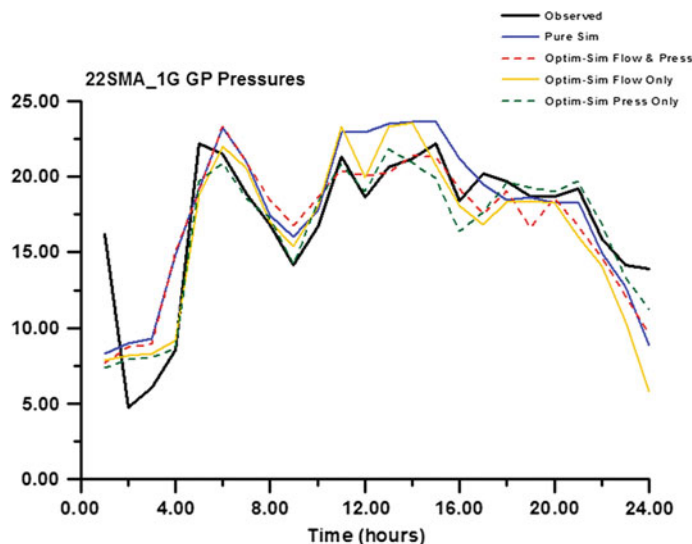


**Fig. 9.8** Time series plots of observed pressures and computed pressures with optimization including pure simulation for gaging station 22SMA-1G

model demonstrates the ease and efficiency in model calibration and estimation of demand patterns of an actual pipe network problem. Other capabilities of this model are for planning for expansion, rehabilitation, or optimal layouting of pipe networks; detection and surveillance of NRW due to pilferage; and optimal water delivery (amount and service period) and pressure distribution.

## References

- Box MJ (1965) A new method of constrained optimization and a comparison with other methods. *Comput J* 8(1):42–52
- NHRC (National Hydraulic Research Center) (2009) Enhancement, incorporation, optimization module and calibration of MWSI Water Distribution Network Model, Report submitted to Maynilad Water Services, Inc. (MWSI), July
- Rossman LA (2000) EPANET 2: user's manual. National Risk Management Research Laboratory, U.S. Environmental Protection Agency, Report No. EPA/600/R-00/07, September
- Tabios GQ III (2010) EPANET pipe network model with COMPLEX optimization. In: Proceedings of 5th conference on Philippine competitiveness through ERDT, Sofitel Philippine Plaza, Manila, September 10

# Chapter 10

## Reliability Studies of Reservoirs Under Climate Change



**Abstract** These studies were conducted to assess the performance and reliability of Upper Agno Reservoirs and Angat Reservoir to deliver water and generate hydropower with 2050 climate change scenario. In the case of Angat Reservoir, a comparison was made on the reliability of the reservoir with 2050 climate change versus future reservoir sedimentation. For the 2050 climate change parameter in Upper Agno Reservoirs, the appropriate global climate model (GCM) and output data set were selected from four (4) candidate GCMs, and the downscaled rainfall projection for 2050 was translated into monthly ratios to be used to rescale the historical rainfall data to represent the future rainfall. For Angat Reservoir, the climate change parameters were derived based on first screening 25 GCMs and then were shortlisted into 6 (six) appropriate GCMs for the Philippines, then finally downscaled rainfall data from this six GCMs were evaluated to select the most appropriate one to be used. Since future Angat River Basin streamflows were already calculated from the downscaled future rainfall, the ratios of future streamflow over the historical streamflows were used to rescale the historical streamflows to represent the future reservoir inflows to Angat Reservoir under climate change.

### 10.1 Upper Agno Reservoir Operations with Climate Change

The Upper Agno Reservoirs composed of Ambuklao, Binga, and San Roque Reservoirs have been described in detail in Sect. 5.3, Chap. 5, in a study of their reliability to deliver hydropower generated from the three (3) reservoirs and irrigation water supply (for San Roque Reservoir). For ease in reference, Fig. 10.1 (same as Fig. 5.7) shows the locations of the three major reservoirs in the Upper Agno River Basin. The study area is 1225 km<sup>2</sup>. The basin boundary on the north is Mankayan of Benguet Province and runs south through Ambuklao, Binga, and San Roque Reservoirs and finally ends on the south at the small re-regulation dam of NIA for the Agno River Integrated Irrigation Project (ARIIP) at San Manuel, Pangasinan.

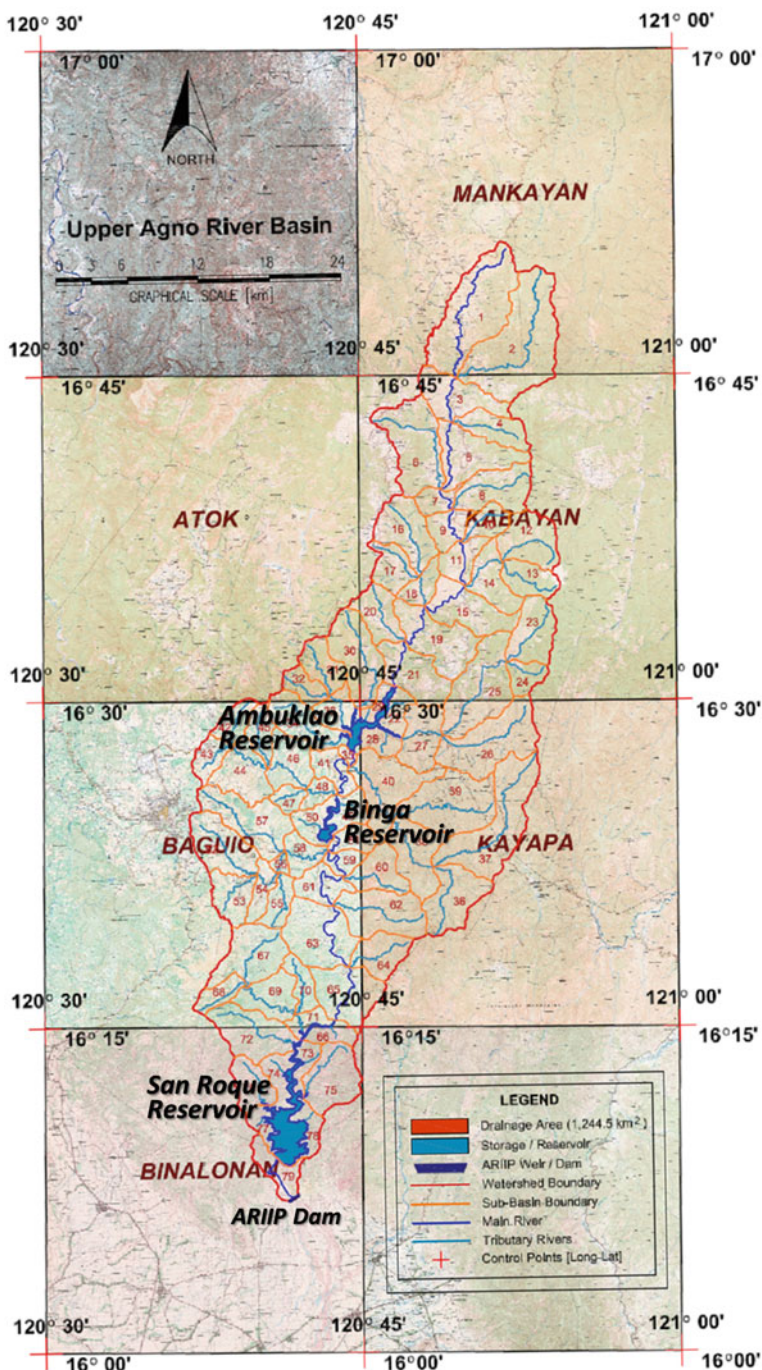


**Fig. 10.1** Assembly of 1:50,000 scale NAMRIA topographic maps covering the Upper Agno River Basin. Also shown is the watershed delineation into sub-basins and the three (3) major reservoirs Ambuklao, Binga, and San Roque (in the order from north or upstream to south or downstream) and the AIIP Dam

Since the three major reservoirs have been discussed in Sect. 5.3, Chap. 5, very brief descriptions of each are given as follows: (1) Ambuklao Dam is located 36 km east of Baguio and 64 km upstream from San Roque Dam, where its dam and hydropower station was commissioned in 1956 with an installed capacity of 75 MW and was designed to supply power during peak demand; (2) Binga Dam constructed in 1959 is situated 50 km upstream of San Roque Dam, and its purpose is only for hydropower generation with an installed capacity of 100 MW; and (3) San Roque Multipurpose Dam which was constructed in 2002 provides flood control, water storage for irrigation, and hydropower with a total installed hydropower capacity of 402 MW and currently supplies irrigation to about 12,000 ha of land although its irrigation water deliveries can be as high as  $27 \text{ m}^3/\text{s}$ .

Presented below is a reservoir operations study and associated reliability analysis using the optimization-simulation model presented in Sect. 5.3 for the Upper Agno Reservoirs with the 2050 climate change scenario. The watershed model presented in that section is the same model used to generate the reservoir inflows with rescaled historical rainfall to represent the 2050 climate change scenario. Details of this study may be referred to Woodfields (2017) which was conducted by the author as principal investigator.

### 10.1.1 2050 Climate Change Scenario

In the study by Woodfields (2017), four (4) global climate models (GCMs), namely, *BCC-CSMS1.1* of the Beijing Climate Center; *CanESM2* of the Canadian Center for Climate Modeling and Analysis; *CNRM-CM5* of Centre National de Recherches Meteorologiques, Center European de Recherche et de Formation; and *FGOALS-g2* of the Institute of Atmospheric Physics, Chinese Academy of Science, were compared and evaluated to determine which GCM is appropriate for the Upper Agno River Basin. Based on the comparison of precipitation predictions for 2050 climate scenario, the most appropriate GCM to represent the Upper Agno River Basin is FGOALS-g2. Based on the downscaled rainfall in the river basin, the ratios of future rainfall over the historical rainfall were determined on monthly basis and used to rescale the historical rainfall as input to the watershed model to finally generate the reservoir inflows representing the 2050 climate change scenario. Figure 10.2 shows the monthly ratios of future rainfall over historical rainfall. During the months of December, January, February, March, and April, the ratio was 1.0 or less; then went up in May and June to around 6.0 to 8.0; then peaked during the months of July, August, and September by as much as 11.0 to 13.0; and then tapered from 6.0 to 2.5 in October and November. Generally, with the 2050 climate change scenarios, the ratio would increase 10 times more during the wet month of July to September.

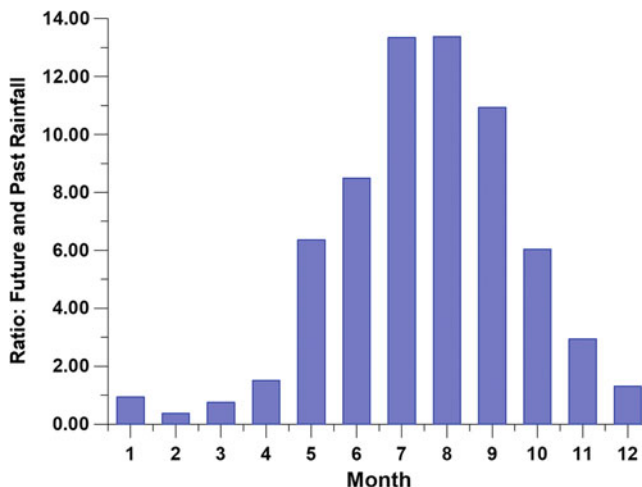


**Fig. 10.2** Ratios of 2050 future climate daily rainfall and historical daily rainfall on monthly basis based on global climate change model, FGOALS

### 10.1.2 *Reliability Analysis of Upper Agno Reservoirs Under Climate Change*

As mentioned earlier, the future rainfall used in the watershed model and subsequently in the optimization-simulation model were derived by rescaling the historical daily rainfall data of 65 years (1950 to 2015) on a monthly basis to represent the 2050 climate change scenario. With the 2050 future climate rainfall and corresponding reservoir inflows computed, the optimization-simulation runs were conducted, and the results of reliability analysis are given in Tables 10.1, 10.2, and 10.3 for the three (3) sets of target reservoir release policies (see Sect. 5.3.4, Chap. 5), respectively, and for the three (3) reservoirs, namely, Ambuklao, Binga, and San Roque. These tables include the reservoir end-of-month (EOM) elevations, reservoir inflows, releases and spills, hydropower generation in Ambuklao, Binga, and San Roque Reservoirs, as well as the final outflow (in  $\text{m}^3/\text{s}$ ) to ARIIP Reservoir. Admittedly with all these results, one has to study carefully these tables to be able to compare across different scenarios and target release policies. Further discussions are presented in the next section which compares the results of hydropower generation, the major purpose of the Ambuklao-Binga-San Roque system.

With regard to irrigation releases which is the only other major purpose of the Upper Agno Reservoirs but only released at San Roque Reservoir, it may be noted in the tables that the outflow to ARIIP always satisfies the irrigation daily requirements

**Table 10.1** Reservoir end-of-month elevations (m); inflows, releases, and spills ( $\text{m}^3/\text{s}$ ); and power generation (MW) for Ambuklao, Binga, and San Roque and outflow to ARUIP Reservoir for target release policy Set 1 with climate change scenario

	Ambuklao reservoir				Binga reservoir				San Roque reservoir				ARUIP Outflow
	EOM Elev	Inflow	Release	Power	EOM Elev	Inflow	Release	Power	EOM Elev	Inflow	Release	Power	
<b>January</b>													
90%	720.0	2.6	2.3	8.3	0.0	547.1	1.0	4.3	13.3	0.0	263.8	4.1	60.0
80%	720.8	3.8	7.0	26.1	0.0	567.6	1.5	22.1	79.7	0.2	269.6	6.2	61.1
50%	749.8	46.1	29.3	121.6	4.5	575.0	19.0	32.4	120.6	21.3	283.5	75.2	117.1
20%	750.0	121.4	34.8	149.2	85.5	575.0	50.2	34.8	131.4	133.9	285.0	197.1	124.7
10%	750.0	180.0	35.0	150.3	145.2	575.0	75.0	35.0	131.9	220.3	285.0	293.4	124.9
<b>February</b>													
90%	720.0	2.9	2.2	7.9	0.0	545.6	1.1	3.2	10.0	0.0	255.3	4.6	60.0
80%	720.9	4.9	4.9	19.4	0.0	569.2	2.0	17.8	64.4	0.1	265.1	8.0	60.6
50%	748.2	23.1	26.6	108.7	0.9	575.0	9.5	31.2	116.0	6.5	282.3	38.1	110.3
20%	750.0	60.4	34.5	146.9	25.8	575.0	24.6	34.7	130.5	46.7	285.0	97.1	124.2
10%	750.0	97.8	34.9	150.0	67.1	575.0	39.6	35.0	131.7	106.3	285.0	159.9	124.8
<b>March</b>													
90%	720.2	3.0	2.1	7.8	0.0	556.4	1.2	3.1	9.8	0.0	249.7	4.9	60.0
80%	728.1	5.6	14.0	56.0	0.0	572.7	2.3	24.1	88.1	0.3	259.6	9.6	65.1
50%	748.7	39.8	30.7	125.9	3.0	575.0	16.2	33.4	124.3	15.0	281.2	65.7	120.4
20%	750.0	106.3	34.8	149.0	65.5	575.0	41.7	34.9	131.5	104.5	285.0	166.6	124.8
10%	750.0	173.5	35.0	150.3	136.9	575.0	68.3	35.0	131.9	200.5	285.0	272.7	124.9
<b>April</b>													
90%	723.3	3.2	2.3	8.2	0.0	572.8	1.3	4.4	16.3	0.2	258.0	5.2	60.9
80%	734.0	7.0	21.3	84.3	0.0	574.7	2.9	25.0	91.9	1.9	269.8	11.8	86.0
50%	750.0	66.6	33.5	139.5	21.0	575.0	26.4	33.6	126.6	49.6	284.5	107.4	123.1
20%	750.0	188.6	34.8	149.6	151.8	575.0	74.8	34.9	131.5	224.8	285.0	301.8	124.8

(continued)

**Table 10.1** (continued)

<i>Ambuklao reservoir</i>				<i>Binga reservoir</i>				<i>San Roque reservoir</i>								
EOM	Inflow	Release	Power	EOM	Inflow	Release	Power	Spill	EOM	Inflow	Release	Power	Spill	Outflow		
10%	750.0	290.9	35.0	150.3	256.8	575.0	119.0	35.0	131.9	374.2	285.0	472.8	124.9	551.6		
<b>May</b>																
90%	720.2	3.2	2.2	8.0	0.0	568.8	1.3	2.5	8.3	0.1	268.0	5.4	60.9	261.1	0.0	67.0
80%	744.3	9.1	18.7	74.7	0.1	575.0	3.7	24.9	89.6	3.0	279.6	15.5	98.1	415.1	1.3	112.8
50%	750.0	163.6	33.1	141.8	126.3	575.0	63.5	33.4	126.1	189.3	285.0	270.3	122.7	538.9	329.1	468.2
20%	750.0	823.8	34.8	149.4	789.0	575.0	330.8	34.8	131.1	1101.4	285.0	1338.4	124.7	550.2	2318.7	2521.1
10%	750.0	1589.8	34.9	150.3	1562.6	575.0	619.1	34.9	131.9	2164.8	285.0	2510.1	124.9	551.7	4580.4	4820.3
<b>June</b>																
90%	728.1	3.4	2.3	8.5	0.0	572.7	1.3	3.9	13.5	0.2	271.3	5.5	60.8	260.5	0.0	65.0
80%	743.3	6.1	21.7	87.1	0.0	574.7	2.4	24.8	90.5	1.9	278.9	10.0	87.8	371.8	0.5	104.0
50%	750.0	128.1	32.4	137.2	91.8	575.0	54.2	33.2	124.7	143.4	285.0	214.6	121.9	531.8	228.9	360.9
20%	750.0	930.0	34.7	149.1	874.6	575.0	367.8	34.7	130.9	1238.2	285.0	1436.0	124.5	548.4	2533.9	2734.8
10%	750.0	2008.6	34.9	150.2	1992.6	575.0	784.2	34.9	131.7	2786.5	285.0	3147.8	124.9	551.3	5845.6	6134.7
<b>July</b>																
90%	728.2	3.6	2.7	10.1	0.0	570.8	1.4	6.4	23.5	0.2	271.6	5.9	64.3	272.8	0.0	74.4
80%	742.9	6.7	19.8	79.3	0.0	574.7	2.8	24.8	89.8	2.1	279.0	11.6	98.5	404.3	0.8	117.1
50%	750.0	90.6	32.6	138.1	52.4	575.0	37.5	33.0	123.6	89.8	285.0	153.7	122.0	532.6	117.1	238.9
20%	750.0	1158.7	34.7	148.9	1129.1	575.0	465.3	34.7	130.9	1576.6	285.0	1905.6	124.5	548.3	3403.8	3632.5
10%	750.0	3077.1	34.9	150.2	3043.1	575.0	1220.8	34.9	131.7	4256.9	285.0	4799.2	124.9	551.0	8939.1	9313.9
<b>August</b>																
90%	732.3	3.6	4.3	17.0	0.0	573.9	1.5	6.0	21.4	0.5	272.1	6.0	62.5	267.1	0.0	70.2
80%	742.8	5.7	23.2	92.2	0.0	575.0	2.4	25.0	90.8	2.9	278.5	9.8	104.0	444.9	1.9	120.3
50%	750.0	85.8	33.0	139.1	44.8	575.0	35.5	33.3	125.7	79.3	285.0	144.7	122.4	533.0	98.4	229.1

	20%	750.0	803.0	34.8	149.1	755.4	575.0	322.4	34.8	131.2	1096.4	285.0	1266.4	124.7	549.2	2219.6	2410.9
	10%	750.0	2169.5	35.0	150.2	2123.6	575.0	847.7	35.0	131.9	2972.9	285.0	3446.2	124.9	551.3	6309.1	6617.4
<b>September</b>																	
90%	730.3	3.7	4.8	19.5	0.0	573.6	1.5	10.0	35.6	0.3	273.9	6.0	62.0	266.1	0.0	76.1	
80%	743.7	5.9	22.4	89.5	0.0	574.8	2.4	25.7	96.3	2.3	280.0	9.9	96.2	404.1	1.9	113.4	
50%	750.0	80.8	33.2	140.1	28.9	575.0	31.2	33.5	125.9	59.1	285.0	128.4	122.8	536.6	59.5	184.0	
20%	750.0	469.4	34.8	149.3	429.8	575.0	194.4	34.8	131.3	639.1	285.0	786.0	124.7	549.7	1300.5	1483.4	
10%	750.0	1266.4	35.0	150.3	1233.2	575.0	514.9	35.0	131.9	1712.7	285.0	2009.7	124.9	551.4	3576.9	3841.4	
<b>October</b>																	
90%	734.9	3.6	12.5	51.8	0.0	573.2	1.4	21.6	80.9	0.4	275.6	5.8	60.1	259.9	0.0	66.1	
80%	743.0	4.5	24.1	95.9	0.0	574.6	1.8	25.8	97.0	1.6	278.9	7.5	69.2	296.8	1.9	87.1	
50%	750.0	54.4	32.8	139.0	11.9	575.0	22.7	33.6	126.1	37.4	284.8	88.7	122.3	529.7	38.5	152.7	
20%	750.0	327.5	34.8	149.3	295.8	575.0	136.2	34.8	131.4	449.9	285.0	561.3	124.7	550.2	895.3	1055.3	
10%	750.0	729.8	35.0	150.3	698.1	575.0	313.3	35.0	131.9	1013.4	285.0	1199.9	124.9	551.7	2121.5	2323.3	
<b>November</b>																	
90%	723.9	3.1	3.4	12.9	0.0	571.5	1.3	19.9	73.1	0.1	272.7	5.1	60.0	250.6	0.0	60.9	
80%	736.4	3.8	19.7	78.1	0.0	574.0	1.5	25.0	94.0	0.8	276.6	6.2	62.1	265.2	0.0	70.9	
50%	749.6	34.9	31.0	128.9	5.9	575.0	14.3	33.5	125.6	16.4	284.0	57.5	120.5	519.8	25.5	136.3	
20%	750.0	190.5	34.8	149.5	156.4	575.0	77.1	34.9	131.5	234.9	285.0	317.6	124.8	550.7	458.1	596.2	
10%	750.0	369.9	35.0	150.3	335.2	575.0	148.9	35.0	132.0	476.6	285.0	592.5	124.9	551.9	961.6	1117.5	
<b>December</b>																	
90%	720.1	2.8	2.4	8.7	0.0	561.8	1.1	4.2	13.9	0.0	267.3	4.5	60.0	246.5	0.0	60.5	
80%	726.5	3.3	18.3	70.6	0.0	572.5	1.3	24.7	89.8	0.4	273.0	5.4	62.0	260.5	0.0	64.6	
50%	749.7	42.2	30.3	125.1	3.0	575.0	17.9	32.8	122.2	18.2	283.9	69.1	119.0	511.0	12.4	130.5	
20%	750.0	140.3	34.8	149.8	107.1	575.0	57.1	34.9	131.6	165.4	285.0	227.8	124.8	551.1	301.9	437.7	
10%	750.0	205.0	35.0	150.4	173.8	575.0	82.8	35.0	132.0	257.9	285.0	328.7	125.0	551.9	492.8	632.0	

**Table 10.2** Reservoir end-of-month elevations (m); inflows, releases, and spills ( $\text{m}^3/\text{s}$ ; and power generation (MW) for Ambuklao, Binga, and San Roque and outflow to ARUP Reservoir for target release policy Set 2 with climate change scenario

	Ambuklao reservoir				Binga reservoir				San Roque reservoir				ARUP			
	EOM Elev	Inflow	Release	Power	EOM Elev	Inflow	Release	Power	EOM Elev	Inflow	Release	Power	Spill	Outflow		
<b>January</b>																
90%	720.0	2.6	2.4	8.7	0.0	546.6	1.0	3.8	11.7	0.0	235.2	4.1	80.0	295.6	0.0	81.3
80%	720.1	3.8	6.3	23.3	0.0	557.9	1.5	24.6	86.3	0.0	252.2	6.2	88.3	324.3	0.0	90.7
50%	749.4	46.1	33.0	136.9	3.2	575.0	19.0	33.9	126.1	20.1	282.3	75.2	121.0	491.4	1.2	129.6
20%	750.0	121.4	34.9	149.9	82.7	575.0	50.2	34.9	131.7	131.3	285.0	197.1	124.8	550.6	209.7	342.9
10%	750.0	180.0	35.0	150.5	144.6	575.0	75.0	35.0	132.0	216.6	285.0	293.4	125.0	551.9	407.5	546.3
<b>February</b>																
90%	720.0	2.9	2.4	8.6	0.0	546.0	1.1	3.8	11.7	0.0	216.1	4.6	80.0	250.5	0.0	80.9
80%	720.3	4.9	8.4	30.2	0.0	557.0	2.0	25.6	89.8	0.0	240.5	8.0	84.3	307.7	0.0	88.3
50%	747.3	23.1	31.6	129.6	0.7	575.0	9.5	33.9	126.5	7.3	279.3	38.1	117.7	456.5	1.2	125.6
20%	750.0	60.4	34.8	148.9	19.4	575.0	24.6	34.9	131.6	42.5	285.0	97.1	124.7	546.1	39.8	159.3
10%	750.0	97.8	35.0	150.3	62.0	575.0	39.6	35.0	132.0	102.1	285.0	159.9	125.0	550.6	139.7	268.3
<b>March</b>																
90%	720.1	3.0	3.0	11.1	0.0	552.7	1.2	13.4	44.3	0.0	198.0	4.9	82.0	228.1	0.0	83.9
80%	725.1	5.6	22.8	90.5	0.0	571.4	2.3	29.8	108.0	0.2	222.6	9.6	93.0	309.1	0.0	98.3
50%	747.1	39.8	33.8	135.8	2.0	575.0	16.2	34.4	128.6	15.3	275.2	65.7	122.8	468.2	0.4	129.2
20%	750.0	106.3	34.9	149.6	59.2	575.0	41.7	35.0	131.8	94.8	285.0	166.6	124.9	549.2	115.1	245.4
10%	750.0	173.5	35.0	150.4	130.5	575.0	68.3	35.0	132.0	195.9	285.0	272.7	125.0	551.5	327.6	463.2
<b>April</b>																
90%	721.0	3.2	7.5	27.2	0.0	567.8	1.3	24.9	91.2	0.1	220.3	5.2	87.2	302.1	0.0	89.9
80%	731.6	7.0	28.1	109.6	0.0	574.1	2.9	30.9	114.9	1.8	248.4	11.8	108.5	350.9	0.0	115.2
50%	750.0	66.6	34.3	144.8	18.3	575.0	26.4	34.5	129.9	45.7	281.9	107.4	123.7	519.4	12.1	139.8
20%	750.0	188.6	34.9	149.9	149.4	575.0	74.8	34.9	131.7	223.5	285.0	301.8	124.8	550.1	347.9	487.2

	10%	750.0	290.9	35.0	150.4	253.9	575.0	119.0	35.0	132.0	368.8	285.0	472.8	124.9	551.5	657.2	805.4	
<b>May</b>																		
90%	720.0	3.2	3.6	13.5	0.0	552.5	1.3	7.6	25.4	0.0	247.0	5.4	90.3	327.4	0.0	94.5		
80%	742.6	9.1	28.6	118.8	0.0	575.0	3.7	30.4	113.2	3.1	269.3	15.5	114.2	426.9	0.0	123.3		
50%	750.0	163.6	34.1	146.0	120.5	575.0	63.5	34.4	129.6	184.8	285.0	270.3	123.5	542.3	292.7	433.1		
20%	750.0	823.8	34.9	149.9	787.7	575.0	330.8	34.9	131.7	1104.0	285.0	1338.4	124.7	550.3	2263.6	2457.3		
10%	750.0	1589.8	35.0	150.4	1555.0	575.0	619.1	35.0	132.0	2166.2	285.0	2510.1	124.9	551.7	4550.2	4783.9		
<b>June</b>																		
90%	725.9	3.4	14.8	61.1	0.0	570.7	1.3	25.4	91.6	0.1	250.4	5.5	86.8	328.5	0.0	93.0		
80%	742.4	6.1	28.8	117.0	0.0	574.7	2.4	30.8	115.8	2.0	273.4	10.0	109.7	410.5	0.0	121.7		
50%	750.0	128.1	33.9	144.5	88.0	575.0	54.2	34.2	128.7	141.3	285.0	214.6	123.0	537.1	218.1	352.4		
20%	750.0	930.0	34.9	149.7	861.6	575.0	367.8	34.9	131.6	1227.8	285.0	1436.0	124.6	549.6	2534.0	2734.8		
10%	750.0	2008.6	35.0	150.3	1974.4	575.0	784.2	35.0	131.9	2786.3	285.0	3147.8	124.9	551.3	5837.5	6134.7		
<b>July</b>																		
90%	722.6	3.6	10.4	38.1	0.0	569.9	1.4	26.1	93.5	0.1	251.5	5.9	89.8	348.5	0.0	97.2		
80%	741.1	6.7	28.6	114.9	0.0	574.7	2.8	30.9	114.7	2.4	273.3	11.6	111.1	429.9	0.0	121.9		
50%	750.0	90.6	34.0	144.6	48.1	575.0	37.5	34.2	128.9	84.4	285.0	153.7	123.2	538.1	99.8	231.5		
20%	750.0	1158.7	34.9	149.7	1124.2	575.0	465.3	34.9	131.6	1577.3	285.0	1905.6	124.7	549.6	3370.3	3613.6		
10%	750.0	3077.1	35.0	150.3	3045.3	575.0	1220.8	35.0	132.0	4259.4	285.0	4799.2	124.9	551.4	8937.8	9313.9		
<b>August</b>																		
90%	727.4	3.6	14.7	60.0	0.0	573.1	1.5	26.1	94.8	0.3	261.3	6.0	90.5	351.0	0.0	97.7		
80%	741.6	5.7	29.9	123.7	0.0	575.0	2.4	31.0	116.4	2.8	274.4	9.8	113.7	456.2	0.0	123.6		
50%	750.0	85.8	34.2	144.9	39.8	575.0	35.5	34.3	129.3	79.0	285.0	144.7	123.4	539.0	79.1	209.9		
20%	750.0	803.0	34.9	149.7	746.9	575.0	322.4	34.9	131.7	1096.0	285.0	1266.4	124.8	550.2	2180.0	2375.6		
10%	750.0	2169.5	35.0	150.4	2124.6	575.0	847.7	35.0	132.0	2973.6	285.0	3446.2	124.9	551.6	6299.5	6615.8		
<b>September</b>																		
90%	728.1	3.7	17.4	71.0	0.0	570.9	1.5	28.0	103.8	0.4	262.2	6.0	90.4	353.7	0.0	99.3		

(continued)

Table 10.2 (continued)

<i>Ambuklao reservoir</i>						<i>Binga reservoir</i>						<i>San Roque reservoir</i>							
	EOM Elev	Inflow	Release	Power	Spill	EOM Elev	Inflow	Release	Power	Spill	EOM Elev	Inflow	Release	Power	Spill	Outflow	<i>ARIIP</i>		
80%	742.8	5.9	29.4	119.2	0.0	574.6	2.4	31.8	118.8	2.5	276.9	9.9	113.4	449.1	0.5	122.8			
50%	750.0	80.8	34.2	145.1	23.8	575.0	31.2	34.4	129.2	56.2	285.0	128.4	123.6	540.4	51.4	178.9			
20%	750.0	469.4	34.9	149.8	420.9	575.0	194.4	34.9	131.7	639.5	285.0	786.0	124.8	550.2	1292.0	1446.2			
10%	750.0	1266.4	35.0	150.3	1203.7	575.0	514.9	35.0	132.0	1695.1	285.0	209.7	124.9	551.6	3577.2	3829.2			
October																			
90%	731.9	3.6	20.6	80.0	0.0	572.9	1.4	28.9	106.7	0.3	263.9	5.8	85.0	347.3	0.0	90.2			
80%	741.9	4.5	28.9	115.7	0.0	574.5	1.8	31.5	118.3	1.6	273.1	7.5	100.7	400.7	0.0	109.7			
50%	750.0	54.4	34.1	144.5	9.7	575.0	22.7	34.5	129.7	31.8	284.6	88.7	123.2	534.6	30.9	150.7			
20%	750.0	327.5	34.9	149.9	291.4	575.0	136.2	34.9	131.8	449.2	285.0	561.3	124.8	550.3	890.0	1040.1			
10%	750.0	729.8	35.0	150.4	697.7	575.0	313.3	35.0	132.0	1005.5	285.0	1199.9	124.9	551.6	2101.4	2315.3			
November																			
90%	720.3	3.1	5.8	21.1	0.0	562.1	1.3	25.5	91.3	0.0	258.5	5.1	81.2	325.9	0.0	83.3			
80%	733.6	3.8	25.9	103.6	0.0	573.2	1.5	30.0	112.4	0.5	267.8	6.2	89.1	362.4	0.0	94.6			
50%	749.2	34.9	33.7	141.6	4.4	575.0	14.3	34.3	129.1	15.7	282.9	57.5	122.8	523.7	14.0	133.8			
20%	750.0	190.5	34.9	149.8	155.1	575.0	77.1	34.9	131.7	234.6	285.0	317.6	124.8	550.6	445.4	587.0			
10%	750.0	369.9	35.0	150.4	326.4	575.0	148.9	35.0	132.0	472.8	285.0	592.5	124.9	551.7	960.4	1112.1			
December																			
90%	720.0	2.8	2.9	10.3	0.0	552.1	1.1	13.7	46.5	0.0	243.8	4.5	80.6	312.0	0.0	81.9			
80%	723.0	3.3	19.0	74.3	0.0	570.3	1.3	29.0	103.8	0.3	261.1	5.4	87.6	338.0	0.0	89.9			
50%	749.4	42.2	33.3	137.0	2.8	575.0	17.9	34.1	127.8	17.8	283.2	69.1	122.0	500.6	8.0	130.4			
20%	750.0	140.3	34.9	150.1	105.3	575.0	57.1	34.9	131.8	163.9	285.0	227.8	124.9	551.2	294.3	428.8			
10%	750.0	205.0	35.0	150.5	170.2	575.0	82.8	35.0	132.0	252.3	285.0	328.7	125.0	552.0	486.3	628.2			

**Table 10.3** Reservoir end-of-month elevations (m); inflows, releases, and spills ( $\text{m}^3/\text{s}$ ); and power generation (MW) for Ambuklao, Binga, and San Roque and outflow to ARUIP Reservoir for target release policy Set 3 with climate change scenario

	Ambuklao reservoir				Binga reservoir				San Roque reservoir				ARUIP Outflow
	EOM Elev	Inflow	Release	Power	EOM Elev	Inflow	Release	Power	EOM Elev	Inflow	Release	Power	
<b>January</b>													
90%	720.0	2.6	2.4	8.5	0.0	545.5	1.0	3.5	10.8	0.0	243.3	4.1	70.0
80%	720.1	3.8	6.4	23.3	0.0	551.8	1.5	18.9	66.3	0.0	255.9	6.2	76.7
50%	749.4	46.1	32.1	132.5	3.2	575.0	19.0	34.5	127.8	20.2	282.7	75.2	118.3
20%	750.0	121.4	34.8	149.6	83.6	575.0	50.2	35.0	131.8	129.4	285.0	197.1	124.7
10%	750.0	180.0	35.0	150.4	144.8	575.0	75.0	35.0	132.0	216.1	285.0	293.4	124.9
<b>February</b>													
90%	720.0	2.9	2.5	9.1	0.0	545.4	1.1	3.8	11.8	0.0	227.8	4.6	70.0
80%	720.3	4.9	9.9	36.8	0.0	553.4	2.0	24.0	83.9	0.0	247.5	8.0	74.5
50%	747.1	23.1	30.6	126.3	0.6	575.0	9.5	34.5	128.6	6.9	280.6	38.1	111.4
20%	750.0	60.4	34.7	148.3	20.6	575.0	24.6	35.0	131.7	42.3	285.0	97.1	124.5
10%	750.0	97.8	35.0	150.0	62.2	575.0	39.6	35.0	132.0	97.7	285.0	159.9	124.9
<b>March</b>													
90%	720.1	3.0	3.1	11.2	0.0	550.7	1.2	10.4	33.9	0.0	218.2	4.9	72.1
80%	725.3	5.6	21.4	85.8	0.0	568.5	2.3	31.2	112.9	0.2	234.0	9.6	85.5
50%	747.5	39.8	33.2	134.4	2.1	575.0	16.2	34.7	129.6	15.0	278.3	65.7	121.1
20%	750.0	106.3	34.9	149.2	59.1	575.0	41.7	35.0	131.8	95.9	285.0	166.6	124.8
10%	750.0	173.5	35.0	150.3	131.8	575.0	68.3	35.0	132.0	198.2	285.0	272.7	124.9
<b>April</b>													
90%	721.0	3.2	4.3	16.4	0.0	566.0	1.3	19.9	72.1	0.0	233.5	5.2	76.5
80%	731.2	7.0	27.5	108.4	0.0	573.0	2.9	32.5	120.2	2.2	255.5	11.8	105.0
50%	750.0	66.6	34.0	143.5	18.6	575.0	26.4	34.6	130.1	44.4	282.9	107.4	123.4
20%	750.0	188.6	34.9	149.8	150.5	575.0	74.8	35.0	131.8	223.9	285.0	301.8	124.8

(continued)

**Table 10.3** (continued)

<i>Ambuklao reservoir</i>				<i>Binga reservoir</i>				<i>San Roque reservoir</i>					
EOM	Inflow	Release	Power	EOM	Inflow	Release	Power	EOM	Inflow	Release	Power	Spill	Outflow
Elev				Elev				Elev					
10%	750.0	290.9	35.0	150.4	233.0	575.0	119.0	35.0	132.0	368.9	285.0	472.8	124.9
May													
90%	720.0	3.2	2.8	10.5	0.0	550.7	1.3	5.5	17.4	0.0	254.0	5.4	78.6
80%	743.1	9.1	25.7	106.9	0.0	574.8	3.7	31.4	116.3	2.5	274.6	15.5	110.2
50%	750.0	163.6	33.8	144.2	123.6	575.0	63.5	34.5	130.1	181.5	285.0	270.3	123.0
20%	750.0	823.8	34.8	149.7	788.8	575.0	330.8	34.9	131.8	1103.1	285.0	1338.4	124.7
10%	750.0	1589.8	35.0	150.3	1557.7	575.0	619.1	35.0	132.0	2164.4	285.0	2510.1	124.9
June													
90%	725.9	3.4	5.2	20.6	0.0	568.6	1.3	22.3	80.0	0.1	257.3	5.5	77.4
80%	742.7	6.1	26.5	108.3	0.0	574.0	2.4	32.1	119.3	2.1	274.8	10.0	101.9
50%	750.0	128.1	33.5	142.7	90.1	575.0	54.2	34.5	129.5	140.0	285.0	214.6	122.3
20%	750.0	930.0	34.8	149.3	872.9	575.0	367.8	34.9	131.6	1227.1	285.0	1436.0	124.6
10%	750.0	2008.6	34.9	150.2	1974.1	575.0	784.2	35.0	131.9	2785.5	285.0	3147.8	124.9
July													
90%	723.0	3.6	7.5	28.4	0.0	566.0	1.4	24.4	88.4	0.1	260.2	5.9	81.9
80%	741.2	6.7	26.7	105.3	0.0	574.4	2.8	31.7	116.8	2.2	275.2	11.6	107.1
50%	750.0	90.6	33.5	142.2	49.7	575.0	37.5	34.4	129.2	86.5	285.0	153.7	122.4
20%	750.0	1158.7	34.8	149.3	1122.8	575.0	465.3	34.9	131.7	1577.4	285.0	1905.6	124.6
10%	750.0	3077.1	35.0	150.3	3042.2	575.0	1220.8	35.0	132.0	4256.7	285.0	4799.2	124.9
August													
90%	728.7	3.6	7.7	32.0	0.0	570.3	1.5	24.3	89.4	0.3	265.3	6.0	85.2
80%	741.8	5.7	28.3	114.6	0.0	574.8	2.4	32.1	120.0	3.1	275.5	9.8	111.7
50%	750.0	85.8	33.8	143.2	38.9	575.0	35.5	34.5	129.7	78.4	285.0	144.7	122.9

20%	750.0	803.0	34.8	149.4	749.8	575.0	322.4	34.9	131.7	1090.5	285.0	1266.4	124.7	549.3	2216.9	2399.7
10%	750.0	2169.5	35.0	150.2	2124.7	575.0	847.7	35.0	132.0	2978.2	285.0	3446.2	124.9	551.4	6301.4	6615.8
<b>September</b>																
90%	729.0	3.7	13.6	53.9	0.0	569.1	1.5	27.8	102.3	0.3	266.5	6.0	84.7	336.2	0.0	96.3
80%	743.1	5.9	28.1	113.8	0.0	574.1	2.4	33.0	121.5	2.4	277.8	9.9	106.6	431.5	0.7	120.4
50%	750.0	80.8	33.9	143.9	23.9	575.0	31.2	34.6	130.1	56.8	285.0	128.4	123.1	537.2	57.9	188.2
20%	750.0	469.4	34.9	149.6	423.7	575.0	194.4	35.0	131.8	639.3	285.0	786.0	124.7	549.9	1297.4	1475.4
10%	750.0	1266.4	35.0	150.3	1204.8	575.0	514.9	35.0	132.0	1695.2	285.0	2009.7	124.9	551.5	3582.5	3841.4
<b>October</b>																
90%	731.9	3.6	18.6	73.6	0.0	570.5	1.4	29.7	109.2	0.3	267.7	5.8	77.1	314.0	0.0	84.3
80%	742.1	4.5	27.5	110.4	0.0	573.9	1.8	33.0	122.2	1.6	275.2	7.5	95.8	394.1	0.0	108.4
50%	750.0	54.4	33.8	143.1	10.7	575.0	22.7	34.7	130.3	31.0	284.7	88.7	122.5	529.4	34.4	151.0
20%	750.0	327.5	34.9	149.5	291.8	575.0	136.2	35.0	131.8	451.2	285.0	561.3	124.7	549.7	888.0	1040.1
10%	750.0	729.8	35.0	150.3	695.0	575.0	313.3	35.0	132.0	1004.7	285.0	1199.9	124.9	551.6	2105.1	2321.1
<b>November</b>																
90%	720.3	3.1	4.2	15.2	0.0	557.2	1.3	19.5	70.5	0.0	262.4	5.1	71.0	292.0	0.0	73.8
80%	733.8	3.8	24.2	96.9	0.0	571.7	1.5	32.8	120.7	0.7	270.8	6.2	82.8	340.7	0.0	90.3
50%	749.3	34.9	33.2	139.2	4.9	575.0	14.3	34.7	130.2	15.5	283.3	57.5	121.7	517.0	19.1	135.1
20%	750.0	190.5	34.9	149.7	156.1	575.0	77.1	35.0	131.8	235.3	285.0	317.6	124.8	550.5	449.8	587.0
10%	750.0	369.9	35.0	150.4	334.1	575.0	148.9	35.0	132.0	472.6	285.0	592.5	124.9	551.7	958.4	1112.1
<b>December</b>																
90%	720.0	2.8	2.8	10.0	0.0	550.1	1.1	6.8	23.2	0.0	250.4	4.5	71.2	279.6	0.0	72.5
80%	722.5	3.3	19.1	74.9	0.0	565.8	1.3	30.4	109.4	0.2	263.5	5.4	80.0	316.7	0.0	82.8
50%	749.3	42.2	32.6	134.0	2.6	575.0	17.9	34.6	128.9	18.0	283.5	69.1	120.8	507.7	8.6	130.5
20%	750.0	140.3	34.9	149.9	106.5	575.0	57.1	35.0	131.8	163.8	285.0	227.8	124.8	551.0	299.9	434.2
10%	750.0	205.0	35.0	150.5	171.8	575.0	82.8	35.0	132.0	253.6	285.0	328.7	125.0	552.0	492.4	628.6

(maximum of 27 m<sup>3</sup>/s) for all months at even more than 90 percent-of-the-time reliability. In fact, in almost all months, the average daily releases are as high as 80 m<sup>3</sup>/s (at 90 percent reliability) so that ARIIP can even increase its irrigation service area to even twice as much as the current service area.

### ***10.1.3 Comparison of Hydropower Generation Between Existing and 2050 Climate Change Scenarios***

Since maximizing hydropower generation is the major objective in the Ambuklao-Binga-San Roque Reservoir system, it is worthwhile to focus the discussion on comparison of hydropower generation between the existing climate and for the case with 2050 climate change scenario. Tables 10.4, 10.5, and 10.6 show the hydropower generation of the Ambuklao, Binga, and San Roque reservoirs, respectively, for the existing reservoir and 2050 climate change scenarios and for the three sets of target release policies.

For the hydropower generation of Ambuklao Reservoir in Table 10.4, it shows that in the three release policies (Set 1, Set 2, and Set 3), the target release of 30 m<sup>3</sup>/s in Set 2 provides higher hydropower generation compared to the more conservative release policy of only 25 m<sup>3</sup>/s in Set 1 for the different scenarios. However, for the same target release of 30 m<sup>3</sup>/s in Set 3, it resulted in lower hydropower generation which is most likely due to the higher target release in Binga Reservoir of 35 m<sup>3</sup>/s in Set 3 rather than only 30 m<sup>3</sup>/s (at Binga) in Set 2. This implies that optimal hydropower generation or water delivery should not be too conservative, or too aggressive. Note that part of this reservoir operation study was to seek for this best or optimal target release.

For the hydropower generation in Binga Reservoir in Table 10.5, a similar trend is observed as in Ambuklao where the target release policy Set 2 results in higher hydropower generation. Similarly, the scenario with 2050 climate change results in the lowest hydropower generation.

In Table 10.6 for the hydropower generation of San Roque Reservoir, it appears that best reservoir release policy that results in highest optimal hydropower generation depends on the month of the year. During the months of August through March, the best release policy is Set 1 which is a conservative release policy, while the aggressive release policy Set 3 is best only for the month of July, and for the remaining month from April through June and September, the best release policy is Set 2. This result can be observed in both existing and climate change scenarios.

**Table 10.4** Comparison of Ambuklao Reservoir generated hydropower (MW) for the existing reservoir and 2050 climate change scenarios for the three sets of target release policies (RP)

	Existing scenario			Climate change scenario		
	Set 1 RP	Set 2 RP	Set 3 RP	Set 1 RP	Set 2 RP	Set 3 RP
January						
90%	6.8	7.2	7.4	8.3	8.7	8.5
80%	11.4	15.3	14.1	26.1	23.3	23.3
50%	119.5	133.5	130.4	121.6	136.9	132.5
20%	149.7	150.0	149.8	149.2	149.9	149.6
10%	150.4	150.4	150.4	150.3	150.5	150.4
February						
90%	7.8	10.6	10.7	7.9	8.6	9.1
80%	45.3	84.6	73.6	19.4	30.2	36.8
50%	136.6	144.4	141.1	108.7	129.6	126.3
20%	149.8	150.1	150.0	146.9	148.9	148.3
10%	150.4	150.5	150.4	150.0	150.3	150.0
March						
90%	10.1	24.9	30.0	7.8	11.1	11.2
80%	86.6	108.9	108.5	56.0	90.5	85.8
50%	136.7	144.1	142.1	125.9	135.8	134.4
20%	149.8	150.1	149.9	149.0	149.6	149.2
10%	150.4	150.5	150.4	150.3	150.4	150.3
April						
90%	29.7	65.7	61.6	8.2	27.2	16.4
80%	90.0	111.2	109.6	84.3	109.6	108.4
50%	137.9	145.4	143.3	139.5	144.8	143.5
20%	149.9	150.1	150.1	149.6	149.9	149.8
10%	150.4	150.5	150.5	150.3	150.4	150.4
May						
90%	7.7	9.6	8.8	8.0	13.5	10.5
80%	69.8	91.0	79.1	74.7	118.8	106.9
50%	132.2	143.2	140.1	141.8	146.0	144.2
20%	149.8	150.1	149.9	149.4	149.9	149.7
10%	150.5	150.5	150.4	150.3	150.4	150.3
June						
90%	7.8	8.3	8.0	8.5	61.1	20.6
80%	48.4	35.2	28.4	87.1	117.0	108.3
50%	114.4	131.9	130.0	137.2	144.5	142.7
20%	149.3	149.9	149.6	149.1	149.7	149.3
10%	150.3	150.4	150.3	150.2	150.3	150.2
July						
90%	7.1	7.1	7.2	10.1	38.1	28.4
80%	13.2	10.8	11.1	79.3	114.9	105.3
50%	102.6	121.8	118.1	138.1	144.6	142.2
20%	147.0	149.0	148.6	148.9	149.7	149.3

(continued)

**Table 10.4** (continued)

	<i>Existing scenario</i>			<i>Climate change scenario</i>		
	Set 1 RP	Set 2 RP	Set 3 RP	Set 1 RP	Set 2 RP	Set 3 RP
10%	149.9	150.3	150.2	150.2	150.3	150.3
August						
90%	6.8	7.0	6.7	17.0	60.0	32.0
80%	11.0	11.0	10.3	92.2	123.7	114.6
50%	99.6	116.0	114.4	139.1	144.9	143.2
20%	144.8	148.0	146.7	149.1	149.7	149.4
10%	149.6	150.0	149.9	150.2	150.4	150.2
September						
90%	7.3	7.5	7.1	19.5	71.0	53.9
80%	14.1	12.3	11.2	89.5	119.2	113.8
50%	95.5	112.8	110.8	140.1	145.1	143.9
20%	141.2	146.4	144.5	149.3	149.8	149.6
10%	148.8	149.8	149.3	150.3	150.3	150.3
October						
90%	7.2	7.4	7.3	51.8	80.0	73.6
80%	11.6	12.3	11.7	95.9	115.7	110.4
50%	98.6	118.5	114.7	139.0	144.5	143.1
20%	143.4	147.2	145.7	149.3	149.9	149.5
10%	149.4	149.9	149.6	150.3	150.4	150.3
November						
90%	6.2	6.5	6.6	12.9	21.1	15.2
80%	10.1	10.4	10.2	78.1	103.6	96.9
50%	98.8	117.1	114.5	128.9	141.6	139.2
20%	146.5	148.9	148.1	149.5	149.8	149.7
10%	149.9	150.3	150.2	150.3	150.4	150.4
December						
90%	7.0	7.0	7.1	8.7	10.3	10.0
80%	12.4	11.5	11.9	70.6	74.3	74.9
50%	105.5	124.3	120.6	125.1	137.0	134.0
20%	148.7	149.6	149.2	149.8	150.1	149.9
10%	150.2	150.4	150.4	150.4	150.5	150.5

### 10.1.4 Other Issues and Challenges of the Upper Agno Reservoir Operations

#### 10.1.4.1 Present and Future Water Demand

As mentioned earlier, the Ambuklao, Binga, and San Roque Reservoirs of Upper Agno are mainly operated by maximizing hydropower generation, and only San Roque Reservoir has an irrigation water demand for ARIIP. As noted in the reliability analysis presented earlier, the current daily irrigation demand (with a

**Table 10.5** Comparison of Binga Reservoir generated hydropower (MW) for the existing reservoir and 2050 climate change scenarios for the three sets of target release policies (RP)

	Existing scenario			Climate change scenario		
	Set 1 RP	Set 2 RP	Set 3 RP	Set 1 RP	Set 2 RP	Set 3 RP
January						
90%	8.4	9.0	9.2	13.3	11.7	10.8
80%	28.9	28.8	22.9	79.7	86.3	66.3
50%	119.9	126.7	127.2	120.6	126.1	127.8
20%	131.5	131.8	131.8	131.4	131.7	131.8
10%	132.0	132.0	132.0	131.9	132.0	132.0
February						
90%	10.2	15.5	16.8	10.0	11.7	11.8
80%	79.0	105.0	112.9	64.4	89.8	83.9
50%	126.4	130.0	130.5	116.0	126.5	128.6
20%	131.7	131.9	131.9	130.5	131.6	131.7
10%	132.0	132.1	132.1	131.7	132.0	132.0
March						
90%	21.4	89.3	96.7	9.8	44.3	33.9
80%	94.4	116.4	121.5	88.1	108.0	112.9
50%	127.1	130.1	130.5	124.3	128.6	129.6
20%	131.7	131.9	131.9	131.5	131.8	131.8
10%	132.0	132.0	132.1	131.9	132.0	132.0
April						
90%	70.6	102.8	106.4	16.3	91.2	72.1
80%	95.5	117.8	122.4	91.9	114.9	120.2
50%	127.3	130.3	130.6	126.6	129.9	130.1
20%	131.7	131.9	131.9	131.5	131.7	131.8
10%	132.0	132.0	132.1	131.9	132.0	132.0
May						
90%	11.8	21.0	12.9	8.3	25.4	17.4
80%	90.4	109.5	117.8	89.6	113.2	116.3
50%	124.4	129.4	130.3	126.1	129.6	130.1
20%	131.7	131.8	131.9	131.1	131.7	131.8
10%	132.0	132.0	132.0	131.9	132.0	132.0
June						
90%	11.0	12.1	10.4	13.5	91.6	80.0
80%	81.1	93.2	90.0	90.5	115.8	119.3
50%	114.3	126.6	129.1	124.7	128.7	129.5
20%	131.2	131.7	131.7	130.9	131.6	131.6
10%	131.9	132.0	132.0	131.7	131.9	131.9
July						
90%	8.7	8.8	8.6	23.5	93.5	88.4
80%	61.4	29.1	19.9	89.8	114.7	116.8
50%	109.6	123.0	127.0	123.6	128.9	129.2
20%	130.9	131.4	131.6	130.9	131.6	131.7

(continued)

**Table 10.5** (continued)

	<i>Existing scenario</i>			<i>Climate change scenario</i>		
	Set 1 RP	Set 2 RP	Set 3 RP	Set 1 RP	Set 2 RP	Set 3 RP
10%	131.8	131.9	132.0	131.7	132.0	132.0
August						
90%	8.4	9.0	8.7	21.4	94.8	89.4
80%	23.3	19.4	16.1	90.8	116.4	120.0
50%	104.2	120.5	125.3	125.7	129.3	129.7
20%	129.8	131.4	131.5	131.2	131.7	131.7
10%	131.7	132.0	132.0	131.9	132.0	132.0
September						
90%	9.1	9.5	8.9	35.6	103.8	102.3
80%	33.6	25.3	19.6	96.3	118.8	121.5
50%	102.3	118.2	123.6	125.9	129.2	130.1
20%	129.5	131.2	131.3	131.3	131.7	131.8
10%	131.5	132.0	132.0	131.9	132.0	132.0
October						
90%	8.8	9.0	9.1	80.9	106.7	109.2
80%	20.3	18.4	16.0	97.0	118.3	122.2
50%	103.4	119.9	124.6	126.1	129.7	130.3
20%	129.3	131.5	131.7	131.4	131.8	131.8
10%	131.6	132.0	132.0	131.9	132.0	132.0
November						
90%	7.7	8.3	8.3	73.1	91.3	70.5
80%	24.3	17.4	14.9	94.0	112.4	120.7
50%	101.3	118.1	125.0	125.6	129.1	130.2
20%	130.5	131.7	131.7	131.5	131.7	131.8
10%	131.8	132.0	132.0	132.0	132.0	132.0
December						
90%	8.3	8.7	8.7	13.9	46.5	23.2
80%	29.1	30.2	19.7	89.8	103.8	109.4
50%	107.5	121.1	124.5	122.2	127.8	128.9
20%	131.2	131.6	131.7	131.6	131.8	131.8
10%	131.9	132.0	132.0	132.0	132.0	132.0

maximum amount of  $27 \text{ m}^3/\text{s}$  on any month to irrigate about 12,000 hectares) is more than satisfied every month since even as much as  $80 \text{ m}^3/\text{s}$  is released at San Roque Dam at 90 percent-of-the-time reliability. Thus, with the present irrigation water demand at ARIIP, as long as there is enough water, hydropower generation is maximized and that the irrigation demand is always satisfied. In the future, ARIIP is planning to expand the irrigable service from 12,000 hectares to perhaps 25,000

**Table 10.6** Comparison of San Roque Reservoir generated hydropower (MW) for the existing reservoir and 2050 climate change scenarios for the three sets of target release policies (RP)

	Existing Scenario			Climate Change Scenario		
	Set 1 RP	Set 2 RP	Set 3 RP	Set 1 RP	Set 2 RP	Set 3 RP
January						
90%	225.6	174.7	197.8	240.3	295.6	266.5
80%	244.1	254.4	260.1	251.3	324.3	292.5
50%	450.9	433.0	429.5	500.7	491.4	491.5
20%	550.6	550.2	549.9	549.9	550.6	549.8
10%	551.8	551.7	551.8	551.7	551.9	551.7
February						
90%	226.1	211.3	218.8	232.9	250.5	240.7
80%	260.1	268.8	279.1	248.6	307.7	276.0
50%	497.7	493.7	480.8	461.7	456.5	449.3
20%	551.0	550.9	550.6	544.2	546.1	543.2
10%	551.9	551.9	551.9	550.1	550.6	550.0
March						
90%	243.7	224.2	250.6	236.2	228.1	232.5
80%	274.4	327.6	322.4	265.1	309.1	298.4
50%	506.6	505.2	491.7	481.8	468.2	462.2
20%	550.6	550.6	550.1	548.9	549.2	549.0
10%	551.9	551.8	551.7	551.5	551.5	551.4
April						
90%	255.2	300.7	277.3	255.4	302.1	285.2
80%	285.3	344.2	325.0	352.5	350.9	351.7
50%	522.1	520.7	515.2	529.1	519.4	518.6
20%	550.7	550.8	551.0	550.2	550.1	550.1
10%	551.9	552.0	551.9	551.6	551.5	551.6
May						
90%	246.7	308.5	277.5	261.1	327.4	309.5
80%	263.5	348.7	325.2	415.1	426.9	430.7
50%	509.9	510.4	505.7	538.9	542.3	539.5
20%	550.8	550.9	550.7	550.2	550.3	549.9
10%	552.0	551.9	551.9	551.7	551.7	551.5
June						
90%	236.2	271.2	263.5	260.5	328.5	302.7
80%	253.3	317.7	292.9	371.8	410.5	402.2
50%	448.6	496.4	483.7	531.8	537.1	533.0
20%	550.3	550.1	549.9	548.4	549.6	549.2
10%	551.9	551.8	551.7	551.3	551.3	551.2
July						
90%	230.3	221.7	237.1	272.8	348.5	318.9
80%	245.0	292.0	272.8	404.3	429.9	422.4
50%	342.9	426.0	413.7	532.6	538.1	533.7
20%	547.6	548.9	547.7	548.3	549.6	548.9

(continued)

**Table 10.6** (continued)

	<i>Existing Scenario</i>			<i>Climate Change Scenario</i>		
	Set 1 RP	Set 2 RP	Set 3 RP	Set 1 RP	Set 2 RP	Set 3 RP
10%	551.3	551.5	551.4	551.0	551.4	551.1
August						
90%	219.9	185.2	204.0	267.1	351.0	344.6
80%	238.4	260.6	256.1	444.9	456.2	450.3
50%	303.7	373.0	367.8	533.0	539.0	534.8
20%	539.0	541.8	538.2	549.2	550.2	549.3
10%	550.0	550.7	550.0	551.3	551.6	551.4
September						
90%	215.9	151.2	187.0	266.1	353.7	336.2
80%	239.5	238.2	245.8	404.1	449.1	431.5
50%	297.5	349.6	339.3	536.6	540.4	537.2
20%	522.6	526.5	525.9	549.7	550.2	549.9
10%	547.0	547.3	545.5	551.4	551.6	551.5
October						
90%	218.1	170.4	194.0	259.9	347.3	314.0
80%	234.9	234.2	243.0	296.8	400.7	394.1
50%	304.0	345.1	343.0	529.7	534.6	529.4
20%	524.9	518.4	518.4	550.2	550.3	549.7
10%	546.2	545.7	544.4	551.7	551.6	551.6
November						
90%	215.1	134.3	184.5	250.6	325.9	292.0
80%	237.4	208.4	226.9	265.2	362.4	340.7
50%	305.1	350.8	335.7	519.8	523.7	517.0
20%	538.0	530.8	532.2	550.7	550.6	550.5
10%	550.3	550.1	549.6	551.9	551.7	551.7
December						
90%	224.0	131.8	179.8	246.5	312.0	279.6
80%	240.1	237.8	237.9	260.5	338.0	316.7
50%	365.2	352.5	347.9	511.0	500.6	507.7
20%	546.3	542.8	543.6	551.1	551.2	551.0
10%	551.4	551.2	551.1	551.9	552.0	552.0

hectares which implies that the irrigation water demand from San Roque Reservoir can be twice the current amounts. In this case, since the reservoir releases at San Roque is even as much as  $80 \text{ m}^3/\text{s}$  at 90 percent-of-the-time reliability, then this future irrigation water demand can be easily satisfied.

#### **10.1.4.2 Water Supply and Demand Management**

With regard to water supply and demand management, with the existing or current conditions of the Upper Agno watersheds and reservoirs, it appears that there is no pressing issue or concern. However, with future reservoir sedimentation, there may be a reduction in irrigation water releases during the months of November and December. In this case, with regard to water demand management, there may be some adjustments to be made in the timing of cropping schedules during this period especially when the irrigable service area is increased. With climate change, it may be noted that only during 3 months of January through March that rainfall is reduced but for the rest of the year the rainfall increases so that water supply management is not an issue also.

#### **10.1.4.3 Institutional Arrangement on Upper Agno Reservoir Operations**

Currently, the hydropower asset of Ambuklao and Binga is owned by SN-Aboitiz while that of San Roque's is owned by the San Roque Power Corporation (SRPC). The ARIIP irrigation water delivery from San Roque is the concern of National Irrigation Administration (NIA). During normal reservoir operations, SN-Aboitiz and SRPC in coordination with NIA direct the reservoir operations (when and how much to release) on day-to-day basis with National Power Corporation (NAPOCOR) overseeing the operations. However, during emergency reservoir operations (under storm or typhoon conditions), the reservoir operation is directly under NAPOCOR in coordination with PAGASA and to some extent, in consultation with NWRB. The Ambuklao and Binga Reservoir operations are not quite as critical during emergency operations since they do not have significant flood control function compared to San Roque Reservoir which has a flood allocation storage of almost 130 million m<sup>3</sup> (MCM) from 280 to 290 m reservoir elevations which can contain a sustained inflow of about 3000 m<sup>3</sup>/s for 12 hours without spilling during that period. Under normal reservoir operations, the above institutional arrangement is fairly adequate. However, during emergency reservoir operations, government agencies including private organizations downstream of San Roque Dam such as the local government units, the provincial or even national disaster risk management units must be involved to ensure that flood risk management is adequate at the downstream of San Roque Dam. In particular, the flood risk management scheme should include flood inundation modeling and forecasting together with real-time monitoring in the Central and Lower Agno River Basin (downstream of San Roque Dam) and the proper dissemination of this information for purposes of early warning as well as emergency response and recovery protocols in the affected communities (Tabios et al. 2010).

## 10.2 Angat Reservoir Reliability Analysis with Climate Change and Future Reservoir Sedimentation

In Sect. 5.1, the Angat Reservoir system and the various reservoir operations studies were presented to evaluate their performance and for reliability analysis especially in the context of the competing uses of its water. Also presented was the Angat Reservoir monthly allocation scheme with accompanying monthly inflow forecasting model. In this section, the reservoir operations studies presented evaluated the performance of the Angat Reservoir under 2050 climate change. In addition, a comparison was also made between its performance and reliability to deliver contractual requirements for domestic and irrigation water supply under climate change and with future reservoir sedimentation. In this case, the optimization-simulation studies conducted were with climate change and with future reservoir sedimentation, both in 2050. The water demands imposed are 46 CMS MWSS domestic water demand and the NIA's irrigation water demand on monthly basis is the same as those presented in Sect. 5.1. This presentation below is also contained in the papers by Tabios (2014, 2016).

### 10.2.1 Angat River Basin 2050 Climate Change Parameters

For Central Luzon and Angat River Basin in particular, Koike (2012) found out that 6 global climate models (GCMs) are appropriate for this area out of 25 GCMs used by the Intergovernmental Panel on Climate Change (IPCC). The results of these six GCMs were then downscaled for the Angat River Basin as shown in Table 10.7, which shows that half of the six GCMs resulted in higher (and half lower) annual mean discharge inflow to the Angat Reservoir for the future climate scenario (around 2046–2065) compared with the past climate scenario (circa 1981–2000). However, all the standard deviations for the future climate scenario resulted in higher values than the past climate. For the Angat River climate change scenario, the result of downscaling from Koike (2012) using the GFDL\_0 global climate model was used

**Table 10.7** Annual average discharge to Angat Reservoir for past and future climate scenarios from six global climate models (GCMs)

GCM	Annual average discharge ( $m^3/s$ )			
	Past(1981–2000)		Future (2046–2065)	
	Average	Stdev	Average	Stdev
MIROC	28.30	80.30	27.80	114.60
IPSL	35.30	94.40	63.70	159.70
INGV	32.80	85.00	35.40	105.40
GFDL_1	32.60	85.40	31.30	109.79
GFDL_0	35.00	90.30	34.20	101.66
CSIRO	28.50	67.10	30.30	152.80
<i>Average</i>	32.08	83.75	37.12	123.99

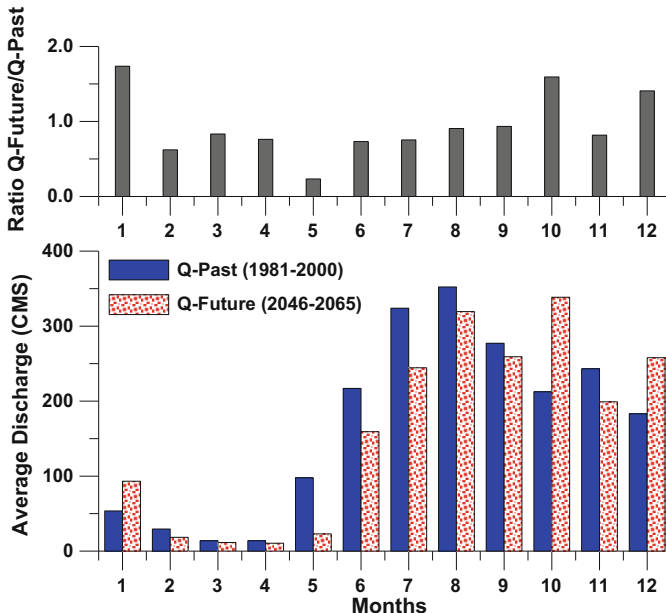


**Fig. 10.3** Monthly average discharges to Angat Reservoir for past (Q-past) and future (Q-future) climate change scenarios from GFDL\_0 GCM including the monthly ratios (Q-future/Q-past) of monthly past and future climate inflows

here, and Fig. 10.3 shows the time series plots of the monthly mean discharges of inflows to the Angat Reservoir for past and future climate scenarios as well as the ratio of future (Q-future) and past (Q-past) monthly discharges. In 9 of 12 months, the ratios (Q-future/Q-past) were less than 1.0; thus, the inflows were lower in the future climate than in the past climate. For this optimization-simulation scenario, the daily watershed inflows from 1974 to 2012 were multiplied by the ratios (Q-future/Q-past) on a monthly basis as inputs to the Angat Reservoir watershed model with Sacramento soil-moisture accounting (see Sect. 5.1.1, Chap. 5). Also, for this particular scenario, the MWSS domestic water demand was set at 46 CMS.

### 10.2.2 Angat Reservoir Sedimentation in 2050

This scenario was used to assess the reliability of the Angat Reservoir system to deliver water to MWSS and NIA-AMRIS with future sediment deposition in Angat Reservoir around 2050. The future sediment scenario was created based on the historical reservoir sediment accumulated or deposited in Angat Reservoir, estimated to be about 4.128 million cubic meters (MCM) per year. This was computed from the difference between the original reservoir volume of 1050 MCM in 1967 at 217 m reservoir elevation and the current volume of about 855 MCM (in 2013), also

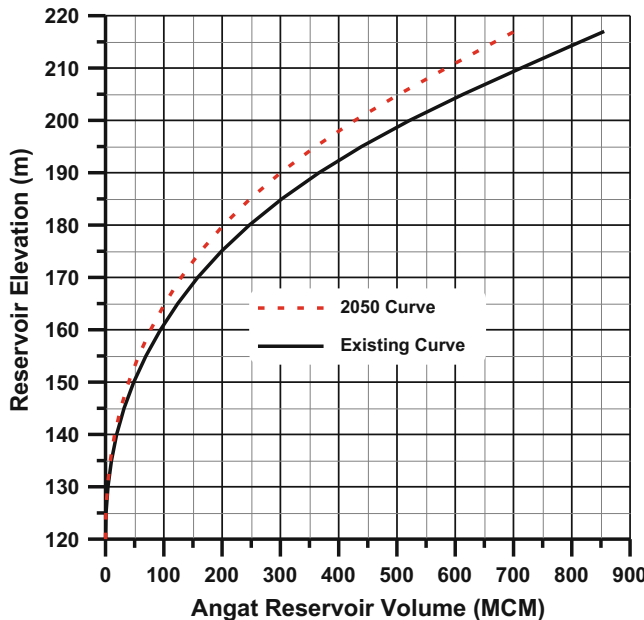


**Fig. 10.4** Angat Reservoir elevation-volume curves for existing case (circa 2013) and with 2050 future reservoir sedimentation

at 217 m reservoir elevation. Assuming the same sediment inflow rate in the future, the reservoir volume at 217 m elevation would be about 702 MCM in 2050, which is a total of 153 MCM reservoir sediment deposited by 2050 from 2013. The future reservoir sediment deposition scenario is accounted for in the optimization-simulation model with the 2050 reservoir storage-elevation curve as shown in Fig. 10.4. Also shown in this figure is the current storage-elevation curve. This future sediment scenario storage-elevation curve assumes that the sediment deposition is uniformly deposited in the reservoir at the ratio 0.82 (from the quotient of 702/855).

### 10.2.3 Results of Angat Reservoir Operations Under 2050 Climate Change and Future Sedimentation

With 38 years of daily streamflow generated (January 1974 to December 2012) from the watershed model, the optimization-simulation model runs were conducted to determine the reservoir releases and associated hydropower generation. Then the flow duration curves (as the basis of reliability analysis) were calculated on a monthly basis by pooling all the daily reservoir releases and hydropower generated by month. For the climate change and future sedimentation scenarios, the flow duration curves are given in Tables 10.8 and 10.9 for Angat Reservoir releases to

**Table 10.8** Angat Reservoir daily releases to Ipo Dam for MWSS domestic water supply for the three optimization-simulation scenarios: (a) with 46 CMS MWSS demand; (b) with reservoir sedimentation and 46 CMS demand; and (c) with climate change and 46 CMS demand

Month	Percent of time	Angat Releases to Ipo Dam (CMS)		
		Existing 46 CMS MWSS demand	2050 Climate change scenario	Future reservoir sedimentation
<i>Jan</i>	80	46.00	46.00	<b>4.59</b>
	60	46.00	46.00	<b>9.79</b>
	40	46.00	46.00	<b>19.13</b>
<i>Feb</i>	80	<b>29.77</b>	<b>31.49</b>	<b>3.37</b>
	60	46.00	46.00	<b>5.79</b>
	40	46.00	46.00	<b>10.78</b>
<i>Mar</i>	80	<b>5.70</b>	<b>4.91</b>	<b>3.06</b>
	60	<b>36.70</b>	<b>39.95</b>	<b>5.26</b>
	40	46.00	46.00	<b>9.74</b>
<i>Apr</i>	80	<b>4.09</b>	<b>2.98</b>	<b>3.67</b>
	60	<b>19.43</b>	<b>14.31</b>	<b>7.09</b>
	40	46.00	46.00	15.50
<i>May</i>	80	<b>14.38</b>	<b>3.13</b>	<b>8.41</b>
	60	<b>46.00</b>	<b>14.18</b>	<b>23.85</b>
	40	46.00	46.00	46.00
<i>Jun</i>	80	46.00	<b>38.19</b>	<b>27.29</b>
	60	46.00	46.00	46.00
	40	46.00	46.00	46.00
<i>July</i>	80	46.00	46.00	43.32
	60	46.00	46.00	46.00
	40	46.00	46.00	46.00
<i>Aug</i>	80	46.00	46.00	44.30
	60	46.00	46.00	46.00
	40	46.00	46.00	46.00
<i>Sep</i>	80	46.00	46.00	<b>38.06</b>
	60	46.00	46.00	46.00
	40	46.00	46.00	46.00
<i>Oct</i>	80	46.00	46.00	<b>23.32</b>
	60	46.00	46.00	45.76
	40	46.00	46.00	46.00
<i>Nov</i>	80	46.00	46.00	<b>13.52</b>
	60	46.00	46.00	<b>29.94</b>
	40	46.00	46.00	46.00
<i>Dec</i>	80	46.00	46.00	<b>9.32</b>
	60	46.00	46.00	<b>19.79</b>
	40	46.00	46.00	46.00

Written in italic bold are cases that did not meet water demand

**Table 10.9** Angat Reservoir daily flow releases to Bustos Dam for NIA-AMRIS irrigation water supply for the three optimization-simulation model scenarios

Month	Percent of time	Angat Releases to Bustos Dam (CMS)		
		Existing 46 CMS MWSS demand	2050 Climate change scenario	Future reservoir sedimentation
<i>Jan</i>	80	36.00	36.00	<b>0.00</b>
	60	36.00	36.00	<b>0.00</b>
	40	45.98	45.98	<b>0.00</b>
<i>Feb</i>	80	<b>27.49</b>	<b>29.34</b>	<b>0.00</b>
	60	39.82	39.82	<b>0.00</b>
	40	39.86	39.86	<b>0.00</b>
<i>Mar</i>	80	<b>1.31</b>	<b>0.83</b>	<b>0.00</b>
	60	<b>22.07</b>	<b>23.83</b>	<b>0.00</b>
	40	31.00	31.00	<b>0.00</b>
<i>Apr</i>	80	<b>0.00</b>	<b>0.00</b>	<b>0.00</b>
	60	<b>0.00</b>	<b>0.00</b>	<b>0.00</b>
	40	15.50	15.50	0.00
<i>May</i>	80	0.00	0.00	0.00
	60	0.00	0.00	0.00
	40	0.00	0.00	0.00
<i>Jun</i>	80	27.90	<b>6.27</b>	<b>0.00</b>
	60	27.90	27.90	<b>5.57</b>
	40	27.90	27.90	27.90
<i>July</i>	80	28.00	25.00	<b>0.00</b>
	60	28.00	28.00	25.00
	40	28.00	28.00	28.00
<i>Aug</i>	80	25.00	25.00	<b>0.00</b>
	60	25.00	25.00	22.73
	40	25.00	25.00	25.00
<i>Sep</i>	80	22.73	22.73	<b>0.00</b>
	60	22.73	22.73	<b>13.00</b>
	40	22.73	22.73	22.73
<i>Oct</i>	80	13.00	13.00	<b>0.00</b>
	60	13.00	13.00	<b>0.81</b>
	40	13.00	13.00	13.00
<i>Nov</i>	80	17.57	17.57	<b>0.00</b>
	60	17.57	17.57	<b>0.00</b>
	40	17.57	17.57	15.96
<i>Dec</i>	80	36.00	36.00	<b>0.00</b>
	60	36.00	36.00	<b>0.00</b>
	40	45.99	45.99	<b>10.60</b>

Written in italic bold are cases that did not meet water demand

Ipo Dam and Bustos Dam, respectively. For comparison purposes, also included in these two tables are results of the reservoir releases for the existing or base case scenario which was also presented in Sect. 5.1, Chap. 5.

With reference to the existing or base case, at 46 CMS MWSS water demand, the reliability of water deliveries is 80 percent-of-time for the months of January and June through December, but only 60 percent-of-time during the dry months of February through May. At 60 percent-of-time, it can be expected that the reservoir release to MWSS (through Ipo Dam) is greater than or equal to 46 CMS, 220 days a year, on the average and in the long term. Note that as mentioned in Sect. 5.1, the natural Angat River flows at the Angat Reservoir damsite (assuming no reservoir) at 46 CMS are only about 40 percent-of-time (i.e., natural river flows are equal to or greater than 46 CMS about 146 days a year); thus the Angat Reservoir is able to increase the reliability of the water availability of 46 CMS to 80 percent-of-time or about 292 days available.

With climate change, the results show that, on a monthly basis, the Angat-Ipo-Bustos-Umiray water resource system can still deliver the imposed water demands at fairly reasonable reliability, with slightly higher amounts during the months of February and March but slightly lower amounts during the months of May and June. Since the future climate scenario is around 2050 (during the 2046–2065 period) and there are only slight deficiencies during those months, either new water sources should be developed or changes in cropping patterns are made to reallocate (in time) irrigation water demand to avoid deficiencies in domestic water supply, especially since domestic water supply has higher priority over irrigation water supply during dry years or periods of low watershed inflows.

With future sediment deposition, the ability of the Angat Reservoir to deliver the water demand is already compromised compared with the other scenarios, even without climate change. In fact, there are practically no irrigation water deliveries (through Bustos Dam) during the months of December through May and subsequently no power generation at the main HP. It is seen here that the future reservoir sediment deposition appears to be a bigger issue as far as the ability of the Angat Reservoir to deliver water for domestic and irrigation purposes and consequently hydropower generation is concerned. Proper and serious watershed protection and sediment yield control measures should be employed in the Angat River basin to preserve or prolong the life of the Angat Reservoir.

## References

- Koike T (2012) Climate change impact assessment and hydrological simulation, study of Water Security Master Plan for Metro Manila and Its Adjoining Areas. JICA-University of Tokyo and Nippon Koie Co., Ltd., August
- Tabios GQ III (2014) Reliability analysis of Angat Reservoir operations with climate change and future reservoir sedimentation. In: Proceedings of the Nakdong River International Water Week 2014, Gyeongju City, Gyeongbuk Province, Korea, October 20–22

- Tabios GQ III (2016) Competing water uses of Angat multipurpose reservoir with increased domestic water demand under future reservoir sedimentation and climate change. In: Banta SJ (ed) Water in agriculture: status, challenges, and opportunities. Published by The Asia Rice Foundation, College, Laguna, pp 73–90
- Tabios GQ III, Monsod SC, Arcilla C, Momo RS, Rabonza GJ, Salazar CS, M.S. Chiu, Nilo PD, Ordona PM, Loyzaga MA, Connell WB. (2010) San Roque Dam during typhoon Pepeng of October 2009, Report of Investigating Committee Created under Department Order DO2009-10-0015 by Secretary Angelo T. Reyes, Department of Energy, Republic of the Philippines
- Woodfields (Woodfields Consultants, Inc.). (2017). Climate-resilient management of the dams and reservoirs in the upper Agno River Basin, Project, Report submitted to National Water Resources Board, Quezon City, June

# Chapter 11

## Modeling for Environmental Assessment Studies



**Abstract** Two modeling studies are presented here. First is the hydrodynamic and water quality modeling of Subic Bay which is a major shipping port (formerly a US Naval Airbase) to provide information for environmental impact assessment studies and likewise for the development of an integrated coastal management plan. Second is to assess possible groundwater pollution of the Novaliches Reservoir which is a major water supply reservoir of Metro Manila. The Payatas dumpsite is an open household and industrial garbage pit located about 700 m away on the northwest portion of the Novaliches Reservoir.

### 11.1 Subic Bay Hydrodynamic-Water Quality Modeling as a Tool for Developing Integrated Coastal Management Plan (ICMP)

In order to protect the ecologically diverse and productive state of Subic Bay and to sustain its economic and environmental benefits, management of the bay system must aim to achieve and maintain its physical, chemical, and biological integrity. The purpose of the hydrodynamic and water quality modeling of Subic Bay is to provide information and scientific basis for developing policies and strategies for integrated coastal management planning. Specifically, the hydrodynamic-water quality model was used to describe the physical, chemical, and biological processes in the bay as well as to assess the consequences, effects or impacts of possible actions, and alternative management schemes imposed on the bay through water quality model simulation studies. Specifically, the model was used as one of the tools to guide in developing the integrated coastal management plan (ICMP) of Subic Bay. This work is reported by MAXXIA (2006) in which the author was the principal investigator of Subic Bay modeling component of this study.

The major factors affecting the hydrodynamics and water quality processes of Subic Bay as depicted in Fig. 11.1 are as follows:

- Rainfall.
- River inflows from surrounding watersheds.

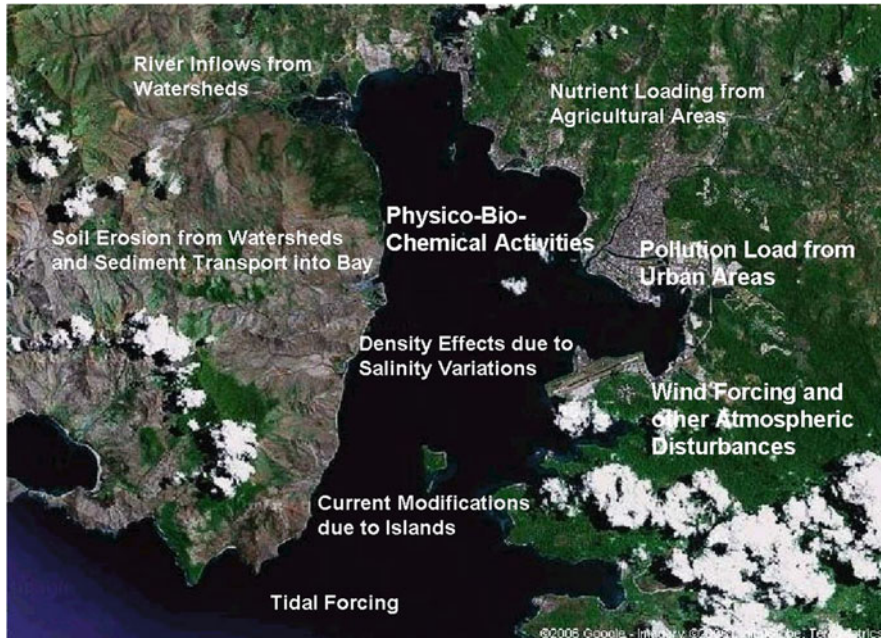


**Fig. 11.1** Major factors affecting Subic Bay hydrodynamics and water quality process

- Tidal forcing from China Sea.
- Wind forcing.
- Density driven currents due to salinity-freshwater balance and stratification due to temperature effects.
- Presence of islands, offshore structures.
- Nutrient and pollution loadings from watersheds and urban areas.
- Sediment load from watershed.

Based on the above factors, the hydrodynamic and water quality model including the watershed model for Subic Bay was designed to capture as close as possible the various factors affecting its physical processes as listed above.

### **11.1.1 Subic Bay Hydrodynamic-Water Quality Model**

A short discussion on the choice of models used here is now in order. Subic Bay is considered a deepwater body so that a three-dimensional (3-d) treatment of its hydrodynamics is necessary. The salinity and temperature gradient or stratification inherent in deep waters such as Subic Bay give rise to secondary currents that create

vertical motions superposed on horizontal motions driven by tidal forcing from China Sea, lateral inflows from the watersheds and wind forcing. Although, the 3-d model can be computationally time consuming, it is important that the model used properly captures the bay hydrodynamics. This is in contrast to previous modeling studies in Subic Bay where two-dimensional models were employed (Woodward 2001). With regard to the water quality model, a two-dimensional water quality model was used since of primary importance is only in the near-shore coastal areas that are relatively shallow water bodies. Water quality movement in shallow waters is normally well-mixed so that two-dimensional, horizontal treatment is assumed adequate.

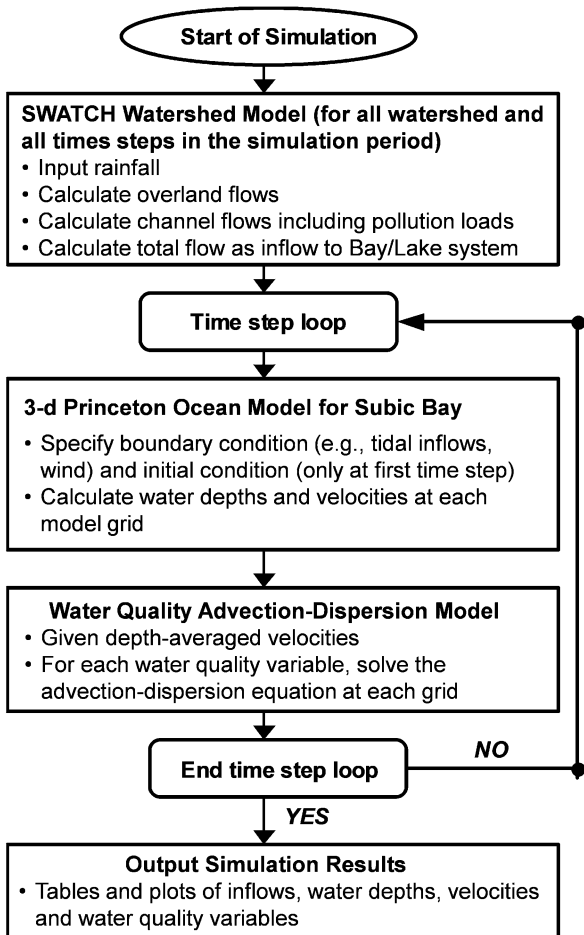
In view of these considerations, the Subic Bay model structure adopted consists of three parts: (1) a watershed model to calculate the watershed inflows into the bay given the rainfall input data; (2) hydrodynamic water model to calculate water depths and velocities; and (3) advection-dispersion model to describe the movement and evolution of water quality constituents (e.g., suspended solids, biological oxygen demand BOD, or any conservative tracer particle). The computed velocities from the hydrodynamic model are the major driving variables in the advection-dispersion model. Figure 11.2 shows the program flowchart of the Subic Bay model which may be noted that this is similar to the program flowchart in Fig. 7.5, Sect. 7.4 for the Manila Bay hydrodynamic model but using a different watershed model and without the 2-d hydraulic model of the lake and estuaries.

Table 11.1 summarizes how the different physical factors are entered or parameterized in the Subic Bay hydrodynamic-water quality model.

**Table 11.1** Physical variables and model parameterization of Subic Bay hydrodynamic and water quality model including the watershed model

Variables	Model parameterization
Rainfall	Historical data and input to watershed model
Watershed inflows	Computed in watershed model for specific development scenario and used as input to hydrodynamic model
Tidal forcing from China Sea	Historical tide data and input to hydrodynamic model as boundary condition
Density and temperature	Computed in hydrodynamic model
Offshore structure or islands	Specified in model geometry of hydrodynamic model
Nutrient and pollution load	Source or sink term in the water quality model
Sediment load from watersheds	Computed as function of watershed inflows using sediment-discharge rating curve for specified land use or development scenario
Land use changes	Accounted for as impervious areas, land use cover, interception, and infiltration parameters in the watershed model

**Fig. 11.2** Program flowchart of Subic Bay hydrodynamic and water quality model



### 11.1.2 Major Components of the Subic Bay Hydrodynamic-Water Quality Model

Referring to Fig. 11.2, the three major model components of the Subic Bay hydrodynamic-water quality model described below are as follows: (1) SWATC<sub>H</sub> watershed model to generate river inflows from watershed surrounding Subic Bay; (2) 3-d hydrodynamic model using the Princeton Ocean model; and (3) the 2-d water quality advection-dispersion model. It may be noted that these three models are used in tandem and uncoupled as depicted by the flowchart in Fig. 11.2.

### 11.1.2.1 SWATC H Watershed Model

A major input to the Subic Bay model is the watershed inflows which are calculated using SWATC H model which is a physically based, continuous simulation watershed model developed by Morel-Seytoux and Alhassoun (1987) and likewise described in Morel-Seytoux et al. (1999). SWATC H models the surface and sub-surface flows in a soil-aquifer-stream system with the following components: rainfall, infiltration, excess rainfall, interception and retention storage, soil moisture storage in the root zone, evapotranspiration, interflow storage, interflow discharge, groundwater recharge flow, stream-aquifer return flow, overland flow, and channel flow. Details of the SWATC H model are given in Appendix D.

Figure 11.3 shows the watershed delineation and river network of Subic Bay River Basin. The watershed is delineated into 109 sub-basins (see Table 11.2) and each sub-basin is represented in SWATC H like an open book where the pages are the left and right overland flow planes and the book spine is the stream channel. This open book representation is the same as that for the watershed model with Sacramento soil-moisture-accounting model shown in Fig. 4.2, Sect. 4.1.1. The land use map is also superposed in Fig. 11.3 which is the basis for deriving the model parameters of the SWATC H model.

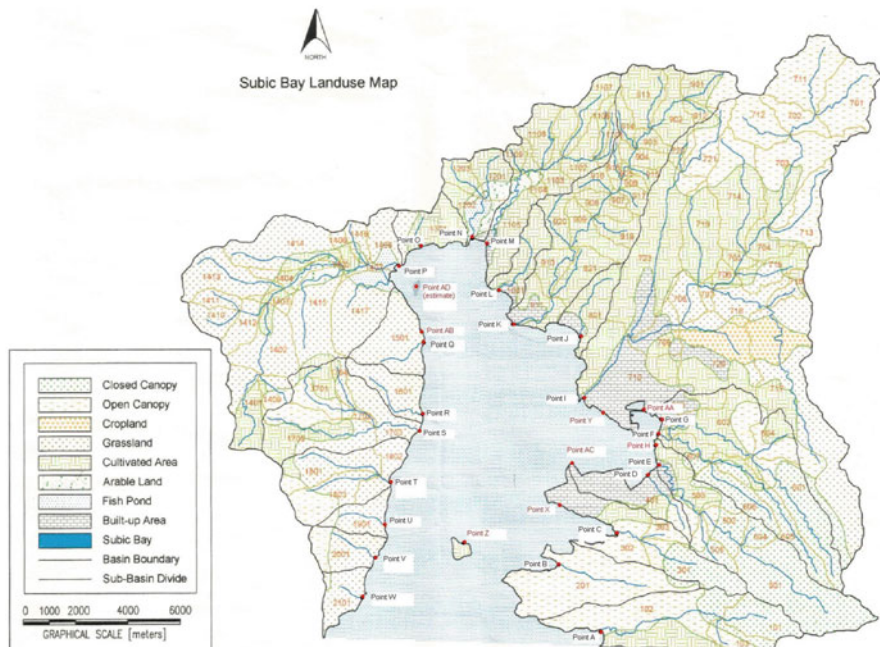


**Table 11.2** Number of sub-sub-basins and drainage areas of Subic Bay River sub-basin delineation

Sub-basin no.	Sub-basin area (km <sup>2</sup> )	No. of sub-sub-basins	Sub-basin no.	Sub-basin area (km <sup>2</sup> )	No. of sub-sub-basins
1	17.228	3	12	6.297	3
2	10.947	1	13	4.056	1
3	10.772	3	14	42.429	17
4	4.907	1	15	5.204	1
5	18.449	5	16	3.484	1
6	24.067	7	17	13.788	5
7	100.200	23	18	9.894	3
8	3.653	1	19	2.675	1
9	30.344	21	20	3.740	1
10	3.423	1	21	2.797	1
11	17.578	9	<b>Total ----&gt;</b>		<b>335.930</b>
					<b>109</b>

### 11.1.2.2 Subic Bay Hydrodynamic Model by Princeton Ocean Model (POM)

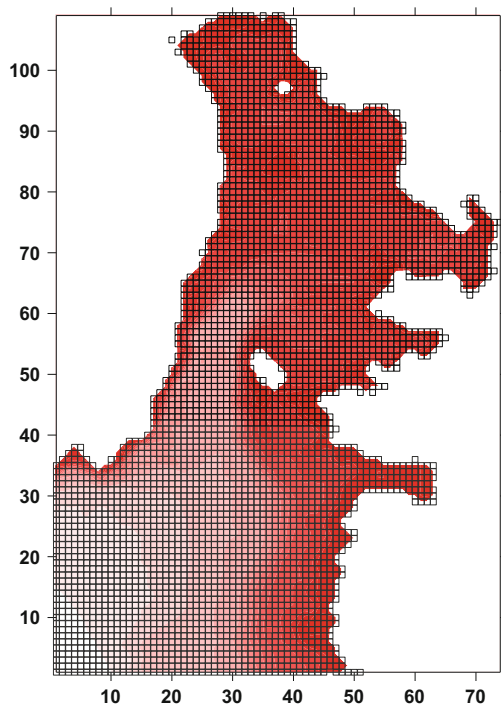
The Princeton Ocean Model (POM) developed by Blumberg and Mellor (1983, 1987) was used here to model the hydrodynamics of Subic Bay. This model has been presented in Sect. 7.4.2, Chap. 7 as applied to Manila Bay. Details of the Princeton Ocean model may be referred to Blumberg and Mellor (1987) and Mellor (2004).

Figure 11.4 shows the finite difference grid of Subic Bay as the model geometry of the Princeton Ocean model which consist of 4126 horizontal grids of 200 m x 200 m and 15 vertical layers on a *dual-sigma* coordinate system (Nadaoka et al. 2000) where the computation is divided between the upper layer and the lower layer by a horizontal sigma interface as done for Manila Bay. The model geometry covers the entire Subic Bay and extends about 5 km into China Sea. Figure 11.5 shows the bathymetry of the Bay that is specified in the model.

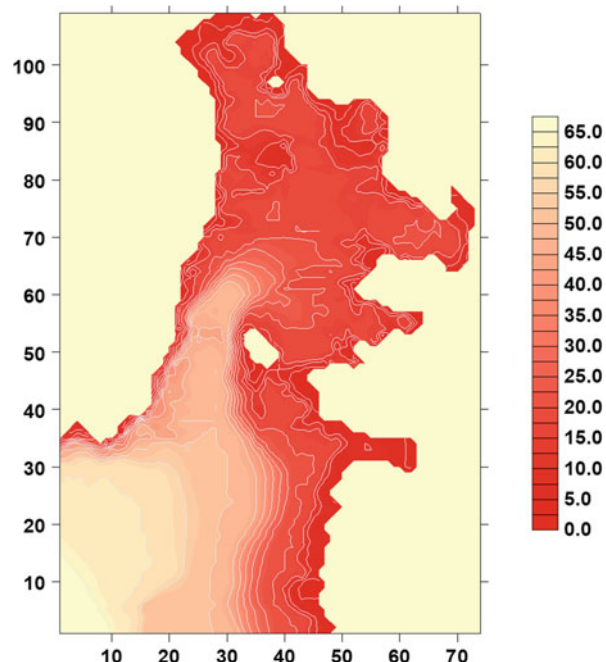
### 11.1.2.3 Subic Bay Two-Dimensional, Advection-Dispersion Water Quality Model

For the water quality model, a two-dimensional, horizontal formulation is adopted. For each finite difference cell, the advection-dispersion equation for the various water quality constituents with depth-averaged velocities is given by:

**Fig. 11.4** Subic Bay hydrodynamic-water quality model finite-difference grids composed of 4133 active horizontal grids and 15 vertical layers



**Fig. 11.5** Subic Bay bathymetry in downward depths (m) from mean low-low water (MLLW)



$$\frac{\partial C}{\partial t} = \frac{\partial}{\partial x} \left( D_x \frac{\partial C}{\partial x} - U_x C \right) + \frac{\partial}{\partial y} \left( D_y \frac{\partial C}{\partial y} - U_y C \right) + \text{sink/source term} \quad (11.1)$$

where  $C$  = concentration of a particular water quality constituent;  $D_x$  and  $D_y$  = dispersion coefficients in the  $x$ - and  $y$ -directions;  $U_x$  and  $U_y$  = velocities;  $t$  = time; and the *sink/source term* may include reactions terms.

For a given cell, the velocities obtained in the 3-d hydrodynamic model of Subic Bay are averaged over the water depth and used in the above equation. Various water quality constituents can be modeled such as dissolved oxygen (DO), suspended solids, biological oxygen demand (DO), salinity, and coliform bacteria. Other water quality variables may be modeled such as the case of the oil spill problem below.

In the case of modeling dissolved oxygen, details of the interaction with other water quality constitutes are described in Sect. 7.4.4 of Chap. 7 in its application to Manila Bay. As discussed in that section, DO is affected by the amount of organic matter present, photosynthesis which is parameterized by algae, ammonia ( $\text{NH}_3$ ) and nitrate ( $\text{NO}_2$ ) oxidation, benthic animals, and zooplankton, among others, so that these variables would become source/sink terms in the model above for the DO concentration. For purposes of this Subic Bay study, the hydrodynamic and water quality model was used for pollutant transport represented by biological oxygen demand (BOD) parameter and for an oil spill problem assuming a conservative tracer particle.

### 11.1.3 Subic Bay Hydrodynamic-Water Quality Simulations

As part of the integrated coastal management planning (ICMP) in Subic Bay, the results of this hydrodynamic-water quality simulation studies were presented as part of the several public consultations held in the course of this study to update and revise the ICMP of Subic Bay in 2006 (MAXXIA 2006).

Two (2) applications are presented here to illustrate the use of the Subic Bay hydrodynamic-water quality model which were actually used as part of the public consultations for the ICMP. The first application is to simulate the movement and describe the spatial distribution of BOD for various wastewater or pollutant discharges in terms of BOD loading for existing or base case and three (3) future cases with BOD loadings depending on BOD reduction measures adopted. The second is an oil spill movement simulation based on actual oil spill incident in Subic Bay.

Before conducting the Subic Bay hydrodynamic-water quality model simulations, the first step is to generate the streamflows from the watershed model as inflows to the hydrodynamic model of the bay. Historical rainfall from Olongapo City stations from a typical year over a period of 150 days was selected as input to the SWATCII watershed model. Then, the generated inflows were entered as flow fluxes in the hydrodynamic model. Another major driving factor of the bay circulation is the tidal forcing from China sea and also the wind forcing. The tide time series

**Fig. 11.6** China Sea tidal forcing southwest of Subic Bay

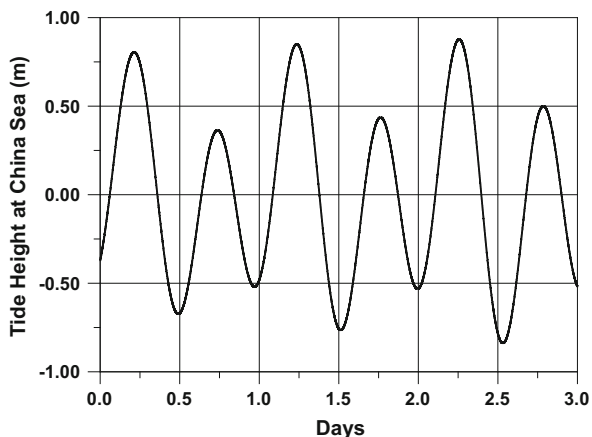
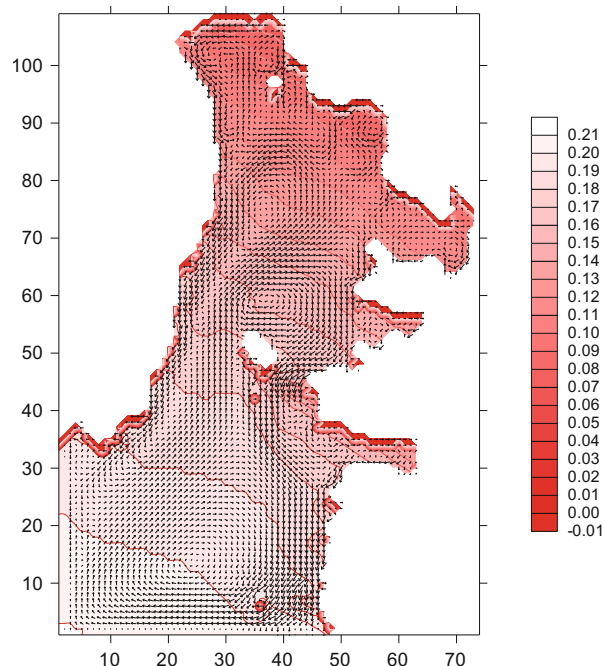


**Fig. 11.7** Typical velocity vector of Subic Bay



specified in the model is shown in Fig. 11.6. There are several model parameters and other input variables in the hydrodynamic but are too lengthy to enumerate here. With the hydrodynamic model component completely specified, the model is run, and a typical velocity vector plot and water surface elevation of the simulation run is given in Fig. 11.7.

With the results from the hydrodynamic model, especially the velocities and water depths, the water quality simulations proceeded and a brief description of

the simulation scenarios or cases are given below together with the discussion of results.

### 11.1.3.1 Spatial Distribution of BOD Over Time

Table 11.3 below shows the BOD loadings (milligram per liter or mg/l) for base (existing) case and three (3) future cases at various points along the shoreline of Subic Bay indicated in Fig. 11.3. The base case BOD loadings were estimated by first fitting a regression equation between observed BOD data and the population at

**Table 11.3** BOD loadings in mg/l at various locations in the Subic Bay as indicated in Fig. 11.2

Station number	Station label	Existing	Future case 1	Future case 2	Future case 3
1	A	3.09	3.09	3.09	3.09
2	B	1.09	1.09	1.09	1.09
3	C	0.88	0.88	0.88	0.88
4	D	9.31	9.31	9.31	9.31
5	E	0.69	0.69	0.69	0.69
6	F	4.28	4.28	4.95	4.95
7	G	2.42	2.42	2.47	2.47
8	H	6.63	6.63	6.63	6.63
9	I	522.56	250.45	652.90	311.66
10	J	45.12	21.00	57.71	27.47
11	K	58.05	23.91	77.44	44.36
12	L	60.41	14.89	81.22	37.12
13	M	43.31	23.29	57.32	30.21
14	N	38.15	18.13	50.50	23.39
15	O	2.03	2.03	5.79	5.79
16	P	16.43	16.43	16.43	16.43
17	Q	2.46	2.46	3.45	3.45
18	R	1.65	1.65	1.65	1.65
19	S	5.49	5.49	5.49	5.49
20	T	3.51	3.51	3.51	3.51
21	U	1.16	1.16	1.16	1.16
22	V	1.36	1.36	1.36	1.36
23	W	0.98	0.98	0.98	0.98
24	X	4.21	4.21	4.25	4.25
25	Y	12.89	2.58	12.89	2.58
26	Z	0.32	0.06	0.54	0.11
27	AA	0.08	0.08	0.08	0.08
28	AB	7.37	1.48	7.37	1.48
29	AC	0.57	0.57	0.57	0.11
30	AD	3.43	3.09	3.43	3.09

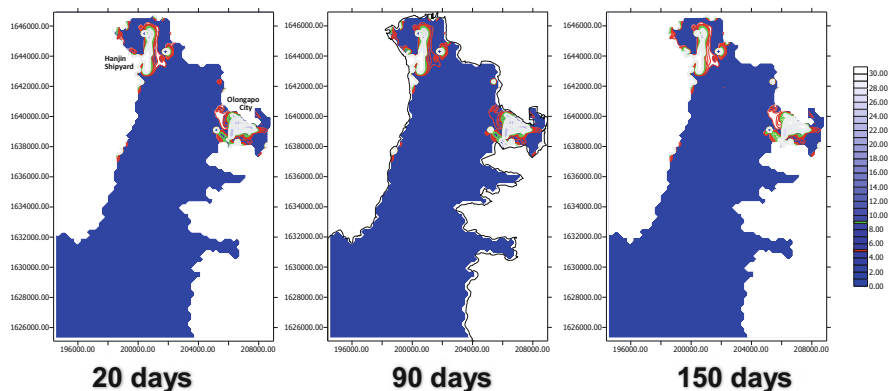


**Fig. 11.8** Spatial distribution of BOD concentrations after 20, 90, and 150 days for a specific waste discharge scenario around Subic Bay with significant concentration from Olongapo City and Hanjin Shipyard

those cities or municipalities where the BOD was observed in its coastal waters, then this regression equation was used to estimate the BOD loadings at ungaged points (without BOD readings) given the population of the associated cities or municipalities.

For these simulations, the models were ran for 4 months on an hourly time interval. It may be noted that running the Princeton Ocean model takes tremendous computer time compared to the watershed model and the water quality model. As shown in the Fig. 11.8, the bulk of high BOD concentrations after 20 days were around Olongapo City (around 1639000 northing and 207000 easting) and the Hanjin Shipyard (around 1644000 northing and 200800 easting) reaching as high as 30 mg/l, then after 90 days there was some BOD concentration reduction in those same area and again reaching high BOD concentrations after 150 days. The Olongapo City and Hanjin Shipyard areas are notable for their relatively high waste discharges but the presence of high BOD concentration may be exacerbated hydrodynamically since the currents or velocities (see Fig. 11.7) in the embayment around these areas tend to go around in a circulating manner. In effect, the embayment in these areas prolongs residence time thus the inability of the waters to assimilate waste to effectively reduce BOD concentrations. It may be mentioned that there were other areas in the bay where BOD loads were present but the concentrations were too small to be displayed in the contour plots.

Figure 11.9 shows the plots of BOD concentrations after 90-day simulation, and three future case scenarios with BOD loadings are also given in Table 11.3. In these future case scenarios, the amount of BOD loadings is reduced accordingly and judiciously depending on which area in the Subic Bay where BOD mitigation measures were imposed. In fact, the basis of what mitigation measures to adopt were decided through the public consultations depending on what type of wastewater treatment technology and investment to adopt and of course the commitment by

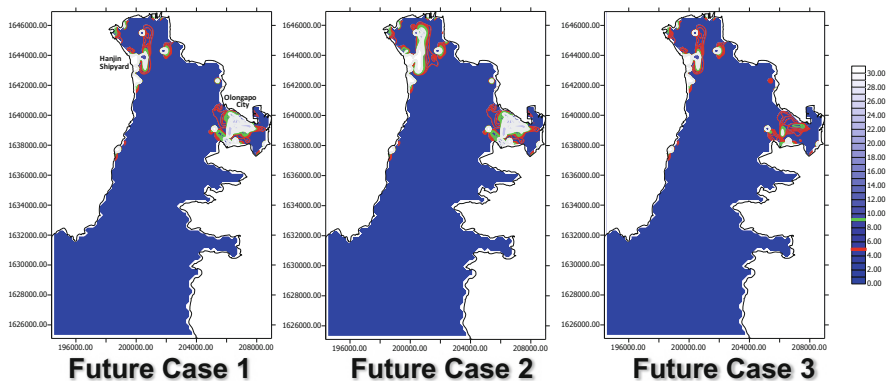


**Fig. 11.9** Spatial distribution of BOD concentrations after 90 days for three (3) BOD waste discharge scenarios around Subic Bay depending on sewerage and septage reduction schemes specially in the identified hot spot areas

the local government units and communities. In view of these BOD reduction or mitigation measures, the future case 1 offers some reduction in BOD load most especially on the northwest corner of the bay as shown in Fig. 11.9, while the future case 3 resulted in the most significant BOD loading reduction especially in the northwest corner of the bay as well as in the Olongapo City area (Mideastern section of Bay). The future case 2 resulted in insignificant reduction in BOD loading compared to future cases 1 and 3, and in fact this case is almost indiscernible to the contour plots of BOD concentration of the base case scenario (see Fig. 11.8 at 90 days) especially around Olongapo City.

### 11.1.3.2 Oil Spill Movement Simulation

In the course of this modeling study at Subic Bay, there was an actual oil spill incident that occurred which was identified coming from a ship southwest of Grande Island as indicated in Fig. 11.10. There was a news blackout when this happened sometime August, 2006. The oil spill measured about  $5000 \text{ m}^2$  and affecting about 7 km of the Subic Bay coastline where prime beaches and tourist-oriented resorts are located. The oil spill that was allegedly deliberately dumped was of petroleum-based sludge including used bunker oil. Thus, the motivation for this oil spill simulation.

The oil spill simulation was conducted with almost, pure advective transport (i.e., with very small dispersion coefficient) thus assumes that oil is a conservative tracer. As shown in Fig. 11.10, the actual ship oil spill incident occurred in the lower, left-hand portion of the figure and actual sighting of oil had been observed 5 days after the incident at the White Rock Resort indicated in the upper, right-hand side of the figure.

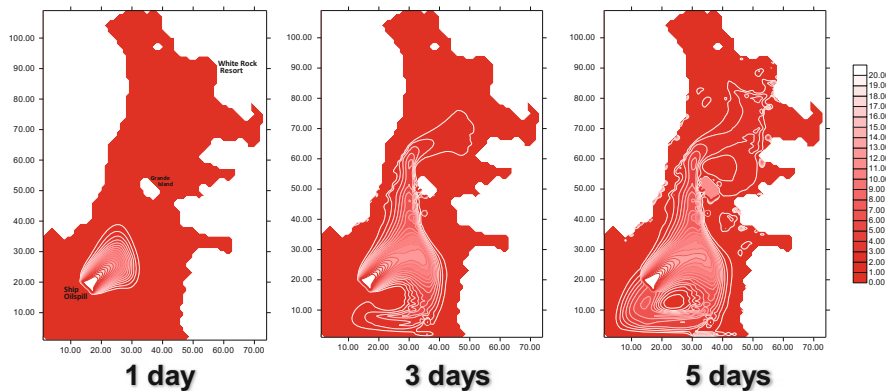


**Fig. 11.10** Oil spill simulation with almost, purely advective (no advection) transport assuming that oil is a conservative tracer. This simulation was motivated by an actual ship oil spill incident indicated in the lower, left-hand portion of the figure and actual sighting of oil had been observed 5 days after the incident the White Rock Resort indicated in the upper, right-hand side of the figure



**Fig. 11.11** Aerial photo of Novaliches Reservoir and the location of the Payatas open dumpsite and a closeup view of the dumpsite looking northeast

## 11.2 Risk of Polluting Novaliches Reservoir from Payatas Dumpsite Through Groundwater Contaminant Transport

The Payatas dumpsite is an open household and industrial garbage pit in Quezon City located about 700 m away on the northwest portion of the Novaliches Reservoir (see Fig. 11.11). The Novaliches Reservoir is part of the water supply system of the Metropolitan Waterworks and Sewerage System (MWSS) of Metro Manila. Transport of pollutants from the Payatas dumpsite can either be through atmospheric, surface runoff or groundwater flow transport. This modeling study investigates the

risk of polluting the Novaliches Reservoir through groundwater flow and pollutant transport from the Payatas dumpsite.

The movement of contaminants in the subsurface zone is a combination of unsaturated and saturated groundwater flow and contaminant transport. Saturated groundwater flow in the upper portion of the dumpsite and also in the area between the dumpsite and the reservoir can only be sustained by prolonged, uninterrupted rainfall. Prolonged, sustained rainfall is however an infrequent event. In the lower portion of the study area, saturated groundwater flow is sustained by the seepage from the reservoir that has a down gradient from the reservoir to the surrounding area. Right below the dumpsite, this reservoir seepage face may be hovering from 5 meters to 10 meters below the dumpsite area. Contaminants or leachate from the Payatas dumpsite is known to have already reached the groundwater table below it.

In the modeling study presented here, an unsaturated-saturated finite element model is employed to simulate the groundwater flow and contaminant transport from the dumpsite to the reservoir. Two major forcing functions in the groundwater model are the rainfall sequences, and the reservoir levels both of which have been stochastically generated to be able to conduct long-term risk analysis. The rainfall sequences are generated using a Poisson-based rectangular pulse model and the reservoir levels from an autoregressive-moving average model. Details of this study have been reported by NHRC (2002) as well as in Tabios et al. (2003).

### ***11.2.1 Groundwater Flow and Contaminant Transport Model with FEMWATER***

The groundwater flow and contaminant transport model used is the three-dimensional saturated-unsaturated, finite-element model FEMWATER. The FEMWATER is designed to simulate the movement of moisture and contaminant through density-dependent, unsaturated-saturated porous media. Details of the model are described by Lin et al. (1997) and Yeh et al. (1992). The GMS software of BYU (1998) which contains FEMWATER as one of the model options was used in this study. The governing equation for flow of water through an unsaturated-saturated porous medium in FEMWATER is given by:

$$F(h) \frac{\partial h}{\partial t} = \nabla \cdot [K(h) \cdot (\nabla h + \nabla z)] + q \quad (11.2)$$

where  $h$  = pressure head (L),  $z$  = distance above a datum (L),  $K(h)$  = effective hydraulic conductivity ( $L/T$ ),  $F(h)$  = water (storage) capacity ( $1/L$ ),  $q$  = source/sink term ( $L^3/T/L^3$ ),  $t$  = time (T),  $\nabla$  = del operator for gradient, and  $\nabla \cdot$  = del operator for divergence. Equation (11.2), often referred to as Richard's equation, differs from the saturated flow equation through porous media because of the nonlinearity of the hydraulic conductivity and storage terms with respect to the prevailing moisture

content (in terms of pressure head) of the soil. Note that the letters in parenthesis are physical units M, L, and T for mass, length, and time, respectively.

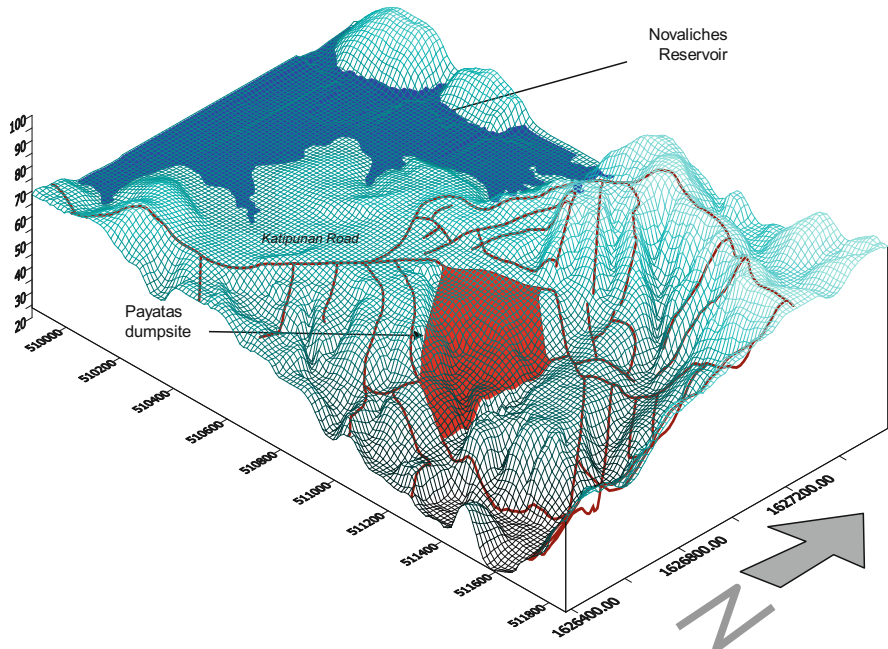
The advective-dispersion solute transport equation through the unsaturated-saturated porous media in FEMWATER is given by:

$$\theta \frac{\partial C}{\partial t} + \rho_b \frac{\partial S}{\partial t} = \nabla \cdot (\theta D \cdot \nabla C) - V \cdot \nabla C - \lambda(\theta C + \rho_b S) + Q C_{in} - Q C \quad (11.3)$$

where  $\theta$  = moisture content ( $L^3/L^3$ ),  $\rho_b$  = bulk density of the porous medium ( $M/L^3$ ),  $C$  = concentration of the dissolved species ( $M/L^3$ ),  $S$  = species concentration in the adsorbed phase ( $M/M$ ),  $t$  = time (T),  $V$  = Darcy velocity or specific discharge ( $L/T$ ),  $D$  = dispersion coefficient tensor ( $L^2/T$ ),  $\lambda$  = material decay constant (T),  $Q$  = water source/sink rate ( $M/T$ ), and  $C_{in}$  = dissolved species concentration of the source/sink fluid ( $M/L^3$ ).

### 11.2.2 Groundwater Modeling of Novaliches Reservoir-Payatas Dumpsite

For a 3-d topographic perspective of the Novaliches Reservoir-Payatas dumpsite, Fig. 11.12 shows the CAD drawing of the area. In the groundwater model, the



groundwater aquifer properties needed include soil porosity, hydraulic conductivity, storage coefficients, soil matric potential, and others. For unsaturated groundwater flow simulation in particular, data such as hydraulic conductivity and soil moisture relationships are also needed. The modeled area has been classified into five different soil layers (types) as shown in the finite element discretization of the study area in Fig. 11.13, namely, (1) top layer is sandy clay; (2) second layer is conglomerate with sandstone; (3) third layer is mudstone; (4) bottom layer is pebbly/silty sandstone; and (5) the dumpsite with a special porous media type. Table 11.4 lists the major

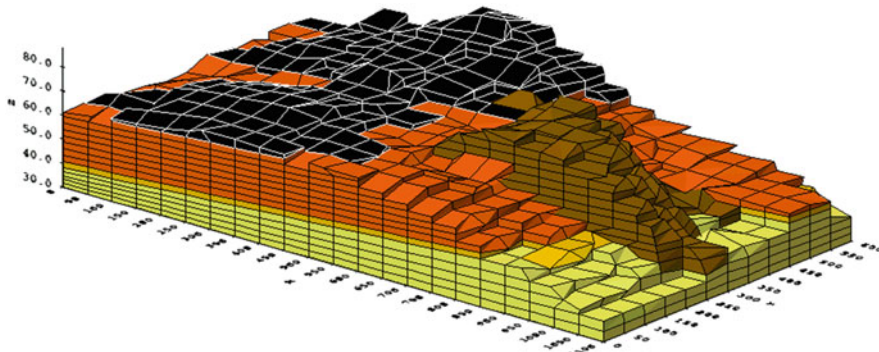


**Fig. 11.13** Finite element discretization of the Novaliches Reservoir-Payatas dumpsite

**Table 11.4** Groundwater flow and contaminant transport model parameters of Novaliches Reservoir-Payatas dumpsite

Parameter	Sandy clay (top layer)	Conglomerate with sandstone (second layer)	Mudstone (third layer)	Pebby/silty sandstone (bottom layer)	Dumpsite
Saturated hydraulic conductivity (m/d)	0.01296	0.4536	0.06523	0.4536	6.912
Specific storage ( $m^{-1}$ )	$10^{-2}$ to $10^{-4}$	$10^{-4}$ to $10^{-6}$	$10^{-3}$ to $10^{-5}$	$10^{-4}$ to $10^{-6}$	$10^{-4}$ to $10^{-5}$
Soil compressibility ( $pa^{-1}$ )	$10^{-7}$ to $10^{-8}$	$10^{-8}$ to $10^{-9}$	$10^{-9}$ to $10^{-10}$	$10^{-7}$ to $10^{-9}$	$10^{-8}$ to $10^{-10}$
Porosity $\Theta$	0.38	0.43	0.39	0.43	0.41
Residual moisture content $\Theta_s$	0.1	0.045	0.1	0.045	0.057
Van Genuchten $\alpha$	0.027	0.145	0.059	0.145	0.124
Van Genuchten $\beta$	1.23	2.68	1.48	2.68	2.28
Longitudinal dispersivity (m)	0.3	0.65	0.4	0.65	1.25
Thickness ranges (m)	10 to 15	20	2 to 5	5 to 10	30 to 35

model parameters for each of the five different soil layers. These model parameters were obtained from various sources such as field data, previous studies, and the literature especially from Van Genuchten (1980).

### 11.2.3 Stochastic Modeling of Reservoir Levels and Rainfall Sequence

Two major forcing functions in the groundwater model are the rainfall and Novaliches reservoir levels. These two boundary conditions are the major factors that drive the contaminant transport in the unsaturated, saturated groundwater system. For purposes of this study, long sequences of rainfall and reservoir levels were stochastically generated to properly assess the risk and uncertainty associated to the groundwater contaminant transport problem.

Figure 11.14 shows the observed daily rainfall and reservoir levels in the La Mesa Dam from year 1987 to 1997. Since there is only 10 years of historical data available

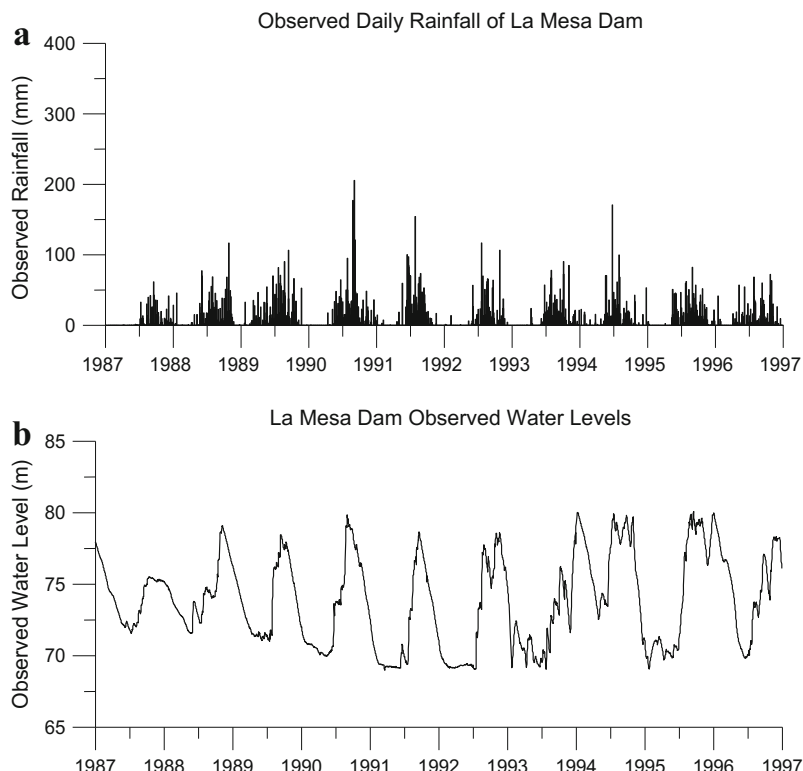


**Fig. 11.14** Observed (a) daily rainfall and (b) water level at Novaliches Reservoir

and the study is intended to investigate the risk of pollutant transport over a 30-year period or more, thus the need for stochastic data generation to extend the data to be used in the simulation studies. A cursory examination of the historical time series plots shows the typical features of stochastic time series such as seasonality and randomness superposed on this seasonality. Statistical and stochastic analyses were performed on these data and specifically for purposes of stochastic modeling of these data.

Based on the time series features of the Novaliches Reservoir water levels, the time series model used was a daily autoregressive-moving average model ARMA(P,Q) of orders P (autoregressive part) and Q (moving average part), with a seasonal component written as follows (Box and Jenkins 1976):

$$Z_{\nu,t} = Z_{\nu,0} + \sum_{j=1}^P \phi_{\nu,j} Z_{\nu,t-j} + \sum_{j=1}^P \theta_{\nu,k} e_{\nu,t-k} + e_{\nu,t} \quad (11.4)$$

in which  $Z_{\nu,t}$  is the time series variable at month  $\nu$  and day  $t$ ,  $e_{\nu,t}$  is the random variable with mean zero and finite variances, and  $\phi_{\nu,j}$  as well as  $\theta_{\nu,t}$  are model parameters on monthly basis. To account for seasonality in the original domain of the time series variable, the raw data (observed reservoir levels) were standardized with daily means and standard deviations. Furthermore, since it is preferable to model the time series data in the normal (Gaussian) domain of the time series variables, the reservoir levels were transformed first using the Wilson-Hilferty transformation (Wilson and Hilferty, 1931).

The resulting stochastically generated daily water levels for 30 years at Novaliches Reservoir are shown in Fig. 11.15.

For stochastic modeling of rainfall, two types of models were tried, namely, the Poisson rectangular pulse (PRP) model and Neyman-Scott white noise (NSWN) model (Waymire et al. 1984). Appropriate model identification, parameter estimation, and diagnostics checks were performed to find the most appropriate model. It is found that the PRP model is the most appropriate model to be used to represent the rainfall in the area. In the PRP model, the rainfall process is characterized by a Poisson process in which the interarrival times between rainfall events are exponentially distributed. Associated with each event is an intensity and a duration that are assumed to be independent and exponentially distributed. To account for seasonality in the rainfall process, the rainfall model parameters were estimated on a monthly basis. Further details of these rainfall models may be referred to Waymire et al. (1984) or likewise Obeysekera et al. (1987).

The resulting stochastically generated daily rainfall in the vicinity of Novaliches Reservoir-Payatas dumpsite for 30 years is shown in Fig. 11.16.

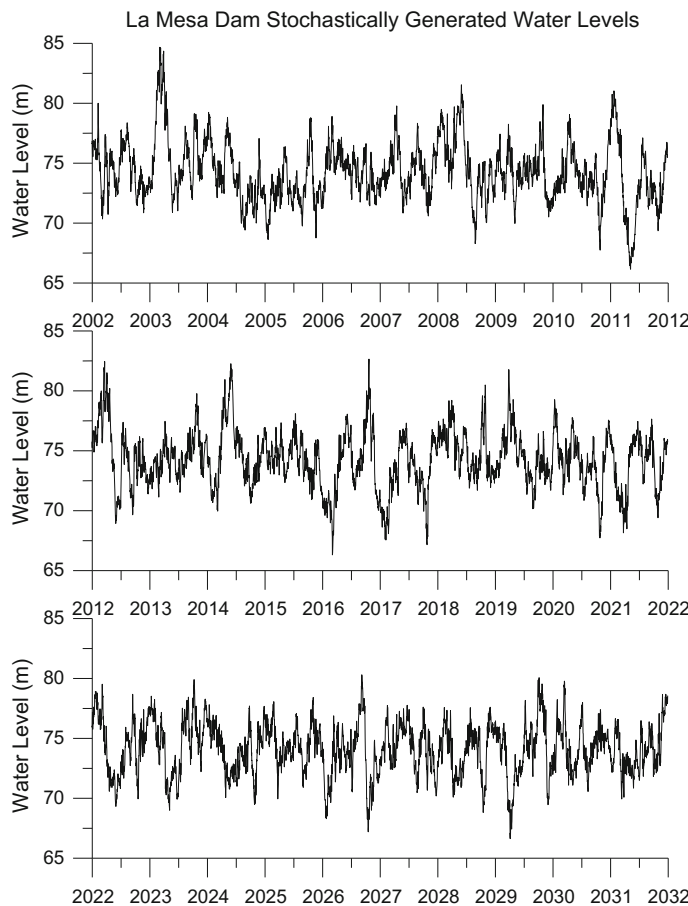


**Fig. 11.15** Stochastically generated daily water levels for 30 years at Novaliches Reservoir

#### 11.2.4 Results of Groundwater Contaminant Transport Simulations

Figures 11.17 and 11.18 show, respectively, typical results of contaminant concentration after 24 h and 2 years of simulation for one particular trace of stochastically generated rainfall and reservoir level. Initially, the contaminants are concentrated only around the dumpsite. Then, the contaminants migrated in the direction of the reservoir area and within a period of over a year; the contaminants reached the 350 km mark (x-axis) east of the reservoir (the reservoir being 0 km, x-axis).

In running the model with full scale coverage of the modeled area as shown in Fig. 11.13, it required several days of computing time. In view of this, a scaled-down geometry of the modeled area reducing on its transverse side was adopted for long-

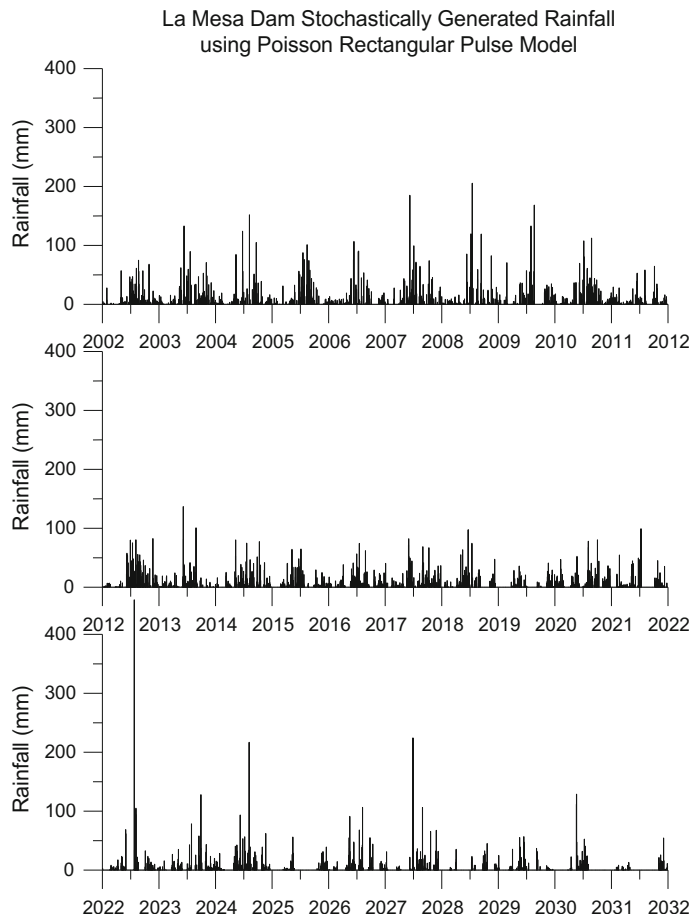


**Fig. 11.16** Stochastically generated daily rainfall for 30 years in the vicinity Novaliches Reservoir-Payatas dumpsite

term simulation. The longitudinal side of the model was retained which is 1100 m, while the width was scaled-down to 150 m from the original width of 400.

For the scaled-down modeled area, Fig. 11.19 shows the pollutant concentration at 24 h, 3 years, 8 years, and 25 years of simulation for one trace of stochastically generated rainfall and reservoir level. Initially, only the dumpsite area was polluted as shown below after 24 h simulation. Then, the pollutants migrated in the direction of the reservoir but hovering around the 350 km mark east of the reservoir (reservoir is at 0 km, left-hand side of figure) for the next several years of simulation. In the saturated portion, the pollutant plume virtually remained in the same position during the entire simulation period, that is, the 350 km mark was the interface between the

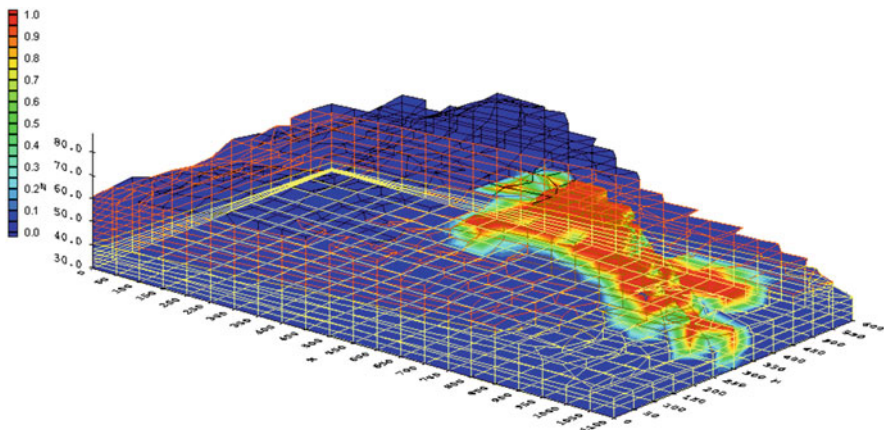


**Fig. 11.17** Contaminant concentration after 24-hour simulation

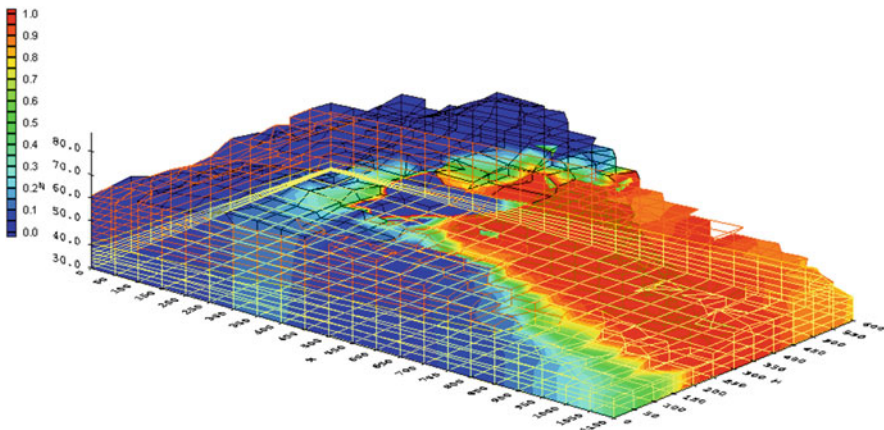


**Fig. 11.18** Contaminant concentration after 2-year simulation

reservoir seepage field and the pollutant front. In the unsaturated portion, this pollutant front oscillated around the 300–400 km distance from the reservoir, attributed to the seasonal occurrence of rainfall. Generally, the movement of contaminant in this unsaturated zone was very, very slow that it could hardly reach the reservoir area. Thus, it can be concluded that it is a nil risk for pollutants from Payatas dumpsite to be transported to Novaliches Reservoir through groundwater contaminant transport.

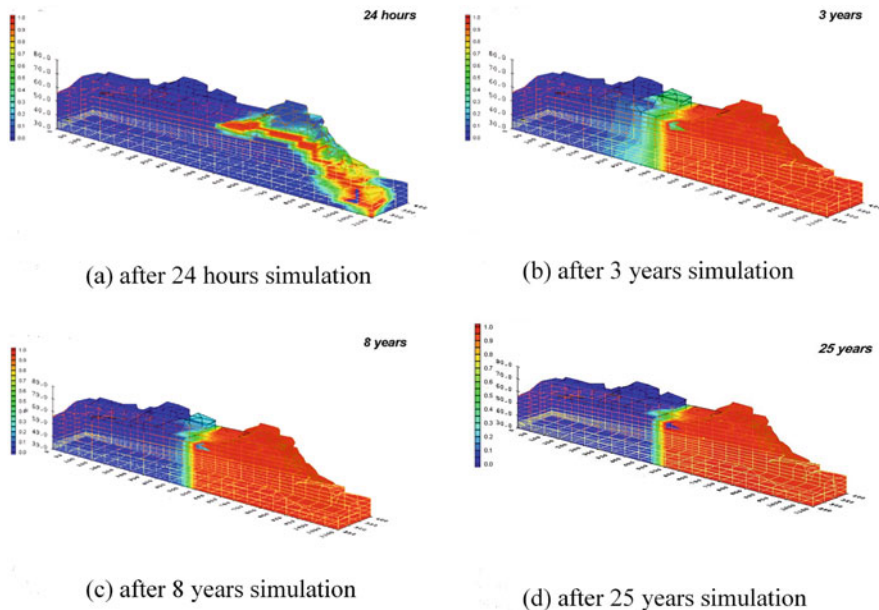


**Fig. 11.19** Contaminant concentration after **(a)** 24 h, **(b)** 3 years, **(c)** 8 years, and **(d)** 25 years from start of simulation

### **11.2.5 Atmospheric Pollution Posing a Bigger Concern than Groundwater Contamination in Novaliches Reservoir**

Based on the simulation presented above, it is concluded that there is a very low chance or risk for the Payatas dumpsite contaminants to reach the Novaliches reservoir dumpsite. As mentioned earlier, the movement of contaminants in the Payatas dumpsite to the Novaliches Reservoir may be through atmospheric dispersion, surface runoff, or groundwater flow. Since groundwater contamination poses a very small risk and there is no surface water link or channel connecting the Novaliches Reservoir and Payatas dumpsite, the remaining issue is the atmospheric dispersion of pollutants from the dumpsite into the reservoir.

It may be noted that typically from dumpsites, some of the dioxins coming from the burning materials are inhalable particulates with sizes less than 10 microns. Usually these finer particles contain more toxic components than the total suspended particulates normally monitored by air pollution agency, that is, the Environmental Management Bureau (EMB) of the Department of Natural and Environmental Resources (DENR) in the Philippines. The gaseous pollutants in the air such as carcinogenic volatile organic compounds (VOCs) and aromatic hydrocarbons especially benzene should be analyzed. Smoke from open burning of plastic at low temperature (less than 800 °C) is especially harmful since it contains toxic

compounds. Public exposure to these toxicants through direct inhalation and the possible ingestion via drinking water are a huge concern that requires serious investigation.

In view of this, a worthwhile modeling study in this case would be to investigate the movement of airborne pollutants from the Payatas dumpsite, through atmospheric dispersion, and the possible arrival of these pollutants in the Novaliches Reservoir. This may be accompanied by modeling of the advection and dispersion of these pollutants that reach and settle in the reservoir (now waterborne pollutants) including the movement of pollutants that settled in the La Mesa watershed (of Novaliches Reservoir) that can be entrained in the watershed overland and channel flows to the reservoir.

Since the movement of pollutants especially by atmospheric dispersion is a fairly random process due generally to more turbulent mixing in the atmosphere, determining where the plume of pollutants travel, at what concentrations, and at what time they arrive at various locations (i.e., in the reservoir) can be so uncertain. Thus, the modeling and analysis should incorporate the probabilistic nature or uncertainty of the pollutant movement. Also, the advection and dispersion of airborne pollutants would require perhaps a three-dimensional model formulation and the advection-dispersion in the reservoir may require only a two-dimensional treatment.

## References

- Blumberg AF, Mellor GL (1983) Diagnostic and prognostic numerical circulation of the South Atlantic Bight. *J Geophys Res* 88:4579–4592
- Blumberg AF, Mellor GL (1987) A description of a three-dimensional coastal ocean circulation model. In: Heaps N (ed) *Proceedings of three-dimensional coastal ocean models*, vol 4. American Geophysical Union, Washington, DC, p 208
- Box GEP, Jenkins GM (1976) *Time series analysis: forecasting and control*. Holden-Day, San Francisco, p 575
- BYU (Brigham Young University) (1998) *The Department of defense: groundwater modeling system, GMS v2.1, reference manual*, engineering computer graphics laboratory, Provo, Utah
- Lin HJ, Richards DR, Talbot CA (1997) FEMWATER: a three-dimensional finite element computer model for simulating density-dependent flow and transport in variably saturated media, technical report CHL-97-12. U.S. Army Corps of Engineers, Waterways Experiment Station, Vicksburg
- MAXXIA (MAXXIA Consulting Company) (2006) Subic bay integrated coastal management planning project, report submitted to Ecology Center, Subic Bay Metropolitan Authority (SBMA)
- Mellor GL (2004) User's guide for a three-dimensional, primitive equation, numerical ocean model. Program in Atmospheric and Oceanic Sciences, Princeton University, Princeton, New Jersey, 56 p
- Morel-Seytoux HJ, Alhassoun SA (1987) A multi-process watershed model for simulation surface and subsurface flows in a soil-aquifer-stream hydrologic system, report. No. 87.3. HYDROWAR Publications, Atherton
- Morel-Seytoux HJ, Alhassoun SA, Tabios GQ III, Liogson LQ, Rojas DS Jr (1999) SWATCH – a distributed hydrologic watershed model. In: *Proceedings of 19th annual hydrology days*. American Geophysical Union, Colorado State University, Fort Collins. August 16–20

- Nadaoka K, Yoshino T, Nihei Y (2000) Dual-sigma coordinate system for improvement of coastal ocean model. *J Hydraul Coast Environ Eng JSCE* 656/II-52:183–192
- NHRC (2002). A study of the effect of the Payatas open dumpsite to the Novaliches (la Mesa) Reservoir, final report to metropolitan waterworks and sewerage system, National Hydraulic Research Center, University of the Philippines, Diliman, Quezon City, Report No. 121, February
- Obeysekera JTB, Tabios GQIII, Salas JD (1987) On parameter estimation of temporal rainfall models. *Water Resour Res* 23(10):1837–1850
- Tabios GQ III, Liogson LQ, Peralta GL (2003) A study on the possible pollution of Metro Manila water supply reservoir from an open dumpsite through groundwater contaminant transport modeling with stochastic inputs, In: Proceedings of first international symposium on Southeast Asian water environment, AIT Conference Center, Bangkok, Thailand, October 23–25, pp 419–424
- Van Genuchten MT (1980) A closed-form equation for predicting the hydraulic conductivity of unsaturated soils. *Soil Sci Soc J* 44:892–898
- Waymire E, Gupta VK, Rodriguez-Iturbe I (1984) A spectral theory of rainfall intensity at the meso- $\beta$  scale. *Water Resour Res* 20:1453–1465
- Wilson EB, Hiltferty MM (1931) The distribution of chi-square. In: Proceedings of the National Academy of Sciences of the United States of America, Washington, DC, vol 17, pp 684–688
- Woodward (Woodward Clyde Consultants, Inc) (2001) Resource inventory: resource inventory integration report, Volume 1, Final summary report. Subic Bay Protected Areas Management Plan Project of Ecology Center-SBMA
- Yeh GT, Sharp-Hansen S, Lester B, Strobl R, Scarbrough J (1992) 3DFEMWATER/3DLEWASTE: numerical codes for delineating wellhead protection areas in agricultural regions based on assimilative capacity criterion, EPA/600/R-92/223, environmental research laboratory. U.S. Environmental Protection Agency, Athens

# Chapter 12

## Imperatives of Water Resources Modeling and Applications in the Philippines



**Abstract** This chapter presents the needs and imperatives of modeling and simulation studies for planning, design, and management of water resources systems in the Philippines. The importance of continuous monitoring and data collection of water-related data is also discussed and the need for research and capacity building (with creation or sustained outsourcing of modeling support) especially in government agencies related to water resources project implementation and operations. In relation to sustainable water resources development in the Philippines, discussions are given on the role of sustainability science and the need for transdisciplinary approach. The chapter ends with building urban resilience to water-related disasters.

### 12.1 Key Considerations in Modeling Water Resources Systems

Modeling and simulation studies are useful tools in the planning and management of river basins. With modeling tools, one can assess the existing or future impacts and implications of any water resources development in the river basin through model simulation studies. When developing models as well as choosing the model to be utilized either for descriptive, predictive, or prescriptive purposes, they must have been formulated and designed to properly capture the properties of the water resources systems being modeled to sufficiently and efficiently address the purpose by which the models are employed in the first place. The following are key considerations in the design and choice of models to be utilized in modeling water resources systems.

#### 12.1.1 Modeling Approach: Scientific Versus Data Analytic Method

It is worthwhile to revisit a discussion by Eddy (1979) with reference to modeling approaches which distinguishes between the so-called scientific method and data

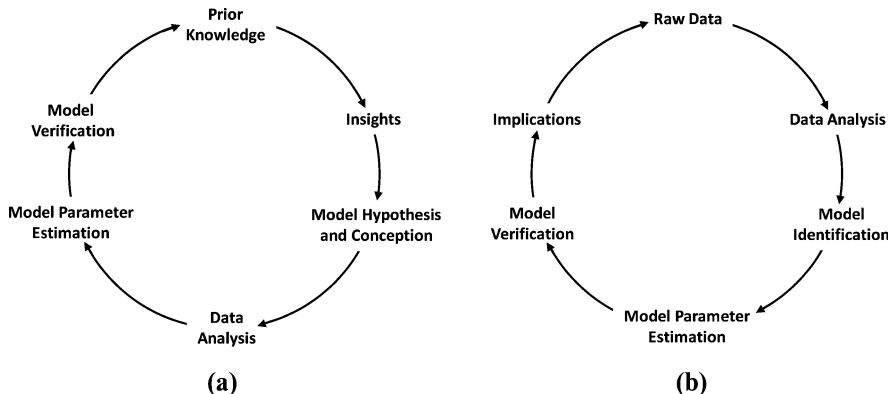


**Fig. 12.1** Illustrative definition of modeling approaches by (a) scientific method and (b) data analytic method

analytic method as shown in Fig. 12.1. Briefly, the scientific method begins and ends with the background knowledge underlying the physical process, while the data analytic method evolves around the data; thus the only knowledge is empirical. As argued by Eddy (1979):

*The crucial difference between the data analytic and scientific method is the role of the data. Obviously, for data analysts, the data are central. The scientific method uses data only at a late stage when the correctness of a model is being formally verified.*

It is advocated here that one must strive as much as possible to employ the scientific method of modeling water resources before resorting to data analytic method. The continuous loop in Fig. 12.1 signifies that as new data and/or knowledge come in, one keeps on improving and updating the model and modeling process.

In the mid-1970s, there was somewhat a clash between deterministic and stochastic approaches in modeling water resources systems where the deterministic approach was associated to the scientific method while the stochastic approach was associated to the data analytic method.

Deterministic approaches appealed to a number of researchers because models of this type are considered more physically based to give considerable insight into the physics and system dynamics of the water resources systems. To some however, the degree of theoretical and mathematical development has become numerically intractable and that accuracy cannot be guaranteed because of inadequate or insufficient data for model identification and parameter specification resulting in some modelers to look for alternative approaches. Stochastic approaches then started to become popular dominated by black-box models so that given the system inputs, an output response is apparently produced. In some cases, these stochastic models have been purely based on probabilistic formulations. An early attempt to reconcile stochastic and deterministic approaches started with the claim that the deterministic approach is actually a subset of stochastic approach since models can be formulated with a deterministic component and a probabilistic or random component. One formalization of this idea was done by Finney et al. (1982) where they presented deterministic

water quality models and transformed them into stochastic differential equations so that the mechanistic form of the system dynamics is explicitly retained in the model, while the uncertainties in the input, parameters, and likewise the output of the water quality process are considered. To further close the gap between deterministic and stochastic approaches, Klemes (1978) has ironically insisted and said that:

*Since any model can be either deterministic or stochastic depending on whether its variables and parameters do or do not contain an element of randomness, there is a real and legitimate challenge in seeking efficient combination of deterministic and stochastic approaches in order to obtain better insights into specific problems.*

Until now, this challenge seems to be still the same, and in fact in the Philippines, the deterministic approach is still the dominant mode of modeling water resources systems thus ignoring the complex dynamics due to uncertainty, stochastic disturbances, and unpredictability of water resources systems.

### ***12.1.2 Incorporating the Hydrologic, Geomorphologic, and Ecologic Interactions***

Understanding of the mechanistic interactions of hydrology, geomorphology, and ecology is required in the proper understanding of the river environment (Tabios 2008, 2018). Also, special attention must be given to the temporal and spatial scales of fluctuations and interactions of these processes in the river system so that proper tools can be employed in the analysis and characterization of such processes.

In the case of geomorphologic and hydrologic interactions, Tabios (2018) stated that the river morphology influences the shape and magnitude of the basin hydrograph while the river flow regimes changes the river morphology (Solyom and Tucker 2004). High-flow regimes remove or mobilize sediments, while the low-flow regimes promote deposition of sediments.

With respect to hydrologic and ecologic interactions, the river ecology in terms of species, composition, and communities and life cycles of the flora and fauna highly depends on the seasonal variations of discharges, transverse and longitudinal channel velocity distribution, floodplain-river interaction, time-space frequencies, and floodplain wetting and drying as well as water residence times and dilution effects on water quality (Shen et al. 1994).

In terms of ecologic and geomorphologic interaction, it is noted that the biogeography and the spawning, refuge, and survivability of aquatic flora and fauna depend on the river bed form, bed material composition, and sediment loads. For instance, the fish prefer spawning in cobble bars and then rest and feed in the pool or deeps in the riffle-pool sequence of the river during spawning forays (Milhous 1995). On the other hand, bioturbation due to burrowing organisms can cause resuspension of sediments in streambeds thus modifying the river morphology.

One must also recognize the importance of the temporal and spatial scales of fluctuations of the various processes in the hydrologic, geomorphologic, and

ecologic interactions. For example, flood flows carrying high sediment loads can abruptly change the river morphology in a few hours or few days in contrast to river morphologic changes due to burrowing organisms which could take several months or years. Another example is the disappearance of a wetland due to river water diversion over a long period that after several years, the wetland flora and fauna are also disappearing. In fact, there are cases when it is already too late to notice or realize that the wetland has disappeared and its associated flora and fauna.

In view of these interactions, when the river environment is modified such as by construction of roadways, bridges, and other types of obstructions, the natural hydrologic/hydraulic, geomorphologic, and ecologic interactions in the river system are drastically modified.

## 12.2 Monitoring and Data Needs for Future Modeling Efforts

When modeling water resources systems in the Philippines, one is usually handicapped because of lack or inadequate data to conduct model calibration or model validation. This is always the issue in developing countries where investments toward long-term, sustainable sampling in time and space are not forthcoming. For instance, a rigorous model validation procedure is to test whenever possible the forecasting or predictive ability of the model using a remotely different data with unique characteristics from those used in the calibration period in order to objectively and properly assess the accuracy and reliability of the model (Sorooshian 1983). Of course, this will not be at all possible with short, fragmentary data available or where there is no data.

As far as rainfall data is concerned, there are currently 144 rainfall gaging stations over the country operated by PAGASA, and these data are published and can be procured from this agency. There are also rainfall data collected by other agencies such as NIA for their major irrigation systems or at major reservoir sites and likewise by certain universities but mostly on short-term, project basis and are usually not published. The Philippines has a total area of about 340,000 km<sup>2</sup>, so that with PAGASA's 144 rainfall stations, the sampling density is one (1) station per 2360 km<sup>2</sup> which is definitely sparse compared to the sampling densities suggested by WMO which is one station per 25 km<sup>2</sup> for small islands, 250 km<sup>2</sup> for mountainous areas, and 575 km<sup>2</sup> for plains and hilly, undulating areas.

With regard to streamflow gaging, there were 778 stream gaging stations during the period from the late 1950s to the early 1980s, installed in 421 principal river basins in the Philippines. Currently, however, there are only 249 that are still operational (IWAVE 2012). The major agency that collects and publishes the streamflow data is the Bureau of Research and Standards (BRS) of the Department of Public Works and Highways (DPWH) except during the period between mid-1975 and early 1980 when this was transferred to the National Water Resources Council

(NWRC), which is now named the National Water Resources Board (NWRB). But many of the 249 streamflow gaging stations collect discontinuous and fragmentary data so that in the last 30 years, the effective number of years of record is only about 10 years. The country has 216 lakes and 22 major marshes, swamps, and reservoirs, but only 7 of the lakes and at least 7 of the major reservoirs (i.e., Magat, Pantabangan, Angat, Ambuklao, Binga, San Roque, Pulangi) are currently monitored. As far as groundwater monitoring is concerned, the local water districts, which are the domestic water provider of the country, mostly source their water supply from groundwater. They also conduct monitoring and collect groundwater data such as water levels and water quality data, but most of them are not on regular basis, and these data are not usually published.

In view of the above, investments in climatologic and hydrologic data collection in the long term and at appropriate sampling frequency in time and space are needed which are useful for various types of water resources analysis and modeling studies such as for flood forecasting and flood mitigation plans (i.e., requiring short-time interval, hourly data) and for domestic water supply (daily to weekly) or irrigation water supply (weekly to monthly data). There are a lot more data needed such as water quality data, sediment transport data, and river survey data that are collected on project basis or periodically (e.g., quarterly basis) but that are equally important to be monitored regularly and ideally at least on a weekly or monthly basis.

On a separate note, nowadays, satellite data, remote sensing (imaging) data, or high-resolution LIDAR data have also become available and affordable for water resources modeling studies. Acquisition of these data may require bigger investments, but they have more sophisticated uses (aside from deriving elevation, soils, or land use maps), such as in monitoring watershed activities that adversely impact the environment like illegal logging that leads to deforestation denudation and consequently to increased soil erosion and sedimentation in rivers or even in long-term degradation of ecological integrity of the watersheds. These data can likewise be used for detection and surveillance purposes against water quality violations or water pilferage.

## **12.3 Science-Based Management and Decision Tools and Capacity Building**

In terms of water resources management, the Philippines still lacks investments in science-based management and decision tools. Most water-related agencies in the Philippines do not even have dedicated scientific division or group in their offices to employ science-based analysis or modeling tools. Thus, the Philippine government should seriously consider developing a science-based culture and institutionalized within their agencies the use of science-based tools, maintained by a permanent and sustained modeling group or division. Resources and budget should be allocated to establish this scientific division or modeling group in targeted water institutions with

long-term, periodic capacity building and training programs including sustained upgrading of software and hardware tools and equipment. With a dedicated science-based group or division in a water agency, research and development should become part of the routine task of the group.

To reiterate what was already mentioned in Chap. 1, having a permanent modeling group will allow the government to employ adaptive and continuous updating of its master plans and operational studies of water resources system recognizing that plans cannot be static since watersheds or natural resource systems in general are evolutionary in nature due to land use change, anthropogenic activities, economic change, and climate change. In fact, adaptive planning is best employed under the framework of sustainability science and transdisciplinary approach as discussed below.

With the science-based support or modeling group, not only that adaptive planning can be accomplished with development and continuous updating of water resources management plans, but also the computerized decision support system to be used in adaptive planning can likewise be maintained and continuously upgraded by the modeling group as new knowledge, data and technologies come in.

## **12.4 Need for Sustainability Science and Transdisciplinary Approach for Sustainable Water Resources Development**

The sustainable utilization and development of water resources systems must balance economic development and environmental protection. Economic development is to satisfy basic needs, to alleviate poverty, to enhance economic and social equity, and to improve the quality of human life. Environmental protection is to ensure ecological integrity of the environment to support biological life in general and to maintain genetic diversity, resilience, and biological productivity in particular. Thus, a sound and enhanced water resources environment is a necessary condition to ensure economic efficiency and sustainability in that region.

Watershed planning and management studies should be conducted in the context of sustainable development. In this case, water studies should cover periods of 100 to 150 years (planning horizon) encompassing two to three generations. In this case, future scenario setting as far as land use plans, economic developments, and demographic change including climate change will be important to such planning studies. For instance, assessment studies on watersheds with proposed building of large-scale, urban centers in the countryside, conversion of farmlands into residential subdivision or industrial zones that balances economic development, and ecological integrity of the watersheds will be required.

The following subsections discuss holistic water resources management, sustainability science, transdisciplinary approach, and planning horizon for sustainable water development. It may be noted that the concept of transdisciplinarity is the inspiration of the birth of sustainability science.

### ***12.4.1 Holistic Water Resources Management***

It is advocated here that holistic water resources management is needed, which requires integrated management of land, water, coastal, and even air environments. In this context, since we now deal with large-scale, complex, dynamic, and uncertain water resources systems, holistic water management requires a new approach which can no longer be based on traditional science but rather based on sustainability science which views that planning, design, and management of water systems is interwoven and demands understanding of the physical system (natural processes, climate, weather), social system (societal, political, economic), and human system (cultural, behavioral, lifestyles).

In the context of flood risk management as an example, meteorological factors such as climate and weather and specifically the weather elements such as rainfall, wind, temperature, and evaporation are significant factors that govern the hydrology and hydraulic of flow and sediments. However, two other aspects of flood management are the hydrological or river management factors and human factors. These other factors include reduction of river capacities because of sedimentation of soils eroded from forest denudation; dumping of solid waste in the river and encroachment of river banks especially by illegal settlers; poor land use planning or implementation that allows legal or illegal settlements in flood prone areas; and obliteration of pervious areas due to urbanization, thus virtually obliterating opportunity for rainwater infiltration into the ground. The issue of illegal settlements has also been tainted with political accommodation of the urban poor. Other factors include insufficient design level of protection of flood infrastructure, lack of maintenance of drainage system for de-clogging drains or desilting river channels, and fragmented and lack of coordination among flood agencies.

In view of the above, transdisciplinary approach is required which utilizes scientific and technological tools to address the physical system, sociopolitical-economic studies to address the social system, and psychological and cultural studies to address the human system and, most importantly, engages stakeholders to solve problems through integrated, participatory, and collaborative learning, research, and consensus building.

### ***12.4.2 Role of Sustainability Science***

Holistic water resources management recognizes that a water resources system is a complex system, dynamic, thus continuously changing, as well as uncertain and thus unpredictable and capable of surprise. For this reason, a new approach is required which can no longer be based on traditional science but rather based on sustainability science (Komiyama and Takeuchi 2011). Yoshikawa (2011) described the five (5) elements of sustainability science according to (1) aim of study, (2) mode of change, (3) truth verification, (4) result of research, and (5) expected outcomes as

shown in Table 12.1. To describe the elements of sustainability science, flood risk management in particular is illustrated and discussed below with reference to Table 12.1 (Tabios 2015a, 2015b).

**Table 12.1** Flood risk management in the context of sustainability science (SS) versus traditional science (TS)

Elements	Traditional Science (TS)	Sustainability Science (SS)	Difference TS vs SS	Flood Management with TS	Flood Management with SS
<b>Aim of Study</b>	To understand everything and manage individuals	To understand everything and manage their relations	Separate Disciplines vs Transdisciplinary	Understand flood and mitigate flood to protect human life and property	Understand flood and its relations to flora, fauna and people for its adverse impacts and/or benefits
<b>Mode of Change</b>	Unchangeable (deduced from existence)	Slow change	Stable vs Unstable	Design flood and return period assuming stationary conditions	Flood changes with climate, weather, social, political and economic changes at micro/macro levels
<b>Truth Verification</b>	Experiments in laboratory	Evolution in reality	Certain (historicism) vs Uncertain (evolutionary)	Observation (2d/3d lenses) and estimation based on historical data	Include computer simulations (4d lens) to account for uncertainties and dynamic changes
<b>Result of Research</b>	Knowledge for understanding	Knowledge for action	Analysis vs Synthesis	Flood frequency analysis and flood design at point or river stretch	Integrated flood management that covers land, coastal and hazard management
<b>Expected Outcome</b>	Prosperity of human beings	Sustainability of the earth	Prosperity vs Sustainability	Minimize loss of life and property	Optimize impacts and benefits of floods to enhance and sustain ecosystem functions to support flora, fauna and especially human life

#### **12.4.2.1 Aim of Study**

Sustainability science aims “to understand everything and manage the relations among the various components of the system,” thus transdisciplinary in nature in contrast to traditional science which is monodisciplinary (based on separate disciplines). In relation to flood management, traditional science aims to “understand flood and mitigate flood to protect life and property” in contrast to the use of sustainability science which aims to “understand flood and its relations to flora, fauna, and people for its adverse impacts and/or benefits and recognizing the geomorphologic-hydrologic-ecologic interactions.”

#### **12.4.2.2 Mode of Change**

In terms of mode of change, flood management in the context of traditional science utilizes “design flood and return period assuming stationary conditions,” but sustainability science views that “flood changes with climate, weather, social, political, and economic changes both at microscopic and macroscopic levels” with the view that the earth is unstable and slowly changing although it can attain at certain periods what is referred to as dynamic equilibrium.

#### **12.4.2.3 Truth Verification**

Under truth verification, traditional science had fairly relied on “experiments in the laboratory,” thus a historicist and “certain or almost sure” perspective as opposed to sustainability science where nature is an “evolution in reality” and is therefore “uncertain and evolutionary and requires piecewise engineering.” In the context of flood management, traditional science employs observations referred to as two-dimensional (2-d) lenses or tools in line/time or three-dimensional (3-d) lenses in 2-d space/time and that estimates are based on historical data, in contrast to sustainability science which employs four-dimensional (4-d) lenses through computer simulations and scenario building to account for uncertainties due to socio-economic or climate and ecosystem dynamics and future changes.

#### **12.4.2.4 Result of Research**

The result of research in traditional science is “knowledge for understanding” which entails analysis and can be simply a fancy or for the sake of science, referred to as dream research. This is in contrast to sustainability science which is “knowledge for action” requiring synthesis and entails nightmare research. In the context of flood management, traditional science would employ “flood frequency analysis and flood design at a point or river stretch,” while sustainability science would employ

“integrated flood management which covers physical, socioeconomic, and environment dimensions including land management and drought mitigation.”

#### **12.4.2.5 Expected Outcome**

With regard to expected outcomes, traditional science is for “prosperity of human beings,” while sustainability science is for “sustainability of the earth.” In the context of flood management, this translates to “minimizing loss of life and property” in traditional science as opposed to “optimal management of impacts and benefits of floods to enhance and sustain ecosystem functions and support flora, fauna, and especially human life.”

### ***12.4.3 Transdisciplinary Approach to Holistic Flood Risk Management***

Transdisciplinary approach is described here in the context of flood risk management (Tabios 2015b, 2018). In an urban setting like Metro Manila, flood risk management is a complex problem which is an interaction of a dynamic and uncertain physical system, social system, and human system as shown in Box 12.1 owing to the various factors affecting floodings in Metro Manila from meteorological (typhoons, monsoons), hydrological (sedimentation, river changes, inadequate infrastructure), and human (garbage disposal, illegal settlement in rivers, river encroachment). Consequently, holistic flood risk management must encompass the various disciplines from physical sciences, socioeconomics, and political science as well as cultural and behavioral sciences. As a footnote on *culture of disaster* under human system in Box 12.1, Bankoff (2004) observed that:

*Disasters, are not simply geophysical or meteorological events but are psychological matters as well. In some societies, natural hazards occur with such historical frequency that the constant threat of them has been integrated into the schema of both daily life and attitude to form what can be called cultures of disaster.*

In this case, transdisciplinary approach is needed which according to van Kerckhoff (2013) “transcends disciplinary pre-conceptions but is capable of understanding and synthesizing across a range of disciplinary and non-disciplinary ideas and theories.” As shown in Box 12.2, transdisciplinary approach can be contrasted to monodisciplinary (isolated approach by individual experts), to multidisciplinary (additive approach bringing together a wide range of experts), and to interdisciplinary (interactive approach of several experts solving a problem together).

The platform of transdisciplinary approach is shown in Box 12.3 which involves the following: (1) stakeholder engagement, (2) iterative process, (3) working collectively, and (4) hierarchical levels of decision-making.

**Box 12.1 Elements of Physical, Social, and Human Systems Inherent in a Complex, Dynamic, and Uncertain Flood Problem**

Physical system	Social system	Human system
Global and local climate extremes and variabilities	Socioeconomic objectives	Individual lifestyles and behaviors
Weather dynamics	Social norms and traditions	Culture of disaster
River dynamics and sedimentation	Political ambitions	Informal settlements in rivers
River ecological integrity	Investments and financing	Garbage disposal practices

**Box 12.2 Differences of Monodisciplinary, Multidisciplinary, Interdisciplinary, and Transdisciplinary Approaches**

Monodisciplinary	Multidisciplinary	Interdisciplinary	Transdisciplinary
Reactive	Proactive	Integrative	Interactive and holistic
Isolated approach by individual experts	Additive approach bringing together a wide range of experts	Experts and stakeholders solve a problem by parts then integrate	Experts and stakeholders solve problem as a whole through interaction of parts

**Box 12.3 Platform of Transdisciplinary Approach**

---

*Stakeholder engagement and collaboration* involving academics, professionals, government units, nongovernment organizations, communities, and individuals

---

*Iterative process* of project development in consultation with stakeholder

---

*Work collectively* from problem identification and then knowledge generation to development of sustainable solutions and final project implementation

---

*Decisions are made on hierarchical levels* in the order of (i) satisfying physical laws and constraints, (ii) then sustainable ecological solution, (iii) sound economic basis, and finally (iv) socially justifiable and (v) politically acceptable solutions

---

To reiterate, the important components of IWRM as well as holistic water resources management are to ensure the active participation of stakeholders and to engage or at least consult them in problem identification, knowledge generation, project implementation, and monitoring. This can be guided by experts with experiences in community-based planning (bottom-up planning policy) rather than planning handed down from the national government (top-down planning).

#### **12.4.4 Planning Horizon for Sustainable Development of Water Resources Systems: Case of Reservoir and Dam Projects**

There is a debate whether a reservoir and dam project for water supply, hydropower, and/or flood control purposes is a renewable resource or not – due to reservoir sedimentation. In particular, a reservoir is nonrenewable resource if it has a finite or useful economic life when it becomes filled with sediments. Tabios (2018) discussed that for a reservoir to become renewable, it has to be planned, designed, and operated in the timeframes of sustainable development so that it is not *only for the current human generation but future generations to come*. It may be noted that reservoir and dam projects are commonly justified based on an economic life of 50 years to at most 70 years which essentially covers only one human generation. This concept or practice that reservoirs have a finite design life is to accede to nature that rivers carry sediments and then reservoirs trap them and simply become filled-up. However, a reservoir can be planned, designed, and operated to have a very prolonged life, with proper sedimentation management strategies implemented and that the dam structure should have a facility to flush or remove sediments instead of being retained in the reservoir. In fact, the river downstream of a reservoir should not be deprived of sediments which are useful to channel morphodynamic equilibrium as well as maintain and enhance aquatic habitats as advocated by Kondolf et al. (2014). Admittedly, it is quite difficult for governments including private investors to appreciate and more so justify projects with economic planning horizons beyond 150 years or more.

As discussed by Tabios (2018), with planning horizons of 50 to 70 years, either the available historical data or stochastically generated data is used in the feasibility study of the reservoir and dam project which includes water demand projections and the business or economic model of the design life of the reservoir. However, for a reservoir life of more than 150 years or so, covering four to five future generations, the feasibility study of such reservoir and dam project requires long-term visioning, life cycle analysis and scenario setting for the next two centuries. Thus, creative and imaginative skills will be needed in order for planners, design engineers, economists, and stakeholders to project future projections in water demand, land use, river landscape, climate, and ecosystem including changes in political and socioeconomic structures that influence the physical environment. Admittedly, this visioning and

scenario setting exercise could have all elements of uncertainty, but hopefully this will not prevent decision-makers to seriously consider making long-term investments for the sustainable development of major water infrastructure.

## **12.5 On Building Urban Resilience to Water-Related Disasters**

Finally, this chapter ends with building urban resilience to water-related disasters, the importance of which cannot be overemphasized. Nowadays, building urban resilience has become a complex problem due to the dynamics and uncertainties of the climate, land, water, and ecosystem including the economic, social, and political environment. Thus, understanding and planning for urban resilience encompasses spatiotemporal variations of physical, economic, social, and political factors and that building urban resilience covers infrastructural, institutional, economic, and social resilience. Davoudi (2012) has given three types of resilience worth examining here, namely, engineering, ecological, and evolutionary. Evolutionary resilience in particular has been defined by Prof C.S. Holling in 1973, a Canadian theoretical ecologist (Davoudi 2012).

### ***12.5.1 Engineering Resilience***

It is the ability of a system to resist and return to an equilibrium or steady state after a disturbance such as a natural disaster or a social upheaval. The faster the system bounces back to a single, stable equilibrium, the more resilient it is.

### ***12.5.2 Ecological Resilience***

It is the ability to absorb and persist before the system changes its structure and ability to adapt to disturbance, recognizing the existence of multiple equilibria and possibility of systems to flip into alternative stability domains.

### ***12.5.3 Evolutionary Resilience***

It is the ability of a socio-ecological system to change, adapt, and transform in response to perturbations and disturbances and that system is not conceived to return

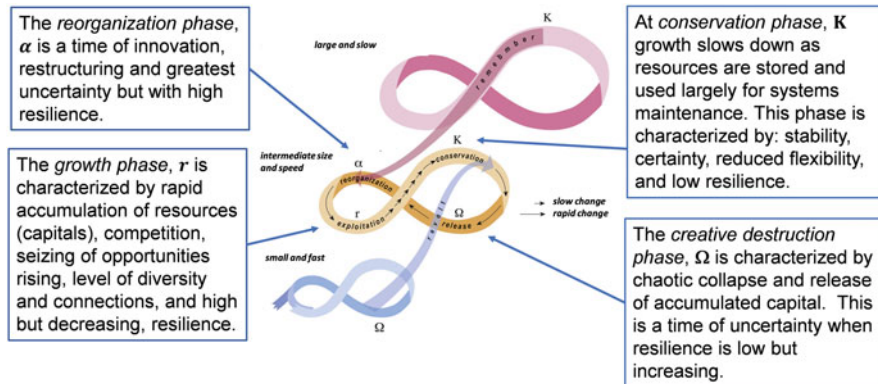


**Fig. 12.2** Panarchy model of adaptive change to illustrate evolutionary resilience. [Taken from Davoudi (2012); Davoudi et al. (2013)]

to normality. It acknowledges that systems are complex, nonlinear, and self-organizing permeated by uncertainty and discontinuities. In the context of panarchy model of adaptive change of Prof. C.S. Holling (Davoudi 2012), evolutionary resilience has four phases as shown in Fig. 12.2 as follows (Davoudi et al. 2013): (1) growth phase characterized by high but decreasing resilience, (2) conservation phase characterized by low resilience, (3) creative destruction with increasing resilience, and (4) reorganization which is the opening up of new and unpredictable possibilities. This implies that as systems mature, their resilience reduces and they become “an accident waiting to happen,” and when systems collapse, “a window of opportunity” opens up for alternative systems configuration. Holling uses the “omega” symbol for the creative destruction phase to denote the end phase, but one which is rapidly followed by an alpha phase of reorganization and renewal. The omega phase is, therefore, a time of greatest uncertainty yet high resilience, a time for innovation and transformation, and a time when a crisis can be turned into an opportunity.

With the above discussion, it appears that the most appropriate approach for building urban resilience to water-related disasters is evolutionary resilience in view of the complex dynamics and uncertainties of the water resources systems and the associated social, economic, and political dimensions (Tabios et al. 2016). Also, it can be concluded that building urban resilience can no longer be based on traditional science but rather on sustainability science since evolutionary resilience logically fits into the framework of sustainability science. In this case, one can also draw Table 12.2 for building urban resilience in the context of sustainability science in the same manner as that shown in Table 12.1 for flood risk management.

**Table 12.2** Building urban resilience in the context of sustainability science

<b>Elements</b>	<b>Sustainability Science (SS)</b>	<b>Evolutionary Urban Resilience</b>
<b>Aim of Study</b>	To understand everything and manage their relations	Understand and manage together infrastructural, institutional, economic and social resilience (i.e., avoid whole system to suffer by improving only part of it)
<b>Mode of Change</b>	Slow change	Urbanization also changes with climate, land use, social, political and economic changes at micro/macro levels
<b>Truth Verification</b>	Evolution in reality	Include computer simulations and scenario settings over so many years to account for uncertainties and dynamics of changes in climate, land use, socio-economics and politics
<b>Result of Research</b>	Knowledge for action	Resilience planning is iterative, inclusive and integrative to reduce the uncertainty and complexity of urban growth and hydromet-climate changes
<b>Expected Outcome</b>	Sustainability of the earth	Not a single outcome but series of outcomes and actions building upon each other, enhanced and progressed over time as people and institutions learn from past experiences and decisions

## References

- Bankoff G (2004) In the eye of the storm: the social construction of the forces of nature and the climatic and seismic construction of god in the Philippines. *J Southeast Asian Stud* 35(01):91–111
- Davoudi S (2012) Resilience: a bridging concept or a dead end? *Plan Theory Pract* 13(2):299–307. <https://doi.org/10.1080/14649357.2012.677124>
- Davoudi S, Brooks E, Mehmood A (2013) Evolutionary resilience and strategies for climate adaptation. *Plan Pract Res* 28(3):307–322. <https://doi.org/10.1080/02697459.2013.787695>
- Eddy WF (1979) Comment on nonparametric statistical data modeling by E. Parzen. *J Am Stat Assoc* 74(365):124–126
- Finney BA, Bowles DS, Windham MP (1982) Random differential equations in river water quality modeling. *Water Resour Res* 18(1):122–134
- IWAVE (IAEA Water Availability Enhancement Project) (2012) Investment needs for resource assessment capability in the Philippines to improve planning and management of water infrastructure. Joint report by International Atomic Energy Agency (IAEA), Philippine Nuclear Research Institute (PNRI)/National Water Resources Board (NWRB), Quezon City, p 130
- Klemes V (1978) Physically based stochastic hydrologic analysis. In: Chow V e (ed) *Advances in hydroscience*, vol 11. Academic Press, New York, pp 285–356
- Komiyama H, Takeuchi K (2011) Sustainability science: building a new academic discipline. In: Komiyama H, Takeuchi K, Shiroyama H, Mino T (eds) *Sustainability science: a multidisciplinary approach*. United Nations University Press, Tokyo, pp 2–19
- Kondolf GM, Gao Y, Annandale G, Morris GL, Jiang E, Zhang J, Cao Y, Carling P, Kaidao F, Guo Q, Hotchkiss R, Peteuil C, Sumi T, Wang H-W, Wang Z, ZhilinWei BW, Caiping W, Yang CT (2014) Sustainable sediment management in reservoirs and regulated rivers: experiences from five continents. *Earth's Future* 2:256–280. <https://doi.org/10.1002/2013EF000184>

- Milhous RT (1995) Changes in sediment transport capacity in the lower Gunnison River, Colorado, USA. In: Proceedings of man's influence on freshwater ecosystems and water use, vol 230. IAHS Publishing, Wallingford, pp 275–280
- Shen HW, Tabios GQIII, Harder JA (1994) Kissimmee river restoration study. J Water Resour Plann Manage ASCE 120(3):330–349
- Solyom PB, Tucker GE (2004) Effect of limited storm duration on landscape evolution, drainage basin geometry and hydrograph shapes. J Geophys Res 109(F03012):13
- Sorooshian S (1983) Surface water hydrology: on-line estimation. U.S. National Report to Int'l Union of Geodesy and Geophysics 1979–1982, contributions in hydrology, Amer. Geophys. Union, Washington, D.C. Rev Geophys 21:706–721
- Tabios GQ III (2008) Hydrology and related ecology-based aspects of managing the Agusan Marsh. In: Primavera JH (ed) Proceedings of the first Agusan Marsh scientific conference. PCMARD-DOST and UNESCO Jakarta Office, Jakarta, pp 21–31
- Tabios GQIII (2015a) Need for holistic flood risk management: Case of Pasig-Marikina River Basin of Metro Manila. In: Proceedings of 11th Association of Pacific Rim Universities (APRU) research symposium on multi-hazards around the Pacific Rim. University of the Philippines, Diliman, 3 pages, October
- Tabios GQIII (2015b) Holistic flood risk management of Pasig-Marikina River basin in metro Manila. In: Proceedings of the international symposium of integrated actions for global water and environmental sustainability. UNESCO-IHP (Jakarta Office), Medan, pp 75–79
- Tabios GQIII (2018) Multiple and integrated water resource utilization. In: Rola A, Pulhin J, Alcala Hall R (eds) Water policy in the Philippines global issues in water policy, vol 8. Springer, Cham, pp 163–184
- Tabios GQ III, Gaerlan NA, Hipolito DM (2016) Urban resilience to climate change: challenges and initiatives for Philippine urban setting. In: Proceedings of 4<sup>th</sup> national climate conference: addressing climate risk for sustainable development. National Academy of Science and Technology, Tagaytay City
- Van Kerckhoff L (2013) Developing integrative research for sustainability science through complexity principles-based approach. Sustain Sci. <https://doi.org/10.1007/s11625-013-0203-y>
- Yoshikawa H (2011) Science and technology for society. In: Komiyama H, Takeuchi K, Shiroyama H, Mino T (eds) Sustainability science: a multidisciplinary approach. United Nations University Press, Tokyo, pp 256–271

# Appendices

## Appendix A

### *Sacramento Soil-Moisture Accounting Model*

Described in detail below is the Sacramento soil moisture accounting (SAC-SMA) model adopted in the watershed model computer program developed by Tabios et al. (1986). At the end of this Appendix A, briefly described are the flow routing model options for overland flow and channel routing as well as the Rosenbrock optimization algorithm (Kuester and Mize, 1973) employed for automatic model parameter calibration.

The SAC-SMA model developed by Burnash et al. (1973) when it was incorporated in the National Weather Service River Forecasting System (NWSRFS) sometime mid-1980s for real-time river forecasting over 4,000 river systems in the United States (Burnash, 1985), it was too large a computer program and can only be implemented in mainframe computers. During that period, the IBM Personal Computer (IBM-PC) also came out so that in order to use the SAC-SMA model, Tabios et al. (1986) developed a small version of the NWSRFS model for IBM-PC application, hence the name NWS model-PC version. Also, instead of using the flow routing models in the original NWSRFS model, the kinematic wave routing model adapted from HEC-1 computer model of the US Army Corps of Engineers (USACE, 1985) for overland flow and channel routing, including the unit hydrograph method for overland flow planes and Muskingum method for channel routing, were utilized as optional methods. For model calibration, the constrained Rosenbrock optimization routine given by Kuester and Mize (1973) was used as an option to automatically calibrate selected model parameters in the SAC-SMA model.

Referring to the model structure of SAC-SMA as shown in Fig. A.1, the model utilizes conceptual storages to represent the watershed hydrology starting with precipitation, the subsequent vertical and horizontal movement of water through and over the soil, and finally the production of runoff.

In the model, the subsurface layer or soil moisture storage is divided into the upper zone and lower zone. The upper zone represents the upper soil layer and interception

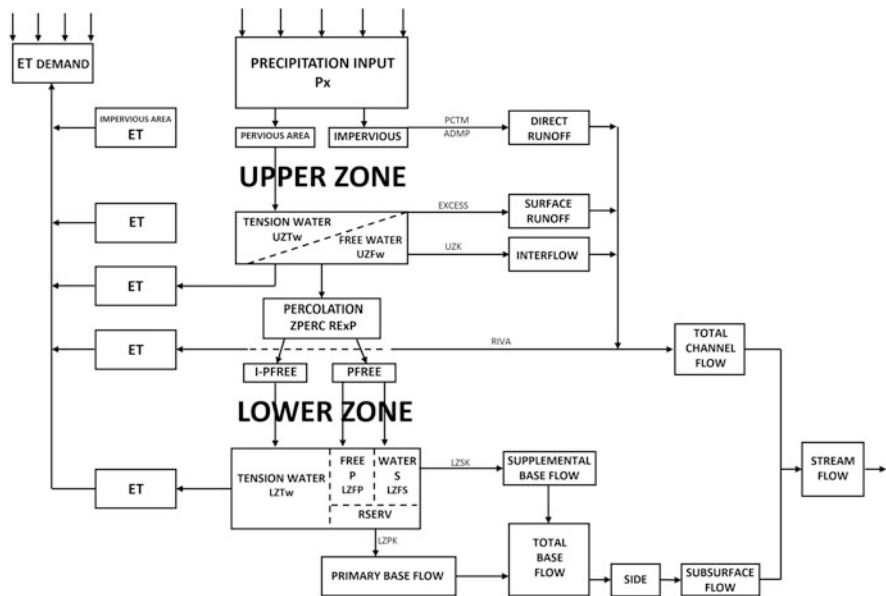


**Fig. A.1** Model structure of Sacramento soil-moisture accounting model. Also indicated are key model parameters described in the main text (from Burnash et al. 1973)

storage, while the lower zone represents the bulk of the soil moisture and groundwater storage. Each zone stores water in the form of tension water and free water. Tension water is that which is closely bound to the soil particles by tension or electrostatic forces in contrast to the water that is free to move by gravitational forces. In these conceptual storages, tension water storage must be filled before free water storage is supplied. Tension water can only be removed by evaporation, and free water can be depleted by evapotranspiration as vertical percolation. In the lower zone storage, there are two types of free water storages: primary which is slow draining and provides baseflow over long periods of time; and, supplementary which is fast draining and provides baseflow after relatively short period from recent rainfall. Movement of water from the upper zone to lower zone is by percolation process which is a nonlinear function of the available free water in the upper zone and the soil moisture deficiency in the lower zone.

Finally, the model generates five flow components, namely, (1) direct runoff from impervious areas; (2) surface runoff which occurs when the upper zone free water storage is full and the rainfall intensity exceeds the rate of percolation and interflow rates; (3) interflow resulting from lateral drainage of the upper zone free water storage; (4) supplemental baseflow; and (5) primary baseflow. The first three flow components represent the total channel inflow, while the latter two is the total baseflow. The total channel inflow constitutes the entire surface runoff contribution to the stream flow hydrograph routed via kinematic wave or combined unit hydrograph-Muskingum routing and a portion of total baseflow is the subsurface runoff contribution to streamflow. This subsurface flow contribution is added to the

routed streamflow at the basin or sub-basin outlet using a linear, decay weighting function similar to unit hydrograph routing.

Described below are the various components and processes of the SAC-SMA model especially the mechanics of water movement in the upper zone storages and the lower zone storages including the evapotranspiration and runoff processes. Also, described briefly are the kinematic wave routing for both overland flow and channel flow as well as the use of combined unit hydrograph routing for overland flow and Muskingum channel routing.

### Upper Zone Water Storages

As mentioned earlier, the upper zone is divided into tension water storage and free water storage. Tension water is water in the upper shallow soil layer that is tightly bound to the soil molecules but can be removed by evapotranspiration. Any deficit in the tension water storage is rapidly replaced by rainfall before sufficient moisture can accumulate in the free water storage to initiate the runoff process. The upper zone tension water (UZTW) storage must be filled first before moisture becomes available to enter other storages. On the other hand, the upper zone free water (UZFW) storage provides water to produce fully effective wetting front which percolates as rapid drainage to form interflow and any excess water move laterally to deeper portions of the soil mantle until reaching the lower zone storage. Anytime when the upper zone tension water storage has a deficit due to evapotranspiration loss, water from the free water or rainfall immediately replenishes the tension water storage deficit. Internally in the model, the computation time step is made small enough that not more than 5 mm of water is moved from any soil moisture storage over this time step. In view of the above, the water balance and mechanics of water movement in the upper zone water storages can be described by the following equations.

Letting the upper zone tension water content and maximum storage capacity be denoted by UZTWC and UZTWM, respectively, and the corresponding upper zone free water content UZFWC and maximum capacity UZFWM, then the water contents at any given time are:

$$UZTWC = UZTWM \cdot UZRAT \quad (\text{A.1a})$$

and

$$UZFWC = UZFWM \cdot UZRAT \quad (\text{A.1b})$$

in which UZRAT is given by:

$$UZRAT = \frac{UZTWC + UZFWC}{UZTWM + UZFWM} \quad (\text{A.2})$$

The above computation is done following evapotranspiration computations of the UZTW storage to ensure proper balance of relative soil moisture loadings of the upper zone storages. The portion of UZFW that goes to interflow is computed assuming an outflow from a linear reservoir such that interflow is the product of UZFWC and UZK where UZK is the upper zone free storage depletion coefficient. However, prior to interflow computation, water that percolates to deeper soils is first obtained.

### Lower Zone Water Storages

The water stored in the lower zone tension (LZTW) storage is the remaining volume of tension water in excess of the UZTW storage which is necessary to fully satisfy moisture requirements based on molecular attraction between dry soils and moisture (excluding free water). Physically, water from LZTW storage is utilized by plants for evapotranspiration but not readily transferred from roots to leaf systems as in the shallow UZTW. Since tension water deficiencies are associated with a suction force, they tend to absorb all percolating water until the moisture deficiencies are satisfied. To account for variations in soil conditions and rainfall amounts in the basin, the model diverts a fraction of the percolated water into the lower zone free water (LZFW) storages before the tension water (LZTW) moisture deficiencies are fully satisfied. This fractional split is defined by *PFREE* parameter such that the fraction *PFREE* of percolated water goes to free water and the remainder ( $1.0 - \text{PFREE}$ ) goes to tension water. Once the LZTW storage is filled, the percolated water goes to LZFW.

The lower zone free water storage is composed of primary storage which is slowly draining and provide longer lasting subsurface flow referred to as primary baseflow and the supplemental storage is rapidly draining source of subsurface flow referred to as supplementary baseflow. Both primary and supplementary storages fill simultaneously from percolated water but drain independently at different drainage rates acting as linear reservoirs with depletion coefficients denoted by *LZPK* and *LZSK*, respectively, thus generating different baseflow recessions. The LZFW storages can be depleted by water transfer to LZTW storage, by evapotranspiration and by drainage to become baseflow. Computationally, the water transfers are accomplished as follows. First, the ratios *RATLZT* and *RATLZ* are computed such that:

$$\text{RATLZT} = \text{LZTWC} / \text{LZTWM} \quad (\text{A.3})$$

where RATLZT is the ratio for tension water and:

$$\text{RATLZ} = \frac{\text{LZTWC} + \text{LZFPC} + \text{LZFSC} - \text{SAVED}}{\text{LZTWM} + \text{LZFPM} + \text{LZFSM} - \text{SAVED}} \quad (\text{A.4})$$

in which  $RATLZ$  is the ratio for primary and supplemental water, including tension water but excluding the reserved free water  $SAVED$  computed as:

$$SAVED = RSERV \cdot (LZFPM + LZFSM) \quad (\text{A.5})$$

where  $RSERV$  is the fraction of the amount of water in LZFW storage that is unavailable to such transfers.

With the above ratios, the transfer of water is made if  $RATLZT$  is less than  $RATLZ$  and the amount to be transferred is such as to make the two ratios equal. Denoting this quantity by  $DEL$  defined as:

$$DEL = (RATLZ - RATLZT) \cdot LZTWM \quad (\text{A.6})$$

then, the water transfers are made by first, adding the amount  $DEL$  to the lower zone tension water content ( $LZTWC$ ), which is taken out from the lower zone supplemental free (LZFS) water content ( $LZFSC$ ), so that  $LZFSC$  is reduced by the amount  $DEL$ . However, if  $DEL$  is greater than the amount of water available in LZFS storage, then the remaining water is taken from the lower zone primary free water (LZFP) by such amount.

## Percolation

The percolation process allows the flow of water from the upper to lower zone storages through vertical drainage. Computation of water that percolates is done prior to interflow calculation. The rate of vertical drainage is controlled by the contents of the UZFW and the deficiency of the lower zone moisture contents by a power decay function between the maximum percolation rate when the upper zone is full and lower zone is empty and the minimum rate equal to the maximum baseflow when the lower zones are full. Functionally, the minimum percolation rate denoted by  $PERCM$  is computed as:

$$PERCM = LZFSM \cdot LZSK + LZFPM \cdot LZPK \quad (\text{A.7})$$

On the other hand, the maximum is equal to  $PERCM \cdot (1 + ZPERC)$  in which  $ZPERC$  is a model parameter.

Given the above quantities, the actual percolation rate is given by:

$$PERC = PERCM \left[ 1 + ZPERC \cdot DEFR^{REXP} \right] \frac{UZFWC}{UZFWM} \quad (\text{A.8})$$

where  $REXP$  is a model parameter and  $DEFR$  is defined by:

$$DEFR = 1 - \frac{LZTWC + LZFPC + LZFSC}{LZTWM + LZFPM + LZFSM} \quad (\text{A.9})$$

## Evapotranspiration

The evapotranspiration process consists of evaporation from areas covered by surface water and riparian or vegetation which occurs at a potential rate and evapotranspiration from upper zone and lower zone storages that vary with the volume and distribution of tension water storage. The actual amount of evapotranspiration in the model is based on the evapotranspiration demand data (*EDMND*) entered into the model. The evapotranspiration computations are performed sequentially starting from upper zone storage, lower zone storages, temporary impervious area, and finally permanent impervious area covered by riparian vegetation, streams, and lakes.

Computationally, the evapotranspiration from upper zone tension water (UZTW) denoted by *E1* is given by:

$$E1 = \min \left[ EDMND \frac{UZTWC}{UZTWM}, UZTWC \right] \quad (\text{A.10})$$

Following this, the *UZTWC* is updated by subtracting the amount *E1*. The evapotranspiration from the UZFW storages is simply calculated as:

$$E2 = \min [EDMND - 1, UZFWC] \quad (\text{A.11})$$

Likewise, *UZFWC* is reduced by *E2*, and the upper zone moisture storages are properly maintained through transfer of water from free water to tension water.

Evapotranspiration loss from the lower zone tension water is computed as follows:

$$E3 = \min \left[ (EDMND - E1 - E2) \frac{LZTWC}{UZTWM + LZTWM}, LZTWC \right] \quad (\text{A.12})$$

Then, *LZTWC* is likewise reduced by *E3*. No evapotranspiration takes place in the lower zone free water storages. As in the upper zone storages, the lower zone moisture contents must be updated and balanced which involves transfer of water from LZFW to LZTW.

The evapotranspiration from temporary impervious areas *E4* is taken equal to *E1* plus an additional amount based on tension water in temporary impervious areas in excess of the moisture in UZTW before withdrawal of *E1*. In equation form, this is given by:

$$E4 = ADIMP$$

$$\cdot \min \left[ E1 + (EDMND - E1) \frac{ADIMC - E1 - UZTWC}{UZTWM + LZTWM}, ADIMC \right] \quad (\text{A.13})$$

Then, the content of the conceptual storage representing the temporary impervious area,  $ADIMC$  is reduced by  $[E4/ADIMP]$  where  $ADIMP$  is the fraction of temporary impervious area.

Evaporation from portions of the catchment area covered by streams, lakes, and riparian vegetation is as the residual rate which is equal to:

$$E5 = (EDMND - E1 - E2 - E3) \cdot RIVA \quad (\text{A.14})$$

in which the model parameter  $RIVA$  is the fraction of total catchment area covered by streams, lakes and riparian vegetation. The evaporation amount  $E4$  is subtracted from the total channel inflow after drainage and runoff computations are made for the given computational time step.

The total evapotranspiration  $ET$  used for a given time step is given by:

$$ET = (E1 + E2 + E3) \cdot PCIAR + E4 + E5 \quad (\text{A.15})$$

where  $PCIAR = 1 - (ADIMP + PCTIM)$  is the fraction of pervious area in the catchment over which the evapotranspiration processes  $E1$ ,  $E2$ , and  $E3$  take place.

## Runoff Components

The SAC-SMA generates five runoff components, namely, direct runoff, surface runoff, interflow, supplementary baseflow, and primary baseflow.

Direct runoff results from rainfall that falls on permanent impervious area as well as temporary impervious area. From permanent impervious areas, direct runoff is simply computed from:

$$ROIMP1 = PXV \cdot PCTIM \quad (\text{A.16})$$

where  $PXV$  is the rainfall for the given computational time step and  $PCTIM$  is the fraction of permanent impervious area in the catchment or sub-basin.

The direct runoff from temporary impervious area is computed as:

$$ROIMP2 = (PXV + UZTWC - UZTWM) \cdot RATIO \cdot ADIMP \quad (\text{A.17})$$

where:

$$RATIO = [(ADIMC - UZTWC)/LZTWM]^2 \quad (\text{A.18})$$

The total direct runoff is the sum of  $ROIMP1$  and  $ROIMP2$ .

The surface runoff  $SUR$  is computed from the previous portion of the catchment area which is the converse of  $ROIMP2$  which is equal to:

$$SUR = (PXV + UZTWC - UZTWM) \cdot (1 - RATIO) \cdot ADIMP \quad (\text{A.19})$$

The interflow  $SIF$  which results from lateral drainage of the upper zone free water storage operates as a linear reservoir given by:

$$SIF = UZK \cdot UZFWC \cdot PCIAR \quad (\text{A.20})$$

where  $PCIAR = 1 - ADIMP - PCTIM$  is the pervious area and  $UZK$  is model parameter of the linear reservoir representation.

The primary baseflow  $BFP$  and supplementary baseflow  $BFS$  which come from lateral drainage from the lower zone primary free water storage  $LZFP$  and supplementary storage  $LZFS$  are given by:

$$BFP = (LZPK \cdot LZFPC \cdot PCIAR)/(1 + SIDE) \quad (\text{A.21})$$

and

$$BFS = (LZSK \cdot LZFSC \cdot PCIAR)/(1 + SIDE) \quad (\text{A.22})$$

where the  $LZPK$  and  $LZSK$  are recession coefficients and the model parameter  $SIDE$  is to account for a portion of the baseflow components that may bypass the channel flow points in the basin due to some natural features in the basin.

In the flow routing component of the watershed model, the first three components of runoff, namely, direct runoff ( $ROIMP1+ROIMP2$ ), surface runoff ( $SUR$ ), and interflow ( $SIF$ ), constitute the total channel inflows which are routed from overland flow planes to the sub-basin outlet, while the sum of the primary ( $BFP$ ) and supplementary ( $BFS$ ) constitutes the subsurface or baseflow runoff component which is added to the routed flows at the sub-basin outlet.

## Flow Routing Model

In the watershed computer program of Tabios et al. (1986), there are two methods available for flow routing, namely, kinematic wave routing technique for both overland flow and channel routing or the combined use of unit hydrograph for overland flow and Muskingum method for channel routing. For the kinematic wave routing, in particular, the Fortran computer program in HEC-1 model of the US Army Corps of Engineers (USACE, 1985) was modified and adopted to fit into the watershed computer program in Tabios et al. (1986). The reader is referred to the computer manual of HEC-1 for detailed description of the kinematic wave routing technique. The methodologies in the unit hydrograph overland flow routing and Muskingum channel routing have been extensively discussed in the literature in

several hydrology textbooks so the reader may be referred to classic hydrology textbooks such as Bedient and Huber (1992) or Chow et al. (1988).

### Automatic Model Calibration by Rosenbrock Optimization

The SAC-SMA soil moisture accounting model has 18 model parameters in addition to a few in the flow routing models. Model parameter estimation can be an arduous task if all these parameters had to be calibrated manually. Thus, this watershed model developed by Tabios et al. (1986) includes an automatic model calibration technique using the Rosenbrock optimization algorithm adapted from the Fortran computer code of Kuester and Mize (1973) for selected parameters in the SAC-SMA. The objective function in the optimization algorithm is to minimize the sum of observed and computed streamflows at specified sub-basin flow points in the river basin modeled where observed data are available. For this optimization method to properly and efficiently perform the automatic model calibration, fairly reasonable, initial values of the model parameters should be specified at the start and guidelines to arrive at this initial parameters values are described in Tabios et al. (1986).

## References

- Bedient PB, Huber WC (1992) Hydrology and Floodplain Analysis, 2nd edn. Addison-Wesley Publication Company, New York
- Burnash RJC (1985) Real-time forecasting with the Sacramento watershed model. In: Proceedings of 14th Annual Hydrology Days. Colorado State Univ, Fort Collins, pp 103–113
- Burnash RJC, Fernal RL, McGuire RA (1973) A generalized streamflow simulation system: Conceptual modeling for digital computers. National Weather Service, California, Dept of Water Resources, Sacramento
- Chow VT, Maidment DR, Mays LW (1988) Applied Hydrology. Mc-Graw Hill, New York
- Kuester JL, Mize JH (1973) Optimization techniques with FORTRAN. McGraw Hill Book, Co., New York
- Tabios GQ III, Obeysekera JTB, Salas JD (1986) National Weather Service model – PC version. Dept. of Civil Engineering, Colorado State University, Fort Collins
- USACE (U.S. Army Corps of Engineers) (1985) HEC-1 flood hydrograph package user's manual, (Revised Edition). Hydrologic Engineering Center, Davis

## Appendix B

### ***WATPOW Model and COMPLEX Algorithm***

#### **Brief Description of WATPOW Model**

The WATPOW model originally developed by Tabios and Shen (1993) is a generalized optimization-simulation model. This model is formulated based on the network representation of the physical system. The model basically consists of a simulation module and an optimization module. The simulation module is nested in the optimization module. The model may be used for pure simulation studies or for combined simulation optimization studies. In implementing this scheme, both simulation and optimization models would interact by generating the inputs to each other sequentially (or iteratively). The results obtained from one model should converge with those of the other model to achieve the desired accuracy as the cycle of optimization-simulation calculations is repeated. At the end, an optimal solution should be obtained which does not violate any of the system idiosyncrasies. The combined optimization and simulation scheme has been advocated by Jacoby and Loucks (1972).

The major model components in the simulation module of WATPOW are (1) inflow nodes, (2) demand nodes, (3) combination or junction nodes, (4) diversion nodes, (5) hydropower plants, (6) reservoirs, (7) pumped storage system, and (8) special nodes. These eight model components constitute the nodes of the network. Another major model component is the links or arcs which connect the various nodes in the network. Essentially, the links represent watercourses such as closed conduits, diversion canals, fish links, or rivers. Along with the major model, components are processes such as reservoir evaporation, reservoir leakage, and canal conveyance losses. The simulation model of WATPOW performs mass balance calculations from node to node throughout the network. The nodal calculations may be in any order, provided that when calculations are performed for a given node, all its inflows, demands, outflows, and operation rules are known. The order or sequence of the nodal calculations is specified by the user.

There are three optimization procedures available in the WATPOW model, namely, (1) the constrained simplex algorithm called COMPLEX due to Box (1965); (2) incremental dynamic programming (IDP) procedure; and (3) genetic algorithm. For purposes of this study, the COMPLEX optimization method is utilized since it is a fast and efficient method compared to the other techniques.

The COMPLEX method is a nonlinear optimization algorithm using a sequential search technique. To initiate the search technique, a set of alternative feasible solutions are randomly generated based on the constraints on the decision variables. The technique tends to find the global solution due to the fact that the initial set of solution are randomly scattered throughout the feasible region of the optimization problem. No derivatives are required in the technique, and the technique is generally applicable in solving optimization problems with nonlinear objective function and nonlinear equality and inequality constraints. The decision variables are flow

releases at designated release outlets of specified reservoirs as well as flow amounts at specified flow links in the network. In the WATPOW program, the subprogram to perform the COMPLEX optimization technique was adapted from Kuester and Mize (1973). The use of the COMPLEX algorithm in reservoir operations had been demonstrated by Ford et al. (1981), and its application to wastewater treatment design was presented by Craig et al. (1978).

Optimization with the COMPLEX technique can be conducted on a day-to-day or month-to-month or multi-day or multi-month basis. Say for month-to-month or multi-month optimization, the COMPLEX optimization is conducted as follows. For a certain *planning horizon*, say a length of 12 months (from January to December of the first year), perform the combined simulation-optimization for this 12-month period. After this, discard the results for the months of February to December of the first year, but keep the solution for the month of January. Then proceed with the optimization-simulation scheme for the months of February of the first year to January of the second year (i.e., moving or sliding forward the 12-month planning horizon by a month) with initial conditions (such as beginning-of-month storage) already computed for January of the first year. After this, discard the results for the months March (this year) to January (succeeding year), but keep the solution for the month of February of the current year. The above process is repeated until the entire period of study is covered. The same procedure is applied for month-to-month optimization by setting the planning horizon equal to 1 month. Note that in month-to-month optimization, there is no month where the results are discarded.

Another scheme to account for foresight (i.e., future flow conditions) aside from the multiple-month *moving planning horizon* scheme is through month-to-month optimization with a *future benefit function*. An example of a future benefit function would be a function of end-of-month reservoir storage level plus current month's inflow to provide a trade-off between releasing water right away to fully satisfy the current demands (high immediate benefit but low future benefit) and holding the water in storage to prevent future severe shortages (low immediate benefit but high future benefit).

## **COMPLEX Optimization Algorithm**

The COMPLEX algorithm is used to solve the optimization (maximization) problem given by:

$$\text{Max } F(x_1, x_2, \dots, x_N) \quad (\text{B.1})$$

which is a general nonlinear function of  $N$  explicit (independent) variables  $x_1, x_2, \dots, x_N$  subject to  $M$  constraints of the form:

$$x_{\min} \leq x_i \leq x_{\max} \quad (\text{B.2})$$

in which  $x_{N+1}, x_{N+2}, \dots, x_M$  are implicit variables and are functions of the explicit variables  $x_1, x_2, \dots, x_N$  and the lower and upper constraints  $x_{\min}$  and  $x_{\max}$ ,

respectively, are either constants or functions of  $\mathbf{x}_1, \mathbf{x}_2, \dots, \mathbf{x}_N$ . Constraints on the variables  $\mathbf{x}_1, \mathbf{x}_2, \dots, \mathbf{x}_N$  are called explicit constraints, and the constraints on  $\mathbf{x}_{N+1}, \mathbf{x}_N, \dots, \mathbf{x}_M$  are called implicit constraints. Note that  $M$  should be greater or equal to  $N$ .

In the WATPOW model, the explicit variables can be any system variables computed in the simulation model such as flow amounts in the links, reservoir flow releases, and hydropower energy or capacity generated. Also, values of the objective function  $F(\mathbf{x}_1, \mathbf{x}_2, \dots, \mathbf{x}_N)$  and the implicit variables  $\mathbf{x}_{N+1}, \mathbf{x}_{N+2}, \dots, \mathbf{x}_M$  as well as the lower and upper constraints  $x_{\min}$  and  $x_{\max}$ , respectively, are calculated in user-supplied subroutines in the WATPOW model.

To find the solution of the above optimization problem using COMPLEX optimization, the algorithm proceeds as follows:

*S1.* Generate the initial  $P$  feasible sets of solution. A value of  $P \geq 2N$  is suggested. It is suggested that one initial set of points  $(\mathbf{x}_{1,1}, \mathbf{x}_{2,1}, \dots, \mathbf{x}_{N,1})$  that satisfies all  $M$  constraints must be known and entered as input. The remaining  $P - 1$  points are generated by:

$$x_{i,k} = x_{\min} + (x_{\max} - x_{\min}) \cdot U \quad \text{for } i = 1, 2, \dots, N; k = 2, 3, \dots, P \quad (\text{B.3})$$

in which  $U$  is a uniformly distributed random number over the interval [0,1].

After generating each point of the  $k$ th set of solution, a check is made if it satisfies all the constraints. While the generating equation in (B.3) assures that the explicit constraints are satisfied, the implicit constraints may not be satisfied. If the  $i$ -th generated point of the  $k$ th solution set violates the constraints, calculate the new points:

$$x_{i,k} = (\bar{x}_i + x_{i,k})/2 \quad \text{for } i = 1, 2, \dots, N \quad (\text{B.4})$$

where  $k$  is the number of solution sets that have already been generated in which  $2 \leq k \leq P$  and the centroid of the remaining points  $\bar{x}_i$  is defined as:

$$\bar{x}_i = \frac{1}{k-1} \left[ \sum_{j=1}^k x_{i,j} - x_{i,k} \right] \quad \text{for } i = 1, 2, \dots, N \quad (\text{B.5})$$

The use of Eqs. (B.4) and (B.5) is repeated as many times as necessary to satisfy all implicit constraints.

*S2.* For each feasible set, evaluate the objective function  $F(\cdot)$  for  $k = 1, 2, \dots, P$ . Then, select the point having the lowest objective function say solution set  $m$ , and carry out the reflection step to compute new values for this solution set using the following formula:

$$x_{i,m} = \bar{x}_i + \alpha[\bar{x}_i - x_{i,m}] \quad \text{for } i = 1, 2, \dots, N \quad (\text{B.6})$$

where the centroid is computed as:

$$\bar{x}_i = \frac{1}{P-1} \left[ \sum_{j=1}^P x_{i,j} - x_{i,m} \right] \quad \text{for } i = 1, 2, \dots, N \quad (\text{B.7})$$

In Eq. (B.6) a value of 1.3 is recommended for  $\alpha$ .

After the above procedure, one of the following actions is taken:

- (a) If the new computed point is feasible and its corresponding objective function value is worse than its previous objective function value, then recompute a new set of points using Eq. (B.4) until a better objective function value is obtained. Then go to step **S4**.
- (b) If the new computed point is feasible and its corresponding objective function value is better than its previous value, then go to step **S4**.
- (c) If the new computed point is infeasible, go to step **S3**.

**S3.** Adjust for feasibility as follows:

- (a) If an explicit constraint is violated, the point is moved inside the constraint by setting it equal to the upper or lower bound of the constraint whichever is applicable.
- (b) If an implicit constraint is violated, the point is moved one-half distance toward the centroid of the remaining points using Eq. (B.4).

**S4.** Check for convergence. Convergence is attained if the objective function values can no longer be improved for a specified maximum number of iterations. An iteration is defined as the calculations required to select a new point that satisfies the constraints and does not repeat in yielding the lowest objective function value.

## References

- Box MJ (1965) A new method of constrained optimization and a comparison with other methods. Computer J 8(1):42–52
- Craig EW, Meredith DD, Middleton AC (1978) Algorithm for optimal activated sludge design. J Environ Eng 104(EE6):1101–1117
- Ford DT, Garland R, Sullivan C (1981) Operation policy analysis: Sam Rayburn reservoir. J Water Resour Plan Manag ASCE 107(WR2):339–350
- Jacoby HD, Loucks DP (1972) Combined use of optimization and simulation models in river basin planning. Water Resources Research 8(6):1401–1414
- Tabios GQ III, Shen HW (1993) WATPOW (water and power) simulation-optimization model: Program documentation and user's manual, Document submitted to the Electric Resource Planning, Pacific Gas and Electric Company, San Francisco

## Appendix C

### **Coupled Solution of the Shallow Water and Advection-Dispersion Equations by Finite Volume Method**

#### **Shallow Water and Advection-Dispersion Equations**

The two-dimensional shallow water equations are composed of the mass continuity equation and the two components (in the x- and y- directions) of the momentum equations. These equations given by the first three equations below describe the lake flow hydraulics in terms of the changes of water stages and velocities in time and space. The fourth equation is the two-dimensional advection-dispersion equation to describe the salinity transport process in the lake.

*Continuity equation:*

$$\frac{\partial h}{\partial t} + \frac{\partial hu}{\partial x} + \frac{\partial hv}{\partial y} = q_L \quad (\text{C.1})$$

*Momentum equation in the x-direction:*

$$\begin{aligned} \frac{\partial hu}{\partial t} + \frac{\partial (hu^2 + gh^2)}{\partial x} + \frac{\partial huv}{\partial y} &= gh(s_{ox} - s_{fx}) + \varphi hv \\ &+ \frac{1}{\rho} \left[ \tau_x^s + \frac{\partial h\tau_{xx}}{\partial x} + \frac{\partial h\tau_{xy}}{\partial y} \right] - \frac{gh^2 \partial \rho}{2\rho_0 \partial x} \end{aligned} \quad (\text{C.2})$$

*Momentum equation in the y-direction:*

$$\begin{aligned} \frac{\partial hv}{\partial t} + \frac{\partial huv}{\partial x} + \frac{\partial (hv^2 + gh^2/2)}{\partial y} &= gh(s_{oy} - s_{fy}) - \varphi hv \\ &+ \frac{1}{\rho} \left[ \tau_y^s + \frac{\partial h\tau_{yx}}{\partial x} + \frac{\partial h\tau_{yy}}{\partial y} \right] - \frac{gh^2 \partial \rho}{2\rho_0 \partial y} \end{aligned} \quad (\text{C.3})$$

*Advection-dispersion equation:*

$$\frac{\partial hC}{\partial t} + \frac{\partial huC}{\partial x} + \frac{\partial hvC}{\partial y} = \frac{\partial}{\partial x} \left( D_x \frac{\partial hC}{\partial x} \right) + \frac{\partial}{\partial y} \left( D_y \frac{\partial hC}{\partial y} \right) + C_s \quad (\text{C.4})$$

In the above equations, the variable  $h$  denotes the water depth;  $u$  and  $v$  denote the depth-averaged velocity components in the  $x$ - and  $y$ -directions, respectively;  $q_L$  is the lateral inflow;  $s_{ox}$  and  $s_{fx}$  are the bed slope and friction slope in the  $x$ -direction, respectively;  $s_{oy}$  and  $s_{fy}$  are bed slope and friction slope in the  $y$ -direction, respectively;  $g$  is the gravitational acceleration;  $\varphi$  is the Coriolis parameter;  $\tau_x^s$  and  $\tau_y^s$  are

surface stresses such as wind stresses;  $\tau_{xx}$ ,  $\tau_{xy}$ ,  $\tau_{yx}$ , and  $\tau_{yy}$  are the turbulent shear stresses in which  $\tau_{xy}$ , for instance, is the shear stress in the  $x$ -direction on a plane perpendicular to the  $y$ -direction;  $C$  is the solute (salinity) concentration;  $D_x$  and  $D_y$  are the dispersion coefficients;  $\rho = \rho(C)$  is the density of water mixture which is a function of the solute concentration  $C$ ; and  $\rho_o$  is the density of water.

In the finite volume method formulation, it is convenient to rewrite the above equations in vector form as follows:

$$\frac{\partial q}{\partial t} + \frac{\partial f(q)}{\partial x} + \frac{\partial g(q)}{\partial y} = b(q) \quad (\text{C.5})$$

where  $q = [h, hu, hv, hC]^T$  is the conserved physical vector,  $f(q) = [hu, hu^2 + gh^2/2, huv, huC]^T$  is the flux vector in the  $x$ -direction, and  $g(h) = [hv, hvu, hv^2 + gh^2/2, hvC]^T$  is the flux in the  $y$ -direction.

The source term  $b(q)$  in Eq. (C.5) is written as:

$$b(q) = \begin{bmatrix} gL \\ gh(s_{0x} - s_{fx}) - \varphi hv + \frac{1}{\rho} \left( \tau_x^s + \frac{\partial h\tau_{xx}}{\partial x} + \frac{\partial h\tau_{xy}}{\partial y} \right) - \frac{gh^2 \partial p}{\rho_o \partial x} \\ gh(s_{0y} - s_{fy}) + \varphi hv + \frac{1}{\rho} \left( \tau_y^s + \frac{\partial h\tau_{yx}}{\partial x} + \frac{\partial h\tau_{yy}}{\partial y} \right) - \frac{gh^2 \partial p}{2\rho_o \partial y} \\ \frac{\partial}{\partial y} \left( D_x \frac{\partial hC}{\partial x} \right) + \frac{\partial}{\partial y} \left( D_y \frac{\partial hC}{\partial y} \right) + C_s \end{bmatrix} \quad (\text{C.6})$$

## Finite Volume Method Formulation

Following the model development in Zhao et al. (1994), integration of Eq. (C.5) over an arbitrary element  $\Omega$  yields the basic equation of the FVM obtained using the divergence theorem as:

$$\int_{\Omega} \int q_i d\omega = - \int_{\partial\Omega} F(q) \cdot n dL + \int_{\Omega} \int b(q) d\omega \quad (\text{C.7})$$

in which  $n$  is a unit outward vector normal to the boundary  $\partial\Omega$ ;  $d\omega$  and  $dL$  are the area and arc elements, respectively. The integrand  $F(q) \cdot n$  is the normal flux vector in which  $F(q) = [f(q), g(q)]^T$ .

The vector quantity  $q$  is assumed constant over an element. Thus, discretizing Eq. (C.7), the basic equation of the FVM is:

$$A \frac{dq}{dt} = - \sum_{j=1}^m F_n^j(q) L^j + Ab(q) \quad (\text{C.8})$$

where  $A$  is area of an element;  $m$  is the total number of sides for an element;  $j$  is the index for the side of the element;  $L^j$  is the length of the side; and  $b(q)$  is the source term of the Eq. (C.8). For each side of the element,  $F_n^j(q)$  denoted hereafter by  $F_n(q)$  is defined as [Spekreijse 1988]:

$$F_n(q) = \cos \Phi f(q) + \sin \Phi g(q) \quad (\text{C.9})$$

As shown by Spekreijse (1988),  $f(q)$  and  $g(q)$  have a rotational invariance property satisfying the relation:

$$T(\Phi)F_n(q) = f[T(\Phi)q] = f(\bar{q}) \quad (\text{C.10})$$

or

$$F_n(q) = T(\Phi)^{-1}f(\bar{q}) \quad (\text{C.11})$$

where  $\Phi$  is the angle between vector  $n$  and the  $x$ -axis (measured counterclockwise from the  $x$ -axis);  $T(\Phi)$  and  $T(\Phi)^{-1}$  are the transformation and inverse transformation matrices, respectively.

Finally, Eq. (C.8) can be rewritten as:

$$A \frac{dq}{dt} = - \sum_{j=1}^m T(\Phi)^{-1}f(\bar{q}) L^j + Ab(q) \quad (\text{C.12})$$

Note that the quantity  $\bar{q}$  is transformed from  $q$ , with velocity components in the normal and tangential directions. The quantity  $q$  (or likewise  $\bar{q}$ ) can have different values for each element in the computation domain, and thus the value of  $q$  is discontinuous across the interface between elements.

### Normal Flux Estimation as a Riemann Problem

In view of the discontinuity of  $q$  across the interface between elements, the estimation of the transformed flux  $f(\bar{q})$  in Eq. (C.12) translates into the problem of solving a local one-dimensional Riemann problem in the direction normal to the

element interface. The local one-dimensional Riemann problem is an initial value problem written as follows:

$$\frac{\partial \bar{q}}{\partial t} + \frac{\partial f(\bar{q})}{\partial \bar{x}} = 0 \quad (\text{C.13})$$

with

$$\bar{q}(\bar{x}, 0) = \begin{cases} \bar{q}_L & \bar{x} < 0 \\ \bar{q}_R & \bar{x} > 0 \end{cases} \quad (\text{C.14})$$

The origin of the  $\bar{x}$ -axis is located at the midpoint of that side, and it is directed to the outward normal. The quantity  $f(\bar{q})$  is a normal outward flux at the origin of the  $\bar{x}$ -axis. The quantities  $\bar{q}_L$  and  $\bar{q}_R$  are the properties on the left and right, respectively, of the element interface. Initially, states of  $\bar{q}$  at time  $t = 0$  are assumed to be known. By solving the Riemann problem, the desired outward normal flux  $f(\bar{q})$  which is at the origin  $\bar{x} = 0$  and at time  $t = 0^+$  can be obtained.

### Estimation of Normal Flux by Osher Scheme

There are several numerical procedures to solve the Riemann problem above. Zhao et al. (1996) have examined three of these methods. The Osher scheme developed by Osher and Solomone (1982) is the scheme adopted to the model presented here. This scheme is based on characteristics theory. Based on the developments done in Zhao et al. (1996), the flux  $f(\bar{q})$  is given by:

$$f(\bar{q}) = f_{LR}(\bar{q}_L, \bar{q}_R) = \begin{cases} f^+(\bar{q}_L) + f^-(\bar{q}_R) \\ f(\bar{q}_L) + \int_{\bar{q}_L}^{\bar{q}_R} J^-(\bar{q}) d\bar{q} \\ f(\bar{q}_R) + \int_{\bar{q}_L}^{\bar{q}_R} J^+(\bar{q}) d\bar{q} \end{cases} \quad (\text{C.15})$$

where  $J^+(\bar{q})$  and  $J^-(\bar{q})$  are the Jacobian matrices associated to the positive and negative eigenvalues of the Jacobian matrix of Eq. (C.15) given by:

$$J(\bar{q}) = \frac{df}{d\bar{q}} = \begin{bmatrix} 0 & 1 & 0 & 0 \\ c^2 - \bar{u}^2 & 2\bar{u} & 0 & 0 \\ -\bar{u}\bar{v} & \bar{v} & \bar{u} & 0 \\ -C\bar{u} & C & 0 & \bar{u} \end{bmatrix} \quad (\text{C.16})$$

where  $c = \sqrt{gh}$  is the wave celerity. The flux  $f(\bar{q})$  in Eq. (C.15) is determined through integration over a continuous integral path as described in Zhao et al. (1994). The reader may refer to this paper for details of the numerical algorithm.

## References

- Osher S, Solomone F (1982) Upwind difference schemes for hyperbolic systems of conservation laws. *Math. Computer Simulation* 38:339–374
- Spekreijse SP (1988) Multigrid solution of steady Euler Equations, CWI Tract 46 Amsterdam
- Zhao DH, Shen HW, Tabios GQ III, Lai JS, Tan WY (1994) Finite volume two-dimensional unsteady-flow model for river basins. *Jour. of Hydraulic Engineering, ASCE* 120:863–883
- Zhao DH, Shen HW, Lai JS, Tabios GQ III (1996) Approximate Riemann solvers in FVM for 2D hydraulic shock wave modeling. *J Hydraul Eng, ASCE* 122:692–702

## Appendix D

### *SWATCH Model and Components*

The SWATC<sub>H</sub> was originally developed by Morel-Seytoux et al. (1987) and likewise described in Morel-Seytoux et al. (1999). SWATC<sub>H</sub> models surface and subsurface flows in a soil-aquifer-stream system as shown in Fig. D.1. The various components of the hydrologic process considered in the SWATC<sub>H</sub> model are as follows:

- Rainfall
- Infiltration, excess rainfall, and retention storage
- Soil moisture accounting in the root zone
- Evapotranspiration
- Interflow zone and interflow discharge
- Groundwater flow and stream-aquifer return flow
- Overland flow and channel flow routing

The model being a continuous simulation model has a soil-moisture accounting scheme that tracks the state of moisture of the watershed that could generate streamflow (from interflow or/and baseflow) during periods of no rainfall. Figure D.1 also shows the pertinent equations to model various components of the

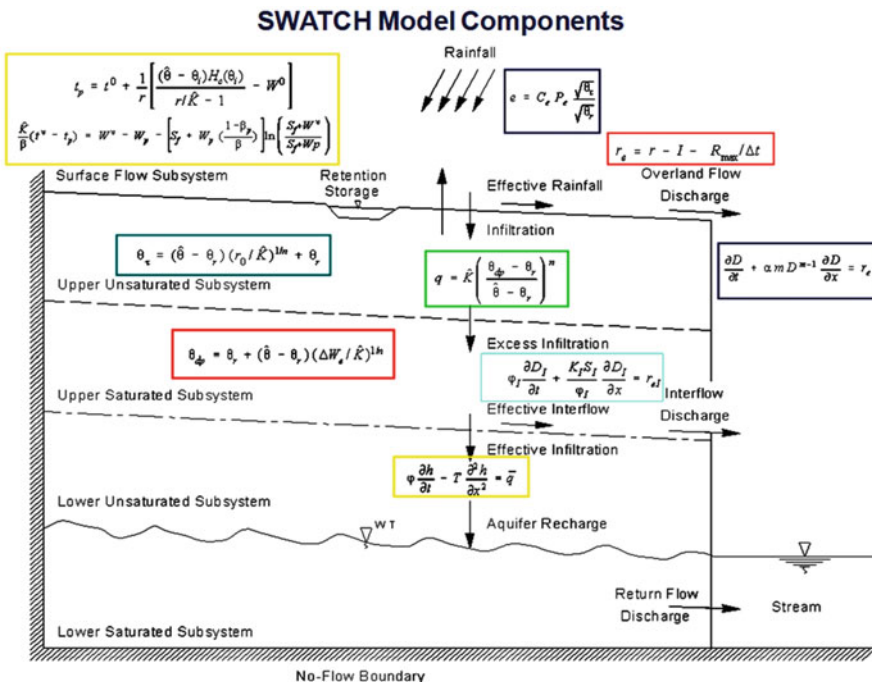


**Fig. D.1** Schematic diagram of the SWATC<sub>H</sub> model structure and components

hydrologic processes. The various equations are solved analytically as well as semi-analytically with the use of discrete kernels. Also, it may be noted below that the model parameters of SWATC<sub>H</sub> are mostly physically based and in fact some of them can be specified directly knowing the soil types and vegetal cover, among others.

Each of these components is described in detail below.

## Rainfall

In the model, a watershed is divided into river systems, reaches, and units. Also, the study area is divided into various climatological zones, with uniform rainfall rate for each zone. Given several rain gage stations in the study area, the uniform rainfall rate for each river system and each unit is given by the weighting function:

$$r(i_R, i_U) = \sum_{j=1}^{N_{ZU}} r(k_j) w(k_j) \quad (\text{D.1})$$

where  $r(i_R, i_U)$  is the areal rainfall rate at river basin  $i_R$  and unit  $i_U$ ,  $r(k_j)$  is the rainfall rate at gaging station  $k_j$ ,  $w(k_j)$  is the corresponding weight of the gaged rainfall, and  $N_{ZU}$  is the number of gaging stations. Note that in the model, an important input parameter are the weights  $w(k_j)$ .

## Infiltration, Excess Rainfall, and Retention Storage

The amount of water that infiltrates into the soil depends on whether the upper soil layer has ponded or not. Ponding occurs when the upper soil layer (surface) has attained natural saturation. Before ponding, the infiltration rate is taken equal to the rainfall supply. In this case, the excess rainfall which is the difference of rainfall supply rate and infiltration rate is equal to zero. Symbolically, the infiltration rate before ponding time  $t_p$  is defined as:

$$I = r \quad (\text{D.2})$$

in which  $I$  is the infiltration rate and  $r$  is the rainfall supply rate taken equal to  $r(i_R, i_U)$  [computed in Eq. (D.1)]. Note that the time subscripts have simply been omitted in the infiltration and rainfall variables in Eq. (D.2) for the sake of brevity. The excess rainfall is of course equal to zero since all rainfall supply goes to infiltration.

The ponding time  $t_p$  is calculated based on the Green-Ampt infiltration equation written as:

$$t_p = t^0 + \frac{1}{r} \left[ \left( \frac{\theta - \theta_i H_c(\theta_i)}{r/K - 1} \right) - W_0 \right] \quad (\text{D.3})$$

in which  $t^0$  is the time at the beginning of the time step,  $\theta$  is the water content at natural saturation taken equal to porosity,  $\theta_i$  is the initial soil moisture content,  $K$  is the hydraulic conductivity at natural saturation, and  $W^0$  is the cumulative infiltration depth since the beginning of the currently, *ongoing* rainfall up to time  $t^0$ . In Eq. (D.3),  $H_c(\theta_i)$  is the effective capillary drive defined by:

$$H_c(\theta_i) = \left[ 1 - \left( \frac{\theta_i - \theta_r}{\theta - \theta_r} \right)^6 \right] H_{\max} \quad (\text{D.4})$$

where  $H_{\max}$  is the maximum value of the capillary drive, that is, when the soil moisture content is equal to the residual moisture content  $\theta_r$ . The residual moisture is usually taken equal to the soil moisture condition at field capacity.

After ponding time, the infiltration rate is calculated as follows:

$$I = \frac{W^v - W^0}{\Delta t} \quad (\text{D.5})$$

where  $W_0$  is the cumulative infiltration depth at the beginning of the time step and the cumulative infiltration depth  $W^v$  in Eq. (D.5) is calculated from the nonlinear function:

$$\frac{K}{\beta}(t^v - t_P) = W^v - W_P - \left[ S_f + W_P \left( \frac{1 - \beta_P}{\beta} \right) \right] \ln \left( \frac{S_f + W^v}{S_f + W_P} \right) \quad (\text{D.6})$$

where  $W_P$  is the cumulative infiltration depth at ponding time,  $\beta$  is the viscous correction factor,  $\beta_P$  is the viscous correction factor at ponding time, and  $S_f$  is the storage-suction factor defined by:

$$S_f = (\theta - \theta_i)H_c(\theta_i) \quad (\text{D.7})$$

Equation (D.6) together with Eq. (D.7) must be solved numerically for  $W^v$ .

As mentioned earlier, there is no excess rainfall before ponding. However, after ponding time  $t_P$ , the effective excess rainfall is calculated by:

$$r_e = r - I - R_{\max}/\Delta t \quad (\text{D.8})$$

where  $r_e$  is the excess rainfall rate,  $I$  is the infiltration rate using Eq. (D.5), and  $R_{\max}$  is the maximum retention storage depth over the time interval  $\Delta t$ .

In the various equations given above, there are several parameters and initial variables to be specified in the model. In Eqs. (D.3) and (D.4), the porosity  $\theta$ , initial soil moisture content  $\theta_i$ , the residual moisture  $\theta_r$ , the hydraulic conductivity  $K$ , and the maximum capillary drive  $H_{\max}$  are model parameters to be specified. The parameters to be specified in Eqs. (D.6) and (D.8) are the viscous correction factor  $\beta$  and the maximum retention storage depth  $R_{\max}$ .

## Soil Moisture Accounting in the Root Zone

Water that infiltrates into the soil surface after ponding time and also while the rainfall event is ongoing is assumed to pass through the root zone (upper layer of soil) at the rate governed by the infiltration rate. The infiltration rate is calculated based on the Green-Ampt type equation given by Eq. (D.6) at which the soil is at saturated (ponded) conditions. Eventually, the infiltrated water reaches the interflow zone which is the portion of the unsaturated zone below the root zone layer. After the cessation of rainfall or when the rainfall rate becomes less than the hydraulic conductivity (i.e., when the potential infiltration rate is greater than the rainfall supply), the soil moisture content in the root zone reduces in time from fully saturated to an unsaturated condition. In this case, the moisture content in the soil  $\theta_\tau$  is computed by:

$$\theta_\tau = (\theta - \theta_r)(r_0/K)^{1/n} + \theta_r \quad (\text{D.9})$$

where  $r_0$  is the last rainfall intensity before cessation of the rainfall event (i.e., entire storm episode) and  $n$  is an exponent in power law for relative permeability to water. The position of the wetting front (i.e., distance below the ground at that  $\theta_\tau$  moisture content from the ground surface) is given by:

$$z_f = \frac{W - e - q_i t}{\theta_\tau - \theta_r} \quad (\text{D.10})$$

in which  $z_f$  is the wetting front distance from the ground surface,  $e$  is the evapotranspiration rate, and  $q_i$  is the water flux across a plane coinciding with the bottom of the root zone at time  $t$ .

In the above equations, the model parameters to be specified are the exponent  $n$ .

## Evapotranspiration

Evapotranspiration occurs in the unsaturated zone of vegetated areas. The actual evapotranspiration rate is computed by:

$$e = C_e P_e \frac{\sqrt{\theta_\tau}}{\sqrt{\theta_r}} \quad (\text{D.11})$$

where  $e$  is the actual evapotranspiration rate,  $C_e$  is evapotranspiration coefficient,  $P_e$  is the average daily pan-evaporation rate,  $\theta_\tau$  is the current soil moisture content in the root zone, and  $\theta_r$  is the residual water content. The variables  $C_e$ ,  $P_e$ , and  $\theta_r$  are part of

the model inputs to be supplied by the user, while the variable  $\theta_\tau$  is computed in Eq. (D.9) every time step.

### Interflow Zone and Interflow Discharge

The interflow zone which is right below the root zone is fed by excess infiltration from the root zone. The excess infiltration rate is computed by:

$$q = K \left( \frac{\theta_{dp} - \theta_r}{\theta - \theta_r} \right)^n \quad (\text{D.12})$$

where  $q$  is the excess infiltration rate which depends on the soil moisture content of the interflow zone  $\theta_{dp}$  and  $K$  is the hydraulic conductivity of the interflow zone. The soil moisture content in the interflow zone is updated after accumulating some excess infiltration over a certain time period as follows:

$$\theta_{dp} = \theta_r + (\theta - \theta_r)(\Delta W_e/K)^{1/n} \quad (\text{D.13})$$

where  $\Delta W_e$  is the effective recharge depth (cumulative excess infiltration depth) calculated as the sum of the excess infiltration rate multiplied by the time interval for some specified time period.

Soil moisture accumulated from the interflow is drained to become interflow discharge to the overland flow (and eventually to the river) or water that deep percolates into the saturated groundwater zone. Interflow discharge to the overland flow plane is calculated as follows:

$$q_I = K_I S_I D_I \quad (\text{D.14})$$

where  $q_I$  is the discharge per unit width,  $K_I$  is the hydraulic conductivity,  $S_I$  is the bed slope, and  $D_I$  is the flow depth. The interflow discharge is routed to the flow outlet using the kinematic wave equations of mass and momentum. Specifically, the mass continuity equation is written as:

$$\varphi_I \frac{\partial D_I}{\partial t} + \frac{\partial q_I}{\partial x} = r_{el} \quad (\text{D.15})$$

where  $\varphi_I$  is the porosity in the interflow zone (n.b. a model parameter to be specified) and  $r_{el}$  is any lateral inflow to the interflow zone.

The momentum equation under the kinematic wave assumption is obtained by neglecting the acceleration and external pressure terms, such that the friction slope is equal to bed slope. Thus, with an appropriate friction equation, the friction slope

term can be simply replaced by the bed slope. For Darcy-type friction equation, this essentially results in Eq. (D.14). Replacing the flow variable  $q_I$  in Eq. (D.15) by Eq. (D.14) results in:

$$\varphi_I \frac{\partial D_I}{\partial t} + \frac{K_I S_I}{\varphi_I} \frac{\partial D_I}{\partial x} = r_{el} \quad (\text{D.16})$$

Equation (D.16) is now a partial differential equation with only one unknown variable  $D_I$ .

### Groundwater Recharge and Stream-Aquifer Return Flows

The one-dimensional linearized Boussinesq equation is used to describe the head distribution due to aquifer recharge. This is given by the following equation:

$$\varphi \frac{\partial h}{\partial t} - T \frac{\partial^2 h}{\partial x^2} = q \quad (\text{D.17})$$

in which  $h$  is the head in the aquifer measured from the stream level,  $q$  is the mean aquifer recharge rate,  $\varphi$  is the effective (drainable) aquifer porosity, and  $T$  is the aquifer transmissivity. The distance  $x$  is measured perpendicular to the stream direction and originates at the stream bank, and  $t$  is for time.

In the model, the groundwater equation above is not directly used. Instead the problem is translated into calculating the mean return flow (baseflow) discharge from the groundwater to the stream or river using discrete kernels of the unit hydrograph theory with the mean aquifer recharge rate  $q$  as input (excitation) function and that the discrete kernels are evaluated based on the groundwater equation defined by Eq. (D.17). It is quite lengthy to show the equations here, and the reader is referred to the original model documentation by Morel-Seytoux and Alhassoun (1987).

The aquifer porosity ( $\varphi$ ) and transmissivity ( $T$ ) are model parameters to be specified.

### Overland Flow and Channel Flow Routing

The excess rainfall is routed through the overland flow plane using the kinematic wave equations composed of the mass and momentum equations. The mass (conservation) equation is given by:

$$\frac{\partial D}{\partial t} + \frac{\partial q}{\partial x} = r_e \quad (\text{D.18})$$

where  $D$  is the flow depth,  $q$  is the discharge per unit width, and  $r_e$  is the effective rainfall depth on the overland flow plane. The momentum equation under the kinematic wave assumption simply reduces to the following:

$$S_f = S_0 \quad (\text{D.19})$$

in which  $S_f$  and  $S_0$  are the friction slope and bed slope, respectively. Using any friction equation such as the Manning's equation or Chezy's equation, we can generally write the equation relating flow depth and discharge as follows:

$$q = \alpha D^m \quad (\text{D.20})$$

Assuming a wide rectangular channel (normally assumed for an overland flow plane) the relevant parameters above can be written as  $\alpha = \sqrt{S_0}/n_M$  in which  $n_M$  is the Manning's roughness coefficient and  $m = 5/3$ . In this particular case, the kinematic wave equation can be rewritten as:

$$\frac{\partial D}{\partial t} + \alpha_m D^{m-1} \frac{\partial D}{\partial x} = r_e \quad (\text{D.21})$$

which is an equation that can be solved for the flow depth  $D$ . The above equation can be readily solved using method of characteristics or other means such as finite difference schemes.

For channel flow routing, the same kinematic wave equations given above are used. Rectangular shaped channels are also assumed and appropriate bed slope and Manning's roughness coefficient are used. However, the effective rainfall variable in Eq. (D.18) or Eq. (D.21) is replaced by lateral inflows which consist of overland flow, interflow, and baseflow components.

In the above equations, the model parameters to be specified are the Manning's roughness coefficient  $n_M$  and the bedslope  $S_0$ .

## References

- Morel-Seytoux HJ, Alhassoun SA (1987) A multi-process watershed model for simulation surface and subsurface flows in a soil-aquifer-stream hydrologic system, Report. No. 87.3. HYDROWAR Publications, Atherton
- Morel-Seytoux HJ, Alhassoun SA, Tabios GQ III, Liongson LQ, Rojas DS Jr (1999) SWATC – A distributed hydrologic watershed model. In: Proceedings of 19th Annual Hydrology Days. American Geophysical Union, Colorado State University, Fort Collins, pp 16–20